STRUCTURES IN FIRE

PROCEEDINGS OF THE FIRST INTERNATIONAL WORKSHOP

STRUCTURES IN FIRE - PROCEEDINGS OF THE FIRST INTERNATIONAL WORKSHOP

Second edition

Editor

Jean-Marc Franssen
Univ. of Liege, 1, Chemin des Chevreuils, 4000, Liège, 1, Belgium
jm.franssen@ulg.ac.be

FIRST INTERNATIONAL WORKSHOP - STRUCTURES IN FIRE

COPENHAGEN, the 19th and 20th of June, 2000

Co-organised by

University of Liege,

Danish Institute of Fire Technology,

CIB-W14 Fire.

Responsible for

the local organising committee:

Henrik Bygbjerg,

Danish Institute of Fire Technology

the concept, the proceedings:

Jean-Marc Franssen,

University of Liege

the program:

Alexander Ptchelintsev,

Technical Research Centre of Finland.

Sponsor

Danish Institute of Fire Technology

Why this workshop?

Looking back some 10 or 20 years ago, the scientific community dealing with the problem of fire in buildings could, schematically, be divided into two separate groups; one group was dealing with the fire side of the problem and was considering that the temperature of 540°C was anything which had to be known concerning the structure of the building; the other group was investigating the behaviour of the structure, quite happy with the comfortable feeling that the ISO curve was a perfect representation of the fire.

The disadvantages of this situation with very little, if any, communication between the two groups progressively became more and more evident and people started to consider talking to each other and, even more, to widen their field of investigation and have a look into the other guy's garden. Other aspects also came into consideration such the behaviour of human beings, risk analysis, etc. This evolution lead to the now widely accepted concept of Fire Safety Engineering which, simply saying, is nothing more than the fact that we are starting to treat the problem of Fire Safety in the way that engineers treat other problems, i.e. trying to do their best in order to take into consideration every phenomenon which is suspected to play a role.

There was anyway a positive aspect to the situation prevailing in these old days: it was very easy and common to meet and discuss with the few people who had a real expertise in your field of application. Specialised meetings were regularly organised in which all the experts who counted would normally show up. For the structural analysis, some examples are:

the ECCS workshop on material properties at elevated temperatures, by ECCS committee 3 - Fire safety of steel structures, in Arnhem, The Netherlands, in June 1986,

the EGOLF seminar "Protection contre l'incendie des structures en acier. Harmonisation Européenne", in Brussels, Belgium, in November 1986,

the Abschlusskolloquium "Bauwerke unter Brandeinwerkung", Technische Universität Braunschweig, in Braunschweig, Germany, in April 1987,

the Eurocodes, Structural Fire Design, Seminar organised by the Eurocode fire drafting groups, in Luxembourg, in June 1990,

the 3rd CIB/W14 Fire Safety Engineering Workshop on Modelling, in Rijswijk, The Nederlands, in January 1993,

or, to some extend, the First European Symposium on Fire Safety Science, IAFSS, in Zürich, Switzerland, in August 1995.

The field of interest was certainly too narrow, but the progress were spectacular. Nowadays, the same specialists and their presentations tend to be disseminated in different places and various meetings: for the organiser of every structural conference on steel, on concrete or on wood, this looks much smarter if he has a session on such an exotic topic as fire, and a couple of papers are indeed published in these general conferences but the interest of the public is generally poor, and very few of those who would really be interested are present. The same problem holds for the publications that, as academic, many researchers have to present in some journals which are prestigious but have only a marginal interest for fire.

Concerning the big conferences specifically dedicated to the fire – and leaving apart that some of them appear now to be concurrent which is another reason of dissemination – if they are of the highest importance because they allow to open your eyes to other aspects than those that you treat in your everyday life, it has to be recognised that the number of presentation is so high that very short time can be dedicated to discussion and that it is not easy to have detailed information on a specific topic.

At the end of 1998 and during the year of 1999, the idea was circulating that a specific association could be created on the topic of structural fire modelling. An exchange of e-mail messages followed and, finally, the topic was discussed in July at an informal meeting in Poitiers during the IAFSS symposium. The general opinion was that it would be better not to have a new association, because there are already so many of them. In order to promote a more intense circulation of information among those interested by the subject, two actions were decided: one was the creation of the SiF discussion list on internet, and the second one was the organisation of this workshop.

Why a second edition of the proceedings?

Every effort was made by the authors and by the editor to have a first version of the proceedings available to the delegates on the morning of the 19th of June and, indeed, most of the papers could be incorporated in due time, only 4 communications being represented in the proceedings by a summary. Having more time to think better since they sent their copy, several authors decided to sent at a later date a revised version of their paper. These revised versions are presented in this second edition. They are marked as [*] in the list of content.

The first edition was only available to those delegates who ordered a copy when they registered to the workshop. This second edition will give the opportunity to obtain a copy of the proceedings to those who could not attend the workshop

PROGRAM AND LIST OF CONTENT

Monday 19.06.2000

9:00 – 9:30   <u>**Opening of the Workshop**</u>

10:45 – 11:00   **Coffee Break**

12:40 – 13:40   **Luncheon**

Session 3 (chairman: P. Vila Real)

13:40 –14:05   **G.Kuznetsov, A.Ptchelintsev & V. Rudzinskii**   **107-115**
*High-Temperature Heat and Mass Transfer in a Concrete Layer Used
for Biological Protection of Nuclear Reactors at Critical Heat Loads*[*]

14:05 – 14:30   **S. Welch**   **117-136**
*Developing a model for thermal performance of masonry
 exposed to fire*[*]

14:30 – 14: 55   **J. Pålsson & U. Wickström**   **137-150**
*A Scheme for Verification of Computer Codes for Calculating
Temperature in Fire Exposed Structures*

14:55 – 15:10   **Coffee Break**

Session 4 (chairman: P. Vila Real)

15:10 – 15:35   **A. Ptchelintsev**   **151-159**
*A Comparative Thermal Analysis of Structures Exposed to Fire
with Advanced Calculation Models*[*]

15:35 –16:00   **L. Twilt, P.H.E. v.d. Leur & C. Both**   **161-174**
*Characteristics of the Heat Transfer for Calculating the Temperature
Development in Structural Steelwork Exposed to Standard Fire
Conditions under Plate Thermocouple Control*[*]

16:00 – 16:25   **M. Green**   **179**
The recent U.K. BS9999 – Presentation and worked examples

18:00   Technical visit of the ***Tivoli*** amusement park in the center of Copenhagen

Tuesday 20.06.2000

Session 5 (chairman: L. Twilt)

9:00 –9:25	**Y. C. Wang & J. M. Davies** *Design of thin-walled steel channel columns in fire using* *Eurocode 3 Part 1.3*	**181-193**
9:25- 9:50	**D. Talamona & J.-M. Franssen** *New quadrangular shell element in SAFIR*	**195-210**
9:50- 10:15	**J. Myllymäki & M. Kokkala** *Thermal Exposure to a High Welded I-Beam Above a Pool Fire*	**211-224**
10:15 –10:40	**B. Zhao & D. Joyeux** *Evaluation of fire resistance of open car park under natural fire* *condition with advanced calculation models*	**225**

10:40 – 11:00 **Coffee Break**

Session 6 (chairman: L. Twilt)

11:00 – 11:25	**G. Faller** Towards a *Performance Based Design Approach for Fire Resistance* *Grading of Buildings*	**227-241**
11:25 – 11:50	**W.E. Koffel** *With Performance Codes Who Needs Structural Fire Resistance?*	**243**
11:50 – 12:15	**M. Gillie & A.S. Usmani** *An Analysis of the Behaviour of the First Cardington Test Using* *Stress-Resultant Shell Elements*	**245-266**
12:15 – 12:40	**J. Outinen, O. Kaitila & P. Mäkeläinen** *A Study for the Development of the Design of Steel Structures* *in Fire Conditions*	**267-281**

12:40 – 13:30 **Luncheon**

THERMAL EFFECTS

J.M. Rotter and A.S.Usmani
School of Civil and Environmental Engineering, University of Edinburgh

ABSTRACT

Behaviour of composite structures in fire has long been understood to be dominated by the effects of strength loss caused by thermal degradation and that large deflections and runaway resulted from the action of imposed loading on a 'weakened' structure. Thus 'strength' and 'loads' are quite generally believed to be the key factors determining structural response (fundamentally no different from ambient behaviour). The exceptional longevity of this view derives in no small measure from observations in the standard fire tests. These observations have little relevance to realistic structural configurations present in large multi-storey composite frame structures. The investigations as part of the DETR, PIT project on composite structure behaviour in fire has clearly shown that this understanding is gravely in error. A 'new understanding' has been produced from the PIT project, sponsored by DETR (UK) and executed by a consortium led by Edinburgh University and including British Steel (now CORUS) and Imperial College. The key message from this new understanding is that, composite framed structures of the type tested at Cardington possess enormous reserves of strength through adopting large displacement configurations, and that thermally induced forces and displacements, not material degradation, governs the response in fire. Degradation (mainly steel yielding and buckling) can even be helpful in developing the large displacement load carrying modes safely. This paper attempts to lay down some of the most important and fundamental principles that govern the behaviour of composite frame structures in fire in a simple and comprehensible manner. This is based upon the analysis of the response of single structural elements under a combination of thermal actions and end restraints representing the surrounding structure.

INTRODUCTION

The assessment of the adequacy of composite steel frame structures in fire continues to be based upon the performance of isolated elements in standard furnace tests. This is despite the widespread acceptance amongst structural engineers that such an approach is over-conservative and even more importantly, *unscientific*. Current codes such as BS 5950 Part 8 and EC3 (draft) allow designers to take advantage of the most recent developments in the field by treating fire related loading as another limit state. The advances in understanding of structural behaviour in fire achieved in the last few years have been considerable. In theory, these advances make it possible for designers to treat the design for fire in an integrated manner with the design of a structure for all other types of loading by using the numerical modelling tools that have been instrumental in developing this understanding. However the use of such tools, which are indispensable for research, is not practical in the design office. Exploitation of the new knowledge can only become feasible if this understanding is further developed into simpler analytical expressions, enabling consulting engineers and designers to undertake performance-based design of steel frame structures without having to resort to large scale computation.

This paper builds upon earlier work presented at the INTERFLAM conference (Report TM1). The most fundamental relationship that governs the behaviour of structures when subjected to thermal effects is:

$$\varepsilon_{total} = \varepsilon_{thermal} + \varepsilon_{mechanical}$$

$$\text{with} \quad \varepsilon_{mechanical} \to \sigma \quad \text{and} \quad \varepsilon_{total} \to \delta \tag{1}$$

The total strains govern the deformed shape of the structure δ, through kinematic or compatibility considerations. By contrast, the stress state in the structure σ (elastic or plastic) depends only on the mechanical strains.

axial expansion or thermal bowing results from

$$\varepsilon_{total} = \varepsilon_{thermal} \quad \text{and} \quad \varepsilon_{total} \to \delta \tag{2}$$

By contrast, where the thermal strains are fully restrained without external loads, thermal stresses and plastification result from

$$0 = \varepsilon_{thermal} + \varepsilon_{mechanical} \quad \text{with} \quad \varepsilon_{mechanical} \to \sigma \tag{3}$$

The single most important factor that determines a real structures response to heating is the manner in which it responds to the unavoidable thermal strains induced in its members through heating. These strains take the form of thermal expansion to an increased length (under an average centroidal temperature rise) and curvature (induced by a temperature gradient through the section depth). If the structure has insufficient end translational restraint to thermal expansion, the considerable strains are taken up in expansive displacements, producing a displacement-dominated response. Thermal gradients induce curvature leads to bowing of a member whose ends are free to rotate, again producing large displacements (deflections).

Members whose ends are restrained against translation produce opposing mechanical strains to thermal expansion strains and therefore large compressive stresses (see Equation 1). Curvatures strains induced by the thermal gradient in members whose ends are rotationally restrained can lead to large hogging (negative) bending moments throughout the length of the member without deflection. The effect of induced curvature in members whose ends are rotationally unrestrained, but translationally restrained, is to produce tension.

Therefore for the same deflection in a structural member a large variety of stress states can exist; large compressions where restrained thermal expansion is dominant; very low stresses where the expansion and bowing effects balance each other; in cases where thermal bowing dominates, tension occurs in laterally restrained and rotationally unrestrained members, while large hogging moments occur in rotationally restrained members. This variety of responses can indeed exist in real structures if one imagines the many different types of fire a structure may be subjected to. A fast burning fire that reaches flashover and high temperatures quickly and then dies off can produce high thermal gradients (hot steel and relatively cold concrete) but lower mean temperatures. By contrast, a slow fire that reaches only modest temperatures but burns for a long time could produce considerably higher mean temperature and lower thermal gradients.

Most situations in real structures under fire have a complex mix of mechanical strains due to applied loading and mechanical strains due to restrained thermal expansion. These lead to combined mechanical strains which often far exceed the yield values, resulting in extensive plastification. The deflections of the structure, by contrast, depend only on the total strains, so these may be quite small where high restraint exists, but they are associated with extensive plastic straining. Alternatively, where less restraint exists, larger deflections may develop, but with a lesser demand for plastic straining and so less destruction of the stiffness properties of the materials. These relationships, which indicate that larger deflections may reduce material damage and correspond to higher stiffnesses, or that restraint may lead to smaller deflections with lower stiffnesses, can produce structural situations which appear to be quite counterintuitive if viewed from a conventional (ambient) structural engineering perspective.

The ideas presented above will be more formally explored in the following sections in the context of simple structural configurations and analytical expressions will be developed for many cases of fundamental importance.

STANDARD FIRE TEST AND RUNAWAY FAILURES

Figure 1 shows a simple comparison of two geometrically non-linear analyses. The first case is heated, simply supported (laterally unrestrained) steel beam with a uniformly distributed load and the second is a laterally restrained (but rotationally unrestrained) beam with the same uniformly distributed load. Initial
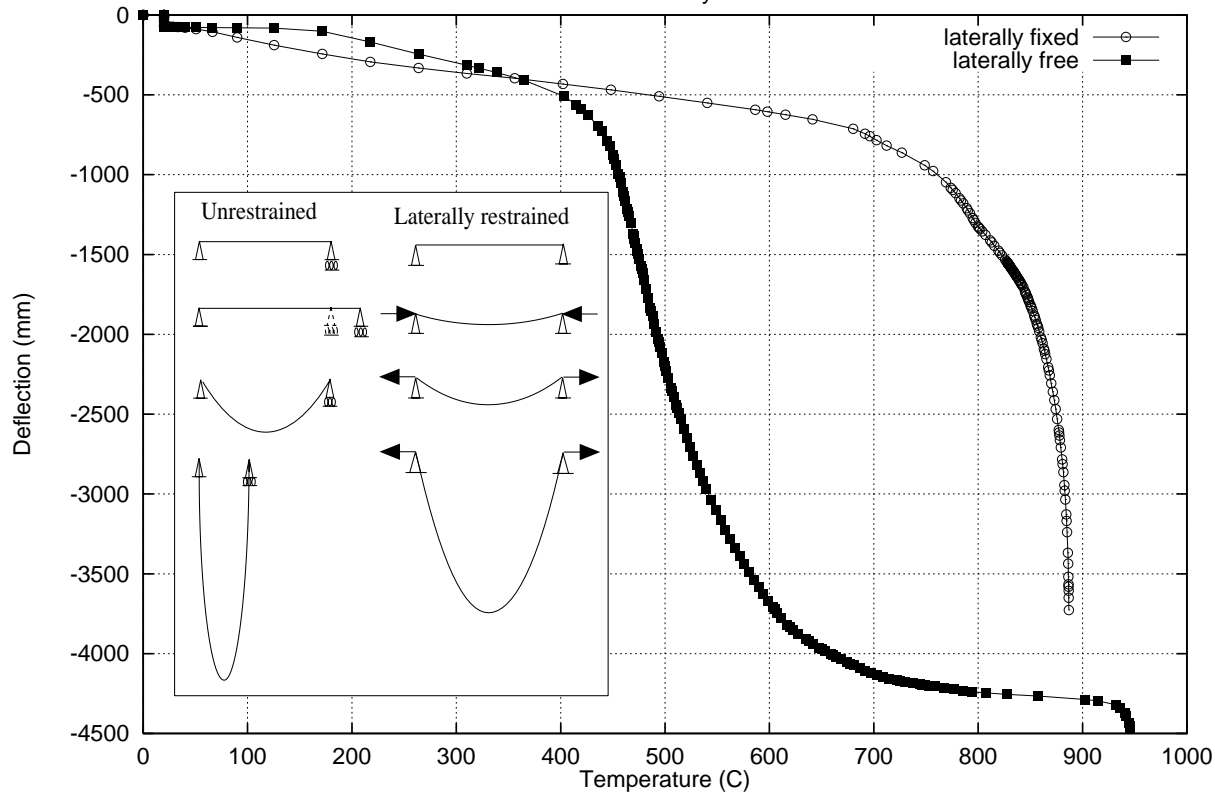
Figure 1: Runaway in unrestrained and restrained beams

deflections are lower in the first beam because the supports are able to translate outwards upon expansion. However, 'runaway' occurs at around $450°$C (even though considerable steel strength remains) mainly because of pulling in of the supports when the flexural stiffness of the beam reduces to a point where it cannot sustain the imposed load and there is nothing to restrain the growing deflections. In the second beam larger initial deflections occur because the beam 'buckles' due to the restraining forces very early on ($70°$C) and further increases in length due to thermal expansion can only be accommodated in deflection. But runaway does not occur until much later ($900°$C) when the steel properties are completely lost. This illustrates that the presence of restraints to end translation delays 'runaway' to much higher temperatures because of development of catenary action to replace the highly depleted flexural stiffness.

The second beam is a much more appropriate model for beams in large redundant structures. In real structures not only is this restraint available but the steel beam is in composite action with the concrete slab which produces a much stronger and more robust structure. This strength and robustness is enhanced by the redistribution mechanisms present in redundant structures (for instance the load may be carried by the transverse slab supported in tensile membrane action which retains its strength for much longer than the steel beams). Large deflections seen in real structures are often misinterpreted as impending runaway failure. Figure 1 clearly shows that for temperatures below $300°$C, the deflections for the restrained beam are much larger than that for the simply supported beam, however they have nothing to do with runaway. These deflections are caused entirely by the increased length of the beam through thermal expansion and are not a sign of loss of 'strength' or 'stiffness' in the beam until much later. In fact approximately 90% of the deflection at $500°$C and 75% at $600°$C is explained by thermal expansion alone. Most of the rest is explained by increased strains due to reduced modulus of elasticity. However the behaviour remains stable until about $700°$C when the first signs of runaway begin to appear.

THERMAL EXPANSION

Heating induces thermal expansion strains (say ε_T) in most structural materials. These are given by,

$$\varepsilon_T = \alpha \Delta T \tag{4}$$

If a uniform temperature rise, ΔT, is applied to a simply supported beam without axial restraint, the

total strain (say ε_t) is equal to the thermal strain and there is no mechanical strain (say ε_m) which means that no stresses develop in the beam.
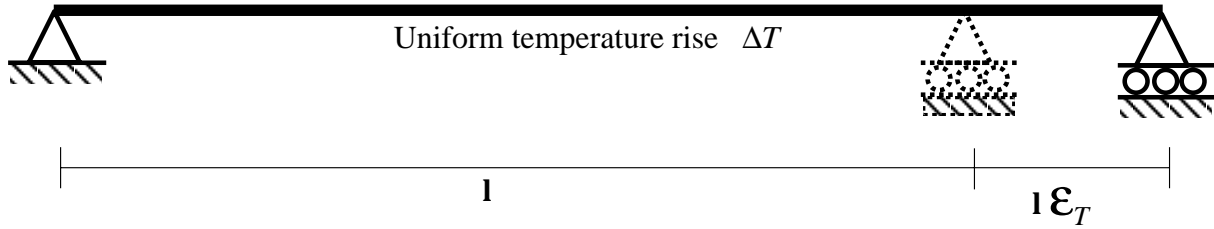

Figure 2: Uniform heating of a simply supported beam

Thermal expansion against rigid lateral restraints

Clearly beams in a real structures do not have the freedom to elongate in the manner described above. Therefore a more realistic case is to consider an axially restrained beam subjected to a uniform temperature rise, ΔT (as shown in Figure 3). It is clear to see that in this case the total strain ε_t is zero (no displacements). This is because the thermal expansion is cancelled out by equal and opposite contraction caused by the restraining force P (*i.e.* $\varepsilon_t = \varepsilon_T + \varepsilon_m = 0$ therefore $\varepsilon_T = -\varepsilon_m$). There exists now a uniform axial stress σ in the beam equal to $E\varepsilon_m$. The magnitude of the restraining force P is,

$$P = EA\varepsilon_m = -EA\varepsilon_T = -EA\alpha\Delta T$$
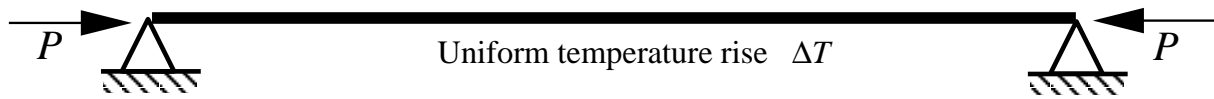
Figure 3: Axially restrained beam subjected to uniform heating

If the temperature is allowed to rise indefinitely, there are two basic responses, depending upon the slenderness of the beam:

1. If the beam is sufficiently stocky the axial stress will sooner or later reach the yield stress σ_y of the material and if the material has an *elastic-plastic* stress-strain relationship, the beam will continue to yield without any further increase in stress, but it will also store an increasing magnitude of *plastic strains*. The *yield temperature increment ΔT_y* is,

$$\Delta T_y = \frac{\sigma_y}{E\alpha}$$

2. If the beam is slender then it will buckle before the material reaches its yield stress. The Euler buckling load P_{cr} for a beam/column as in Figure 3 is,

$$P_{cr} = \frac{\pi^2 EI}{l^2}$$

equating this to the restraining force P, we have,

$$EA\alpha\Delta T = \frac{\pi^2 EI}{l^2}$$

which leads to a critical buckling temperature of,

$$\Delta T_{cr} = \frac{\pi^2}{\alpha}\left(\frac{r}{l}\right)^2 \tag{5}$$

$$\Delta T_{\mathrm{cr}} = \frac{\pi^2}{\alpha\lambda^2} \tag{6}$$

where r is the radius of gyration and λ is the slenderness ratio ($\frac{l}{r}$). This expression is valid for other end-restraint conditions if l is interpreted as the *effective length*.

In this case, if the temperature is allowed to rise further, the total restraining force will stay constant (assuming elastic material and no thermal degradation of properties) and the thermal expansion strains will continue to be accommodated by the outward deflection of the beam δ as shown in Figure 4.

Uniform temperature rise ΔT
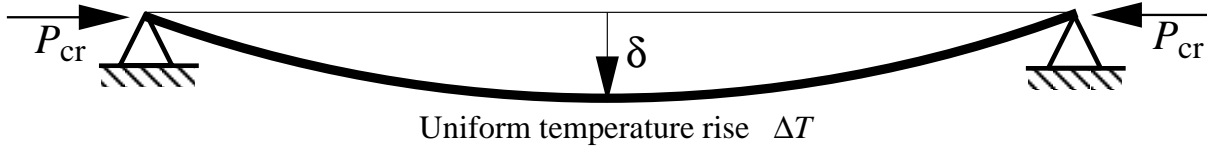
Figure 4: Buckling of an axially restrained beam subjected to uniform heating

The above cases represent the two fundamental responses in beams subjected to restrained thermal expansion. Either of the two (yielding or buckling) may occur on its own (based upon the slenderness of the beam) or a more complex response consisting of a combination of yielding and buckling may occur.

The pattern of development of deflections, axial compression forces and moments with increase in temperature in slender restrained elastic beams is as shown in Figures 5and 6. The deflection and axial force figures clearly show a pre-buckling and post-buckling type response. The sharp bifurcation pattern is absent as a uniformly distributed load is imposed on the beam, imparting an initial displacement to it. The midspan moment continues to rise even after buckling as it consists mainly of the $P - \delta$ moment generated by the axial restraint force times the midspan deflection (which continues to rise beyond buckling).

(a)

(b)
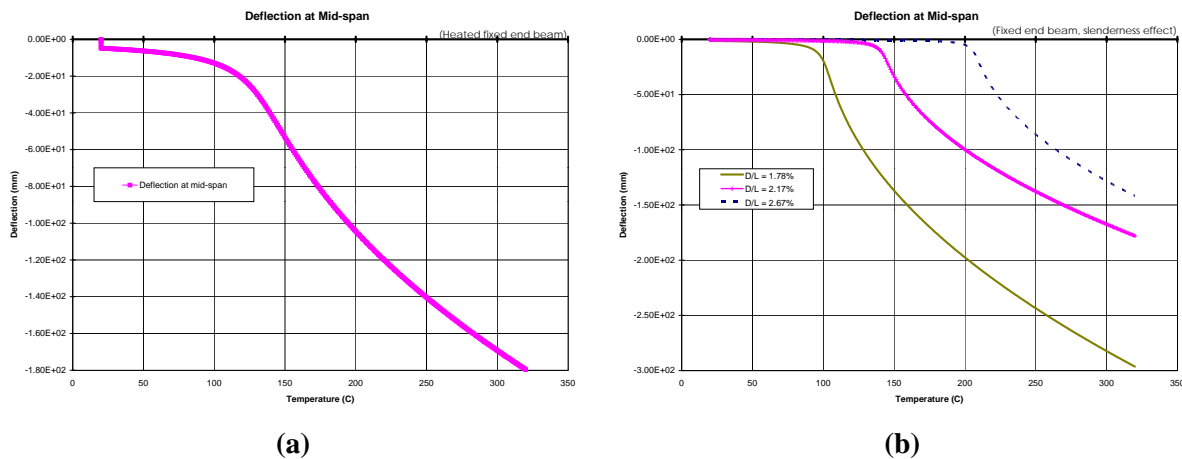
Figure 5: Deflection of axially restrained elastic beams subjected to heating: (a) Single beam, (b) Three beams of varying slenderness

Ideal elastic properties were assumed when discussing the case of buckling above. If the properties are ideal elasto-plastic the deflections and axial compression variations will have a pattern as shown in Figure 7. If the properties remain elastic albeit with a uniform degradation with temperature, the pattern of deflection and axial compression in the beam changes to the one shown in Figure 8. Clearly the response of real composite beams subject to restrained thermal expansion will consist of a combination of the responses shown here. That this is indeed the case, can be seen in report AM1, where the results of modelling the British Steel *restrained beam* Test are shown (which comes closest to the ideal case of rigid lateral restraint). There are other factors in that Test that govern the response of the heated

(a)

(b)
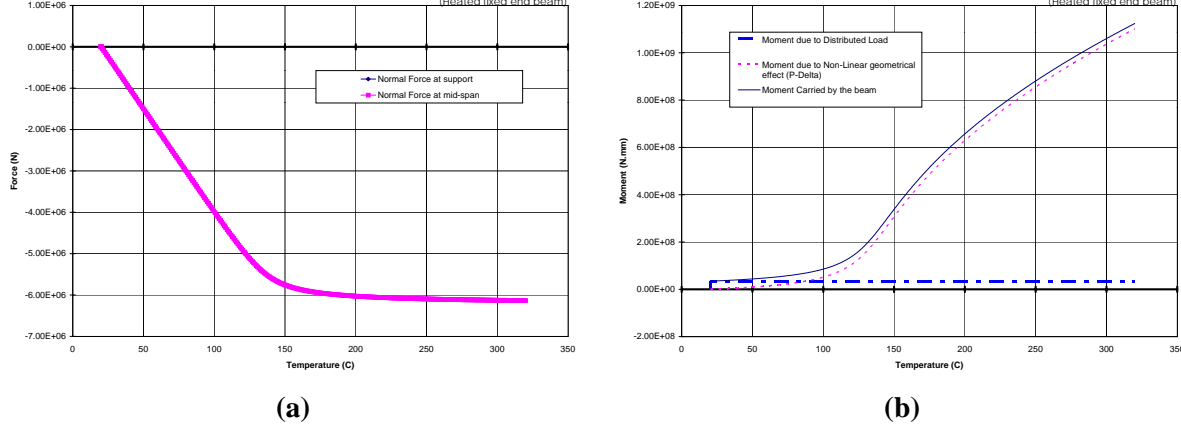
Figure 6: Forces in an axially restrained elastic beam subjected to heating: (a) Axial Forces, (b) Moments

composite beam, particularly the effect of deflection compatibility in the two directions, however the similarity of the development of axial forces in the steel joist and the composite beam to the patterns shown here is clear to see.


(a)

(b)
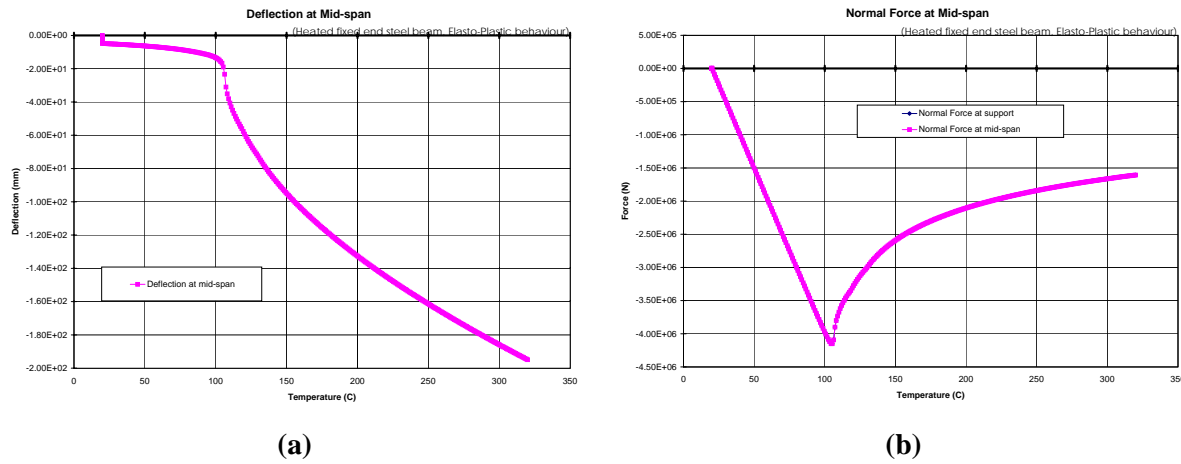
Figure 7: Deflections (a), & Axial forces (b), in an axially restrained elastic-plastic beam

Thermal expansion against finite lateral restraints

In the previous discussion we have assumed the axial restraints to be perfectly rigid. This is an upper limit and practically impossible to achieve in real structures which offer only finite restraints. Figure 9 shows such a beam restrained axially by a translational spring of stiffness k_t. The compressive axial stress developed by thermal expansion is,

$$\sigma = \frac{E\alpha\Delta T}{\left(1 + \frac{EA}{k_t L}\right)} \tag{7}$$

and critical buckling temperature is now given by,

$$\Delta T_{\mathrm{cr}} = \frac{\pi^2}{\alpha\lambda^2}\left(1 + \frac{EA}{k_t L}\right) \tag{8}$$

From Equation 8 it can be seen that buckling and post-buckling phenomena should be observable at moderate fire temperatures in structures with translational restraint stiffnesses (k_t) which are quite comparable with the axial stiffness of the member ($\frac{EA}{L}$). Figure 10 shows a plot derived from Equation 8, where critical buckling temperatures are plotted against slenderness ratio for different restraint stiffnesses. The results clearly show that the amount of restraint required is not large for slender sections to
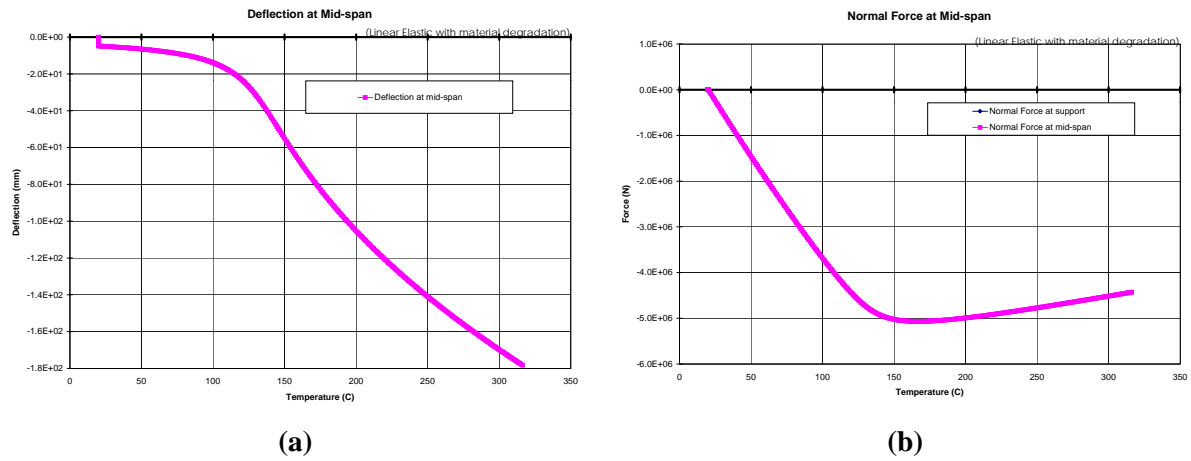
Figure 8: Deflections (a), & Axial forces (b), in a restrained beam with reducing elastic stiffness
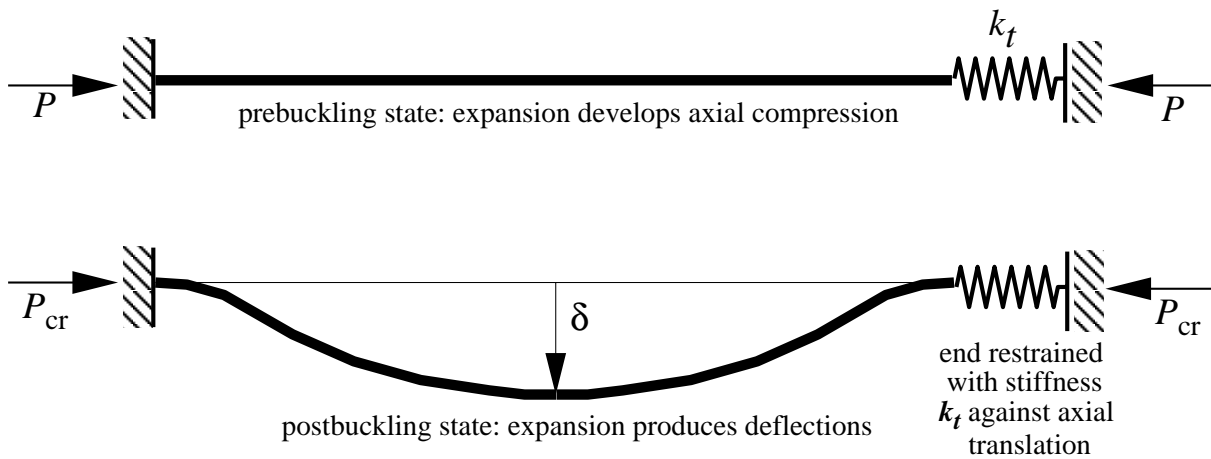

Figure 9: Heating of beam with finite axial restraint

by heating through the reduction in E, so these post-buckling phenomena are **very likely** to be observed in beams in typical fires.
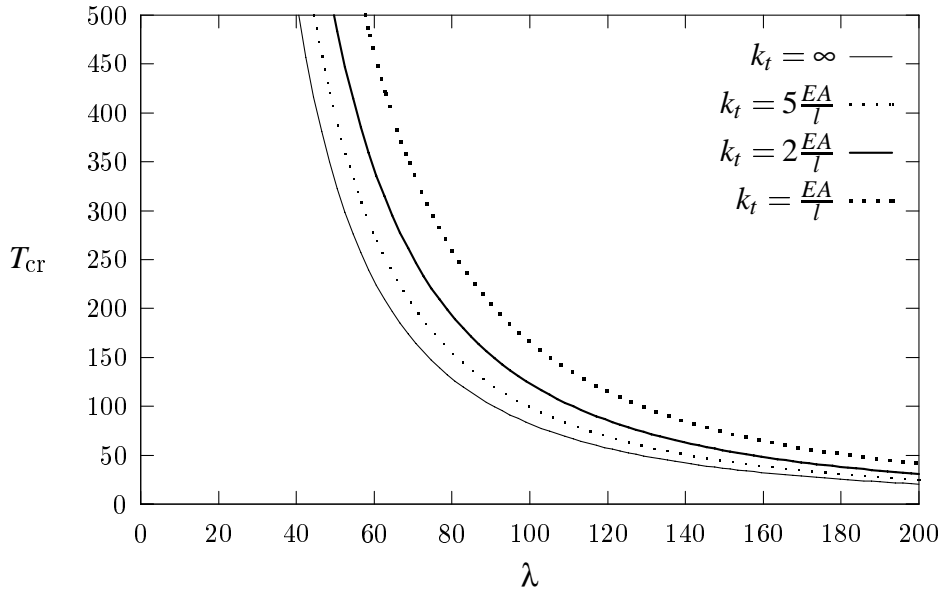

Figure 10: Buckling temperatures for thermal expansion against finite lateral restraint

THERMAL BOWING

In the previous section we discussed the effects of uniform temperature rise on axially restrained beams. In real fires the temperature distributions are anything but uniform. In a small to moderate size compartment of a regular shape one may assume that the compartment temperature will be roughly uniform at a given time. The temperature of the structural members in the compartment depends upon the material they are made of and other details of geometry, construction and design (such as insulation). Concrete beams and slabs on the ceiling of the compartment can be subjected to very high temperature gradients due to the very slow rates of heat transfer to concrete. Therefore the surfaces exposed to fire will be at a much higher temperature than the surfaces on the outside of the compartment. This causes the inner surfaces to expand much more than the outer surfaces inducing bending in the member. This effect is called *thermal bowing* and is one of the main reasons of the deformations of concrete slabs and masonry walls in fires. Another very important source of thermal bowing in composite beams/slabs is the large difference between the temperatures of the steel joist and the slab. This effect is much more important in the early stages of the fire when steel retains most of its strength.

Relationships can be derived for thermal bowing analogous to the one derived earlier for thermal expansion. Figure 11 shows a beam subjected to a uniform temperature gradient through its depth (d) along its whole length (l). Assuming the beam is simply supported (as shown in Figure 11) we can derive the following relationships:

1 The thermal gradient ($T_{,y}$) over the depth is,

$$T_{,y} = \frac{T_2 - T1}{d}$$

2 A uniform curvature (ϕ) is induced along the length as a result of the thermal gradient,

$$\phi = \alpha T_{,y}$$

3 Due to the curvature of the beam the horizontal distance between the ends of the beam will reduce. If this reduction is interpreted as a contraction strain (not literally) ε_ϕ (analogous to the thermal

$$\varepsilon_\phi = 1 - \frac{\sin \frac{l\phi}{2}}{\frac{l\phi}{2}} \tag{9}$$
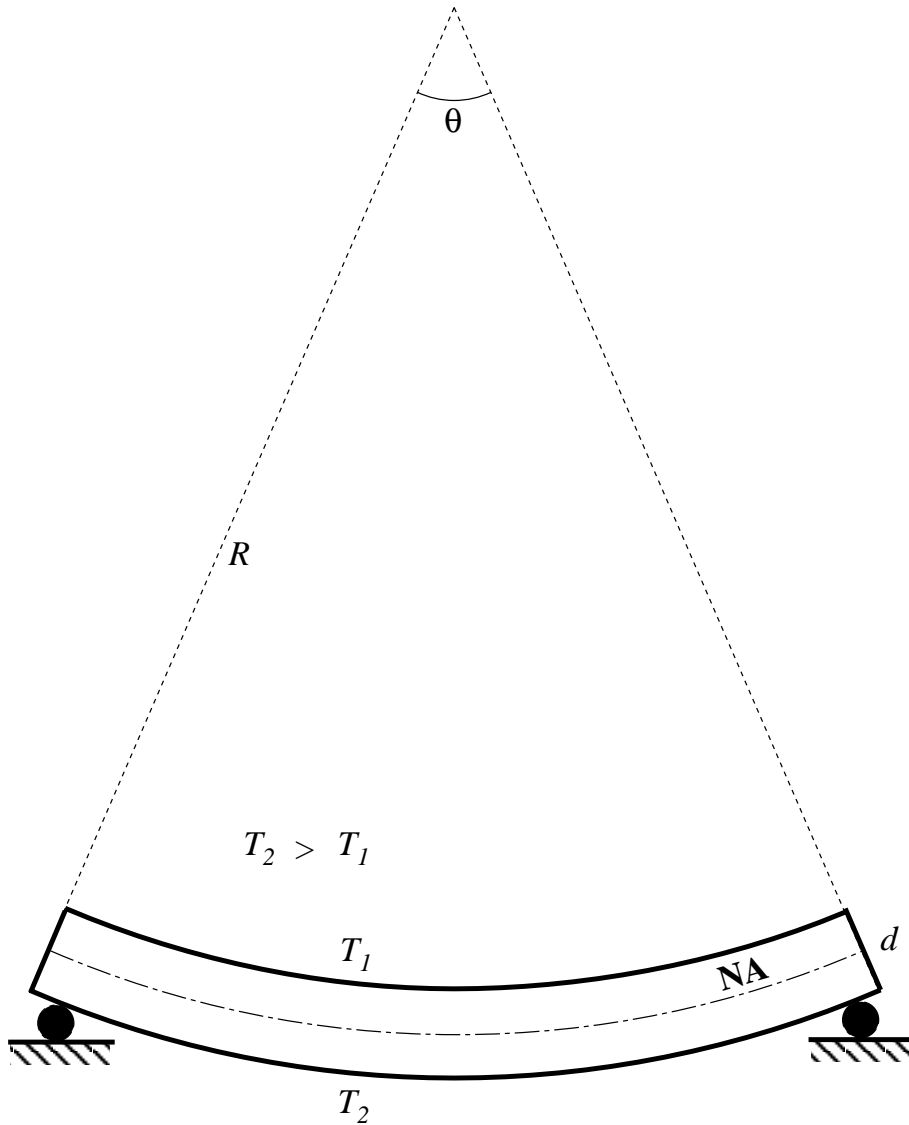
Figure 11: Simply supported beam subjected to a uniform thermal gradient

Now consider the laterally restrained beam of Figure 4. If a uniform thermal gradient $T_{,y}$ is applied to this beam (as shown in Figure 12), the result (in the absence of any average rise in temperature, *i.e.* mean temperature remaining constant) is a thermally induced tension in the beam and corresponding reactions at the support (opposite the the pure thermal expansion case discussed earlier). This is clearly caused by the restraint to end translation against the contraction strain (ε_ϕ) induced by the thermal gradient.

Uniform temperature gradient $T_{,y}$
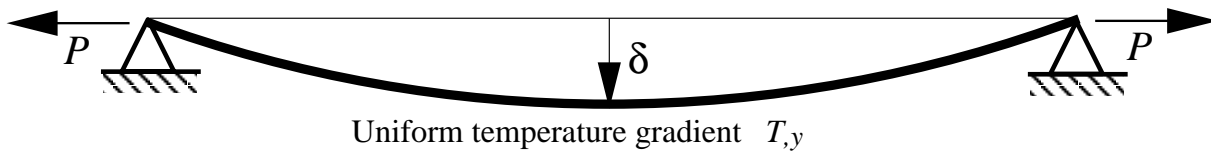
Figure 12: Laterally restrained beam subjected to a uniform thermal gradient

Figure 13 shows a fixed ended beam (by adding end rotational restraints to the Beam of Figure 12) subjected to a uniform temperature gradient through its depth. Recalling that a uniform curvature $\phi = \alpha T_{,y}$ exists in a simply supported beam subjected to gradient $T_{,y}$. If that beam is rotationally restrained

moments cancels out the thermal curvature and therefore the fixed ended beam remains 'straight' with a constant moment $M = EI\phi$ along its length.
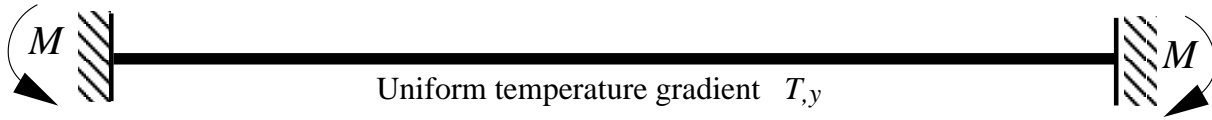
Figure 13: Fixed end beam subjected to a uniform thermal gradient

From the above discussion it is clear that the effect of boundary restraints is crucial in determining the response of structural members to thermal actions. The key conclusion to be drawn from the discussion so far is that, *thermal strains will be manifested as displacements if they are unrestrained or as stresses if they are restrained through counteracting mechanical strains generated by restraining forces.*

As discussed earlier for lateral restraint, perfect rotational restraint is also not very easily achieved in real structures (other than for symmetric loading on members over continuous supports, without any *hinges* from strength degradation). Figure 14 shows a beam restrained rotationally at the ends by rotational springs of stiffness k_r. In this case the restraining moment in the springs as a result of a uniform thermal gradient $T_{,y}$ can be found to be,

$$M_k = \frac{EI\alpha T_{,y}}{\left(1 + \frac{2EI}{k_r l}\right)} \tag{10}$$

This equation implies that if the rotational restraint stiffness is equal to the rotational stiffness of the beam itself ($\frac{EI}{l}$) then the moment it will attract will be about a third of a fixed support moment.
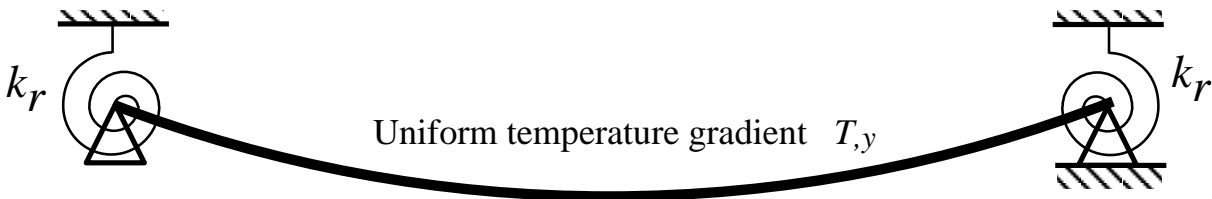
Figure 14: Beam with finite rotational restraint with a uniform thermal gradient

DEFLECTIONS

In the previous sections we have looked at the overall behaviour of beams subjected to expansion and bowing for various restraint conditions. One interesting aspect of structural response to fire is the large deflections that are found in structural members such as beams and slabs. Large deflections are normally associated with loss of strength in structures under ambient conditions. In case of fire such a simple interpretation can be highly misleading. Both the thermal mechanisms discussed earlier (thermal expansion and thermal bowing) result in large deflections, however the state of stress associated with a member subjected to varying degrees of these two mechanisms is not unique for a given deflection and a large range of stress states exist (large compression or tension or very low stresses) depending upon the temperature distribution in the member and its material properties and restraint conditions.

The chief reason for large deflections is that the structural member tries to accommodate the *additional length* generated by thermal expansion, given that it is not possible for it to expand longitudinally due to end restraints. Consider a slender beam (very low buckling temperature) subjected to uniform heating against rigid lateral restraints (as in Figure 4). Buckling will occur very early on (at very low elastic strains) after which any further expansion will make the beam deflect outwards. The resulting midspan deflection δ can be approximated quite accurately by,

$$\delta = \frac{2l}{\pi}\sqrt{\varepsilon_T + \frac{\varepsilon_T^2}{2}} \tag{11}$$

expansion strain ($\alpha\Delta T$).

If the same beam is subjected to a uniform thermal gradient producing no net expansion, only bowing as in Figure 12, the response is then determined by the flexure-tension interaction. The tensile $P - \delta$ moments restrain the curvature imposed by the thermal gradients and limit deflections. The deflections result from the tensile strains produced in the beam, *i.e.*

$$\varepsilon_t = \frac{P}{EA} \tag{12}$$

and the deflections can then be determined by

$$\delta = \frac{2l}{\pi}\sqrt{\varepsilon_t + \frac{\varepsilon_t^2}{2}} \tag{13}$$

The tensile force P_t can be determined from substituting Equation 12 in Equation 13 and solving a quadratic equation for P_t,

$$P_t = \left(\sqrt{\frac{1}{2}\left(\frac{\pi\delta}{l}\right)^2 + 1} - 1\right)EA \tag{14}$$

To determine the deflection $y(x)$ in the beam of Figure 12 for a given curvature ϕ (arising from a thermal gradient), a differential equation solution can be written as follows:

For a simply supported beam subjected to a uniform curvature ϕ one can write,

$$\frac{d^2y}{dx^2} = \phi$$

If the beam is laterally restrained as in Figure 12, a tensile force P will be generated causing a moment Py over the length of the beam, therefore,

$$\frac{d^2y}{dx^2} = \phi + \frac{Py}{EI} \tag{15}$$

or

$$\frac{d^2y}{dx^2} - k^2y = \phi$$

where,

$$k = \sqrt{\frac{P}{EI}}$$

The solution of this equation is,

$$y(x) = -\frac{\phi}{k^2}\left(\frac{\cosh kl - 1}{\sinh kl}\sinh kx - \cosh kx + 1\right) \tag{16}$$

It may be seen that Equations 14 and 16 form a set of nonlinear equations. These equations can be solved using an appropriate iterative technique (bisection, Newton-Raphson) to obtain the tensile forces and deflections for thermal gradient dominated problems.

COMBINATIONS OF THERMAL EXPANSION AND THERMAL BOWING

In the previous sections the response of beams to either thermal expansion or thermal bowing have been considered in isolation. To study the combined response let us first consider the case of a fixed ended beam as shown in Figure 15 which is both rotationally and translationally restrained at both ends. If this beam is subjected to a mean temperature rise and a through depth thermal gradient, it will experience a uniform compressive stress because of restrained expansion and a uniform moment because of the thermal gradient. The stresses on any typical cross-section because of the combined effect of the two
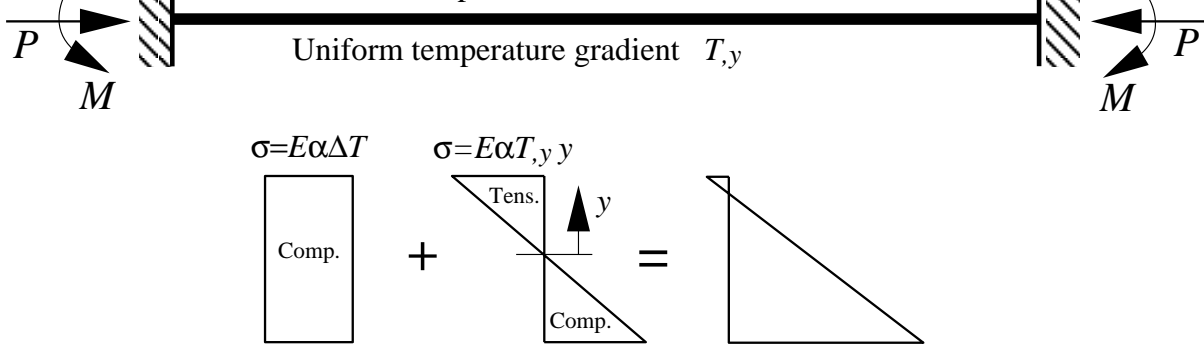
Figure 15: Combined thermal expansion and bowing in a fixed ended beam

thermal actions are also shown in Figure 15. It is clear that the bottom of the beam will experience very high compressive stresses, while the top may be anywhere between significant compression to significant tension.

The above scenario is a common one in composite frame structures such as Cardington. The composite action of a steel joist, framing into an interior column, with a continuous slab over it, produces conditions very close to a fully fixed support (as in Figure 15). The high compressions resulting from the combined effect of thermal actions as described above almost invariably produce local buckling in the lower flange of the steel joist very early on in a fire. This why local buckling of the lower flanges is such a common occurrence in fires (seen in all Cardington tests and other fires).

Once local buckling has occurred the pattern of stresses at the ends of the composite beam changes. The hogging moment is relieved by the *hinge* produced by local buckling and the end restraint conditions change to the one shown in Figure 12. As this happens quite early in real fires, the end conditions described by Figure 12 are the ones that govern the behaviour of a composite beam for most of the duration of the fire.

Combined thermal expansion and bowing in laterally restrained beam

The fundamental pattern of behaviour of a beam whose ends are laterally restrained (but rotationally un-restrained, see Figure 12) subjected to thermal expansion and thermal bowing separately was established in previous sections. Restrained expansion resulted in compression and bowing resulted in tension. This helped to illustrate that two opposite stress regimes can occur depending upon the thermal regime applied, however the apparent response of the beam is the same (*i.e.* downward deflection).

To study the effects of the applying combinations of thermal expansion and thermal bowing we define and effective strain as follows,

$$\varepsilon_{\text{eff}} = \varepsilon_T - \varepsilon_\phi \tag{17}$$

The variation of ε_{eff} (for various thermal regimes) can produce a large variety of responses. Positive values of ε_{eff} imply compression (or the effect of mean temperature rise is dominant) and negative values imply tension (or the effect of thermal gradients is dominant). Figure 16 shows the variation of ε_{eff} for different values of thermal gradient when the temperature is increased from 0 to 400°C (ε_{eff} is plotted for a linear increase in gradient against temperature).

Case 1: Zero stress in the beam ($\varepsilon_{\text{eff}} = 0$)

Figure 17 shows an interesting theoretical case. If the implied combination of ε_ϕ and ε_T are applied:

- There are no stresses in the beam. All thermal strains are converted into displacement as seen in the figure.

- The deflection of the beam is **entirely** due to *thermal bowing* to accommodate the *excess length* generated by expansion.
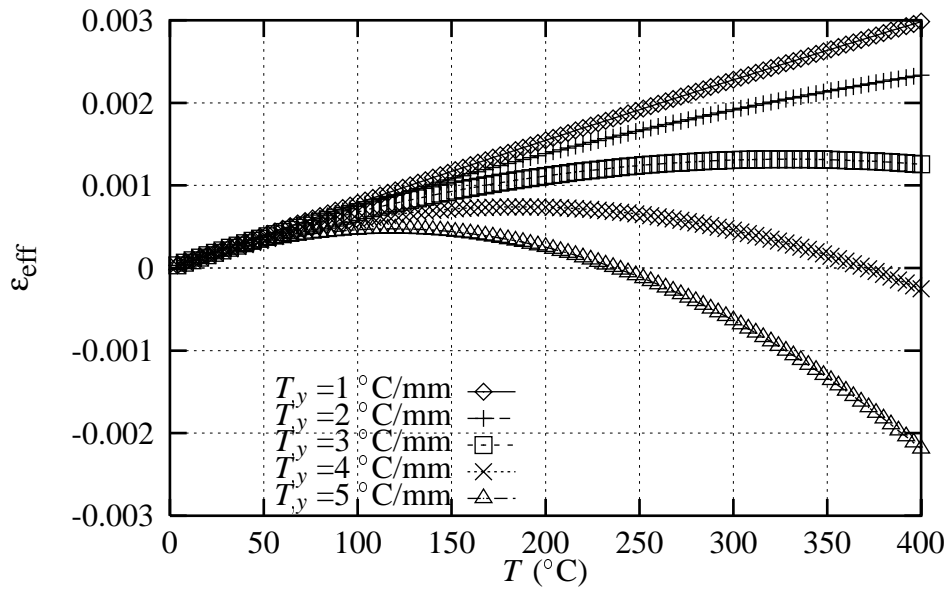
Figure 16: Effective expansion strains

Step 1 : Impose a temperature rise ΔT

Step 2 : Impose a curvature αT,y to return support to the original position

Figure 17: Case 1: Zero Stress

elastic curve of the beam versus its deflection. Figure 18 shows a number of length increase vs midspan deflection plots based on assumed curve shapes. The figure shows that the shape of the curve chosen does not matter much, therefore the formula given earlier based upon the sin curve (Equation 11) can be used to get a good approximation of the midspan deflection y_m, *i.e.*

$$y_m = \frac{2l}{\pi} \sqrt{\varepsilon_T + \frac{\varepsilon_T^2}{2}}$$
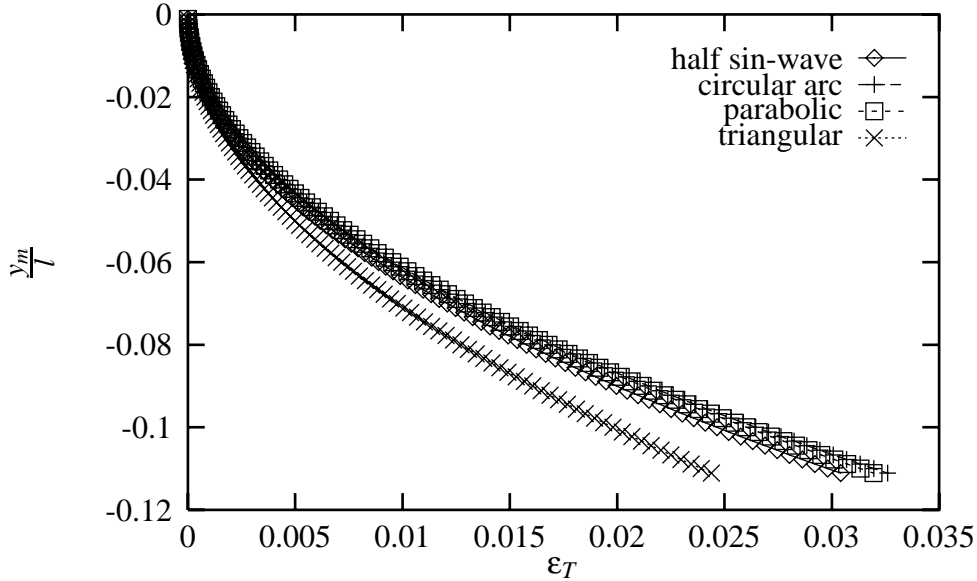
Figure 18: Strain v non-dimensional midspan deflection (per unit length)

Case 2: Thermal expansion dominant ($\varepsilon_{\text{eff}} > 0$)

If $\varepsilon_T >> \varepsilon_\phi$, thermal expansion dominates and a two stage response is produced consisting of *Prebuckling* and *Postbuckling* phases. The thermal expansion produced is partly used up in generating mechanical strains and partly in generating deflections. This is governed by the magnitude of ε_{eff} which is the component that generates stresses to progress the beam towards buckling. The ε_ϕ component annihilates part of the expansion and produces deflections by imposing curvature with the available excess length. The prebuckling deflections (y_m^-) will for a small part result from the elastic bending of the beam and a larger part will generally come from the deflection resulting from the imposed curvature ($y_m(\phi)$).

$$y_m^- = \frac{y_0}{1 - \frac{\Delta T}{\Delta T_{cr}}} + y_m(\phi) \tag{18}$$

Here y_0 can be interpreted as the initial elastic deflection before the fire because of the imposed loads on the beam and $y_m(\phi)$ is the extra deflection due to thermal bowing given by,

$$y_m(\phi) = \frac{2l}{\pi} \sqrt{\varepsilon_\phi + \frac{\varepsilon_\phi^2}{2}} \tag{19}$$

The presence of the gradient clearly delays the buckling event and the critical buckling temperature (ΔT_{cr}) is increased to,

$$\Delta T_{cr} = \frac{1}{\alpha} \left(\frac{\pi^2}{\lambda^2} + \varepsilon_\phi \right) \tag{20}$$

Figure 19 shows the typical variation in buckling temperature with the change in gradient (for a beam of slenderness ratio $\frac{l}{r}$ equal to 70).
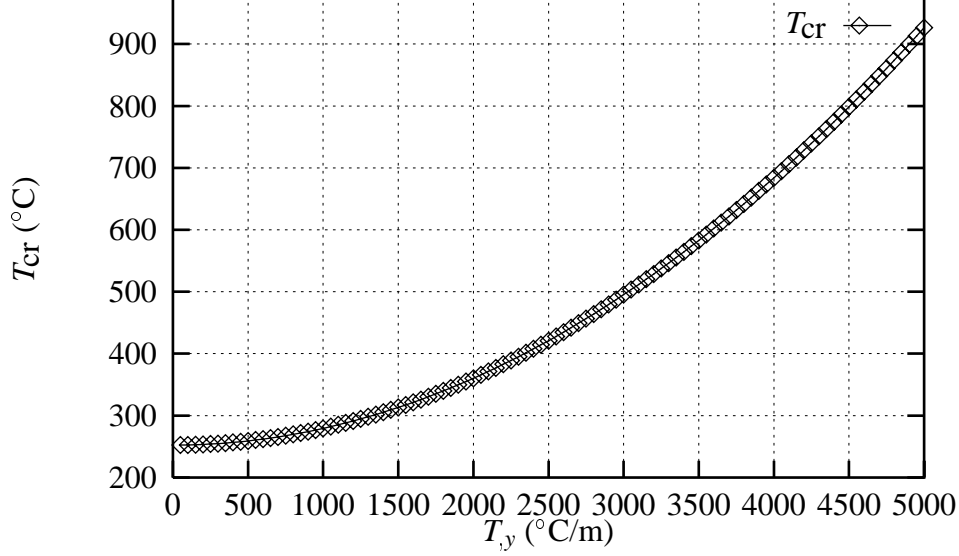
Figure 19: Critical Buckling temperatures vs Thermal gradient

The *postbuckling* deflections will carry on increasing because of all further expansion strains ε_T^+ as in Equation 11, *i.e.*

$$y_m^+ = \frac{2l}{\pi}\sqrt{\varepsilon_T^+ + \frac{\varepsilon_T^{+2}}{2}}$$

The thermal bowing deflection added to the elastic deflections (due to $P - \delta$ moments and loading) will again act as 'imperfections' to 'straightness' of the beam and produce a smooth variation of beam midspan deflection with temperature until the large displacement post-buckling mode begins (identified by the change of curvature of the temperature deflection curve). This also has the effect of reducing the development of compression forces in the beam (as the beam displaces more for lower compressions because of the additional bowing displacements increasing the $P - \delta$ moments).

Case 3: Thermal bowing dominant ($\varepsilon_{\text{eff}} < 0$)

When $\varepsilon_\phi >> \varepsilon_T$, the deflection response will be the sum of two components,

1 Deflection caused by bowing of the excess length generated through expansion, as before *i.e.*

$$(y_m)_1 = \frac{2l}{\pi}\sqrt{\varepsilon_T + \frac{\varepsilon_T^2}{2}}$$

2 The tensile strain ε_t produced by the tension (P_{eff}) caused by the excess contraction strain (ε_{eff}) as in the case of pure thermal gradients.

$$\varepsilon_t = \frac{P_{\text{eff}}}{EA}$$

which will produce further deflections as,

$$(y_m)_2 = \frac{2l}{\pi}\sqrt{\varepsilon_t + \frac{\varepsilon_t^2}{2}}$$

The tension P_{eff} and the deflections can then be determined according to the iterative procedure suggested in the previous section on deflections.

Finally Figure 20 shows the main types of deflection responses that may be observed if a laterally restrained beam is exposed to combinations of thermal actions discussed above.
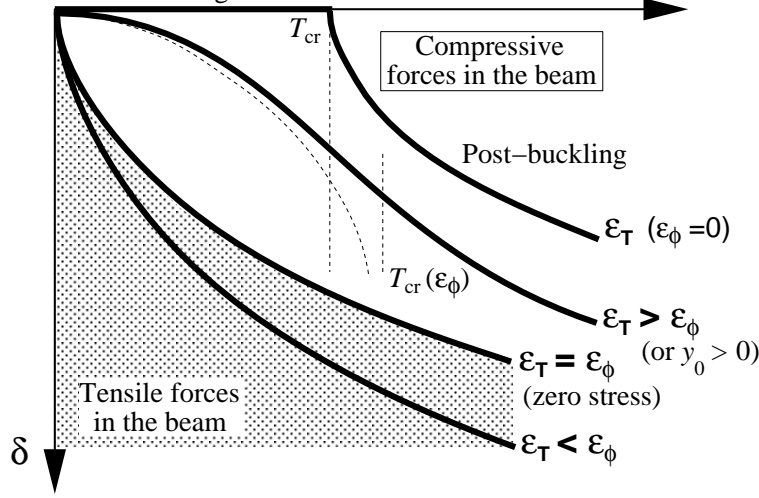
Figure 20: Temperature deflection responses for combinations of ε_T and ε_ϕ

CRITERION FOR THE VARIOUS TYPES OF RESPONSES

From the discussion above a simple criterion for all the various types of responses observed can be developed. If ε_{eff} is close to $\frac{\pi^2}{\lambda^2}$ then there will be no buckling as not enough compression is generated. A dimensionless number ζ may be defined as follows to categorise the various responses:

$$\zeta = \frac{\varepsilon_T - \varepsilon_\phi}{\frac{\pi^2}{\lambda^2}} \tag{21}$$

To summarise,

1 $\zeta \gg 1$

typically generates pre and postbuckling type deflection responses with thermal expansion and compression dominant. The compression force patterns are as discussed earlier in the restrained thermal expansion section.

2 $\zeta \simeq 1$

generates responses where most of the thermal expansion is converted into deflection but there are negligible stresses in the beam (close to the *zero stress* case discussed earlier).

3 $\zeta \ll 1$

generates thermal bowing dominated response with deflection patterns similar to the *zero stress* case and with considerable tensile forces in the beam which grow with the increase in the gradient.

NUMERICAL ANALYSIS OF THE SIMPLE BEAM MODEL

The analytical approach developed above to fully understand the structural response to the heating regime has been checked numerically by modelling the same simple beam examples in ABAQUS. The data for beam analysed was as follows:

- length (l)=9000 mm

- Modulus of Elasticity (E)=210000 N/mm^2

- Coefficient of thermal expansion (α)=8×10^{-6}

- Area A=5160 mm^2

- Second moment of area I =8.55×10^7 mm^2

to investigated the simple beam model restrained laterally but free to rotate at its ends as in Figure 12. The results confirm the theoretical solutions derived for the response of the beam to thermal bowing and thermal expansion. Figure 21 shows the results of the numerical analysis in terms of the deflections and axial forces produced when the beam is subjected to a mean temperature rise (uniform over the length) of $400°C$ and an effective thermal gradient through the depth of the beam. The temperature increase, ΔT and thermal gradient, T,y were applied to the simple numerical beam model at a constant rate from zero to their maximum values. The deflection as a result of pure restrained thermal expansion shows the double curvature shape of the pre-buckling/post-buckling response (see Figure 21). When a gradient is also applied to the model and the response of the beam is governed by the interaction between thermal bowing and restrained thermal expansion the deflected shape becomes smoother, indeed for a specific combination of mean temperature rise and temperature gradient the response will be very close to linear. At large gradients ($T,y = 10°C/mm$) when the response is dominated by thermal bowing the deflected shape is very non-linear.

The corresponding axial forces are also plotted in Figure 21. When a mean temperature rise of $400°C$ alone is applied to the model and the response of the beam is governed purely by restrained thermal expansion and the axial force is in high compression. When the model is subjected to a combination of mean temperature rise and temperature gradient the axial force becomes smaller in compression and at high gradients moves into tension. The axial force at the beginning of the analysis is always in compression because the mean temperature and the gradient are applied to the model linearly from zero to their maximum values and are governed by the development of the effective strains, ε_{eff}, as shown in Figure 16.

The actual values of deflections and forces in the numerical exercise above can be estimated using the formulas given here. For instance for the case of a temperature rise of $400°C$ the compression force is simply the Euler buckling load ($\frac{\pi^2 EA}{\lambda^2}$) equal to 2170 kN (approx.). The deflection for this case can be obtained from subtracting the elastic compression strain ($\frac{\pi^2}{\lambda^2}$) from the thermal strain (ε_T) to obtain the strain that produces the deflections, therefore,

$$y_m \simeq \frac{2l}{\pi}\sqrt{\varepsilon_T - \frac{\pi^2}{\lambda^2}}$$

which produces a value of approximately 200mm (within 10%) of the numerical calculation above. The difference is because the numerical calculation is fully geometrically non-linear while the above formulas are based on 1st order definitions of strain.

If all the thermal strains were to produce deflection (by appropriate combination of ε_T and ε_ϕ) then the internal forces would be very low and the deflection would be approximately 324 mm (from Equation 11) which lies between the cases of $T,y = 3°C/mm$ to $T,y = 5°C/mm$. It may be noted from Figure 21 that the axial force in the beam moves from compression to tension between these values (suggesting that for the deflections in the region of 324 mm) the forces in the beam will be insignificant.

The tensile forces and deflections for large gradients can be calculated from iteratively solving the set of nonlinear Equations 14 and 16.

The above analysis clearly highlights the large range of deflected shapes and axial forces possible as a result of the interaction between thermal expansion and thermal bowing.

OTHER IMPORTANT FACTORS

The discussion above has focussed upon the effects of thermal expansion and thermal bowing and illustrated the large variety of responses possible in real composite frame structures. Analytical expressions have been presented which allow a good quantitative estimate of forces and deflections to be made for simple structures.

Deflection at mid-span due to thermal expansion and thermal bowing
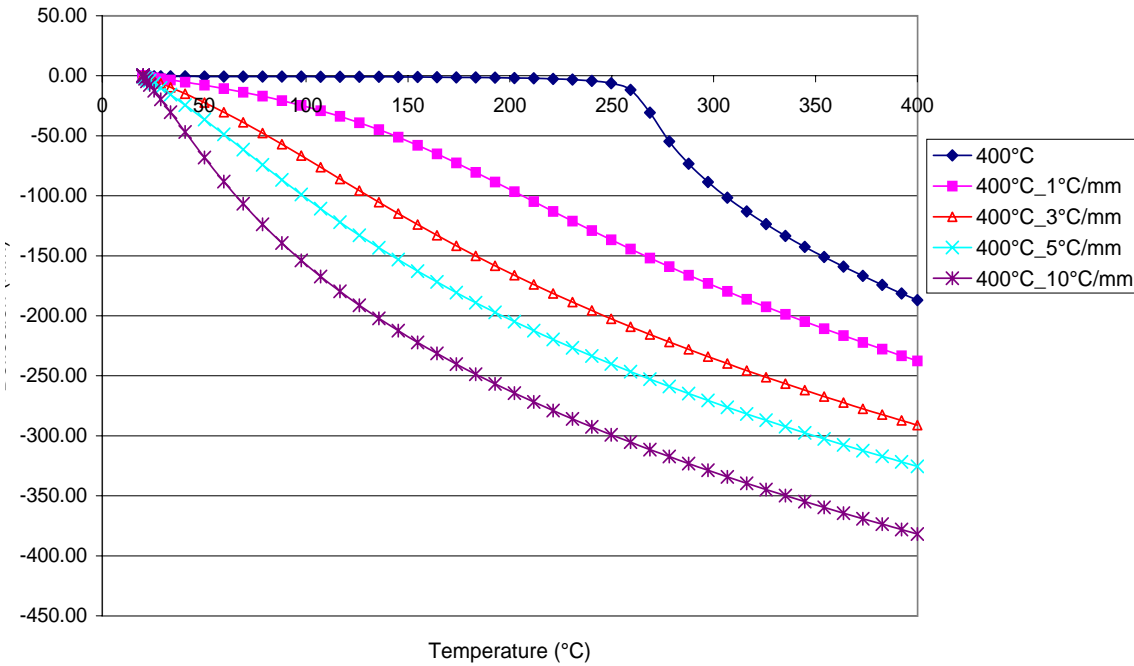

(a)

Axial Force in the model
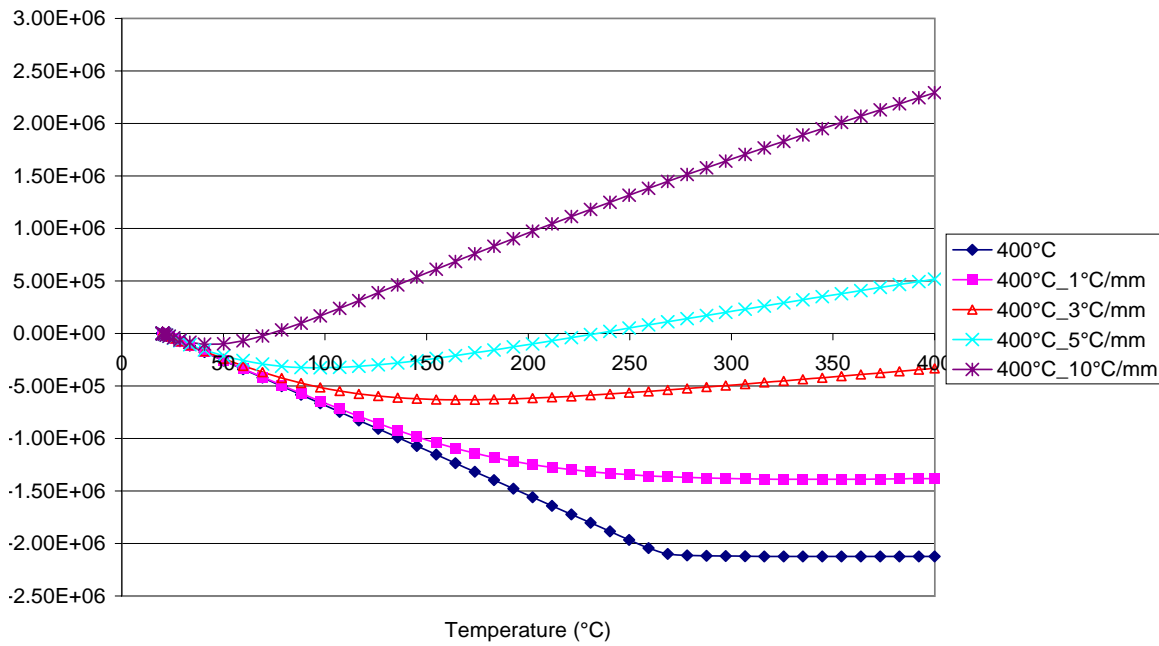
(b)

Figure 21: Numerical model results for combined thermal expansion and thermal bowing: (a) Deflections (b) Axial forces

modelling of Cardington Tests (see reports SM1-2). The effect of strength degradation was shown to change the development of compressive forces in a restrained beam in Figures 7 and 8. The loading on a beam in a large displacement configuration (through thermal effects) will be carried very effectively in a *catenary* (or tensile membrane) behaviour. It is clear from the above discussion that for the most likely combinations of thermal actions (ε_T and ε_ϕ) the mechanical strains in a member are likely to be very low (compression or tension). If this is true and that thermal degradation has been contained in the surface layers, then the tensile strains induced by membrane mechanisms should be carried quite reliably. This is however an area which needs further extensive investigation using all standard research techniques, experimental, computational and theoretical.

Restraint conditions can certainly have a major effect on the distribution of the internal forces and the displacements that occur as has been illustrated by the simple theoretical and computational analyses in this paper. The degree of restraint available also changes during a fire , for instance the rotational restraint available to the composite beam at the beginning is lost quite early on (around 200 C) [1] due to the local buckling of the steel joist and tensile capacity of the slab being reached. Rotational restraints result in increasing hogging moments until a 'plastic hinge' is achieved. Lateral translation restraints produce compression forces if thermal expansion was dominant and tension forces if thermal bowing is dominant. The amount of restraint required is not large to produce buckling as floor structures usually very slender. The source of this restraint is obvious for interior compartments - the colder and stiffer surrounding structure. For exterior compartments it is not so clear if sufficient restraints are still available. It is likely that sufficient restraint to lateral expansion is available at exterior boundaries through the actions of tension rings [2]. At large deflections lateral restraints provide an anchor to the tensile membrane mechanisms. Again, it is likely that sufficient lateral restraint is available at exterior boundaries through the action of compression rings [3]. This however is a matter of much greater importance than the restraint to thermal expansion as the survival of the floor system ultimately depends upon the reliability of the tensile membrane mechanism. This again is a key question for further investigation.

Another very important factor that has not been investigated here is the effect of the compartment geometry. This can have a large effect on the development of thermally induced forces and deflections in the heated structural members. The principle that allows one to make a quantitative assessment of the effect of compartment geometry, is **compatibility**. For instance for a rectangular fire compartment, the thermal expansion in the shorter direction will be smaller than the expansion the longer direction. This can lead to an increase in compression in the longer direction (because compatibility does not allow it to deflect as much as its thermal expansion demands). In the shorter the reverse happens, compatibility forces the deflections in this direction to be somewhat larger than thermal expansion would allow resulting in lower compressions or even tensile forces. This has been identified clearly in the modelling of the British Steel restrained beam test (3m×8m) where the midspan ribs are in tension. This allows redistribution of the thermally induced forces.

CONCLUSIONS

The fundamental principles presented in this paper provide a means of estimating forces and displacements in real structures with appropriate idealisations. Such estimates can be of considerable use in assessing the results from more rigorous numerical analyses or they can be used in design calculations. Examples of such usage will be presented in a subsequent paper. There are however a considerable number of very important issues that remain to be investigated as mentioned in the previous section. Considerable effort is required to address these issues to satisfaction before a complete set of principles can be developed.

REFERENCES

1 A.M.Sanad, J.M.Rotter, A.S.Usmani, and M.O'Connor. Composite beams in buildings under fire - numerical modelling and structural behaviour. *Fire Safety Journal*. submitted, 2000.

2 J.M.Rotter, A.M.Sanad, A.S.Usmani, and M.Gillie. Structural performance of redundant struc-

ence, pages 1069–1080, Edinburgh, Scotland, 29 June - 1 July 1999.

3 Y.C. Wang. Tensile Membrane Action in Slabs and its Application to the Cardington Fire Tests. Technical report, Building Research Establishment, 1996. Paper presented to the second Cardington Conference 12-14 March 1996.

APPLICATION OF FUNDAMENTAL STRUCTURAL MECHANICS PRINCIPLES IN ASSESSING THE CARDINGTON FIRE TESTS

AS Usmani
School of Civil and Environmental Engineering
University of Edinburgh

ABSTRACT

The understanding of the fundamental principles of mechanics that govern the behaviour of structures subjected to thermal actions is vital to the understanding the behaviour of composite frame structures (like the Cardington frame) in fire. A set of basic principles have been developed and presented in various reports and presentations, and form one of a number of important outputs from the PIT project, sponsored by DETR (UK). The PIT project was about developing computational models of the full-scale fire tests on the multi-storey steel frame at Cardington (UK).

However in executing this massive computational exercise properly, and interpreting the voluminous results from the many computational models developed, it was found necessary, time and again, to go back to the basics and develop the appropriate theory. This paper will discuss a cross-section of the results from the Cardington computational models with corresponding test data and assess it for consistency with the fundamental principles presented in an earlier paper. It will be shown that these principles not only provide a good basis for checking the qualitative accuracy of the results, but also provide a reasonable order-of-magnitude type quantitative prediction of the key measures of structural behaviour. Such an analysis is an enormously practical and powerful tool to allow engineers to make quick preliminary calculations for real life engineering problems and also provides a means to check results from large and complex numerical models to ensure that they are consistent with the basic principles.

Thermal and Structural Behavior of Continuous Steel Construction under Fire Conditions

R. Becker, Ph.D.
Assoc. Prof. of Civil Eng. at the Technion – Israel Institute of Technology, Haifa 32000, ISRAEL, E-mail: becker@tx.technion.ac.il

ABSTRACT

Temperature evolution within structural members is the driving mechanism of structural response under fire conditions. Longitudinal non-uniformity of temperature variation along a structural steel component is an inherent outcome of the continuity of the steel columns beyond the fire story. Heat sinks exist at both ends of the story-high column, that stem from its contact with the floor slabs while passing through them, and from the cooler air temperature in the stories below and above the fire story. The extent of cooling exerted by these sinks on the column and the attached beams has not been investigated.

This paper presents first the procedure and models, which were developed for analyzing the longitudinal thermal response and for predicting the extent of its non-uniformity. Some typical results are presented to demonstrate the general longitudinal thermal behavior of steel assemblies. Factors affecting the extent of non-uniformity of temperature distributions along the beams and columns were depicted. They are used for a compact presentation of the results. The presentation concludes with a simple example demonstrating the effects of this non-uniformity on the structural behavior of a simple frame, including a comparison to the structural behavior of the uniformly heated one. The structural response has been predicted by means of SAFIR.

The presentation emphasizes the heating processes along typical structural components and assemblies and their effects on the evolution of displacements, stress (and moment) redistribution and on the formations and locations of plastic hinges.

KEY WORDS

Steel Construction, Fire Behavior, Thermal Response, Structural Response

INTRODUCTION

Temperature evolution within structural members is the driving mechanism of structural response under fire conditions. Under the sustained loads that prevail at the onset of fire, strains within structural components increase as they are heated, leading to increasing rotations and displacements and to redistribution of stresses and internal forces. Failure would usually occur due to instability associated with the formation of an excessive number of plastic hinges, or an almost infinite rate of growth of strains (and relevant deformations).

Conservative analysis of structural response addresses only small deformations of uniformly heated structural components without any redistribution of internal forces. Fire-resistance thus predicted practically coincides with the value obtained from equating the relative stress with the loading ratio, leading to a simple procedure for establishing the structural fire resistance of steel structures. This commonly used procedure is composed of measuring or calculating the temperature evolution at the central part of a virtually infinitely long structural member. The fire resistance is then identified with the time of occurrence of the so-called critical temperature (for regular structural steel: Tcrit. ≈ 540C). The simplicity of these tools and the lack of motivation for establishing more sophisticated ones (which stemmed probably from the prescriptive approach in the existing building codes) inhibited, for many years, more thorough investigation of the actual behavior of structures under fire conditions.

In recent years, there is an emerging worldwide tendency to implement a performance-based approach to fire-safety design of buildings. To apply this approach to structural fire protection requires foremost a thorough understanding of the partial contributions of the various factors that may affect the actual structural behavior during fire. As temperature evolution is the main driving mechanism for structural response of steel construction, rigorous investigation of the heating processes of typical structural components and assemblies is of primary significance.

Some investigators have developed predictive tools and analyzed the effects of temperature variation across steel beams and columns, addressing also the variation in steel thermal properties with temperature [Gilvery 1997]. Theoretical [Franssen 1995, Liu 1996, Anderberg 1996] and some experimental works [Jeans 1986] have demonstrated that when beams are in full contact with a cooler floor slab along the entire width of their upper flange, they may experience a temperature difference of some hundreds degree C between the upper and lower flange. All these works, however, assumed a uniform temperature distribution along the structural components. A state-of-the-art paper by Witteveen, published already in 1981, [Witteveen 1981] addressed some points that were not sufficiently pursued in previous research efforts. Amongst these, it includes longitudinal non-uniformity of temperature distributions. However, the only paper that was published on the topic is from a much earlier period, by Culver [Culver 1972]. It shows significant effects of some specific non-uniform linear temperature distributions on the buckling resistance of slender steel columns. Despite these early results and the later mention of neglecting this issue, none of the published works has addressed it since Witteveen's paper.

Longitudinal non-uniformity of temperature variation along a structural steel component is an inherent outcome of the continuity of the steel columns beyond the fire story. Heat sinks exist at both ends of the story-high column, that stem from its contact with the floor slabs while passing through them, and from the cooler air temperature in the stories below and

above the fire story. The extent of cooling exerted by these sinks on the column and the attached beams has not been investigated. On the other hand, investigations [Chiou 1992, Wang 1995] have indicated that joint flexibility and frame action may have some significant effects on the structural response patterns of steel structures. The difference between the temperature evolution at the vicinity of the joint and the main sections may thus be an ameliorating factor, that deserves some special attention.

This paper presents first a two-stage procedure, which was utilized for analyzing the longitudinal thermal response and for predicting the extent of its non-uniformity. It then presents and discusses some typical results that demonstrate the general thermal behavior of steel assemblies. Factors affecting the extent of non-uniformity of temperature distributions along the beams and columns were depicted and used for a compact presentation of the results. The paper concludes with simple examples demonstrating the effects of this non-uniformity on the structural behavior of an isolated beam, column and simple frame (in comparison to the structural behavior of uniformly heated ones).

STAGE 1 - A SIMPLIFIED DISCRETE LUMPED-MASS MODEL

The main objective of this stage was to obtain a very fast indication of the order of magnitude of temperature differences between the central parts of steel columns and beams and their joints, which are closer to the heat sinks. An additional aim of this stage was to obtain a fast indication to the extent of influence of some parameters.

The left hand side of figure 1 depicts schematically the construction features of steel columns and beams within a given fire-story and the heat sinks that present themselves at the floor levels and beyond. The scheme on the right hand side of this figure presents a discrete lumped-mass model that was developed for a fast and simplified heat transfer analysis. The assumptions that were applied in the model are presented in appendix I.

Energy balance at each mass yielded a set of differential equations that depend on the various parameters listed in the appendix. The equation set is driven by the gas-temperature evolution in the fire story. A fast solution was obtained by an explicit numerical integration procedure. For the sake of accuracy, the time step was chosen as the smallest amongst the values of $d_{jk}^2/(2\alpha_{jk})$, where α_{jk} is the thermal diffusivity between the mass points j and k.

Some of the results obtained during this stage, for the ISO fire curve and a floor temperature, Tfl, of $Tfl = 0.1 \cdot Tf + 0.9 \cdot Ta$ (where Tf is the fire-room gas temperature and Ta the cool-room air temperature), are presented below.
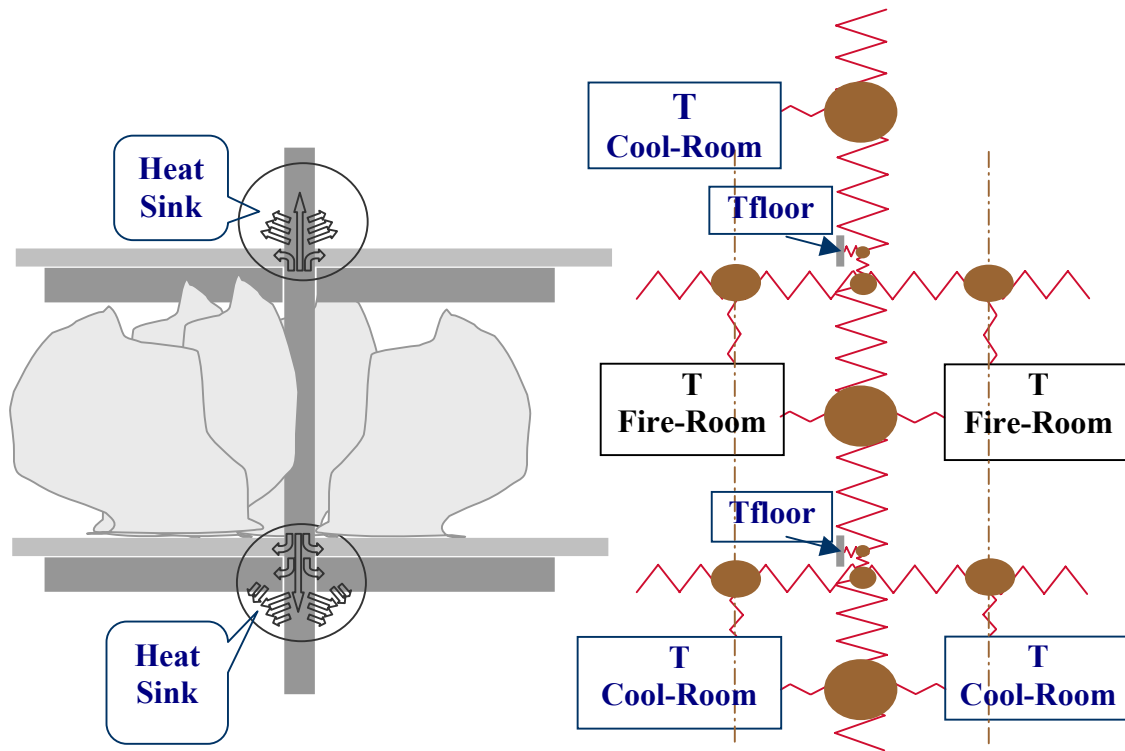
Figure 1: Schematic of Simplified Discrete Lumped-Mass Model.

Results in Figure 2 are for various combinations of non-insulated steel profiles and in Figure 3 for insulated ones. Varying parameters in these figures are the combination of the steel column and beam's sizes (virtual thickness ratios from 0.86 to 2.71and cross-sectional area ratios from 1.0 to 4.15) and within each group the lumped lengths γ_c and γ_b (each pair varying from 70% to 95%). One can notice that, as expected, only the profile sizes had some effect on the predicted temperatures of the column's or beam's lumped-masses. On the other hand, both parameters affected the temperature of the joint's lumped mass, indicating that close to the fire-room joint, the heat sink may have a significant effect. The solutions at 60 minutes for the non-insulated components showed a difference of up to only some 120C between the joint and the main sections, while for the insulated cases a difference of up to some 500C was indicated. The total set of results indicated that for insulated structures the effect of the heat sinks may be of some structural significance as well. This conclusion motivated a more accurate procedure for predicting longitudinal temperature evolution, as described in the next chapter.

This further analysis indicated, as expected, that the fast procedure predicted for the main sections' lumped-masses temperatures equal to those predicted by the "accurate" procedure. Nevertheless, the fast procedure predicted a larger temperature for the joint's lumped-mass than the average "accurate" temperature of this mass. For this reason, despite its simplicity, the fast procedure cannot be recommended for the detailed analysis of continuous steel construction.
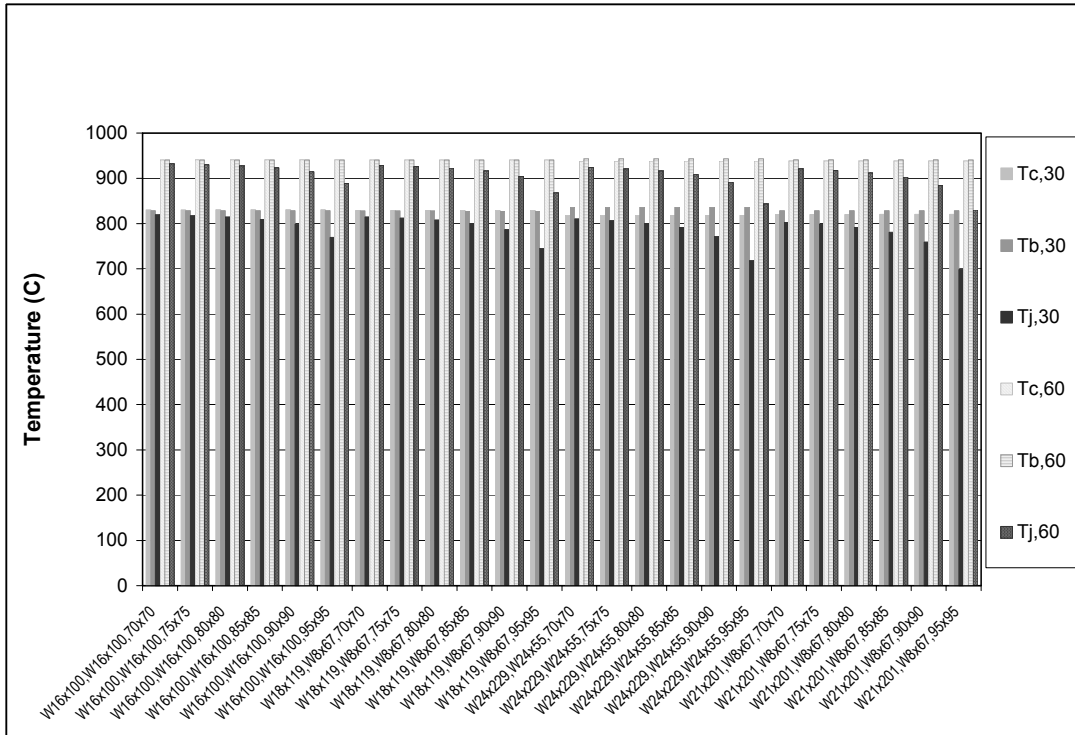
Figure 2: Some Temperature Results Obtained by the Simplified Procedure for Non-Insulated Steel Components.
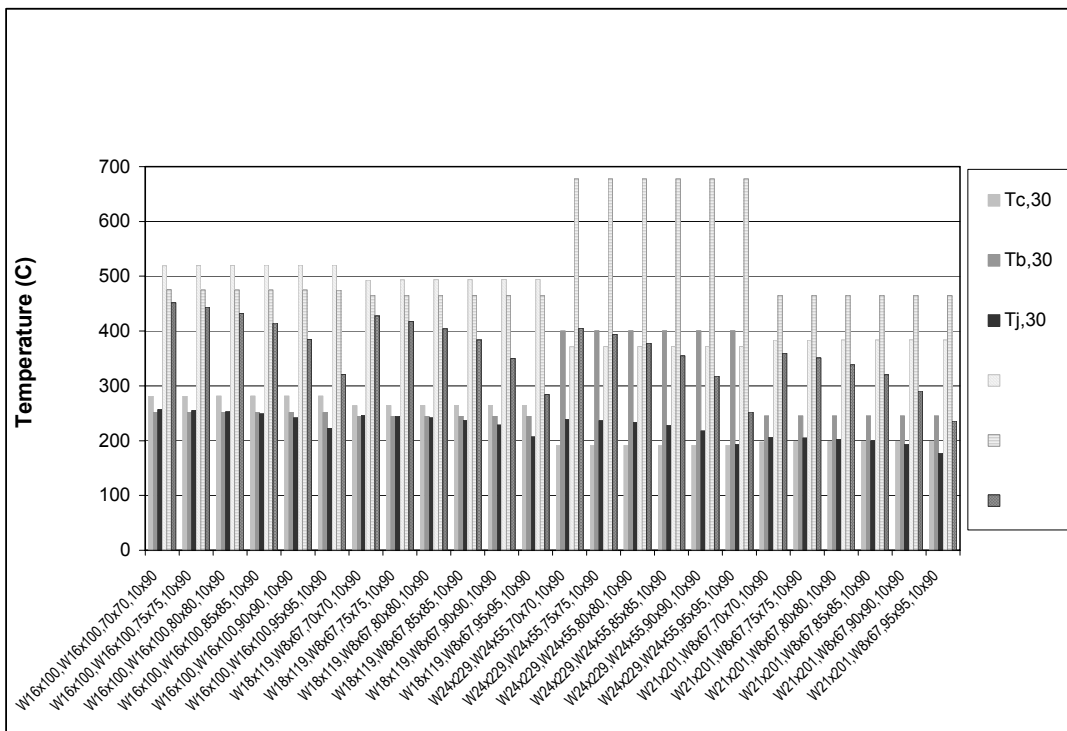

Figure 3: Some Temperature Results Obtained by the Simplified Procedure for Insulated Steel Components.

**STAGE 2 - A CONTINUOUS "ACCURATE" HEAT TRANSFER MODEL**

The purpose of this stage was to provide thermal data for the structural analysis of continuous steel construction in order to obtain an indication to the effects of the longitudinal temperature evolution on structural response. A set of 2-D partial differential equations for transverse and longitudinal heat transfer in the continuous frame components was established. The steel component was lumped in the transverse direction into its center by means of its cross-sectional area, A, and virtual-thickness, r, (where the virtual-thickness is defined by the ratio of the cross-sectional area to the heated perimeter). Within the insulation layer, a dense mesh was applied in all directions. To gain better accuracy, the longitudinal mesh size varied along the component. It was established to be compatible with the virtual thickness of the steel profiles and the insulation-mesh. Temperature-dependant material properties were considered. The set of reduced algebraic equations with varying coefficients was solved numerically by means of an implicit scheme, thus ensuring stability and fast convergence of the iterative procedure. Effects of various parameters were analyzed for a wide range of beam-column combinations.

Some representative results of the longitudinal temperature variation for an insulated frame with W14X61 beams and W14X120 columns, exposed to the ISO fire curve and the same floor temperature as in Figures 2 and 3, are given in Figures 4. The left graphs represent the variations along the height of the column at various times, and the right graphs the variations along the beam. The upper figures present components passing through thick insulation sleeves within the floor slabs, thus representing a case with heat sinks generated only by the room-air temperatures above and below the fire-room. The lower figures present the same components but in contact with the floor slabs' concrete, thus representing the actual case of heat sinks at the slab's levels. It is obvious that in the first case, the remote heat sinks hardly affect the joint temperatures. In the second case, however, the heat sink generated by the upper slab of the fire-room affects the adjacent joint temperatures significantly. Results for non-insulated components showed the same trend, but the temperature drop was much smaller, and was considered insignificant for further pursuing the subject.

Figures 5 to 8 present summarized results for the parametric influence of steel profiles' characteristics on the various temperatures at 60 minutes. The parameters considered were combinations of the virtual-thickness (rc and rb for the columns and beams respectively) and the cross-sectional areas (Ac and Ab). Only relations with large values of the correlation coefficients are presented. These indicate that the main geometric parameters affecting the temperature variation along the components are r, rc/rb, and $(Ac/2Ab)^2/(rc/rb)$. Figure 5 presents results for the temperatures at the mid-section of columns and beams. Figure 6 - results for the joint temperatures. Figure 7 - the ratio of the differences between joint and mid-section temperatures. Figure 8 - the influence distance from the joint.
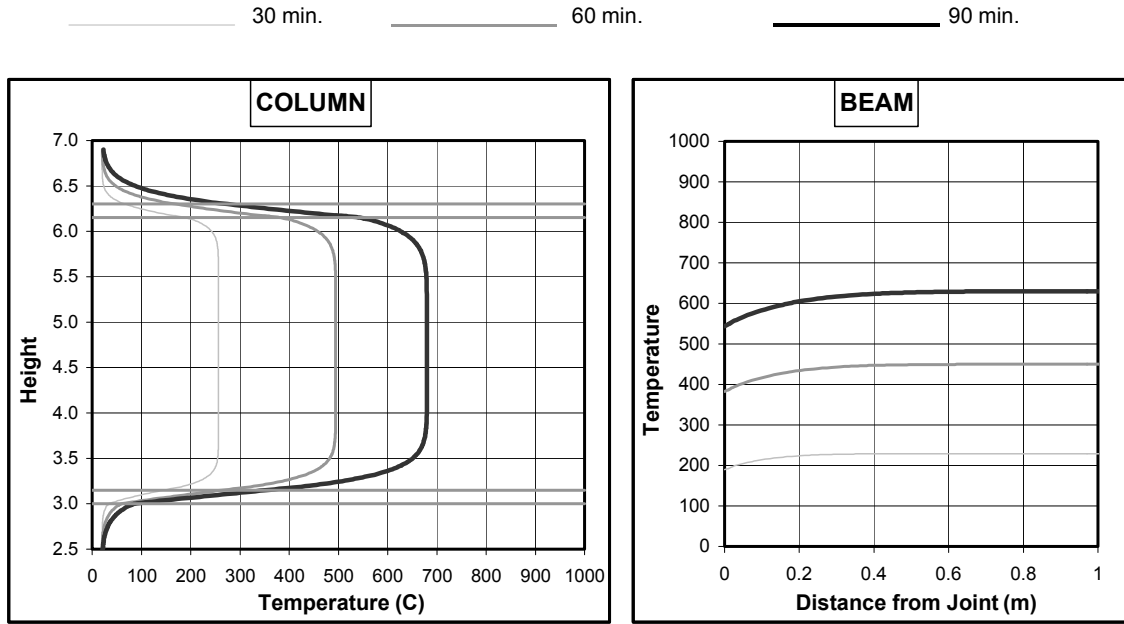
Components Passing through Insulation Sleeves within Floor Slabs
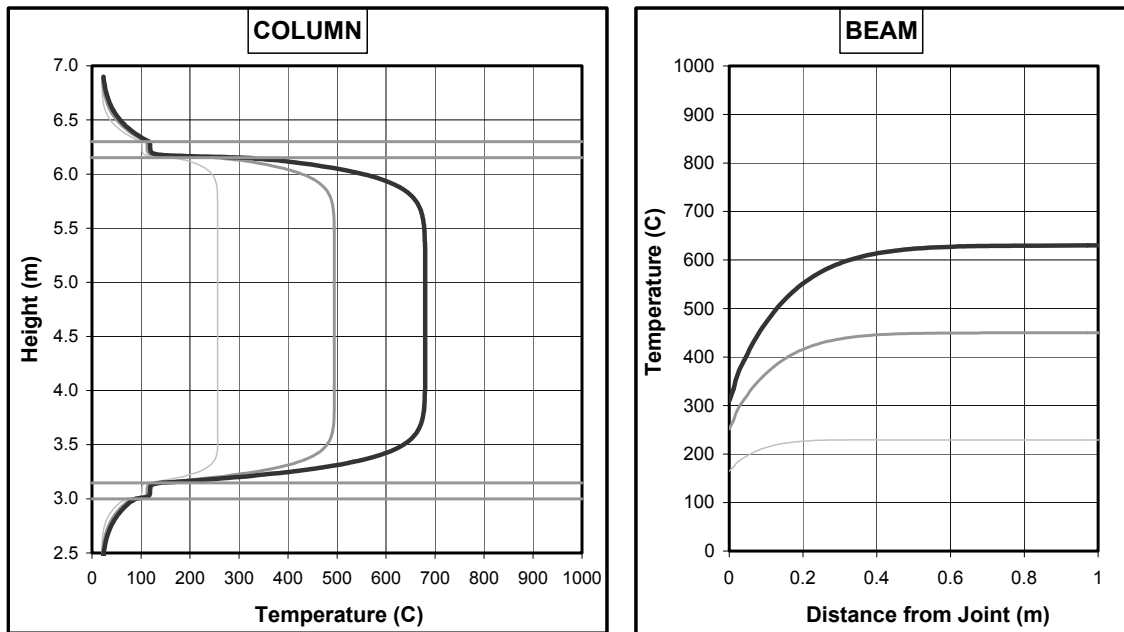
Components Passing through Floor Slabs in Full Contact with the Slab's Concrete

Figure 4: Longitudinal Temperature Variation for Insulated Columns and Beams.

It can be observed that the temperature drop towards the joint and the influence-distance increase as the component's virtual-thickness, r, decreases. For small r-values the drop at 60 minutes may reach some hundreds of C, and the influence-distance is approaching 1m.

The results of this stage strengthened the general conclusions from stage I. They confirmed the tendency of the temperature-drop to increase with the decrement of the virtual-ratio, but, in addition, indicated that the size of the drop maybe much larger. It is thus clear that for structural analysis temperature results from a simplified tool are not sufficient.

STAGE 3 - ANALYSIS OF STRUCTURAL RESPONSE

Structural response was obtained by SAFIR, from the Univ. of Liege in Belgium. Effects of uniform temperature distributions and longitudinally varying ones were compared. Results of the analysis in the former chapter were used as thermal input to the program, instead of the uniform temperature distributions predicted by its own thermal algorithm. Figures 9 to 11 include some results comparing evolutions and distributions of displacements, relative stresses (ration of current stress to yield stress at the given temperature), and moments along structural members of a one-bay frame with fixed ends. The frame was designed to carry the loads that match the maximum capacity of the individual members, with an initial maximum loading-ratio of 0.61-0.62 at the joint (only vertical loads were concerned). Calculated according to EuroCode 3, the beam and columns were expected to have maximum fire-resistances of 56 and 67 minutes respectively (for the clamping support conditions and a rigid joint). Structural response of the frame was analyzed for various evolutions of uniform and non-uniform temperature distributions. In order to isolate the behavior of a heated beam or a heated column within the frame the analysis included cases where only the isolated component was heated. Table 1 presents the symbols used for the analyzed cases whose results are presented in Figure 12. Figure 12 summarizes the results for the fire-resistance obtained for the same frame by the various case/methods.

Table 1: Description of symbols for analyzed cases presented in figure 12.

| Symbol	Description of Case/Method
EC3-B	Eurocode3 calculation for beam with clamped end supports
EC3-C	Eurocode3 calculation for column with various end conditions
U-B	SAFIR analysis for a beam with a longitudinally uniform temperature distribution in a frame with cooler columns
U-C	SAFIR analysis for columns with a longitudinally uniform temperature distribution in a frame with cooler beams
NU-B	SAFIR analysis for a beam with a longitudinally non-uniform temperature distribution in a frame with cooler columns
NU-C	SAFIR analysis for columns with a longitudinally non-uniform temperature distribution in a frame with cooler beams
U-F	SAFIR analysis for a frame with a longitudinally uniform temperature distribution
NU-F	SAFIR analysis for a frame with a longitudinally non-uniform temperature distribution
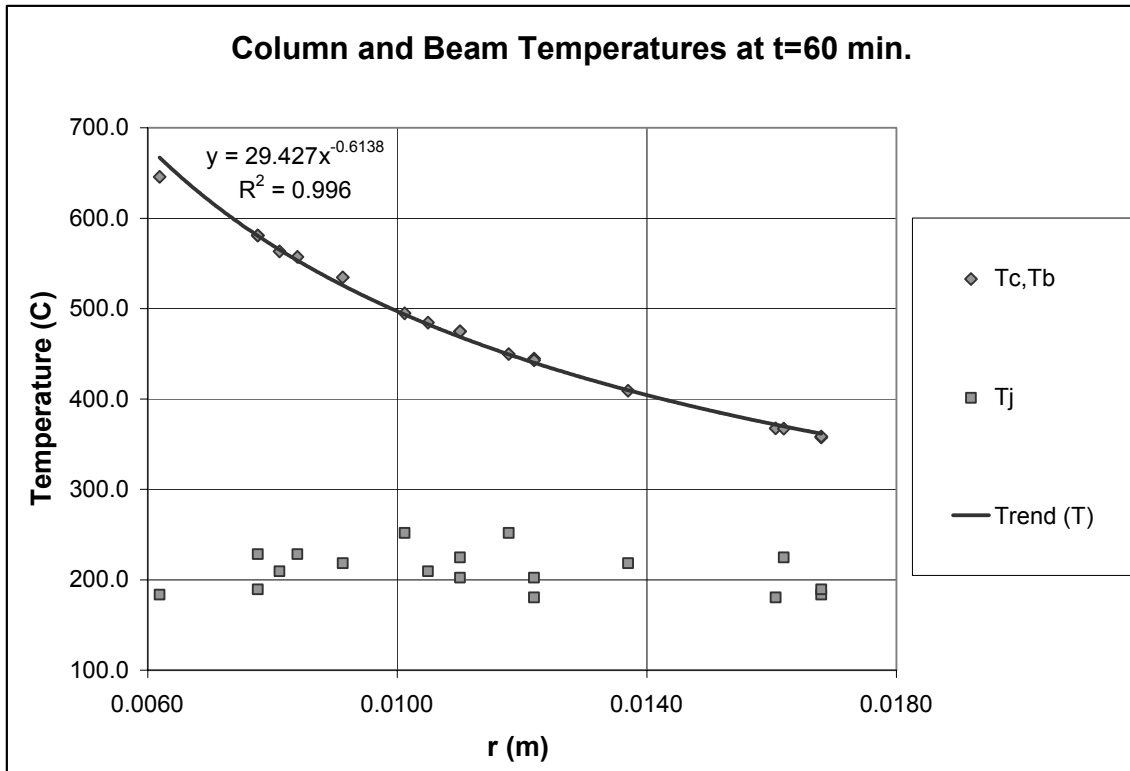
Figure 5: Component Temperatures at 60 minutes vs. Virtual Thickness.
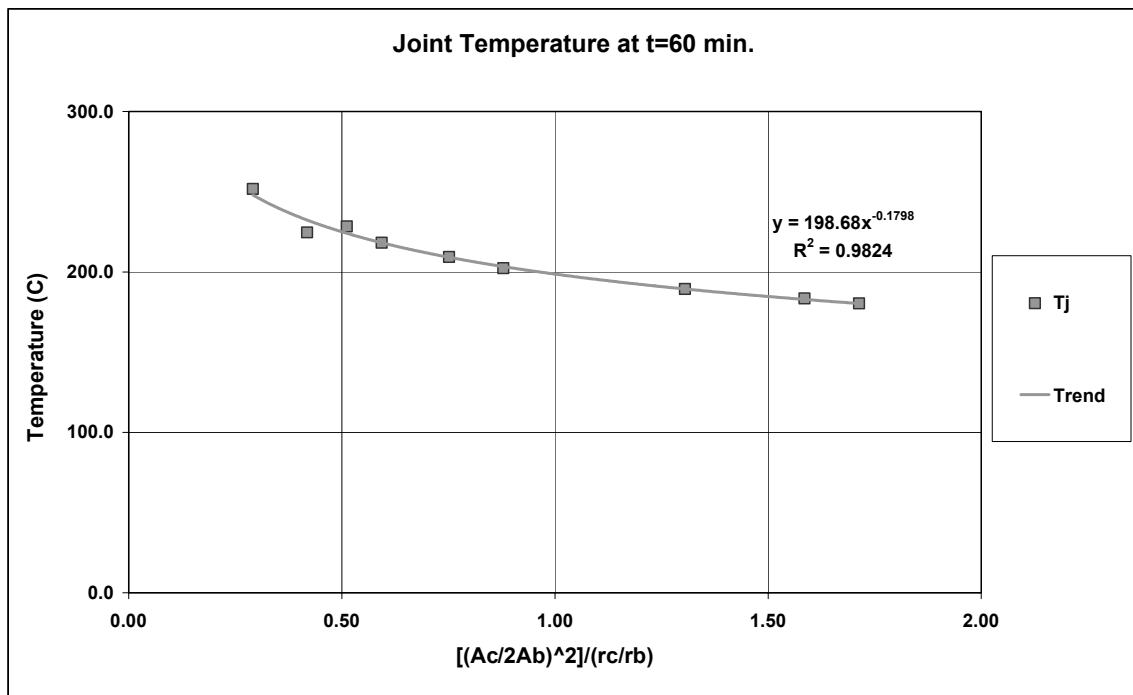

Figure 6: Joint Temperatures at 60 minutes vs. a Non-Dimensional Geometric Factor.
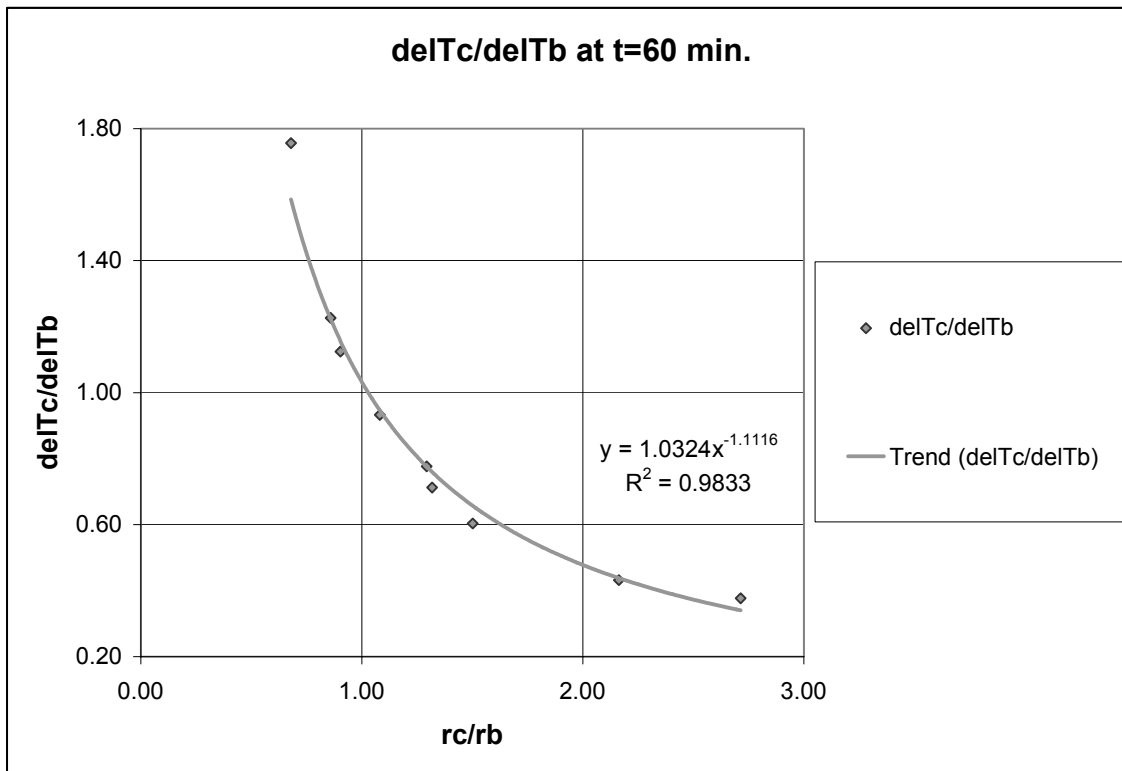
Figure 7: Temperature Difference Ratio at 60 minutes vs. Virtual Thickness Ratio.
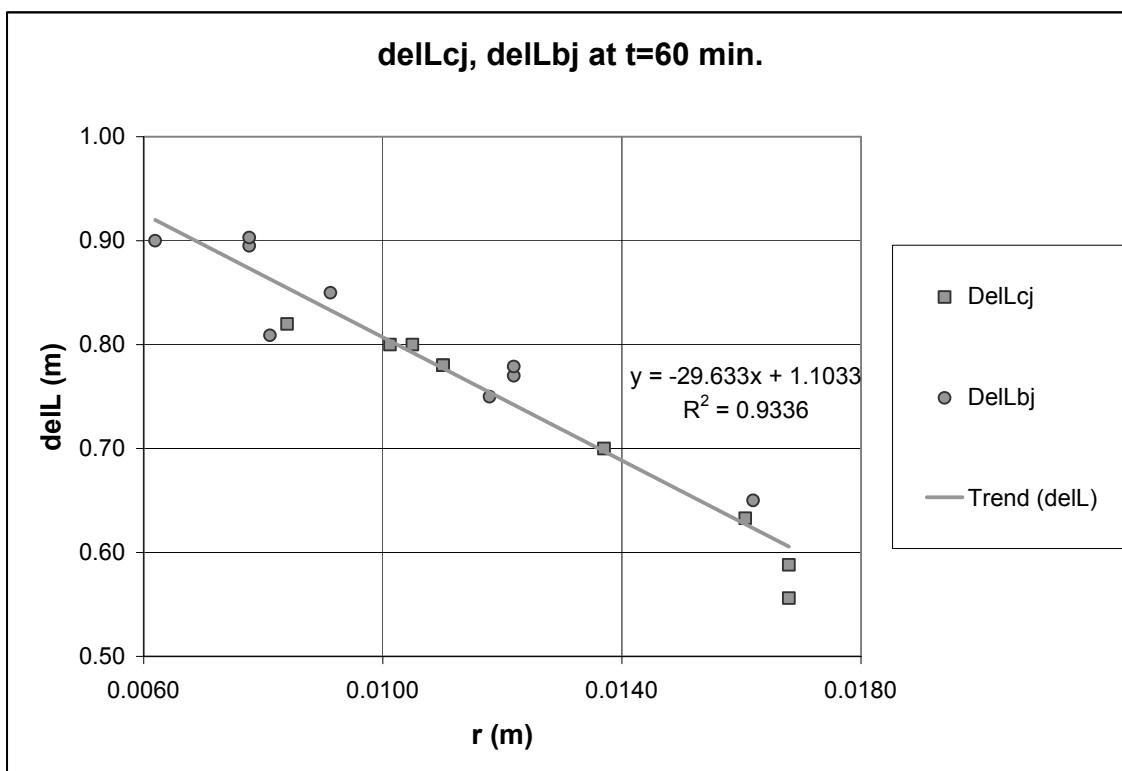
Figure 8: Influence Distances at 60 minutes vs. Virtual Thickness.

Some of the main observations from the results are discussed below:

1. The cases with non-uniform longitudinal temperature distributions show much slower development of rotations that those with uniform distributions. The same is observed for deflections along the beam, whereas the effect on the columns deflections is marginal.

2. The effect of the non-uniformity of temperature distribution along the beam on its total expansion is small. The deflection of the columns is mainly affected by the longitudinal expansion of the beams. Thus, the longitudinal non-uniformity of the temperature distribution has almost no effect on the columns deflections.
    This actually explains the last observation in 1.

3. In some cases analysis predicted non-symmetrical failure due to a snap-through of one of the deflected columns, with the other column experiencing a sudden increase in its deflections. The author could not find evidence to this phenomenon in the experimental literature.

4. Within the frame situation, heating of the columns affects mainly their expansion, thus hardly affecting the beam rotations and differential deflections.
    This explains the similarity of the fire-resistances obtained for the cases with non-heated columns (U-B and NU-B) to those derived for the cases with heated columns (U-F and NU-F) respectively.

5. When the beams are kept cool (cases U-C and NU-C) they do not expand, and the columns experience smaller rotations and deflections, thus exhibiting larger fire-resistances than when the whole frame is heated. These fire-resistances are larger by some 15 minutes than those established according to EC3. The influence of the longitudinal temperature variation along the column has almost no effect in this case, as failure occurs due to the onset of yield and not due to buckling.

6. In the cases with uniform temperature distributions, the plastic hinges formed at the joints, and their timing (so called fire-resistance) could be predicted by the critical temperature relevant to the actual load-ratios at the joint.

7. In the cases with non-uniform temperature distributions: As heating progressed, the location of the maximum relative stress moved away from the joint. Eventually, plastic hinges formed in the beam some 70 cm away from the joint. Formation of the first plastic hinge occurred some 10 minutes later than in the uniform temperature case. Experimental results from the Cardington facility [Kirby 1996] also indicate that the plastic hinges in the beam occurred somewhat away from the joint.

8. Within the delay period of first-plastic-hinge formation heating continued. Thus, deflections and relative stresses in the central region of the beam continued to increase. Consequently, the utilization factor of the central section increased and a second plastic hinge has almost formed when the first one occurred. This behavior stems from the specific nature of the ISO fire curve. From this point of view, it is thus most interesting to investigate the influence of actual-fire's temperature-time curves on the structural behavior of structures with non-uniform temperature distributions.
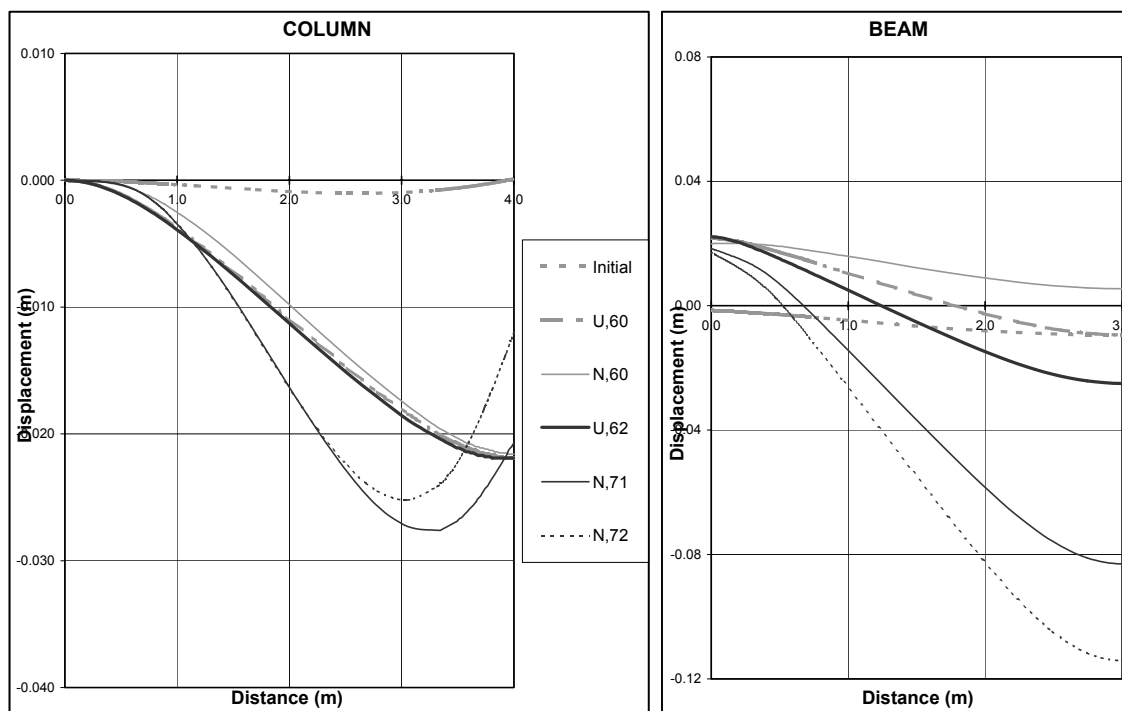
Figure 9: Time Evolution of Displacements along Column and Beam of a One-Bay Frame with Fixed Supports.
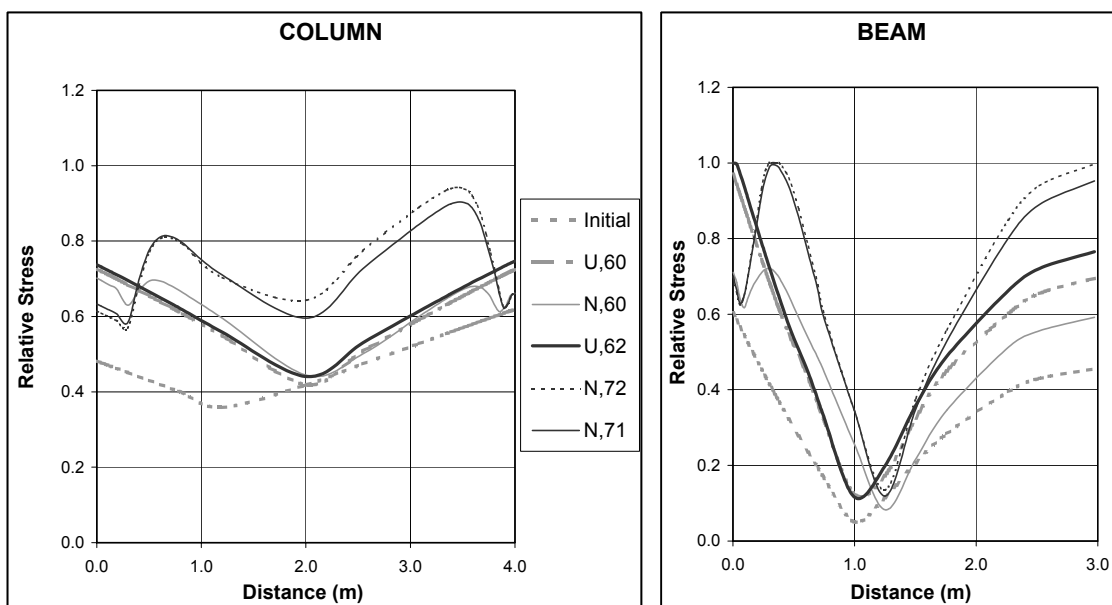
Figure 10: Time Evolution of Relative-Stress Distributions along Column and Beam of a One-Bay Frame with Fixed Supports.
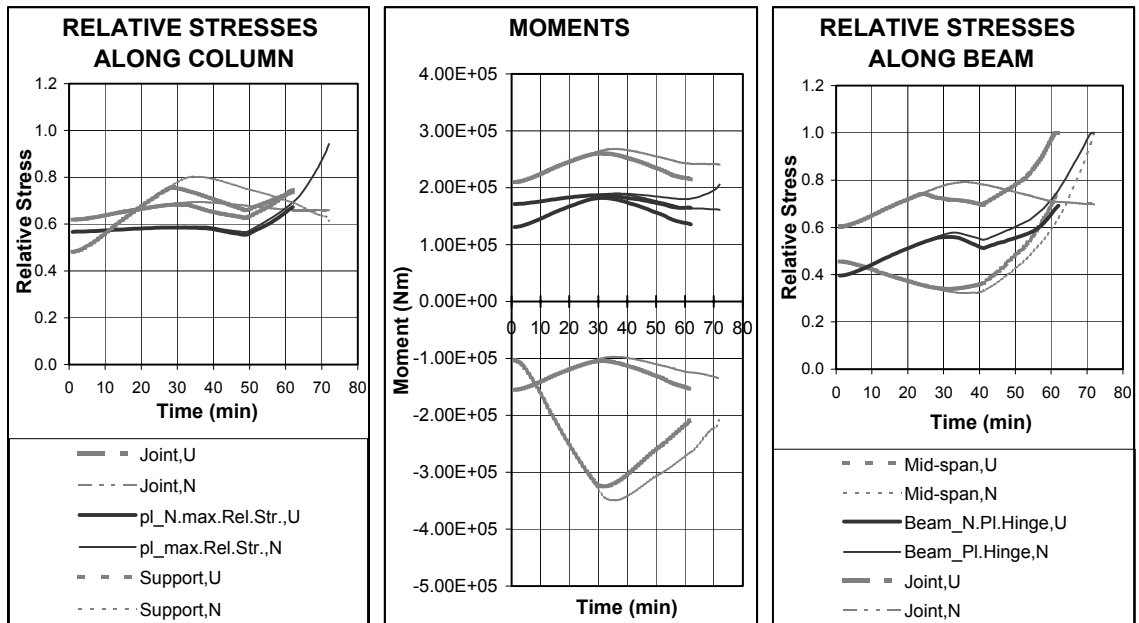
Figure 11: Time Evolution of Relative-Stress Distributions and Moment at Specific Locations of a One-Bay Frame with Fixed Supports.
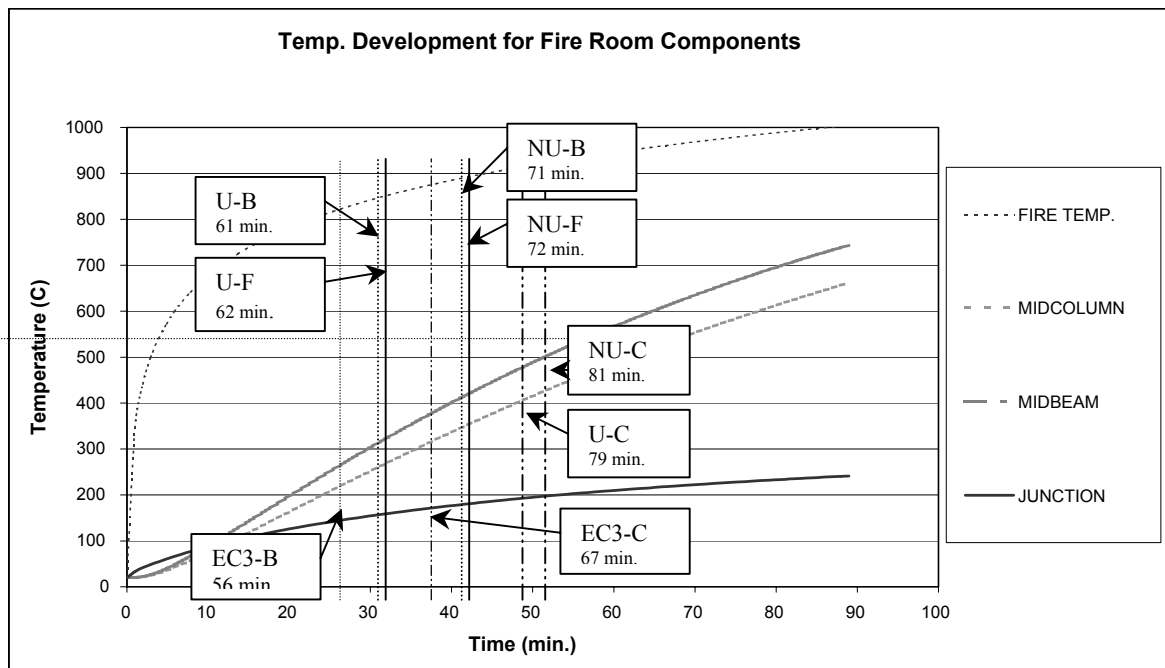
Figure 12: Summary of Fire Resistance Results for Various Cases.

CONCLUSIONS

It can be concluded that for continuous steel construction:
1. The heat sinks generated by the cooler room-air temperatures above and below the fire-story have practically no effect on the temperature near the fire-story beam-column joints.
2. The heat sinks generated by the cooler temperature of the concrete slabs may affect the joint temperature quite significantly, causing a temperature drop that depends on a combination of the properties of both components. Simplified fast tools, relying on lumped-mass calculations, predict the trend, but cannot predict the extent of the temperature-drop and influence-distance. The evolution of longitudinal temperature variation can be well estimated only with an accurate thermal analysis, which accounts for the parts of the columns that are embedded in the concrete slabs. However, for all practical purposes of this calculation only the fire-story may be considered, with columns extending into the cool rooms some 50 cm only.
3. For practical purposes, the temperature-drop expected for non-insulated steel construction after 30 to 60 minutes from the start of an ISO-fire is too small to be of any structural significance.
4. For insulated steel construction, the effect of these heat sinks on the non-uniformity of longitudinal temperature distribution is much more significant. For components with a small virtual thickness it may reach some hundreds Degree C at 60 minutes, with an influence-distance of up to 1 m. Studies of the effect of temperature-time curves better representing actual fires should still be done, as they are expected to have even a stronger effect.
5. The evolution of the non-uniform longitudinal temperature distribution is accompanied by a moving location of the maximum relative stress, thus prohibiting the use of the initial loading-ratio as an indicator for the critical temperature.
6. The longitudinal temperature non-uniformity may have some significant practical implications on the structural response as well. The predicted fire-resistance of a structure taking into account a uniform temperature distribution is always conservative. For the one-bay frame example presented in the paper the difference was 16% ($\approx$60 min. for the uniform temperature and $\approx$70 min. for the non-uniform). The implications on more complicated structures need further studies.

Nomenclature:

Ab, Ac   -   beam and column Cross-sectional areas (m^2)

d_{jk} -   distance between centers of lumped masses (m)

rb, rc   -   beam and column virtual thicknesses (m)

Ta   -   cool-room air temperature (C)

Tb, Tc   -   temperature of beam's and column's main areas (C)

Tfl   -   floor temperature (C)

Tg   -   fire-room gas temperature (C)

Tj   -   temperature of joint (C)

delLbj   -   influence distance from fire-room joint into beam (m)

delLcj   -   influence distance from fire-room joint (downwards) into column (m)

α_{jk} -   diffusivity between lumped masses j and k (m^2/s)

References:

1. Anderberg, Y., 1998, "European Experience in Fire Design of Structural Steel". Proceedings of the 24th Structures Congress on "Building an International Community of Structural engineers" ASCE - American society of Civil Engineers. Part 1. pp. 357-364.
2. Chiou, Y.J. and Lin, Y.R., 1992, "Study on the fire Response of Flexibly Jointed Steel Frames". Computers and Structures, Vol. 45, No. 3, pp. 439-451.
3. Culver, C.G., 1972, "Steel Column Buckling under Thermal Gradients". Journal of the Structures Division, ASCE - American society of Civil Engineers, v99 No. ST8
4. Franssen, J.M., Cooke, G.M.E. and Latham, D.J., 1995, "Numerical simulation of a Full Scale Fire Test on a Loaded Steel Framework". Journal of Constructional Steel Research, v35 n3, pp. 377-408.
5. Gilvery, K.R. and Dexter R.J., 1997, "Evaluation of Alternative Methods for Fire Rating Structural Elements". NIST-GCR-97-718, Building Fire research Laboratory, National Institute of standards and Technology, Gaithersburg MD.
6. Jeans, D.C., 1986, "The performance of a Large Scale Structural Steel Frame During exposure to Fire environment". Internal Report, Building Fire research Laboratory, National Institute of standards and Technology, Gaithersburg MD.
7. Kirby, R.B., 1996, "British Steel Technical European Fire Test Programme - Design, Cnstruction and Results".Proceedings of the 2nd Cardington Conference on "Fire, Static, Dynamic Tests at the The Large Building Test Facility", Cardington.
8. Liu, T.C.H., 1996, "Finite element modelling of Behaviours of Steel Beams and connections in fire". Journal of Constructional Steel Research, v36 n3, pp. 181-199.
9. Wang, Y.C., Lennon, T. and Moore, D.B., 1995, "The Behavior of Steel Frames Subject to Fire". Journal of Constructional Steel Research, v35 n3, pp. 291-322.
10. Witteveen, J. and Twilt, L., 1981/82, "a Critical View on the Results of Standard Fire Resistance Tests on Steel Columns". Fire Safety Journal, 4 (1981/82) pp. 259-270.

Appendix I: Basic Assumptions for the Simplified Discrete Lumped-Mass Model

- Each lumped steel-mass i is heated uniformly and represented by a unique temperature evolution T_i.
- Steel thermal properties are constant.
- Resistance to heat transfer between adjacent lumped steel masses j and k is given by:

$$r_{jk} = d_{jk} / \lambda_s \qquad (1)$$

Where:

d_{jk} - the distance between the centers of the adjacent masses

λ_s - steel thermal conductivity

- Heat transfer between the masses during an infinitesimal time period dt is given by:

$$q_{jk} = dt \cdot A_{jk} \cdot (T_j - T_k) / r_{jk}$$

Where:

A_{jk} - is the cross-sectional area of the actual member between masses j and k.

- Horizontal symmetry. I.e.: the centers of the joint and the beam's lumped mass are at their actual centers.
- The joint's lumped length along the column is given by $\gamma_c \cdot H$, where:

H - the actual distance between the top of the floor slab and the joint

γ_c - variable for the parametric investigation.

- The joint's lumped length along the beam is given by $\gamma_b \cdot L$, where:

L - the actual beam length

γ_b - variable for the parametric investigation.

- The lumped length of the column's part within the floor is given by $\gamma_{fl} \cdot D$, where:

D - the actual floor thickness

γ_{fl} - variable for the parametric investigation.

- When fire protected: the temperature of the insulation above the i'th mass is represented by a unique temperature evolution $T_{in,i}$.
- Heat transfer from the room air-temperature T_a towards a lumped mass i is given by:

$$q_{a,i} = dt \cdot (\sum_m L_{im} p_{im}) \cdot [h_v \cdot (T_a - T_{s,i}) + \sigma \cdot \varepsilon_j \cdot (T_a - T_{s,i}) \cdot (T_a + T_{s,i})(T_a^2 + T_{s,i}^2)] \quad (2)$$

Where:

σ - the Stefan-Boltzman constant equals $5.76 \cdot 10^{-8}$ W/(m^{2}K^4).

h_v - the convective heat transfer coefficient. It is well known not to have major significant effect during fire. Thus in the fire story the value: $h_{v,f} = 25$ W/(m^{2}K) was used, and in the other stories: $h_{v,a} = 8$ W/(m^{2}K)

ε_j - the resultant emmissivity. It is the significant parameter for heat transfer during fire. Thus, in the fire story ε_f was a variable for parametric investigation, and in the other stories the value: $\varepsilon_a = 0.9$ was used

$T_{s,i}$ - equals T_i for the non-insulated case, and $T_{in,i}$ for the insulated case

$T_{a,j}$ - equals the gas-temperature in the fire-story (taken in this case from the standard ISO curve given by: $T_f = 20 + 345\log(8t+1)$), and the room air temperature (in this case : 20C) in the other stories.

p_{im} - is the heated perimeter of the m'th part along the i'th mass (for most parts m=1. For the joint's mass m=1 stands for the part that stems from the column and m=2 for the one related to the beams).

- Floor temperature at contact with steel column is given by:

$T_{fl} = \gamma_1 T_f + (1 - \gamma_1) \cdot 20$

Where:

γ_1 - is a variable for parametric investigation.

COMPARISON OF FINITE ELEMENT MODELS OF COMPOSITE STEEL FRAMED BUILDINGS BEHAVIOUR IN FIRE

O'Callaghan, D.J & O'Connor M.A,
Corus Research Development & Technology, Swinden Technology Centre, Rotherham, United Kingdom, S60 3AR

ABSTRACT

This paper summarises some of the results obtained from an extensive numerical study into the behaviour of composite structures in fire. This work is part of a major research initiative involving both UK and European partners in a programme to establish important principles for modelling structures in fire. As part of the study, rigorous models were developed and calibrated against a large experimental testing programme carried out at the Cardington test facility to develop an understanding of the structural behaviour. These models were developed using finite element analysis and included temperature profiles extracted from the Cardington tests applied to each structural element in the FE model so that a direct comparison between model and test could be made. This paper compares the results of three variations of FE models namely, grillage, beam/shell and shell representation of the fire loaded area. The results comparison highlights the sensitivity of each modelling methodology along with the observed behaviour.

The results showed the overall behaviour to be highly complex with the effects of each structural member affected by such phenomena as; temperature profile through the member, degree of thermal restraint offered by the surrounding structure, degradation in material properties with increasing temperature and development of alternative load carrying paths. Various results are plotted showing the change in member behaviour throughout the application of fire loading and reveal the development of alternative complex load paths which enable the structure to retain its structural integrity.

The grillage model used beam elements to represent the primary and secondary beams and the concrete slab. Such models fail to include in-plane shear transfer across the slab but offer reasonable accuracy when the primary mode of failure is by flexure. To account for shear transfer the second model type included a shell representation of the slab. Finally, observations from the Cardington tests showed extensive local buckling of flanges and webs in both the primary and secondary steel beams. This would not be captured using beam elements so a further rigorous model was generated. This rigorous model discretisation included a shell representation of all the fire-loaded area so events such as local buckling of webs and flanges were captured.

INTRODUCTION

With the development of composite deck slabs to enhance the competitiveness of steel framed buildings, a growing concern has arisen of their under utilisation when designing against fire attack. Current design practice for the fire limit state is based on tests that are carried out on determinate, unrestrained, single members. In reality, composite structures possess a high degree of redundancy, which contributes to load redistribution within the structure during and after a fire, as found in the Cardington test frame and other structures [3,4].

To incorporate this into current design practice, a thorough understanding of the structural behaviour of composite structures must be established. The development of this understanding has been a central theme of a recent UK DETR funded project involving the University of Edinburgh (project leaders), Corus RD&T, Imperial College, Steel Construction Institute (SCI), Building Research Establishment (BRE) and with interest from various fire engineering specialists.

The research forms part of series of objectives which are aimed at developing a rational approach to designing steel framed buildings with composite deck slabs under fire. The structure of the overall research can be divided as follows:

1. Demonstration of the structural behaviour of steel framed buildings in fire
2. Development and calibration of rigorous models to understand the structural behaviour
3. Application of models in parametric studies to understand a wide variety of structural scenarios
4. Generation and dissemination of design guidance based on thorough understanding, for use in everyday design of structures against fire attack.

This paper describes some of the modelling work carried out at Corus RD&T in pursuit of the second objective. The modelling work concerns the third or corner test carried out at BRE Cardington as part of an earlier project.

DESCRIPTION OF TEST 3, CORNER TEST

The corner test was carried out on the second floor of the 8-storey steel framed building at the BRE large building test facility (LBTF) at Cardington. The LBTF structure was a braced frame conforming in design to EC3&4 [5,6] with three stiff cores located at either end and in the center of the building (Figure 1). The composite deck slab was 130 mm thick, containing lightweight concrete reinforced with A142 anti-cracking mesh on CF70 profile decking. This was designed for an imposed load of $2.5 kN/m^2$ and the test load ($5.48 KN/m^2$) was in the form of uniformly distributed sand bags each weighing 11 kN to represent typical operational loads, representing a third of normal imposed load.
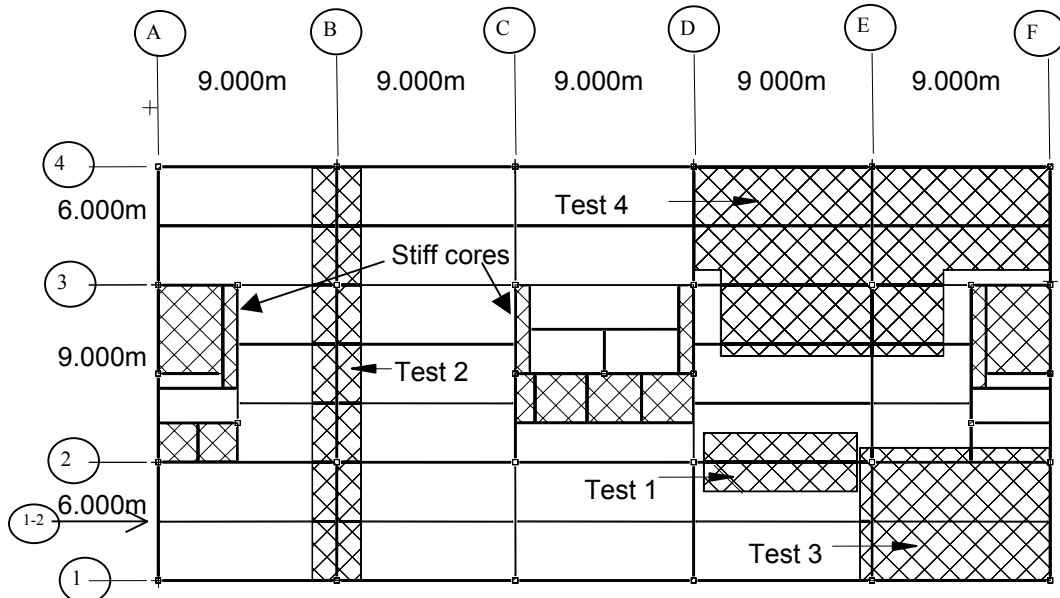
Figure 1: Plan of Cardington showing Cores and Test Compartments

The test area covered $80m^2$ at one corner with the nearby gable end bracing removed to prevent load transfer. A 7m wide opening provided ventilation, assisted with an adjustable screen and calculated to provide an effective opening factor of $0.31m^{1/2}$.

The columns and edge beams were protected using 25mm ceramic fibre blanket leaving the primary beams, secondary beams and connections fully exposed.

The maximum temperature reached was over 1000^oC provided by a fire loading of $45kg/m^2$ of wood cribs over the first floor compartment.

DEVELOPMENT OF RIGOROUS MODELS

It is important in any modelling procedure that the key structural behaviour is captured in the developed model. This was achieved in this project by developing models of varying complexity to examine the differences in various modelling assumptions on overall structural behaviour. This process is not only necessary in the development of robust models but is an essential part in developing understanding of structural behaviour.

General Modelling Assumptions

To ensure that restraint from the surrounding structure was adequately represented, half of the second floor was modelled to represent the corner test compartment and the immediate surrounding structure. Each model was developed using the general-purpose FE package, ABAQUS/Standard [7], having 2 noded beams and 4 noded shell elements. The columns extended to the floors above and below and were represented by beam elements. This is sufficient, as they were protected in the test.

It was important to obtain a good representation of the composite action. This was achieved by modelling the top 70 mm of the concrete slab at the centreline of the top of the slab. Beam element representations of the steel beam were located on their neutral axis at the midpoint of the webs. Constraint equations were incorporated between the slab and beams, which assumes full composite action. The beams connections to columns and other beams

were modelled using constraint equations (usually pinned) and included torsional restraint. The slab elements were not connected directly to the columns but were continuous over columns and primary beams. The downstand ribs in the slab spanning direction were modelled as a series of stiffener beams representing the concrete trapezoidal section. A schematised version of this representation is given in Figure 2 below.
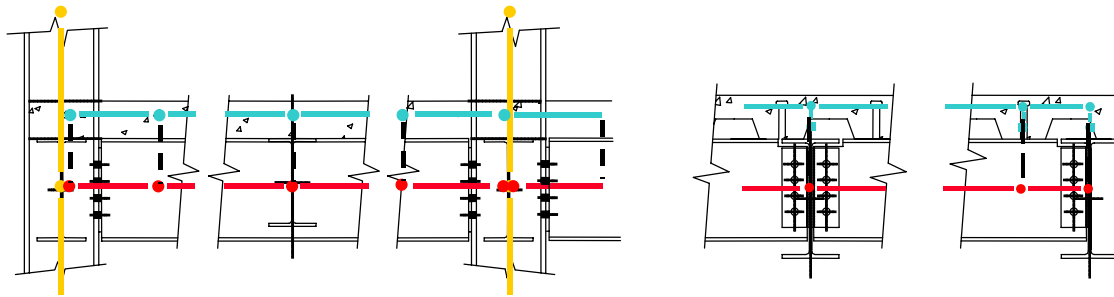
Figure 2: Modelling of composite deck arrangement

Representing the slab and beams as described above was necessary to capture the correct restraint conditions and to ensure that the flexural stiffness of the slab and composite beam, the membrane stiffness of the slab and composite beam and the stiffness of supporting structure (lateral, vertical and torsional) were correctly captured.

Grillage Model
It is still uncertain how representative a grillage approach is, but due to its simpler slab representation, it offered a means of explaining the complex 3D effects of structural restraint and load transfer paths. Beam elements were used to represent both the primary and secondary steel beams and the concrete slab. The slab spanning in the primary beam direction was modelled as a series of 500 mm wide strips. These included the properties of the downstand in an overall representation of slab behaviour consisting of temperature varying moment-curvature and axial-strain relationships to represent decoupled bending and membrane stiffness in this direction.

The portion of slab acting composite with the secondary beams was again modelled as a strip over the beams, which represented the top 70 mm of the slab. This method relies on transferring load directly into the column or primary beam, ignoring in-plane load transfer by means of shear. This should be adequate if the main mode of slab load transfer is one-way decoupled flexural and membrane action. The grillage representation of the corner test is illustrated in Figure 3(a).

Beam/Shell Model
A beam/shell model, consisting of a shell representation of the floor, was developed to further understand the 3D effects such as tensile membrane action in the slab and in particular the contribution of in-plane shear within the highly deflected regions of the slab. This model used beam elements for the primary and secondary steel beams and shell elements for the slab. Minor changes were also incorporated as further understanding of the structural behaviour due to thermal effects became apparent [8], for example preventing the outer edge of the slab from being heated allowing for the correct form of edge restraint. The beam/shell representation of the corner test is illustrated in Figure 3(b).

44

Full Shell Model of Test Compartment

It was observed from examination of the test that severe local buckling of webs and flanges occurred particularly at intersections of continuous beams. To capture the local buckling effects and associated complex action of the composite behaviour at elevated temperatures, a full shell model of the test compartment was generated. The primary and secondary beam connections were included with the use of gap contact and spring elements. The gap contact elements modelled the effect of the partial depth end plate and fin plate connections closing against the columns as the beams expanded upon heating. To include slab non-linearity, discontinuities were placed in the slab at locations of max sagging and hogging using a moment curvature relationship described in the material model representation. The shell representation of the corner test is illustrated in Figure 3(c).

(a): Grillage Model

(b): Beam/Shell Model

(c): Shell Model
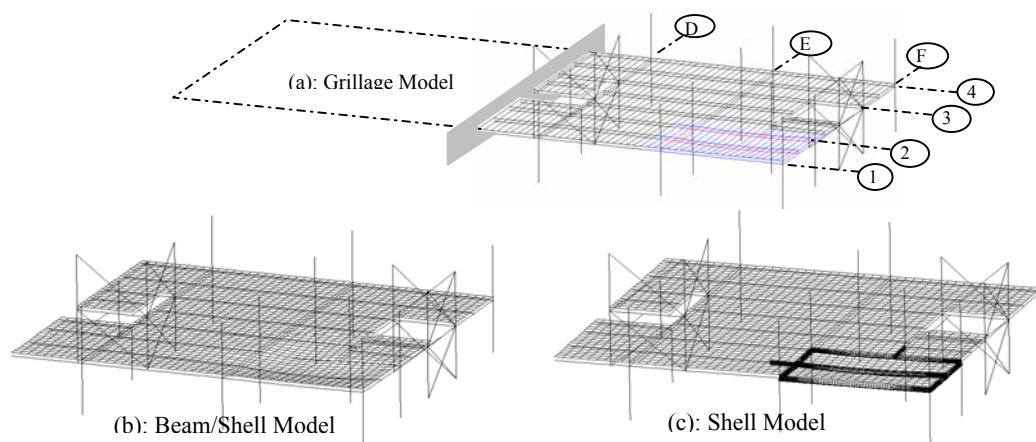
Figure 3: Discretisation of half a Cardingtion floor for modelling test 3

Material Model Representation

Various material modelling approaches were used as part of the development of the rigorous model. Initially, the slab was modelled linear elastically. This later changed to incorporate non-linear effects of axial force with strain and moment curvature relationship for increasing temperature profile, along with anisotropic effects between tensile and compressive concrete behaviour. These properties were incorporated into spring elements placed at locations of maximum bending in both hogging and sagging in the slab i.e. at mid span and over beam supports (Figure 4a). The properties were calculated by dividing the trapezoidal sections of the slab into horizontal slices and determining the axial force with strain and the moment curvature relationships for each slice as the neutral axis changed with increased bending [9]. This was calculated for the slab temperature profiles observed in the test for both in plane and out of plane spans (Figure 4b).

The heated beams were modelled using nonlinear properties with temperature. Analyses were carried out using both isothermal and an-isothermal material models, namely EC1: Part 1-2 [10] and the Anderberg model [11] respectively. These were applied to both the primary (S355 grade steel) and secondary beams (S275 grade steel). It was found that due to the steeper gradient of stress temperature curves found with the Anderburg material model, this proved to be more stable at temperatures above 350^0C. Both material models are illustrated in Figure 5. The non-heated beams were given linear elastic properties.

(a): Plan of model showing location of springs at mid spans and over

(b) **Moment rotation relationship applied to slab at max hogging & bending**
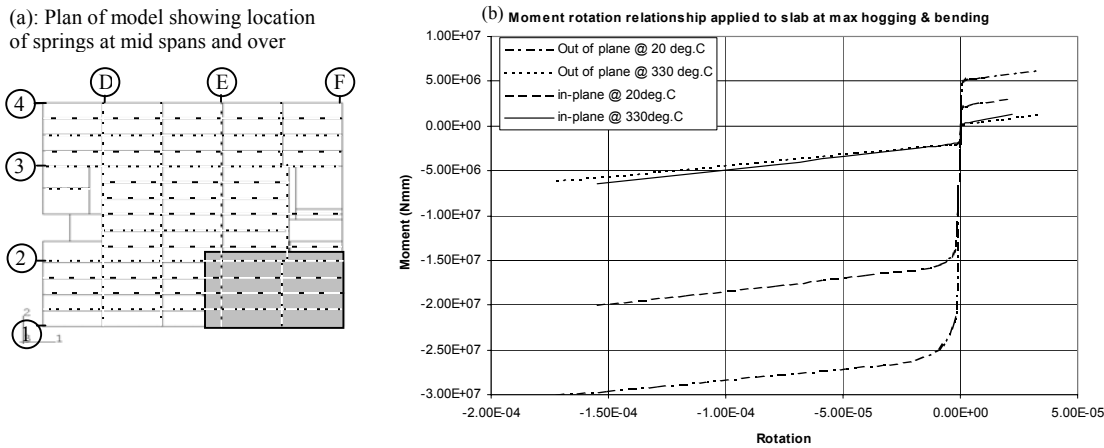
Figure 4: Material non-linearity used in concrete slab

(a): EC 3 pt.1 stress strain relationship   (b): Anderburg stress strain relationship
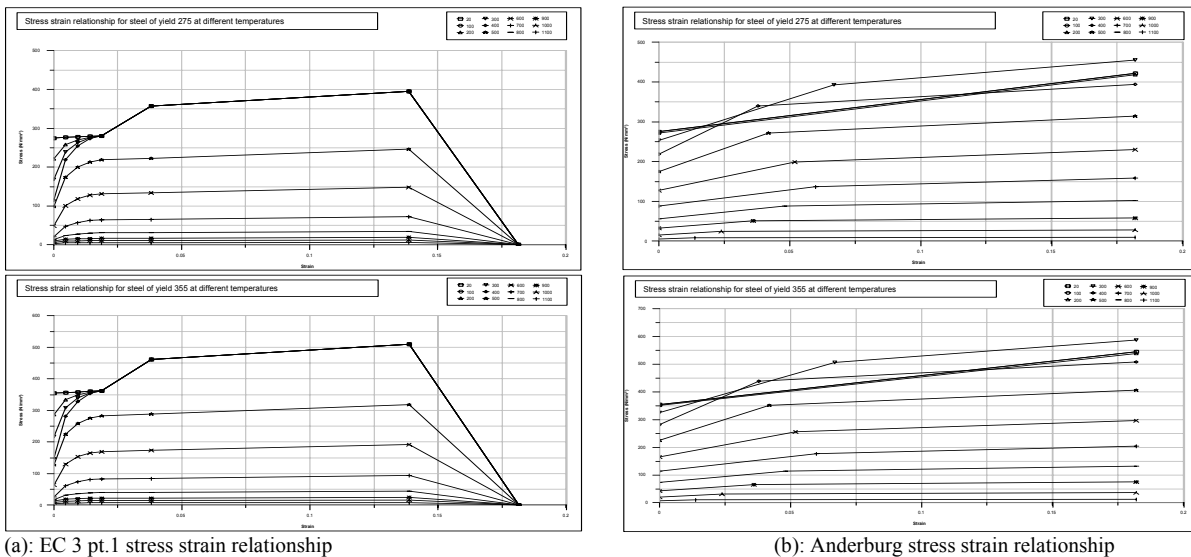
Figure 5: Stress strain relationship for grade 275 and 355 steel with increasing temperatures

Loading and Boundary Conditions

The temperature loading applied to the heated area was taken directly from measured values of each member in the test (Figure 6) and applied at increments of five minutes. The boundary conditions consisted of fixing the column ends at the floor levels above and below the heated floor. Since a model representing half the floor was adequate the cut edge was restrained from moving in plane, thus mirroring the restraint provided by the remaining floor (Figure 3a).
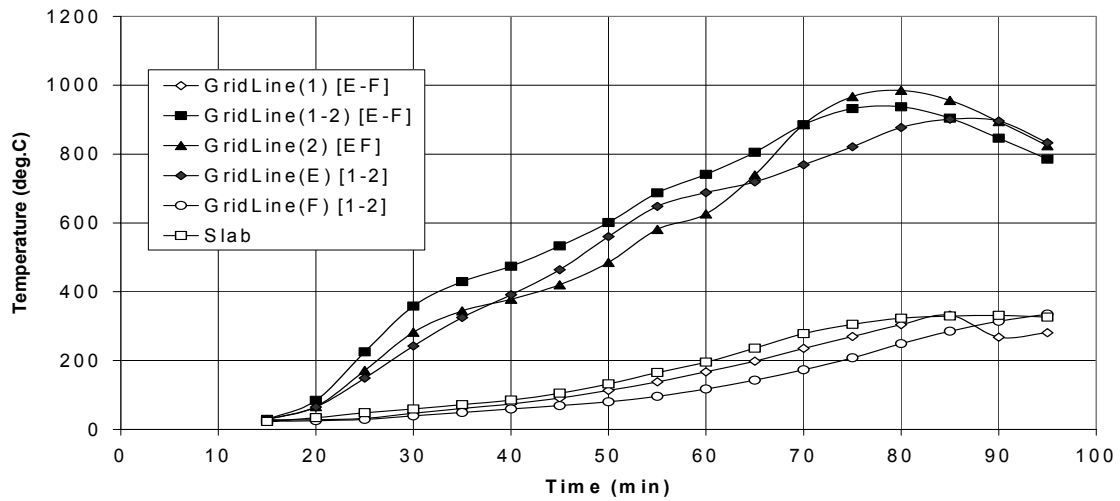
Figure 6: Temperature profiles applied to bottom flange of beams and slab

DISCUSSION OF RESULTS

A level of confidence was generated in the models by comparing slab vertical deflections, column lateral displacements and column strains to test results. The more rigorous the model, the better the agreement and hence confidence in structural behaviour to a real scenario. Understanding the structural behaviour was based on examination of member forces to reveal load redistribution paths. For this purpose all the models were extensively post processed.

Figure 7 shows slab deflection across the heated compartment over the heated secondary beams with the shell rigorous model offering closest agreement to test results. Column lateral displacements at floor level for edge columns E1 (y-direction) and F2 (x-direction) (refer to Figure 1 for location) were compared. The level of agreement compared favourably well for each model, indicating simplified models provide an adequate representation of the overall structural restraint (Figure 8). Comparison of column vertical strains at locations 500 mm above the heated floor also showed good agreement to test results considering the sensitivity of strain gauge readings (Figure 9).
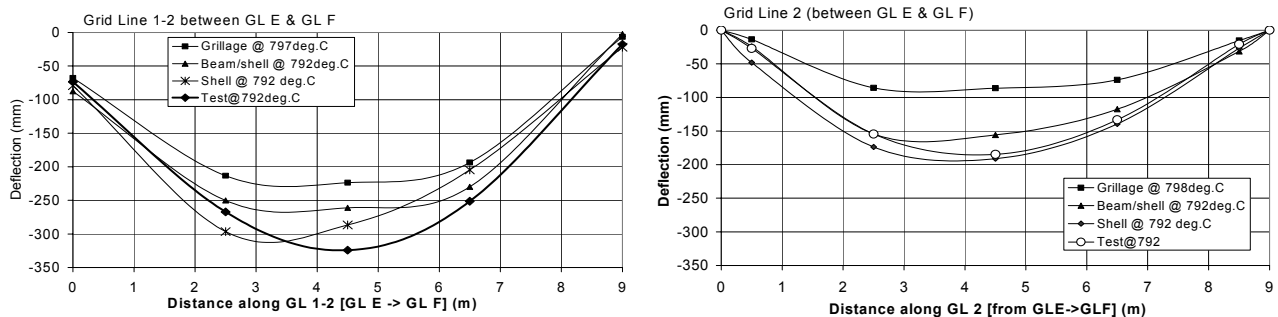
Figure 7: Comparison of slab deflections over heated secondary beams

Primary and secondary beam forces were plotted at 100° C intervals for both grillage and beam/shell models (Figure 10). The similarity between grillage and beam/shell indicated

both approaches captured the same structural behaviour in the steel frame. However, the slab forces across the test compartment showed less agreement particularly in the primary direction (y-direction, Figure 11). This is almost certainly due to the lack of in-plane shear transfer capability in the grillage model. Although it could also be attributed to the density of the grillage representation of the slab.
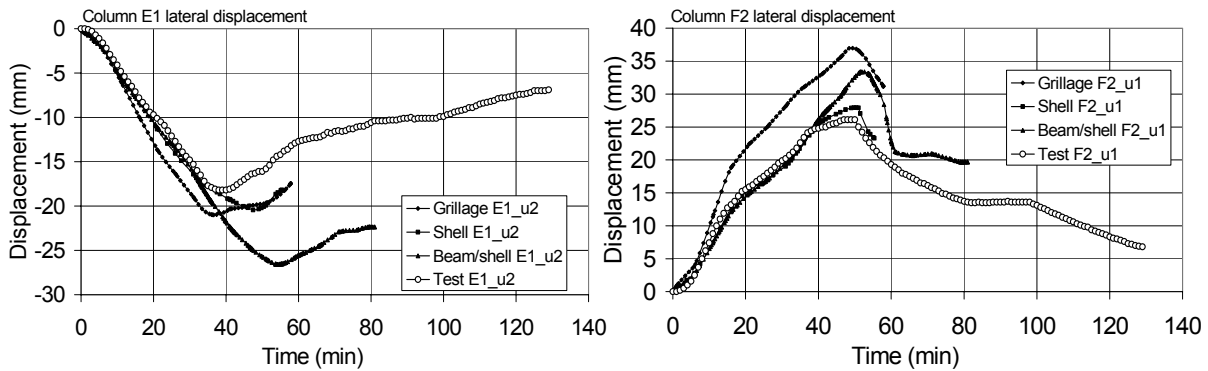
Figure 8: Comparison of Column lateral displacements at floor level
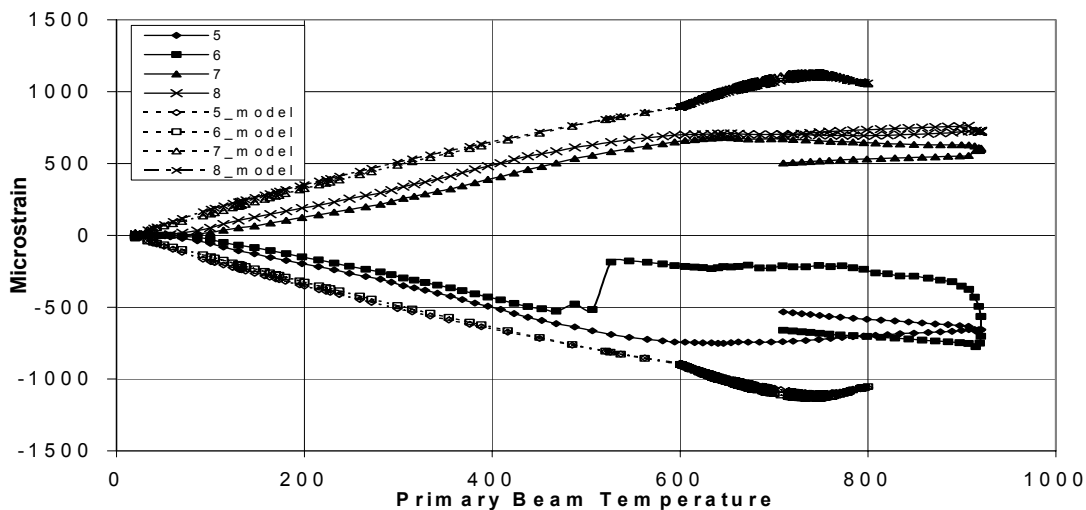
Figure 9: Column E1 vertical strains (500 mm above heated floor)

Composite Behaviour

Examination of longitudinal forces in the steel beam and concrete slab along secondary beam GL 1-2 in Figures 10 and 11 reveals the composite beam behaviour in fire. The steel beam, initially in tension, expands upon heating. However, restraint against thermal expansion is provided by both the cold edge beam (GL F) and the unheated part of the secondary beam GL 1-2, causing the beam to compress. Considering that plane sections remain plane and that the rate of heating of the concrete slab is slower than the steel beam, the slab is forced vertically downwards and into tension, similar to the scenario of a bi-metallic strip. The composite beam continues to expand but when the steel beam reaches temperatures of around 300 to 400°C it is unable to sustain an increasing axially compressive force due to local buckling at the end of the beam. However, deflections continue to increase due to the thermal differential between the steel beam and the concrete slab. At steel beam temperatures of 500°C, material degradation means that axial compressive forces in the steel beam gradually reduce and the beam begins to lose its stiffness. However, the

concrete slab temperatures start to rapidly increase at this moment in time continuing to drive vertical deflections down and beginning to dominate the structural behaviour.

Restraining Effects

Towards the end of the test where the slab dominates, it is conventionally believed that it demonstrates tensile membrane action which transfers load outside the heated compartment, thus providing structural stability. Examination of slab forces along the secondary beam, however, reveals significant areas of both compression and tension between the mid span and compartment edges (Figure 11). The compression is provided by restraint to thermal expansion from that part of the slab outside the heated compartment and by other structural elements such as the stiff cores. This is illustrated Figure 12, where strips of slab forces through the heated compartment reveal tension at the first quarter strip leading to compression at the third quarter strip where the stairwell core provides restraint. This means that the slab does not act as a simple tensile net but exhibits a complex stress field dependent upon the overall deflected shape of the slab, the temperature in the slab and the degree of restraint provided by the surrounding structure. Furthermore, in this case, the magnitude of the tensile forces and hence tensile strains is small. This means that the straining requirement placed on the steel mesh within the concrete slab is also low. In effect the compressive forces generated due to restrained thermal expansion of the slab offset any tensile forces due to the slabs deflected shape.
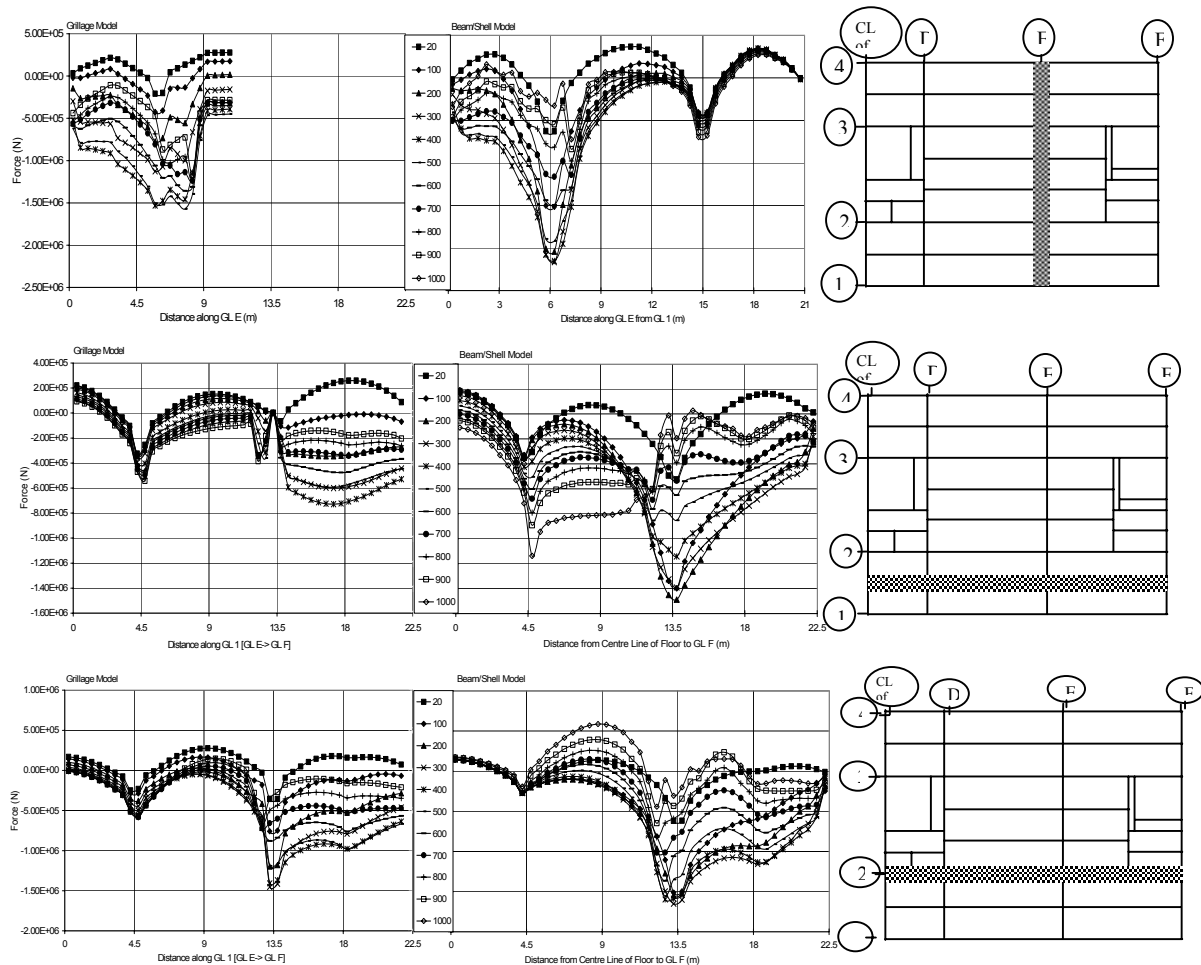
Figure 10: Comparison of Beam Axial Force between grillage and beam/shell models at temperatures between 20 and 1000°C

Model Comparisons

The grillage model underestimates deflections (Figure 7). However, the midspan deflection along GL1-2 is comparatively close to that of the beam shell model. This shortfall in deflection can be attributed to the grillage approach, which only contains allowance for flexure and would be enhanced if the contribution of in-plane shear were present. This grillage model is relatively coarse; consequently a finer grillage would most likely offer closer agreement with test results. The lateral restraint offered by the columns, although slightly over predictive for column F2, is reasonable in magnitude for such a coarse model. The secondary composite beam along GL 1-2 did not provide load transfer across the connection with the primary beam (Figures 10,11). This maybe attributed to the lack of transverse shear, otherwise found in the shell representation of the slab, permitting the composite beam to deflect upon thermal expansion.

The beam/shell model gives a better estimation of deflection at midspan in the test compartment (Figure 7). Close agreement is also achieved in the lateral displacement of column F2, but column E1 lateral displacement is over predicted probably caused by over expansion of the primary beam (Figure 8). Apart from the lack of load transfer across the connection at E2 found in the grillage model, the secondary beam forces responded similar to that of the grillage model, going into compression until 400 to 500°C where the capacity to carry load subsequently diminished (Figure 10). This model illustrates the increased accuracy that can be achieved by adapting a more rigorous approach to capturing the composite behaviour and restraint to thermal expansion from the surrounding unheated structure.

This point is further illustrated by the comparisons of deflections from the full shell model, which show a further improvement in vertical displacements (Figure 7) and also with column lateral displacements against test results (Figure 8). This can be attributed to capturing local buckling effects of beams (Figure 13). However, the global response is essentially the same as the beam/shell model meaning that it not important to capture local buckling effects for this case.
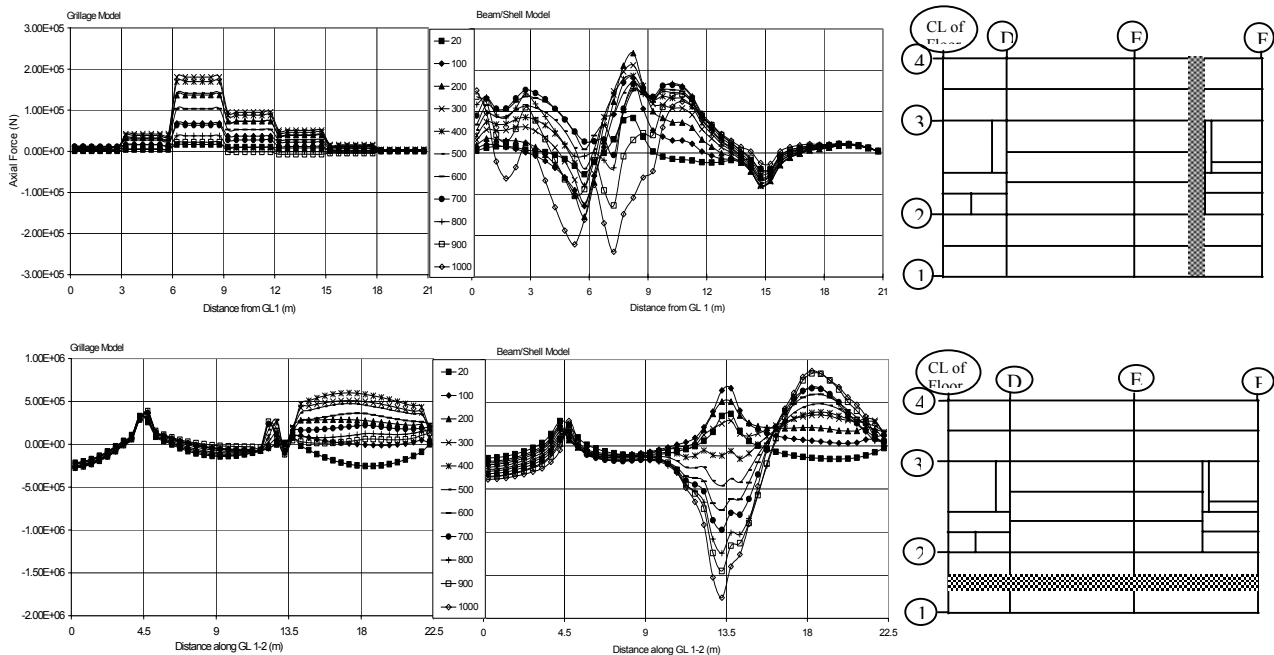
Figure 11: Comparison of Slab Axial Force between grillage and beam/shell models at primary and secondary midspan at temperatures between 20 and 1000°C
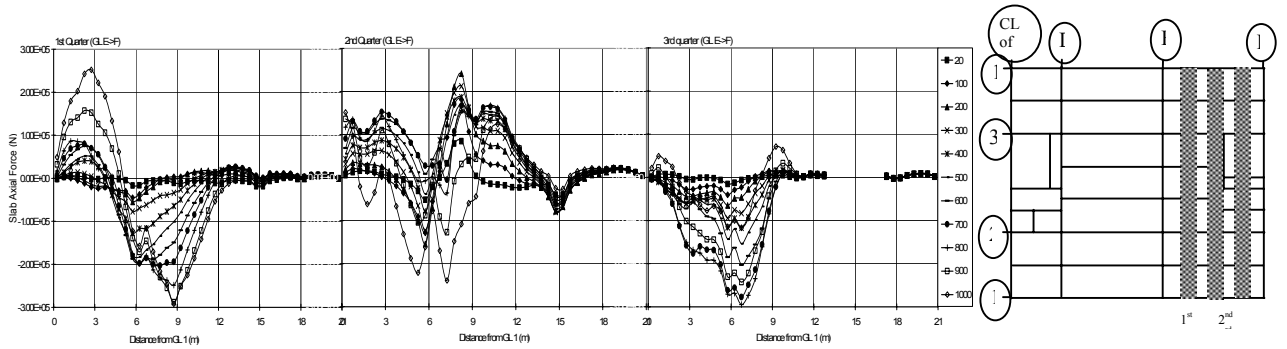
Figure 12: In-plane slab axial force for beam/shell model at temperatures between 20 and 1000ºC
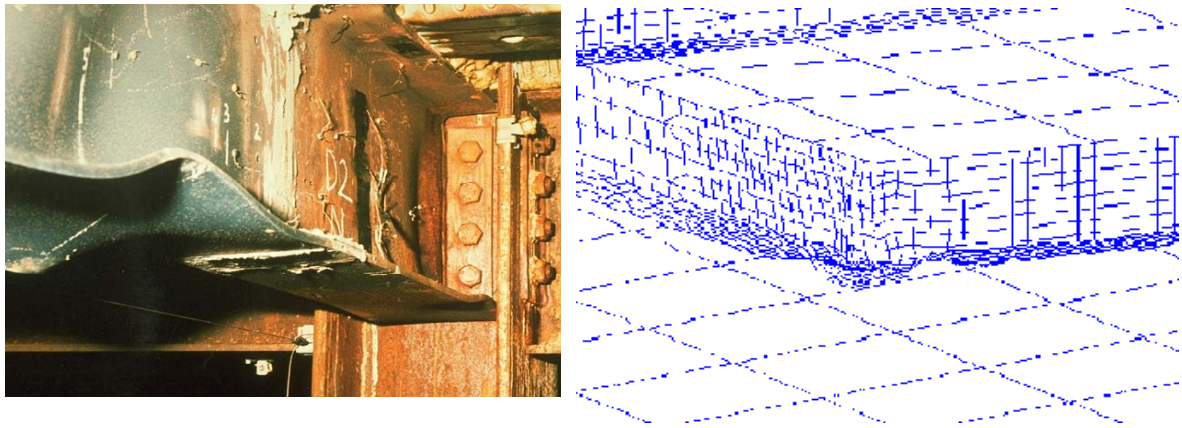
Figure 13: Local bucking captured using shell representation of steel beams

CONCLUSIONS

An understanding of the structural behaviour under fire attack has been developed through the development of rigorous models. Forces plotted in both beams and slabs show the high degree of redundancy offered by the composite floor. The main conclusions deduced are:

- A high level of confidence in the development of rigorous models has been generated due to the extensive calibration against test results.
- The composite behaviour is initially dominated by the underlying steel beam, which drives the slab down, until the steel temperature reaches approximately 500ºC where material degradation occurs. The slab temperatures at this stage start to rapidly increase and subsequently the slab dominates the overall response of the structure.
- At high temperatures the slab exhibits a complex stress field dependent upon its overall deflected shape, its temperature and degree of restraint provided by the surrounding structure. The tensile forces at midspan are low as they are offset by compressive forces generated due to restraint to thermal expansion, hence the strain requirements on the steel mesh are also low.
- The model comparison has demonstrated that the grillage approach achieves reasonable agreement with deflections, lateral restraint and exhibits similar magnitudes of forces to the beam/shell model and is thus a good numerical representation of the structure. However, this approach does lack the capability to transfer load by means of in-plane and transverse shear, particularly with a coarse grillage representation.

- The beam/shell and full shell models have demonstrated that, with a more rigorous approach, better accuracy can be achieved in capturing the composite behaviour.

Now that this understanding of the behaviour of composite structures in fire has been developed, the simplified models can be used to conduct parametric studies on various fire and structural scenarios to generate design guidance.

REFERENCES

1   *The Behaviour of Multi-Storey Steel Framed Buildings in Fire*, ISBN 0 900206 50 0, British Steel plc, Swinden Technology Centre, 1999.
2   Bailey, C.G., Lennon, T., Moore, D.B., The behaviour of full-scale steel framed buildings subjected to compartment fires, *The Structural Engineer*, Vol 77, No. 8, pp 15-20, 20 April 1999.
3   Steel Construction Industry Forum: *Structural Fire Engineering: Investigation of Broadgate Phase 8 Fire*, The Steel Construction Institute, 1991.
4   Churchill Plaza, *Basingstoke: Fire Damage Structural Report*, Amos Broom Associates, April 1991.
5   BS ENV 1993:*Eurocode 3; Design of Steel Structures*, Part 1.1: Basis of Design, British Standards Institution, 1994.
6   BS ENV 1994:*Eurocode 4; Design of Composite Steel and Concrete Structures*, Part 1.1: Basis of Design, British Standards Institution, 1994.
7   Hibbitt, Karlsson & Sorensen, Inc., *'ABAQUS Theory Manual'* v5.8, HKS Inc., 1080 Main Street Pawtucket, RI 02860-4847 USA.
8   Rotter, J.M, Sanad, A.M., Usmani, A.S., Gillie, M., Structural Performance of Redundant Structures under Local Fires, *Proceedings of Interflam '99*, pp1069-1080, Edinburgh, Scotland, June-July, 1999.
9   O'Connor, D.J., B. McAllister, J. Munro, H.R. Bennett, 'Determination of the fire endurance of model concrete slabs using a plastic analysis methodology', *The Structural Engineer*, Volume 73, No. 19, October 1995.
10 ENV 1993-1-2:1985: *'Eurocode 3 – Design of Steel Structures'*, Part 1-2: General Rules – Structural Fire Design.
11 Practical Design Tools for Composite Steel-Concrete Construction Elements Submitted to ISO-Fire Considering the Interaction Between Axial Load N and Bending Moment M, Commission of the European Communities Technical Steel Research, France 1991.

NON-LINEAR MODELLING OF THREE FULL-SCALE STRUCTURAL FIRE TESTS

by Huang, Z.[1], Burgess, I.W.[1] and Plank, R.J.[2]

[1] Department of Civil & Structural Engineering, University of Sheffield, S1 3JD, UK.
[2] School of Architectural Studies, University of Sheffield, S10 2TN, UK.

ABSTRACT

A computer program VULCAN has been progressively developed for some years at the University of Sheffield, with the objective of enabling three-dimensional modelling of the behaviour of composite buildings in fire. In this paper the current theoretical basis of the program is very briefly outlined.

Three of the fire tests carried out in 1995-96 on the composite frame at Cardington, representing cases in which different degrees of in-plane restraint are provided by the adjacent structure, are modelled to show how this restraint affects the structural behaviour within the heated zone. In order to illustrate the influence of membrane action and its relationship with boundary restraint, all cases have been analysed using both geometrically linear and non-linear slab elements. A series of parametric studies has been carried out as an initial investigation into the characteristics of steel reinforcement which allow this action to take place. It is evident that the influence of membrane action in slabs can be very important to the ultimate integrity of compartments, and should be accounted for in the modelling of this type of structure in fire conditions.

Keywords: Numerical Modelling, Composite Structures, Structural Behaviour in Fire.

1. INTRODUCTION

In 1995-96 six large fire tests were carried out on a full-scale composite multi-storey building at the BRE Fire Research Laboratory at Cardington UK. The tests appeared to confirm that composite beams with unprotected downstand steel sections have a significantly greater fire resistance when incorporated in the floors of real buildings than when they are tested as isolated members. Although steel temperatures became considerably greater than EC4 [1] critical temperatures for the loading levels used, no run-away failures were observed. This appears to be largely due to interaction between the heated members and slabs within the fire compartment and the adjacent cool structure. The resistance provided by this adjacent structure to both vertical and horizontal movement seems to play a large part in the behaviour. The cost of such full-scale fire testing, and of fire tests in general, is very high. It is therefore very important that the phenomena involved should be understood, and that analytical methods should be developed to model the behaviour of such structures when subjected to fire.

The numerical software VULCAN [2-4] has been developed in recent years at the University of Sheffield, for three-dimensional analysis of the structural behaviour of composite and steel-framed buildings in fire. In this paper the current theoretical basis of the program is very briefly outlined. Three of the Cardington fire tests, representing cases in which markedly different degrees of restraint are provided by the adjacent structure, are modelled to show how this restraint affects the behaviour within the heated zone. The effect of tensile membrane action in slabs has been suggested recently as being an important mechanism for supporting the loading and maintaining the integrity of the fire compartment at the high deflections which eventually occur as temperatures rise. In order to illustrate the influence of membrane actions and their relationship with boundary restraint, all cases have been analysed using both geometrically linear and non-linear slab elements. A series of parametric studies has been carried out as a pilot study within an investigation into the slab design parameters which allow this action to take place.

2. THEORETICAL BASIS OF THE PROGRAM

In this 3-D non-linear finite element procedure which is the theoretical basis of VULCAN the composite steel-framed building are modelled as an assembly of finite beam-column, spring, shear connector and slab elements. It is assumed that the nodes of theses different types of element are defined in a common reference plane, as shown in Fig. 1. The reference plane is assumed to coincide with the mid-surface of the concrete slab element. Its location is fixed throughout the analysis.
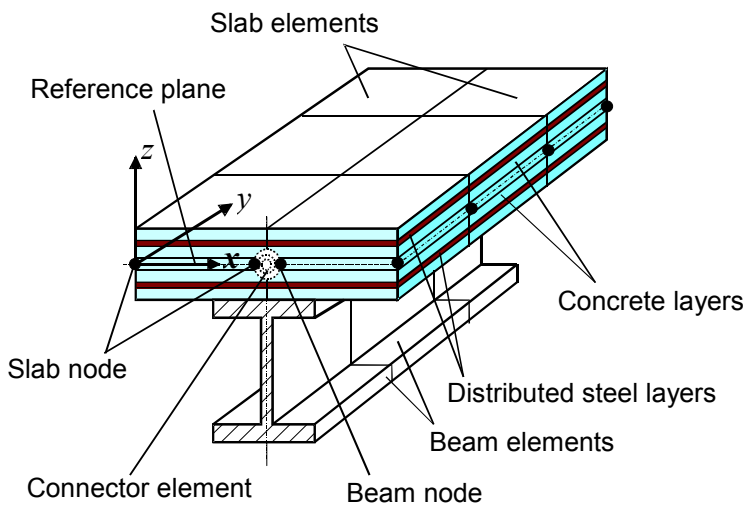
Fig. 1. Division of composite structure into beam, slab and shear connector elements.

The beam-columns are represented by 2-noded line elements. The cross-section of each element is divided into a number of segments to allow consideration of distributions of temperature, stress and strain through the cross-section. To model the characteristics of steelwork connections a 2-noded spring element of zero length, with the same nodal degrees of freedom as a beam-column element, is used. The details of the formulations of these elements and the constitutive modelling of steel at elevated temperatures have been presented previously [2, 3].

In order to model the composite slabs including their ribbed lower part a modified layered orthotropic slab element has been developed. This element is based on the previously developed layered procedure [5] in which the slab elements are modelled using a layered flat shell element based on Mindlin/Reissner theory and each layer can have a different

temperature and material properties. An effective stiffness model has been incorporated into the layered procedure to account for the orthotropic properties of composite slabs. The basic idea is to use a stiffness-reduction factor (or effective stiffness factor) to modify the material stiffness matrix for the properties parallel and orthogonal to the ribs. The calculation of effective stiffness factors is based on the theory of elastic beam bending and determined from the geometric dimensions of the cross-section of the composite slab. The stiffness matrix in local co-ordinates can be transformed into global co-ordinates using a standard transformation matrix.

A maximum-strain failure criterion has been adopted in this model. When the principal mechanical strains at any Gauss point exceed the maximum tensile or compressive strains then cracking or crushing will occur. A smeared crack model has been used, in which cracking at any Gauss point is identified layer by layer. After the initiation of cracking in a single direction, the concrete is treated as an orthotropic material with principal axes normal and parallel to the cracking direction. Upon further loading of singly cracked concrete, if the tensile strain in the direction normal to the first set of smeared cracks exceeds the maximum tensile strain then a second set of cracks forms. After crushing concrete is assumed to lose all stiffness. The uniaxial properties of concrete and reinforcing steel at elevated temperatures which are specified in EC4 have been adopted in this model. The details of this modified layered procedure can be found in [6].

In order to model the interaction of the steel beam and the concrete slab the shear connector element has been developed to link slab and beam elements. The details of connection of the three elements are shown in Fig. 1. The shear connector element in Fig. 1 is a specialised element, which has zero length and three translational and two rotational degrees of freedom at each node. Because the shear studs prevent the relative movement of slab and beam elements in the vertical direction it is assumed that there is no relative vertical movement between their nodes. It is also assumed that common nodes of slab and beam have the same rotations. The shear connector element permits the modelling of full, partial and zero interaction at the interface between the concrete slab and the steel beam. The details of the formulation are given in [7].

The authors have recently further extended the layered procedure mentioned above to include geometric non-linearity in the modelling of reinforced concrete slabs in fire [8]. A quadrilateral 9-noded higher-order isoparametric element is used in place of the previous 4-noded geometrically linear element, and a total Lagrangian approach is adopted. In this non-linear layered procedure all previous developments in the modelling of material non-linearity are retained, including the effective stiffness modelling of ribbed composite slabs. This development is intended to enable VULCAN to model the membrane action caused by *"P-Δ"* interaction of concrete floor slabs in fire.

3. MODELLING OF THE RESTRAINED BEAM TEST

A full-scale eight-storey composite test building was constructed by BRE at its Cardington Laboratory during 1994 to resemble a modern city-centre medium-rise office development typical of current UK practice. Composite action was achieved between both primary and secondary steel beams and the floor slabs using shear studs. The Restrained Beam Test was carried out by British Steel plc [9,10] on the frame in January 1995. It was the first, and the smallest, of six fire tests carried out in 1995 and 1996, and involved heating a single secondary beam and an area of the surrounding slab on the seventh floor. The major objective of this test was to study the effects of restraint from the large area of surrounding cool structure, including floor slabs, on the behaviour of the heated structure. The member

tested consisted of a 305x165UB40 section spanning between columns D2 and E2, and was heated using a specially constructed gas-fired furnace along the middle 8m of its 9m length. The location of the test is shown in Fig. 2. The extent of the structure incorporated within the model is also indicated in Fig. 2, with a more detailed representation including the finite element mesh layout shown in Fig. 3.
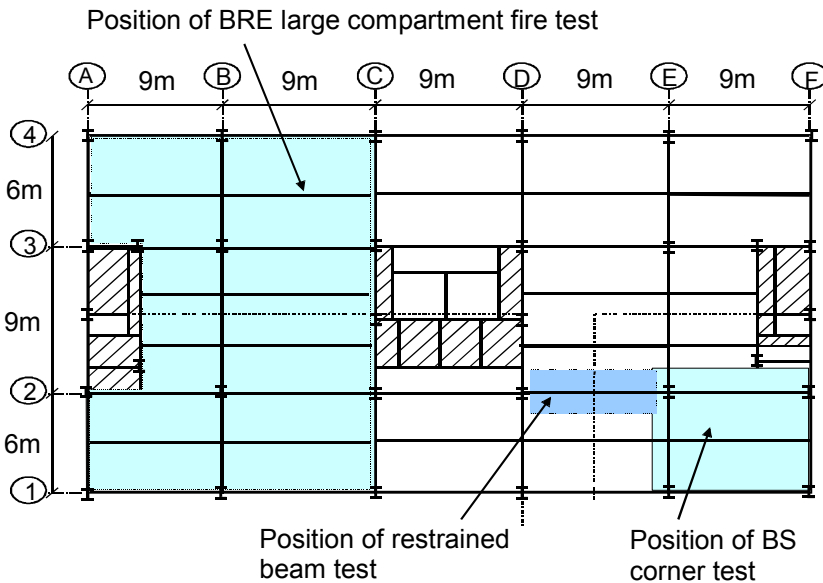
Fig. 2   Locations of the three fire tests in the Cardington test frame.
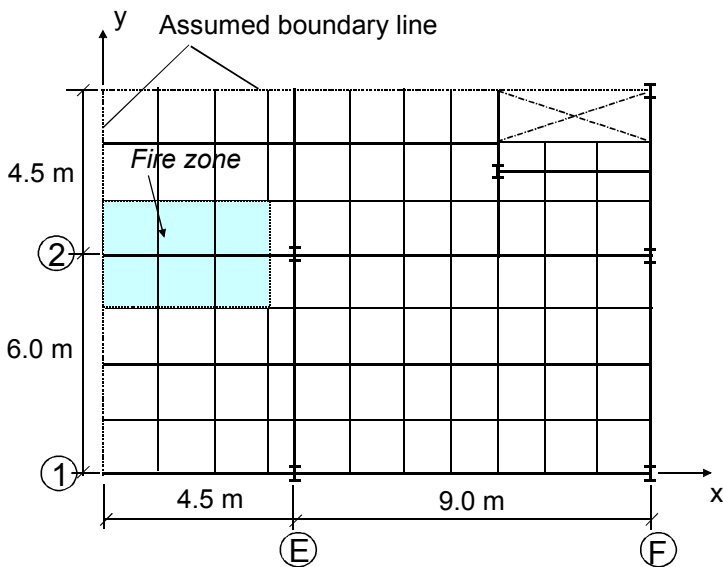
Fig. 3   Finite element layout adopted in the analysis of the Restrained Beam test.

In the Cardington test building the total nominal thickness of the composite slabs was 130mm, with a 75mm top continuous portion, giving effective stiffness factors of 0.72 and 0.34 parallel and perpendicular to the rib direction. The ambient-temperature material properties used in the modelling, based on tested values where these were available, were as follows:

- The yield strength of steel was 308MPa for Grade 43 steel (S275) and 390MPa for Grade 50 steel (S355);

- The yield strength of the steel used in the anti-crack mesh was assumed to be 460 MPa;

- The elastic modulus of steel was 2.1×10^5 MPa;

- The average compressive strength of concrete test samples was 35 MPa, and this is used.

A uniform floor load of 5.48kN/m^2 was applied to the whole building using sand-bags, and this is assumed in the modelling. The temperature distributions across the section of the steel beam and the depth of the slab are assumed to be invariant with position within the fire compartment. These temperature distributions at any time in the test are the averages of the recorded test temperature distributions at this time across the beam and slab. The maximum recorded temperatures of the bottom flange, web and top flange were 834°C, 816°C, and 764°C respectively, and the maximum recorded temperatures of the bottom and top layers of the slabs were 481°C and 129°C respectively. In order to investigate the structural behaviour of the restrained beam up to extremely high temperatures, these temperatures have been extrapolated linearly, so that the maximum temperatures of the bottom flange of the beam and bottom layer of the slab become 1005°C and 637°C respectively. The temperature of the bottom flange of the tested beam is used as the "key temperature" which is quoted in all figures.

The test is modelled using geometrically linear and non-linear slab elements, and the orthotropic nature of the slabs is included in the modelling. The test results showing the variation of mid-span deflection of the heated beam against the bottom flange key temperature are given in Fig. 4, together with the analytical results. Then results shown for the geometrically linear slab element are for the complete orthotropic cross-section; in previous modelling the best agreement had been obtained by using only the upper continuous portion. It is evident that the influence of membrane action is very significant in this situation of high restraint, especially when the key temperature is higher than 500°C. The predictions of the present model, in which geometric non-linearity of slab element is included, are in remarkably good agreement with the test results. Due to the high restraint from surrounding cool structure the second-order forces caused by geometric non-linearity in the beam and slab within the fire compartment become very significant and eventually dominate the structural behaviour.

Fig. 5 shows the distributions of the two principal membrane tractions in the slab at ambient temperature. It can be seen that the slabs above the composite secondary and primary beams act very much in line with the normal engineer's assumption for the flanges of composite beams, being in compression in the spanning direction. This reduces somewhat in the zones mid-way between parallel beams due to the well-known phenomenon of shear lag (see Fig. 6).

Mid-span deflection (mm)
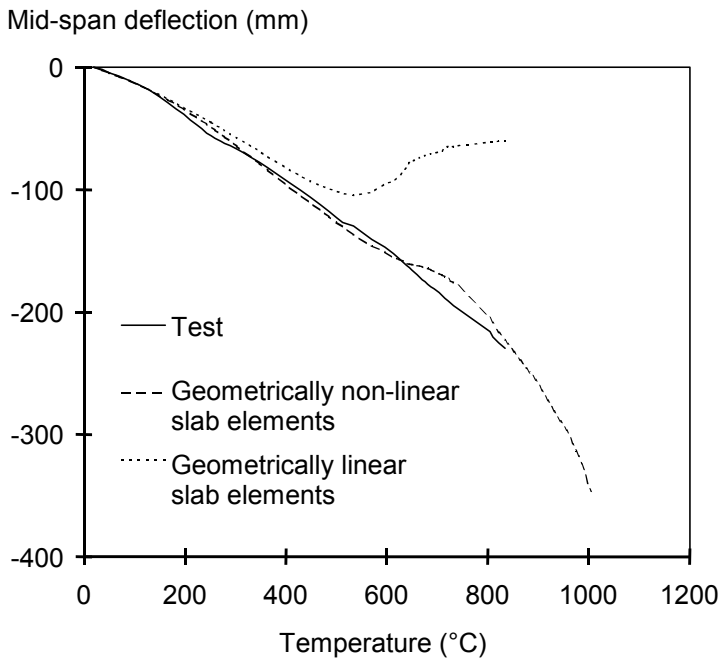
Fig. 4. Comparison of predicted and measured deflections for the Restrained Beam test using geometrically linear and non-linear slab elements.
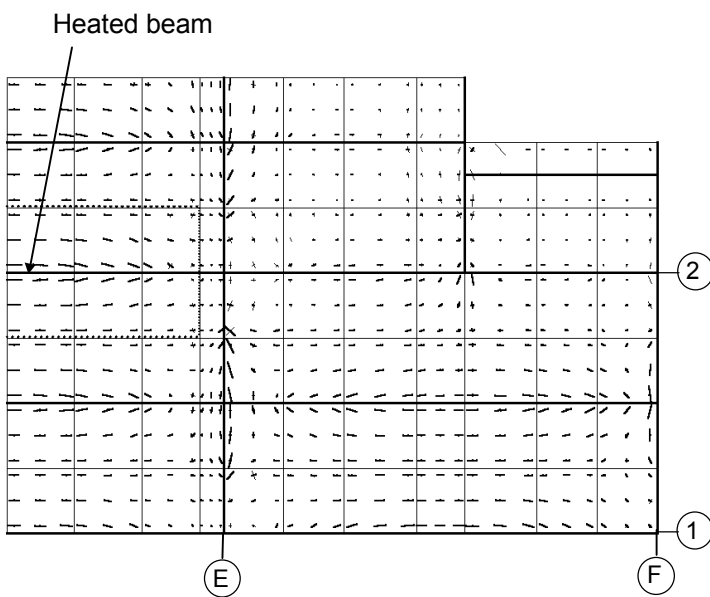
Fig. 5 Distribution of two principal membrane tractions at 20°C for the Restrained Beam test (thick line = compression; thin line = tension).

At the beam-ends, which are zones of hogging action, these slab membrane tractions are in tension. In contrast, the membrane tractions within the slabs at very high temperature are presented in Fig. 7.

Membrane force in x-direction (N/mm)
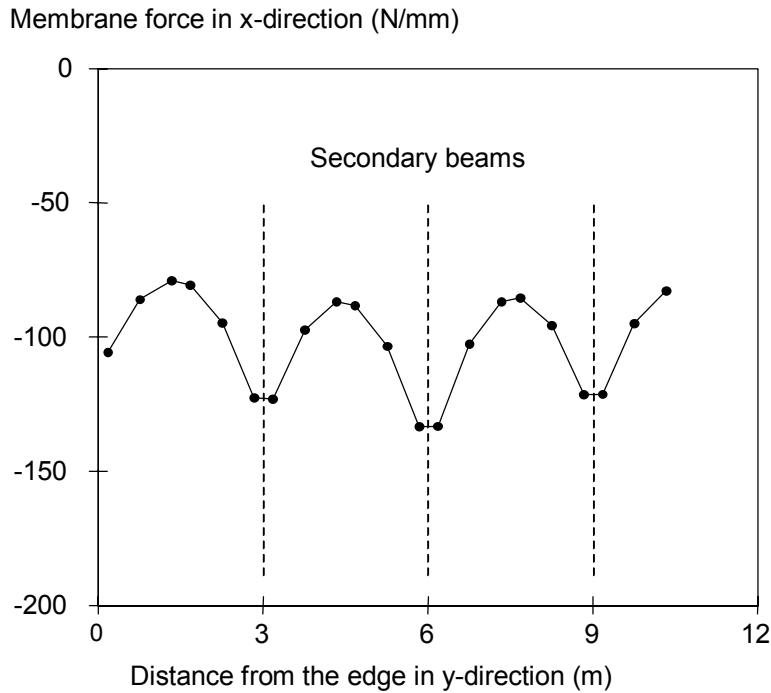
Fig. 6 Distribution of normal membrane tractions along the assumed boundary line in the y-direction at 20°C for the Restrained Beam Test.
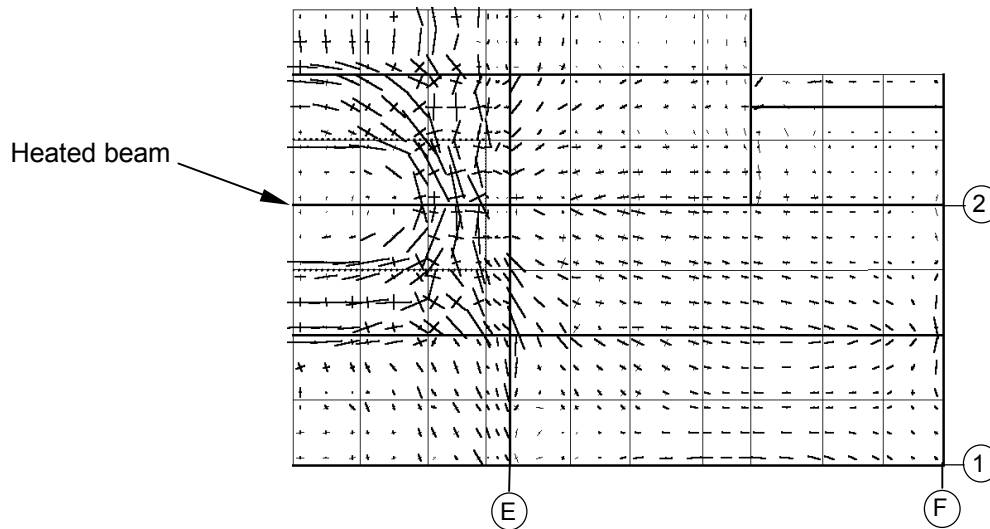
Fig. 7   Distribution of two principal membrane tractions at 1000°C for the Restrained Beam test (thick line = compression; thin line = tension).

It can be seen that very high compressive tractions are formed surrounding the edges of the fire compartment, and within the fire compartment the compressive tractions at the edges gradually change to tensile in the central areas. The central zone of the fire compartment is subject to tensile membrane forces which are carried mainly by the anti-crack mesh. If the tensile forces are large enough to cause the steel reinforcement to yield then the slabs within the fire compartment will fail, at least in terms of maintaining the integrity of the compartment.
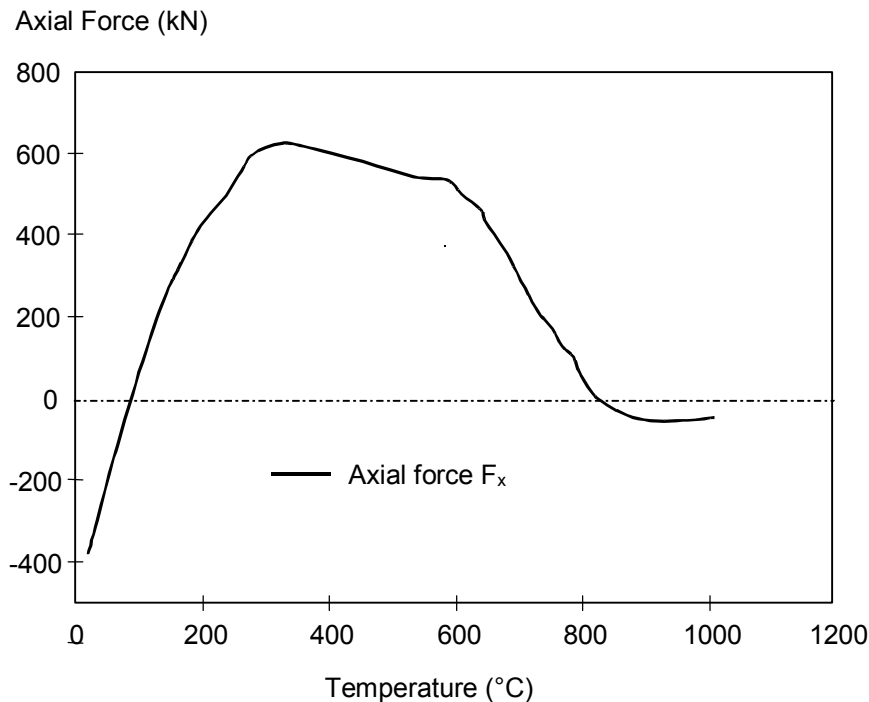
Axial Force (kN)

Fig. 8 Predicted axial force at mid-span of tested beam for Restrained Beam test.

Fig. 8 shows the change of the internal force F_x of the heated steel beam at its mid-span position as its temperatures increase. It can be seen that the beam is in tension at ambient temperature, when the steel beam is acting as the tension zone of a composite beam. As temperatures rise the steel beam heats more rapidly than the concrete slab and attempts to expand against both the cool surrounding structure and the slab itself. Due to the high restraint provided by these cooler elements the axial force in the heated beam changes rapidly from tension to compression in the initial heating stage, reaching a peak at about 350°C. On further heating, the steel's progressive loss of strength and stiffness gradually becomes more significant than the restrained expansion, and so the axial force in the beam gradually reduces. It eventually passes into low, and almost constant, tension as the deflection becomes very high due to the weakening of the slab. At this stage the beam is acting similarly to a catenary cable of finite strength, helping to support the slab.

4. MODELLING OF THE BRITISH STEEL CORNER FIRE TEST

In July 1995 a fire test (Test 3 of the British Steel series) was carried out [11,12] on a corner bay of the structure 9.98m wide by 7.57m deep. The walls of the fire compartment, shown schematically in Fig. 2, were constructed using lightweight concrete blockwork, the top of which was detached to allow free deflection of the structure above. All columns and perimeter beams were wrapped with ceramic fibre, but all other structural elements were left unprotected. The test was fired using timber cribs giving an overall fire load of 45kg/m^2 to produce a natural fire. During the fire test the maximum recorded atmosphere temperature in the compartment was 1028°C, which occurred after 80 minutes. Steel temperatures and structural deflections were recorded at key locations and at required intervals throughout the test, providing information for comparison with analytical results. A description of the test and comprehensive records of temperatures and deflections are given in Refs. [11, 12].

The test location, the extent of the structure incorporated within the numerical model and the finite element mesh layout are shown in Figs. 2 and 9. The material properties at ambient temperature and the uniform floor load were the same as in the Restrained Beam test. In

order to rationalise the test temperature profiles of the beams and columns the following assumptions were made (see Fig. 9 for the beam positions):

- Unprotected beams B1/2, B2, BE have the same temperature distributions, in which the maximum temperatures of the bottom flange, web and top flange are 900°C, 860°C, and 800°C respectively;

- Protected beams B1 and BF have the same temperature distributions, in which the temperatures of the bottom flange, web and top flange were 250°C, 180°C, and 110°C respectively;

- The cross-sections of all protected columns have uniform temperature distributions with a maximum temperature of 160°C.

The average test temperature distribution through the thickness of the concrete slab was used with the maximum temperatures of bottom and top layers at 360°C and 70°C respectively.
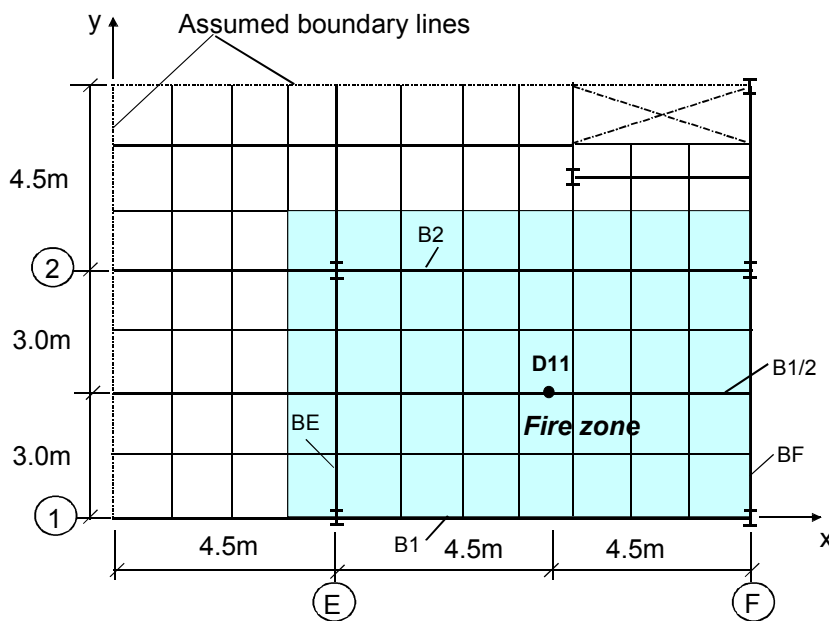
Fig. 9. Finite element layout for Corner Fire test, with locations of comparisons.

Again the test has been modelled using both geometrically linear and non-linear slab elements. Fig. 10 shows the test results with the predicted deflections for the mid-span (point D11) of the central secondary beam B1/2, against the bottom flange temperatures of the beam.
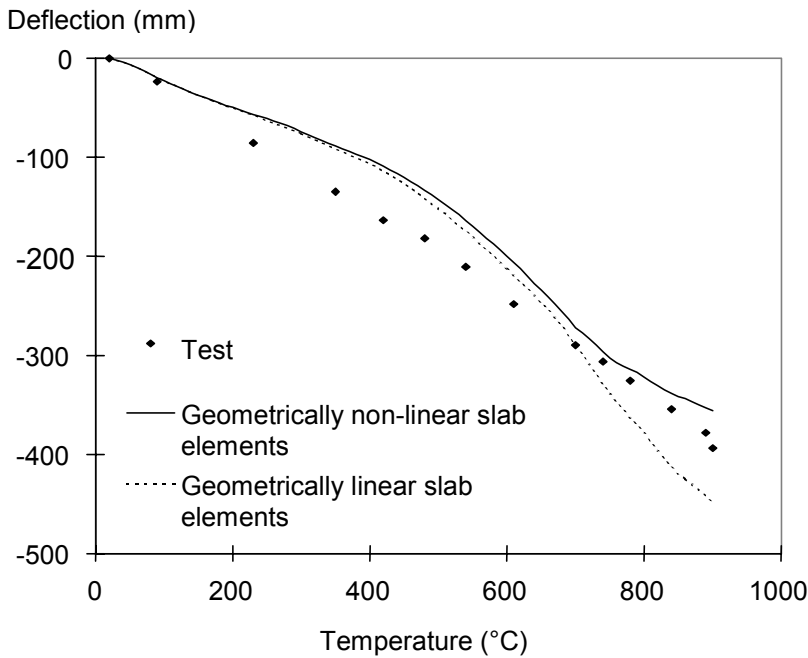
Fig. 10 Comparison of predicted and measured deflections for the BS Corner Fire Test using geometrically linear and non-linear slab elements.
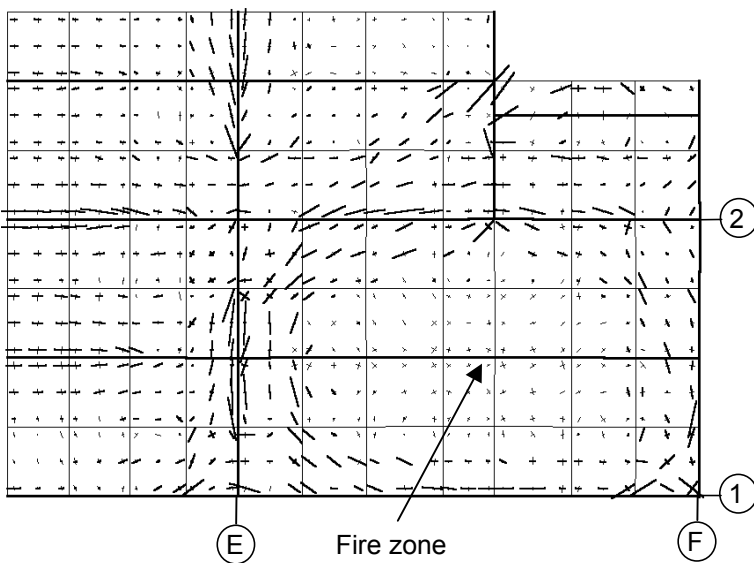

Fig. 11 Distribution of the principal membrane tractions at 900°C for the BS Corner Fire Test (thick line = compression; thin line = tension).

The distribution of the two principal membrane tractions at 900°C is shown in Fig. 11. It can be seen that when the vertical deflections were less than 300mm in which the temperatures of the steel beam were less than 700°C, there was little influence of tensile membrane action. After further increase of temperature the steel beams had lost most of their strength, and the loads above fire compartment were largely carried by the floor slab. In this corner test little restraint was provided by surrounding cool structure, and so the floor slabs within the corner bay need to be almost self equilibrating. This means that the tensile membrane forces within the central zone of the floor slab were balanced by the compression forces formed around the perimeter of the fire compartment. The load-carrying capacity of

the slabs was increased significantly due to this tensile membrane action in which the anti-cracking mesh is the key component. This phenomenon is confirmed visually in Fig. 11.

The area of steel reinforcing mesh used in the concrete slabs of the Cardington tests was 142mm^2/m. In order to demonstrate the effect of reinforcement on the structural behaviour two fictitious reinforcing meshes, with half and double the actual area, were employed for comparison, and the geometrically non-linear slab element was used. The predictions and test results for the vertical deflection at the mid-span (D11) of secondary beam B1/2 are shown in Fig. 12.
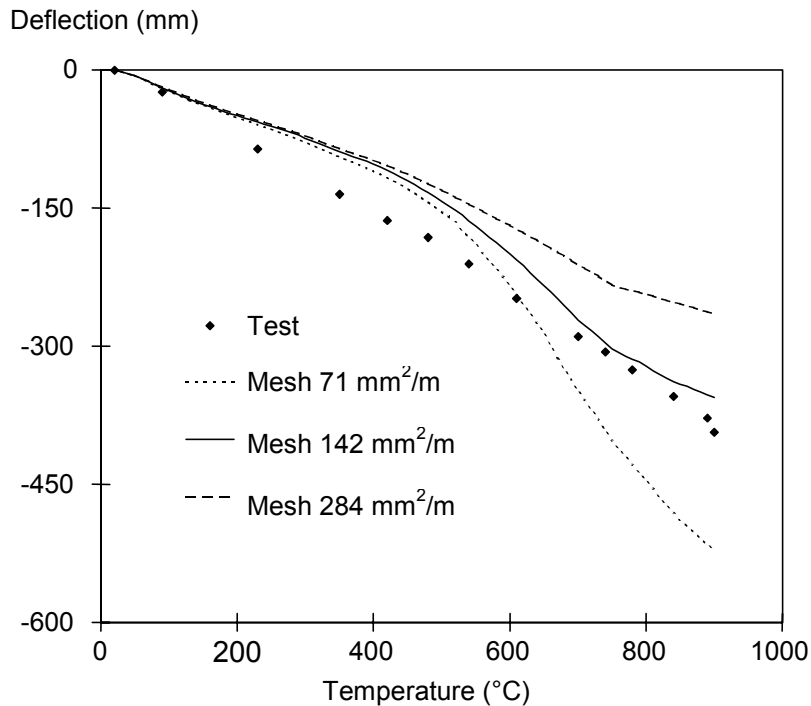
Deflection (mm)

Fig. 12 Comparison of predicted deflections at D11 with different areas of reinforcement against test results for the BS Corner Fire Test.

Fig. 13 shows the cracking patterns of the bottom and top floor slab layers at 500 °C. It can be seen that at this stage the concrete was subjected to intensive cracking, so that the tensile membrane forces within the floor slabs were mainly carried by the steel mesh. Hence the load capacity of concrete slabs depends strongly on the reinforcement area and strength. As the temperatures of the steel beams increase their strength and stiffness is decreasing so that the influence of steel reinforcement becomes more and more significant. In an extreme situation, when slabs are subjected very large deflections, the reinforcement will become a key element in maintaining the integrity of the structure, and if the reinforcement fails this may initiate a major structural failure. Ensuring that fracture of slabs does not occur may necessitate either higher reinforcement ratios, higher ductility or placement of the mesh further from the heated surface of the concrete.

TOP LAYER
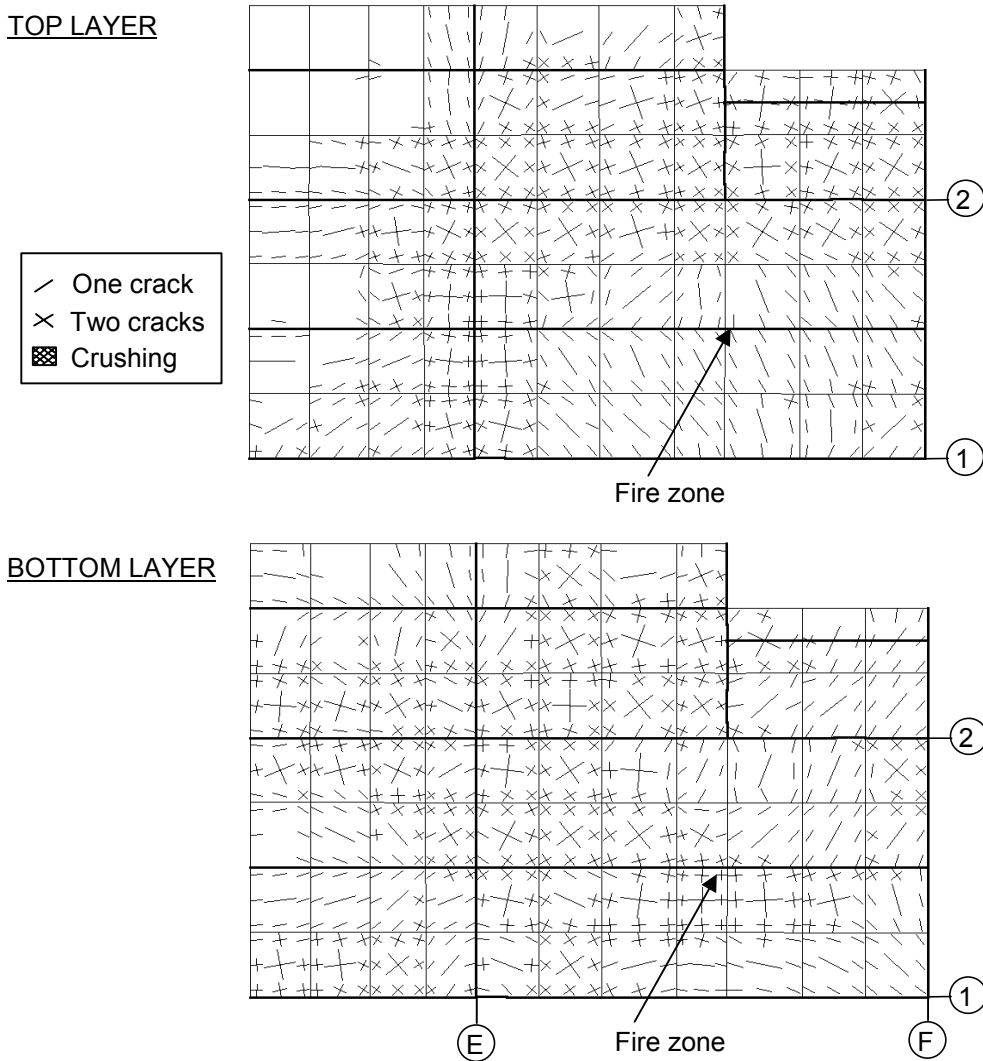
BOTTOM LAYER

Fig. 13 Predicted crack patterns of the top and bottom layers of the floor slab at 500°C in the BS Corner Fire Test.

5. MODELLING OF BRE LARGE COMPARTMENT FIRE TEST

In April 1996 BRE carried out their second fire test [13] on the Cardington Test Frame, in a large compartment between the second and third floors. This extended across the full width of the building, between grid-line A and a line 0.5m from grid-line C (see Fig. 2). This is considered to be the largest fully instrumented fire test which has taken place to date, covering an area of 340m^2. A fire load of 40kg/m^2 of wood was provided by timber cribs. All the internal steel beams were unprotected, but the columns were protected over their full height, including their connections. The maximum recorded atmospheric and steelwork temperatures were 763°C and 691°C, respectively. The average maximum temperature of the slab soffit was about 260°C. The extent of the structure incorporated within the numerical model is shown in Fig. 2, and more detail, together with the finite element mesh layout adopted, is shown in Fig. 14.
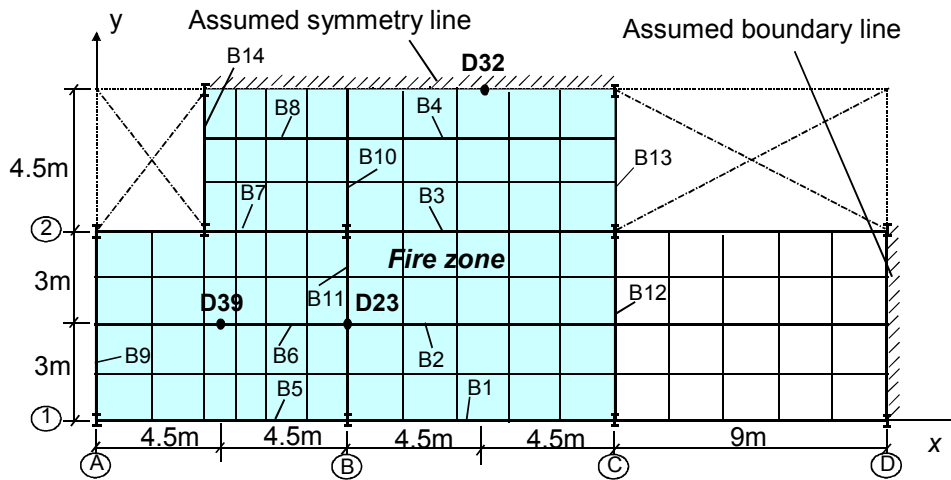
Fig. 14 Finite element layout adopted in the analysis of the BRE Large Compartment Fire Test, together with the locations of comparisons.

In the analysis the rotational and horizontal movements perpendicular to the assumed symmetry and boundary lines were fixed. The ambient-temperature material properties assumed were the same as for the corner test, and a uniform floor load of 5.48kN/m^2 was again assumed. In order to investigate the structural behaviour of this large fire test up to extremely high temperatures the measured temperatures have been extrapolated linearly, so that the following assumptions have been made for the modelling:

- Beams B2, B3, B4, B6, B7, B8, B10, B11 had identical temperature distributions, with the maximum temperatures of the bottom flange, web and top flange being 1000°C, 957°C and 885°C respectively;

- Beams B1, B5, B9, B12, B13 and B14 had the same temperature distributions, with the maximum temperatures of the bottom flange, web and top flange being 640°C, 640°C and 567°C respectively;

- The cross-sections of all columns inside or surrounding the fire compartment had uniform temperature at any time, with a maximum temperature of 92°C;

- The average temperature distribution through the thickness of the concrete slab was used, with the maximum temperatures of bottom and top layers being taken as 366°C and 106°C respectively.

In order to demonstrate the influence of membrane action the test was modelled using both geometrically linear and non-linear slab elements. The comparisons between the predicted and test results for vertical deflections taken at the 3 key positions shown in Fig. 14 are plotted in Figs. 15-17.
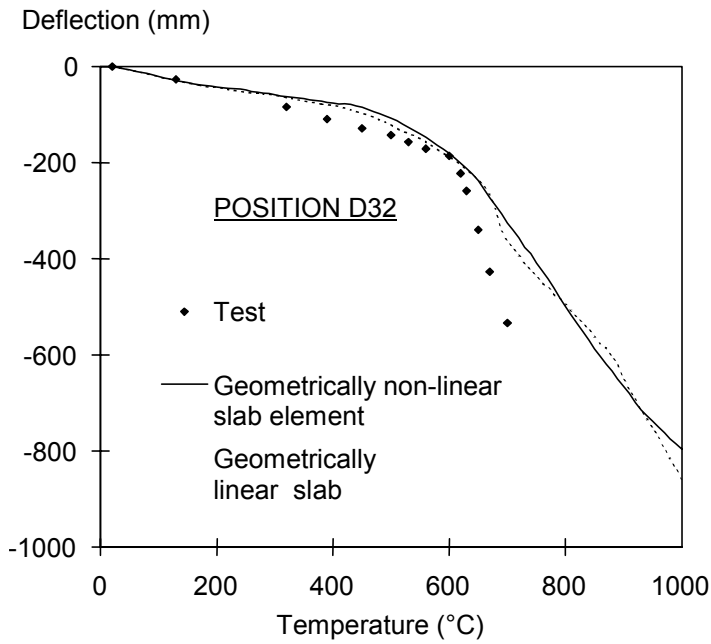
Deflection (mm)

Fig. 15 Comparison of predicted and measured deflections at position D32 for BRE Large Compartment Fire Test using geometrically linear and non-linear slab elements.
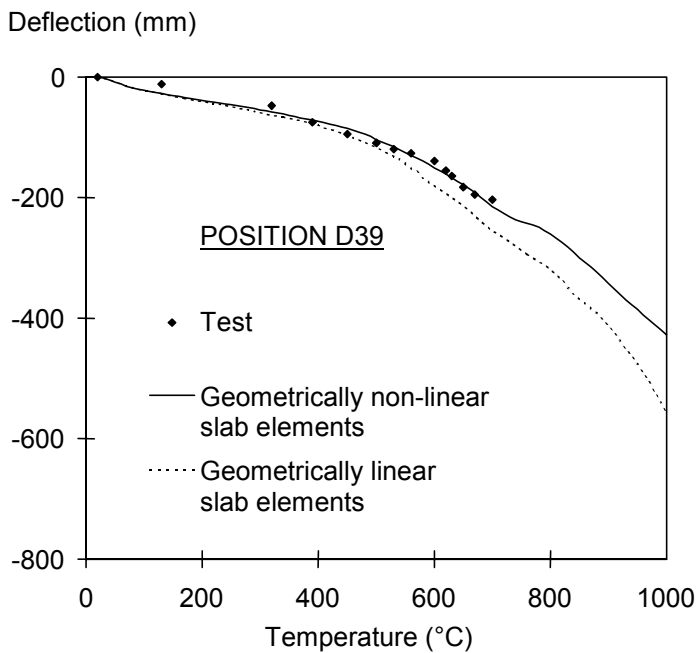
Deflection (mm)

Fig. 16 Comparison of predicted and measured deflections at position D39 for BRE Large Compartment Fire Test using geometrically linear and non-linear slab elements.
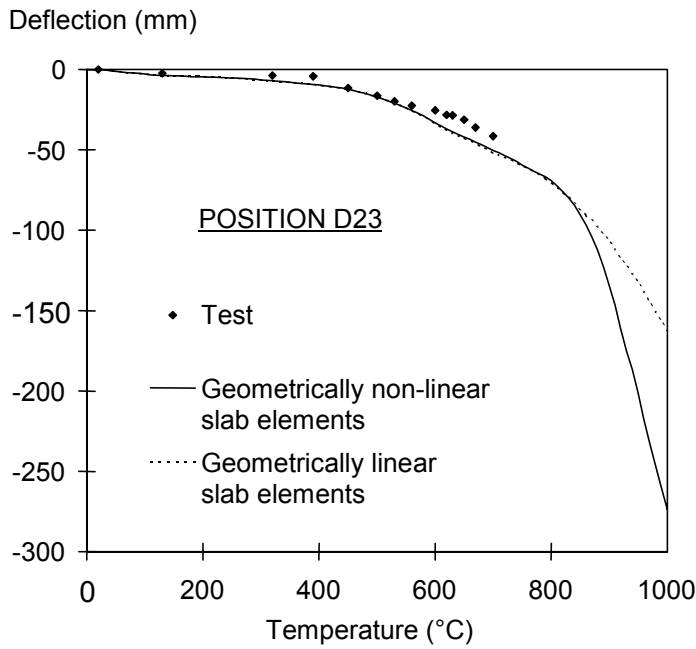
Deflection (mm)

Fig. 17 Comparison of predicted and measured deflections at position D23 for BRE Large Compartment Fire Test using geometrically linear and non-linear slab elements.

Fig. 18 shows the predicted distribution of membrane tractions at a steel key temperature of 1000°C, and the deflection profile of the composite slab is shown in Fig. 19 at the same temperature, including the cracking patterns of the top concrete layer.
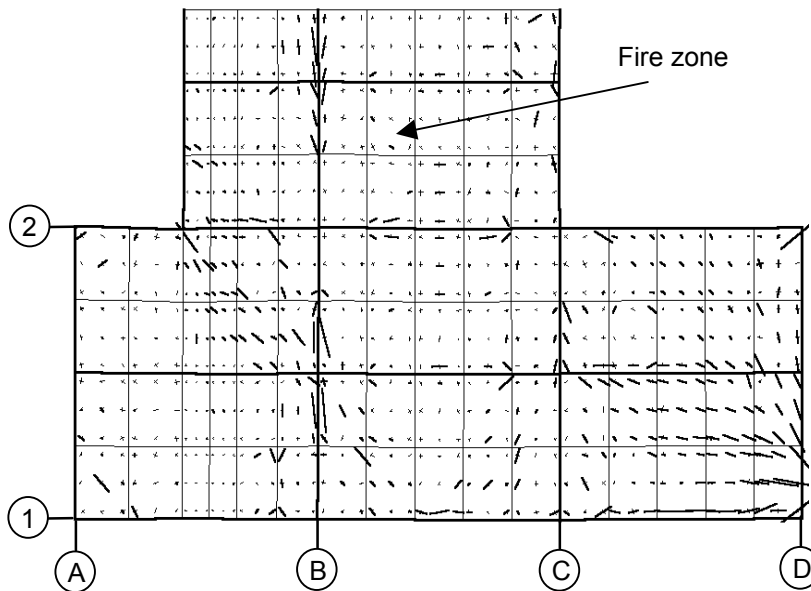
Fig. 18 Distribution of two principal membrane tractions at 1000°C for BRE Large Compartment Fire Test (thick line = compression; thin line = tension).

It can be seen from Figs. 15-17 that the predictions are in good agreement with test results at positions D39 and D23. There are some discrepancies concerning position D32, for which the predictions are in good agreement with test results up to 600°C, beyond which the program produces less deflection than the actual test data. In this test, because of the large amount of instrumentation the sand-bags used to add imposed load had to be moved in some locations, so that a fully uniform floor load could not really be guaranteed. With such a deep fire compartment, ventilated at both sides, it is also impossible to be certain that the heating was uniform at any time or across the whole area. In spite of these uncertainties the program produces very reasonable predictions compared with the test results for such a large-scale fire test.

From Fig. 15 it can be seen that the influence of geometric non-linearity of the slab elements is small. The reason for this is that the floor slab essentially deforms in single curvature in the region of position D32 (see Fig. 19). The restraint provided by some structural bracing in the stair-well and the atrium at the ends of the compartment was ignored in the modelling. Hence relatively small tensile membrane forces are generated within the slabs above the fire compartment.
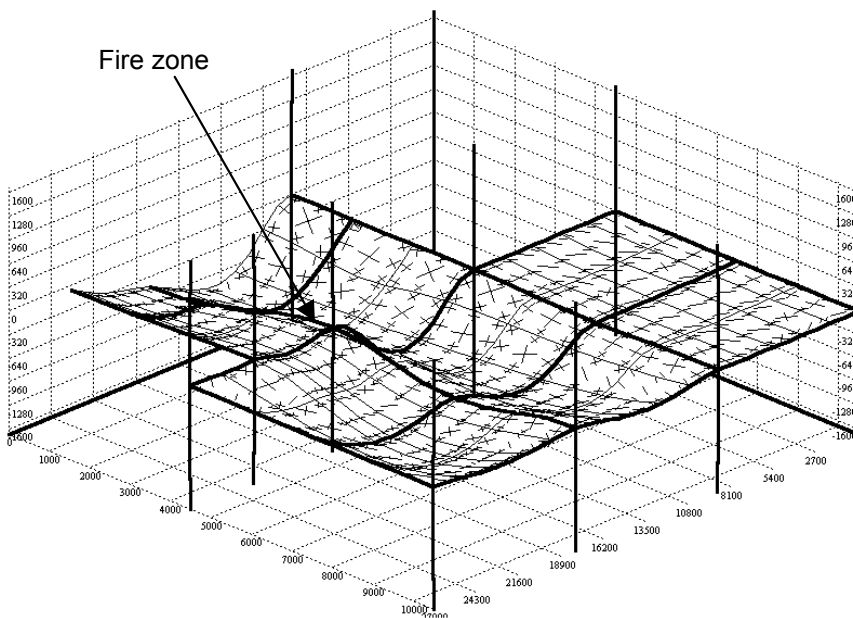
Fig. 19 Deflection profiles at 1000°C for BRE Large Compartment Fire Test, with cracking patterns of top layer of floor slab.

Comparing the results for this test with those presented in Figs. 16-17 some effect of geometric non-linearity is apparent, especially when the key temperatures are above 800°C and the deflections of primary beam B11 are increasing sharply. At this stage the floor slabs at positions D23 and D39 are forced to some extent to deform in double curvature, and thus the influence of membrane action becomes more significant.

6. CONCLUSIONS

The basic features of purpose-written computer program, VULCAN developed at the University of Sheffield, have been outlined in this paper. The program has been used to model the structural behaviour of three full-scale fire tests carried out by British Steel plc (now Corus Group plc) and BRE on the Cardington composite test frame. From this study some conclusions can be drawn as follows:

- VULCAN can predict the structural behaviour of a composite steel-framed building subjected to fire with quite reasonable accuracy. The program is a useful tool to perform intensive parametric studies aimed at a deeper understanding of the structural behaviour of such structures under fire attack.

- When the temperatures of steel beams are less than 300-400°C the influence of the concrete slabs on the structural behaviour of a composite building is small, but when temperatures are above 500°C the effect of the slab increases greatly. It then becomes very important to model concrete slabs correctly. The influence of membrane action cannot be ignored, particularly when the fire compartment is subject to high restraint because it is surrounded by cool, stiff structure.

- When the deflections of floor slabs become large the influence of tension membrane action in the slabs can become important in supporting the slab loading. Whether this is capable of preventing final fracture of the slabs depends mainly on the properties of the steel reinforcement used and the degree to which it is insulated from temperature rise by its concrete cover, even if this is cracked.

- It has been seen that tensile membrane action is not necessarily dependent on in-plane restraint, since the mid-slab tensions can be balanced by peripheral compressions, provided that the slab is forced to deform in double curvature because of vertical support to its edges. The benefit of tensile membrane action to the load-carrying capacity of the floor slabs is minimised when they deform in single curvature. If this is the case, then slabs may probably undergo much higher deflections before the tractions reach critical values at which fracture occurs. In these circumstances the relative movement of the column-ends may become unacceptable, or unsafe, before there is fracture of slabs

These three full-scale fire tests span a wide range in terms of the restraint to horizontal movement of slabs or beams. It is apparent that the slab reinforcement, which has been employed mainly for control of cracking during the curing process and may not be subject to any structural calculation in design, may be vitally important in ensuring integrity when a building is subject to high deflection in the fire limit state. Design of this reinforcement for tensile membrane action in fire may be the price to be paid for design processes based on the real performance of such systems rather than that of isolated elements.

REFERENCES

[1] European Committee for Standardisation, " Eurocode 4, Design of composite steel and concrete structures, Part 1.2: Structural fire design (Draft)", Commission of the European Communities, Brussels, (1992).

[2] Najjar, S.R. and Burgess, I.W., "A non-linear analysis for three-dimensional steel frames in fire conditions", *Engineering Structures*, **18** (1), (1996) pp77-89.

[3] Bailey, C.G., Burgess, I.W. and Plank R.J., "Computer simulation of a full-scale structural fire test", *The Structural Engineer*, **74**(6), (1996) pp93-100.

[4] Huang, Z., Burgess, I.W. and Plank, R.J., "Three-dimensional analysis of composite steel-framed buildings in fire", *J. Struct. Eng. ASCE*, **126**(3), (2000) pp389-397.

[5] Huang, Z., Burgess, I.W. and Plank, R.J., "Non-linear analysis of reinforced concrete slabs subjected to fire", *ACI Structural Journal*, **96**(1), (1999) pp127-135.

[6] Huang, Z., Burgess, I.W. and Plank, R.J., "Effective stiffness modelling of composite concrete slabs in fire", *Engineering Structures*, **22**(9), (2000) pp1133-1144.

[7] Huang, Z., Burgess, I.W. and Plank, R.J., "Influence of shear connectors on the behaviour of composite steel-framed buildings in fire", *J. Construct. Steel Research*, **51**(3), (1999) pp219-237.

[8] Huang, Z., Burgess, I.W. and Plank, R.J., "Non-linear layered procedure for modelling of concrete slabs in fire", Research Report DCSE/2000/F/1, Department of Civil and Structural Engineering, The University of Sheffield, (2000).

[9] Bentley, P.K., Shaw, D. and Tomlinson, I., "ECSC Project: Behaviour of a multi-storey steel framed building subjected to natural fires. Test 1: Restrained beam, Data files: Temperature measurements", Report S423/1/Part T1, Swinden Technology Centre, British Steel plc, Rotherham, UK, (1995).

[10] Bentley, P.K., Shaw, D. and Tomlinson, I., "ECSC Project: Behaviour of a multi-storey steel framed building subjected to natural fires. Test 1: Restrained beam, Data files: Deflection measurements", Report S423/1/Part D1, Swinden Technology Centre, British Steel plc, Rotherham, UK, (1995).

[11] Bann M. S., Bentley P.K., Shaw D. and Tomlinson I., "ECSC Project: Behaviour of a multi-storey steel framed building subjected to natural fires. Test 3: Corner compartment, Data files: Temperature measurements", Report S423/1/Part T1, Swinden Technology Centre, British Steel plc, South Yorkshire, (1995).

[12] Bentley, P.K., Shaw, D. & Tomlinson, L., "ECSC Project: Behaviour of a multi-storey steel framed building subjected to natural fires. Test 3: Corner compartment. Data files: Deflection/Displacement measurements", Report S423/3/Part D1, Swinden Technology Centre, British Steel plc, Rotherham, UK, (1996).

[13] Lennon T., "Cardington fire tests: instrumentation locations for large compartment fire test", Report N100/95, Building Research Establishment, Watford, (1996).

Lateral Torsional Buckling of Steel I-Beams in Case of Fire – Numerical Modelling

Paulo M. M. Vila Real * ; Jean-Marc Franssen *

* Departamento de Engenharia Civil, Universidade de Aveiro – Campus Santiago - 3810 Aveiro, Portugal
(email: pvreal@civil.ua.pt, tel: 351-34-370049)

** Institut de Mécanique et Génie Civil - Service "Ponts et Charpentes", Université de Liége – Chemin des Chevreuils, 1 - B 4000 Liège 1, Belgium
(email: JM.franssen@ulg.ac.be, tel: 32-4-3669251)

ABSTRACT

A geometrically and materially non-linear finite element program, i. e., a general model, has been used to determine the lateral-torsional resistance of steel I-beams under fire conditions, according to the hypotheses of Eurocode 3, Part 1-2. Two yield strengths, one cross section, one type of load and four durations of exposure to the ISO834 standard fire have been considered. The numerical results have been compared to the simple models presented in Eurocode 3, Part 1-2. These simple models lead to a safety level that depends on the slenderness of the beam, being unsafe for intermediate non-dimensional slenderness when compared with the general model. A new proposal has been made for a simple model that ensures a conservative result when compared to the general model.

1. INTRODUCTION

Although the problem of lateral buckling of steel beams at room temperature is well known [12], the same problem at elevated temperature is not. Among the work done in this field there is the paper from Bailey et al. [16] who uses a three-dimensional computer model to investigate the ultimate behaviour of uniformly heated unrestrained beams. In this paper, a simple model for fire resistance of lateral-torsional buckling of steel I-beams is presented. It is based on the numerical results of the SAFIR program, a geometrically and materially non-linear code specially established for the analysis of structures submitted to the fire [3]. The capability of this code to model the lateral buckling of beams has been demonstrated [11] at room temperature by comparisons with the formulas of Eurocode 3, Part 1-1 [1].

71

It has been used a three-dimensional (3D) beam element based on the following formulations and hypotheses:

-   Displacement type element in a total corrotational description;
-   Prismatic element;
-   The displacement of the node line is described by the displacements of the three nodes of the element, two nodes at each ends supporting seven degrre of freedom, three translations, three rotations and the warping amplitude plus one node at mid-length supporting one degree of freedom, the non-linear part of the longitudinal displacement;
-   The Bernoulli hypothesis is considered, i. e., plane sections remain plane and perpendicular to the longitudinal axis and no shear energy is considered;
-   No local buckling is taken into account, reason why the proposal in this paper is valid only for Class1 and Class 2 sections [1];
-   The strains are small (von Kármán hypothesis), i. e.

$$\frac{1}{2}\frac{\partial u}{\partial x} << 1$$

    where u is the longitudinal displacement and x is the longitudinal co-ordinate;
-   The angles between the deformed longitudinal axis and the undeformed but translated longitudinal axis are small, i. e.,

$$\sin\varphi \cong \varphi \text{ and } \cos\varphi \cong 1$$

    where φ is the angle between the arc and the cord of the beam finite element.
-   The longitudinal integrations are numerically calculated using Gauss' method;
-   The cross-section is discretised by means of triangular or quadrilateral fibers. At every longitudinal point of integration, all variables, such as temperature, strain, stress, etc., are uniform in each fiber;
-   The tangent stiffness matrix is evaluated at each iteration of the convergence process (pure Newton-Raphson method);
-   Residual stresses are considered by means of initial, and constant, strains [14];
-   The material behaviour in case of strain unloading is elastic, with the elastic modulus equal to the Young's modulus at the origin of the stress-strain curve. In one cross section, some fibers that have yielded may therefor exhibit a decreased tangent modulus because they are still on the loading branch, whereas, at the same time, some other fibers behave elastically. The plastic strain is presumed not to be affected by a change in temperature [15].

A simply supported steel beam described in [11] has been studied to compare the results between the EUROCODE 3, Part 1-2 [2] and the SAFIR code under fire conditions.

It has been assumed that the beam had a geometrical imperfection of sinusoidal type [4-6] and residual stresses [7] were considered.

The beam has been submitted to a uniform moment (see Figure 1) and has ends that cannot deflect laterally or twist (but are provided with no other restraining effects).
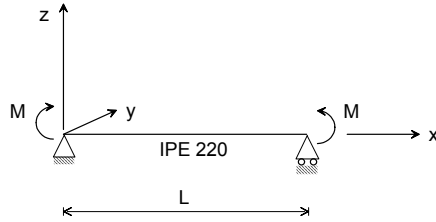
Fig. 1 – Simply supported beam submitted to moments at the ends.

The results of the Eurocode 3 and the SAFIR code were compared for the unprotected beam after 10, 15, 20 and 30 minutes of exposure to the ISO834 standard fire.

2. LATERAL-TORSIONAL BUCKLING UNDER FIRE CONDITIONS

2.1 Analysis according to the Eurocode 3

The temperature of the beam after the desired time has been obtained using the simplified equation of Eurocode 3 Part 1.2 [2]. From this temperature (which is uniform in the beam cross section), the buckling resistance moment $M_{b,fi,t,Rd}$ at time t, provided that the non-dimensional slenderness $\overline{\lambda}_{LT,\theta,com}$ for the maximum temperature in the compression flange $\theta_{a,com}$ reached at time t exceeds the value of 0.4, has been determined according to:

$$M_{b,fi,t,Rd} = \frac{\chi_{LT,fi}}{1.2} w_{pl,y} k_{y,\theta,com} f_y \frac{1}{\gamma_{M,fi}}$$ (1)

where:

$\chi_{LT,fi}$ is the reduction factor for lateral-torsional buckling in the fire deign situation;

$w_{pl,y}$ is the plastic section modulus;

$k_{y,\theta,com}$ is the reduction factor for the yield strength at the maximum temperature in the compression flange $\theta_{a,com}$, reached at time t (see Figure 2, a);

$\gamma_{M,fi}$ is the partial safety factor for the fire situation (usually $\gamma_{M,fi}=1$).

The constant 1.2 is an empirically determined value and is used as a correction factor that allows for a number of effects.

The reduction factor for lateral-torsional buckling in fire design situation, $\chi_{LT,fi}$, must be determined as for room temperature case, except using the non-dimensional slenderness $\overline{\lambda}_{LT,\theta,com}$ for temperature $\theta_{a,com}$ given by

$$\overline{\lambda}_{LT,\theta,com} = \overline{\lambda}_{LT} \sqrt{\frac{k_{y,\theta,com}}{k_{E,\theta,com}}}$$ (2)

where

$\overline{\lambda}_{LT}$ is the non-dimensional slenderness at room temperature;

$k_{E,\theta,com}$ is the reduction factor for the slope of the linear elastic range at the maximum steel temperature in the compression flange $\theta_{a,com}$ reached at time *t* (see Figure 2, a).

The factor $\sqrt{k_{y,\theta,com} / k_{E,\theta,com}}$, which is represented in Figure 2, b), leads to a particular behaviour of the non-dimensional slenderness $\overline{\lambda}_{LT,\theta,com}$. It could be expected that this slenderness should increase with the temperature but, according to the Eurocode 3 material model, this is not the case as it can be seen in Figure 3. In that figure is represented the variation of the non-dimensional slenderness, $\overline{\lambda}_{LT,\theta,com}$, with the temperature, for the Fe 360 and Fe 510 steel and for a IPE 220 beam with 2.0 meters span.
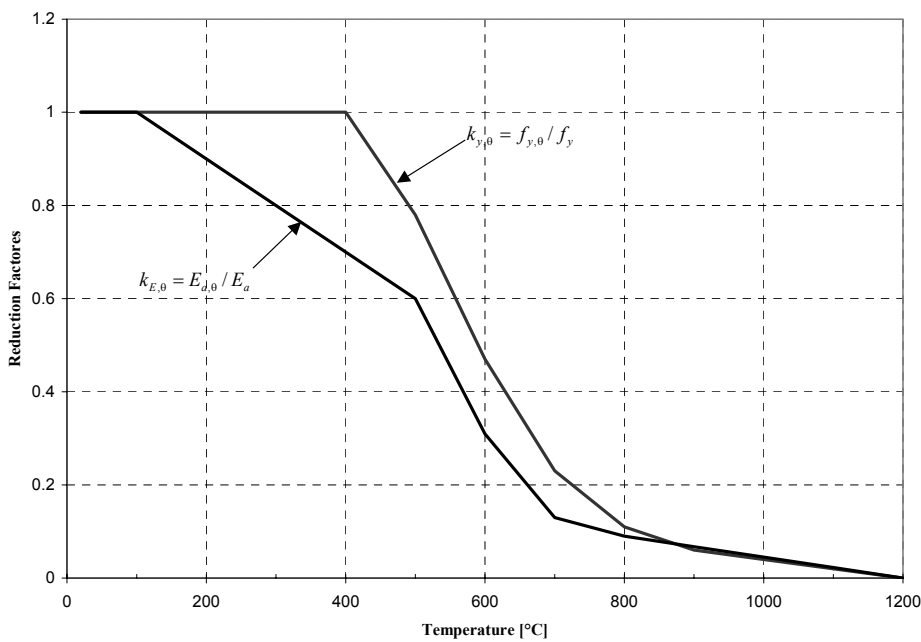
a)   Reduction factors $k_{y,\theta,com}$ **and** $k_{E,\theta,com}$

Fig. 2 – Dependency with temperature.

$$\sqrt{\frac{k_{y,\theta}}{k_{E,\theta}}}$$
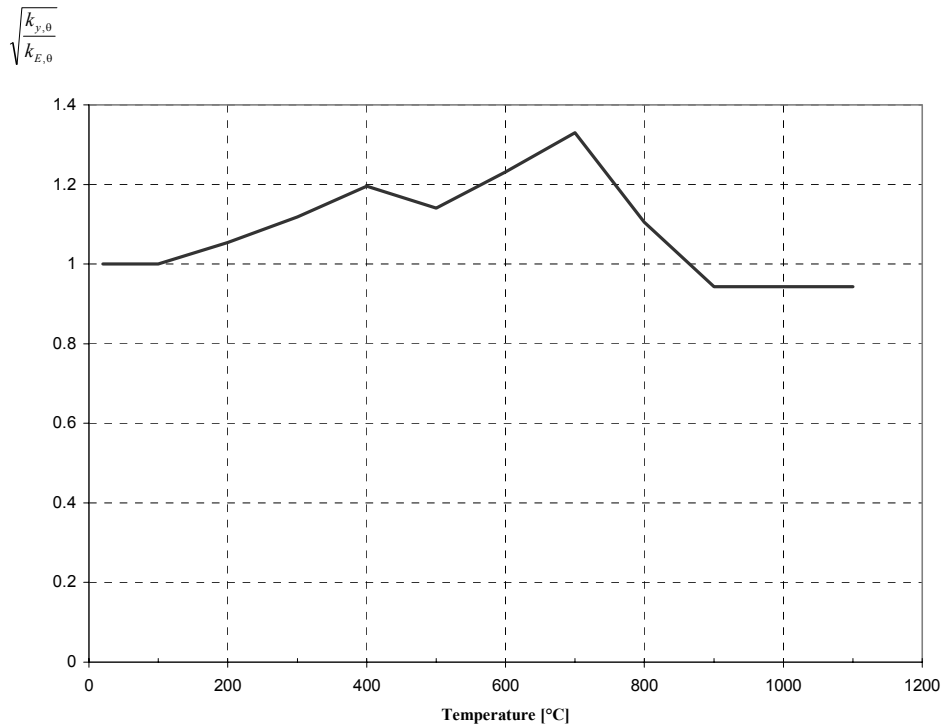
b) Factor $\sqrt{k_{y,\theta,com} / k_{E,\theta,com}}$

Fig. 2 – Dependency with temperature (cont.).
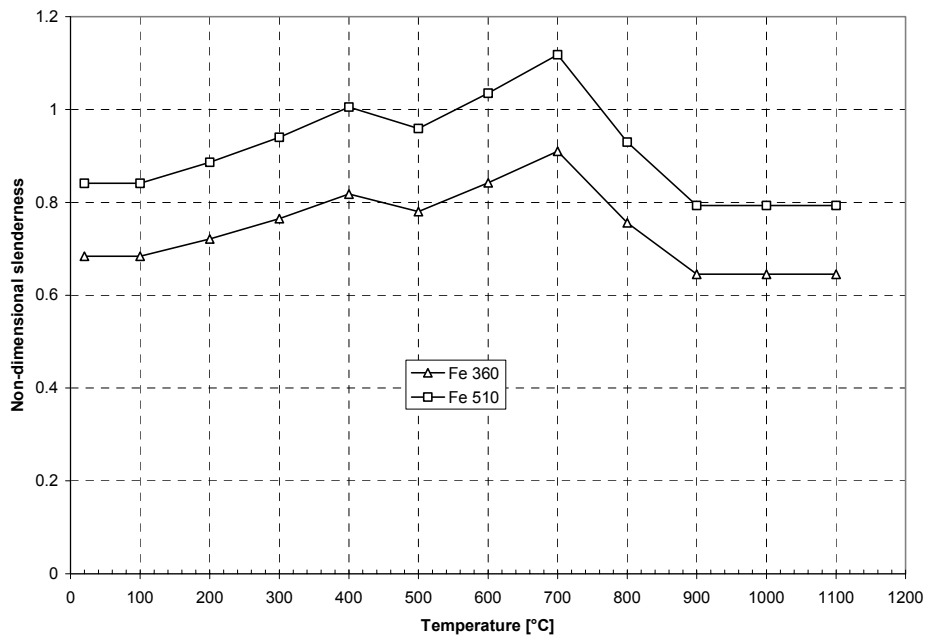
Fig. 3 – Dependency of the non-dimensional slenderness with temperature for a IPE 220 beam with 2 meters span.

    Figure 4 shows the variation with the temperature of the length of a IPE 220 simply supported beam that corresponds to a non-dimensional slenderness of 0.4. As it can be seen this length is shorter than the length at room temperature for temperatures between 100 °C

and approximately 850 °C for the two types of steel. This is also due to the Eurocode 3, Part 1-2, material model.

Dependency of the non-dimensional slenderness with temperature
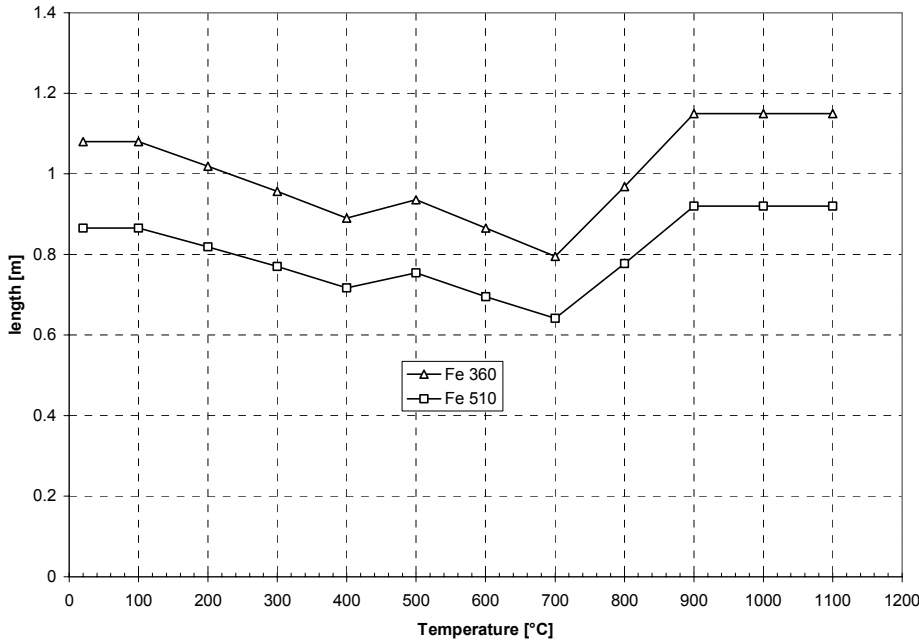
Fig. 4 – Dependency of the length of a IPE 220 simply supported beam corresponding to $\lambda_{LT,\theta,com} = 0.4$ **with the temperature.**

The full line of Figure 5 shows the beam design curve of Eurocode 3. For all the temperatures greater than 20 °C this curve is unique and named EC3,fi in that figure. On the vertical axis is the ratio

$$\frac{M_{b,fi,t,Rd}}{M_{fi,\theta,Rd}} \tag{3}$$

where, $M_{b,fi,t,Rd}$ is the design lateral buckling resistance moment at time t of a laterally unrestrained beam given by equation (1) and the design moment resistance $M_{fi,\theta,Rd}$ of a Class 1 or 2 cross-section with a uniform temperature θ_a may be determined from:

$$M_{fi,\theta,Rd} = k_{y,\theta} \frac{\gamma_{M0}}{\gamma_{M,fi}} M_{Rd} \tag{4}$$

where, $\gamma_{M0} = 1.0$, $\gamma_{M,fi} = 1.0$ and M_{Rd} is the plastic resistance of the gross cross-section $M_{pl,Rd}$ for normal temperature, which is given by

$$M_{Rd} = \frac{w_{pl,y} f_y}{\gamma_{M0}} \tag{5}$$

where $\gamma_{M0} = 1.0$.

76

Beam Design Curves of EC3 and SAFIR. Fe 360
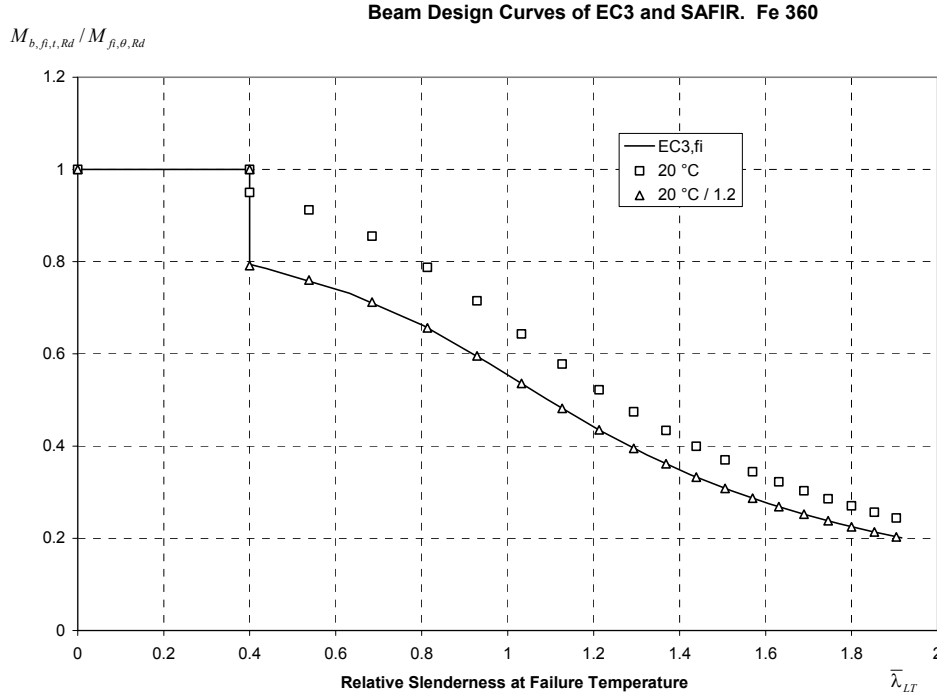
Fig. 5 – Beam design curve of Eurocode 3 for fire situation (EC3,fi) and at room temperature (20°C).

In that figure, it can also be seen that the buckling design curve at 20 °C is different from the curve at elevated temperature due to the empirical factor 1.2. This figure shows that the curve at elevated temperature, EC3,fi, is the curve at 20 °C divided by 1.2.

So it must be emphasised that in the beam design curves used throughout this paper the ratio $M_{b,fi,t,Rd} / M_{fi,\theta,Rd}$ plotted on the vertical axis represents the reduction factor for lateral-torsional buckling in the fire design situation $\chi_{LT,fi}$ divided by 1.2, i. e.:

$$\frac{M_{b,fi,t,Rd}}{M_{fi,\theta,Rd}} = \frac{\chi_{LT,fi}}{1.2} \text{, for the Eurocode 3, Part 1-2 results} \tag{6.a}$$

or

$$\frac{M_{SAFIR}}{M_{fi,\theta,Rd}} \text{, for the SAFIR results} \tag{6.b}$$

It must also be mentioned that the Class of cross-section of the IPE 220 was checked for all the analysed temperatures to see if it maintains as a Class1 cross-section like at room temperature [8] or not. This was done using the modified value of ε given by [2]:

$$\varepsilon = [(235 / f_y)(k_{E,\theta} / k_{y,\theta})]^{0.5} \tag{7}$$

It has been concluded that the Class of the cross-section doesn't change with the temperature.

2.2 Analysis with the SAFIR code

The time evolution of the temperature is obtained using finite element analysis. So the temperature field is not uniform like the one obtained with the simplified equation of Eurocode 3, see Figure 6
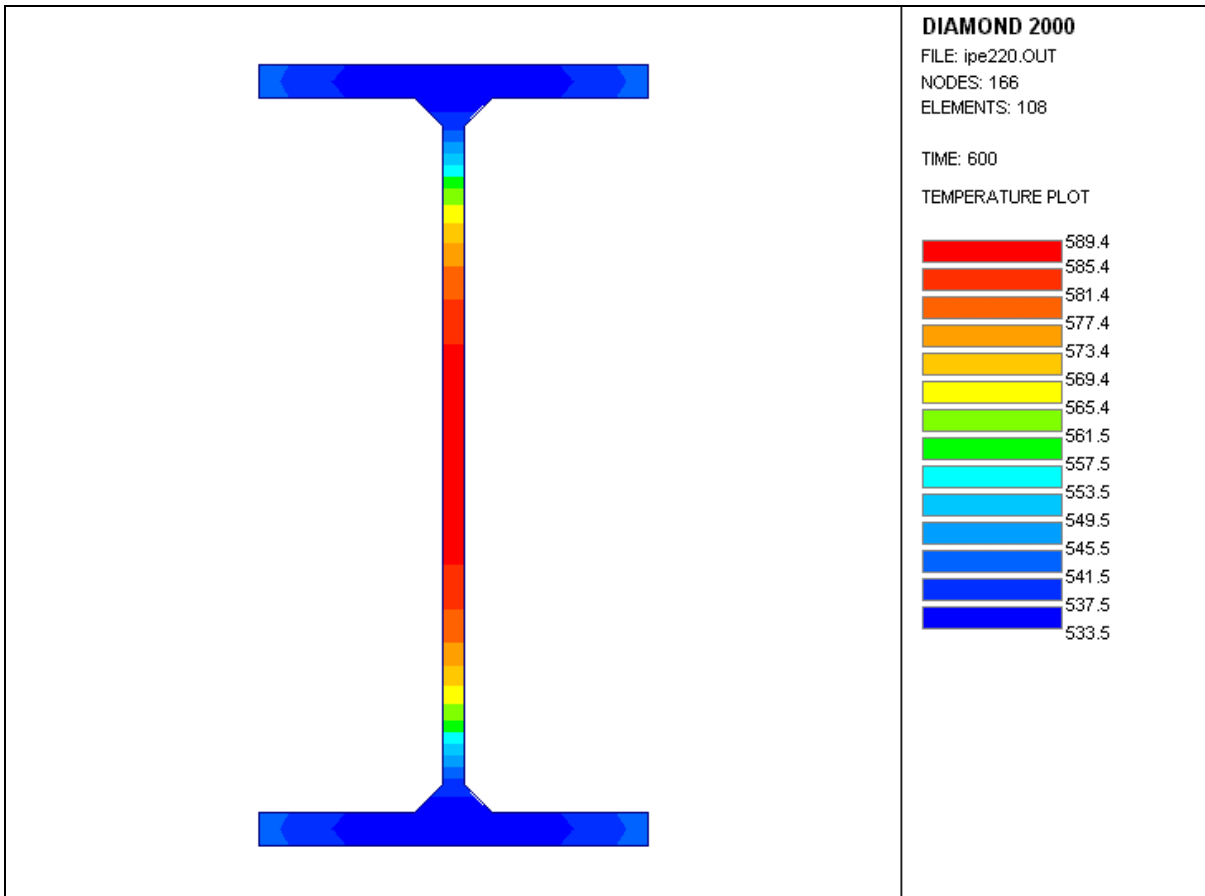
Fig. 6 – Temperature field after 10 minutes, obtained with SAFIR.

For the temperature reached at time *t* (10,15,20 and 30 minutes) the load was applied with step increments of 100 Nm (for the temperature at 10, 15 and 20 minutes) or 50 Nm (for the temperature at 30 minutes).

The numerical simulations were carried out considering the following assumptions:
- End conditions: ends that cannot deflect laterally or twist but are provided with no other restraining effects;
- Beam lateral imperfection: Sinusoidal, with a maximum value of L/1000;
- Longitudinal integration: two Gauss points;
- Residual stresses: constant across the thickness of the web and of the flanges. Triangular distribution with a maximum value of 0.3×235 Mpa [7], for the Fe 360 steel as well as for the Fe 510 steel.

Figures 7, 8 and 9 show for the IPE 220 beam with 2 meters span, the evolution of the vertical and lateral displacement and the rotation around the longitudinal axis of the central node of the beam, with the increasing load for the time instant of 10, 15, 20 and 30 minutes.

Evolution of DOF2
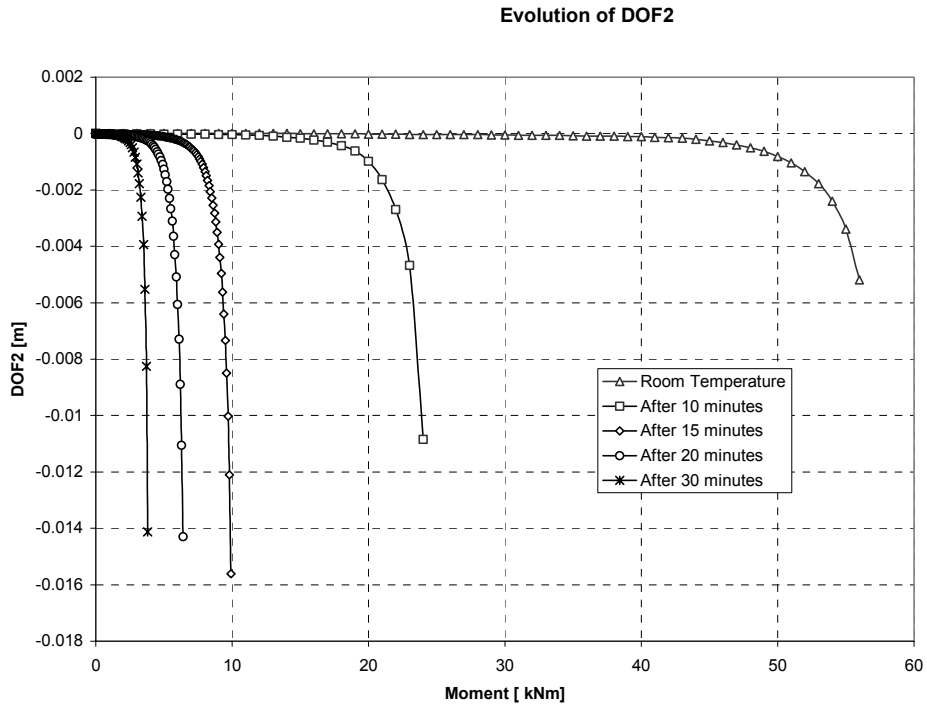
a) Fe 360 steel
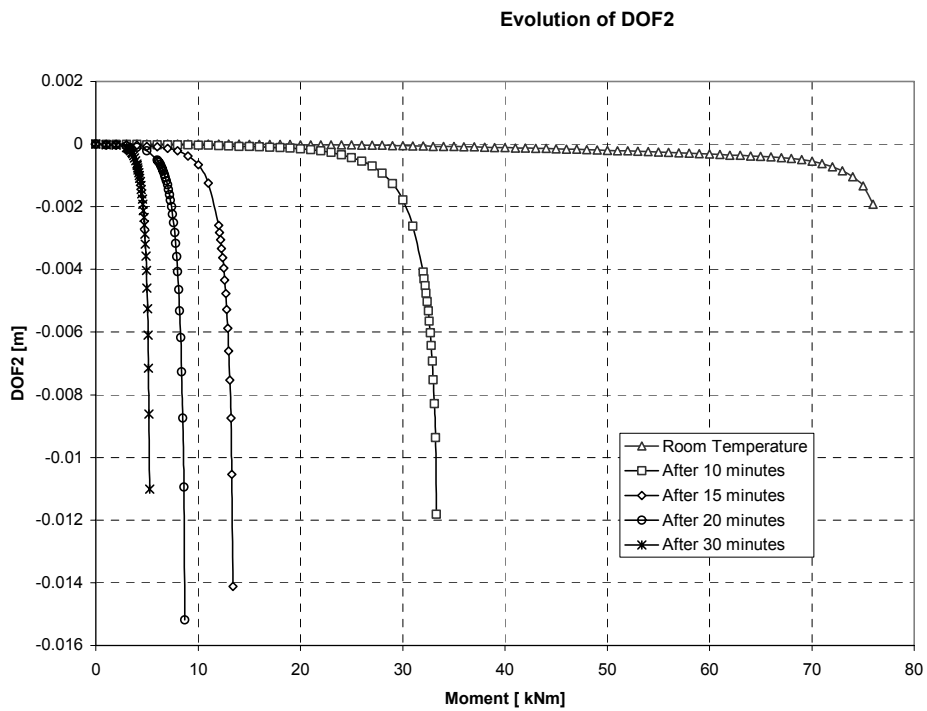
Evolution of DOF2

b) Fe 510

Fig. 7 – Evolution of the lateral displacement of the central node of a 2 meters span beam.

Evolution of DOF3

a) **Fe 360 steel**

Evolution of DOF3
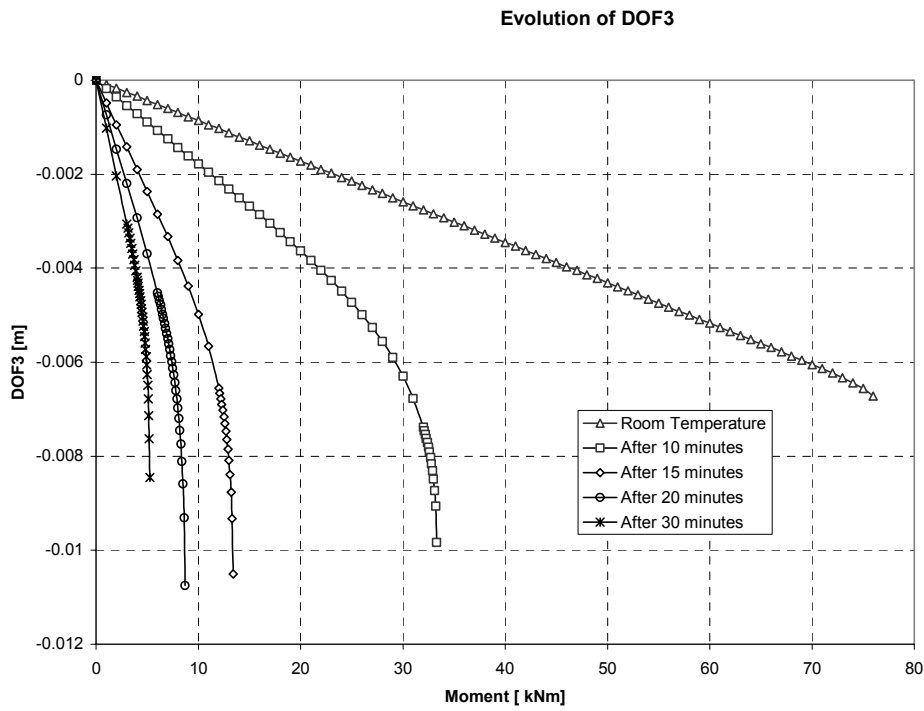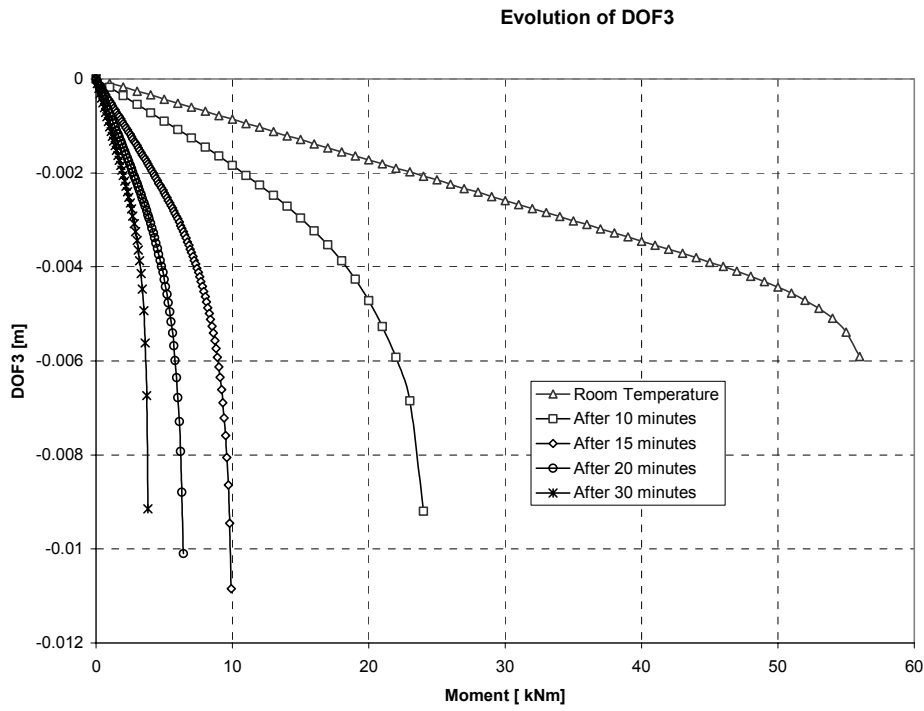
b) **Fe 510**

Fig. 8 – Evolution of the vertical displacement of the central node of a 2 meters span beam.

Evolution of DOF4
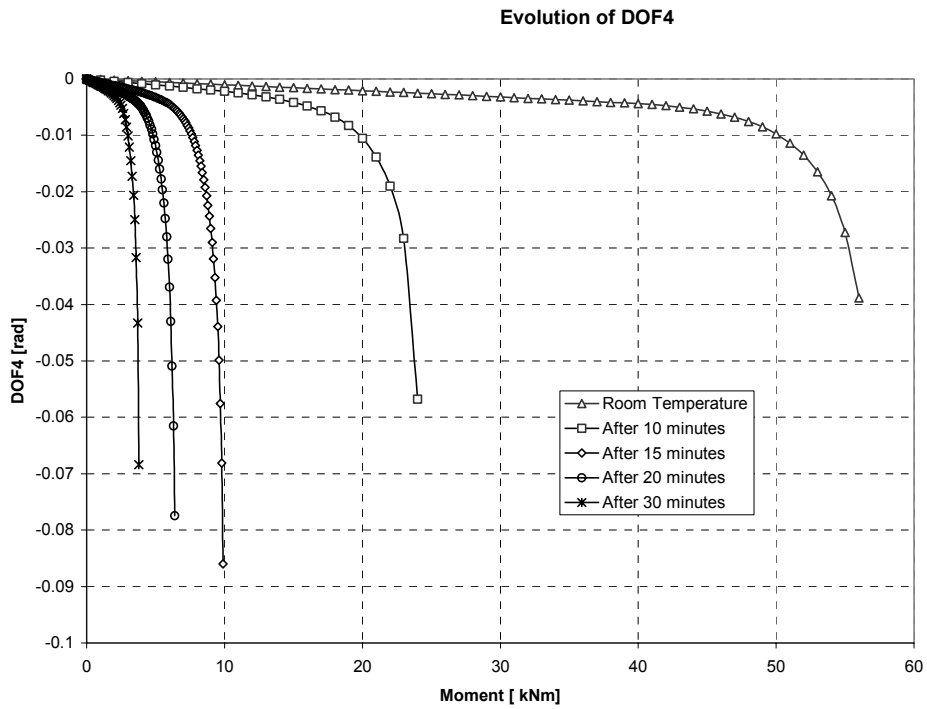
a) Fe 360 steel
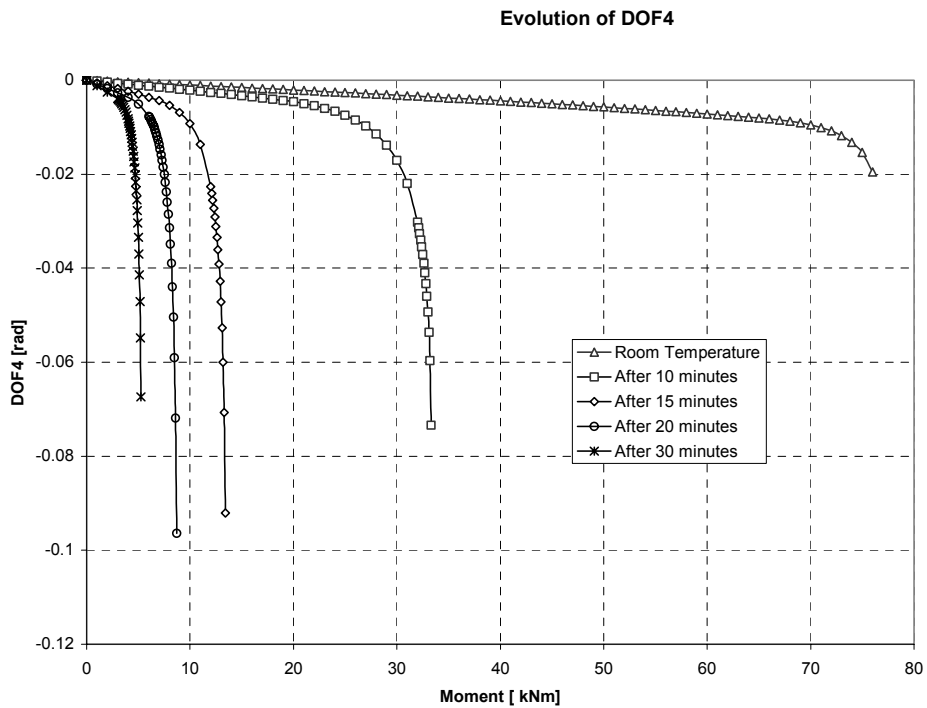
Evolution of DOF4

b) Fe 510

Fig. 9 – Evolution of the longitudinal rotation of the central node of a 2 meters span beam.

The beam design curves for all the time instants studied are shown in Figures 10 to 13 for the Fe 360 and Fe510 steel. In these figures, $M_{b,fi,t,Rd}$ is the design lateral buckling resistance moment at time t of a laterally unrestrained beam given by equation (1) or

calculated by the SAFIR code and the design moment resistance $M_{fi,\theta,Rd}$ of a Class 1 or 2 cross-section is given by equation (4) evaluated for the temperatures obtained with the simplified equation of the Eurocode 3, i. e., 554 °C, 680 °C, 733 °C and 827 °C for the time instants 10, 15, 20 and 30 minutes respectively. The relative slenderness was calculated at failure temperature according to equation (2).
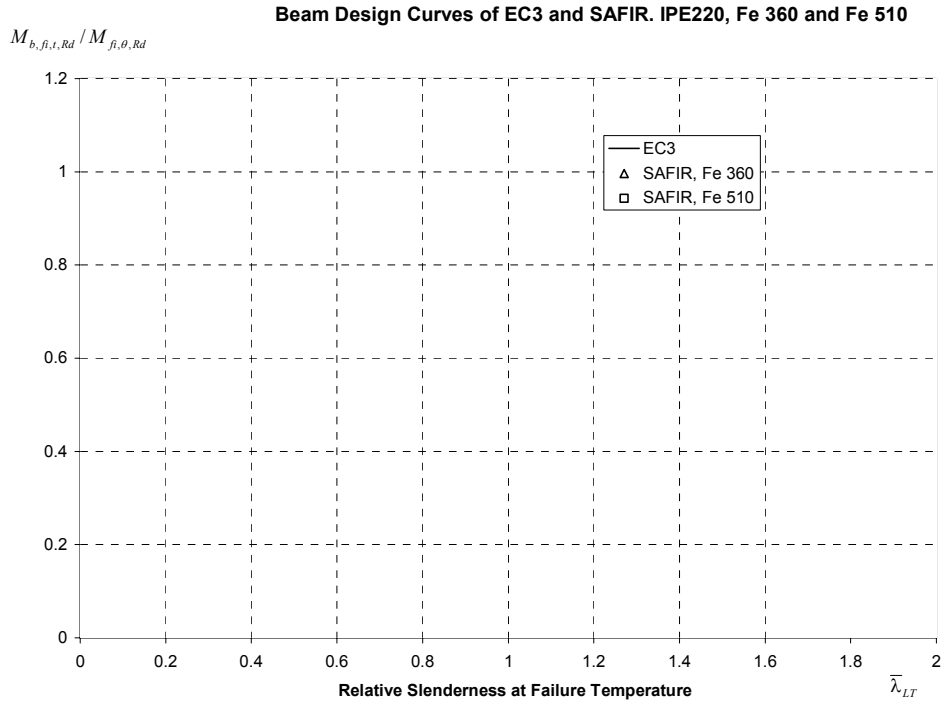
Fig. 10 – Beam design curve after 10 minutes. Comparison between the Eurocode 3 and SAFIR, for Fe 360 and Fe 510 steel.
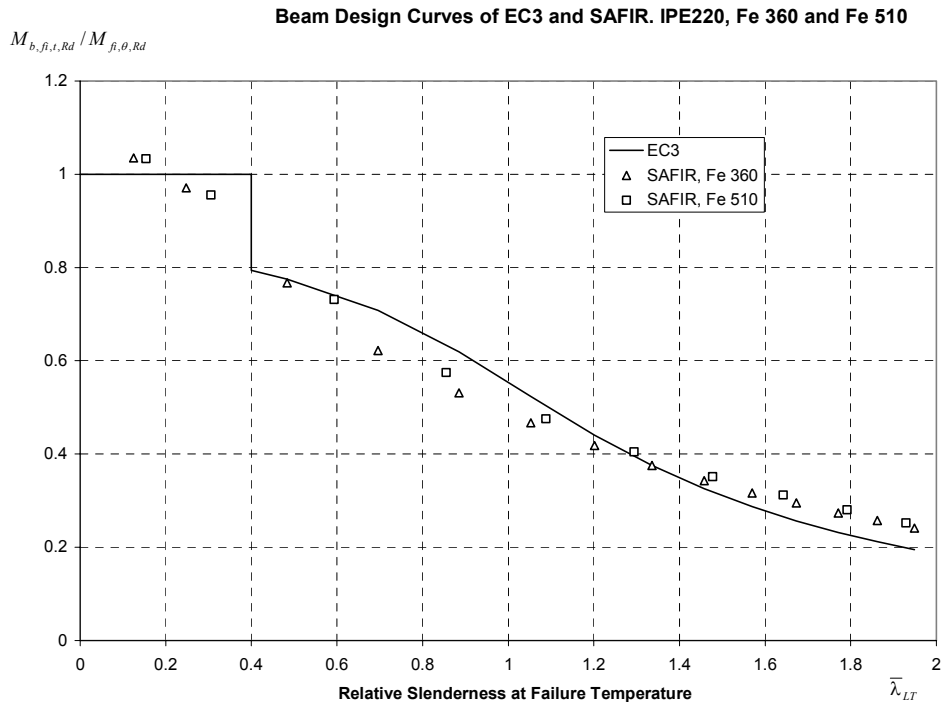
Fig. 11 – Beam design curve after 15 minutes. Comparison between the Eurocode 3 and SAFIR, for Fe 360 and Fe 510 steel.

Beam Design Curves of EC3 and SAFIR. IPE220, Fe 360 and Fe 510

$M_{b,fi,t,Rd} / M_{fi,\theta,Rd}$

Relative Slenderness at Failure Temperature

$\overline{\lambda}_{LT}$
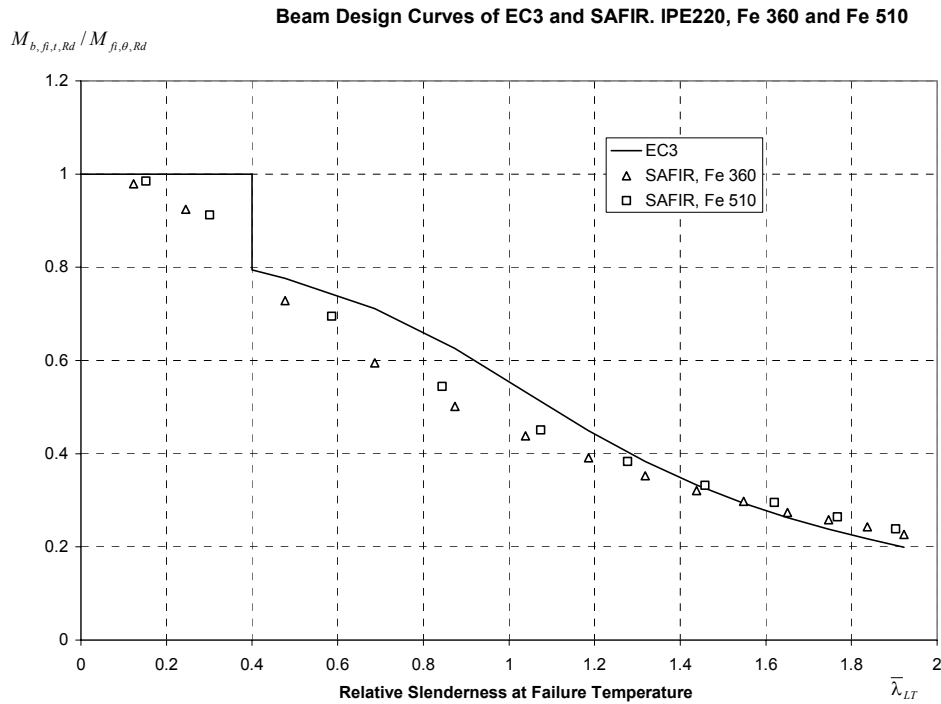
Fig. 12 – Beam design curve after 20 minutes. Comparison between the Eurocode 3 and SAFIR, for Fe 360 and Fe 510 steel.

Beam Design Curves of EC3 and SAFIR. IPE220, Fe 360 and Fe 510

$M_{b,fi,t,Rd} / M_{fi,\theta,Rd}$

Relative Slenderness at Failure Temperature

$\overline{\lambda}_{LT}$
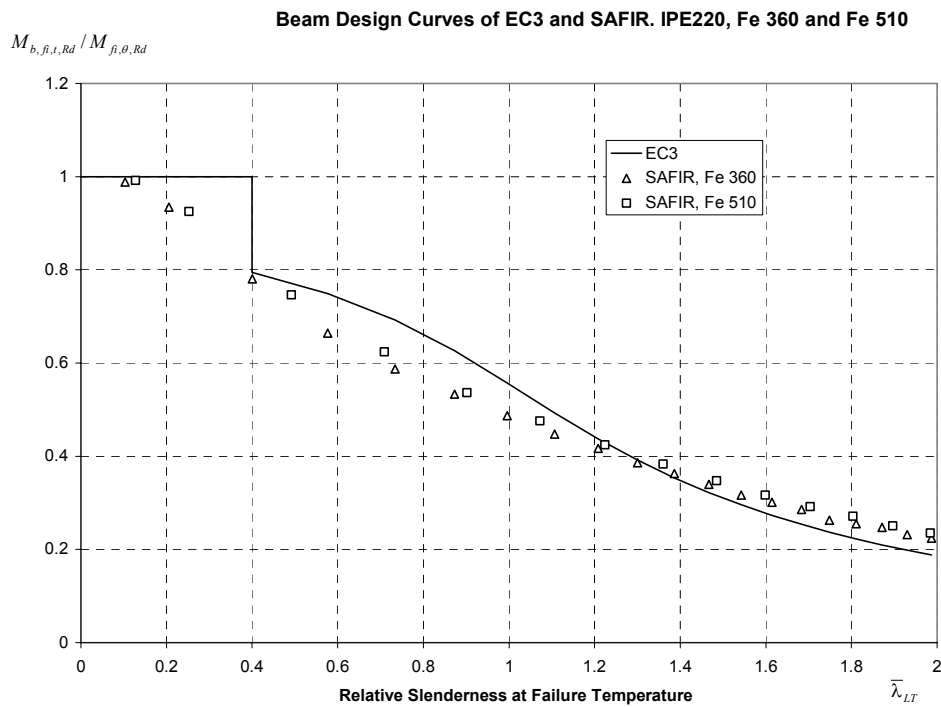
Fig. 13 – Beam design curve after 30 minutes. Comparison between the Eurocode 3 and SAFIR, for Fe 360 and Fe 510 steel.

Figure 14 shows the beam design curve obtained with the SAFIR results for the time instants of 10, 15, 20 and 30 minutes, all plotted at the same chart for the Fe 360 and Fe 510 steel. This curves are not coincident like in the case of the Eurocode 3 curve at elevated temperature (see for instance curve EC3,fi in Figure 5, or curve EC3 in Figures 10 to 13).

Beam Design Curves of EC3 and SAFIR. IPE220, Fe 360

$M_{b,fi,t,Rd} / M_{fi,\theta,Rd}$

a) Fe 360 steel

Beam Design Curves of EC3 and SAFIR. IPE220, Fe 510

$M_{b,fi,t,Rd} / M_{fi,\theta,Rd}$
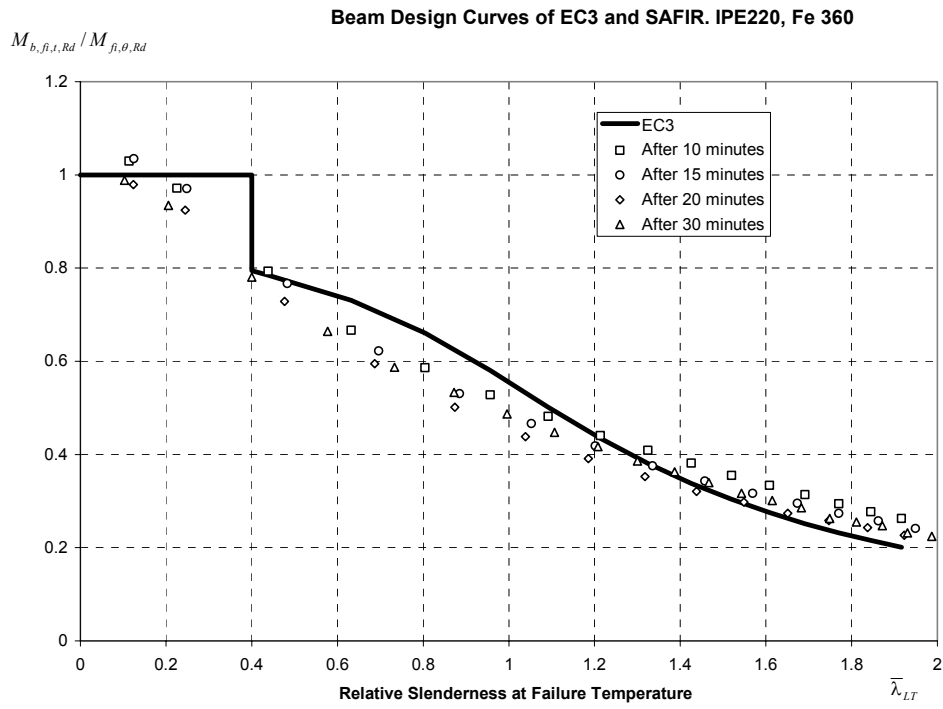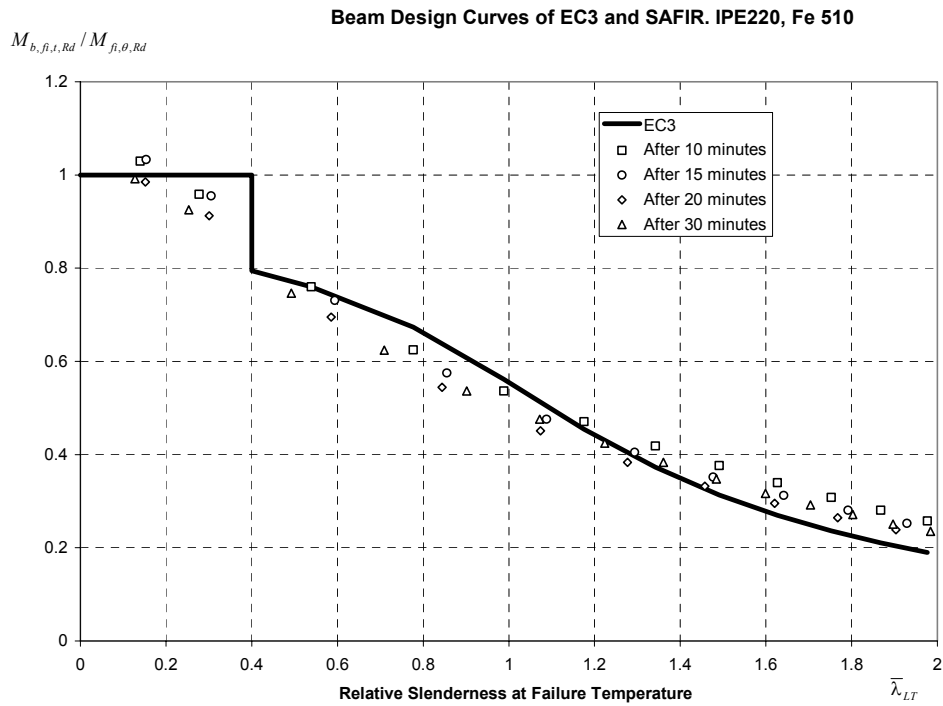
b) Fe 510

Fig. 14 – Beam design curve obtained with Eurocode 3 and SAFIR (after 10, 15, 20 and 30 minutes).

Until now all the charts were plotted with relative slenderness calculated at ultimate temperature. Figure 15 shows the numerical lateral-torsional buckling values using for the figure the relative slenderness at room temperature, i. e., at 20 °C.
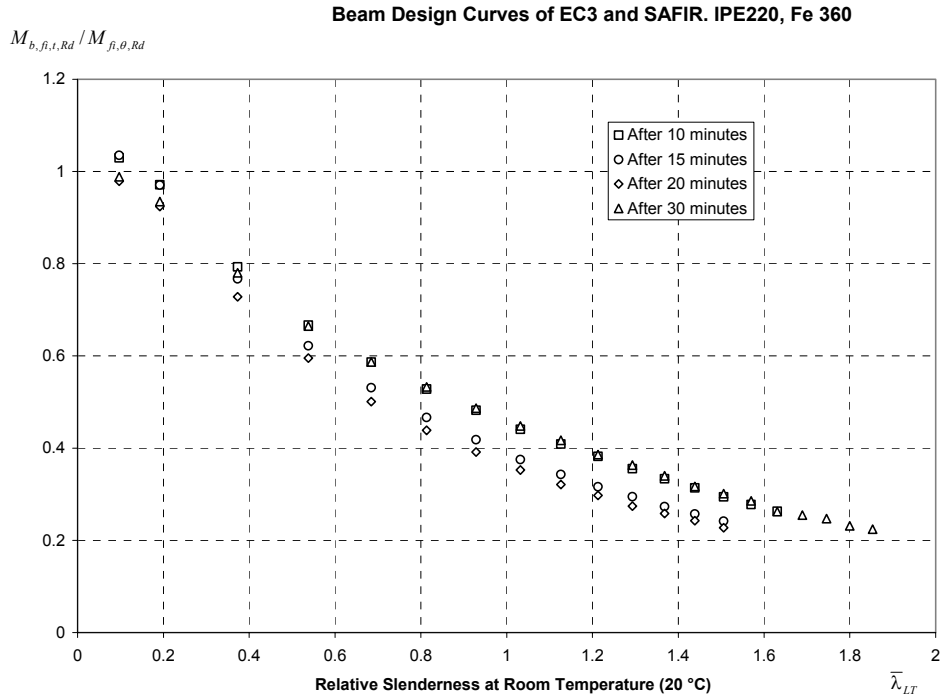
a) Fe 360 steel
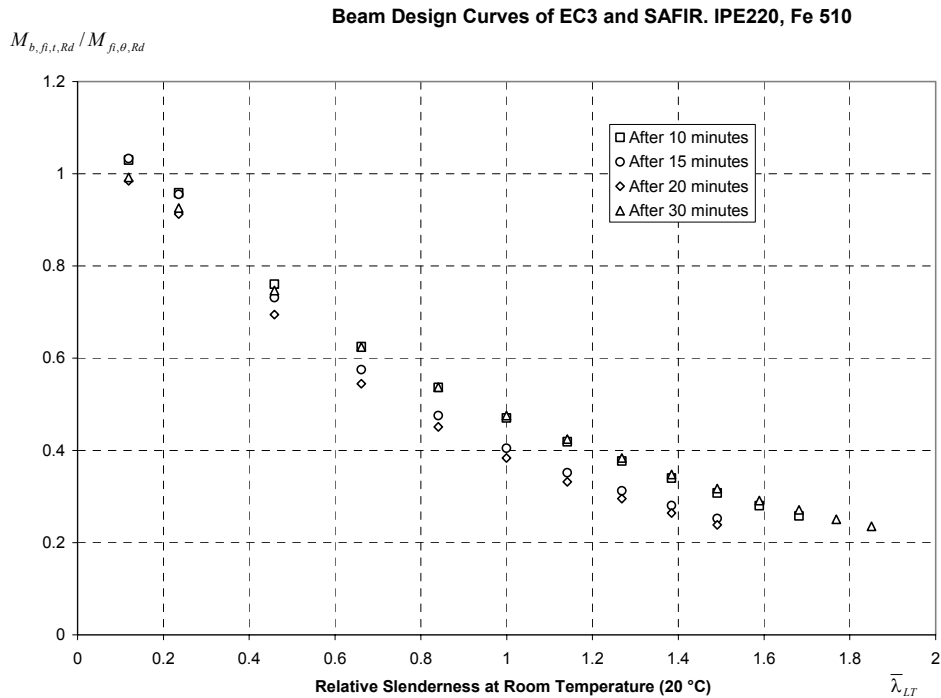
b) Fe 510

Fig. 15 – Beam design curve obtained with Eurocode 3 and SAFIR (after 10, 15, 20 and 30 minutes), using the relative slenderness evaluated at room temperature.

In Figures 10 to 14 all the named EC3 curves corresponds to the buckling curve *c* of the Eurocode 3, Part 1-1 [1], for $\overline{\lambda}_{LT} > 0.4$ divided by 1.2. The only difference between the numerical values in Figures 10 to 14 and the values in Figure 15 is that the variable on the horizontal axis of the diagrams is evaluated in the first case at ultimate temperature and in the last case at room temperature.

Anyway the shape of the distribution of the numerical lateral-torsional buckling curves is too different from the shape of the present analytical curve of Eurocode 3 to allow any hope that a modification of the correction factor used in the simple model could lead to a better correlation [6]. The lateral-torsional curve's distribution is thinner in Figure 14 than it is in Figure 15. This means that there is a better possibility of representing the numerical results, without excessive safety, with an analytical expression when the relative slenderness is evaluated at elevated temperature [6] than if it is evaluated at 20 ℃. This is what will be done in the new proposal presented in the point 3 of this paper.

From Figure 10 to Figure 14 it can be seen that the numerical values are higher on the vertical axis for Fe 510 than they are for Fe 360. As stated in [6], "This is due to the fact that the residual stresses do not depend on the yield strength. Their relative influence is therefore smaller when the yield strength is increased. This phenomena is not accounted for in the simplified model of ref. [2], where the buckling coefficient does not vary with the yield strength". In fact the reduction factor for lateral-torsional buckling, χ_{LT}, depends on the yield strength as well as the non-dimensional slenderness, $\overline{\lambda}_{LT}$, but the lateral-torsional buckling curves do not depend on the yield strength.

The reason why in the Figures 10, 11 and 14 the ratio $M_{SAFIR} / M_{fi,\theta,Rd}$, for low values of the slenderness and for the time instants 10 and 15 minutes, is greater than 1 is due to the fact that the temperature field obtained with SAFIR is not uniform, with temperatures in the flanges lower than the uniform temperature given by the simplified equation of the Eurocode 3 used to calculate $M_{fi,\theta,Rd}$, see Figure 6 for the temperature field after 10 minutes. The uniform temperature after 10 minutes calculated with the Eurocode 3 is 554 °C, which is higher than the temperature in the flanges calculated with SAFIR. For longer duration, this effect tends to disappear because the temperature field becomes more and more uniform as can be seen in Figure 16, which shows the temperature field after 30 minutes obtained by finite elements using the SAFIR code. After 30 minutes the uniform temperature field obtained with the simplified equation of the Eurocode 3 is 827 °C. The maximum temperature difference after 30 minutes, for the SAFIR results, is only 11.9 °C (see Figure 16), while after 10 minutes it is 55.9 °C (see Figure 6).
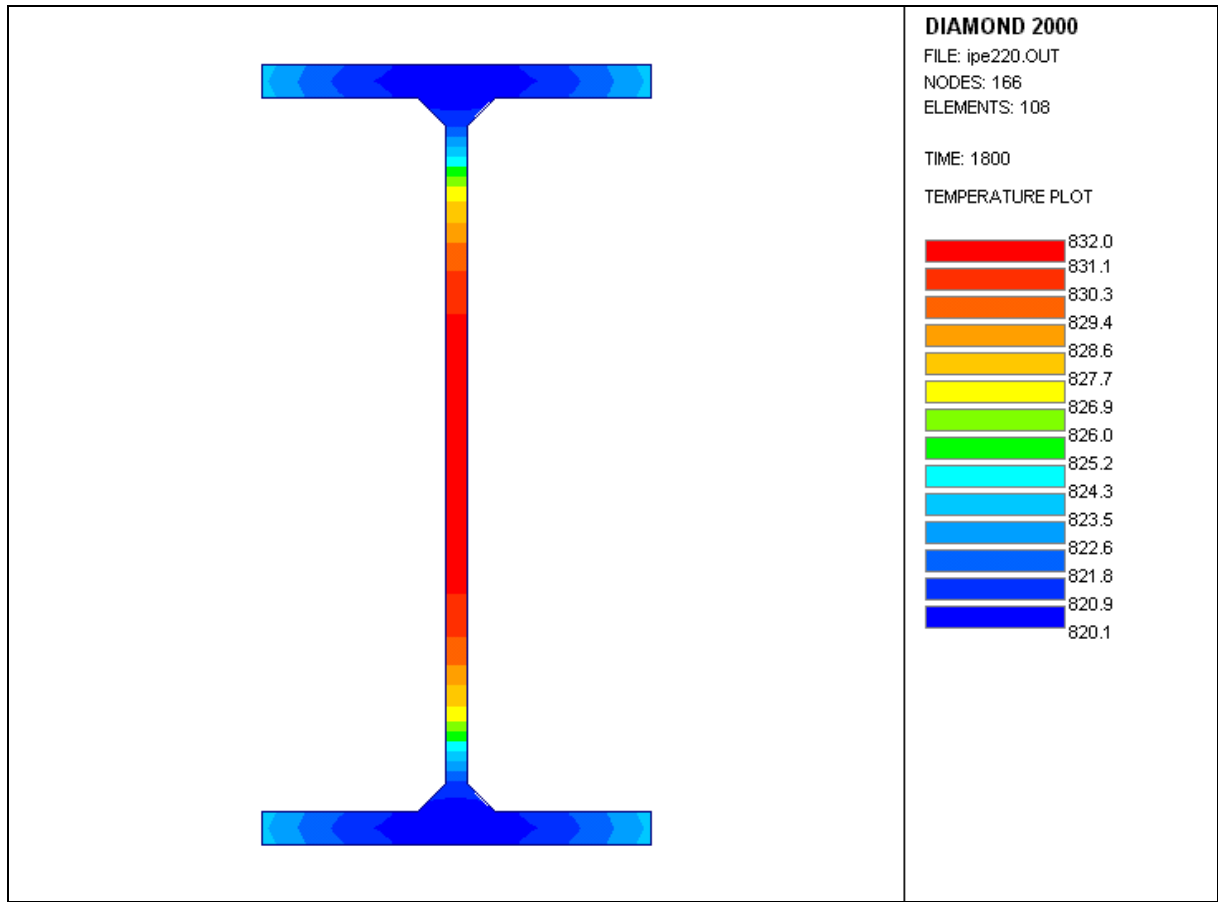
Fig. 16 – Temperature field after 30 minutes, obtained with SAFIR.

3. NEW PROPOSAL

Adopting the same proposal as in Franssen et al. [6] our approach to a new proposal is given bellow. The lateral-torsional buckling resistance moment is

$$M_{b,fi,t,Rd} = \chi_{LT,fi} w_{pl,y} k_{y,\theta,com} f_y \frac{1}{\gamma_{M,fi}}$$

(8)

where

$$\chi_{LT,fi} = \frac{1}{\phi_{LT,\theta,com} + \sqrt{[\phi_{LT,\theta,com}]^2 - [\overline{\lambda}_{LT,\theta,com}]^2}}$$

(9)

$$\phi_{LT,\theta,com} = \frac{1}{2}\left[1 + \alpha\overline{\lambda}_{LT,\theta,com} + (\overline{\lambda}_{LT,\theta,com})^2\right]$$

(10)

and

$$\overline{\lambda}_{LT,\theta,com} = \overline{\lambda}_{LT} \sqrt{\frac{k_{y,\theta,com}}{k_{E,\theta,com}}}$$

87

where $\overline{\lambda}_{LT}$ is the non-dimensional slenderness at room temperature, and with

$\alpha = \beta\varepsilon$ the imperfection factor;

β is the severity factor, to be chosen in order to ensure the appropriate safety level;

$\varepsilon = \sqrt{235/f_y}$, f_y in MPa is the yield strength.

Comparing equations (1) and (8) we can verify that with this new proposal we do not use the empirical constant 1.2 that is used as a correction factor in the proposal of the Eurocode 3.

Equations (9) and (10) are in fact exactly the same as those defined at room temperature in Eurocode 3, Part 1-1 [1], except that the threshold limit of 0.20 for $\overline{\lambda}_{LT}$ does not appear in equation (10). The fact that the threshold limit does not appear changes the shape of the buckling curve. It differs from that at room temperature. The new curve starts at $\chi_{LT} = 1.0$ for $\overline{\lambda}_{LT} = 0.0$ but it decreases even for very low slenderness, instead of having a horizontal plateau up to $\overline{\lambda}_{LT} = 0.4$ (see Fig. 17 to Fig.19).

The lateral-torsional buckling curve varies with the yield strength due to the parameter ε that appears in the imperfection factor.

The beam design curve obtained with this new proposal using a severity factor $\beta = 1.2$ as in [6] is shown in Figure 17. This value of the severity factor seems to be very safe as it can be seen in that figure.

Beam Design Curves of EC3 and SAFIR. IPE220, Fe 360

$M_{b,fi,t,Rd} / M_{fi,\theta,Rd}$

Relative Slenderness at Failure Temperature $\overline{\lambda}_{LT}$

a) Fe 360 steel

Beam Design Curves of EC3 and SAFIR. IPE220, Fe 510
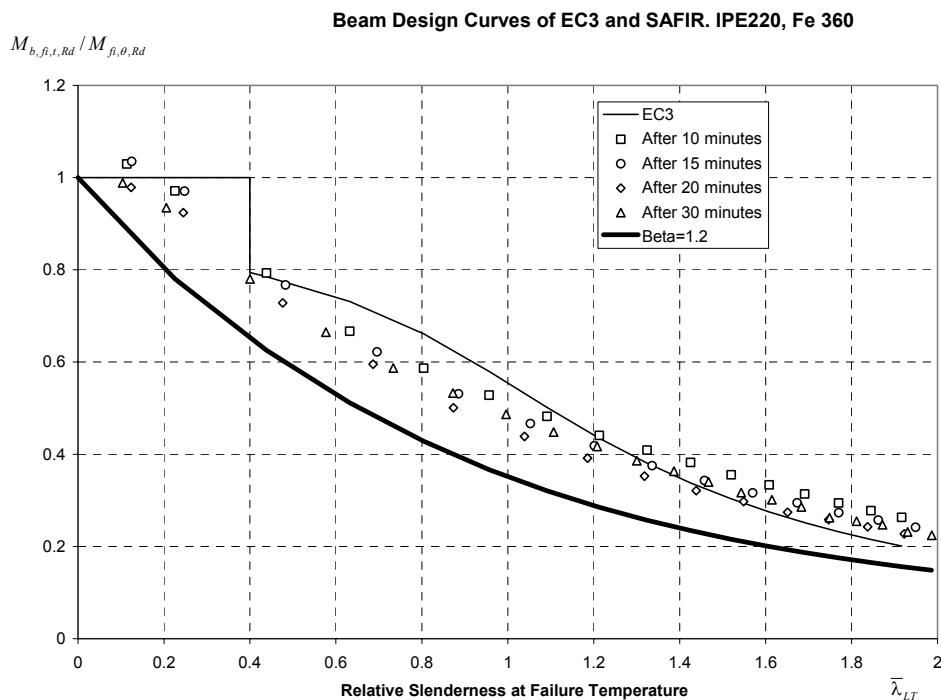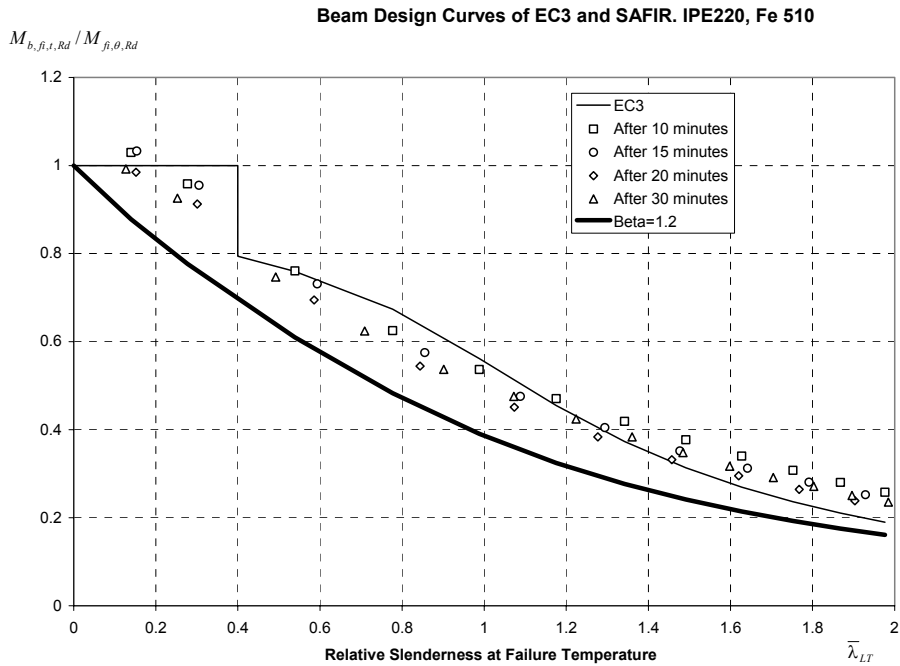
b) Fe 510

Fig. 17 – Beam design curve obtained with Eurocode 3, SAFIR (after 10, 15, 20 and 30 minutes) and with the simply model of reference [6], with $\beta = 1.2$.

When comparing the simple model with experimental results for the fire resistance of axially-loaded members [9], Franssen at al. determined a severity factor with a value of 0.65 instead of 1.2. It must be mentioned that the value of 0.65 for the severity factor is the adopted value in the Belgium and French National Application Documents of Eurocode 3, Part 1-2, [10, 13].

Beam Design Curves of EC3 and SAFIR. IPE220, Fe 360
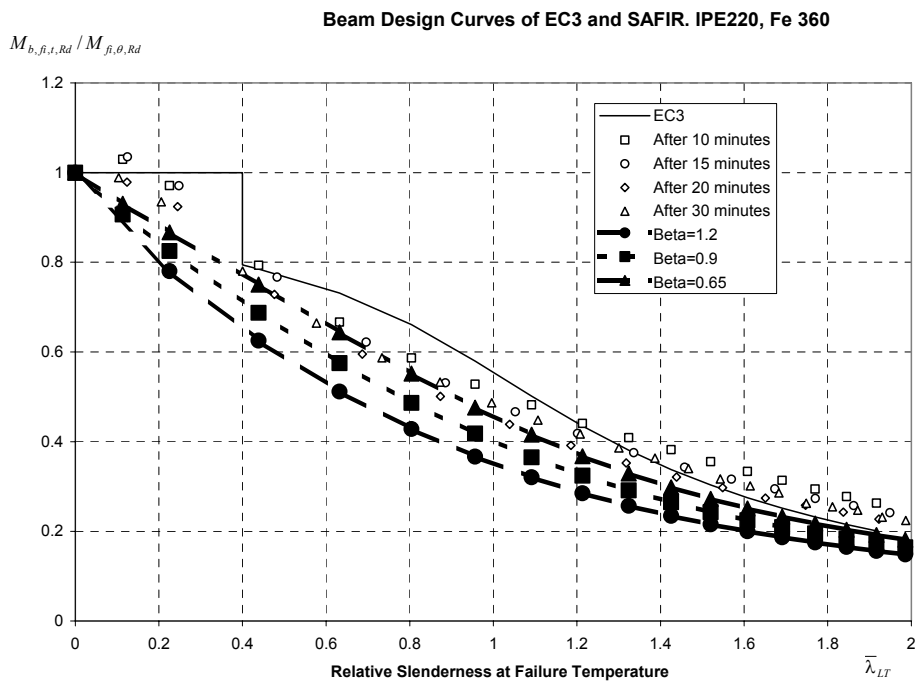
Fig. 18 – Beam design curve obtained with Eurocode 3, SAFIR (after 10, 15, 20 and 30 minutes) and with the simple model of reference [6].

Figure 18 shows the influence of the severity factor in the lateral-torsional buckling curve, for the Fe 360 steel. The values of 1.2, 0.9 and 0.65 have been used.

As the value of 0.65 for the severity factor gives safe results when compared with the SAFIR code, this value has been used in Figure 19 for the Fe 360 and Fe 510 steel.
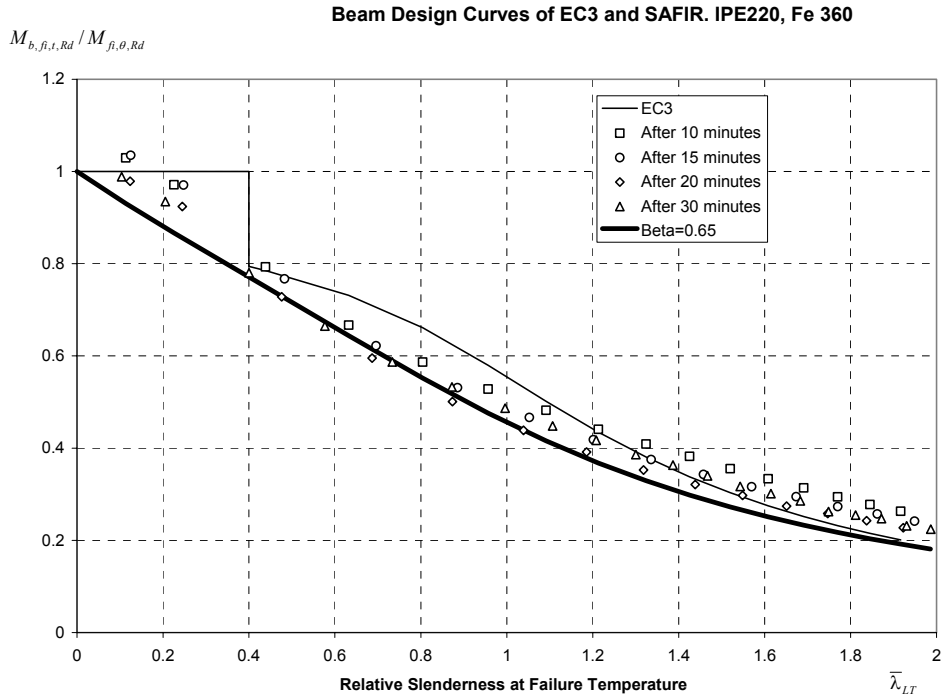

a) Fe 360 steel
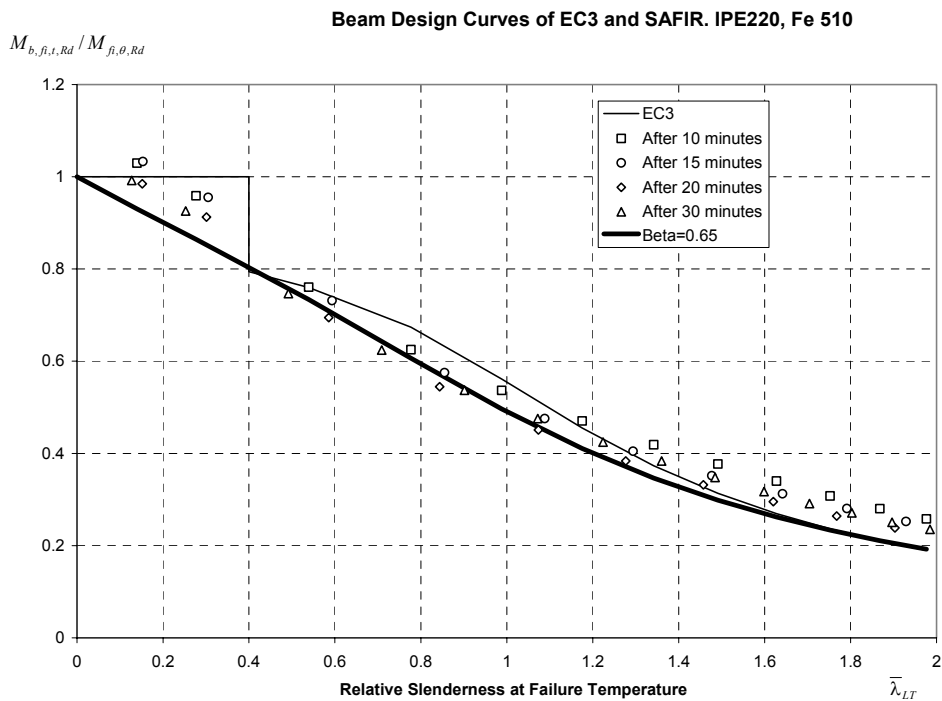
b) Fe 510

Fig. 19 – Beam design curve obtained with Eurocode 3, SAFIR (after 10, 15, 20 and 30 minutes) and with the simple model of reference [6], with $\beta = 0.65$.

As it can be seen in Figure 20, with this new proposal based on the results for axially-loaded columns [6], the beam design curve for lateral-torsional buckling now depends on the steel grade whereas the proposal of the Eurocode 3 does not. This dependence of the lateral buckling curve with the steel grade can be numerically supported with the results already shown in Figure 14.

Beam Design Curves of EC3 and SAFIR. Fe 360 and Fe 510

$M_{b,fi,t,Rd} / M_{fi,\theta,Rd}$

Relative Slenderness at Failure Temperature $\overline{\lambda}_{LT}$
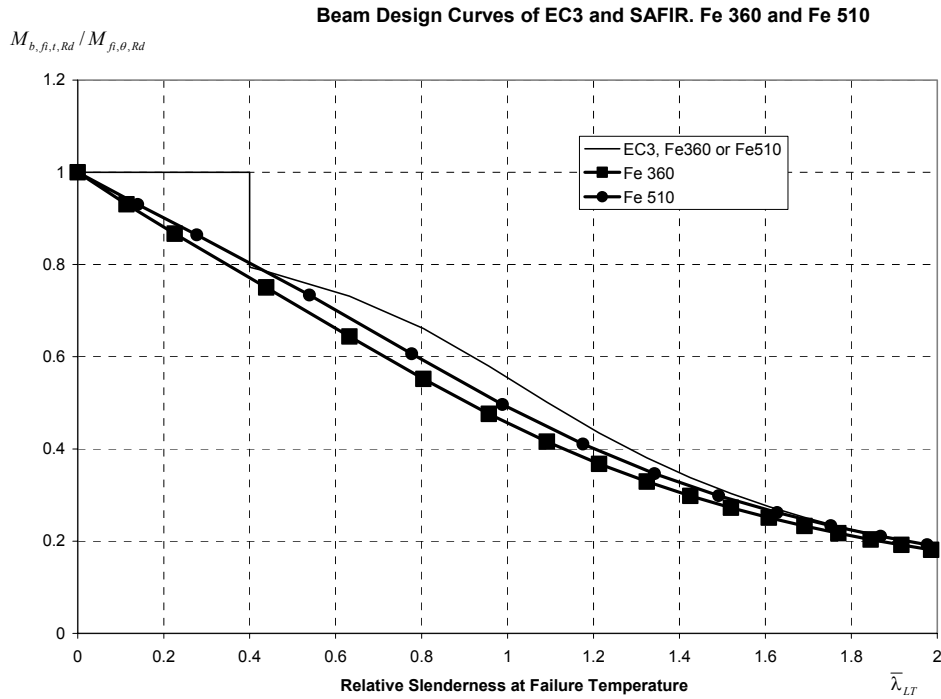
Fig. 20 – Beam design curves at elevated temperature obtained with the proposal of the Eurocode 3 and with the new proposal with $\beta = 0.65$.

4. CONCLUSIONS

The physical fact that Young's modulus decreases faster than the yield strength when the temperature increases, plus the fact that the stress-strain relationship at elevated temperature is not the same as at room temperature, produce a modification of the lateral-torsional buckling curve at elevated temperature. The horizontal plateau valid at 20 °C up to a non-dimensional slenderness of 0.4 vanishes in the case of elevated temperatures [6]. The simple models based on the lateral-torsional buckling curve that is valid at room temperature lead to a safety level that depends on the slenderness of the beam, the results being unsafe for intermediate length beams. It has been possible to make a new proposal of a lateral-torsional buckling curve for hot-rolled I-sections beams submitted to fire, based on the proposal suggested earlier [6] for axially-loaded hot-rolled H-sections submitted to fire. The beam design curve based on the reduction factor for lateral-torsional buckling in fire design situation and the non-dimensional slenderness evaluated at the ultimate temperature now depends on the steel grade, which is not the case in the Eurocode 3, Part 1-2.

It has been found that the same severity factor as the one used for the case of axially-loaded columns, i. e. $\beta = 0.65$ [9] could also be used here. This leads to the same philosophy as the one of Eurocode 3, i. e., to use the same formulas for the reduction factor for lateral-torsional buckling and for flexural buckling.

The severity factor β of the proposed simple calculation model has been established analysing only the behaviour of the IPE 220 profile. Further analysis of the numerical results should be done considering different steel I-sections.

It would also be worth to have results of well instrumented and carefully carried experimental tests to verify whether the present proposal can actually reproduce the test results and to fix definitely the value of the severity factor. As there is a low probability for the two structural imperfections, residual stresses and initial imperfection, to have simultaneously in a test the high amplitude assumed here in the numerical simulations, this could lead to the fact that the final adopted severity factor will be less severe than the one proposed in this paper.

REFERENCES

[1] Eurocode 3, Design of Steel Structures – Part 1.1. General rules and rules for buildings. Draft ENV 1993-1-1, Commission of the European Communities, Brussels, Belgium, 1992.

[2] Eurocode 3, Design of Steel Structures – Part 1.2. General rules and rules. Structural fire design. Draft ENV 1993-1-2, Commission of the European Communities, Brussels, Belgium, 1995.

[3] Jean-Marc Franssen, PROGRAM SAFIR, Ver. 1.3, User's Manual, Universite de Liege, Institut du Genie Civil, Service "Ponts et Charpentes", Dec. 1996.

[4] D. Talamona, J. M. Franssen, J. B. Schleich, J. Kruppa, "Stability of Steel Columns in Case of Fire: Numerical Modelling", Journal of Structural Engineering, Vol. 123, No. 6, pp. 713-720, Jun. 1997.

[5] Jean-Marc Franssen, "Contributions a la Modelisation des Incendies dans les Batiments et de Leurs Effects Sur les Structures", Thèse présentée en vue de l'obtention du grade d'Agrégé de l'Enseignement Supérieur, Année académique 1997-1998.

[6] Jean-Marc Franssen, Jean-Baptiste Schleich & Louis-Guy Cajot, "A Simple Model for Fire Resistance of Axially-loaded Members According to Eurocode 3", Journal Construct. Steel Research, Vol. 35, pp. 49-69, 1995.

[7] ECCS – EUROPEAN CONVENTION FOR CONSTRUCTIONAL STEELWORK, Technical Committee 8 – Structural Stability, Technical Working Group 8.2 – System, "Ultimate Limit State Calculation of Sway Frames With Rigid Joints", first edition, 1984.

[8] ARBED. Sale Programme. Structural shapes. ARBED, Luxembourg, Octobre 1995.

[9] Jean-Marc Franssen, Jean-Baptiste Schleich, Louis-Guy Cajot & Wenceslao Azpiazu "A Simple Model for Fire Resistance of Axially-loaded Members – Comparison with Experimental Results", Journal Construct. Steel Research, Vol. 37, pp. 175-204, 1996.

[10] Eurocode 3 – Calcul des structures en acier – Partie 1-2: Règles générales – Calcul de comportement au feu, DAN belge, Juillet 1998.

[11] Paulo M. M. Vila Real, Jean-Marc Franssen – "Lateral buckling of steel I beams at room temperature - Comparison between the EUROCODE 3 and the SAFIR code considering or not the residual stresses", internal report No. 99/01 , Institute of Civil Engineering – Service Ponts et Charpents – of the University of Liege, Jan. 1999.

[12] Eurocode 3 – Design of steel structures. Part 1 – General rules and rules for buildings. Background documentation. Cap. 5 document 5.03. Evolution of test results on beams with cross-sectional classes 1 – 3 in order to obtain strength functions and suitable model factors – October 1989.

[13] Eurocode 3 - Calcul des structures en acier – Partie 1-2: Règles générales – Calcul de comportement au feu, Document D'Application Nationale française.

[14] Franssen, J. M. – "Modélisation et influence des contraintes résiduelles dans les profils métalliques soumis à l'incendie", Construction Métallique, Vol. 3, pp. 35-42, 1989.

[15] Franssen, J. M. – "The unloading of building materials submitted to fire", Fire Safety Journal, Vol. 16, pp. 213-227, 1990.

[16] C. G. Bailey, IW. Burgess & R. J. Plank, "The Lateral-torsional Buckling of Unrestrained Steel Beams in Fire", Journal Construct. Steel Research, Vol. 36, 1996, pp. 101-119.

Lateral Torsional Buckling of Steel I-Beams in Case of Fire – Experimental Evaluation

Piloto, P. A. G.[1]; Vila Real, P. M. M.[2]

[1] Mechanical Department - Polytechnic of Bragança, Campus Santa Apolonia, Ap 134 5301-857 Bragança Portugal
Email: ppiloto@ipb.pt

[2] Civil Department - University of Aveiro, Campus Santiago 3810 Aveiro -Portugal
Email: pvreal@civil.ua.pt

ABTSRACT

In this paper, experimental tests on lateral torsional buckling of steel I Beams under fire conditions are presented. The beam spans varies from 0.5 to 6.5 [m] length and the temperature was risen up to 600 [ºC]. The initial conditions of the steel beams were measured. The residual stress state was characterized by the hole drilling method, using specific strain gauges. The geometric imperfections was measured by means of a laser beam and the cross section of the beams was dimensionally controlled. The methodology to the thermo-mechanical load was first heat the beam and let it expand for controlling the mechanical load position, and finally increase the load step by step.

The aim of this work is to validate the proposal for lateral torsional buckling design resistance suggested in ref.[1] based on numerical results.

A Set of experimental results are presented, relating the collapse load with the mid span movement of the beam cross section, when submitted to concentrated moments at the ends and to a uniform distributed load, due to the ceramic mat, the insulation material weight and the self weight of the beams.

1 - INTRODUCTION

The lateral torsional buckling resistance of steel beams is well known at room temperature, but in case of fire, the guides for designers are undifferentiated regarding the temperature and they are not supported by experimental results. In this work it is presented a full scale test at elevated temperatures for determining the buckling design resistance of simple supported steel I beams.

Some numerical simulations of the same test are being made and should be presented soon. The behavior will be material and geometrical non linear.

The tests presented were done as a result of a Portuguese R&D national project PRAXIS/P/ECM/14176/1998 "lateral buckling of steel beams under fire conditions" and intend to be a contribution on the knowledge of structures in fire.

The Experimental set-up is presented in the figure 1 and is constituted by two parts. One for the thermal effect simulating of the fire around the beam, and the other for structural purpose.

Fig.1 – Experimental set-up for lateral torsional behavior of structures.

The heating system must have the necessary components for thermal energy generation. The temperature controller connected to several thermocouples along the beam should be able for rise and fall the temperature, maintaining the temperature as uniform as possible. The heating elements should deliver the necessary power, provided the thermal insulation for best efficiency and a set of accessories for mounting the complete system are required.

The structural system should be stable with adjustable supports and load points. The structure used is modular and multi- functional. The Electro Hydraulic system is capable of delivery 60 [ton] force in each point load, and has the possibility of programming the rise and rate of force respect to time. The control unit as the capability of store the pick force value.

According to the Eurocode 3, the design buckling resistance moment of a laterally unrestrained beam with class 1 or 2 cross section, in case of fire is given by

$$M_{b,fi,t,Rd} = \frac{\chi_{LT,fi}}{1.2} w_{pl,y} k_{y,\theta,com} f_y \frac{1}{\gamma_{M,fi}} \qquad (1)$$

Provided that the non dimensional slenderness $\overline{\lambda}_{LT,\theta,com}$ for the maximum temperature in the compression flange $\theta_{a,com}$ reached at time t does not exceed 0.4 no allowance need be made for this situation. When non dimensional slenderness exceed that value the design moment should be calculated by expression (1). In this expression $\chi_{LT,fi}$ represents the reduction coefficient in fire situation, $w_{pl,y}$ is the plastic moment of beam cross section, $k_{y,\theta,com}$ is the reduction factor for the influence in yield by the temperature variation.

The aim of this work is to contribute to an alternative expression for the design moment resistance and validate the numerical results from [1] with full scale tests.

2 - LATERAL TORSIONAL BUCKLING OF STEEL I BEAMS

When a beam is bent about its greatest flexural axis of rigidity it may twist before it reaches its strength limit state. This stability limit state is most commonly referred to as *lateral torsional buckling* of a beam. The twisting of the beam occurs when the compression flange becomes unstable as a result of its being subjected to flexural induced axial stresses. Lateral buckling is of importance when the compression flange is laterally unsupported as is often the case in continuous beams, cantilever beams, frame beams and frame columns.
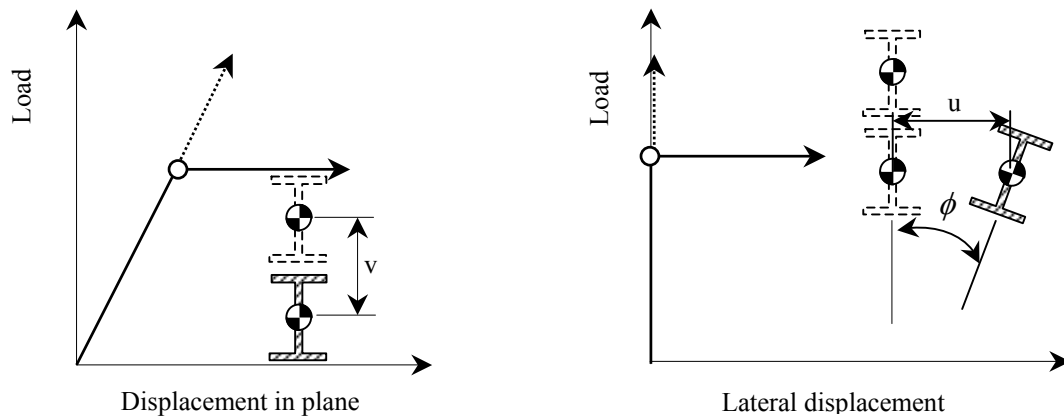
Fig.2- **Graphics representation of the cross section movement.**

The lateral torsional buckling of beams (Figure 2) involves lateral displacement u out of the plane of bending and twist rotations ϕ. In this case, the twist rotations make the applied moments to have components acting out of the original plane of bending, while the lateral rotations du/dz (z is the coordinate along the beam axis) cause the applied moments to have torque components about the axis of twist through the shear center.

Methods for designing against lateral torsional buckling are essential of two types. For the first type, buckling is avoided, and the member in plane capacity is fully utilized. One way of achieving this is to use beam cross sections not susceptible to buckle. A second way of avoiding buckling is to increase bracing, either by reducing its spacing, or else by

increasing its effectiveness. For the second type a reduced capacity is determined which accounts for the effects of flexural torsional buckling [3].

In this paper a simple supported beam with two forks at the supports, uniform distributed load (due to the weight of the heating system) and moment at the ends of the beam, as shown in the figure 3, is studied.
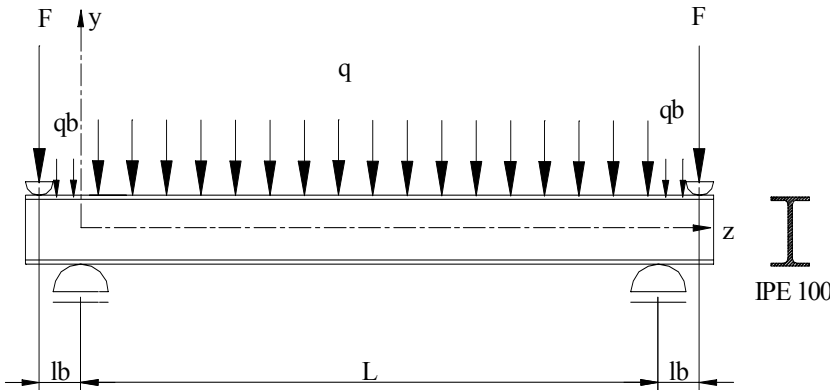
Fig. 3 – Case studied. Simply supported beam with two forks separated by L[m].

The bending moment distribution with transverse load varies along the beam and so the differential equations have some variable coefficients and are difficult to solve.

For the case when the load acts at the shear center, and for double symmetric beams, the elastic critical moment varies with the type of load.

The lateral torsional buckling equilibrium is traduced by the differential equations presented in (2).

$$\left(EI_y u''\right)'' + \left(M_x \phi\right)'' = 0$$
$$\left(EI_w \phi''\right)'' - \left(GJ\phi'\right)' + \left(M_x u''\right) = 0 \tag{2}$$

The first equation expresses the equality between the flexural resistance $\left(EI_y u''\right)''$ and the lateral bending action $-\left(M_x \phi\right)''$ of the bending moment caused by this rotation. The second equation expresses the equality between the sum of internal warping and uniform torsion resistance $\left[\left(EI_w \phi''\right)'' - \left(GJ\phi'\right)'\right]$ and the distributed torque generated by warping and twisting of the beam, during buckling.

It can be verified by substitution that these equations are satisfied by the buckled shapes:

$$\frac{u}{\delta} = \frac{\phi}{\theta} = sin\left(\frac{\pi z}{L}\right) \tag{3}$$

or still by the simply formula

$$\frac{u}{\delta} = \frac{\phi}{\theta} = \frac{z}{L} - \frac{z^2}{L^2} \tag{4}$$

where δ and θ represent the values of u and ϕ at mid span and z the coordinate along the beam axis.

For the present case the beam should verify the equilibrium equations (2) and also the energy equation (5).

$$\frac{1}{2}\int_0^L \left(EI_y u''^2 + EI_w \phi''^2 + GJ\phi'^2\right)dz + \frac{1}{2}\int_0^L 2M_x \phi\, u''dz + \frac{1}{2}\int_0^L q(y_q - y_0)\phi^2\, dz = 0 \tag{5}$$

which represents the equality at buckling between the flexural, warping and torsional strain energy stored and the work done by the bending moment M_x and the distributed load q, acting at a distance y_q from the shear center y_0.

Substituting the equation (4) and all the derivatives into equation (5) and taking into account the moment distribution along the buckling length, it can be verified that the critical load is a function of the material properties, the geometric characteristics of the beam cross section and also a function of the distributed load. This critical force when introduced into the moment distribution, near one of the supports give the critical moment. That result can be compared to the critical elastic moment for the constant moment load case using the buckling factor α_M, as shown in equation (6).

$$M_{cr} = \alpha_M \times \frac{\pi^2 EI_z}{L^2} \times \sqrt{\frac{I_w}{I_z} + L^2 \times \frac{GI_t}{\pi^2 EI_z}} \tag{6}$$

This coefficient is not constant and depends on the buckling length of the tested beam, as can be seen in the figure 4.

The critical moment is necessary for the evaluation of the relative slenderness $\overline{\lambda}_{LT}$ in equation (10).
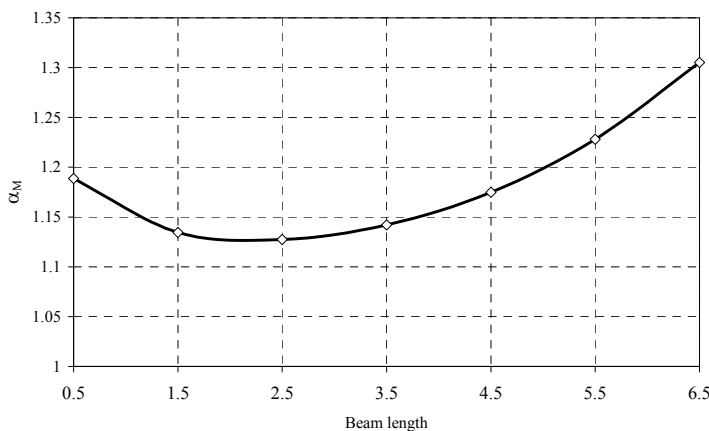
Fig.4- **Coefficient for critical elastic moment.**

99

3 - EXPERIMENTAL SETUP FOR EVALUATE LATERAL TORSIONAL BUCKLING

As a result of the R&D project it was necessary to build a support structure and all the necessary equipment for loading and measuring the necessary parameter during this phenomenon (figure 1). A multifunction structure with 8 x 1.2 [m] was used to fix the beam and apply the forces. The Electro hydraulic power system with two hydraulic jacks with 60 [ton] each gave the possibility to simulate the mechanical action on the beams and the electric ceramic mat were used to simulate a fire condition, rising and controlling the temperature in the way we intended to do.

The initial conditions of the steel beams were measured, specially, the residual stresses, the geometric imperfections and the cross section geometry was dimensionally controlled. Most of this information was a result of the steel process fabrication and of the packing process during transportation and storing.

The rolling process reduces the thickness of the section and changes its shape. After the rolling phase, the steel will gradually cools. The cross sections will have a non uniform temperature distribution and the root of the web maintains its bigger temperature for a long period than the other parts. This differential cooling leads to residual stresses that can influence the behavior of steel work under load.

The residual stresses in a single structural component or in a global structure are always present even without service load. Fabrication processes like foundry, soldering, machining, heat treatment and other factors, are the most common causes in this stress state. Other possible causes are those related to structural repair or modifications in their components. In some cases the stresses can be introduced in the structure by means of installation procedures, over load or other type of variable loads.

The effects of residual stresses in structural components may be positive or negative, depending on the magnitude, signal and their distribution relative to those induced by external loads. Several reported cases presents these residual states as the predominant factor for structural collapse.

3.1 - Auxiliary equipment for experimental setup

A multifunctional and dimensional stable structure was built for the experimental tests of lateral torsional buckling of I beam under fire condition. This structure has two main types of UNP profiles and also HEA200 profiles to build the two movable forks supports. The two other movable point loads (see figure 1) are constituted by parts of UNP350. This flexibility is necessary to leave the beam expands during the fire simulation, and load the structure after fixing the supports

For fire simulation, a heating system with 70 [kVA] and all the necessary components for thermal energy generation were used. The temperature control for rise and fall should be done, the heating elements should deliver the necessary power, provide the thermal insulation for best efficiency.

Two different types of Electro ceramic mat resistance's with 1220 x 45 and 610 x 85 [mm] with the maximum electric power of 2.7 [kW] each were used for thermal delivery into steel I beams. This material is capable to support 1050 [ºC], although our experiments were

done up to 600 [ºC] and at a heat rate of 800 [ºC/h]. The temperature distribution along the beam should be uniform to compare with the numerical simulation. Although there is always a difference near the extremes of the tested beams as it can be proved by the registration of the temperatures of the thermocouples K type used.

The displacements of the three point controlling the cross sections movement were measured by means of displacement transducers as shown in the figure 5.
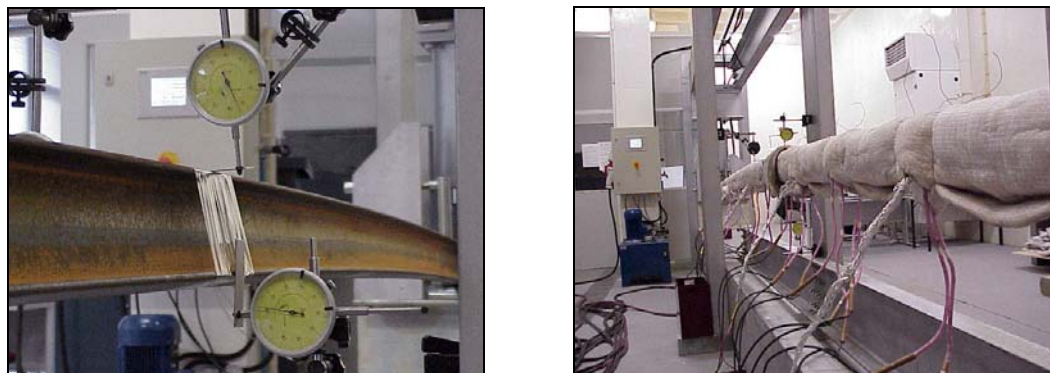
Fig.5- Displacement measuring system at room temperatures and at elevated temperatures.

3.2 - Methodology of the experiments

The geometric imperfections were measured for each I beam. For the beams submitted to elevated temperatures it was necessary to thermocouples to measure the temperature. This thermocouples were micro welded by a special equipment that minimize some possible reading errors with this type of thermal sensor.

During temperature rise the distance between the support and the point load was controlled and fixed after temperature stability was achieved. After that, the mechanical load is applied and incremented up to the collapse load, as can be seen in the figure 6.

From the results presented in the figure 6 it can be seen that the collapse load decrease as the temperature of fire increase. The relation between displacement and force changes due to the variation of the material properties, as it can be shown in the graphics for temperatures above 400 [ºC].

A series of results for other beam lengths were obtained and transposed to the global graphic results presented in figure 7.

In all this graphic representation DV represents the vertical displacement, DLB represents the bottom lateral displacement and DLC the lateral top displacement of the mid span cross section.

Beam 3.5 [m] at room temperature

Beam 3.5 [m] at temperature 200 [ºC]

Beam 3.5 [m] at temperature 300 [ºC]

Beam 3.5 [m] at temperature 400 [ºC]

Beam 3.5 [m] at temperature 500 [ºC]

Beam 3.5 [m] at temperature 600 [ºC]
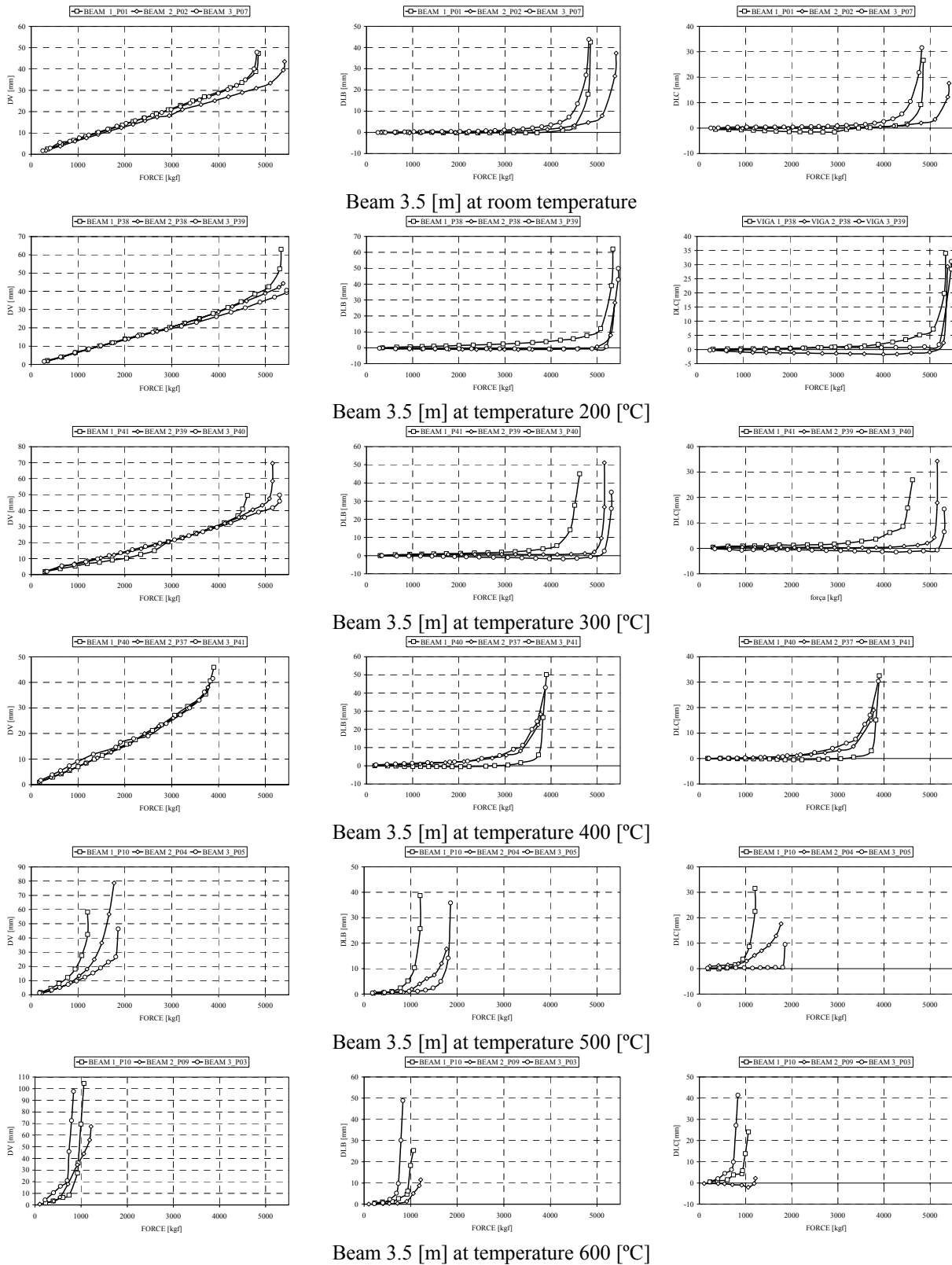
Fig.6- Experimental results from 20[ºC] to 600[ºC] of a 3.5 [m] of buckling length.

4 - A NEW PROPOSAL FOR A SIMPLE MODEL IN LATERAL TORSIONAL BUCKLING OF I-BEAMS.

According to the new proposal from Paulo Vila Real 1999 [1] and adopting for the lateral torsional buckling of beams the same proposal that Franssen used in 1995 [4] to represent the behavior of columns when submitted to fire conditions and with axial mechanical load, the design value to buckling resistance in fire conditions should be:

$$M_{b,fi,t,Rd} = \chi_{LT,fi} w_{pl,y} k_{y,\theta,com} f_y \frac{1}{\gamma_{M,fi}} \tag{7}$$

where $\chi_{LT,fi}$, $\phi_{LT,\theta,com}$ and $\overline{\lambda}_{LT,\theta,com}$ are given by

$$\chi_{LT,fi} = \frac{1}{\phi_{LT,\theta,com} + \sqrt{[\phi_{LT,\theta,com}]^2 - [\lambda_{LT,\theta,com}]^2}} \tag{8}$$

$$\phi_{LT,\theta,com} = \frac{1}{2}\left[1 + \alpha\overline{\lambda}_{LT,\theta,com} + (\overline{\lambda}_{LT,\theta,com})^2\right] \tag{9}$$

$$\overline{\lambda}_{LT,\theta,com} = \overline{\lambda}_{LT}\sqrt{\frac{k_{y,\theta,com}}{k_{E,\theta,com}}} \tag{10}$$

The imperfection factor α now is a function of a severity factor β

$$\alpha = \beta\varepsilon \tag{11}$$

This severity factor β should be chosen in order to ensure the appropriate safety level in the design of beams to lateral torsional buckling, and

$$\varepsilon = \sqrt{\frac{235}{f_y}} \tag{12}$$

In this formulas, f_y represents the nominal yield strength of the material testing, $\overline{\lambda}_{LT}$ the relative slenderness at room temperature, $\overline{\lambda}_{LT,\theta,com}$ the relative slenderness at elevated temperature, $w_{pl,y}$ represents the plastic moment of the cross section, $k_{y,\theta,com}$ the relative coefficient of the yield strength at the temperature $\theta_{a,com}$. The partial security factor in case of fire $\gamma_{M,fi}$ should be taken as 1.0.

Comparing equations (1) and (7) we can verify that with this new proposal we do not use the empirical constant 1.2 that is used as a correction factor in the proposal of the Eurocode 3. Equations (8) and (9) are exactly the same as those defined at room temperature in [2], except that the threshold limit of 0.20 for $\overline{\lambda}_{LT}$ does not appear in equation (9). This fact changes the shape of the buckling curve, beginning at $\chi_{TL} = 1.0$ for $\overline{\lambda}_{LT} = 0.0$ but decreasing even for very low slenderness, instead of having a horizontal plateau up to $\overline{\lambda}_{LT} = 0.4$.

The lateral-torsional buckling curve varies with the yield strength due to the parameter ε that appears in the imperfection factor.

4.1. Experimental results

A set of 120 experimental results were done in the Laboratory of Structures of the Polytechnic of Bragança, with the equipment described in the previous chapters. The geometry of the cross section was averaged from a set of specimens and it could be observed that they didn't correspond exactly to the dimensions presented by the manufacturer.

The mechanical properties were considered from 20 measures on the specimens.

The self weight from the ceramic mat, beam, and insulation material was considered to evaluate the critical buckling moment.

The results of each resistance force were recorded and graphically presented in figure 6. The last value of each experiment was considered to be the buckling resistance force.

Adopting the same value for the severity factor $\beta = 0.65$ that Paulo Vila Real used in his proposal, it can be verified that the buckling moments obtained with this simple model are in the safe side, except for the results corresponding to the smallest beams.
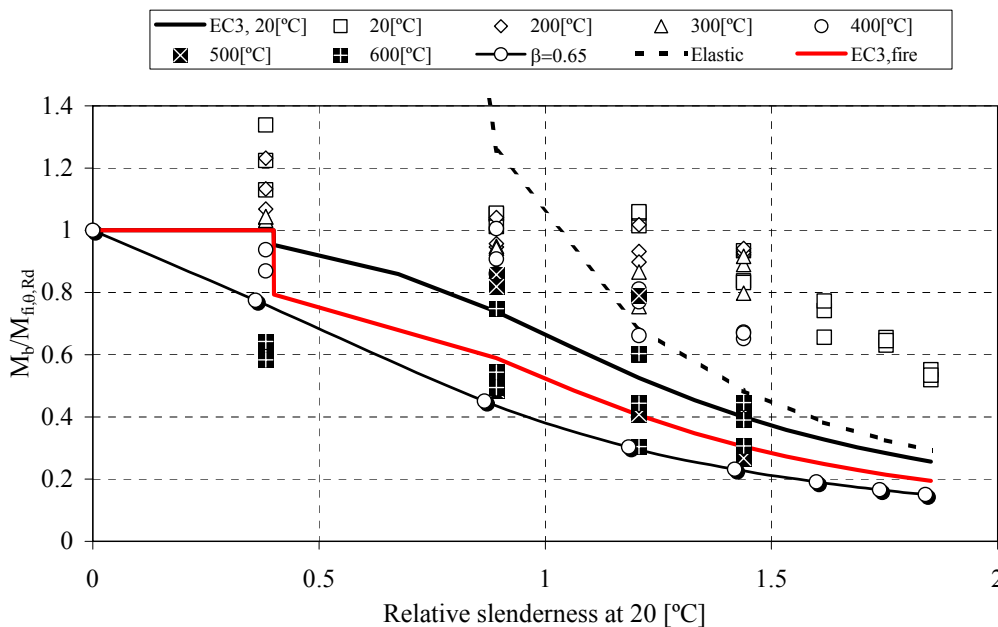
Fig. 7- Beam design curves at elevated temperatures with the new proposals.

5- CONCLUSIONS

The experimental results were done during several days, and the results could be influenced by a lot of parameters. First the temperature should or intended to be uniform, but in reality it does not occur, since the 4 temperature control unit only read the values in each thermocouple and action in conformity on rising and cooling of that region. Despite the beam insulation, this fact may influence the material properties and by consequence the results.

The time that each beam was exposed to the heat was almost constant but those differences may be important for the creep phenomenon.

The physical fact that Young's modulus decreases faster than the yield strength when the temperature increases, plus the fact that the stress-strain relationship at elevated temperature is not the same as at room temperature, produce a modification of the lateral-torsional buckling curve at elevated temperature. The horizontal plateau valid at 20 °C up to a non-dimensional slenderness of 0.4 may vanishes in the case of elevated temperatures like in the new proposal.

The beam design curve based on the reduction factor for lateral-torsional buckling in fire design situation depends, in the new proposal, on the steel grade, which is not the case in the Eurocode 3, Part 1-2.

The severity factor β of the proposed simple calculation model has been established analyzing only the behavior of the IPE 100 profile. Further experimental results should be obtained to confirm the value of this severity factor.

ACKNOWLEDGEMENTS

REFERENCES

[1] Paulo M. M. Vila Real, Jean-Marc Franssen (1999) – "Lateral buckling of steel I beams at room temperature - Comparison between the EUROCODE 3 and the SAFIR code considering or not the residual stresses", internal report No. 99/01 , Institute of Civil Engineering – Service Ponts et Charpents – of the University of Liege, 1999.

[2] ECS ENV 1993-1-2; Eurocode 3 – Design of steel structures – Part 1-2: General rules – Stuctural fire design"; 1995.

[3] Trahair N.S. ; "Flexural Torsional Buckling of structures; E&FN SPON Chapman & Hall; London; 1993.

[4] Jean-Marc Franssen, Jean-Baptiste Schleich & Louis-Guy Cajot, "A Simple Model for Fire Resistance of Axially-loaded Members According to Eurocode 3", Journal Construct. Steel Research, Vol. 35, pp. 49-69, 1995.

High-Temperature Heat and Mass Transfer in a Concrete Layer Used for Biological Protection of Nuclear Reactors at Critical Heat Loads

Genii V. Kuznetsov * , Alexander V. Ptchelintsev ** and Vladimir P. Rudzinskii *

* Research Institute of Applied Mathematics and Mechanics, Tomsk State University, ul. Lenina 36, Tomsk, 634050, RUSSIA, E-mail: rvp@nvkz.kuzbass.net and rvp@rvp.tomsk.su

** Technical Research Centre of Finland, VTT Building Technology, Fire Technology, Kivimiehentie 4, P.O. Box 1803, 02044 VTT, FINLAND, E-mail: Alexander.Ptchelintsev@vtt.fi

ABSTRACT

The problem of high-temperature heat and mass transfer in a layer of concrete of nuclear reactors at critical heat loads or emergency situations like fire is discussed . The processes of evaporations of adsorbed moisture and the reaction of dehydration are taken into account. The set of nonlinear unsteady-state differential equations of heat and mass transfer is solved by the finite difference method. The numerical analysis is performed for a wide range of temperature variation. It is shown that the process of dehydration of concrete during heating to 1000-1200 K leads to formation in concrete of a high-pressure zone (up to 15-20 $\times$ 10^5 Pa) of gaseous products of evaporation and dehydration. The level of attendant stresses exceeds considerably the ultimate strength of typical grades of concrete for respective values of high temperature. It is further found that the process of dehydration of high-grade concrete with low porosity may result in higher pressures as compared with low-grade concrete. The results of numerical analysis serve as a basis for a more exact calculation of temperature fields in the biological protection layer of nuclear reactors, as well as for computation of the stress-strain state of concrete and for prediction of the reliability of operation of power reactors as a whole.

Nomenclature

T temperature (K)

t time (s)

x space coordinate (m)

y space coordinate (m)

c specific heat capacity (kJ/kg · K)

ρ density (kg/m^3)

W rate of physicochemical transformations (kg/m^3 · s)

$Q,$ heat effect of physicochemical transformations (kJ/kg)

λ coefficient of thermal conductivity (W/m · K)

φ volume fraction (m^3/m^3)

V velocity (m/s)

k permeability factor (m/s)

μ dynamic viscosity (kg/m · s)

P pressure (N/m^2)

R   universal gas constant (kJ/kmol · K)

M   molecular weight (kg/kmol)

A   accommodation coefficient

η degree of completeness (depth of reaction) of the dehydration process

ε_{pr} reduced emissivity factor

α heat transfer coefficient (W/m^2 · K)

σ Stefan-Boltzmann constant (W/m^2 · K^4)

P^S pressure of saturated steam (N/ m^2).

Subscripts:

0 initial values

1 concrete at initial state

2 adsorbed moisture

3 gaseous products of dehydration and evaporation

Σ total values

e environment,

h heated concrete surface

c crystalline moisture.

INTRODUCTION

Concrete used as the main structural material for producing the layer of biological protection of nuclear reactors is heated during operation at critical heat loads or emergency situations like fire to fairly high temperatures [1-4]. Under certain conditions, the attendant stresses may cause cracking of the concrete and corresponding reduction of the efficiency of biological protection of the reactor. All these processes are most intensive in power reactors characterized by a high energy release per unit volume and by a significant loss of energy from the external surface of the core [5].

The adsorbed moisture contained in pores may play a special role in forming the stress-strain state of concrete under conditions being treated [1]. It is demonstrated in [1] that, in the case of intensive heating of concrete at elevated temperatures, the presence of adsorbed

moisture leads to a rise of intraporous pressure to values substantially exceeding the limiting permissible values.

At the same time, it is known [5] that the heating of concrete is accompanied by the emission of steam as a result of the process of dehydration. The scale of possible effect of this process on the distribution of interstitial pressure has not yet been investigated in detail.

This paper gives the results of numerical investigation of heat and mass transfer in a layer of concrete with due regard for the evaporation of adsorbed moisture and for the dehydration reaction [5].

PHYSICAL AND MATHEMATICAL MODELS AND METHOD OF SOLUTION

A numerical analysis is performed using the following physical model. Construction is made of concrete or of reinforced-concrete with a porosity other than zero. Pores are partly filled with moisture adsorbed by concrete from the atmosphere. At the initial instant of time, the construction is exposed to heating over the external surface due to the convection and radiation mechanisms of heat transfer. The parameters of heat transfer are predefined. As the temperature rises, the process of evaporation of moisture in micropores begins. The increase of temperature is accompanied with an increase of the evaporation rate. At the same time, the pressure of evaporation products in pores rises. As some pressure drop forms over the thickness of the concrete layer, water vapors start to percolate to the heated and unheated surfaces. The rate of percolation is determined by the gas permeability of concrete. As soon as the temperature reaches a certain value, the process of concrete dehydration begins, accompanied by the gasification of crystalline moisture. The pressure in micropores of concrete and the rate of filtration of gases to the heated and unheated surfaces increase due to additional evolution of gas.

The complex of physicochemical processes occurring in concrete at critical heat loads has in common with the processes taking place in insulating materials at high temperature [7].

The mathematical model of the process being treated, for the adopted flow scheme, includes the equations of conservation for mass, momentum, and energy with the appropriate boundary and initial conditions,

$$(c\rho)_\Sigma \frac{\partial T}{\partial t} = \frac{\partial}{\partial x}\left(\lambda_\Sigma \frac{\partial T}{\partial x}\right) + \frac{\partial}{\partial y}\left(\lambda_\Sigma \frac{\partial T}{\partial y}\right) + \rho_3 V_X c_3 \frac{\partial T}{\partial x} + \rho_3 V_Y c_3 \frac{\partial T}{\partial y} - Q_1 W_1 \pm Q_2 W_2 \quad (1)$$

$$(c\rho)_\Sigma = c_1\rho_1\varphi_1 + c_2\rho_2\varphi_2 + c_3\rho_3\varphi_3, \quad (2)$$

$$\lambda_\Sigma = \lambda_1\varphi_1 + \lambda_2\varphi_2 + \lambda_3\varphi_3, \quad (3)$$

$$\rho_1 \frac{\partial \varphi_1}{\partial t} = - w_1, \quad (4)$$

$$\rho_2 \frac{\partial \varphi_2}{\partial t} = \pm W_2, \quad (5)$$

$$\frac{\partial \rho_3 \varphi_3}{\partial t} + \frac{\partial \rho_3 \varphi_3 V_{3X}}{\partial x} + \frac{\partial \rho_3 \varphi_3 V_{3Y}}{\partial y} = W_1 \pm W_2, \quad (6)$$

$$V_{3X} = - \frac{k}{\mu} \frac{\partial p}{\partial x}, \tag{7}$$

$$V_{3Y} = - \frac{k}{\mu} \frac{\partial p}{\partial y}, \tag{8}$$

$$p = \frac{\rho_3 \, R \, T}{M}, \tag{9}$$

$$\varphi_1 + \varphi_2 + \varphi_3 = 1 \tag{10}$$

$$W_1 = \rho_{10} \, \varphi_c \, \frac{d \eta}{dt}, \tag{11}$$

$$W_2 = \frac{A(p^s - p)}{\sqrt{2 \pi RT / M}}, \tag{12}$$

$$t = 0 \quad T = T_0, \quad \varphi_1 = \varphi_{10}, \quad \varphi_2 = \varphi_{20}, \quad \rho_3 = \rho_{30}, \tag{13}$$

$$x = L_X, \quad \alpha_{H'}(T_H - T) + \varepsilon_{pr} \sigma \left(T_H^4 - T^4\right) = -\lambda_\Sigma \frac{\partial T}{\partial x}, \quad P = P_a, \tag{14}$$

$$y = L_Y, \quad \alpha_H(T_H - T) + \varepsilon_{pr} \sigma \left(T_H^4 - T^4\right) = -\lambda_\Sigma \frac{\partial T}{\partial y}, \quad P = P_a, \tag{15}$$

$$x = 0, \quad 0 \le y \le L_Y, \quad \lambda_\Sigma \frac{\partial T}{\partial x} = 0, \quad V_X = 0, \tag{16}$$

$$y = 0, \quad 0 \le x \le L_X, \quad \lambda_\Sigma \frac{\partial T}{\partial y} = 0, \quad V_Y = 0, \tag{17}$$

concrete–steel:

$$-\lambda_\Sigma \frac{\partial T_-}{\partial x} = -\lambda_\Sigma \frac{\partial T_+}{\partial x}, \quad -\lambda_\Sigma \frac{\partial T_-}{\partial y} = -\lambda_\Sigma \frac{\partial T_+}{\partial y}, \quad T_- = T_+, \quad V_X = V_Y = 0. \tag{18}$$

The following main assumptions were made in formulating the problem: the treated region is not deformed as a result of pressure rise in the porous concrete structure during evaporation of moisture and dehydration of concrete; radiative heat transfer in concrete is negligibly small as compared with conductive and convective modes.

The problem is solved in cartesian coordinates but there is a possibility to use cylindrical coordinate system as well.

The set of equations of boundary and initial conditions (1)-(18) is solved by the finite difference method [8] using the method of iterations and the sweep method diring each iteration. Use was made of an implicit four-point difference scheme [8]. The net parameters were selected from the condition of ensuring the stability of solution for the entire range of rates of physico-chemical processes.

CALCULATION RESULTS

Numerical investigations were conducted for the following characteristic [1,5] values of environmental parameters: $k=1.0\times10^{-11}$, $\alpha_H=29$ W/(m^{2}s), $T_0=293$ K, $Q_1=490$ kJ/kg, $Q_2=2260$ kJ/kg, $\varphi_{10} = 0.91$, $\varphi_{20} = 0.03$, $\varphi_{230} = 0.06$, The dehydration process occurs in the range of temperature variation from 573 to 1173 K.

A scheme of the calculation domain is shown in Figure 1. Because of the symmetry both of model geometry and the boundary conditions imposed on the model, only a quarter of the model's cross-section need to be considered in the analysis. Time variation of the surrounding gas temperature was assumed according to the standard ISO-834 fire.
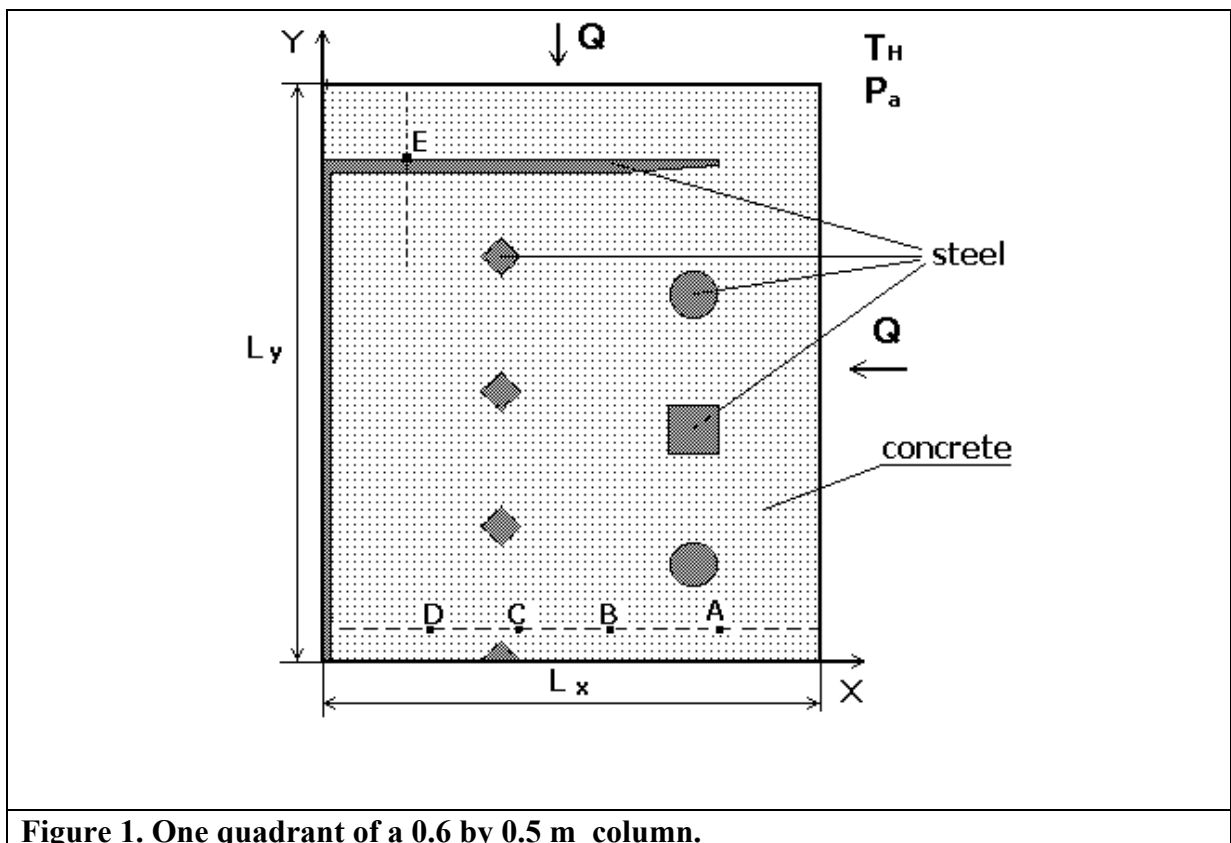
Figure 1. One quadrant of a 0.6 by 0.5 m column.

Temperature isolines corresponding to 30 min of fire are shown for the concrete and reinforced concrete columns in Figure 2.
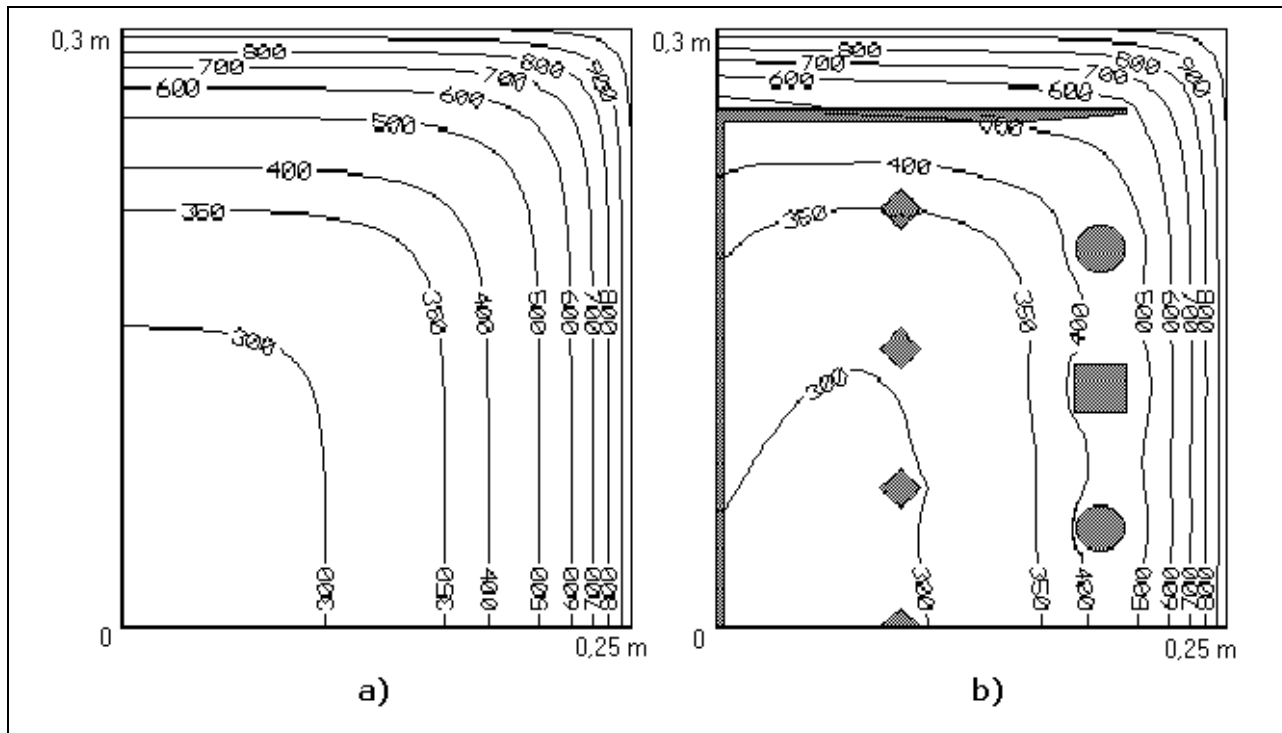
Figure 2. **Temperature Contours (K) after 1800 s: a) concrete, b) reinforced-concrete.**

Pore pressure distribution for the concrete and reinforced concrete columns after 15 min, 30 min and 1 hour of fire is shown in Figures 3-5 respectively.
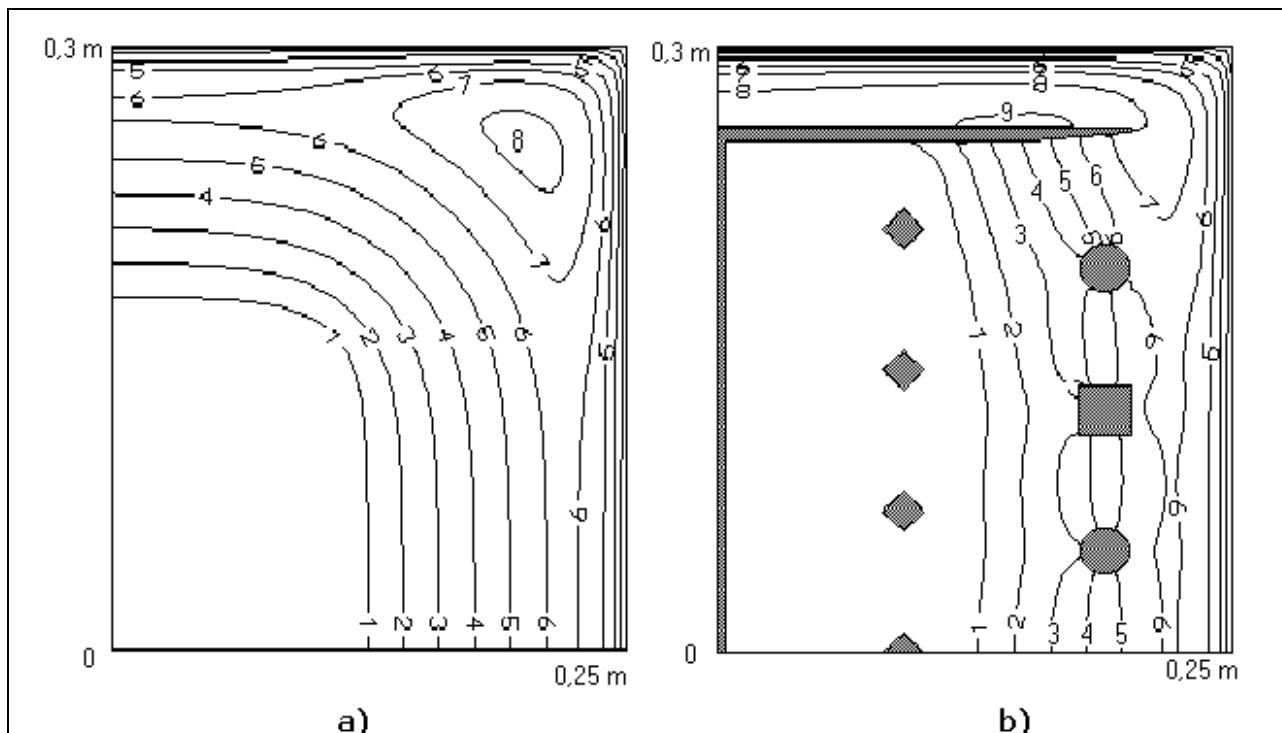
Figure 3. **Pore pressure contours (atm) after 900 s: a) concrete , b) reinforced-concrete.**
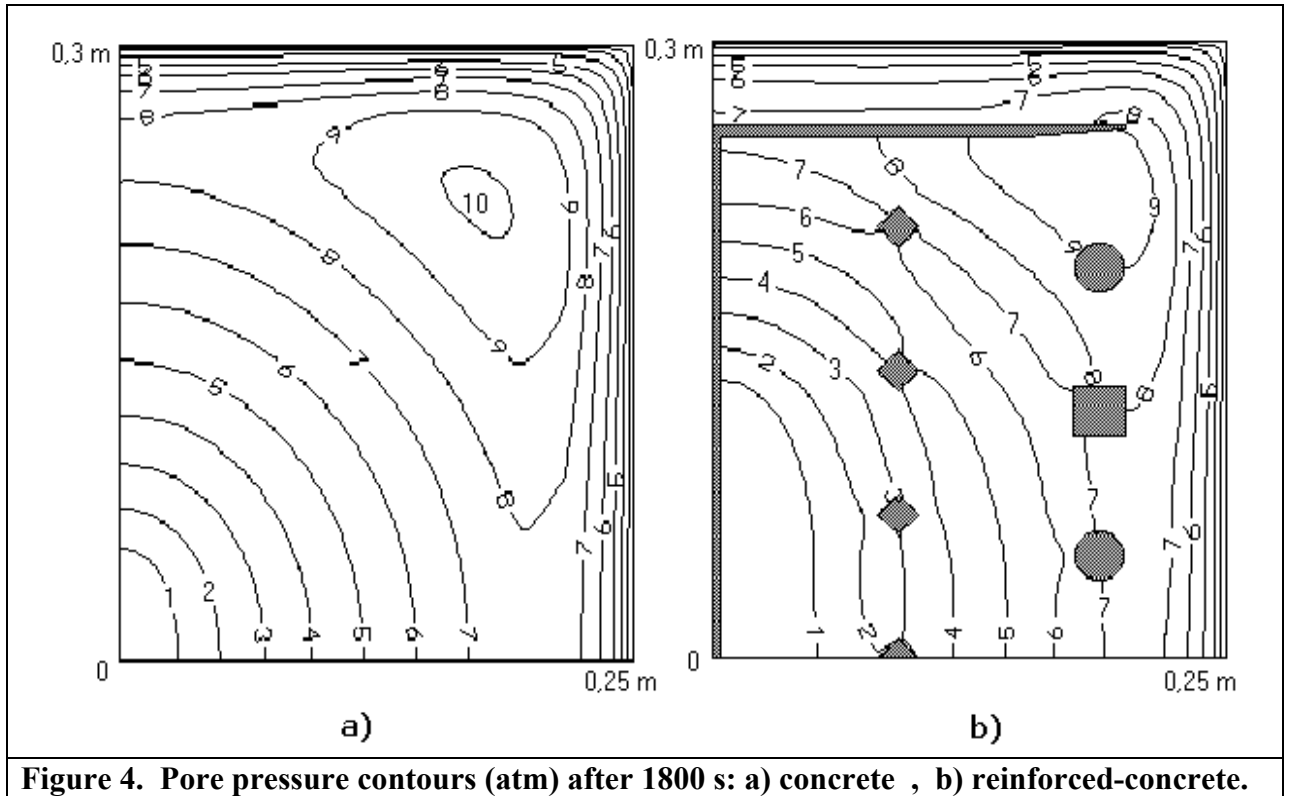
Figure 4. Pore pressure contours (atm) after 1800 s: a) concrete , b) reinforced-concrete.
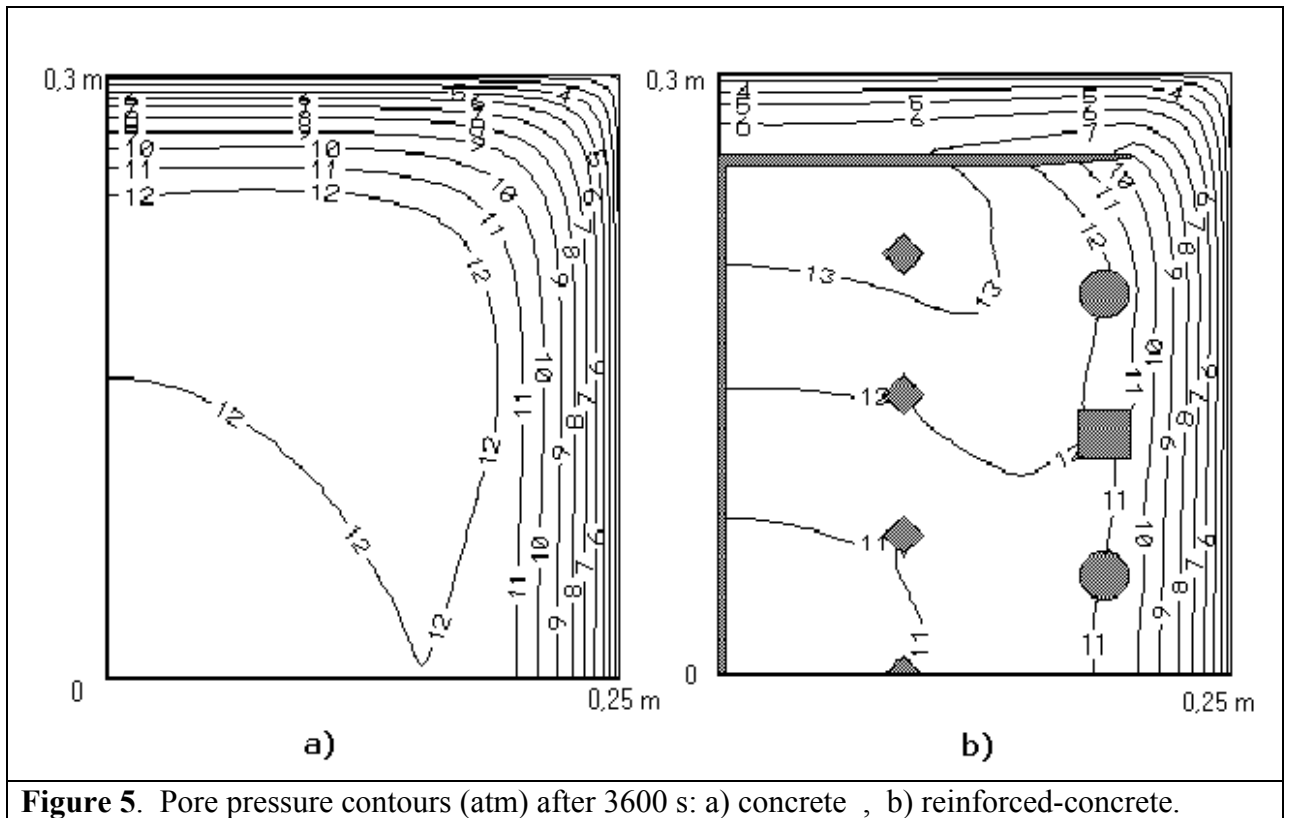
Figure 5. Pore pressure contours (atm) after 3600 s: a) concrete , b) reinforced-concrete.

Characteristic time-temperature curves are shown in Figure 6 corresponding to a number of internal points in the column (Fig.1). Temperature plateau is clearly seen as a result of moisture evaporation.
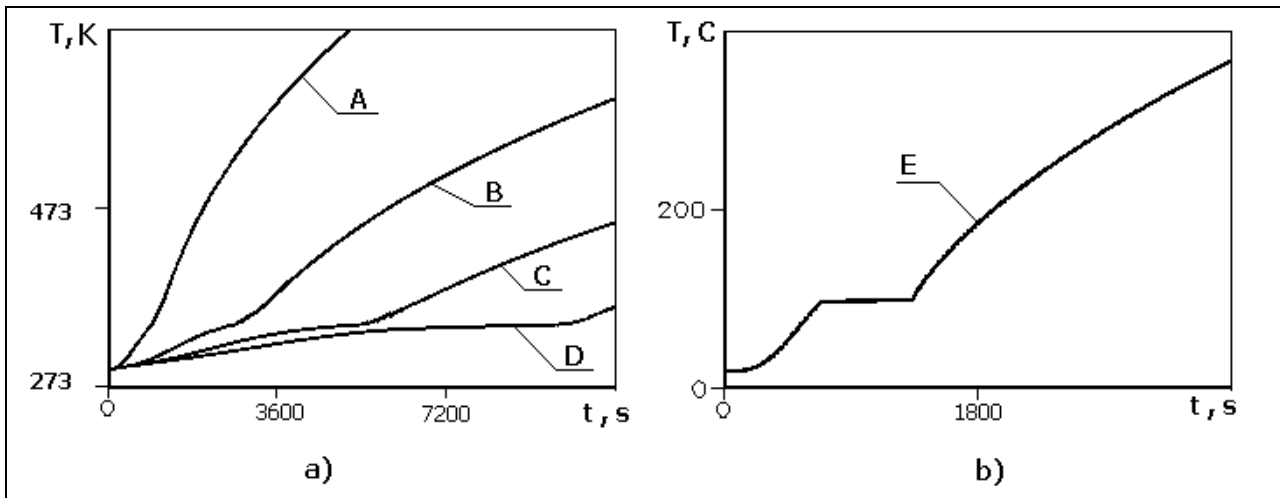
Figure 6. Time variation of temperature of different points (shown in Figure 1).

Note that the rise of pressure during evaporations of moisture and dehydration of concrete is so high that even approximate estimates (by the procedure of [7]) of the level of arising stresses indicate that they exceed substantially the ultimate strength of concrete at such temperatures [6].

CONCLUSIONS

This study involves numerical investigation of the process of formation of high-pressure zones in a layer of concrete used for biological protection of nuclear reactors as a result of gasification of crystalline moisture contained in concrete, at critical heat loads or emergency situations like fire. It has been found that the heating of concrete to a high temperature leads to intensive evolution of gas as a result of dehydration of concrete. The pressure of the gases formed in this process may reach 15×10^5 Pa. The obtained results both create prerequisites for analysis of the operating efficiency of concrete under conditions of intensive heating to temperatures close to 1100 K and serve as a basis for the development of more general models of high-temperature heat and mass transfer in concrete under conditions of critical heat loads. The obtained results further lead one to a conclusion about the possibility of using, with some modifications, mathematical models developed for theoretical analysis of heat shielding [7] when solving problems of heat and mass transfer in concrete at critical heat loads.

REFERENCES

1. Huang, C.D. and Ahmed, G.N., Int. J. Heat Mass Transfer, 1991, vol 34, p. 2535.

2. Kuznetsov, G.V., Rudzinskii, V.P. Heat and mass transfer in a layer used for protection of nuclear reactors. Materials of the international conference: The connected tasks of the mechanics and ecologies. Tomsk: Tomsk State University, 1996.

3. Kuznetsov, G.V., Rudzinskii, V.P. Heat and mass transfer in a concrete layer used for protection of nuclear reactors at critical heat loads. Reports of the All-Russia scientific conference: Fundamental and applied problems modern mechanics. Tomsk: Research Institute of Applied Mathematics and Mechanics, 1998.

4. Kuznetsov, G.V., Rudzinskii, V.P. High-temperature heat and mass transfer in a concrete layer used for protection of nuclear reactors at critical heat loads. High Temperature, 1999, vol 37, no. 5.

5. Fedik, I.I., Kolesov, V.S., and Mikhailov, V.N., *Temperaturnye polya i termonapryazheniya v yadernykh reaktorakh* (Temperature Fields and Thermal Stresses in Nuclear Reactors), Moscow: Energoatomizdat, 1985.

6. Makagonov, V.A., *Beton v usloviyakh vysokotemperaturnogo nagreva* (Concrete under Conditions of High-Temperature Heating), Moscow: Stroiizdat, 1979.

7. Pancratov, B.M., Polezhaev, Yu.V., and Rud'ko. A.K*., Vzaimodeistvie materialov s gazovymi potokami* (Interaction between Materials and Gas Flows), Moscow: Mashinostroenie, 1975.

8. Samarskii, A.A., *Teoriya raznostnykh skhem* (The Theory of Difference Schemes), Moscow: Nauka, 1983.

Developing a Model for Thermal Performance of Masonry Exposed to Fire

WELCH, S.
Fire and Risk Sciences, Building Research Establishment
Bucknalls Lane, Garston, Watford, Herts, WD2 7JR, UK

SUMMARY

This work concerns the development and validation of a simple finite-element based model for prediction of the thermal performance of masonry structures exposed to fire. Given the current period of regulatory change within Europe, which will see some traditional tabular data on fire-resistance performance eventually becoming obsolete, calculation-based methodologies may well play a more significant role in the near future. However, no extensive validations of such model-based approaches have yet been undertaken.

The challenge in modelling the fire performance of porous materials is always in adequately describing the effects of moisture, with even a small amount having a significant impact on observed fire-resistance periods. A number of advanced treatments of this phenomena have been described in the literature in recent years, but these models are generally out of reach of the average engineer. There is some evidence, though, that reasonable results might be obtained through use of simpler models which accommodate moisture movement effects by means of a modified specific heat capacity. The capabilities of such methodologies have been investigated in this study by means of a model validation exercise.

Test data was supplied by UK trade association partners. Simulation results were compared to the through-thickness measurements of temperature from 18 fire-resistance tests covering specimens of different base material (both brick and concrete based), geometry, void content and initial moisture content.

It was found that in order to reproduce the observed experimental moisture plateaux it is necessary to significantly increase the thermal conductivity values below the moisture vaporisation temperature of the material. Reasonable overall estimates of the temperature development within the material depth have been obtained, suggesting that this simple model has significant potential for use as an effective design tool.

KEYWORDS: *Fire resistance, masonry, brick, concrete, finite element, thermal model*

INTRODUCTION

The motivation for this study derives from the current regulatory change afoot within Europe with regard to the fire-resistance assessment of structures. This process will see some traditional tabular data on fire-resistance performance eventually becoming obsolete so that calculation-based methodologies may well become more important in the near future. However, such methods have as yet not been extensively validated for the case of masonry products.

Specifically, the requirements on fire resistance of structures are affected by the forthcoming adoption of new CEN standards covering both testing and product types, which will ultimately replace existing national standards. The relevant CEN standards for 'resistance to fire' testing are now in place whilst the product standard for fire resistance of masonry will soon be converted to a full EN. CEN rules require that the new standards are taken on board by national standards bodies within 6 months of their availability. For this purpose, it has been proposed that CEN regulations may be supported with a national 'equivalence table' that indicates the correspondence between the new European classes and the national classes. Tests and associated classifications conducted/awarded prior to adoption of the CEN standards will be accepted in parallel during a transition period of perhaps 10 years. However, after that date, the data pertaining to the old national tests will no longer be acceptable.

In the UK, guidance in support of the UK Building Regulations (Approved Document B) [1] makes reference to the performance of materials, products or structures in standard fire tests (i.e. BS 476 [2]) in terms of loadbearing capacity, integrity and insulation. Advice on the performance of constructions is provided in the BRE report "Guidelines for the construction of fire-resisting structural elements" (BRE, 1988) [3] and in BS 5628: Part3 (BSI, 1985) [4] for the case of masonry walls. The new European DD ENV 1996-1-2 [5] is also likely to contain tabular fire-resistance data, which is supported by more recent test results.

Much of the data in these documents relates to tests done many years ago on standard-format specimens of the day. Although the results can be supported by more recent test data, they cannot be easily adapted or interpreted to predict the fire-resistance performance of walling which is not of standard fire-test specimen configuration. However, whilst in the short term, i.e. during conversion of the ENVs to EN standards, it is likely that tabular data will be adopted, model-based solutions are a serious contender for the longer term.

Thus, availability of validated methodologies for generalising the interpretation and application of fire-resistance test data would be of great value. Given that brickwork and blockwork tend not to have a standard composition or size, the ability to generalise results, for example to different geometries or constructional forms, would be a significant advantage.

An important point is the desirability of access to methodologies that are no more complex than is necessary, so that their use might be promoted with resulting efficiencies in design.

MODELLING METHODOLOGY

Conventionally, predictions of the thermal response of solid materials exposed to fire are obtained by means of numerical methods based on 'finite element' (or 'finite difference') techniques. However, whilst such techniques are have been well-proven and extensively validated for the case of steel for example, their application to typical masonry products is significantly complicated by the fact that these materials are porous and may contain variable amounts of moisture. In this regard, even a small amount of moisture may considerably extend the fire resistance period of a masonry product, with a 5% increase in time to insulation failure per 1% increase in moisture content being a typical 'ballpark' figure [Harmarthy, T.Z. (1965) [6]] .

In recent years a number of modelling approaches have been applied to this problem, varying greatly in degree of sophistication. A number of these are briefly described in the next section.

Moisture in building elements

Under ambient conditions, masonry and concrete blockwork will normally contain a few percent of moisture. Some of the water is chemically bonded to the base material, whilst the remainder is located in pores of the material, either as liquid or vapour, and is known as 'free water'. Both components of the moisture content will move in response to applied high temperatures and affect heat transfer through the material.

Harmarthy (1965) [6] provides an overview of the chemical composition of concrete. Moisture in concrete is associated primarily with the cement paste. When moisture is present, overall heat transfer through the material will be strongly influenced by latent heat effects of water in the paste, even though the bulk thermal conductivity of the material is dominated by the aggregate matrix.

Cement paste consists predominantly of tobermorite gel (impure calcium silicate hydrate) in which small crystals of calcium hydroxide are embedded. Dehydration of the gel starts at around 93°C (200 F) and continues uninterrupted to about 871°C (1600 F). Superimposed on this is the dehydration of the calcium hydroxide, which takes place at about 427°C (800 F). Both the desorption of moisture and dehydration involve absorption of heat and hence retard flow of heat through the material.

Thus the thermal performance of different materials can be interpreted in terms of their different mineralogical compositions. For example, In autoclaved products, fine quartz added to the cement reacts with it to form crystalline tobermorite instead of tobermorite gel and there is almost no calcium hydroxide present. Normal weight concretes are fairly stable being made with gravel and sand aggregates or with crushed stone but less stable aggregates, i.e. those containing large amounts of hydrated water, undergo decomposition and dehydration reactions at higher temperatures. Lightweight concretes exhibit high chemical stability at elevated temperatures by virtue of their constitution from processed lightweight materials or industrial by-products, e.g. cinder, slag, etc. Thus, the only latent heat effects that must be considered are those associated with the dehydration of the cement paste.

The thermal conductivity of the aggregates also depends on the internal microstructure and the material composition. For highly crystalline materials, the conductivity is high at room

temperature and decreases with rise of temperature whereas amorphous aggregates (e.g. traprock, basalt) have a lower conductivity at room temperature and this rises with temperature. At high temperatures (>800°C), the difference substantially disappears. Thus depending on the mineralogical changes occurring on heating, materials might be expected to exhibit different variations in thermal conductivity.

There are many literature reports of physical properties for building elements, though values which take account of temperature and moisture effects are rather scarce. Harmarthy (1988) [7] reviews information on the properties of building materials, including concrete and brick, with particular reference to high temperature (fire exposure) conditions. The review contains useful information on the temperature dependence of the thermal properties of various types of concrete over the range 0 to 1000°C, but does not provide this information for brick. The International Energy Agency have collated information on material properties (IEA Annex 24, Task 3 - Kumaran, 1996) [8]. Also, Schneider (1985) [9] reported properties of concrete at high temperatures and Garvin (1994) [10] refers to the material properties of aircrete blocks.

Moisture movement in porous materials

When subject to sufficient heat, the liquid water in the pores, and eventually the chemically-bound water, evaporates, giving rise to an increase in the pore pressures. The effect of the gradients in temperature, pore pressure and mass concentration is such that water vapour will be forced to move through the material.

Diffusion processes must consider the possibility of both liquid- and vapour-phase moisture transfer [Phillipson (1996) [11]]. The diffusion processes of the gas and liquid phase are driven by gradients in the respective pressures (i.e. the vapour and capillary pressure) and the moisture in the dominant phase at a particular time/location moves to equilibrate the relevant pressure field across the material. Thus, the description of moisture transport under unsaturated conditions is complicated by the fact that the proportions of each phase cannot be easily determined experimentally and also by hysteresis effects. Thus, simple mathematical descriptions are precluded. Nevertheless, some theoretical treatments have been developed based on the basic laws describing diffusion of each phase through a porous medium.

Modelling methodologies

Reviews of the relevant literature have been provided by Harada & Terai (1988) [12], Šelih et al. (1994) [13], Ahmed & Hurst (1995) [14] and Huang et al. (1996) [15].

Some early model were proposed which made no explicit reference to moisture effects, including the finite element model of Bizri et al. (1974) [16], called FIRES-T, and the model of Ellingwood et al. (1991) [17], both applied to reinforced concrete. Lie et al. (1994) [18] report predictions of the thermal response of a clay brick wall to fire, where it was assumed that the moisture content if the brick was negligible. The predicted temperature gradients within the wall did show a good agreement with experiment.

Other models have been proposed which do attempt to explicitly account for moisture effects, but which make no attempt model the mass transfer of the moisture within the material. Harada & Terai (1988) [12] refer to the early Japanese models of Kawagoe (1965) [19], Wakamatsu (1965) [20], and Fujii (1965) [21] which were all applied to the prediction

of temperature histories of concrete in the case of fire. Though latent heat effects were accounted for, these models neglected the conservation of the water vapour; despite this simplification, the models give reasonable results for engineering purposes.

In the late 1960's and early 1970's, Harmarthy et al. published extensively on the model studies of brick [e.g. Harmarthy, T.Z. (1965) [6], Harmarthy, T.Z. (1970) [22], Harmarthy, T.Z. & Allen, L.W. (1971, 1972) [23,24]], again considering heat absorption effects but neglecting moisture motion per se. A method was derived for determining the fire endurance at some given moisture content, if the fire endurance in the dry condition is known or vice versa [Harmarthy, T.Z. (1965) [6]].

A number of other researchers have described similar models for moisture effects, including Saito & Seki (1977) [25], Wang & Yu (1988) [26], Motakef et al. (1986) [27], Rubin & Schweitzer (1972) [28], Lie et al. [e.g. Lie, T.T. (1984) [29], Lie, T.T. (1992) [30], Lie, T.T. et al. (1994) [31]], Franssen (1986) [32] and Hamerlinck & Twilt (1990) [33].

Of particular note is the model proposed by Wickström (1979) [34], known as TASEF, which has found fairly extensive application in prediction of the response of steel and composite structures for fire. TASEF uses temperature-dependent conductivity and specific heat values and employs a modified enthalpy to account for the effect of moisture subjected to evaporation in concrete. Anderberg & Forsén (1982) [35] have applied this model in conjunction with a model for structural response of the concrete, for prediction of the thermal response of various plate strips. A good agreement is shown in terms of temperature and this was earlier documented by Anderberg & Haksever (1982) [36].

Thermal conductivity effects

The presence of small amounts of water can have a profound effect on the effective specific heat capacities of different materials and hence on the overall heat transfer. However, thermal conductivities are also affected by moisture, with the value for moisture-containing specimens being much greater than that of the dry material even at quite low concentrations. It is therefore essential to account for thermal conductivity dependencies on moisture concentration, particularly in the simple lumped parameter models which neglect moisture migration itself.

Some values and relationships for the thermal conductivity of moisture-containing materials can be found in the literature. Volume 3 of the International Energy Agency report on Heat, Air and Moisture Transfer in Insulating Envelop Parts (HAMTIE) is devoted to materials properties (Kumaran, 1996) [8], and includes data for brick, concrete, lightweight concrete, aerated concrete, mortars etc. In addition to data, relationships are given for the thermal conductivity in terms of the moisture content:

$$k = k_o + Aw\rho$$

where: k is the effective thermal conductivity [W/m/K]
k_o is the thermal conductivity at dry conditions [W/m/K]
A is an empirical constant [Wkgm^2/K]
w is the water content [kg/kg]
ρ is the material density [kg/m^3]

Values of the parameter A are given as follows:

Material	Density [kg/m^3]	Temperature [ºC]	A [Wkgm^2/K]
Concrete	2200	20	3.20e-3
Lightweight concrete	1158-1187	20	2.55e-3
Lightweight concrete	1130-1138	20	1.04e-3
Lightweight concrete	644-674	20	1.50e-3
Aerated concrete	598-626	10	0.801e-3
Aerated concrete	598-626	20	0.980e-3
Aerated concrete	455-492	20	0.904e-3

Table 1 - Values of empirical constant in thermal conductivity expression

Thus, the effect of additional moisture on the thermal conductivity appears to be greater for the heavier materials.

The form of this equation implies a linear relationship between the moisture concentration and the enhancement in thermal conductivity. However, inspection of the individually measured values in the IEA report shows that the true relationship is highly non-linear, with a significant enhancement in conductivity between the dry value and the value at the lowest moisture level (e.g. 63%, 25% and 88% increases in thermal conductivity for 1% moisture in concrete, 0.8% moisture in lightweight concrete and 5% moisture in aerated concrete respectively) and a progressive reduction at higher levels. Therefore, it might be necessary to use non-linear expressions.

Other empirical equations have been suggested, see for example Kingery (1960) [37] and Ahmed and Hurst (1996) [14].

Models accounting for energetic moisture effects, including migration

A number of recent models have been proposed which track moisture movement through the porous medium. Modelling the mass transfer of the moisture introduces considerably more complexity to the problem, since this movement is function of pressure gradients within the material, amongst other things. This generally introduces a requirement for some sort of representation of the state of balance between gaseous and liquid water within the material, which in turn is a function of the local thermodynamic conditions.

Harada & Terai (1988) [12] refer to various early models which account for the movement of liquid and vapour-phase water, including those which have considered both the desorption of physically-adsorbed water and the decomposition of that which was chemically-bound. The model developed by these authors also describes both:

- reversible evaporation of adsorbed water in pores
- irreversible thermal decomposition of chemically adsorbed water

The details of the mechanism for decomposition are not known, but a satisfactory representation of the process can be achieved by means of an empirically-calibrated Arrhenius expression.

In the model of Ahmed & Hurst (1995) [14] it is assumed is that the mobility of the liquid is negligible compared to that of the gaseous mixture. Local equilibrium moisture content is related to the relative vapour pressure and temperature according to a constitutive relation expressed as a set of sorption isotherms. Convective mass transfer is driven by pore pressure gradients and diffusive mass transfer is driven by concentration gradients

Šelih et al. (1994) [13] proposed a detailed model including the free-water flow, adsorbed (bound) water movement and water vapour and air migration. The mass production rate of water vapour is coupled to pressure effects via the continuity equation, which involves the liquid and gaseous water velocities. These velocities are determined from Darcy's law, using appropriate permeability and viscosity constants.

The results were compared to those of two different (simpler) heat transfer models due to Hamerlinck & Twilt (1990) and Franssen (1986). These show that there is little difference in the results in higher temperature regions and even in lower temperature regions beyond an hour or so into the test. Nevertheless, the discrepancy in the temperature region 300-450K in the period up to 1 hour could be significant.

Huang et al. [15] refer to the early work of Sahota (1979) [38] who performed an analysis of the orders of magnitude of terms in the governing equations. This showed that some of the processes described by the more complex models may be reasonably neglected, to a first approximation. The results obtainable from the simpler models, neglecting the movement of moisture *per se* and making no attempt to describe the pore pressure distribution within the solids, may compare favourably with those of the complex models under some circumstances. Thus, in this study, moisture effects were accommodated via the simple methods based on enhanced specific heat values, together with appropriate modification of the thermal conductivities.

MODEL VALIDATION

Data from 33 tests has been identified, amongst which there are 13 for brick, 3 for concrete and 2 for aerated concrete for which through-thickness temperature measurements are reported[1]. Thus there are 18 tests which are well-suited to the model development and validation tasks because of the additional benefit of such data in the fitting of material properties.

A model validation exercise has been undertaken based on test data from these 18 fire resistance tests on specimens of different base material, geometry, void content and initial moisture content. Some basic details about the test specimens are set out in Tables 2 and 3. The precise descriptions of the products cannot be divulged but basic physical characteristics are provided in the table to inform in the interpretation of the results.

---

[1] Test data was supplied by UK trade associations, the Brick Development Association (BDA), the Concrete Block Association (CBA) and the Aerated Autoclaved Concrete Products Association (AACPA).

Test	Brick/block	No. of holes per unit	Initial moisture content (%)
Bricks			
1	A1	Solid	1.1
2	A2	Solid	0.6
3	A1	Solid	5.5
4	B	Solid	1.4
5	C	3	1.0
6	C	3	1.1
7	B	3	5.2
8	B	10	4.7
Concrete products			
9	A	Solid	12.6
10	B	Solid	1?
11	C	2	3.0
12	D	Solid	2.8

Table 2 - Test summary

Brick	Density (kg/m^3)	Thickness (mm)
A1	1650	103
A2	1650	215
B	1990	103
C	1880	103

Block	Product type	Density (kg/m^3)	Thickness (mm) (including render thicknesses)
A	aerated	430	75
B	light-weight aggregate	1550	100+2x(11+2)=126
C	light-weight aggregate	1300	140
D	dense aggregate	1965	100x2+10=210

Table 3 - Summary data on test materials

Model parameters

The use of 'modified' material property values is not a simply a "curve-fitting exercise" but does embody some fundamental physical principles. Notwithstanding this, there are some implicit assumptions built-in to the method and it is useful to consider these and their significance.

When specific heat and thermal conductivity are correlated directly to temperature, there is an implicit decoupling of the moisture concentration parameter itself, such that this is assumed to be directly correlated to the temperature. However, if water is actually moving through the material depth, it is possible that this assumption might be violated. This will

depend on heating rate, amongst other things and the extent to which assumption might be expected to breakdown will have a direct bearing on the anticipated accuracy of such models.

Specific heat modification

A simple approach based on modified specific heat and thermal conductivity has been adopted, using the former parameter to represent both the specific heat itself and latent heat effects. However, unlike the latent heat effect in a pure material at atmospheric pressure, where temperature takes a single constant value during the phase change process, a range of temperatures are found to apply during the evaporation in porous masonry. This is because the boiling point of water is a function of pressure, and the usual value of 100°C can be exceeded by up to 80°C due to a pressure rise of 10 atmospheres. The results of Ahmed & Hurst (1995) showed that pore pressures as high as 6 atmospheres may occur in a typical concrete specimen, and the experimental evidence cited by Anderberg & Haksever (1982), suggests that the boiling point of water in concrete is typically in the range 100 to 140°C.

Therefore, in this study a temperature range of 100 to 140°C has generally been assumed for latent heat effects, though this is a variable parameter in the model.

The upper and lower temperature bounds of the moisture loss regime are set as T_{upper} and T_{lower}, and the midpoint is determined as $T_{mid} = (T_{upper} + T_{lower})/2$.

$$c'_p = 2w \left[\frac{2L}{(T_{upper} - T_{lower})} + c_p \right] \left[\frac{T - T_{lower}}{T_{upper} - T_{lower}} \right]^2 , T_{lower} \leq T < T_{mid}$$

The effective specific heat is thus determined as:

$$c'_p = 2w \left[\frac{2L}{(T_{upper} - T_{lower})} + c_p \right] \left[\frac{T_{upper} - T}{T_{upper} - T_{lower}} \right]^2 , T_{mid} \leq T < T_{upper}$$

and

where: L is the latent heat capacity of water (2.176x10^6 J/kg)
            T is the relevant temperature [K]
            w is the moisture content of the material [kg/kg]

This equation includes an additional scaling factor representing the fact that as the temperature rises, the influence of the moisture progressively reduces due to loss through evaporation. A linear loss over the temperature range of 'boiling' is assumed.

Thermal conductivity modification

Reference was made to the International Energy Agency Annex 24, Task 3 on "Material properties" (Kumaran, 1996) [8]. Various values are given for the thermal conductivity values of brick, concrete, lightweight concrete and aerated concrete at different moisture contents. As noted in Annex 1 of this document, section 2.3.3.1, the value varies with temperature in a non-linear manner, with the largest increase being from the dry condition to the first increment of moisture concentration and a progressive reduction in the steps

thereafter. Linear expressions have been proposed (see section 2.3.3.1), which incidentally indicate that the influence of moisture is roughly in proportion to the density of the base material, but these seem inappropriate.

Therefore, the literature values have been plotted against moisture concentration, see Figure 1. Some dependence on overall material density might be expected, but on normalising further by the respective density values:

> concrete: 2270 kg/m³
> lightweight concrete: 1600 kg/m³
> aerated concrete: 700 kg/m³
> brick: 1800 kg/m³
> lightweight brick: 767 kg/m³

the curves are not collapsed onto a single line.

A best fit curve was fit to the test data in figure 1. Though very approximate, this curve does embody some of the dependence on moisture effects observed in measurements of effective thermal conductivities. The equation for the best fit curve is:

$$k' = k_o (M + 1)^{0.26}$$

where: k_o is the thermal conductivity value for dry conditions [W/m/K]
M is the moisture content of the material [%]
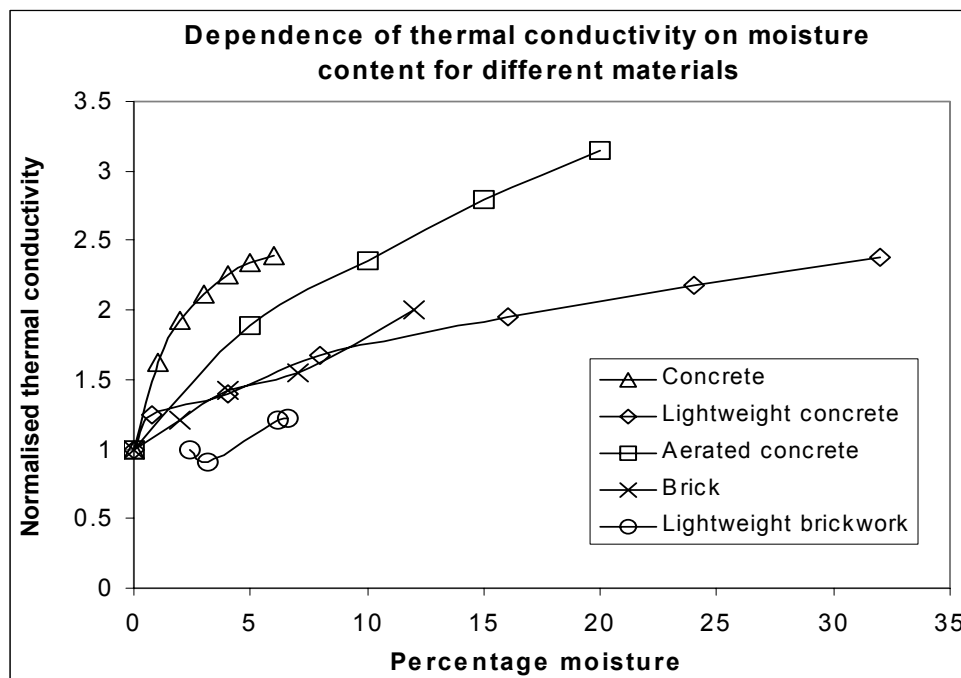
Figure 1 - Normalised thermal conductivity v percentage moisture [IEA Annex 24, Kumaran, 1996]

Assessment of material properties from test data

Some of the key parameters in the simple thermal model were fit by comparison with the test data. Thus, simulations have been run of all of the test cases listed in the upper part of Table 1 (section in italics) and the results carefully compared to the test data.

The basic value of the specific heat capacity of each material is fairly easy to set, since the literature values indicate that there is a fairly narrow range across these types of products [IEA Annex 24, Kumaran, 1996]. The values assumed are listed in Table 3:

Material	Base specific heat capacity [J/kg/K]
Brick	840
Concrete	880
Aerated concrete	1000

Table 4 - Approximate values for specific heat capacity from literature [IEA Annex 24, Kumaran, 1996 [8]]

Thereafter, the main variable parameters are the surface heat transfer parameters (convective heat transfer coefficient and emissivity) and the effective thermal conductivity of the material. Of these, the latter is probably the most critical in terms of prediction of fire resistance periods, and investigations were made into the appropriate values to use in the case of each test material.

The procedure for obtaining an equivalent empirical value is to undertake curve-fitting comparisons with experimental data. The values for low moisture conditions, i.e. the higher temperature regimes and locations nearer to the exposed side of the specimen, are most useful, since in many cases, the interfering effects of the moisture itself are negligible over a substantial proportion of the test period.

In the course of this exercise, it was found that the enhancement to the thermal conductivity due to moisture was insufficient to give a good match to the temperature histories at the rear of the specimen. In most cases, the temperature at the rear of the specimen had begun to rise significantly within an hour of the start of the test. The only way that this could be achieved in the model was by enhancing the thermal conductivity at temperatures below the boiling range. When this was done, with the thermal conductivity being increase by a factor increasing from unity to ten over the temperature range between ambient and the boiling point (and set back to the default again thereafter), much improved matches to the rear surface time-temperature curve could be achieved.

It is not clear precisely why such a large enhancement to the anticipated values was required but it is perhaps some significant transfer of heat taking place by the moisture transfer itself. Thus, hot vapour moving through the specimen heat up material at the rear, particularly if there is a saturated region blocking its exit, so that the effective thermal conductivity is increased. Particularly towards higher temperatures, there are further uncertainties associated with the likely variations in the thermal conductivity values due to decomposition

and chemical changes (referred to above) and these have not yet been incorporated in any systematic manner. Thus more investigation is required to clarify exactly what is occurring. Checks on sensitivities to timestep[2] and number of mesh refinements were performed on a regular basis so as to ensure that there are no significant numerical errors in the results.

The computational mesh adopted for one of the voided brick specimens is shown in Figure 2 below.
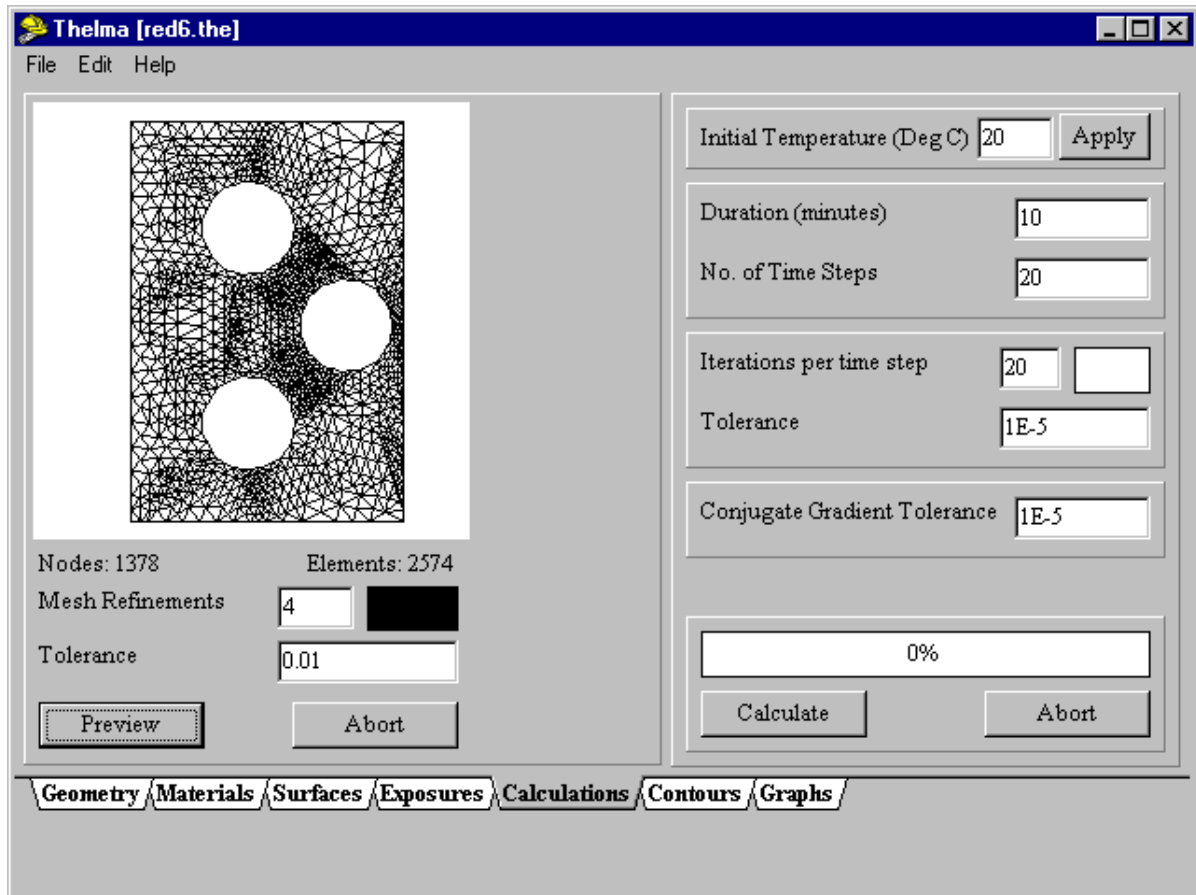
Figure 2 - computational mesh for a brick test case

Figures 3 to 5 (over) show comparisons of the simulation results with the experimental data for 12 selected test cases. These cases were chosen from the eighteen mentioned earlier by neglecting a number which were duplicate tests together with some for which the quality of the test data was rather uncertain. Also, there has been no tuning of the model from one case to another other than in the selection of an appropriate base value of the thermal conductivity for each material, as referred to above.

For each specimen , two graphs are provided - the first (on the left of the page) being an overview of the whole test and the second, on the right, being a more detailed plot of the time-temperature histories in the region of most interest, i.e. below about 150°C. Figure 3 shows data for solid brick materials, figure 4 relates to voided brick materials and figure 5 summarises the results for the concrete-based products (cf Table 2 above).

---

[2] Generally, two iterations per timestep were found to be sufficient

For these particular cases, the best fit to the time-temperature curves was achieved with a base thermal conductivity values spanning 0.1 for the aerated concrete, with 0.3 for most of the bricks, and up to 1.2 for the heaviest concrete.

The temperature profiles throughout the material depth are reproduced reasonably well and the temperature plateau can be clearly seen in the predictions.

It should be noted that there were a number of further assumptions and uncertainties in this comparative exercise. One of these concerns the precise location of the thermocouples in the test specimen. No information was available as to where these were located with respect to the mortar joints, and in the case of the voided specimens, to the holes. Figure 6 (from Test 5) below gives an indication of the magnitude of this effect, with time temperature curves shown for a midpoint between holes and directly adjacent to the void.
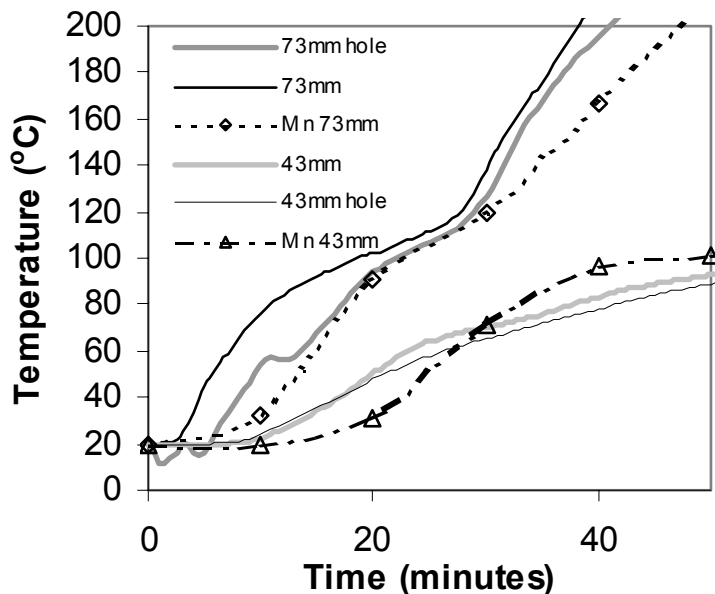
Figure 6 - effect of holes on temperature

In addition the effects of the rendering on some of the test specimens have been neglected, and all simulations were run from a starting temperature of 20°C for simplicity, whereas in reality, some tests began at close to 0°C.
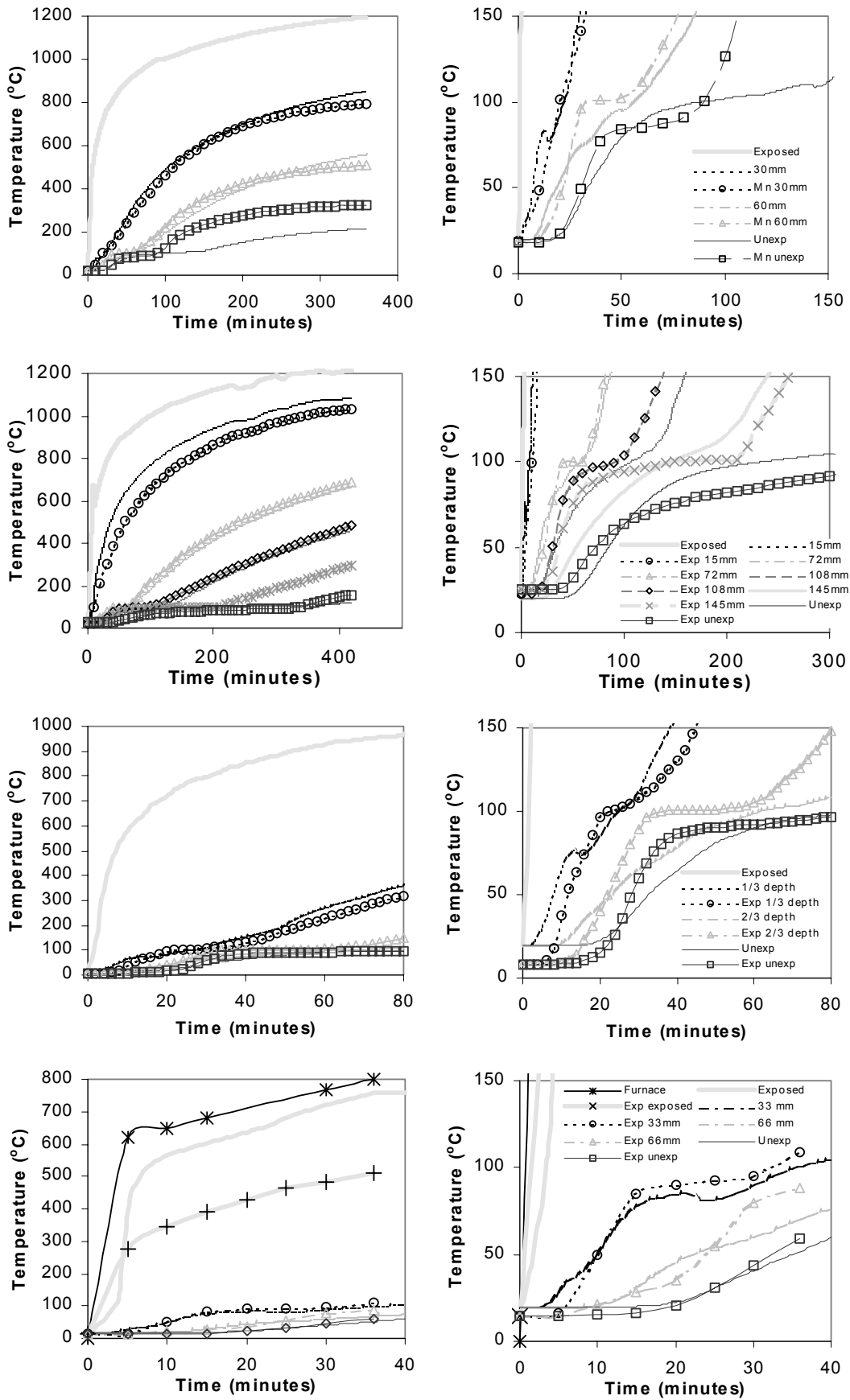
Figure 3 - Comparison of simulation and experiment for tests 1-4 (solid Brick units)
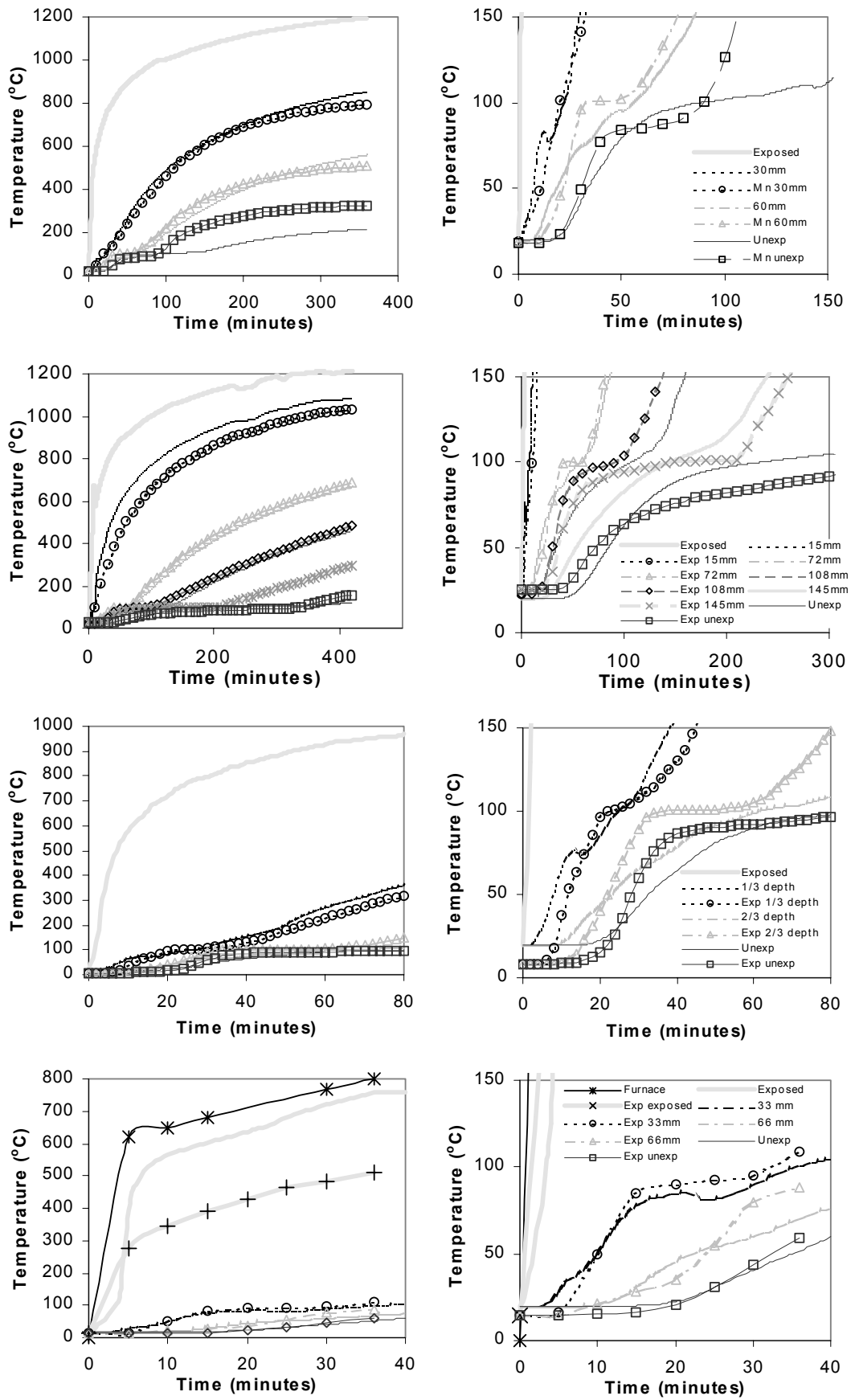
Figure 4 - Comparison of simulation and experiment for tests 5-8 (voided Brick units)
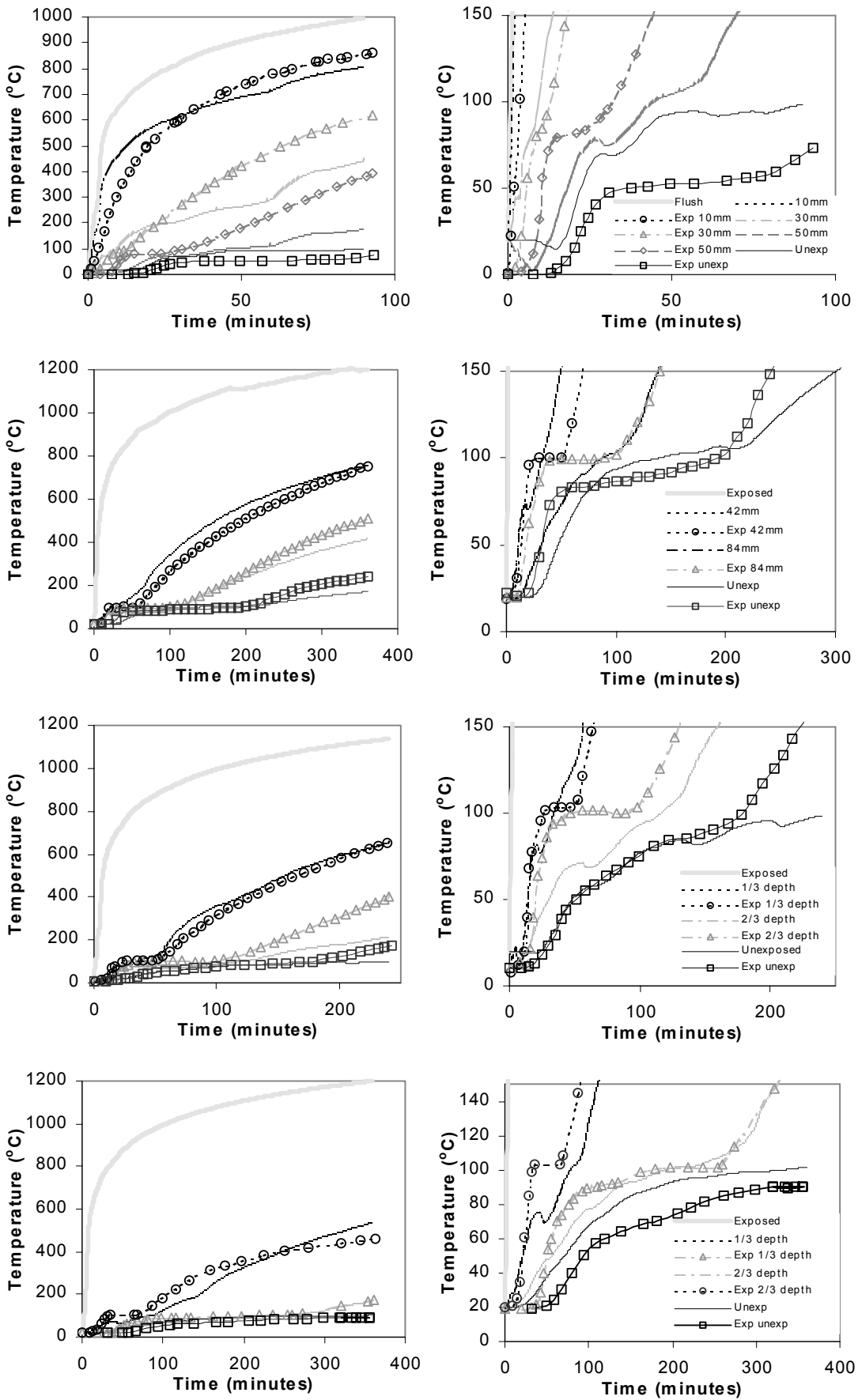
Figure 5 - Comparison of simulation and experiment for tests 9-12 (concrete-based units)

CONCLUSIONS

A review of the relevant literature has assisted in identifying an appropriate modelling methodology for representation of moisture effects. Regarding the essential features of a satisfactory methodology, it can be concluded that it is not strictly necessary to represent all of the relevant physical mechanisms in order to obtain reasonable agreement with experiment. Some of the processes described by the more complex models such as the effect of pore pressure on moisture movement may be neglected, to a first approximation.

Rather, comparative predictions suggest that it may be possible to obtain satisfactory results when the moisture movement itself is neglected, such that the moisture effects are accommodated only by varying the relevant thermal properties of the material, i.e. by means of an additional source term in the energy equation to represent latent heat effects. In addition, it is necessary to include a moisture concentration correction to the thermal conductivity.

In the validation exercise, it was found that in order to reproduce the observed experimental moisture plateaux it is necessary to significantly increase the thermal conductivity values below the moisture vaporisation temperature of the material. Reasonable overall estimates of the temperature development within the material depth have been obtained, suggesting that this type of model has potential for use as an effective design tool.

NOMENCLATURE

A	empirical constant
c_p	specific heat capacity [J/kg/K]
c'_p	effective (moisture-corrected) specific heat capacity [J/kg/K]
k	thermal conductivity [W/m/K]
k'	effective (moisture-corrected) thermal conductivity [W/m/K]
L	latent heat of steam [2176 kJ/kg]
M	moisture content as a fraction of the dry weight [%]
T	temperature [K]
T_{lower}	lower range of moisture evaporation [K]
T_{mid}	midpoint in range of moisture evaporation [K]
T_{upper}	upper range of moisture evaporation [K]
w	water content [kg/kg]
ρ	density [kg/m^3]

Subscripts

o	at dry conditions

ACKNOWLEDGEMENTS

REFERENCES

1. "Building and Buildings", The Building Regulations, 1991, HSMO

2. BS 476: Part 20: 1987, Fire tests on building materials and structures, Method for determination of the fire resistance of elements of construction (general principles), British Standards Institution, 1987

3. Morris, W.A., Read, R.E.H., Cooke, G.M.E., "Guidelines for the construction of fire-resisting structural elements", Building Research Establishment Report, BR 128, 1982

4. BS 5628: Part 3: 1985 "Materials and components, design and workmanship", British Standards Institution, 1985

5. Eurocode 6: "Design of masonry structures", Part 2, DD ENV 1996-1-2, CEN

6. Harmarthy, T.Z. (1965) "Effect of moisture on the fire endurance of building elements", ASTM STP 385, p. 74

7. Harmarthy, T.Z. (1988) "Properties of building materials", in The SFPE Handbook of fire protection engineering, 2nd edition, section 1/chapter 26, pp. 378-391, NFPA, Quincy, Massachusetts

8. Kumaran, M.K. (1996) "Task 3: Material properties", Heat, air and moisture transfer through new and retrofitted insulated envelope parts (HAMTIE), Final Report, volume 3, IEA Annex 24

9. Schneider, U. (ed.) (1985) "Properties of materials at high temperatures - concrete", RILEM

10. Garvin, S.L. (1994) "Mortar and movement in aircrete blockwork: a review", BRE Occasional Paper 62/94, November 1994

11. Phillipson, M.C. (1996) "Effects of moisture in porous masonry", Building Research Establishment Literature Review, BR 304

12. Harada, K., Terai, T. (1988) "Numerical simulation of fire resistance test of a concrete slab", Proc. 2nd Int. Symp. on Fire Safety Science, pp. 707-717

13. Šelih, J., Sousa, A.C.M., Bremner, T.W. (1994) "Moisture and heat flow in concrete walls exposed to fire", Journal of Engineering Mechanics, vol. 120, no. 10, Oct. 1994

14. Ahmed, G.N., Hurst, J.P. (1995) "Modeling the thermal behaviour of concrete slabs subjected to the ASTM E119 standard fire condition", J. of Fire Prot. Engr., vol. 7, no. 4, pp. 125-132

15. Huang, Z., Platten, A., Roberts, J. (1996) "Non-linear finite element model to predict temperature histories within reinforced concrete in fires", Building and Environment, vol. 21, no. 2, pp. 109-118

16. Becker, J., Bizri, H., Bresler, B (1974) "FIRES-T: a computer program for the fire response of structures - thermal", Report No. UCB FRG 74-1, University of California, Berkeley, CA

17. Ellingwood, B., Lin, T.D. (1991) "Flexure and shear behaviour of concrete beams during fires", Journal of structural engineering, vol. 117, no. 2, pp. 440-458

18. Lie, T.T., Gosselin, G.C., Kim, A.K. (1994) "Applicability of temperature predicting models to building elements exposed to room fires", J. Applied Fire Science, vol. 4, no. 2, pp. 83-93, 1994-1995

19. Kawagoe, K. (1965) "Calculation of temperature in double-layer walls heated from one side", Bulletin of the Fire Prevention Society of Japan, vol.13, no. 2, pp. 29-35

20. Wakamatsu, T. (1965) "Heat flow analysis of building members during fire exposure", Trans. Architectural institute of Japan, vol. 109, pp. 73-79 and vol. 111, pp. 31-36

21. Fujii, S. (1965) "The theoretical calculation of temperature of thermally protected steel column exposed to the fire", Bull. Of Fire Prevention Society of Japan, vol.13, no. 1, pp. 13-21

22. Harmarthy, T.Z. (1970) "Thermal performance of concrete masonry walls in fire", ASTM STP 464, p. 209

23. Harmarthy, T.Z., Allen, L.W. (1971) "Thermal performance of concrete masonry walls in fire", CBD-140

24. Harmarthy, T.Z., Allen, L.W. (1972) "Thermal performance of concrete masonry walls in fire", Fire Technology, vol. 8, no. 2, pp. 142-148

25. Saito, H., Seki, N. (1977), "Mass transfer and pressure rise in moist porous material subjected to sudden heating", Journal of Heat Transfer, vol. 99c, pp. 105-112

26. Wang, B.X., Yu, W.P. (1988) "A method for evaluation of heat and mass transport properties of moist porous media", International Journal for Heat and Mass Transfer, vol. 31, pp. 1005-1009

27. Motakef, S., El-masri, M.A. (1986) "Simultaneous heat and mass transfer with phase change in a porous slab", International Journal for Heat and Mass Transfer, vol. 29, pp. 1503-1512

28. Rubin, A., Schweitzer, S. (1972) "Heat transfer in porous media with phase change", International for heat and mass transfer, vol. 15, pp. 43-60

29. Lie, T.T. (1984) "A procedure to calculate fire resistance of structural members", Fire and Materials, vol. 8, no. 1, pp. 40-48

30. Lie, T.T., (ed.) (1992) "Structural fire protection", Manuals and reports on engineering practice No. 78, American Society of Civil Engineers, New York, 1992

31. Lie, T.T., Gosselin, G.C., Kim, A.K. (1994) "Applicability of temperature predicting models to building elements exposed to room fires", J. Applied Fire Science, vol. 4, no. 2, pp. 83-93, 1994-1995

32. Franssen, J.M. (1986) "Etude du comportement au feu des structures mixes acier-beton", These du Docteur en Sciences Appliquées, Université de Liège, Faculté de Science Appliquées, Liège, Belgium (in French)

33. Hamerlinck, A.F., Twilt, L. (1990) "A thermal model for fire-exposed composite steel/concrete slabs", Advanced computational methods in heat transfer, Amsterdam, The Netherlands, vol. 3, pp. 133-144

34. Wickström, U. (1979) "TASEF-2 - A computer program for temperature analysis of structures exposed to fire", Dept. of Structural Mechanics, Lund Institute of Technology, report no. 79-2, Lund, Sweden

35. Anderberg, Y., Forsén, N.E. (1982) "Fire resistance of concrete structures", in Nordic Concrete Research, ed. "The Nordic Concrete Federation", publication no. 1, Oslo, Dec. 1982

36. Anderberg, Y., Haksever, A. (1982) "Comparison between measured and computed structural response of some reinforced concrete columns in fire", Fire Safety Journal, vol. 4 (1981/82), pp. 293-297, Lund Institute of Technology and Technical University, Braunschweig

37. Kingere, W.D. (1960) *An introduction to ceramics*, John Wiley, New York

38. Sahota, M.S., Pagni, P.J., "Heat and mass transfer in porous media subjected to fires", International Journal for Heat and Mass Transfer, Vol.22, pp.1069-1081, 1979

A SCHEME FOR VERIFICATION OF COMPUTER CODES FOR CALCULATING TEMPERATURE IN FIRE EXPOSED STRUCTURES

Pålsson, J. and Wickström, U.

SP Fire Technology, P.O. Box 857, SE-501 15 Borås, Sweden, Telephone: +46 33 16 50 00, Telefax: +46 33 41 77 59, E-mail: johan.palsson@sp.se, Internet: http://www.sp.se

SUMMARY

A number of benchmark reference cases have been suggested for verification of two dimensional temperature calculation computer codes based on the finite element or finite difference methods. First a simple reference case is suggested where an analytical solution is available then more complex cases are introduced assuming non linear boundary conditions and material properties varying with temperature. Finally, cases dominated by heat transferred by radiation in internal voids are defined.

Solutions of all the suggested benchmark reference cases have been modeled numerically with various numbers of elements. The intention is that specialists offering similar computer codes, particularly for fire safety engineers, should have the possibility to carry out similar calculations with given input data and compare the obtained results. Such comparative calculations could then form a basis for discussions on validity and accuracy of various computer codes.

Key words: *temperature calculation, fire, finite element, verification, computer calculation*

INTRODUCTION

Theoretical analysis is gradually more often used to assess fire resistance of structures. A very important step in such an analysis is to evaluate the temperature rise in the structure. Several computer codes are available but their validity and accuracy are sometimes questioned by authorities and certifying bodies.

The quality of an analysis could be verified by considering the validity of the calculation model, the accuracy of used material properties and the accuracy and reliability of the computer code in itself.

- The first point is of course important. Effects of spalling or water migration can for instance not be considered with a code just based on heat transfer according to the Fourier heat transfer equation.
- The second point is crucial. Errors in material property input will certainly be transmitted into output errors. But accurate material properties are often not available even for common materials, and methods for measuring material properties at high temperature are not readily available.
- Finally the verification of the computer code itself. By definition *verification* is here meant: "The process of determining that a model implementation accurately represents the developer's conceptual description of the model and the solution to the model" (see Guide for Verification and Validation of Computational Fluid Dynamics Simulations, AIAA, Guide G-077-1998).

The present paper is focused on the verification of computer codes. A scheme including 8 reference cases of various levels of complexity is suggested to show the expected accuracy in this kind of calculations. It is mainly developed for finite element codes but it may also be used for codes based on finite difference principals. The first reference example is a linear problem which can be solved analytically. When increasing the number of elements the results should converge to the correct value. Similar type of so called patch tests are then suggested for a number of non-linear problems. The principal of this type studies is that codes yielding results that converge smoothly when increasing the number of elements are generally reliable for the type of problems considered. At least it can be seen as a good indication. The scheme suggested here employs problems which are relevant for fire safety engineering including effects of conductivity varying with temperature, latent heat, radiant heat transfer boundary conditions and combinations of materials, concrete, steel and mineral wool. One reference case suggested is the evaluation of a special feature available only in some codes, heat transfer by radiation in voids. The last case is a steel section insulated by boards given rise to voids as in practice. The computer code TASEF [1] has been used to evaluate the suggested scheme.

SCHEME WITH REFERENCE CASES OF VARIOUS LEVELS OF COMPLEXITY

The scheme includes eight reference cases with various level of complexity. The reference cases employ problems which are relevant for fire safety engineering and consider effects of conductivity varying with temperature, latent heat, radiant heat transfer boundary conditions and combinations of materials such as concrete, steel and mineral wool.

The first reference case is a linear problem which has an exact analytical solution in terms of non-dimensional variables. All the other reference cases are non-linear and exact solutions are not available. One of the reference cases deals with the evaluation of a special feature available only in some codes, heat transfer by radiation in voids. The last reference case is a steel section insulated with boards which deals with heat transferred by radiation and convection between interior surfaces of voids.

The calculations have been done with an increasing number of elements. In most cases meshes with 4, 16, 64 and 256 elements were used.

Reference case 1 - Comparison against analytical results, constant material properties
One quarter of a square section with an initial temperature of 0 °C is subjected to ambient gas temperature T_∞ = 1000 °C, see figure 1.
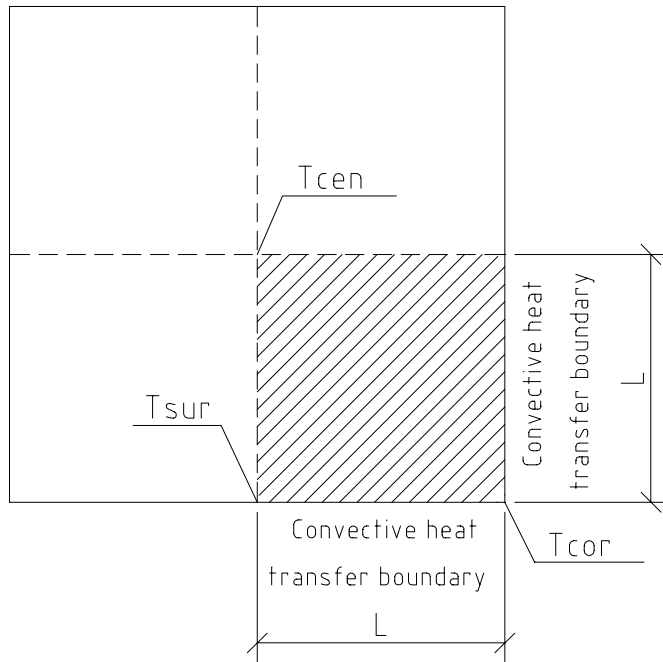
Figure 1 **Quarter of a square with an initial temperature T_i = 0 °C and a surrounding ambient gas temperature T_∞ = 1000 °C.**

The heat transfer at the boundaries to the body surface is given as h $(T_\infty - T_S)$ where h is a heat transfer coefficient assumed constant, T_∞ is the surrounding ambient gas temperature and T_S is the current surface temperature. The convergence of the centre temperature T_C for increasing number of elements n is compared with analytical solutions [5] based on dimensionless time $Fo = at/l^2$ in table 1 where a is the thermal diffusivity $a = k/c\rho$ = 1, t is the time and l is the length of the body side.

Table 1   Constant material properties: Comparison between results from calculations performed with the computer code TASEF and analytical solutions.

Dimensionless time *Fo*	*n* = 4	*n* = 16	*n* = 64	*n* = 256	Analytical
	T_{cen}	T_{cen}	T_{cen}	T_{cen}	solutions
0.1	978	984	986	986	986
0.2	903	904	904	904	904
0.4	703	694	691	691	690
0.6	528	518	516	515	515
0.8	393	386	384	384	383
1	293	287	285	285	285

Reference case 2 - *Non-linear boundary conditions and constant material properties*

A concrete square section with half side length l = 0.1 m and an initial temperature of 0 °C is subjected to a constant fire temperature of 1000 °C or alternatively to the standard-time temperature curve according to ISO 834 [6], see figure 2.
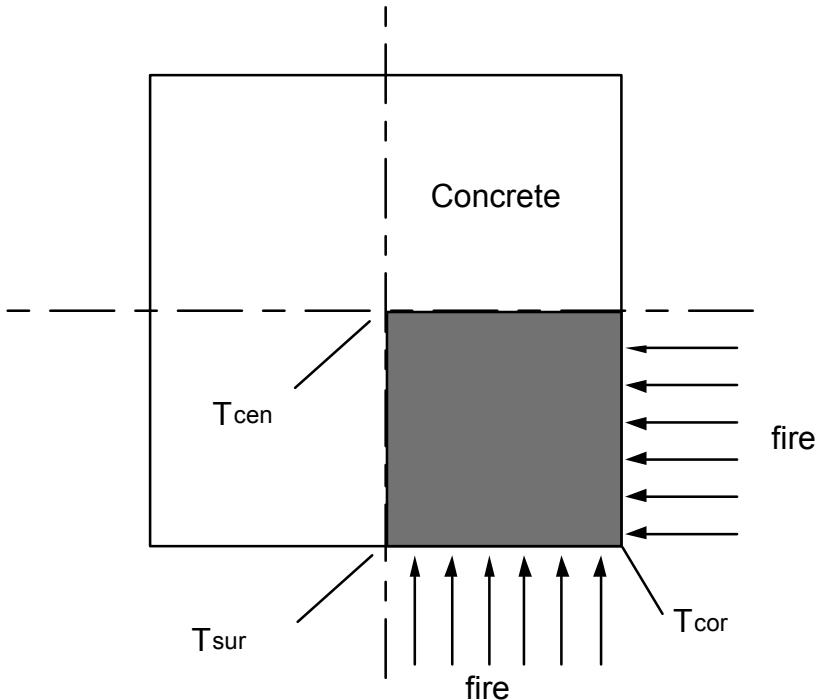
Figure 2   **A concrete square section with half side length l = 0.1 m.**

The thermal properties of the concrete are conductivity k = 1.0 W/mK, specific heat capacity c = 1000 Ws/kg and density ρ = 2400 kg/m^3.

The heat at the boundaries are transferred to the body surface by radiation and convection according to equation $q = \varepsilon\,\sigma\left(T_f^{\,4} - T_s^{\,4}\right) + \alpha\left(T_f - T_s\right)$ with the emissivity ε = 0.8, the convection coefficient α = 10 W/m^{2}K and the Stefan Bolzmann constant σ = 5.67 × 10^{-8} W/m^{2}K^4. T_f is the fire temperature and
T_s is the surface temperature.

The temperatures at the surface in the middle of the sides, in the corners and in the centre after 30, 60, 90, 120, 150 and 180 minutes of fire exposure are presented in table 2a.

Table 2a   Constant material properties and constant fire gas temperature equal to 1000 °C.

Number of elements *n*		time (min)					
		30	60	90	120	150	180
4	T_{sur}	959	970	979	985	989	992
16		947	966	977	984	989	992
64		944	965	977	984	989	992
256		944	965	977	984	989	992
4	T_{cor}	996	997	998	999	999	999
16		996	998	999	999	1000	1000
64		997	999	999	999	1000	1000
256		997	999	999	999	1000	1000
4	T_{cen}	74	247	420	563	675	759
16		44	228	428	588	705	790
64		33	224	434	597	715	799
256		32	224	435	599	716	800

Table 2b   Constant material properties and fire gas temperature according to ISO 834.

Number of elements *n*		time (min)					
		30	60	90	120	150	180
4	T_{sur}	725	879	955	1007	1045	1078
16		725	874	953	1006	1046	1077
64		722	873	952	1006	1045	1077
256		723	873	952	1006	1046	1077
4	T_{cor}	827	921	983	1027	1061	1089
16		811	921	984	1028	1062	1089
64		810	921	984	1028	1062	1089
256		811	922	984	1028	1062	1089
4	T_{cen}	30	156	317	473	608	720
16		15	135	313	485	630	747
64		11	129	314	490	637	755
256		10	128	315	492	639	756

Reference case 3 - Non-linear boundary conditions and temperature dependent material thermal conductivity

The same geometry, boundary conditions and material properties as in reference case 2 except that the heat conductivity *k* varies bi-linearly with temperature *T*: $k_{(T=0)} = 1.5$ W/mK, $k_{200} = 0.7$ W/mK and $k_{1000} = 0.5$ W/mK.

The temperatures at the surface in the middle of the sides, in the corners and in the center of the square section after 30, 60, 90, 120, 150 and 180 minutes of fire exposure are presented in table 3a and 3b.

Table 3a   Heat conductivity varies with temperature. Constant fire gas temperature equal to 1000 °C.

Number of elements *n*		time (min)					
		30	**60**	**90**	**120**	**150**	**180**
4	T_{sur}	973	977	982	985	988	990
16		961	973	980	984	987	990
64		957	971	979	984	987	990
256		957	971	979	984	987	990
4	T_{cor}	999	998	999	999	999	999
16		998	999	999	1000	1000	1000
64		998	999	1000	1000	1000	1000
256		999	999	1000	1000	1000	1000
4	T_{cen}	55	147	250	350	442	522
16		41	137	243	356	459	547
64		36	134	242	361	467	557
256		35	134	243	362	468	558

Table 3b   Heat conductivity varies with temperature. Fire gas temperature according to ISO 834.

Number of elements *n*		time (min)					
		30	**60**	**90**	**120**	**150**	**180**
4	T_{sur}	745	891	961	1011	1048	1078
16		748	886	959	1009	1047	1077
64		745	884	958	1009	1047	1077
256		744	884	958	1009	1047	1077
4	T_{cor}	836	924	985	1028	1062	1089
16		816	923	985	1028	1062	1089
64		815	923	985	1028	1062	1089
256		815	923	985	1028	1062	1089
4	T_{cen}	28	108	199	298	395	485
16		21	101	190	296	403	502
64		19	99	189	299	409	509
256		18	99	189	299	409	510

Reference case 4 - Latent heat due to water content – a concrete block with moisture

The geometry, boundary conditions and heat conductivity varying with temperature are the same as in reference case 3 but this case has been extended with latent heat due to evaporation of 5% by weight water in the range of 100 °C to 120 °C. Influences of water migration have not been considered.

The calculated center, corner and surface temperatures after 30, 60, 90, 120, 150 and 180 minutes of fire exposure are presented in tables 4a and 4b.

Table 4a   Concrete with 5 % content of water. Constant fire temperature equal to 1000 °C.

Number of elements *n*		time (min)					
		30	60	90	120	150	180
4	T_{sur}	975	972	977	981	984	987
16		953	967	974	979	983	986
64		948	965	973	978	982	985
256		948	965	973	978	982	985
4	T_{cor}	1004	998	998	999	999	999
16		997	999	999	999	1000	1000
64		998	999	999	1000	1000	1000
256		998	999	999	1000	1000	1000
4	T_{cen}	35	92	112	185	284	371
16		22	79	104	175	295	392
64		18	75	102	184	301	401
256		17	74	101	186	303	403

Table 4b   Concrete with 5 % content of water. Fire gas temperature according to ISO 834.

Number of elements *n*		time (min)					
		30	60	90	120	150	180
4	T_{sur}	703	884	955	1005	1043	1074
16		732	877	952	1003	1042	1073
64		728	875	951	1003	1042	1073
256		728	875	951	1003	1042	1073
4	T_{cor}	850	924	984	1027	1061	1089
16		816	922	984	1028	1062	1089
64		813	923	985	1028	1062	1089
256		813	923	985	1028	1062	1089
4	T_{cen}	17	66	105	127	231	327
16		11	60	100	115	231	340
64		9	56	98	111	239	348
256		8	56	98	110	241	350

Reference case 5 - Composite, steel and concrete

One quarter of a square section with a concrete core inside a 10 mm thick steel square tube is subjected to a constant fire temperature of 1000 °C or alternatively to the standard-time temperature curve according to ISO 834, see figure 3.
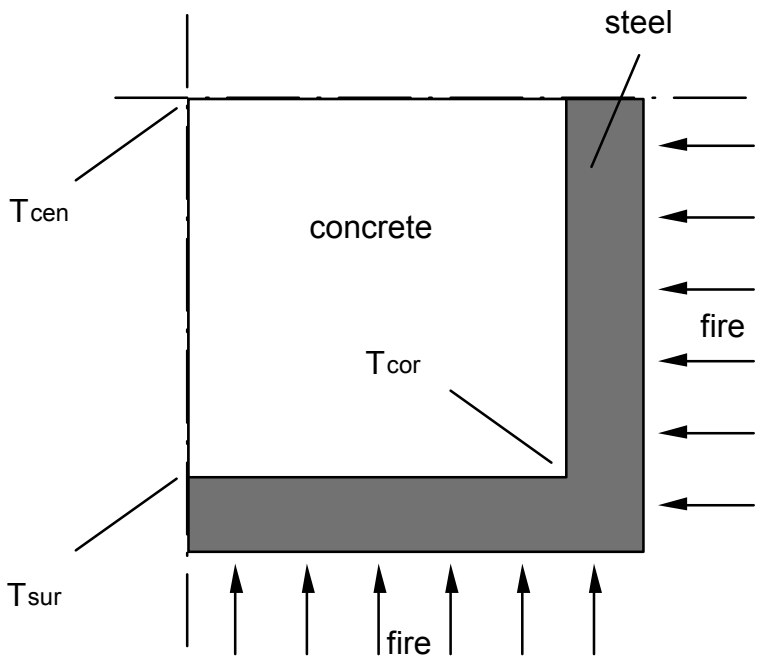
Figure 3   **Concrete core inside a 10 mm thick steel square tube.**

The concrete core has the same thermal properties including latent heat as in reference case 4. The steel square tube is assumed to have thermal conductivity k varying bi-linear with temperature T: $k_{(T=20)} = 54$ W/mK, $k_{800} = 27.3$ W/mK, and $k_{1200} = 27.3$ W/mK, and heat capacity $c = 600$ J/kgK and density $\rho = 7850$ kg/m^3.

The boundary conditions are the same as specified in reference case 2.

The centre temperature and surface temperatures at corner and at the lines of symmetry after 30, 60, 90, 120, 150 and 180 minutes of fire exposure are presented in tables 5a and 5b.

Table 5a   Concrete core inside a 10 mm steel square tube. Constant fire temperature equal to 1000 °C.

Number of elements n		time (min)					
		30	60	90	120	150	180
4	T_{sur}	953	976	981	984	987	989
16		950	969	976	981	985	987
64		944	966	975	981	984	987
256		944	966	975	980	984	987
4	T_{cor}	986	993	995	995	996	997
16		980	989	992	994	995	996
64		975	988	992	994	995	996
256		975	987	991	994	995	996
4	T_{cen}	32	88	111	179	280	369
16		19	75	103	163	286	387
64		14	70	101	172	293	395
256		14	69	101	174	295	397

Table 5b   Concrete core inside a 10 mm steel square tube. Fire gas temperature according to
                 ISO 834.

Number of elements *n*		time (min)					
		30	60	90	120	150	180
4	T_{sur}	581	865	954	1004	1043	1074
16		640	862	950	1002	1041	1073
64		644	860	948	1001	1041	1072
256		645	860	948	1001	1041	1072
4	T_{cor}	646	973	999	1020	1056	1084
16		724	921	992	1040	1076	1084
64		688	890	969	1018	1054	1083
256		688	890	969	1018	1054	1083
4	T_{cen}	14	61	103	119	219	318
16		9	53	96	111	215	328
64		6	49	94	106	222	335
256		6	48	93	106	224	336

Reference case 6 - Composite, steel and mineral wool

One quarter of a square section with a mineral wool core inside a 0.5 mm thick steel square tube is
subjected to a constant fire temperature of 1000 °C or alternatively to the standard-time temperature
curve according to ISO 834, see figure 4.
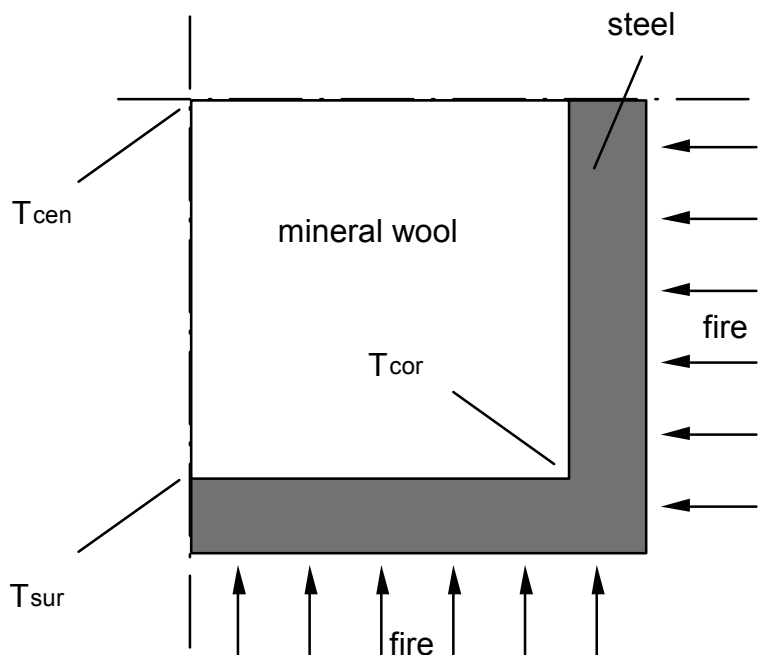
Figure 4   Mineral wool core inside a 0.5 mm thick square steel tube.

The mineral wool core is assumed to have thermal conductivity $k = 0.05$ W/mK, heat capacity
$c = 1\ 000$ J/kgK and density $\rho = 50$ kg/m^3. The thermal properties of steel are the same as in
reference
case 5.

The boundary conditions are the same as specified in reference case 2.

The center temperature and surface temperatures at corner and at the lines of symmetry after 30, 60, 90, 120, 150 and 180 minutes of fire exposure are presented in tables 6a and 6b.

Table 6a   Mineral wool core in a square steel tube. Constant fire temperature equal to 1000 °C.

Number of elements *n*		time (min)						
		15	30	60	90	120	150	180
4	T_{sur}	998	999	999	1000	1000	1000	1000
16		998	999	999	1000	1000	1000	1000
64		998	999	999	1000	1000	1000	1000
256		998	999	999	1000	1000	1000	1000
4	T_{cor}	1000	1000	1000	1000	1000	1000	1000
16		1000	1000	1000	1000	1000	1000	1000
64		1000	1000	1000	1000	1000	1000	1000
256		1000	1000	1000	1000	1000	1000	1000
4	T_{cen}	135	354	682	850	930	967	985
16		91	343	712	877	948	978	990
64		75	341	720	883	952	980	992
256		74	343	722	885	952	980	992

Table 6b   Mineral wool core in a square steel tube. Fire gas temperature according to ISO 834.

Number of elements *n*		time (min)						
		15	30	60	90	120	150	180
4	T_{sur}	711	818	924	985	1029	1062	1090
16		710	818	924	985	1029	1062	1090
64		710	818	924	985	1029	1062	1090
256		710	818	924	985	1029	1062	1090
4	T_{cor}	714	820	925	986	1029	1062	1090
16		714	820	925	985	1029	1062	1090
64		714	820	925	986	1029	1062	1090
256		714	820	925	986	1029	1062	1090
4	T_{cen}	64	222	533	743	875	959	1016
16		38	204	550	766	894	973	1025
64		28	199	555	772	898	976	1027
256		27	199	556	773	899	976	1027

Reference case 7 - Heat transfer by radiation in voids

A rectangle section with outer dimension (width x height) 110 x 20 mm and 5 mm thick walls is analysed regarding heat transfer by radiation across and along a void, se figures 5 and 6.
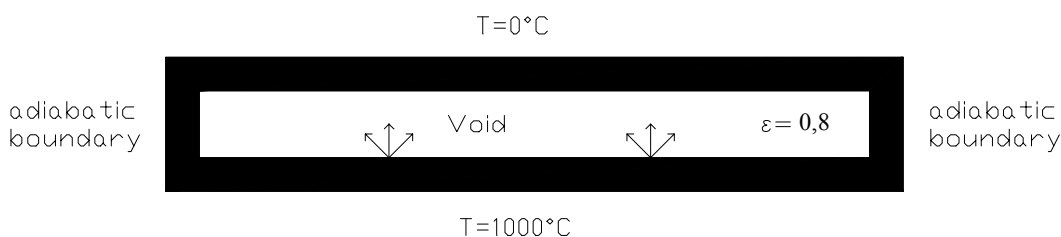
Figure 5   Heat transfer by radiation across a void.
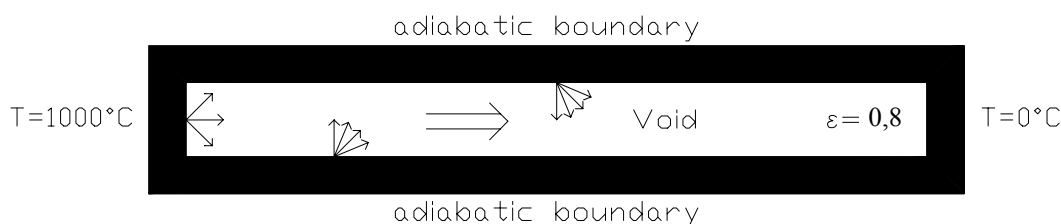
Figure 6   Heat transfer by radiation along a void.

The material of the 5 mm thick walls has the thermal conductivity k = 1.0 W/mK, heat capacity c = 1 000 J/kgK, density ρ = 1000 kg/m^3 and a surface emissivity ε = 0.8.

Heat transfer by radiation across voids is modelled in one approximately one-dimensional case where the results are possible to check analytically and in one two-dimensional case.

One dimensional case

Table 7a shows how the calculated temperature of the wall surface at the center of the void converges to the analytically calculated value when the number of side elements n increases.

Table 7a   Calculated inner wall surface temperature and the exact analytical solution assuming one dimensional heat transfer.

	Number of side elements, *n* in the void	**Lower surface (in the void)**	**Upper surface (in the void)**
TASEF calculation	2	789	198
	4	774	229
	8	779	220
Analytical		779	221

Two dimensional case

Table 7b shows how the temperatures converge nicely. The comparison with results obtained with SAFIR [2] shows reasonably good agreement.

Table 7b   Calculated temperatures along void surface for various numbers of elements *n*.
Comparison with results obtained with SAFIR [2] is shown in the table.

Position	[mm]	0	12.5	25	37.5	50	62.5	75	87.5	100
TASEF	*n* = 2	881				629				117
	n = 4	898		748		675		499		98
	n = 8	906	820	779	723	662	587	485	335	89
SAFIR	*n* = 8	917	820	777	724	662	586	484	344	90

Reference case 8 – Insulated steel section with two voids

Steel section HE200B protected with fire insulation boards is subjected to standard time-temperature curve according to ISO 834, see figure 7.
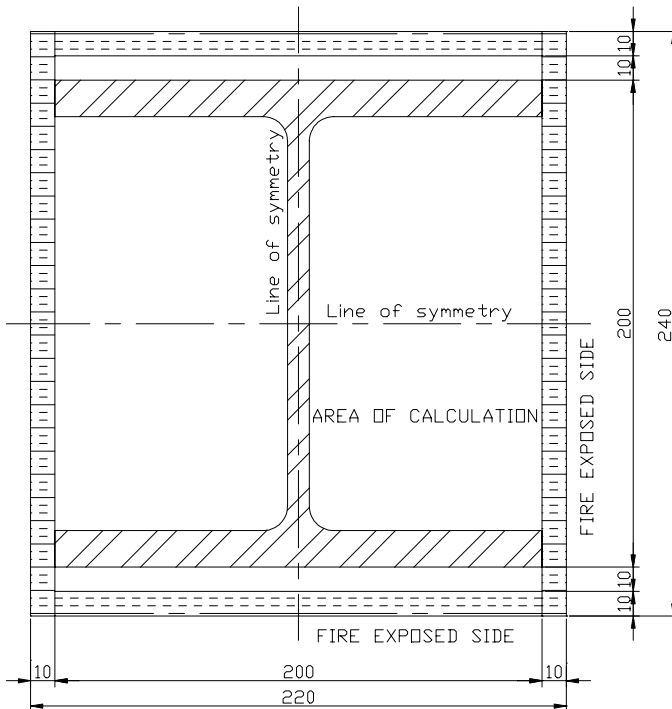
Figure 7   Steel section HE200B protected with fire insulation boards.

The outer boundary is exposed to a standard fire defined by ISO 834 along all four sides with heat transfer conditions as in reference case 2. Heat between the interior surfaces of the void is assumed to be transferred by radiation and convection.

The conductivity of steel is the same as in reference case 5 and the conductivity *k* of the insulation board material varying bi-linear with temperature *T*: $k_{(T=0)} = 0.174$ W/mK, $k_{250} = 0.188$ W/mK and $k_{1100} = 0.188$ W/mK. The emissivity ε of all surfaces is assumed to be 0.8.

Steel temperature in the center of the flange of the section as a function of time and the temperature distribution in the steel section with starting-point in the centre of the web and terminal point at the lower right edge of the bottom flange after 60 minutes fire exposure calculated with various number of elements
n = 12, 30, 99 and 357 (Mesh 0 – Mesh 3) are presented in figures 8 and 9.
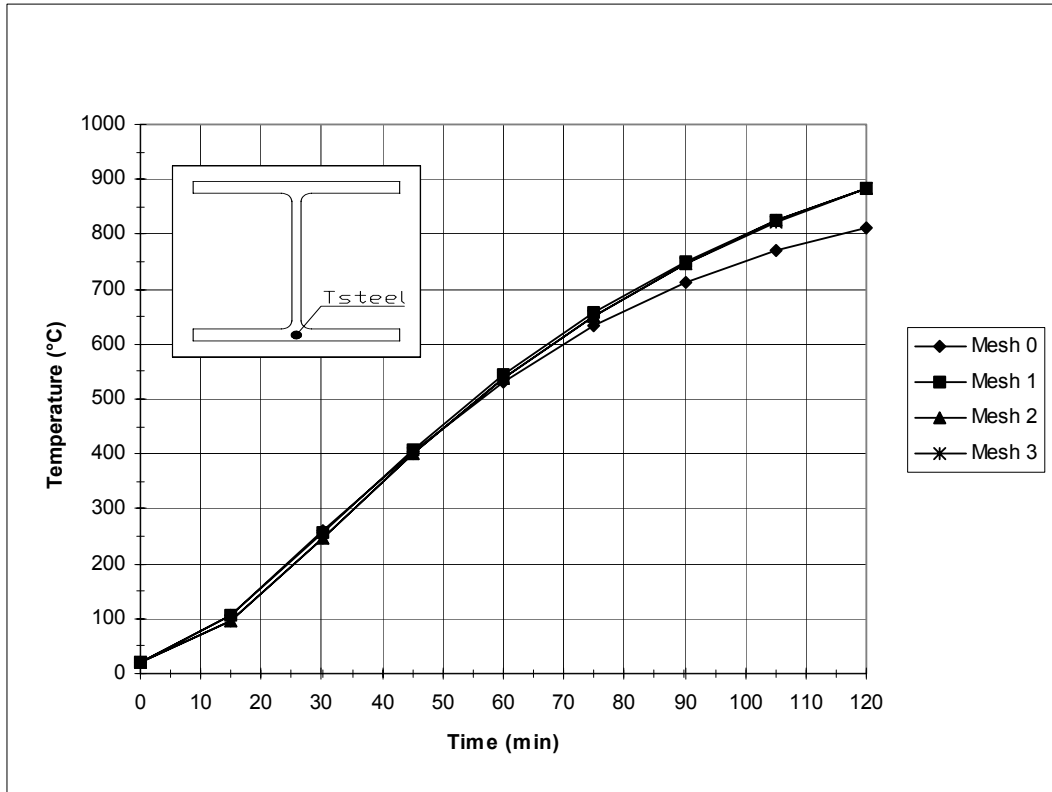
Figure 8 Steel temperature in the centre of the flange as a function of time.
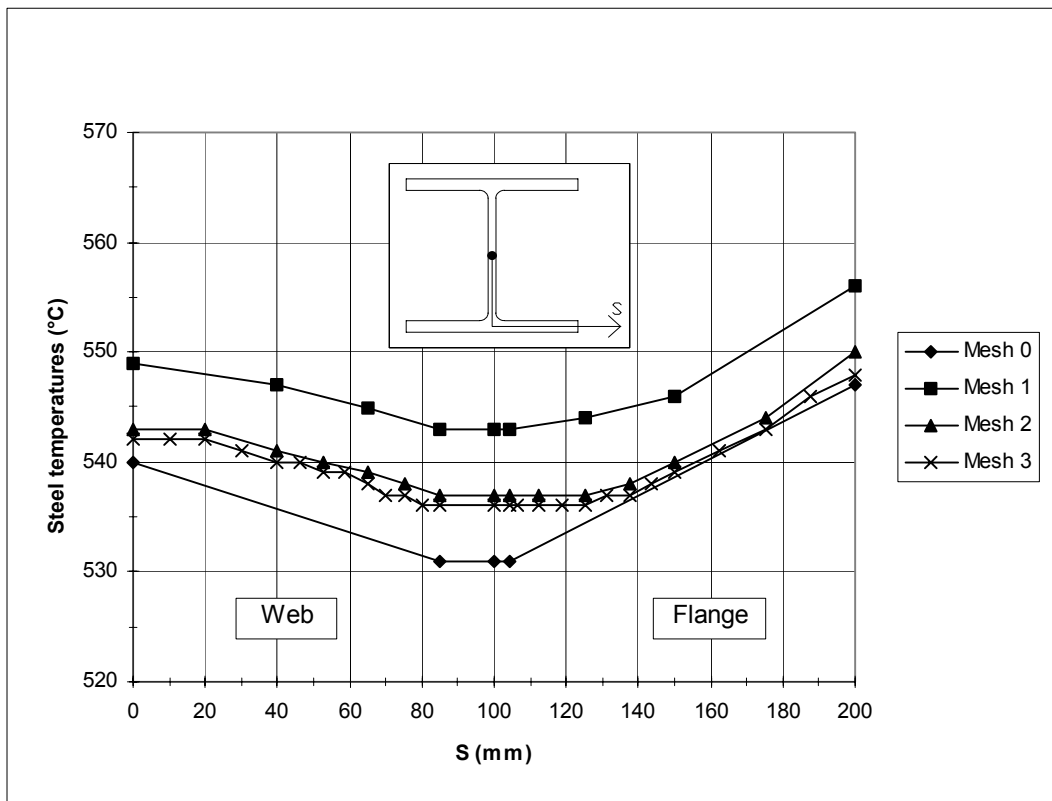
Figure 9   Steel temperature distribution from the center of the web and along the bottom flange (distance s) after 60 minutes of fire exposure.

CONCLUSION

A first outline for a scheme for verification of computer codes for calculation of temperature in fire exposed structures has been developed with the following scenarios:

- case 1: Comparison against analytical results, constant material properties
- case 2: Non-linear boundary conditions and constant material properties
- case 3: Non-linear boundary conditions and temperature dependent material thermal conductivity
- case 4: Latent heat due to water content – a concrete block with moisture
- case 5: Composite, steel and concrete
- case 6: Composite, steel and mineral wool
- case 7: Heat transfer by radiation in voids
- case 8: Insulated steel section with two voids

Other computer program users can now use the same set of reference cases for comparison with the results obtained with the code TASEF. Comparisons of results obtained with various element sizes give indications on the degree of accuracy that can be expected in this kind of calculations and a future possibility to evaluate the validity of different computer codes.

ACKNOWLEDGEMENT

REFERENCES

[1] Sterner, E. and Wickström, U., TASEF - Temperature Analysis of Structures Exposed to Fire, SP Report 1990:05, Swedish National Testing and Research Institute, Borås, 1990.

[2] Pintea, D. and Franssen, J.-M., Evaluation of the thermal part of the code SAFIR by comparison with the code TASEF, Proc. 8th Int. Conf. on Steel Structures, Vol. 2, M. Ivan ed., MIRTON, Timisoara, (1997), 636-643.

[3] Hamann, J., Müller, R., Rudolphi, R., Schriever, R. and Wickström, U., Anwendung von Temperatur-Berechnungsprogrammen auf kritische Referenzbeispiele des Brandschutzes, Bundesanstalt für Materialforschung und -prüfung, Berlin, 1999.

[4] Wickström, U., An evaluation scheme of computer codes for calculating temperature in fire exposed structures, Interflam '99.

[5] Carslaw, H.S. and Jaeger, J.C., Conduction of Heat in Solids, 2nd edition, Oxford University Press, 1969.

[6] SIS 02 48 20, edition 2, dated 1977-07-01 (ISO 834-1975)

A COMPARATIVE THERMAL ANALYSIS OF STRUCTURES EXPOSED TO FIRE WITH ADVANCED CALCULATION MODELS

A. Ptchelintsev

Technical Research Centre of Finland, VTT Building Technology, Fire Technology,
P.O. Box 1803, FIN-02044 VTT, FINLAND
Email : Alexander.Ptchelintsev@vtt.fi

ABSTRACT

The latest trends in the development of CAD/CAM/CAE tools and their influence on fire safety engineering in general and analysis of structures exposed to fire are described and some practical conclusions are made. Importance of development of reliable verification schemes, which can be used by design engineers to evaluate their analysis tools, is explained. As an example the current versions of well-known finite element codes ANSYS and ABAQUS are evaluated against a number of two dimensional benchmark reference cases suggested by U. Wickström. An evaluation scheme employs 8 levels of so called patch tests of various degree of complexity. The cases are relevant for fire safety engineering including effects of temperature dependent material properties, latent heat, combination of different materials and radiative heat transfer in enclosures. Accuracy of results versus mesh density and the convergence properties of the codes are studied.

Importance of parametrization of analysis models is described and an example demonstrates a fully parametric three dimensional analysis of a steel beam exposed to a localised fire conducted with ANSYS.

Keywords: *thermal analysis, finite element, concrete, localised fire*

INTRODUCTION

The latest trends in the development of CAD/CAM/CAE tools open bright perspectives for the computer aided manufacturing, design and analysis in all branches of industries and sciences. Fire safety engineering is not an exception from this rule because the same laws of physics still apply. What are these trends and how they are related to the fire safety engineering and analysis of structures exposed to fire in particular? Only some important trends in the development of the leading finite element programs are discussed in this paper and some practical conclusions are drawn. From the analysis of the latest versions of well-known finite element codes ANSYS and ABAQUS the following main directions of their development can be seen:
- full parametrization of input data,
- geometry driven optimization,

- multifield capabilities,
- probabilistic analysis,
- tight connection with CAD systems.
- open architecture
- move towards cheaper hardware platforms as they become more powerful

As a result of these and other trends a 3-D linear and nonlinear finite element analysis becomes a routine procedure in some branches of industry and science. Improving of multifield capabilities of the finite element codes permit their usage by analysts and design engineers during the whole cycle of design and not only for individual calculations. As more engineers turn their attention to the finite element tools many new problems appear. Since it takes years to become "good" at using a program as complicated as ANSYS or ABAQUS, special tools have been developed in order to provide a possibility to change a Graphical User's Interface of the program and create so called "vertical applications", i.e. specialized versions of the finite element programs with a customized (simplified) user interface tailored for a particular problem(s).

Verification of the analytical capabilities of commercial and research finite element codes is a very important problem in general and in fire safety engineering in particular. When a simulation tool like a FEM based software is used for simulation of a structural element exposed to fire, one has to consider several effects such as:

- temperature dependent material properties;
- convective and radiative boundary conditions;
- latent heat;
- combination of different materials;
- radiation in enclosure.

Although commercial finite element codes are supplied with an extensive set of verification examples it is still necessary to conduct an additional evaluation study if such codes are used for simulation of real-life structures exposed to fire because a combination of the effects mentioned above can cause an error. Another reason is to get necessary experience which is required if an engineer does not use the code on a daily basis.

This paper presents some results of an evaluation study conducted with the current versions of ANSYS (5.61) and ABAQUS (5.8-14) codes. The codes were evaluated against a number of two dimensional benchmark reference cases suggested by U. Wickström [1] and compared with results obtained with TASEF program [2]. Accuracy of results versus mesh density and the convergence properties of the codes are studied.

Implementation of parametrization of input data in ANSYS is briefly described and an example conducted with ANSYS demonstrates a fully parametric three- dimensional analysis of a steel beam exposed to a localised fire.

WICKSTRÖM'S EVALUATION SCHEME

A first outline of a scheme for a grid refinement study has been developed by U. Wickström [1]. The following scenarios have been included:

- case 1: Comparison against analytical results, constant material properties
- case 2: Non-linear boundary conditions and constant material properties
- case 3: Non-linear boundary conditions and temperature dependent material thermal conductivity
- case 4: Latent heat due to water content – a concrete block with moisture

- case 5: Composite, steel and concrete
- case 6: Composite, steel and mineral wool
- case 7: Heat transfer by radiation in voids
- case 8: Insulated steel section with two voids

An evaluation scheme employs 8 levels of so called patch tests of various degree of complexity. The cases are relevant for fire safety engineering including effects of temperature dependent material properties, latent heat, combination of different materials and radiative heat transfer in enclosures.

Most of the cases represent a square 2D section, a quarter of which is analysed using a refining mesh of 4, 16, 64 or 256 elements. This paper presents only some results corresponding to the Reference Cases 4 and 7 which are the most interesting from the analysis point of view. All other reference cases have been calculated and the results are available in [6].

Reference case 4 - Latent heat due to water content – a concrete block with moisture

A concrete square section with half side length $l = 0.1$ m and an initial temperature of 0 °C is subjected to the standard time temperature curve according to ISO 834 [6], see Figure 1.
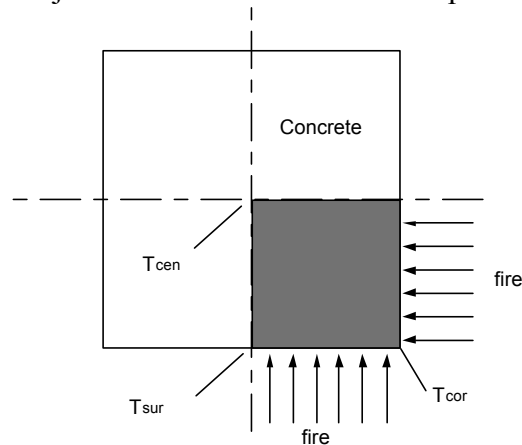
Figure 1   **A concrete square section with half side length l = 0.1 m. [1]**

Material properties:
conductivity $k_{(T=0)} = 1.5$ W/m·K, $k_{200} = 0.7$ W/m·K and $k_{1000} = 0.5$ W/mK.
specific heat capacity $c = 1000$ Ws/kg
density $\rho = 2400$ kg/m^3.
relative emissivity $\varepsilon = 0.8$,

Table 1   Concrete with 5 % content of water. Fire gas temperature
                      according to ISO 834.

Number of elements		time (min)					
		30	**60**	**90**	**120**	**150**	**180**
ANSYS - Diagonalized Specific Heat matrix, Second order elements							
4	T_{sur}	687	866	947	1000	1039	1071
16		717	871	949	1001	1040	1072
64		722	873	950	1002	1041	1072
256		723	874	950	1002	1041	1072
4	T_{cor}	792	916	981	1025	1060	1088
16		807	920	983	1027	1061	1088
64		811	922	984	1028	1061	1089
256		812	922	984	1028	1061	1089
4	T_{cen}	35	48	69	130	241	344
16		9	53	93	120	243	351
64		9	55	96	108	243	353
256		9	56	96	109	243	353
ANSYS - Consistent Specific Heat matrix, Second order elements							
4	T_{sur}	717	874	951	1002	1041	1073
16		725	873	951	1002	1041	1073
64		724	874	951	1002	1041	1073
256		724	874	951	1002	1041	1073
4	T_{cor}	811	922	984	1028	1061	1089
16		812	922	984	1028	1061	1089
64		812	922	984	1028	1061	1089
256		812	922	984	1028	1061	1089
4	T_{cen}	14	51	89	95	258	368
16		9	55	95	102	248	358
64		9	56	96	110	245	355
256		9	56	96	109	244	354
ANSYS - Diagonalized Specific Heat matrix, First-order elements							
4	T_{sur}	665	884	957	1007	1045	1076
16		731	876	952	1003	1042	1073
64		726	875	951	1003	1042	1073
256		725	874	951	1002	1041	1073
4	T_{cor}	792	911	976	1022	1057	1085
16		795	913	979	1024	1058	1086
64		801	917	981	1026	1060	1087
256		807	920	983	1027	1061	1088
4	T_{cen}	16	49	122	203	289	373
16		12	56	90	161	261	360
64		10	55	95	136	251	357
256		9	56	96	113	247	356
1024		9	56	97	110	245	355
ABAQUS - Diagonalized Specific Heat matrix, First-order elements							
16	T_{sur}	713	877	952	1003	1042	1073
16	T_{cor}	795	913	979	1024	1058	1086
4	T_{cen}	21	77	110	177	275	367
16		12	64	101	128	255	359
64		10	58	98	114	246	355
256		9	56	97	111	244	354

convection coefficient $\alpha = 10$ W/m^{2}K

The heat transfer to the boundaries:

$$q = \varepsilon\,\sigma\left(T_f{}^4 - T_s{}^4\right) + \alpha\left(T_f - T_s\right)$$

with the Stefan Bolzmann constant $\sigma = 5.67 \times 10^{-8}$ W/m^{2}K^4,

T_f is the fire temperature and
T_s is the surface temperature.
Latent heat due to evaporation of 5% by weight water in the range of 100 °C to 120 °C should be considered.
The calculated centre, corner and surface temperatures after 30, 60, 90, 120, 150 and 180 minutes of fire exposure are presented in Table 1.

Two finite element types from the ANSYS library of finite elements have been chosen, namely 2D thermal solid elements PLANE55 and PLANE77. PLANE55 is a first order element with 2 Gauss integration points in each direction and PLANE77 is a second order element with 3 integration points. PLANE55 element's specific heat
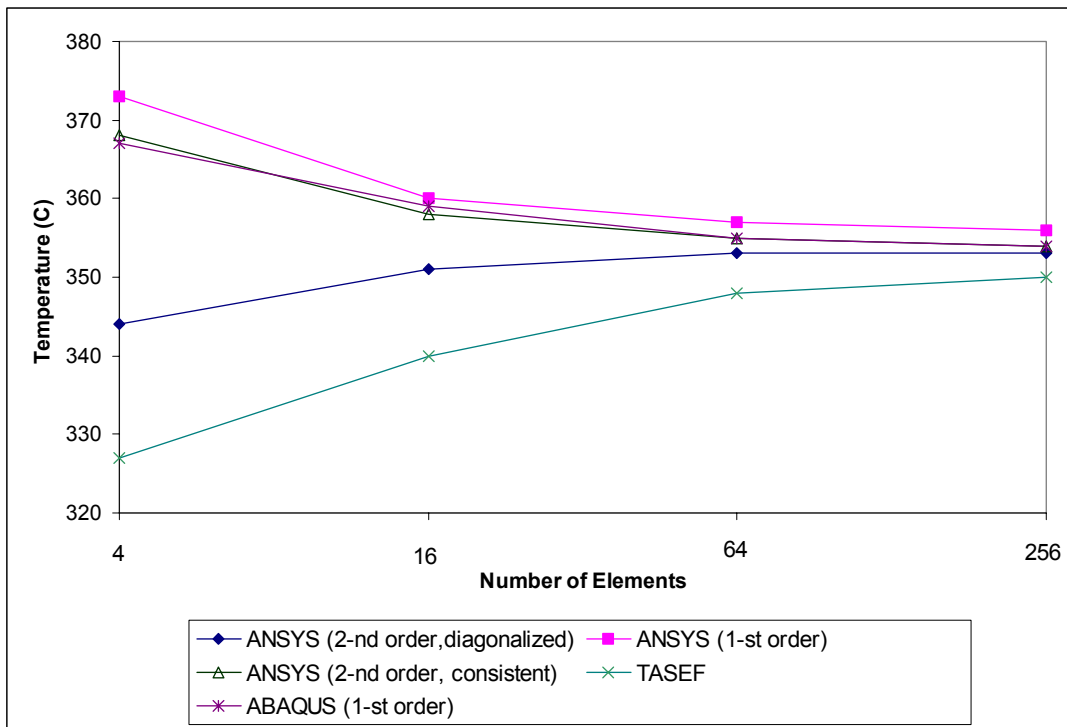
Fig. 2 Centre temperature after 3 hours vs. number of elements

matrix is reduced to a diagonal form but PLANE77 element has an option to choose between a complete and diagonal matrix. Both options were used. In case with ABAQUS only first order elements were used. It can be seen in Figure 2 that ANSYS with PLANE77 elements and ABAQUS have slightly better convergence toward the solution than TASEF. ANSYS post-processor provides an error estimation technique, which estimates the amount of solution error due specifically to mesh discretization. This technique is available only for linear structural and linear/nonlinear thermal analyses using 2-D or 3-D solid elements or shell elements. In the postprocessor, the program calculates an energy error for each element in the model. The energy error is similar in concept to the strain energy. The structural energy error (labelled SERR) is a measure of the discontinuity of the stress field from element to element, and the thermal energy error (TERR) is a measure of the discontinuity of the heat flux from element to element. Using SERR and TERR, the ANSYS program calculates a percent error in energy norm (SEPC for structural percent error, TEPC for thermal percent error). However, it can provide only a qualitative assessment because error estimation is based on stiffness and conductivity matrices that are evaluated at the reference temperatures (TREF). Error estimates, therefore, can be incorrect for elements with

temperature-dependent material properties if those elements are at a temperature that is significantly different than TREF [3]. As an illustration contours of thermal percent error are shown in Figure 3 for two meshes.
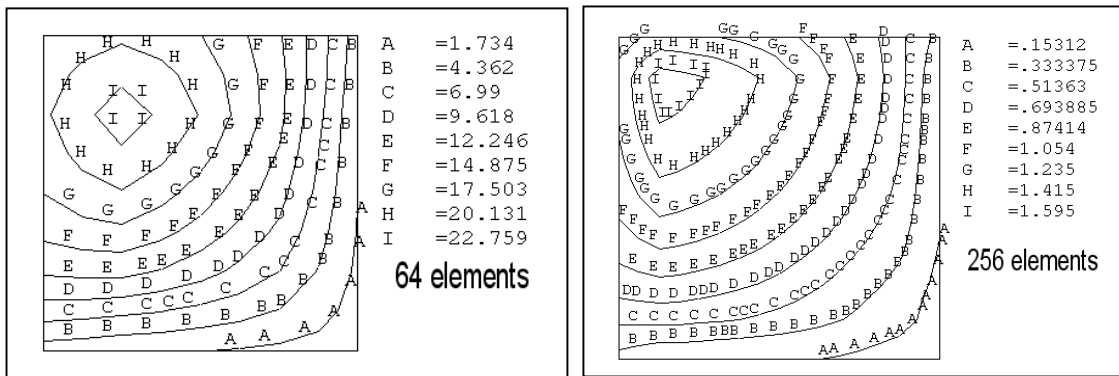
Figure 3. Thermal percent error corresponding to two different meshes of PLANE55 finite elements in ANSYS

Reference Case 7 - Heat transfer by radiation in voids

A rectangle section with outer dimension (width x height) 110 x 20 mm and 5 mm thick walls is analysed regarding heat transfer by radiation along a void, see Figure 4.
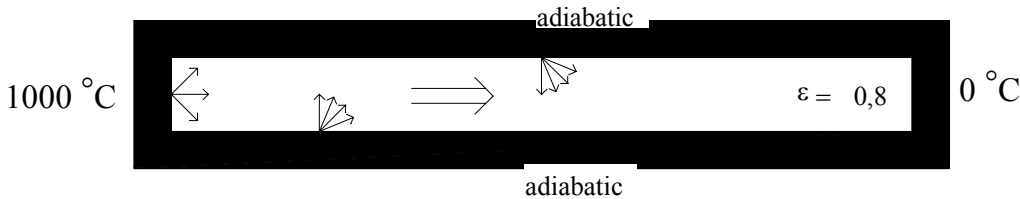
Figure 4   Heat transfer by radiation along a void [1].

The material of the 5 mm thick walls has the thermal conductivity $k = 1.0$ W/mK, heat capacity $c = 1\,000$ J/kgK, density $\rho = 1000$ kg/m^3 and a surface emissivity $\varepsilon = 0.8$.

Table 2   Calculated temperatures along void surface for various numbers of elements n

Position	[mm]	0	12.5	25	37.5	50	62.5	75	87.5	100	TEPC
TASEF	n=8	906	820	779	723	662	587	485	335	89	
SAFIR [4]	n=8	917	820	777	724	662	586	484	344	90	
	n=8	893	833	783	730	669	596	499	356	108	23
ANSYS	n=32	909	834	781	726	662	585	482	333	92	9
(1-st order)	n=64	912	834	781	725	661	583	480	331	91	5
ABAQUS	n=8	911	819	780	723	663	587	486	338	95	
	n=32	913	834	781	725	661	583	480	330	90	

 (TEPC) - THERMAL PERCENTAGE ERROR IN ENERGY NORM

Due to the low thermal conductivity of the material in the walls the heat transfer by conduction is small and the thermal energy is mainly transferred byy radiation. The results presented in Table 2 show that the results obtained by four different programs converge to the same values.

Reasonable results can be obtained with ANSYS only with a fine mesh in this case which corresponds well with the guidelines in the ANSYS manuals.

EXAMPLE OF A FULLY PARAMETRIC 3-D ANALYSIS MODEL

ANSYS Parametric Design Language (APDL) is a powerful tool which makes possible creation of fully parametric models in ANSYS. APDL can now access a large portion of the data held on the ANSYS database and results files. Using APDL for modelling allows generic models to be built. Such models are of significant advantage if a series of analysis are to be performed. Using APDL it is possible to influence all aspects of analysis model including geometry, material properties and boundary conditions.

A series of 2D and 3D calculations was conducted in order to simulate localised fire tests recently conducted at VTT [5].

Computation of steel beam temperature

A series of 2-D and full 3-D numerical simulations of the VTT localised fire tests was conducted with ANSYS program and compared with a simplified engineering method used in Eurocode 3. Only a quarter of the beam had to be modelled due to symmetry. Heat fluxes to the lateral surfaces of the beam were calculated in ANSYS using a modified Hasemi's method [5]. Heat fluxes to the surfaces of the beam and to the slab as functions of time and distance from the center of the beam were applied using array TABLE parameters, which significantly simplified the analysis. Surface elements SURF151 and SURF152 were used in the 2-D and 3-D cases respectively in order to take into account radiation and convection effects, steel emissivity was assumed to be equal 0.85. In the 2-D case the problem was solved as a series of runs in different cross sections of the beam and the main purpose was to study the effect of the heat conduction in the longitudinal direction, which was explicitly considered in a 3-D simulation and neglected in a 2-D analysis. Time-temperature histories for the lower flange, web and upper flange of the beam and temperature contours after 4 minutes of a 3-D simulation are shown in Figures 5 and 6 respectively.

In the calculated example 2-D, 3-D and the simplified method gave very close temperature results. For this particular case it can be explained by the short duration and the fast heating regime, which prevented temperature re-distribution caused by heat conduction. As it can be seen from Figure 4 web of the beam due to its low thickness has the highest temperature. In order to prevent local buckling of the web which was quite possible considering the beam's dimensions it was decided to calculate temperature in the beam with a partial insulation when only a web is protected by a 2 cm of mineral wool (as it is in reality in the existing open car park building). Results of the calculation are shown in Figure 7 and they demonstrate a drastic change in temperature due to the partial insulation
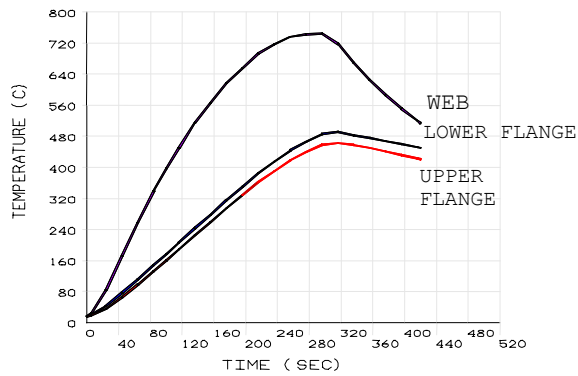
Figure 5. Time-temperature histories at the midspan of the uninsulated beam for the lower flange, web and upper flange
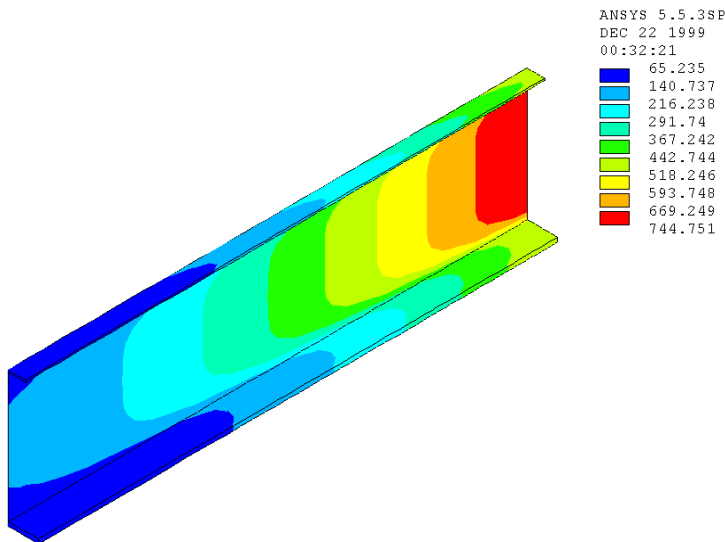
Figure 6. Temperature distribution after 5 minutes.
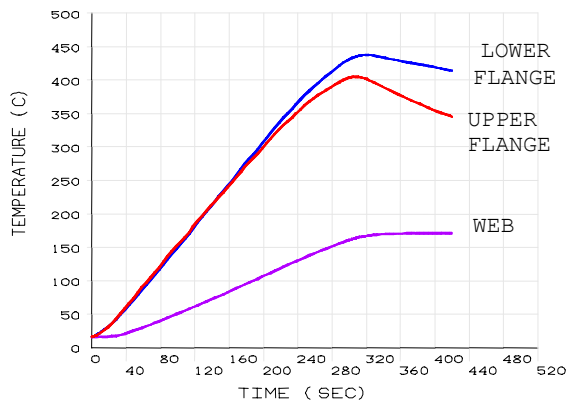
WEB PROTECTED BY 2 CM OF MINERAL WOOL

Figure 7. Time-temperature histories at the midspan of the beam for the lower flange, web and upper flange with the web insulated by 2 cm of mineral wool

CONCLUSIONS

The latest trends in the development of CAD/CAM/CAE tools and their influence on fire safety engineering in general and analysis of structures exposed to fire are described and some practical conclusions are made.

Thermal capabilities of finite element codes ANSYS and ABAQUS have been evaluated against a scheme proposed by U. Wickström. Both programs generally show good convergence properties with second-order elements providing better results for the models with the same number of elements.

Extensive parametric capabilities of ANSYS have been studied and employed during analysis of a steel beam exposed to a localised fire.

ACKNOWLEDGEMENTS

Discussions with Prof. M. Kokkala during preparation of this paper are gratefully acknowledged.

REFERENCES

[1]   Wickström, U., An evaluation scheme of computer codes for calculating temperature in fire exposed structures, Interflam '99.

[2]   Sterner, E. and Wickström, U., TASEF - Temperature Analysis of Structures Exposed to Fire, SP Report 1990:05, Swedish National Testing and Research Institute, Borås, 1990.

[3]   ANSYS 5.6 , On-line manual. Basic Procedures Analysis Guide.

[4]   Pintea, D. and Franssen, J.M., Evaluation of the thermal part of the code SAFIR by comparison with the code TASEF, Proceedingsof the Eight International Conference on Steel Structures, Timosoara, 25- 28 September, 1997, pp. 636-643

[5]   Myllymäki J. and. Kokkala M., Thermal Exposure To A High Welded I-Beam Above A Pool Fire. Proceedings of the First International Workshop "Structures in Fire", Copenhagen, 19-20 June, 2000, pp.

[6]   Ptchelintsev A. Evaluation of ANSYS and ABAQUS thermal capabilities. VTT Research Notes, 2000, (to be published)

CHARACTERISTICS OF THE HEAT TRANSFER FOR CALCULATING THE TEMPERATURE DEVELOPMENT IN STRUCTURAL STEELWORK EXPOSED TO STANDARD FIRE CONDITIONS UNDER PLATE THERMOCOUPLE CONTROL

L. Twilt , P.H.E. van de Leur and C. Both

TNO, The Netherlands

1. Introduction

ENV 1993-1-2: "Fire design on steel structures" [1], gives simple rules for the calculation of the temperature development in bare structural steel members exposed to standard fire conditions. These rules are based on general principles of heat transfer. However semi-empirical heat transfer characteristics are chosen in such a way that the calculation results are in global agreement with the outcomes of conventional standard fire tests.

In such tests the gas temperatures are controlled to follow the standard fire curve in the – so far – common way, i.e. by thermocouples (TC) with a diameter of – typically – 1.5 to 3 mm. With a view to arrive at more harmonized thermal load conditions during standard fire tests, recently new European standards have been accepted, specifying furnace control by so-called plate thermometers (PT) [2]. For a review of the functionality of PT-control, refer to [3].

As shown in [3], the way in which the furnace is controlled (either by TC or PT) will, also depending on the type and dimensions of the furnace, affect the test results in terms of measured steel temperatures. The simple calculation rules of ENV 1993-1-2 referred to above, are directly related to the standard fire test. Therefore, the change from TC to PT control may have consequences for the calculation rules, more in particular on the heat transfer coefficients to be taken into account.

In this paper these consequences are reviewed on the basis of available test results.

2. The Eurocode approach

For a uniform temperature distribution in the cross-section, the increase of temperature $\Delta\theta_{a,t}$ in an unprotected steel member during a time interval Δt may be determined from:

$$\Delta\theta_{a,t} = \frac{A_m/V}{c_a\,\rho_a}\,\dot{h}_{net,d}\,\Delta t \qquad (1)$$

where:

A_m/V is   the section factor for unprotected steel members [1/m];

A_m is   the exposed surface area of the member per unit length [m];

V is   the volume of the member per unit length [m^3];

c_a is   the specific heat of steel[J/kgK];

$\dot{h}_{net,d}$ is   the design value of the net heat flux per unit area   [W/m^2];

Δt is   the time interval   [seconds];

ρ_a is   the unit mass of steel [kg/m^3].

The net heat flux $\dot{h}_{net,d}$ has a radiative ($h_{net,\,r}$) and a convective ($h_{net,\,c}$) component and follows from:

$$\dot{h}_{net,d} = \dot{h}_{net,c} + \dot{h}_{net,r} \qquad (2)$$

with:

$$\dot{h}_{net,r} = \Phi.\varepsilon_{res}.\sigma\cdot\left[(\theta_r+273)^4 - (\theta_m+273)^4\right] \qquad (3^a)$$

and

$$\dot{h}_{net,c} = \alpha_c.(\theta_g - \theta_m) \qquad (3^b)$$

where:

α_{con} is   coefficient of heat transfer by convection [W/m^{2}K];

Φ is   the configuration factor [-];

ε_{res} is   the resultant emissivity coefficient [-];

θ_r is   the radiation temperature of the of the environment of the member [°C];

θ_m is   the surface temperature of the member [°C];

θ_g is   the gas temperature [°C];

σ is   the constant of Stephan-Boltzmann ($= 5.67 \cdot 10^{-8}$ W/m^{2}K^4)

When calculating the fire resistance of structural steel members, the development of the radiation temperature θ_r and the gas temperature θ_g are assumed to follow the ISO standard fire curve. The configuration factor Φ is set equal to unity, assuming a situation in which the steel element is fully engulfed.

Values for the two heat transfer characteristics α_{con} and ε_{res} are conventionally chosen as 25 W/m^2 K and 0.5 respectively. The specified value for α_{con} corresponds globally to gas velocities typical in a furnace environment under standard fire conditions. It has – in practical situations - only a minor effect on the steel temperature development and is for this reason not very critical. The specified value for ε_{res} is a semi empirical factor which accounts for all factors influencing radiative exchange between furnace and member.

3. Basis of analysis

With a view to investigate the effectiveness and practicalities of controlling a fire resistance furnace by means of the Plate Thermometer, CEN/TC127: ad hoc 7 & 14 have performed a large number of fire test [3]. In the scope of those tests, also a series of tests have been performed on bare steel elements in three different European furnaces. The steel elements (I-sections; length: 2 m; section value 90 m^{-1}) are placed in vertical position in the furnace and exposed to standard fire conditions. In each of the furnaces two tests are carried out, one under PT-control and one under TC-control. For some results, refer to Figs. 1 and 2 respectively.

The test results presented in Fig. 1 are based on PT control and are - as such - representative for the new generation of (European) fire resistance tests. Note that the scatter is small, particularly if compared to the results of similar tests, carried out under TC control, see Fig. 2.

In the next section, the Eurocode rules summarized above will be calibrated on the basis of these results. Starting point of the analysis is equation (1) above. In that equation the only factor affected by the furnace control, is the net heat flux h_{net}. It can be shown that under PT control and under certain, simplifying assumptions, the following equation holds [3]:

$$\dot{h}_{net,PTcontrol} = \alpha_c \cdot (\theta_{pt} - \theta_m) + \varepsilon_a \cdot \sigma \cdot \left[\left(\theta_{pt} + 273 \right)^4 - \left(\theta_m + 273 \right)^4 \right] \qquad (4)$$

where:

θ_{pt} is the temperature reading of the PT [°C];
ε_a is the emissivity of steel (= approximately 0.7) [-];

Equ. 4 shows that under PT control the heat flux to the specimen depends only on:

- the properties of the specimen, including the emissivity ε_a determining its temperature response;
- the temperature reading of the PT;
- the convective heat transfer coefficient α_c

Thus, the dependence on furnace properties is – under PT control - limited to the relatively unimportant convective heat flux. This effectively means a harmonized thermal load.

For a detailed discussion under which conditions equ. (4) holds, refer to the Annex[1].
In the next section, calculation results are presented and discussed, in which the numerical value of the emissivity of the steel is systematically varied. In view of its lesser significance for the steel temperature development, the convective heat transfer coefficient is not varied in these calculations, but the conventional value of 25 $W/m^2 K$ has been used.

4. Evaluation & discussion

In Fig. 3 the steel temperature development, calculated with equ. (1) and assuming a net heat flux to the steel element according to equ. (3) is presented for values of ε_{res} varying between 0.1 and 1.0. Comparing the calculated temperatures with the results of the tests, a good correlation is found for $\varepsilon_{res} = 0.5$. This value corresponds with the conventional value for ε_{res} as specified in the current versions of the Eurocode "Fire" but differs quite significantly from the value of approximately 0.7 which one would expect on theoretical grounds. See also Annex. The following explanation for this discrepancy is put forward.

In the above Eurocode equations (1) and (3[a]) the heat flux at a certain moment in time is assumed to be uniform over the cross section of the steel element. For fully engulfed steel members with a convex shape, e.g. rectangular or circular tubes this is a reasonable approximation. For I section however, the assumption of a uniform heat flux is not realistic because parts of the webs and the inner sides of flanges will be protected from direct radiation. This is the so-called shadow effect. See also Fig. 4. The shadow effect is well-known in literature (see e.g. [4], but has not been taken into account in the present version of the Eurocodes "Fire". In [5] rules are given to account for this effect in terms of achieved temperature or necessary insulation thickness, however for insulated sections only. For bare steel it felt to be more appropriate to introduce a correction factor C on the section value. Hence:

$$[A_m / V]_{incl.\ shadoweffect} = C.[A_m/V]_{excl.\ shadow\ effect} \qquad (5)$$

In a first attempt to account for the shadow effect, for $[A_m/V]_{excl.\ shadow\ effect}$ not the contour value for the section value will be taken (as would be done for bare steel I sections) on the basis of [1], but the box-value, i.e.

$$A_m = 2 \cdot [h+b] \qquad (6)$$

where:

 b is the width of the I-section [m];
 h is the height of the I-section [m].

---

1   In the Annex, also an equation for the net heat flux is presented, assuming TC control. In this case the effect of furnace environment on the the net heat flow to the steel member can not be neglected. This explains why TC control is less appropriate as a basis for harmonizing fire resistance tests.

Under this condition, the value of the correction factor C has been determined on the basis of systematic calculations as follows:

- For all listed European I sections (IPE, HEA, HEB etc.) the temperature development has been calculated under standard fire conditions, including the shadow effect. For the way in which the shadow effect has been taken into account, refer to [6]. These calculations (2D), which have been carried out by means of the DIANA finite element computer code [7], lead to a non-uniform temperature distribution over the steel section.
- For various periods of standard fire exposure (10, 20, 30 and 60 minutes), the weighted average steel temperature has been determined for each of the profiles mentioned above; these average temperatures are denoted as $\theta_{av,shadow,t,i}$
- Similar calculations have been carried out, however now based on the Eurocode equation (1), (2) and (3) as described above and with the actual emissivity ε_a of steel (= 0.7); in these calculations the section factor has been chosen such that, for a given period of standard fire exposure, the steel temperature $\theta_{EC,t,i}$ equals $\theta_{av,shadow,t,i}$; this section factor is denoted as $[A_m / V]_{incl.\ shadow\ effect,i}$
- The correction factor C follows from eqs. (5) and (6).

In Fig. 5 the thus determined values of the correction factor C are plotted as function of the average steel temperature calculated by DIANA for various periods of standard fire exposure (10, 20, 30, 60 minutes). Note that for steel temperatures less than approximately 720 °C the correction factor is almost independent of the steel temperature. A fair estimate of the correction factor C in this area would be: $C = 0.9$ For steel temperatures beyond 720 °C the C-values are rather unstable. This is caused by the discontinuous behaviour of the specific heat of steel, as specified in [1]. See also Fig.6. However, the unstable behaviour of C beyond 720 °C is of minor practical significance, since under this condition the steel temperature equals nearly the gas temperature and the section value is of no importance anymore, nor is the actual value of C.

This is illustrated in Fig. 7, in which average temperatures following from the exact calculations($\theta_{av,shadow,t,i}$) are compared with those based on the Eurocode calculations (=$\theta_{EC,t,i}$). For the full temperature range, the agreement between the two sets of temperatures is satisfactory.

On the basis of the above analysis, also the issue whether the change from TC to PT control of fire resistance furnaces will change the severity of the assessment of bare steel members can be dealt with in a quantitative manner. For this purpose, the average steel temperatures following from the systematic calculations including the shadow effect (= $\theta_{av,shadow,t,l}$) been compared with the temperatures calculated on the basis of the present Eurcode rules (=$\theta_{EC,t,i}$), i.e. taking into account $\varepsilon_{res} = 0.5$ and $\alpha_{con} = 25$ W/m^2. The results are presented in Fig. 8. It can be concluded from this Fig. that the present EC rules give rise to conservative results, when compared to more exact solutions. However, in the practical range (i.e. temperatures beyond 500 °C and fire duration beyond 20 minutes) the differences are negligible.

5. Conclusions

Current heat transfer characteristics specified in [1] are semi-empirical and are derived for standard fire test under TC control. If the furnace is controlled by the Plate Thermometer (PT), there no motivation to use a semi-empirical value for the emissivity of steel (0.5 in Eurocode). In stead, the actual physical value (≈ 0.7) should be used. In the paper, the consequences of adopting the physical value of ε_a are discussed. It follows from that discussion that, when applying the simple equations according to Eurocode, the shadow effect must be taken into account. It is shown that this can be done effectively by replacing the section factor specified in the Eurocode equations by:

$$0.9 \cdot [A_m/V]_{box}$$

where:

$[A_m/V]_{box}$ is the box section value of the steel section ($= 2 \cdot [b + h]/V$)

Note that the above modification holds in combination with an emissivity of steel equal to $\epsilon_a = 0.7$ and is not valid for steel members with a convex shape such as rectangular or circular hollow sections. For such cases there is no shadow effect and the nominal value of the section factor should be used.

It has also been shown that – for steel I sections – the above modifications of the heat transfer equations in the Eurocode do not lead to a significant change in the predicted temperatures of bare steel elements under standard fire conditions, when compared to the outcomes following the present semi-emperical Eurocode equations. This is because the latter are globally based on the severity of various European fire resistance furnaces. On the average, this severity is not significantly affected by controlling the fire resistance furnace by plate thermometer rather than by thermocouples

References

[1]   CEN TC250: ENV 1993-1-2: "Eurocode 3 – Design of steel structures – Part 1-2: General rules – Structural fire design"; September 1995

[2]   CEN TC127: EN1363-2: "Fire Resistance Tests – Part 2: Alternative and additional procedures",1999.

[3]   Leur, P.H.E. and Twilt, L.: "Thermal Exposure in Fire Resistance Furnaces".

Proceedings of 6th IAFSS conference held in Poitier, June 5-9, 1999 (to be published).

[4]   CEN TC127: prENV 13381-4: "Test method for determining the contribution to fire resistance of structural member; part 4: applied protection to steel members", 1998.

[5]   Edwards, M.: "Fire Protection of Structural Hollow Sections: Transposition of Spray Protection from 'I' Section Test Data"

British Steel Corporation, CE854/0502.

[6]   C. Both: "The Fire Resistance of Composite Steel-Concrete Slabs".

Thesis Technical University Delft, 1998.

[7]   Witte, F. and Feenstra, P.H.: "DIANA finite element analysis; User's manual release 6.1: Non-linear Analysis, 1996.

[8]   Wickström, U.: "The Plate Thermometer – A simple Instrument for Reaching Harmonised Fire Resistance Tests", SP Report 1989:03, Swedish National Testing Institute, 1989.

ANNEX : PT vs. TC CONTROL: THEORETICAL MODEL

The discussion below is an attempt to theoretically prove the case of the Plate Thermometer as an appropriate instrument for controlling fire resistance furnaces. It will be shown that, under simplifying assumptions, the thermal exposure of a test specimen is almost independent of properties of the furnace if the furnace is controlled such that Plate Thermometers follow a standard curve, whereas the thermal exposure does depend on furnace properties if the furnace is controlled on basis of small thermocouple readings. The treatment is an extension of [8].
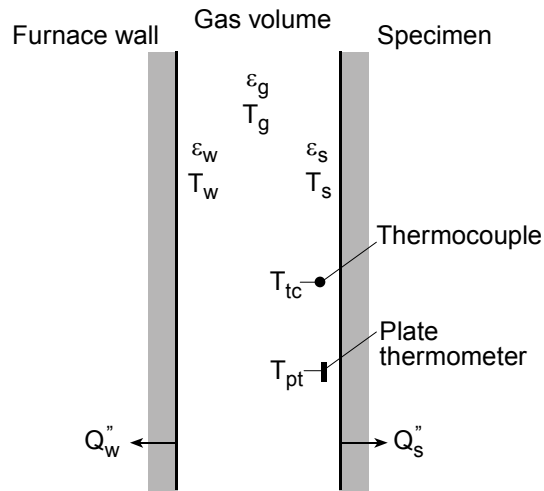
Figure A.1 Thermal parameters

Figure A depicts the model representing a fire resistance furnace in this paper. In the notation, the subscripts refer to the following items: specimen (s), furnace wall (w), furnace gas (g), Plate Thermometer (pt).
The model distinguishes between convective heat transfer to the PT and to a specimen. The convective heat transfer coefficients are denoted as α.

If the furnace geometry approximates an ideal case of two infinite parallel plates, each having an emissivity equal to 1, the net heat flux entering the specimen is given by

$$\dot{h}_{net,d}=\alpha_m \cdot \left(\theta_g - \theta_m\right)+\varepsilon_g.\sigma.\left(\theta_g + 273\right)^4 + \left(1-\varepsilon_g\right)\cdot \sigma \cdot \left(\theta_w + 273\right)^4 - \sigma \cdot \left(\theta_m + 273\right)^4 \qquad (3^a$$

Simplifying this expression by defining θ_r through:

$$\left(\theta_r + 273\right)^4=\varepsilon_g.\sigma.\left(\theta_g + 273\right)^4 + \left(1-\varepsilon_g\right)\cdot \sigma \cdot \left(\theta_w + 273\right)^4$$

and allowing for non-unity emissivity of the test specimen, the first equation reduces to

$$\dot{h}_{net,d}=\alpha_m \cdot \left(\theta_g - \theta_m\right)+ \sigma.\left(\theta_r + 273\right)^4 - \sigma \cdot \varepsilon_a \cdot \left(\theta_m + 273\right)^4$$

Notes :
- When non-unity values for the emissivity of furnace walls and specimen are allowed in the model, the net heat flux cannot be expressed in a simple form any longer (except for some ideal textbook cases). This is because heat emitted by the furnace walls is partly reflected by the specimen, then again partly by the furnace walls etc. This leads to a set of equations that can be solved by e.g. the Hottel zone method. The furnace gases absorbing and emitting make this behaviour more complicated.
- Similarly, the equations are valid for an infinitely large furnace wall opposite an equally infinite specimen. With finite dimensions a more complex expression is needed.

For the net heat flux entering the Plate Thermometer, a similar expression holds:

$$\dot{h}_{net,pt}=\alpha_{pt}\cdot\left(\theta_g-\theta_{pt}\right)+\sigma\cdot\left(\theta_r+273\right)^4-\sigma\cdot\varepsilon_{pt}\cdot\left(\theta_{pt}+273\right)^4$$

But $\dot{h}_{net,pt}$ is zero since a PT has a negligible heat capacity. Subtracting the last two equations and rearranging, we find:

$$\dot{h}_{net,d}=\alpha_{pt}\cdot\left(\theta_{pt}-\theta_m\right)-\left(\alpha_{pt}-\alpha_m\right)\cdot\left(\theta_g-\theta_m\right)+\sigma\cdot\left[\varepsilon_{pt}\cdot\left(\theta_{pt}+273\right)^4-\varepsilon_a\cdot\left(\theta_m+273\right)^4\right]$$

This reduces to a simple expression under the following assumptions:
- The convective heat transfer coefficients α_m and α_{pt} are equal (=α). Typical values of convective heat transfer coefficients are: $\alpha_m = 10$, $\alpha_{pt} = 15$, $\alpha_{tc} = 150$ (W/m^{2}K).
- The surface emissivities ε_a and ε_{pt} are equal (=ε) (and close to 1, see discussion above). Typical values are : $\varepsilon_{pt} = 0.9$ (blackened steel), $\varepsilon_a= 0.7$-0.9 (concrete, ceramic fibre, oxidised metal)

The reduced expression reads:

$$\dot{h}_{net,d}=\alpha\cdot\left(\theta_{pt}-\theta_m\right)+\varepsilon\cdot\sigma\cdot\left[\left(\theta_{pt}+273\right)^4-\left(\theta_m+273\right)^4\right]$$

Under these assumptions, the heat flux to a specimen depends only on:
- The properties of the specimen, determining its temperature response;
- The temperature reading of the Plate Thermometer θ_{pt}
- The convective heat transfer coefficient α

Thus, the dependence of furnace properties is limited to the relatively unimportant convective heat flux. This effectively proves harmonised thermal load. On the other hand, the derivation shows where, how and to what extent harmonisation breaks down when the assumptions made are not all met. It is easy to show that e.g. the furnace gas temperature θ_g enters the expression for if the effective convective heat transfer coefficients for the specimen and for the PT are different; when the radiative properties of the specimen differ substantially from those of the furnace walls, the "radiation temperature" θ_r enters the expression, and thereby θ_w and θ_g .

The above treatment enables –at least in principle- a quantified estimation of the individual effects. For the convective part - for example -   it can be shown that, under circumstances which are typical for a fire resistance tests, the error in the heat flux entering the test specimen by assuming the $\alpha_m = \alpha_{pt}$ is less than 4%.

If the furnace is not controlled by PT but by TC, a similar argument can be made. However, since the thermocouple receives radiation almost equally from the test specimen and from the furnace environment, the equation for heat flux entering the TC reads:

$$\dot{h}_{net,tc}=\alpha_{tc}\cdot\left(\theta_g-\theta_{tc}\right)+\frac{\varepsilon_r\cdot\sigma}{2}\cdot\left(\theta_r+273\right)^4+\frac{\varepsilon_a\cdot\sigma}{2}\cdot\left(\theta_m+273\right)^4-\varepsilon_{pt}\cdot\sigma\cdot\left(\theta_{tc}+273\right)^4$$

and the equation for the heat flux entering the specimen, again after subtracting the above equation, reads:

$$\dot{h}_{net,d} = \alpha_{tc} \cdot (\theta_{tc} - \theta_m) - (\alpha_{tc} - \alpha_m) \cdot (\theta_g - \theta_m) + \sigma \cdot \left[\varepsilon_{tc} \cdot (\theta_{tc} + 273)^4 - \varepsilon_a \cdot (\theta_m + 273)^4 \right] +$$

$$\frac{\sigma}{2} \cdot \left[\varepsilon_r \cdot (\theta_r + 273)^4 - \varepsilon_a \cdot (\theta_m + 273)^4 \right]$$

We see that, due to the large difference between α_m and α_{tc}, the convective term involving $(\theta_g - \theta_m)$ does not disappear; to the contrary, if α_{tc} may indeed be estimated at 150 W/m^{2}K, the term can be significant. The same goes for the radiative terms : the term involving furnace radiation is far from eliminated.

The above observations show that under TC control and the same simplifying assumptions, the heat flux to the specimen depends on furnace properties (θ_g, α_{tc}).

The tests carried out within the proving test programme of CEN TC 127 ad hoc 14 can be seen as corroborating evidence to the theoretical analysis.
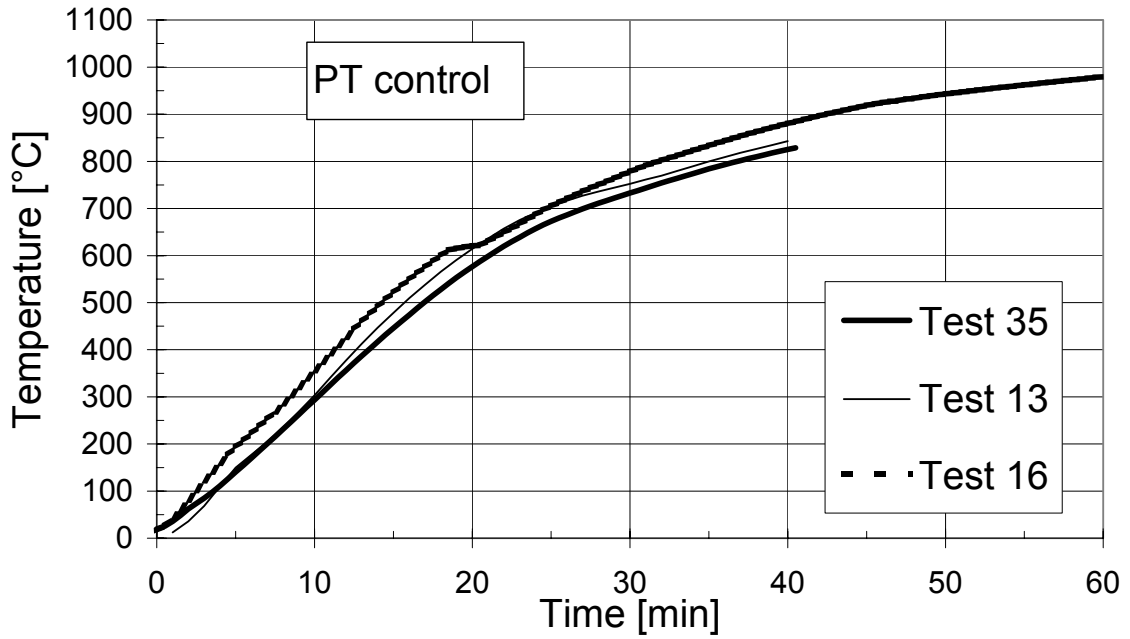
Figure 1: Temperature development in steel sections in different furnaces under PT control.
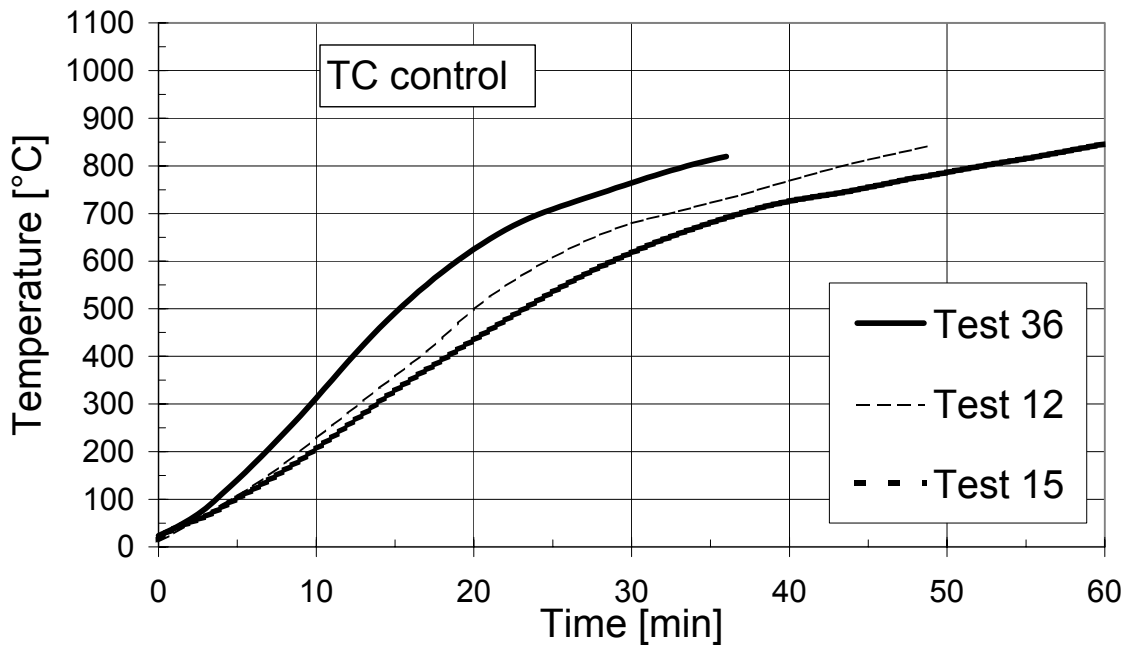
Figure 2: Temperature development in steel sections in different furnaces under TC control.

Calculated vs. measured steel temperature

$F/A = 90 \text{ m}^{-1}$
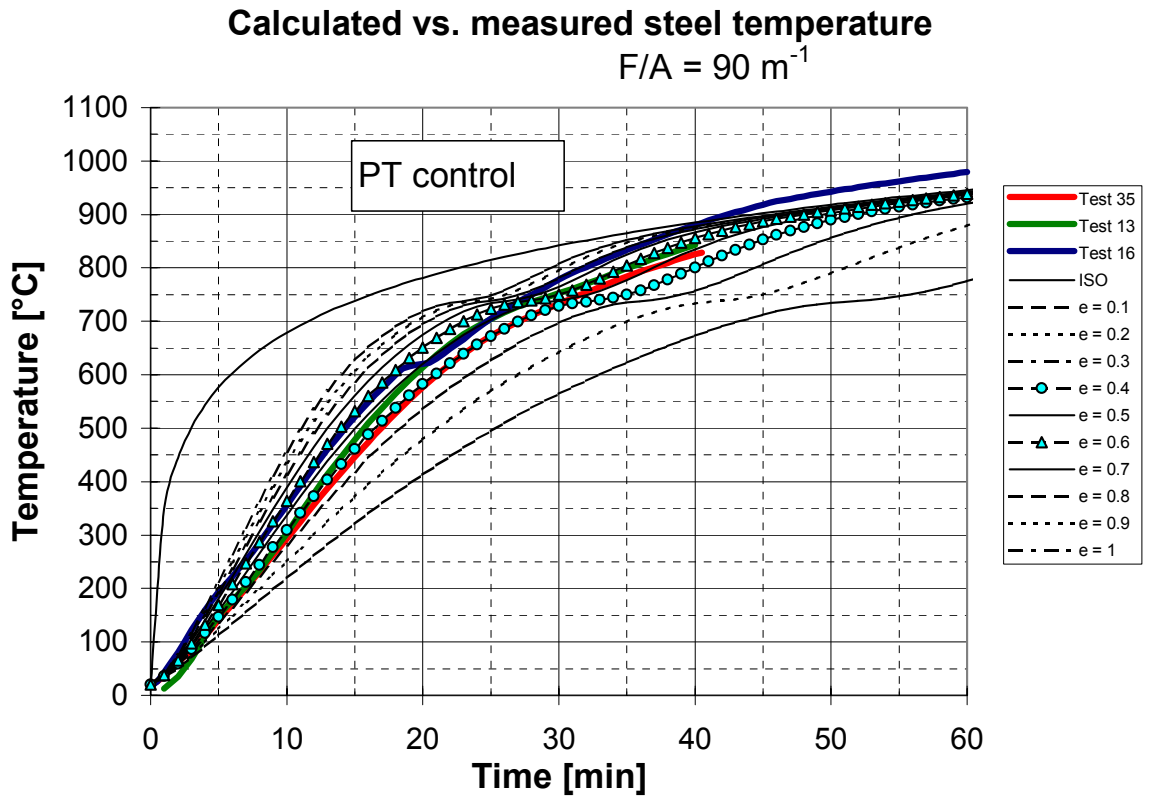
Figure 3: Comparison of measured steel temperatures with calculation results based on the Eurocode rules, however with different values of ε_{res}
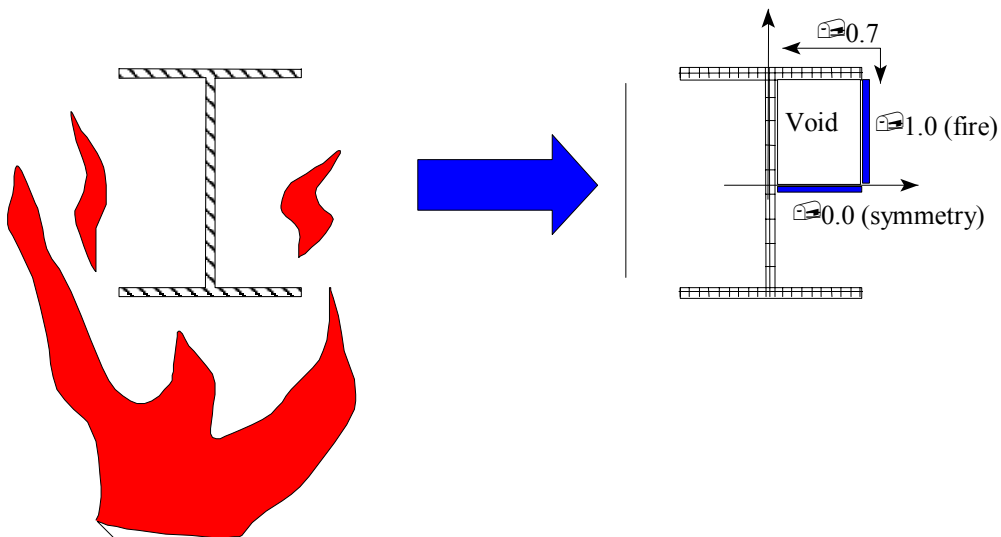
Figure 4: The shadow effect.
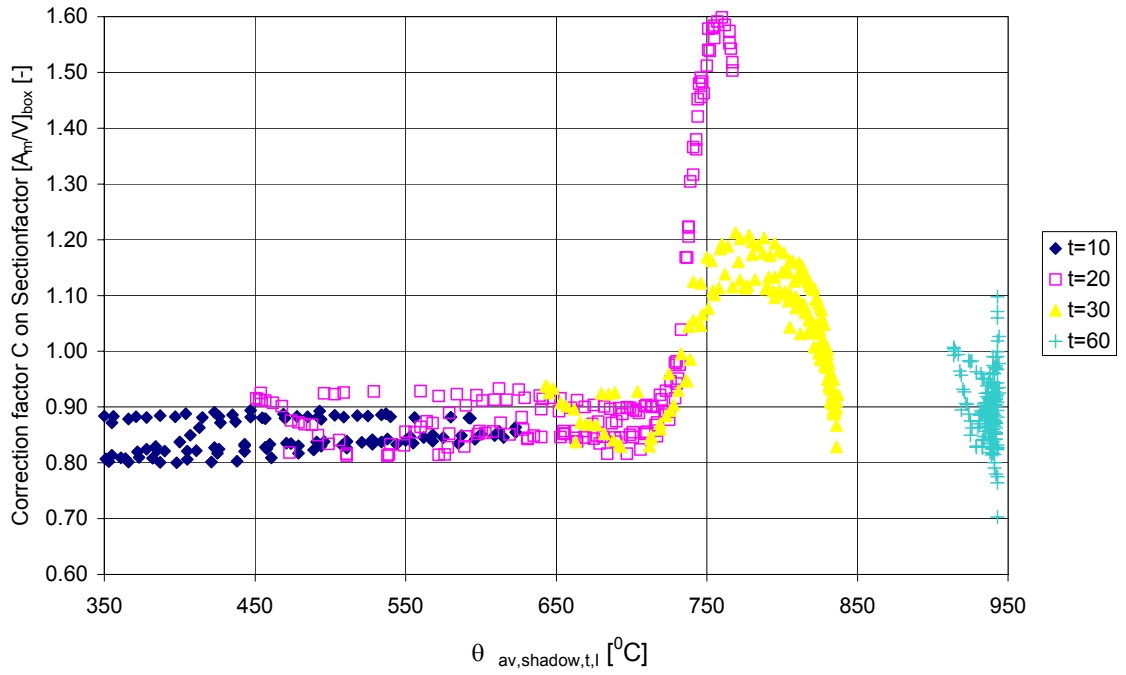
Figure 5: The calculated correction factor C as a function of the steel temperature simulated with finite element program DIANA, including the shadow effect.
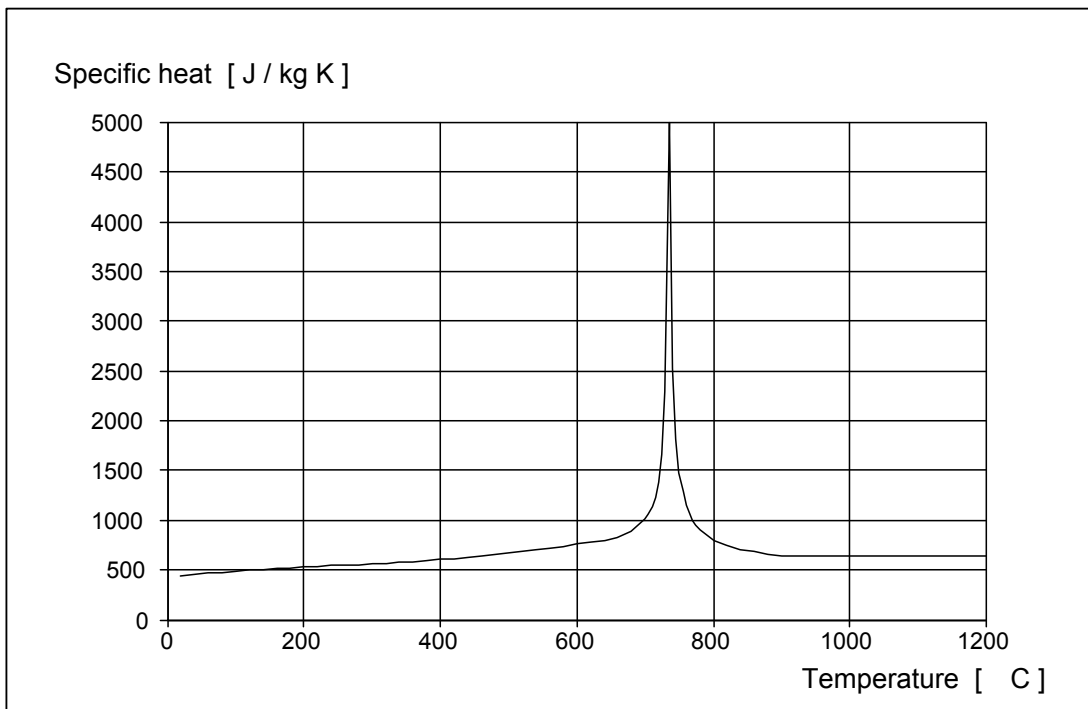
Figure 6: Specific heat of structural steel as a function of temperature [EC3].
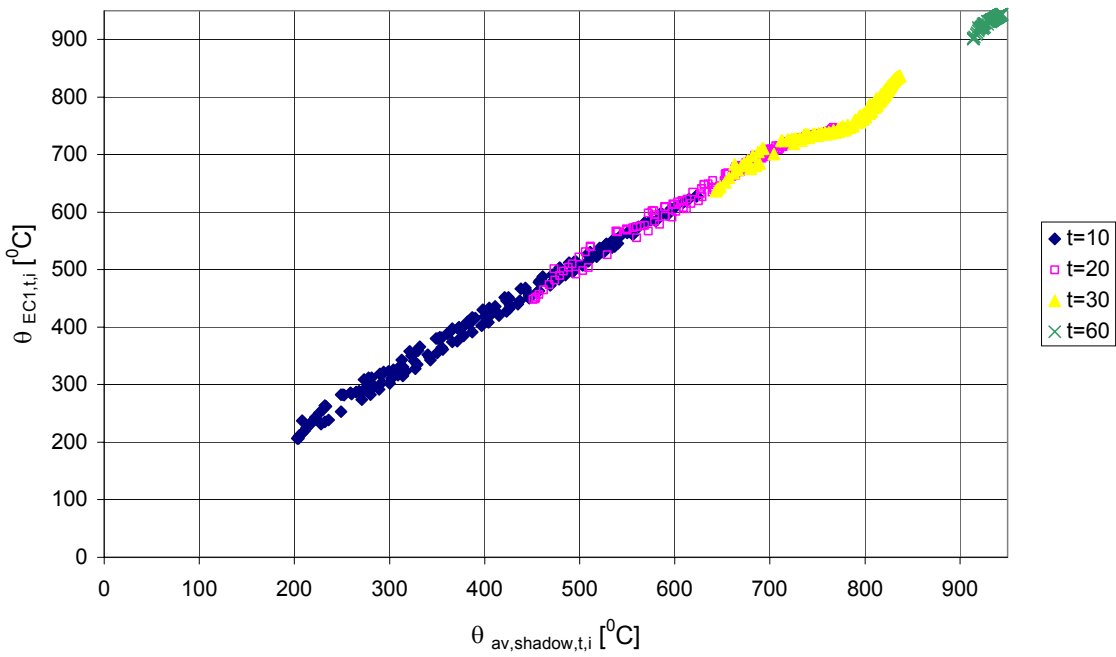
Figure 7:   *Comparison of simple Eurocode rule incorporating the shadow effect by means of a modified section factor to advanced finite element model results.*
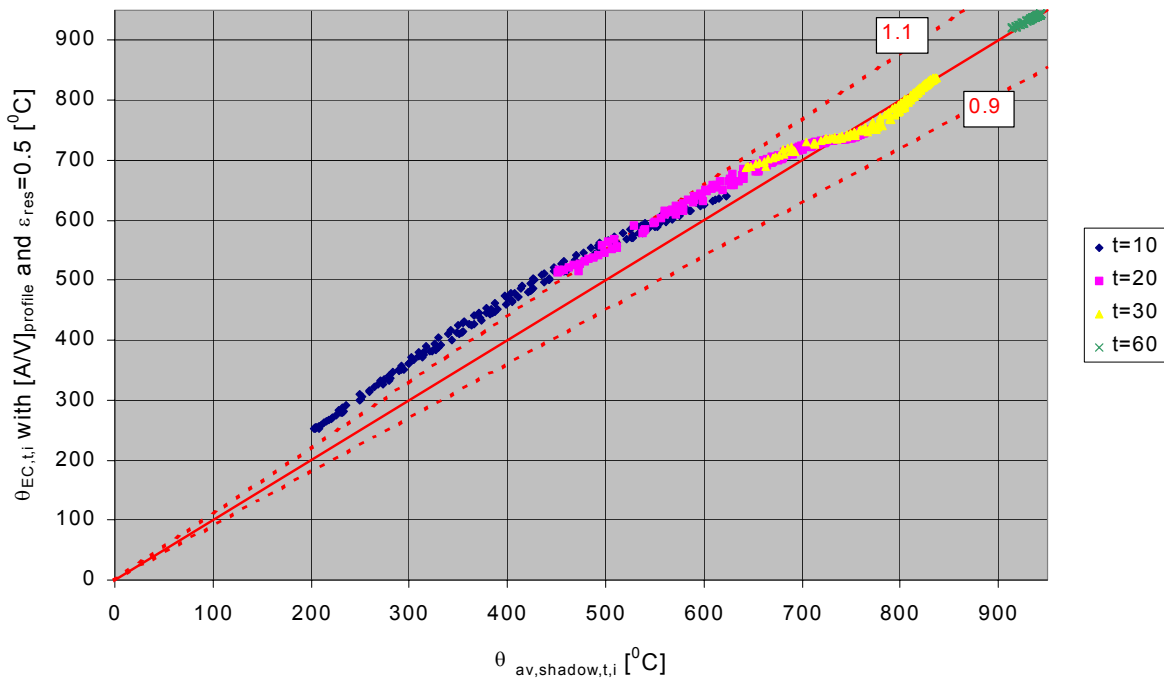
Figure 8: *Comparison of the present Eurocode rule to advanced finite element model results.*

THE RECENT U.K. BS9999 – PRESENTATION AND WORKED EXAMPLES

Mick Green
Buro Happold, Camden Mill, Lower Bristol Road, Bath BA2 3DQ, UK

ABSTRACT

In the UK a new set of prescribed fire precautions standards are being developed (BS9999). They are prescribed standards but fire safety engineering is being used to develop the guidance. This enables a much smoother transition between the normal prescribed approach and a fire safety engineered approach. A description of the impact of this new approach will be provided in combination with an explanation of the scope of the guidance being prepared by the Institution of Structural Engineers.

In addition a number of case studies of buildings where modelling has been used will be presented as follows.

1. SmithKline Beecham, London - headquarters building using whole frame modelling. A risk assessment approach was devised and also output from the Cardington frame fire tests was used.

2. Series of buildings involving external unprotected steelwork using natural fires in a developing architectural theme. This will involve a series of 4 buildings constructed over the last ten years. This includes major HQ building and a major government building in the UK.

Design of thin-walled steel channel columns in fire using Eurocode 3 Part 1.3

Y C Wang, J M Davies
Structures and Fire Research Group
Manchester School of Engineering, University of Manchester, UK

ABSTRACT

This paper presents the results of a preliminary investigation into the strength of cold-formed thin-walled columns under fire conditions. The ambient temperature design method for thin-walled columns in Eurocode 3 is modified to take into account the changes in steel strength and stiffness at elevated temperatures. Limited comparisons against available test results on channel columns in fire indicate that this method can be further developed into a suitable design tool for practical use.

A parametric study has been carried out using the modified design method, in which the influence on column failure temperatures of changing the column section depth, column length, temperature gradient and elevated temperature steel property models have been investigated. The results of this study suggest that the present Eurocode recommendation of limiting the failure temperature of thin-walled members to 350°C is very conservative. These results also indicate that for thin-walled columns with uniform temperature distribution, the limiting temperatures recommended by the SCI and based on the limiting temperatures of hot rolled steel are a good approximation of the column failure temperatures. However, the failure temperatures of columns with non-uniform temperature distribution can be higher or lower than those with uniform temperature, depending on the temperature difference, column section depth and column height. Finally, this paper briefly describes a comprehensive research programme which has recently started at the University of Manchester to experimentally and theoretically investigate the behaviour of cold-formed thin-walled steel structures in fire.

Keywords
Design method, Eurocode, Fire resistance, Thin-walled steel, Columns, Fire testing

Introduction

Due to the high thermal conductivity of steel leading to rapid steel temperature rise in a well developed fire, steel structures have been perceived to have low fire resistance and need expensive fire protection. In an effort to improve the competitiveness of steel structures by eliminating or substantially reducing fire protection to steel structures, many research studies have been carried out worldwide to develop a better understanding of the performance of steel framed structures under fire conditions. These research studies are both experimental and theoretical and concentrate not only on structural behaviour, but also on fire dynamics and heat transfer. They have been fruitful and with careful design considerations, it is now possible to substantially reduce the cost of fire protection to steel structures. Formal codes of practice (BSI 1990, CEN 1995) have been published to disseminate the results of these research studies into practice.

However, these research studies have largely concerned with steel structures made from hot-rolled steel and there are very few studies on the performance of cold-formed thin-walled steel structures in fire (Ala-Qutinen and Myllymaki 1995, Klippstein 1980, Gerlich et al 1996, Lawson 1993, Ranby 1998). As a result, the design of cold-formed steel structures for fire resistance is largely based on the results of manufacturers' standard fire resistance tests (e.g. Redland 1990). This limits the designers' choice of cold-formed steel systems. In addition, as design for fire safety is moving away from the standard fire resistance to natural fires, it will be difficult to make design decisions based on the standard fire resistance test results.

Against this background, with financial support from the UK's EPSRC (Engineering and Physical Science Research Council), the Structures and Fire Research Group at the University of Manchester has started a comprehensive research program to experimentally and theoretically investigate the performance of cold-formed thin-walled steel structures under fire conditions. This paper reports the results of a preliminary study and should be seen as merely making preparations for the more detailed investigations to be carried out within the EPSRC funded project.

In this paper, the design method in Eurocode 3 Part 1.3 (CEN 1996) for cold-formed thin-walled steel structures is adapted for applications under fire conditions. Columns made of channel sections are used as examples. After a brief description of the assumptions made in adapting the Eurocode 3 Part 1.3 method for fire design applications, this paper reports the results of a parametric study using the modified fire design method. The results of this study are then used to assess the accuracy of the preliminary design recommendations given in Eurocode 3 Part 1.2 (CEN 1995) and the Steel Construction Institute publication (Lawson 1993) based on the British Standard BS 5950 Part 8 (BSI 1990).

A brief introduction to the Eurocode design method at ambient temperature

For cold-formed thin-walled steel columns, since its gross-section centroid will inevitably be different from that of the effective section, it is not practical to arrange the column loading so that it is subject to pure axial compression only. Thus, thin-walled steel columns should generally be designed for combined bending and axial compression. Under such a loading condition, the design equations in Eurocode 3 Part 1.3 for cold-formed thin-walled steel columns are:

$$\frac{N_{sd}}{\chi_{min} f_y A_{eff}} + \frac{\kappa_y \left(M_{y,sd} + \Delta M_{y,sd} \right)}{f_y W_{eff,y,com}} + \frac{\kappa_z \left(M_{z,sd} + \Delta M_{z,sd} \right)}{f_y W_{eff,z,com}} \leq 1 \quad (1)$$

$$\frac{N_{sd}}{\chi_{lat} f_y A_{eff}} + \frac{\kappa_{LT} \left(M_{y,sd} + \Delta M_{y,sd} \right)}{\chi_{LT} f_y W_{eff,y,com}} + \frac{\kappa_z \left(M_{z,sd} + \Delta M_{z,sd} \right)}{f_y W_{eff,z,com}} \leq 1 \quad (2)$$

In both equations, the material partial safety factor is assumed to be unity and ignored.

Equation (1) is for checking flexural buckling and (2) for checking lateral torsional buckling of the column.

In these equations, N_{sd} is the applied axial load, M the applied bending moment, ΔM the bending moment due to shift of the column section centroid, f_y the steel design strength, A_{eff} the effective section area and $W_{eff,com}$ the elastic modules of the section with regard to the extreme compression fibre. The subscripts "y" and "z" indicate the major and minor axes of the cross-section. χ_{min} is the smaller of the two flexural buckling reduction factors about y and z axes, χ_{lat} the minimum of the buckling reduction factors among flexural buckling about the two axes and torsional buckling, χ_{LT} the lateral torsional bucking reduction factor under bending about the major (y-y) axis. The κ factors are modification factors to account for non-uniform bending moment distribution in the column.

In order to calculate the various factors in equations (1) and (2), it is first necessary to evaluate the effective cross-section under compression and bending about the y-y and z-z axes. Eurocode 3 Part 1.3 (CEN 1996) gives detailed guidance for ambient temperature calculations and these will not be repeated here.

Assumptions adopted for fire design

For fire design calculations, equations (1) and (2) are also used. Because of the temperature induced changes in steel strength and stiffness, it is necessary to introduce some assumptions in the calculations, especially with regard to evaluating the effective section of the column. These assumptions are:

(1) The elevated temperature stress-strain curve is elastic-perfectly plastic. Studies by Ala-Qutinen and Myllymaki (Ala-Qutinen and Myllymaki 1995) and Ranby (Ranby 1998) suggest to use the 0.2% proof stress for the design yield stress at elevated temperatures. When using the material model in Eurocode 3 Part 1.2 (CEN 1995), this is taken to be the stress for deformation control. When using the SCI guide (Lawson 1993), the stress corresponding to 0.5% total strain is used. In both cases, the same reductions in elasticity as given in Eurocode 3 Part 1.2 (CEN 1995) are used. In addition, Klippstein (Klippstein 1980) suggested the following models for reductions in the cold-formed steel strength and stiffness at elevated temperatures:

$$\frac{f_{y,T}}{f_y} = 1 - 5.3 \frac{T}{10^4} + 4 \frac{T^2}{10^6} - 1.9 \frac{T^3}{10^8} + 1.7 \frac{T^4}{10^{11}}$$

$$\frac{E_T}{E_0} = 1 - 3 \frac{T}{10^4} + 3.7 \frac{T^2}{10^7} - 6.1 \frac{T^3}{10^9} + 5.4 \frac{T^4}{10^{12}}$$

(3)

183

(2) The column section has a uniform temperature in its flange and lip on both the fire and cold sides and the temperature distribution in the web is such that the distribution of steel strength and stiffness is linear.

(3) For the flanges and lips of the section, the same method in Eurocode 3 Part 1.3 (CEN 1996) is used to evaluate the effective width, using the elevated temperature properties to replace those at the ambient temperature.

(4) For the web of the section, due to changing steel properties, the average steel strength and stiffness values are used. Thus, for calculations under pure compression, the average values at the two web-flange junctions are used. For calculations under bending about the y-y axis, the average values at the compressive web-flange junction and at the neutral axis position are used. To avoid iteration, the neutral axis is taken as that calculated for pure compression. With both stress and temperature gradients in the web, the proportioning of the effective width is according to that under stress gradient only.

(5) Calculations for the shear centre location and warping constant are complicated. In the modified design calculations, the shear centre and warping constant of the section remain unchanged at elevated temperatures. The average elasticity of the section is used to calculate the warping rigidity. The lateral torsional slenderness for fire design is 1.2 times that at ambient temperature. This factor is an approximation of $\sqrt{\dfrac{f_{y,T}}{E_T}}$.

(6) The axial load is applied through the centroid of the gross-section. Bending moment about the z-z axis is a result of shift of the centroid only. Bending moment about the y-y axis is a result of the shift of the centroid and thermal bowing. At the column ends, the centroid of the section shifts towards the cold side, thus putting the hot side in compression and the cold side in tension. At the column centre, due to thermal bowing, the column moves towards the fire (hot side), thus the cold side is in compression and the hot side in tension. Thermal bowing is assumed to be more important and calculations of the effective cross-section are carried out assuming the cold side in compression.

For a simply supported member, the temperature gradient induced thermal bowing deflection is given by the following equation:

$$\delta_{th} = \frac{\alpha.\Delta T.H^2}{8D} \qquad (4)$$

where D is the overall depth of the section, H the column height, α (taken as 0.000014/°C) the coefficient of thermal expansion of steel and ΔT the temperature difference between the hot and cold sides of the section.

(7) In equations (1) and (2), compressive strength governs the design. For fire design, since compression is on the cold side thus having a higher strength, and tension is on the hot side thus having a lower strength, either the tension or the compression stress may govern.

Many of these assumptions are based on intuitive reasoning and will be thoroughly examined during the detailed investigations.

Comparison against test results

Fire tests on cold-formed thin-walled steel structures have largely been done for manufacturers and due to associated commercial confidentiality, there are very few reported test results in the public domain to enable a thorough checking of the aforementioned design method. The research programme being conducted at the University of Manchester will provide the necessary experimental data. In the following paragraphs, the results of three tests on channel columns by Gerlich et al (Gerlich et al 1996) are used to give an indication of the validity of the design method.

Gerlich et al (Gerlich et al 1996) reported the results of three standard fire resistance tests on cold-formed thin-walled steel columns in a walling system. The test data are summarised in Table 1. Column strength predicted using the design method is also included. At the ambient temperature, the sheeting material prevented column buckling about the minor axis and torsional buckling. In Test 2, the sheeting performed well under the fire condition and only flexural buckling about the major axis was observed. The calculated flexural failure load agrees well with the test load for Test 2. In Test 3, the sheeting materials degraded near the end of the test and failed to provide restraint to the column against lateral torsional buckling. However, it may be argued that had the sheeting not been present, the test column would have failed under lateral torsional buckling much earlier. Equally, if the sheeting had performed well, flexural buckling failure would have occurred later. Therefore, two predicted values are given in table 1, one being the failure load under lateral torsional buckling (8.1 kN) and the other being the flexural buckling load (14.3 kN). As expected, the test load falls within this range. The predicted flexural buckling load for Test 1 is about 30% higher than the applied load. However, Gerlich et al (Gerlich et al 1996) reported that there had been no actual failure of this column before the column's load was redistributed to other members of the test panel. Thus, the actual failure load of Test 1 may have been somewhat higher.

Therefore, the test results of Gerlich et al (Gerlich et al 1996) may be used to provide an indication that the aforementioned design method may be further developed into a suitable tool for practical use. However, extensive theoretical and experimental studies will be necessary to validate this design method before it can be accepted in practice. The Structures and Fire Research Group has developed a well calibrated finite element program (Liu 1996) that can capture the various failure modes of thin-walled steel structures and this program will be used as part of the detailed investigation currently underway at the University of Manchester.

Table 1: Comparison against test results of Gerlich et al (Gerlich et al 1996)

Test No.	Section size	Steel grade	Column height	Hot face temp.	Cold face temp. (^{o}C)	Test load	Predicted load (kN)

		(N/mm²)	(m)	(°C)		(kN)	
1	Plain C 76x32x1.5	300	2.85	522	460	6	7.85
2	Lipped C 102x51x1.0	450	3.6	508	416	16	15.4
3	Lipped C 102x51x1.0	450	3.6	532	455	12	8.1-14.3

Discussions on results of a parametric study and an assessment of current design recommendations

Using the modified design equations described previously, a parametric study has been carried out to calculate the failure temperatures of channeled columns with a variation of design parameters. The values of these design parameters are:

Section size: three lipped channel sections of 100x55x1.6 mm, 200x55x1.6mm and 200x55x3mm. These sections have been chosen so that the results can give an indication of the effect of section depth and thickness;

Column height: 2m, 3m and 4m;

Temperature levels and gradients: this parametric study assumes that temperatures in the flanges of the section are uniform and the temperature in the web varies linearly from the hot flange to the cold flange. The hot flange temperatures are 400°C, 500°C, 600°C and 700°C. The cold flange temperature is assumed to be 0.4, 0.8 or 1.0 times that of the hot flange temperature. A hot and cold temperature combination of T and 0.8T may be regarded as the realistic distribution in thin-walled columns exposed to fire attack on one side only. A combination of T and 0.4T may be taken as the most severe temperature difference.

Elevated temperature material models: the yield stress of steel changes with temperature either as that in Eurocode 3 Part 1.2 (CEN 1995) for deformation control or as the stress at 0.5% strain given by Lawson (Lawson 1993). The Young's modulus changes as given in Eurocode 3 Part 1.2 (CEN 1995).

The results of this parametric study are presented in figures 1-4. In these figures, the column failure load is normalised with respect to its strength at the ambient temperature.

Figure 1 shows the effect of temperature gradient on column strength for different sections. The maximum temperature was 500°C and the trend for other levels of the maximum temperature is the same. It can be seen that for the three different sections, there is very little difference in the column failure temperature for uniform temperature distribution. The effect of temperature gradient is twofold: it is beneficial with a reduction in the average column temperature and it is detrimental with the associated thermal bowing leading to large bending moment. The column maximum failure temperature is governed by the net effect of these two factors.

Equation (4) gives a larger thermal deflection for longer columns (higher H) or shallower column sections (smaller D), leading to higher bending moments at the same axial load. Therefore, if the temperature in the column cross-section is unchanged, these types of

186

columns are expected to fail at a lower load. Figure 1 clearly shows this type of column behaviour as expected.

Figure 1 also suggests that for short columns when the thermal bowing induced bending moment is small, column failure is mainly due to compression, therefore non-uniform temperature distribution is beneficial and the column failure load is higher than the case of uniform temperature at the same maximum temperature. However, for longer columns, thermal bowing induced bending moments contributes significantly to the column loading, and the failure load is much lower in the case of non-uniform temperature distrbution.

The effect of changing the maximum steel temperature is shown in figure 2. Since the ratio of the lower to the higher steel temperature is fixed at 0.4, a higher steel temperature gives a larger temperature difference, therefore, the effect of temperature gradient is more pronounced for the higher maximum temperature. As previously seen in figure 1, the effect of non-uniform temperature distribution is much more significant on shallower columns.

Figure 3 shows the effect of using different steel strength models. Since the SCI model for 0.5% strain gives lower strength than the Eurocode 3 model for deformation control, lower column strength is predicted using the SCI model. Since the steel modulus is the same in both models, the change in the column strength is not as significant as that in the steel stress.

Figure 4 presents an assessment of the current design guidance for thin-walled structural members. Uniform temperature is assumed in this figure. It is clear that the failure temperature is significantly higher than $350^{o}C$ recommended in Eurocode 3 Part 1.2 (CEN 1995). The SCI recommended limiting temperatures are based on reductions of about 40-$60^{o}C$ from those of hot-rolled slender columns. It seems that the SCI recommendations (Lawson 1993) give a reasonably accurate and safe estimate of the failure temperatures of thin-walled columns obtained using the design equations in Eurocode 3 Part 1.3.

In the same SCI design guidance (Lawson 1993), higher limiting temperatures are given for columns in walls. It is understood that temperature gradients will exist in this type of columns, therefore, their failure temperatures will be similar to the results shown in figures 1 and 2. Whilst short columns with temperature gradient may fail at higher maximum temperatures than those without temperature gradient, longer columns with temperature gradients can have much lower failure temperatures. Therefore, it may not always be safe to recommend improved column failure temperatures when there is temperature gradient.

Future research studies

From previous discussions, it is clear that there is need for a comprehensive investigation of the fire performance of cold-formed thin-walled steel structures. While both experimental and theoretical studies will be necessary, it is vital that some quality test data are obtained to enable proper understanding of the structural element behaviour as well as to provide test data for validating numerical models.

To resolve this problem, the Structures and Fire Research Group has started a comprehensive research programme funded by the UK's EPSRC. This research opportunity has arisen due to the availability of a number of fire testing furnaces and numerical capabilities to the research group.

In this three year research programme, the thermal and structural performance of different types of cold-formed thin-walled structural members will be experimentally studied in the research group' furnaces. The test results will be used to check the accuracy of the thermal and structural analysis programs (Wang 1995, Liu 1996) that have already been developed in the research group. The validated computer programs will then be used to generate parametric data to be used in the development of suitable design guidance.

Conclusions

This paper has presented the results of a preliminary investigation into the strength of cold-formed thin-walled steel channel columns under fire conditions. The ambient temperature design method in Eurocode 3 Part 1.3 (CEN 1996) has been modified to take into account the temperature effect. A very limited comparison against available test results is then carried out. This modified design method is used to study the influence of a number of design parameters on the strength of channel columns. From the results of this preliminary study, the following tentative conclusions may be drawn:

(1) The modified method has the potential to be further developed into a suitable design tool for practical use.
(2) For thin-walled columns with uniform temperature, the Eurocode 3 Part 1.2 (CEN 1995) recommended failure temperature of $350^{o}C$ is very conservative.
(3) The failure temperatures recommended by SCI (Lawson 1993) which are based on the current British Standards for hot-rolled steel (BSI 1990) seem to provide a reasonable and safe approximation to the values obtained using the modified design method.
(4) Temperature gradient can be beneficial or detrimental, thus it may not always be safe to follow the SCI recommendations that only give improved failure temperatures.
(5) Further experimental research studies are necessary to enable better understanding of performance of thin-walled steel structures in fire and to provide results for calibrating numerical procedures. With financial support from the EPSRC, the University of Manchester has recently started a comprehensive research programme.

References

- Ala-Qutinen T. and Myllymaki J. (Ala-Qutinen and Myllymaki 1995), The local buckling of RHS members at elevated temperatures, VTT research notes 1672, Technical Research Centre of Finland, ESPOO, Finland
- British Standards Institution (BSI 1990), British Standard BS 5950: Structural use of steelwork in buildings, Part 8: Code of practice for fire resistant design, BSI
- European Committee for Standatdization (CEN 1995), Eurocode 3: Design of steel structures, Part 1.2: General rules, Structural fire design, CEN
- European Committee for Standardization (CEN 1996), Eurocode 3: Design of steel structures, Part 1.3: General rules, supplementary rules for cold formed thin gauge members and sheeting, CEN
- Gerlich J.T., Collier P.C.R. and Buchanan A.H. (Gerlich et al 1996), "Design of light steel-framed walls for fire resistance", Fire and Materials, Vol. 20, pp. 79-96
- Klippstein K.H. (Klippstein 1980), Strength of cold-formed studs exposed to fire, American Iron and Steel Institute, Washington DC

- Lawson R.M. (Lawson 1993), "Building design using cold formed steel sections: Fire protection", The Steel Construction Institute Publication P129, SCI, Ascot, Berkshire, UK
- Liu T.C.H. (Liu 1996), "Finite element modelling of behaviour of steel beams and connections in Fire", *Journal of Constructional Steel Research*, **36**:2, 181-199
- Ranby A. (Ranby 1998), "Structural fire design of thin walled steel sections", Journal of Constructional Steel Research, Vol. 46:1-3, Paper No. 176
- Redland Plasterboard (Redland 1990), Redland Drywall Manual
- Wang H.B. (Wang 1995), Heat transfer analysis of components of construction exposed to fire, PhD thesis, University of Salford

Acknowledgment
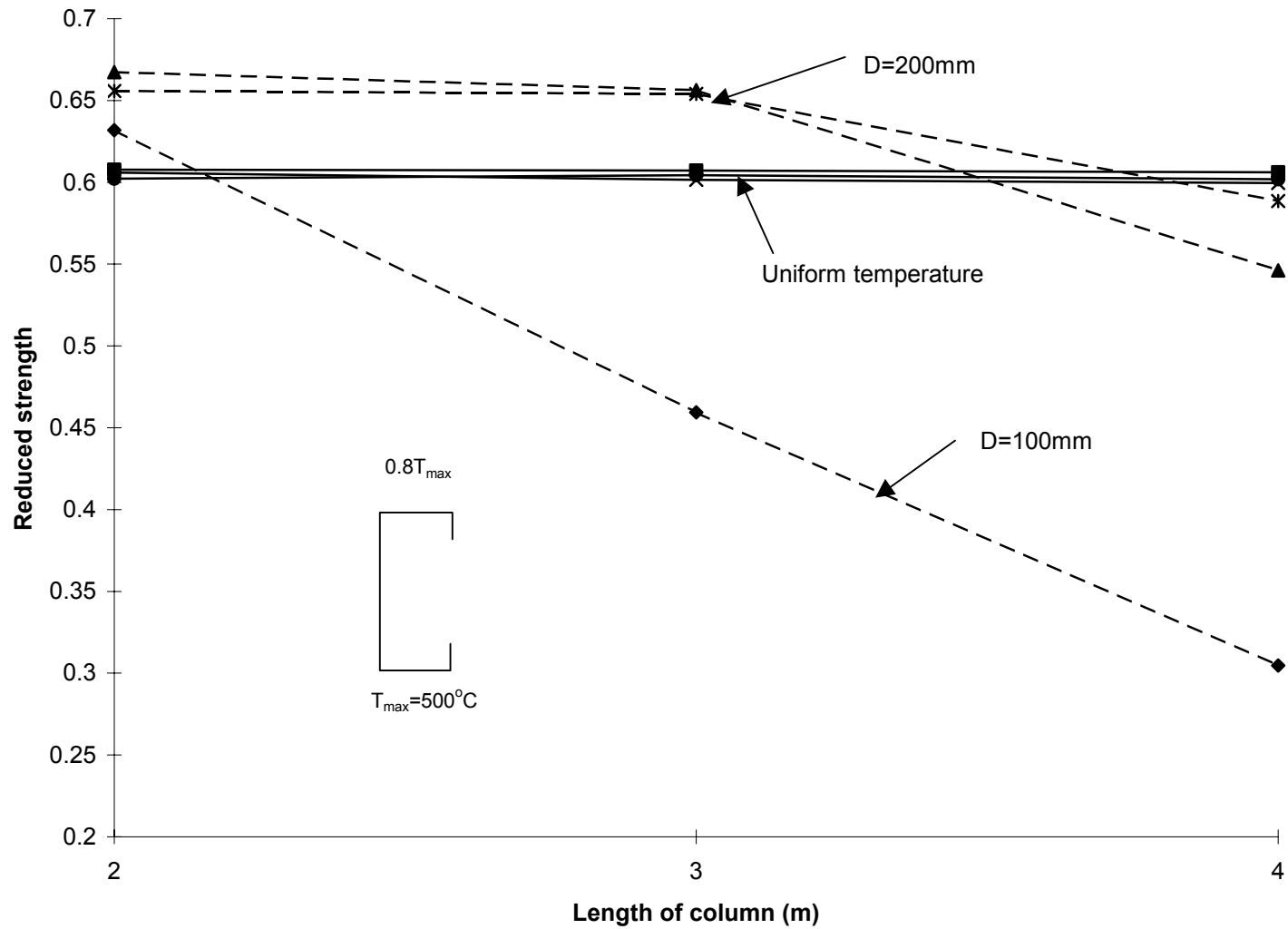
Fig 1 Effect of temperature gradient for different sections, Eurocode material model
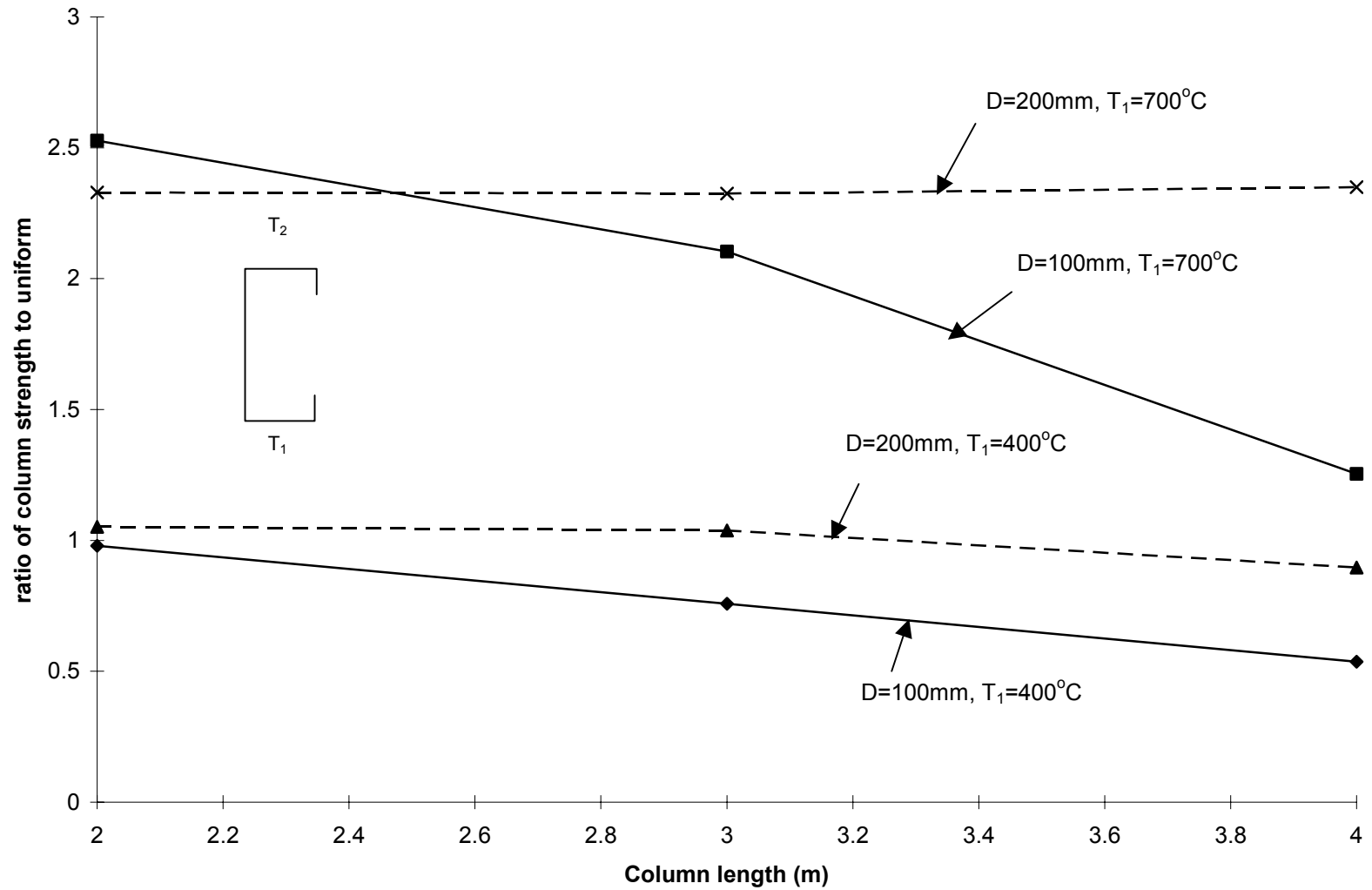
Fig 2. Effect of temperature gradient, T_2/T_1=0.4, Eurocode material model
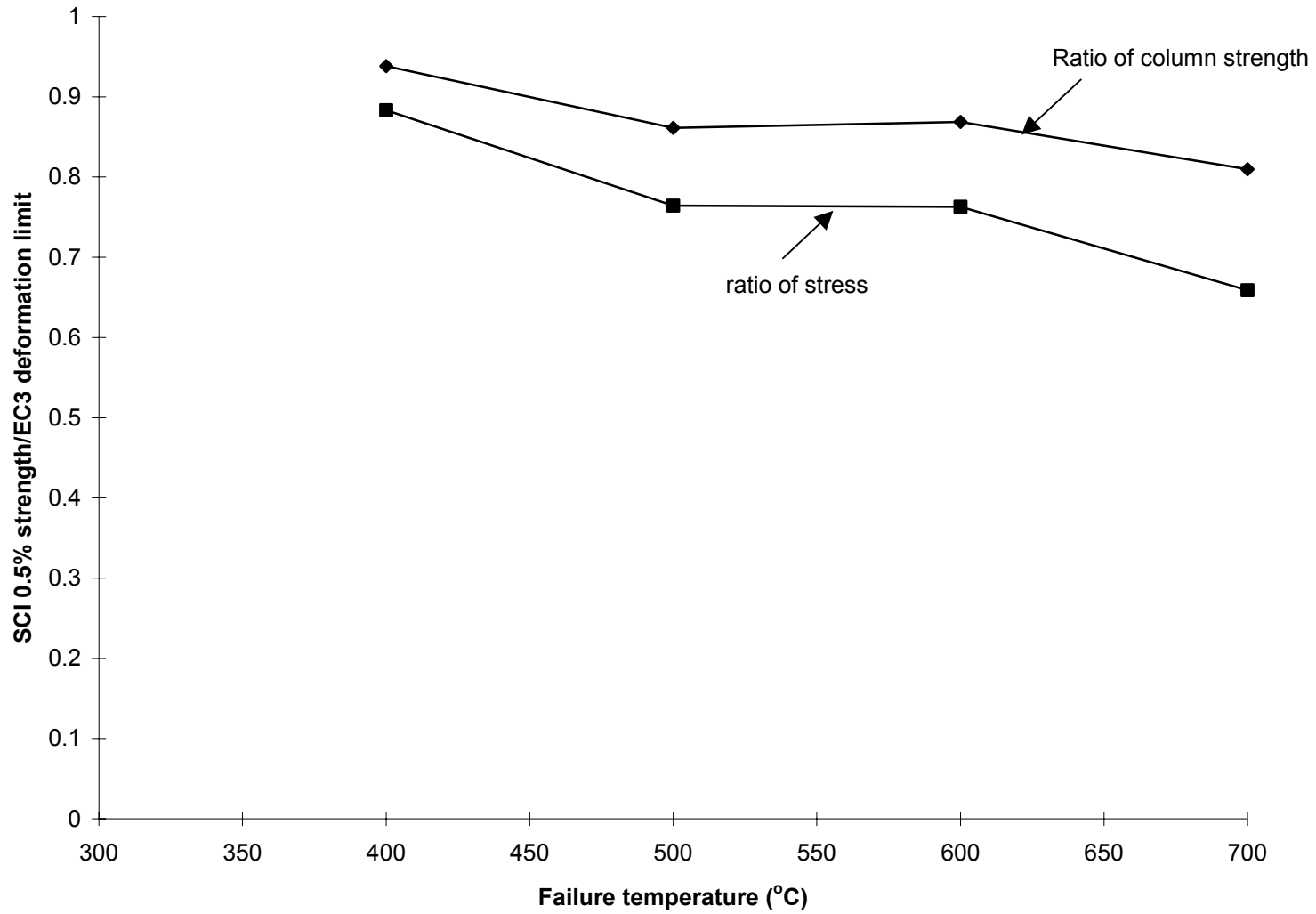
Fig 3 Effect of material models, 100x55x1.6, uniform temperature, H=2m
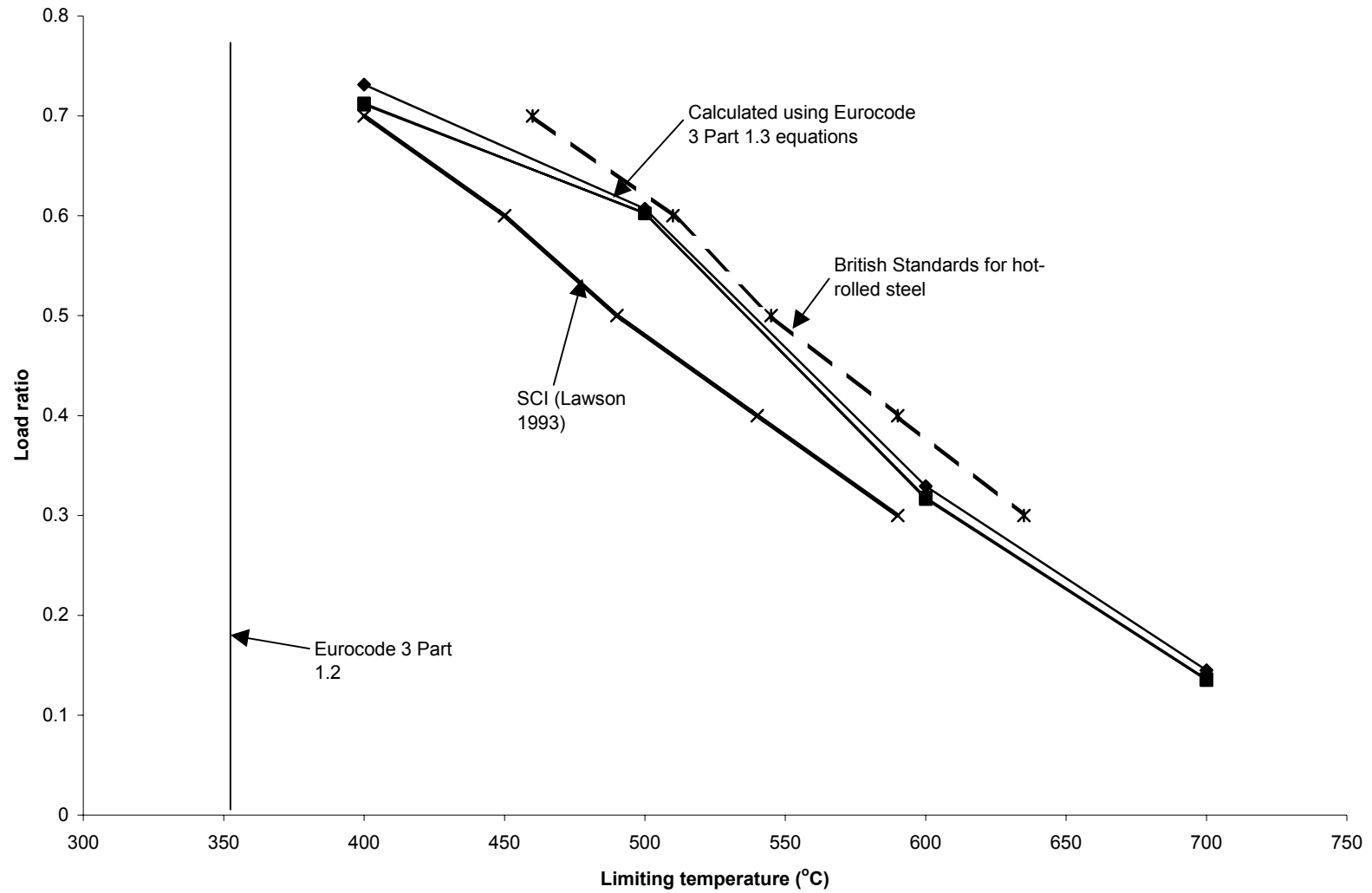
Fig 4 Limiting temperatures: a comparison with design values, uniform temperature

NEW QUADRANGULAR SHELL ELEMENT IN SAFIR

Didier TALAMONA – Jean-Marc FRANSSEN
Univ. of Liège, SPEC, 1 Chemin des Chevreuils, 4000 Liège 1, Belgium
d.talamona@ulg.ac.be – jm.franssen@ulg.ac.be

Abstract

SAFIR is a finite element program for the thermal and mechanical analysis of structures submitted to fire. Usually, thermal calculations are run in a first step to determine the temperatures in the structure subjected to fire. In a second step, mechanical analyses are performed to determine the time when collapse will occur.

In case of mechanical analysis, different elements are available in SAFIR : truss, beam and shell.

The shell element in SAFIR was a triangle with 6 nodes. It gave good results except in case of 'membrane bending' where the answer was too stiff. Furthermore, this element was heavy to use because 3 nodes had 6 DOF and the 3 others had only 1 DOF.

In order to improve SAFIR, it has been decided to introduce a new quadrangular element to eliminate the over-stiffness of the triangular element in case of 'membrane bending'. This element has been taken from the room temperature program FINELG (developed by de Ville at the University of Liège and the Bureau d'Etudes Greisch).

In a first step, this element has been introduced in SAFIR with success. The material law has then been modified to perform calculations under fire conditions. Calculations may be performed using bi-linear or elliptical hardening (according to ENV 1993-1-2). The 2 D yield surface is the Von Mises surface. The ultimate strength, the Young modulus, the limit of proportionality and the thermal expansion also follow the recommendations of ENV1993-1-2.

Some validation examples are presented: a Z-Shaped cantilever, an hemispherical shell and Lee's frame are treated.

Keywords : *SAFIR, finite element, shell, thermal*

FORMULATION OF THE SHELL ELEMENT

This element has been taken (and adapted) from the program Finelg developed by de Ville at the University of Liège and the Bureau d'Etudes Greisch [1, 2, 3, 4, 5].

Reference configuration

For this quadrangular element the *z* axis is obtained as follows:
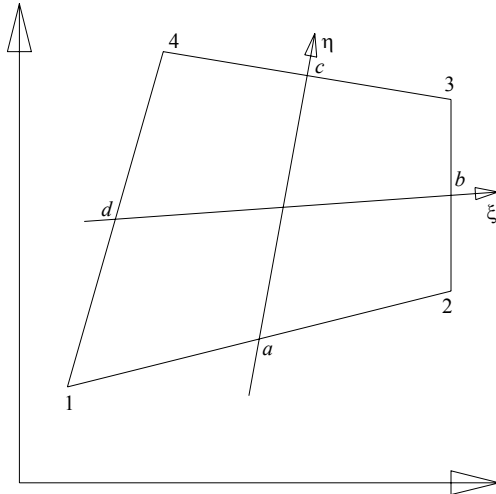
Figure 1 : Reference configuration.

a, *b*, *c* and *d* are the middle edge points, not necessarily located in one plane. The *z* axis is defined as:

$$\underline{z} = \frac{\left(\underline{db} \wedge \underline{ac} \right)}{\left\| \underline{db} \wedge \underline{ac} \right\|} \tag{1}$$

Another way to define the *z* axis could be to find the best plane reference for the element :

$$w_0 = \alpha_1 + \alpha_2 x + \alpha_3 y \tag{2}$$

It can be shown that, if the coefficients α_2 and α_3 are chosen in such a way that the orientation of the reference plane minimizes the slopes between the element and the plane, then the *z* axis defined by eq. 1 is perpendicular to the plane. This proves that eq. 1 minimizes also the slopes.

In eq. 2, α_1 is still undetermined. It will be chosen in such a way that the plane of reference goes through the center of gravity of the quadrangle.

As it will be seen later, the membrane strains are not complete polynomials, so the results will be dependent on the choice of the *x*, *y* local axis. The angle between the *x* axis and $\underline{bd}$ is imposed to be equal to the angle between $\underline{ac}$ and the *y* axis. This determines the choice of the *x*, *y* axis. For a rectangular element, this gives local axes parallel to the edges.
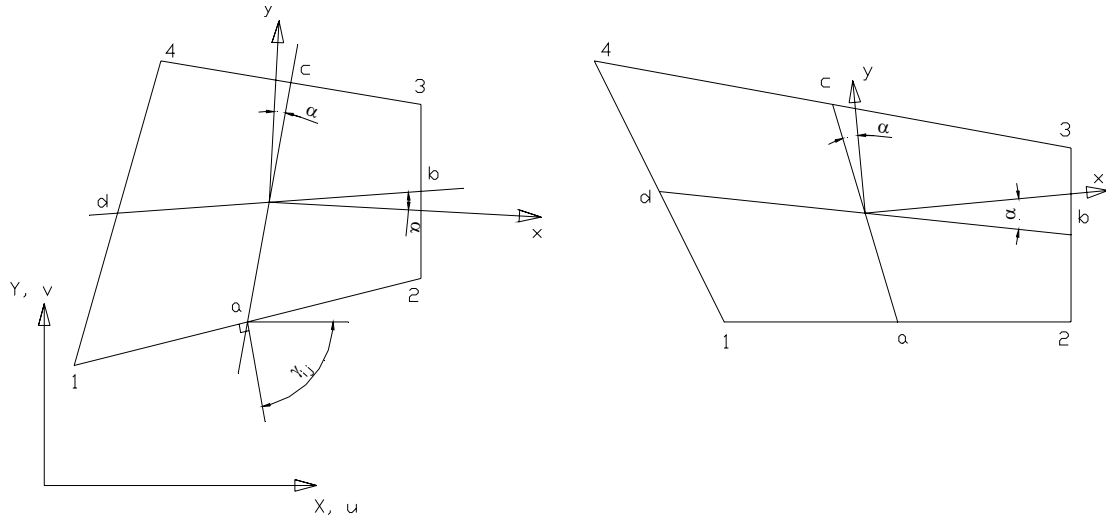
Figure 2 : Local axes *x* and *y*.

The membrane behavior

The classical quadratic membrane displacement field is enlarged to cubic degree by means of cubic (along ξ and η) functions and constants A_{ij}. It is the same development as ALLMAN [6] for a triangle element.

$$u = \frac{1}{4}\left[\sum_{k=1}^{4}(1+\xi\xi_k)(1+\eta\eta_k)u_k + \sum_{sides}\phi_{ij}l_{ij}\cos\gamma_{ij}(\omega_j - \omega_i) + \sum_{sides}\psi_{ij}l_{ij}\cos\gamma_{ij}\ A_{ij}\right]$$

(3)

$$v = \frac{1}{4}\left[\sum_{k=1}^{4}(1+\xi\xi_k)(1+\eta\eta_k)v_k + \sum_{sides}\phi_{ij}l_{ij}\sin\gamma_{ij}(\omega_j - \omega_i) + \sum_{sides}\psi_{ij}l_{ij}\sin\gamma_{ij}\ A_{ij}\right]$$

$$\phi_{12} = \frac{1}{16}(1-\xi^2)(1-\eta) \qquad\qquad \psi_{12} = \frac{1}{8}(1-\xi^2)(1-\eta)\xi\eta^2$$

$$\phi_{23} = \frac{1}{16}(1+\xi)(1-\eta^2) \qquad\qquad \psi_{23} = \frac{1}{8}(1+\xi)(1-\eta^2)\xi^2\eta$$

$$\phi_{34} = \frac{1}{16}(1-\xi^2)(1+\eta) \qquad\qquad \psi_{34} = -\frac{1}{8}(1-\xi^2)(1+\eta)\xi\eta^2$$

(4)

$$\phi_{41} = \frac{1}{16}(1-\xi)(1-\eta^2) \qquad\qquad \psi_{41} = -\frac{1}{8}(1-\xi)(1-\eta^2)\xi^2\eta$$

$$l_{ij} = \sqrt{(x_j - x_i)^2 + (y_j - y_i)^2}$$

(5)

$$A_{ij} = \frac{\omega_i + \omega_j}{2} + \frac{B_{ij} + B_{ji}}{2}$$

(6)

ω_i is the rotation at node i and ω_j is the rotation at node j.
γ_{ij} is the direction of the outward normal along the edge ij.
If i = 1 and j = 2 then B_{ij} and B_{ji} are equal to (for the complete definition see [7]):

$$B_{12} = \frac{1}{4 J_1} \left(x_{41} u_1 + x_{14} u_2 + y_{41} v_1 + y_{14} v_2 \right) \tag{7}$$

$$B_{21} = \frac{1}{4 J_2} \left(x_{23} u_1 + x_{32} u_2 + y_{23} v_1 + y_{32} v_2 \right) \tag{8}$$

$$J_1 = \frac{1}{4} \left(x_{21} y_{41} - x_{41} y_{21} \right) \tag{9}$$

$$J_2 = \frac{1}{4} \left(x_{21} y_{32} - x_{32} y_{21} \right) \tag{10}$$

The function ψ_{ij} are chosen so as to be orthogonal to ϕ_{ij} with respect to integration over the quadrangle.

To improve the convergence, the shear strains are assumed to be constant over the element. After some calculation, the following equations are found:

$$\varepsilon_x = \frac{1}{8J} \left[(y_{42}u_{31} - y_{31}u_{42}) + \xi(y_{21}u_{43} - y_{43}u_{21}) + \eta(y_{41}u_{32} - y_{32}u_{41}) \right]$$

$$\varepsilon_y = \frac{1}{8J} \left[(v_{42}x_{31} - v_{31}x_{42}) + \xi(v_{21}x_{43} - v_{43}x_{21}) + \eta(v_{41}x_{32} - v_{32}x_{41}) \right] \tag{11}$$

$$\bar{\gamma} = \frac{1}{8J_0} \left[(u_{42}x_{31} - u_{31}x_{42}) + (y_{42}v_{31} - y_{31}v_{42}) \right]$$

J is the determinant of the Jacobian matrix, J_0 is the value of J at $\xi = \eta = 0$ and x_{31} is $x_3 - x_1$

Flexural behavior

The formulation used is a Discrete Kirchhoff theory Quadragular (DKQ). This element is fully described in [8, 9, 10, 11]. The principle of this element will be briefly recalled here. The presentation is slightly different from the one given in [8, 9, 10].

The out-of-plane displacement and the rotations are parabolic over each side:

$$w = \sum_{i=1}^{8} N_i w_i \qquad \beta_x = \sum_{i=1}^{8} N_i \theta_{yi} \qquad \beta_y = \sum_{i=1}^{8} N_i \theta_{xi} \tag{12}$$

N_i are the shape functions and they depend on the parametric coordinates ξ and η.
Along the side i, the out-of-plane displacement is given by:

$$w = -\xi \frac{(1-\xi) w_A}{2} + (1-\xi^2) w_C + \frac{\xi(1+\xi) w_B}{2} \tag{13}$$

w_A, w_B and w_C are the normal displacements along z axis normal to xy plane (at the points A, B, and C). If we look to one edge of the element, for example the edge from node 1 to node 2, the node 1 is called A, the node 2 is called B and the middle point is called C, see Figure 3.
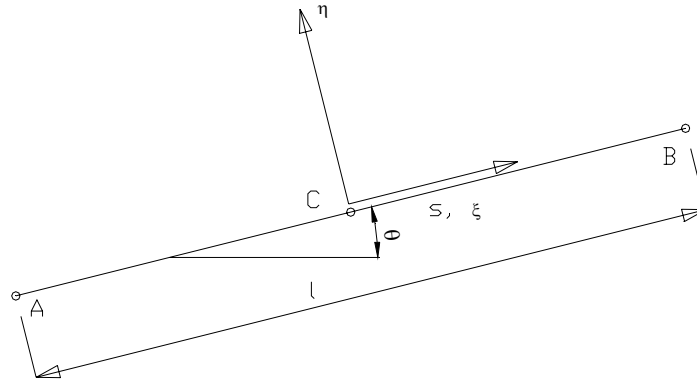
Figure 3 : Local axis on one side.

The contribution of the shear strain energy is neglected.
To reproduce thin plate theory, the Kirshhoff condition is imposed at selected points. In this element, the Kirshhoff constraints are imposed along the edges. The shear strain γ_{sz} at each of the two-point Gauss integration points along the sides is set to zero. Or, which is the same, weighted averages of the shear strain are set to zero:

$$\int_l \gamma_{sz}\, ds = 0 \qquad \int_l \gamma_{sz}\, s\, ds = 0 \tag{14}$$

Moreover, the rotation around the side θ_s is imposed to vary linearly.

$$w_{,s} = \frac{-(1-2\xi)w_A + 4\xi w_C + (1+2\xi)w_B}{l} \tag{15}$$

General features

The thickness is constant over the element.

The integration on the surface is performed with a 2 x 2 points Gauss scheme. The integration on the thickness is performed with a Gauss scheme using a user defined number of points.

The temperature varies on the thickness of the element and comes from a thermal SAFIR analysis which has to be performed before the mechanical analysis. The temperature distribution on the thickness is the same at every surface point of integration.

MATERIAL PROPERTIES

A steel material law has been introduced in SAFIR to perform calculations at elevated temperature. Plane stress relationships have been introduced for isotropic materials.
The thermal strain is taken into account in SAFIR according to ENV 1993-1-2 and it is supposed to be hydrostatic (i.e. $\varepsilon_{thxx} = \varepsilon_{thyy} = \varepsilon_{th}$).
Two types of hardening relationships have been introduced in SAFIR : linear and elliptical.
For linear hardening, the input data are E_0, E^* and f_y, see figure 4.
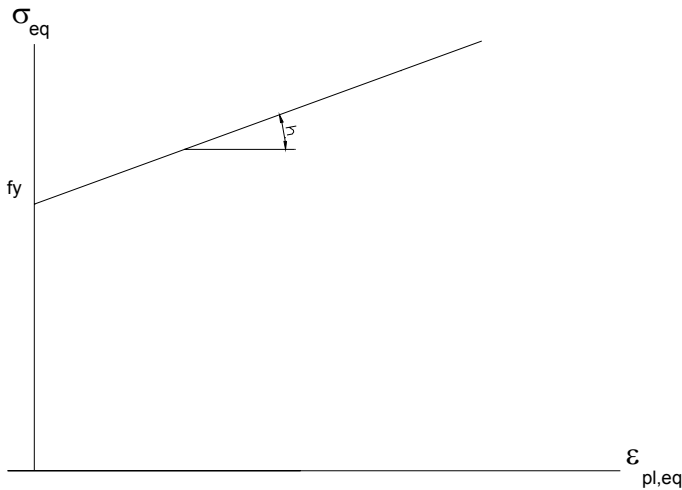
Figure 4 : Linear hardening

With : $h = \dfrac{E * E^*}{E - E^*}$ (16)

The elliptical law is not exactly equal to the function defined as the stress-strain relationship in the EC3. This is because EC3 defines the relationship in the σ-ε plane, whereas the present law is defined in the σ_{eq}-$\varepsilon_{pl,eq}$ plane (figure 5).

The hardening function is defined as:

$$\sigma_{eq} = f_p \sqrt{b \left[1 - \frac{\left(\varepsilon_{pl,eq} - a \right)^2}{a^2} \right]}$$ (17)

$a = 0.02 - f_y / E$ $\qquad\qquad b = f_y - f_p$

f_y : Ultimate strength, $\qquad$ f_p : Limit of proportionality, $\qquad$ $\varepsilon_{pl,eq}$: Equivalent plastic strain
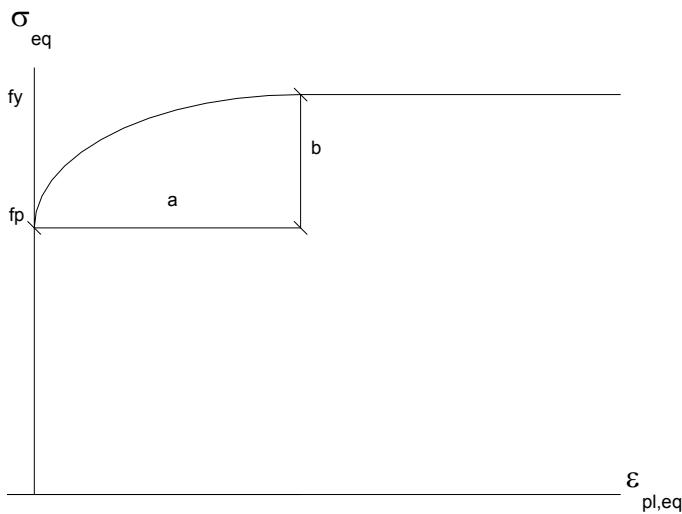
Figure 5 : Elliptic hardening

200

Evolution of the parameters at elevated temperatures

The following equations are used to calculate the Yield strength, the Young modulus, Tangent modulus and the Proportional limit at elevated temperature:

$$\sigma_{y,\theta} = k_{y,\theta}\,\sigma_{y,20} \qquad E_\theta = k_{E,\theta}\,E_{20} \qquad \sigma_{p,\theta} = k_{p,\theta}\,\sigma_{y,20} \qquad E_\theta^* = k_{E,\theta}\,E_{20}^*$$

The coefficients $k_{y,\theta}$, $k_{E,\theta}$ and $k_{p,\theta}$ are defined in ENV 1993-1-2.

Algorithmic strategy

A point of the structure at the time '*t*' (step *n*) is represented by **A** on figure 6. It is defined by:

t_n	: time
T_n	: temperature at the time t_n
σ_{eq} - $\varepsilon_{pl,eq}$	: the hardening function, depending on T_n
$\varepsilon_{pl,eq,n}$	: the equivalent plastic strain
$\{\sigma_n\}$	: the stress vector
$\{\varepsilon_{tot,n}\}$	: the total strain vector
$\{\varepsilon_i\}$	: the initial strain vector
$\{\varepsilon_{th,n}\}$	: the thermal strain vector
$\{\varepsilon_{m,n}\}$	: the mechanical strain vector
$\{\varepsilon_{pl,n}\}$	: the plastic strain vector
$[D_n]$	: elastic constitutive matrix

If the initial strain $\{\varepsilon_i\}$ and the thermal strain $\{\varepsilon_{th,n}\}$ are subtracted from the total strain $\{\varepsilon_{tot,n}\}$, the mechanical strain $\{\varepsilon_{m,n}\}$: is obtained from

$$\{\varepsilon_{m,n}\} = \{\varepsilon_{tot,n}\} - \{\varepsilon_i\} - \{\varepsilon_{th,n}\} \tag{18}$$

It is also possible to calculate the plastic strain, i.e. the mechanical strain that would exist in the structure if it was elastically unloaded. This is point **B** on figure 6. Note that the unloaded structure is not equivalent to the initial structure (non deformed). The equation is

$$\{\varepsilon_{pl,n}\} = \{\varepsilon_{m,n}\} - [D_n]^{-1}\{\sigma_n\} \tag{19}$$

When the temperature changes from T_n to T_{n+1}, it is possible to determine the new Von Mises surface which corresponds to the new hardening parameter, assuming that the plastic strain is not affected by the variation of temperature, i.e. the plastic strain is not modified from the end of step *n* to the beginning of step *n+1*.

In the algorithm used by SAFIR, it is supposed that the structure is 'locked' at the first iteration of each time step, i.e.

$$\{\varepsilon^J_{tot,n+1}\} = \{\varepsilon_{tot,n}\} \tag{20}$$

As the thermal strain is modified by the variation of temperature, the 'mechanical' strain changes accordingly:

$$\{\varepsilon^J_{m,n+1}\} = \{\varepsilon_{tot,n}\} - \{\varepsilon_i\} - \{\varepsilon_{th,n+1}\} \tag{21}$$

It is now represented by the point **D** on figure 6. The segment **A-D** represents the increase of thermal strain from temperature T_n to T_{n+1}. As the thermal strain is hydrostatic, this part is inclined at 45° on figure 6 b.

For each iteration the calculation will start from the unloaded structure (point **B**). The strain increment to be applied from the unloaded state is given by:

$$\{\Delta\varepsilon^1\} = \{\varepsilon^1_{m,n+1}\} - \{\varepsilon_{pl,n}\} \tag{22}$$

The classic plasticity theory is applied at temperature T_{n+1} in order to load the structure from point **A** to point **D**, see figure 6. The stress $\{\sigma^1_{n+1}\}$ and the new tangent matrix $[D^1_{t,n+1}]$ are computed. The return mapping algorithm, and Euler backward algorithm for the integration of the plastic strain, established at ambient temperature are used here.

Of course, the stresses obtained in the structure after the first iteration are not in equilibrium and they generate out of equilibrium forces in the structure which, using the new tangent stiffness matrix allow the calculation of displacement increments and their corresponding strain increments $\{\Delta\varepsilon^{1-2}\}$

At next iteration, the strain increment to be applied from the unloaded state is:

$$\{\Delta\varepsilon^2\} = \{\Delta\varepsilon^1\} + \{\Delta\varepsilon^{1-2}\} \tag{23}$$

In fact, in the calculations, the temperature does not vary during a time step.

When the equilibrium is finally reached, if the point **D** is outside the yield surface calculated at the beginning of the time step T_{n+1}, the hardening has increased and this is taken into account by updating the plastic strain and the equivalent plastic strain of the yield surface.

6.a   6.b   6.c
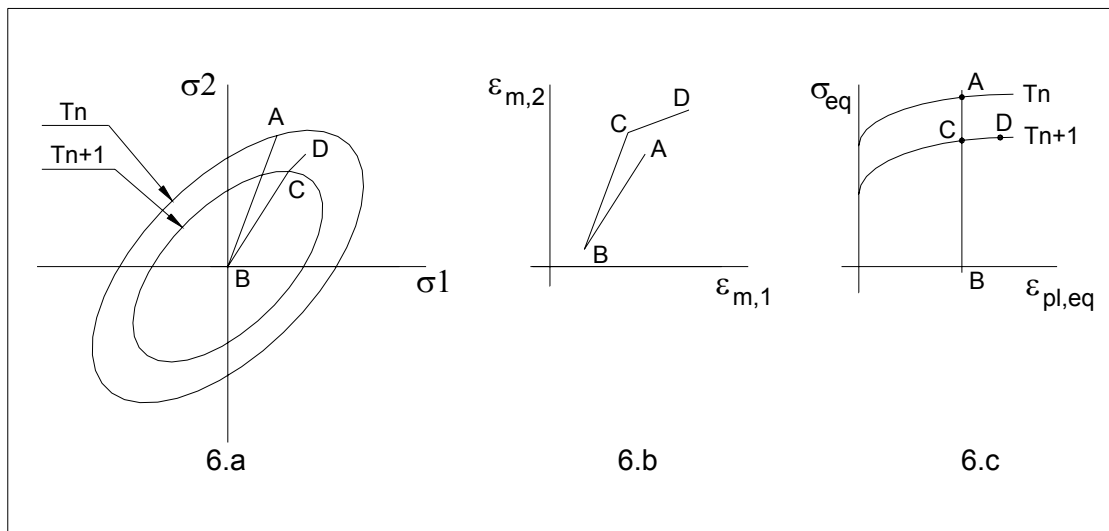
Figure 6 : First iteration of a time step in plastic behavior.

202

NUMERICAL TEST

Response of a Z-shaped cantilever

The structure is a Z-shaped cantilever subjected to a transverse end load (fig. 7).
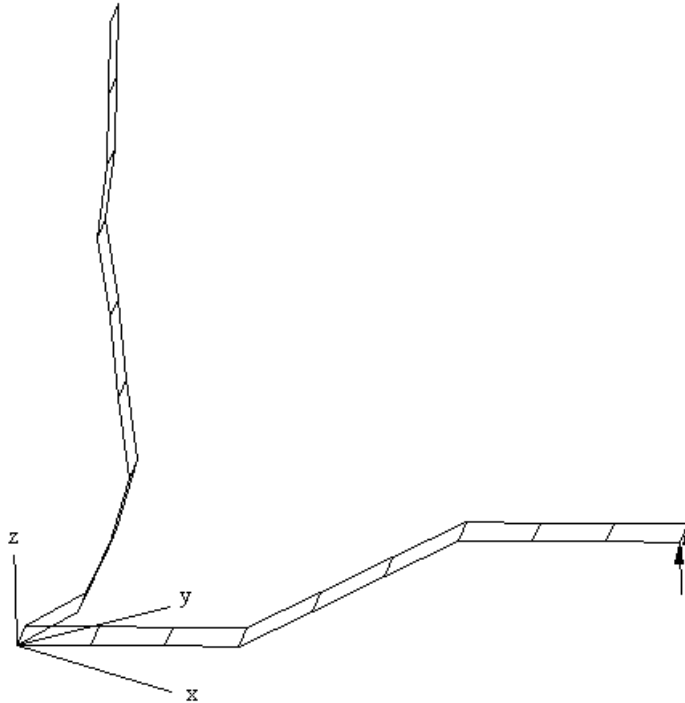
Figure 7 : Initial geometry and deformed shape for a load of 4000.

The solution given in reference [12] is based on nine equal sized element. The structure is oriented at 45° from the x-z plane to activate all three translation and rotations in the element formulation.

The beam is divided into 3 equal parts (each part is meshed with 3 elements). The 2 parts parallel to the x-y plane have a length of 60 and a width of 20. The middle part (inclined) has also a length of 60 and an elevation of 30 in the z-direction, the width is 20. The thickness of the beam is 1.7 (consistent units).

All the six degrees of freedom are restrained at one end and two concentrated nodal forces are applied in the positive z-direction at the other end. The load is increased up to 4000 with a step of 10.

The material is elastic, the Young modulus is equal to 2.0×10^5 and poison's ratio is equal to 0.3. This problem is solved at ambient temperature (20°C).

Two calculations have been performed, the first one "Deflec-Z-Safir" with a load increment of 10, to check that SAFIR gives the same continuous curve as the one given by NAFEMS. The second one with a larger load increment of 500 to check whether SAFIR is able to manage large steps. It can be seen on fig. 7 (displacements not amplified) and 8 that the new element introduced in SAFIR gives good results in case of bending with large geometric non linear behavior. The results obtained for a load step of 500 are also very good even if the first point is a little bit too high compared to the two other curves. It has to be realized that a displacement of nearly 125 has been accommodated within one single step.
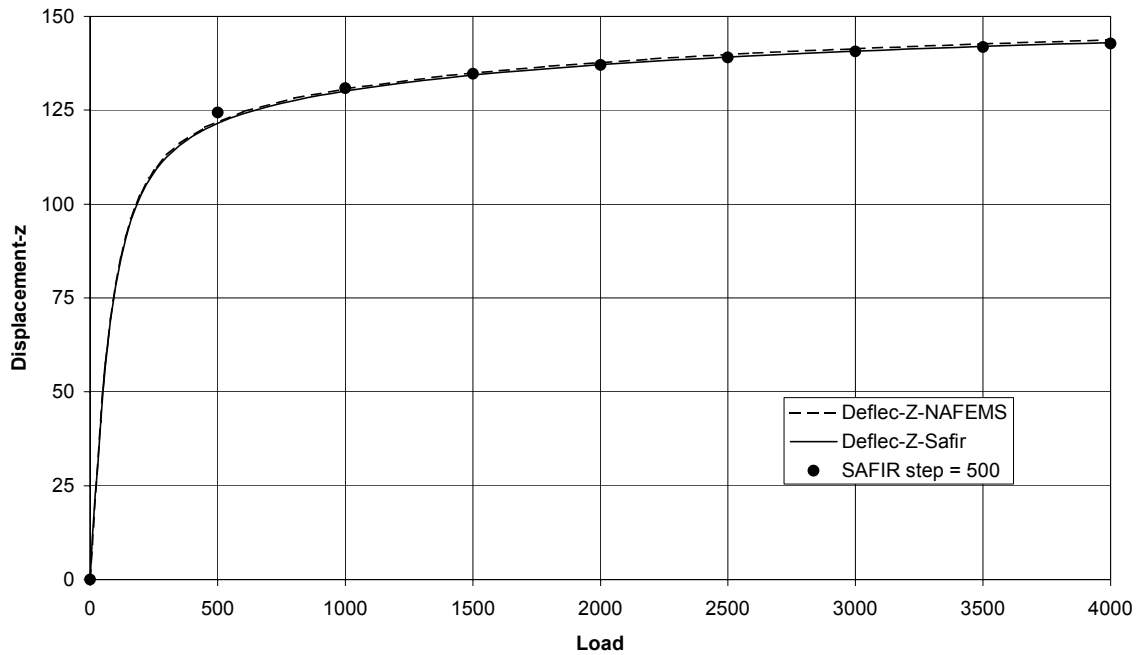
Figure 8 : Load/Displacement.

Hemispherical shell
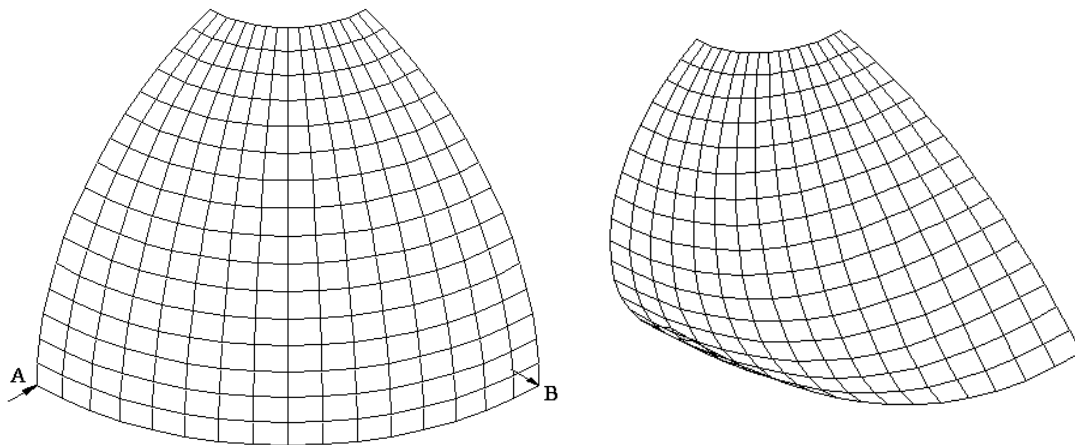
Figure 9 : Hemispherical shell.

The finite element mesh is shown on figure 9. 1/8 of the sphere [12] has been meshed with 16x16 quadrilateral elements. The units are consistent.

The radius of the sphere is 10 and the thickness is equal to 0.04.

The following symmetrical boundary condition have been used:

Symmetry on the plane y = 0

$$U_y = \theta_x = \theta_z = 0$$

204

Symmetry on the plane x = 0

$U_x = \theta_y = \theta_y = 0$

To prevent the rigid body mode in the z-direction, the point A was restrained to have x-translations only, i.e. $U_z = 0$

Inward and outward diametral point loads were applied as concentrated nodal forces at locations A and B respectively. The loads are increased up to a maximum of 100.

The material is elastic, the Young modulus is equal to 6.825×10^7 and poison's ratio is equal to 0.3. This problem is solved at ambient temperature (20°C).
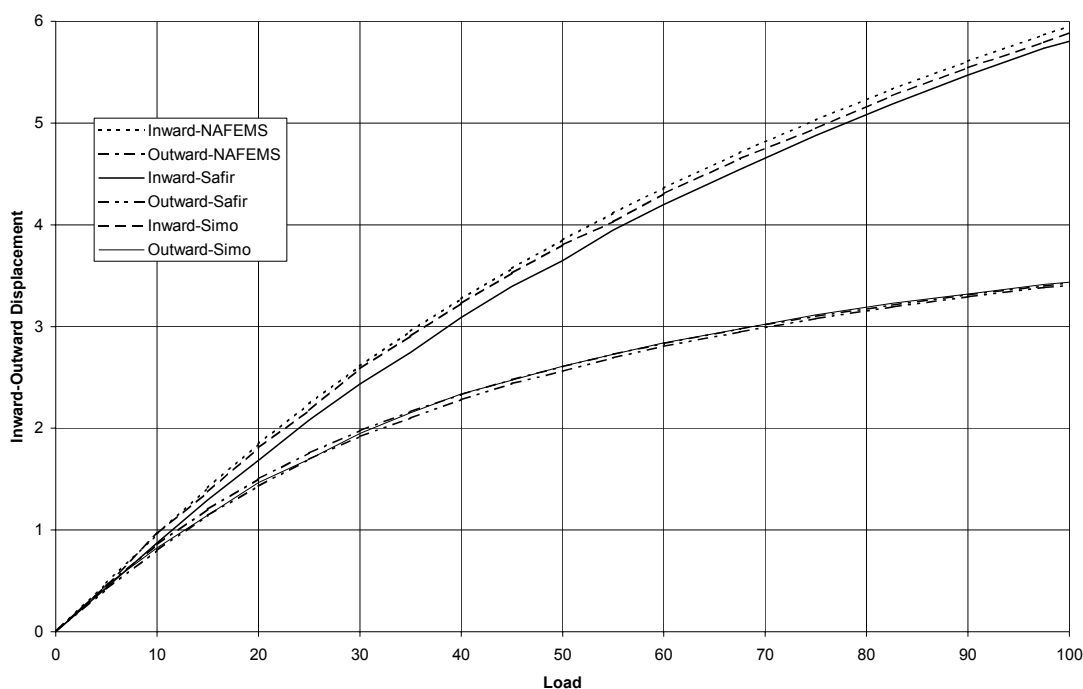
Figure 10 : Inward and outward displacements.

This problem tests the performance of the geometric non-linear formulation for shells under membrane, bending and twisting actions. It can be seen (fig. 10) that SAFIR gives good results in case of large rotations and deflections. For the inward displacement, SAFIR is stiffer than the results obtain by NAFEM [12], but the results are close to the one obtained by Simo. This test confirms that there is no membrane locking in the element.

Note : Simo has performed his calculation for a load going from 0 up to 60. NAFEMS has extrapolated the values up to 100.

Lee's Frame

The finite element mesh is shown on figure 11. The vertical and the horizontal members have a length of 120. Two meshes have been used to check the behavior in case of bending and in case of 'membrane bending'.

205
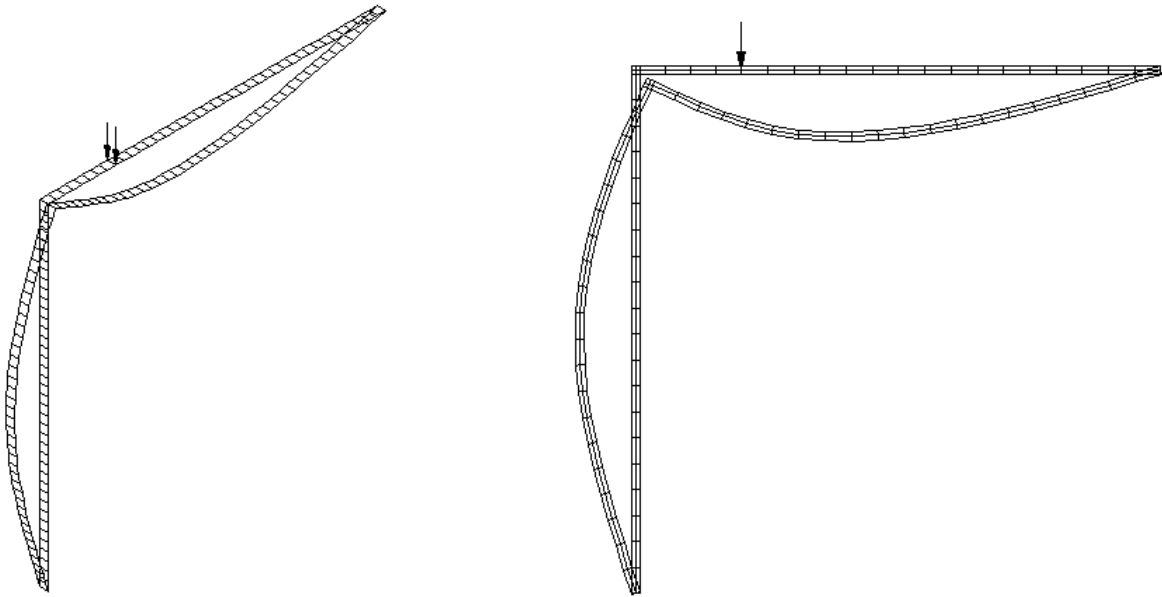
Figure 11 : Lee's frame

At the ends of the frame, the following displacements have been locked:

$$U_x = U_y = U_z = \theta_x = \theta_z = 0$$

The units are consistent. The cross-section of the beam is equal to 6 and the inertia is equal to 2. The elements are divided into 8 layers.

Ambient temperature

A vertical load is applied at a distance of 96 of the top right edge and it is increased until collapse.

The material is elastic, the Young modulus is equal to 720 and poison's ratio is equal to 0.3.
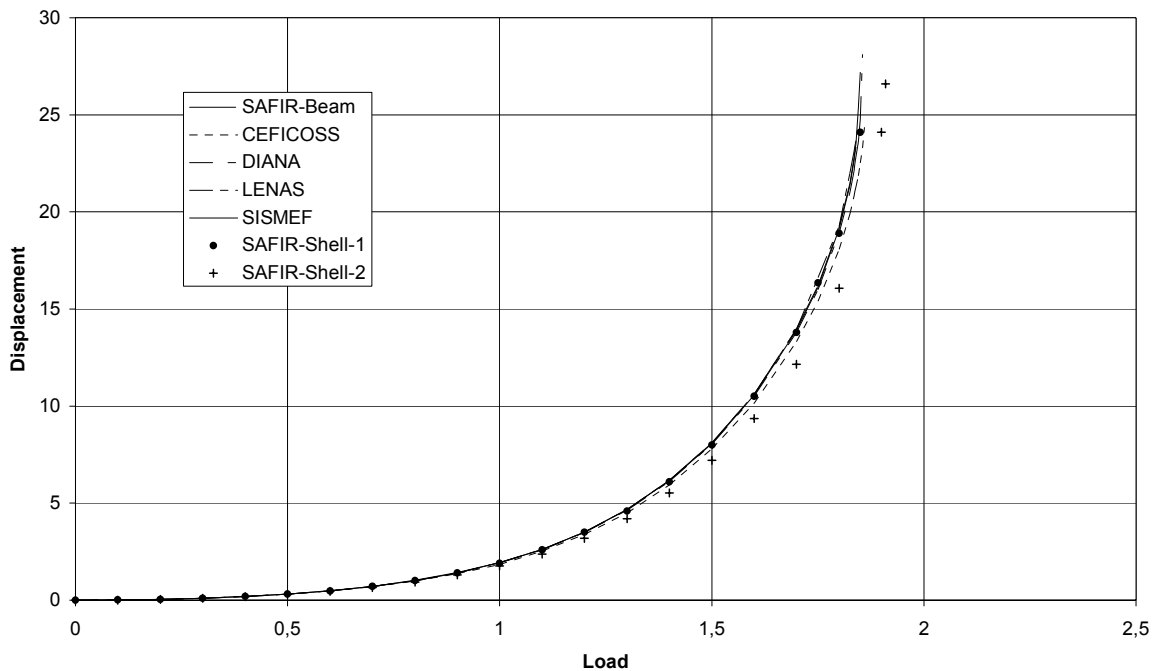
Figure 12 : Horizontal displacement versus load.

A comparison with the results of some beam elements [13] has been performed. It can be seen (fig. 12) that in case of bending (SAFIR-Shell -1) SAFIR gives results close to the been element. In case of "membrane bending" (SAFIR-Shell-2) the element is a little bit too stiff, but the mesh used here is very crude (2 elements on the depth of the beam).

Elevated temperature

A vertical load of 0.2 is applied to the structure at a distance of 96 from the right top edge. The temperature is uniform in the structure and it is increased until collapse.
The elliptic hardening is used, the Young modulus is equal to 720, the yield stress is equal to 3.0 and poison's ratio is equal to 0.3. The material properties decrease with temperature according to ENV 1993-1-2.
A comparison with some beam elements [13] has been performed under fire condition. It can be seen (fig. 13) that in case of bending (SAFIR-Shell-1) SAFIR gives results close to the beam element. In case of "membrane bending" (SAFIR-Shell-2) the results is a little bit higher than the results provided by the other elements. It has to be highlighted that the integration of plasticity on the depth of the beam is performed only at 4 integration points (2 in each of the 2 elements used in the discretisation).
This example shows that the new element takes correctly into account the thermal elongation and the stress-strain relationship according to EC3.
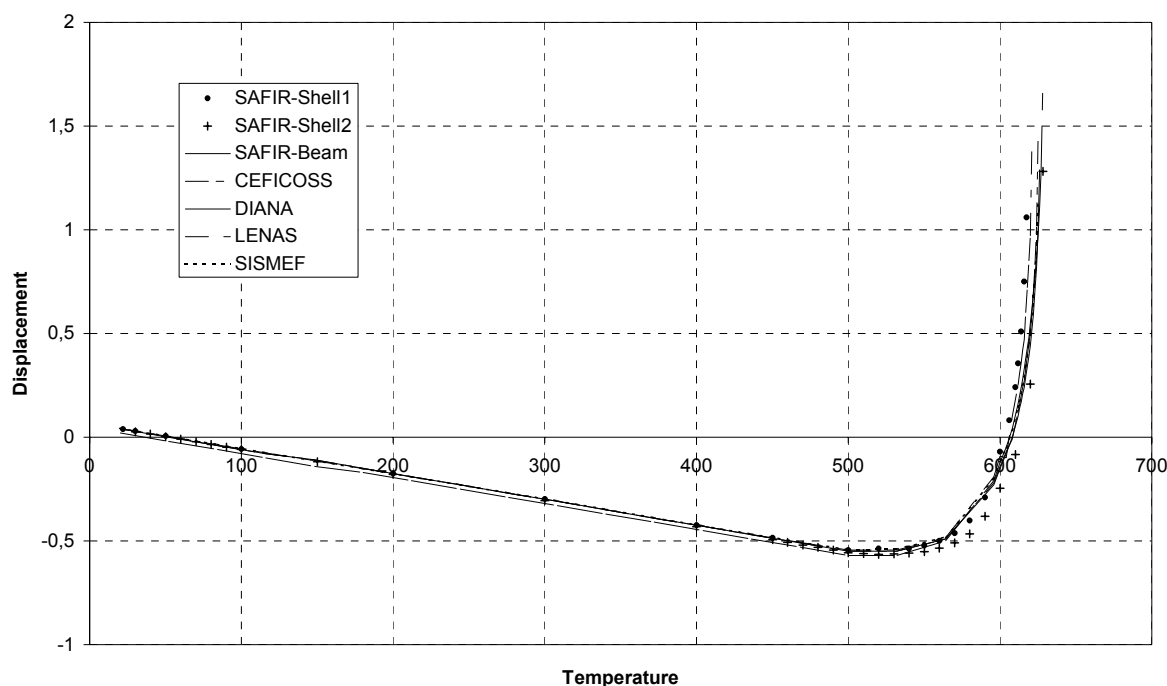
Figure 13 : Horizontal displacement versus temperature

H rolled profile

Calculations have been performed on a S355 HE 300 AA+. The length of the beam is 1 m. The boundary conditions are defined as follow:

First end : All the nodes are locked on the longitudinal displacement and all the rotations. The lateral displacement is locked at all the nodes on the web and all the displacements are locked at the point in the middle of the web.

Second end : All the nodes have an imposed longitudinal displacement in compression and all the rotations are locked. The lateral displacement is locked at all the nodes on the web and all the displacements are locked at the point in the middle of the web.

The temperature is uniform in the structure and it is increased in the same time as the displacement is increased.

An initial sinusoidal imperfection of 10 mm is imposed on the web and the flanges (fig. 14).
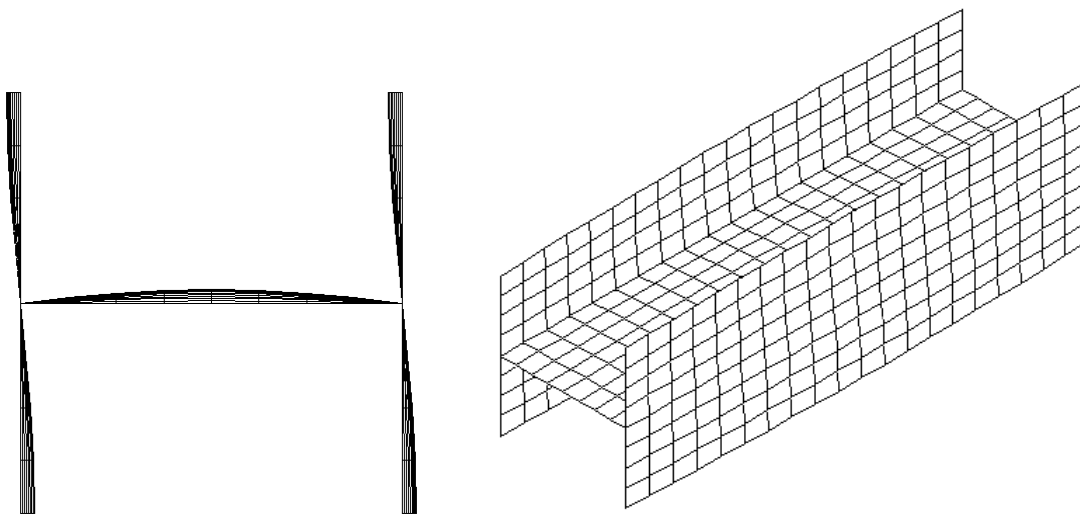
Figure 14 : Initial geometry of the H profile
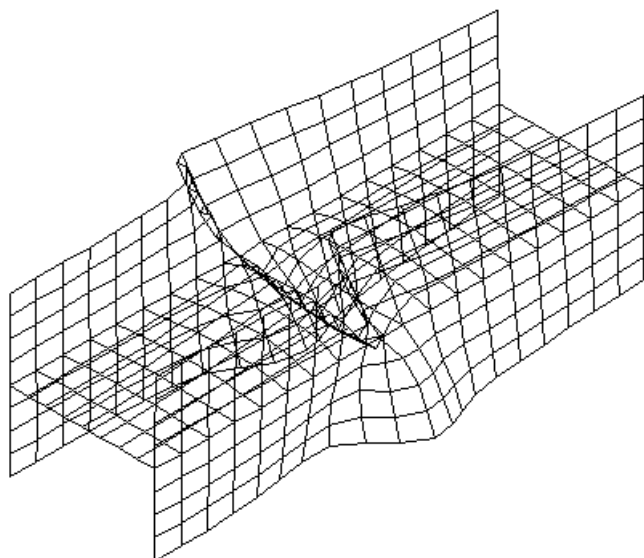
Figure 15 : Deformation of the H profile at the last converged step

In this structure, the stress is function of the imposed longitudinal displacement and the thermal strain (restrained). As the temperature and the displacement are increased at the same time collapse occurred when the temperature in the structure reach 42°C and the longitudinal displacement is equal to 1.8 mm. The ratio between the maximum load applied to the structure and the theoretical crushing compressive load is equal to 0.92. As the calculation has been performed with imposed displacement post-critical behavior can be study. Figure 15 shows the deformation of the beam at the last converged step (displacements not amplified) . It can be seen that large deformations have been obtained in the middle of the beam. The temperature in the structure at this moment is 888°C and the imposed displacement is equal to 72 mm.

CONCLUSION

After a brief description of the new quadrangular shell element introduced in SAFIR and the new material properties, some calculations have been performed to validate this element.
The z-shape cantilever show that the element can be subjected to large geometric non-linear behavior. The hemispherical shell and the calculation performed on Lee's frame at ambient temperature show that this element is not subjected to membrane locking.
Lee's frame at elevated temperature demonstrate that the material properties from EC3 have successfully been introduced in SAFIR in case of plane stress relationship and that the thermal elongation is taken into account.
To complete the validation of this element, more calculations have to be done on benchmark tests at elevated temperature and some comparison with experimental tests have to be performed.

ACKNOWLEDGEMENT

REFERENCES

[1] FINELG – Nonlinear Finite Element Analysis Program – User's Manual Version 6.2 – Feb. 1984.

[2] Jetteur Ph. – Non-Linear Shell Elements Based On Marguerre Theory – IREM Internal Report 85/5 – Swiss Federal Institute Of Technology, Lausanne, Switzerland, Dec. 1985.

[3] Jetteur Ph. – A Shallow Shell Element With In-Plane Rotational Degrees Of Freedom – IREM Internal Report 86/3 – Swiss Federal Institute Of Technology, Lausanne, Switzerland, March 1986.

[4] Jetteur Ph. – Improvement Of The Quadrangular "JET" Shell Element For a Particular Class Os Shell Problems – IREM Internal Report 87/1 – Swiss Federal Institute Of Technology, Lausanne, Switzerland, Feb. 1987.

[5] Jammei S., Frey F., Jetteur Ph. – Elément Fini De Coque Mince Non-Linéaire à Six Defrés De Liberté par Noeud – IREM Internal Report 87/10 – Swiss Federal Institute Of Technology, Lausanne, Switzerland, Nov. 1987.

[6] Allman D.J. – A Compatible Triangular Element Including Vertex Rptations For Plane Elastic Analysis – Comput. Struct., Vol. 19, 1984, pp 1-8.

[7] Jaamei S. – "JET" Thin Shell Finite Element With Drilling Rotations – IREM Internal Report 88/7 – Swiss Federal Institute Of Technology, Lausanne, Switerland, July 1988.

[8] Idelsohn S.. – Analyses Statique et Dynamique Des Coques Par La Méthode Des Eléments Finis – Ph.D. thesis, Liège, 1974.

[9] Batoz J.L., Bathe K.J., Ho L.W. – A Study Of Three Node Triangular Plate Bending Elements – Int. J. Num. Meth. Eng., Vol. 15, pp. 1771-1812, 1980.

[10] Batoz J.L. – An Explicit Formulation For An Efficient Triangular Plate Bending Element – Int. J. Num. Meth. Eng., Vol. 18, pp. 1077-1089, 1982.

[11] Batoz J.L., Ben Tahar M. – Evaluation Of A New Quadrangular Thin Plate Bending Element – Int. J. Num. Meth. Eng., Vol. 18, pp. 1655-1677, 1982.

[12] Prinja N.K., Clegg R.A. – Assembly Benchmark Tests For 3-D Beams And Shells Exhibiting Geometric Non-Linear Behaviour – NAFEMS 1993 – Ref. : R0029

[13] Franssen J.M. and Al.. – A Comparison Between Five Structural Fire Codes Applied To Steel Elements – IAFSS, Fire Safety Science, Proceedings Of the Fourth International Symposium.

THERMAL EXPOSURE TO A HIGH WELDED I-BEAM ABOVE A POOL FIRE

J. Myllymäki and M. Kokkala

VTT Building Technology, Fire Technology,
P.O. Box 1803, FIN-02044 VTT, FINLAND

ABSTRACT

Localized fire tests on an unloaded welded steel beam installed below a lightweight concrete ceiling have been conducted at VTT Building Technology. The fire source in the tests was a heptane pool. Temperature of the beam has been measured. From the plate thermometer and heat flux gage results the heat flux distribution has been computed. Dependence of the flux distribution on the flame length and on the distance from the fire source to the member has been presented. The new engineering method developed by Hasemi for the localized fire design is used. Obtained test results have been compared to the correlation equations used by Wakamatsu and Franssen. Measured heat fluxes to the lower flange agree well with the correlation of Wakamatsu but the measured fluxes to web are much higher. Modified correlations based on the VTT experiments are presented. Simple computation method for the temperature of unprotected web and upper and lower flange are given. This study shows that method of Hasemi with some modifications can be applied to predict thermal behaviour of high steel beams exposed to localized fire in a case of rather high heat release rates.

Keywords: *localized fire, heat flux, unprotected structure, steel structures*

1. INTRODUCTION

Normally, the design of fire resisting structures is based on a fully developed fire. However, for structures located in large compartments, atriums or car parks the assumption of fully developed fire may not necessarily be valid. If the fire load is limited, the fire may maintain localised with flashover never taking place. In the fire resistance tests and design according to standard ISO 834 the gas temperature around the beam is kept uniform along the span. The assumption is valid for fully developed fire, but does not represent the local temperature field caused by a local fire source. Therefore in the case where a load bearing steel member is heated only locally new methods are needed which can accurately predict the temperature of the structure. The method used in this study is experimental and is based on the tests and theory developed by Hasemi and his coworkers in Japan. Hasemi et al. (1995) have presented correlations for distribution of heat flux to ceiling under localized fire as a function of heat release rate, the distance from the fire source and burner size. For an H-section steel beam installed under a ceiling they (Wakamatsu, Hasemi et al. 1996) have shown that the heat flux distribution varies along the span of the beam.

Nomenclature

c_p	The specific heat of air (J/kg/K)
c_s	The specific heat of steel (J/kg/K)
D	Diameter of the fire source (m).
F	area of perimeter of meter of steel section or part of steel section (m^2)
g	gravitational acceleration, 9.81 m/s^2
h	convection coefficient (W/m^{2}K)
H	height (m)
H_B	vertical distance of lower flange from fire source (m)
H_C	vertical distance of ceiling from fire source (m)
H_W	vertical distance of lower flange from fire source (m)
L_{HB}	horizontal length of flame from stagnation point at lower flange level (m)
L_{HC}	horizontal length of flame from stagnation point at ceiling level (m)
L_{HW}	horizontal length of flame from stagnation point at upper flange level (m)
$\dot{Q}$	heat release rate (W)
$\dot{Q}^*$	dimensionless heat release rate
T_∞	ambient temperature of air (K)
T_s	temperature of steel (K)
V	volume of a meter of steel section or part of steel section (m^3)
Greek symbols	
ρ_∞	density of the air (kg/m^3)
ρ_s	density of the steel (kg/m^3)
σ	Stefan-Boltzmann constant 5.670×10^{-8} (W/m^{2}K^4)

The tests in Japan were conducted using a 0,5 m diameter porous gas burner and 1,0 m size square burner producing a constant heat release rate (HRR) that varied in tests in the range from 100 kW to 900 kW. Franssen (1997) has applied Hasemi's method to large compartment fires and car park fires where the HRR was time dependent reaching 8 MW at maximum.

The aim of this research has been to study the applicability of the Hasemi's method for bare steel beam exposed to local fire in a case where the HRR of the local fire is time dependent and is as high as in car park fires. The size of the welded steel beam in VTT tests was typical for car park structures in Finland. Distribution of total net heat flux and temperature of unprotected steel beam were measured for heat release rates 0,56-3,6 MW.

2. TEST ARRANGEMENT AND TEST CONDITIONS

Arrangement of the tests is shown in Figure 1. A welded 570 mm high and 4.5 m long steel section HI 570-6-8*150-18*260 was supported by fire protected steel frame made of RHS-sections. The distance of the lower flange from the floor was 2,3 m. A ceiling made of lightweight concrete Siporex slabs (density =500 kg/m^3) was constructed above the steel beam. The weight of the slabs was not carried by the beam but surrounding steel frame. Bolts prevented formation of a gap during the tests between the ceiling and the welded beam. The bolts were welded to the centre of upper flange and drilled through the ceiling.

A heptane pool was placed on a weighing platform at the centre of the span of the beam. The diameter of the pool D and the amount of commercial heptane LIAV 110 in the pool were
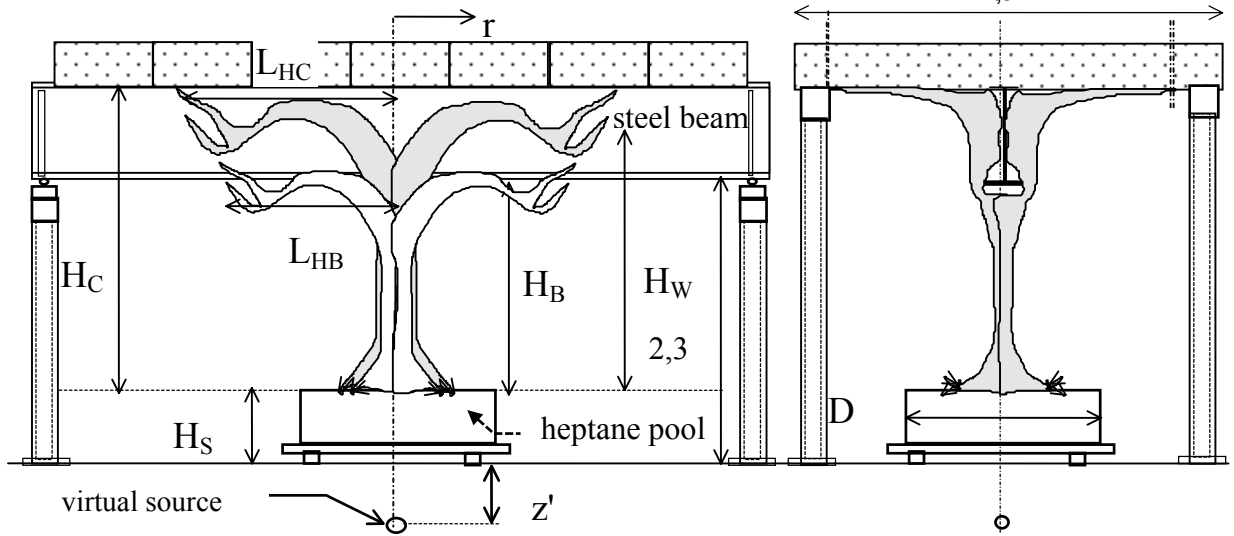
Fig. 1: Test arrangement and flame size measures.

varied. The distance of the upper edge of the pool from the floor *Hs* was varied between 0,42-0,96 m.

Temperature measurements were made both in the beam and in the gas at seven sections of the beam symmetrically located around the stagnation point. Three water-cooled Schmidt-Boelter heat flux gauges were installed flush to the ceiling surface through holes drilled in the lightweight concrete slab (see Figure 2) at three locations near the upper flange of the beam.
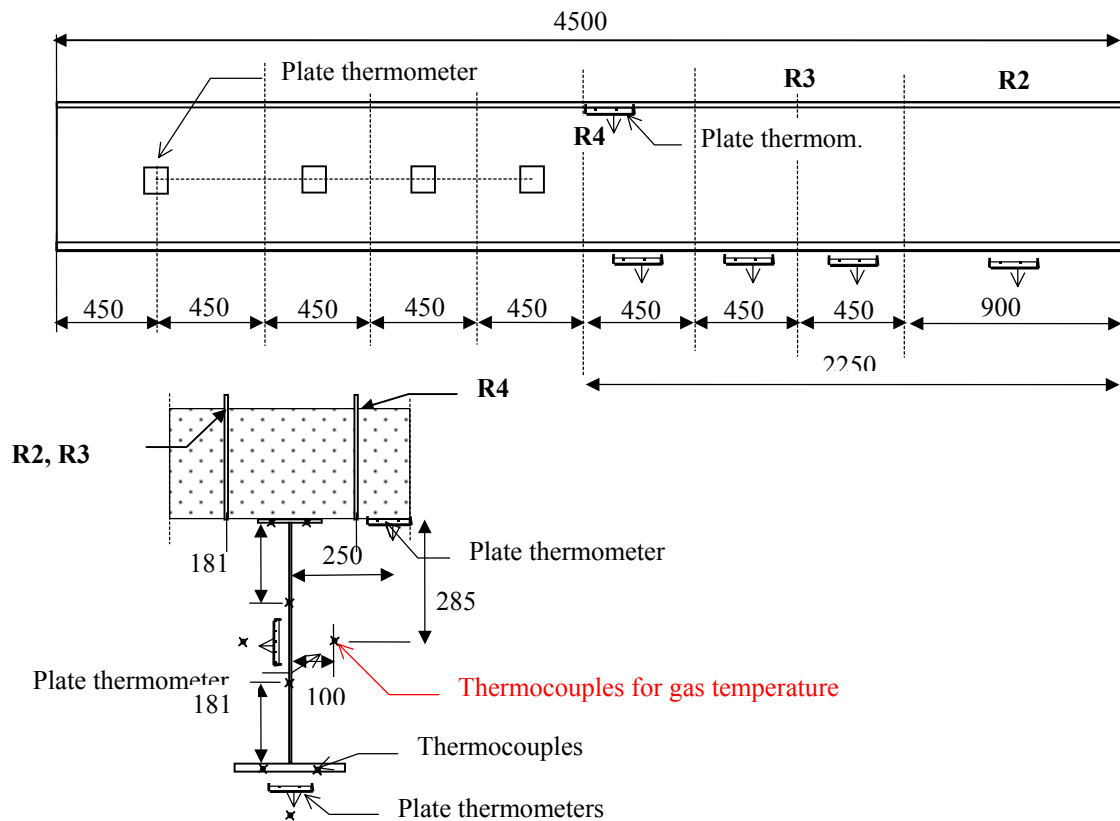
Fig. 2: Location of thermocouples (cross), plate thermometers and heat flux gages (R).

Nine plate thermometers as specified in the standard EN 1363-1 were installed at 20 mm distance from the surface of the beam. Four of them were installed under the lower flange with face of the steel plate looking downwards. The next four plate thermometers were installed near the vertical centre of the web so that the steel plate of the thermometer faced the fire like the web surface. One plate thermometer was fixed below the ceiling near the stagnation point adjacent to a heat flux gage R4.

Totally ten tests were carried out. The diameter of the heptane pool was chosen so that the heat release rate became of the same order of magnitude as that measured for burning passenger cars. Pool diameter, the amounts of heptane in the pool and average heat release rates have been given in the Table 1.

TABLE 1

TEST CONDITIONS

Test	Pool D (m)	Heptane (l)	HRR Q (kW)	Q^* (-)	L_f (m)	Height H_B (m)	L_f/H (-)
1	0.71	10	565	1.21	2.68	1.875	1.43
2	0.88	10	960	1.20	3.31	1.8	1.84
3	0.88	10	890	1.11	3.21	1.8	1.79
4	0.88	15	970	1.21	3.33	1.8	1.85
5	1.17	20	2060	1.26	4.50	1.74	2.58
6	1.17	20	2070	1.27	4.51	1.74	2.59
7	1.17	20	2090	1.28	4.52	1.335	3.39
8	1.60	20	3630	1.02	5.64	1.77	3.19
9	1.60	40	3870	1.09	5.79	1.77	3.27
10	1.60	30	3680	1.03	5.67	1.77	3.20

3. MEASUREMENT RESULTS

3.1 Heat release rate

The heat release rate was calculated from the measured mass loss rate of the heptane during the test using equation

$$\dot{Q} = \dot{m}\,\Delta H_{eff} \tag{1}$$

where $\dot{Q}$ is heat release rate in MW, $\dot{m}$ is mass loss rate (kg/s) and ΔH_{eff} is the effective heat of combustion of heptane 40 MJ/kg. The mass loss rate and also heat release rate was nearly constant during the tests (see Fig. 3a). The mass loss rate per pool area $\dot{m}''$ of LIAV 110 was increasing as a function of the the pool diameter (see Fig 3b) but was not so high as given by Babrauskas or Tewarson for n-Heptane.
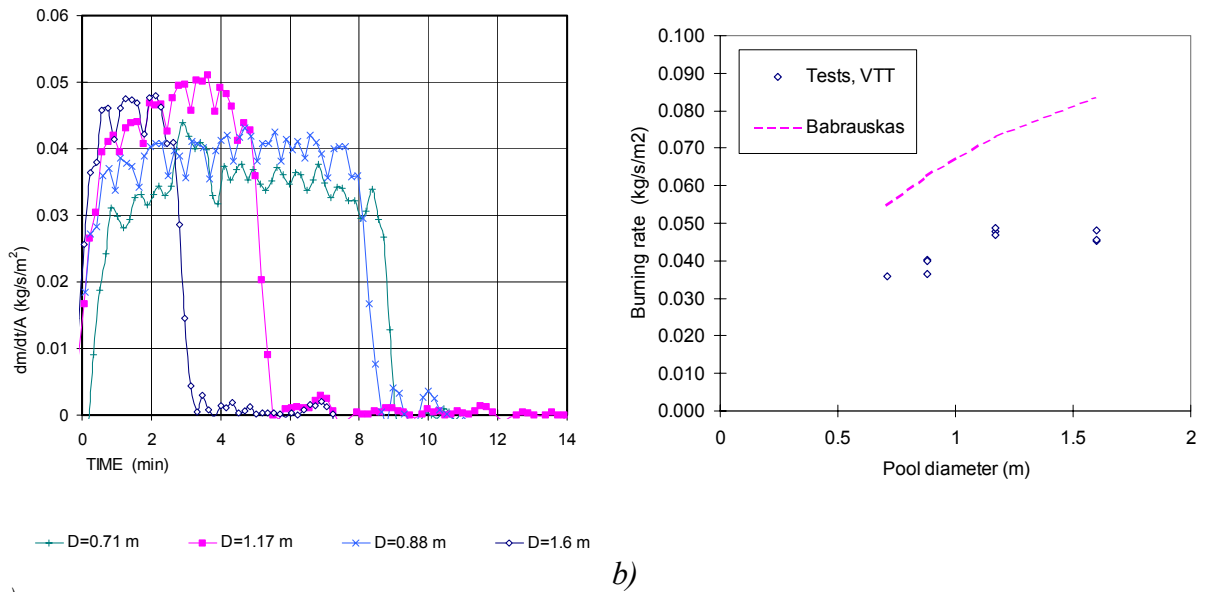
a)

b)

Fig. 3: a) Mass loss rate per pool area in different tests and b) average mass loss rate per pool area as a function of pool diameter.

3.2 Heat flux measurement by plate thermometers

Because the number of the heat flux gages was limited the plate thermometers were used as a cheap flux measurement device. The net heat flux to the plate thermometer was computed from equation

$$\dot{q}'' = c_s \rho_s d_s \dot{T} + h(T_{pl} - T_\infty) + \sigma \varepsilon_r (T_{pl}^4 - T_\infty^4) \qquad (1)$$

The value of convection coefficient h was computed from the fact that the flux measured by gage number R4 and the flux calculated by using equation (1) and temperature measured by the plate thermometer near the flux gage R4 were the same in a least square mean. A typical heat flux time dependence during the test is shown Fig. 4.

3.2 Temperature and heat flux distribution

The duration of each test was so short that the steady state temperature of the steel beam was not reached. Thus the temperature distribution of the beam presented in Fig. 5a at certain time steps. The gas temperature around the beam did reach a steady state value with some fluctuations. Both the gas temperature and the beam temperature followed a Gaussian function of the distance from the stagnation point, where temperatures met their highest values.

A prominent feature in the measured fluxes during the tests was that the flux towards the ceiling (upper flange) and web were as high as the fluxes to the bottom surface of the lower flange (see Fig. 5b) . Wakamatsu and Hasemi (1996) report much lower fluxes to the web and upper flange than to the lower flange. In VTT tests the diameter of the fire source was bigger and the heat release rates higher than in Japanese tests. Also the height of the web was rather high when compared to width of the flange. The large pool with high heat release causes a wide plume;

215

wider than the width of the lower flange. The radiative flux from the plume to the web is not prevented by the lower flange in the VTT tests, which may have been case in the Japanese tests.
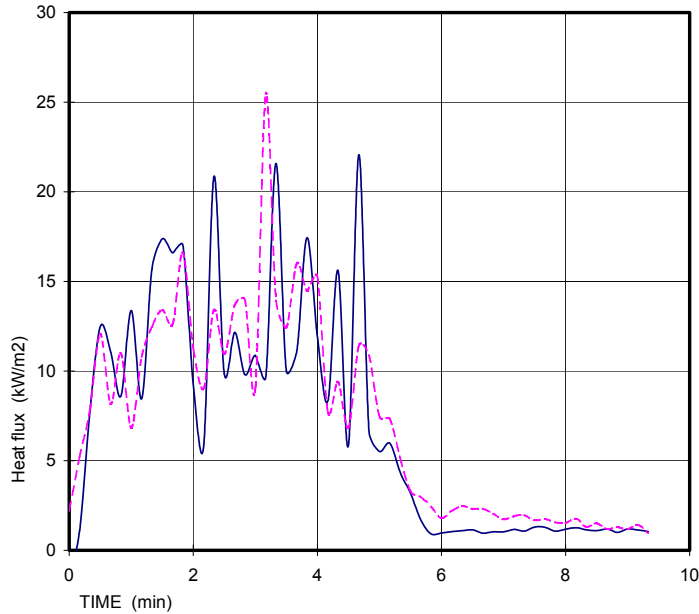
Fig. 4: Heat flux measured by gage R4 (solid line) and heat flux computed from the temperature measurement of the plate thermometer (dotted line). Resultant emissivity 0.8 and convection coefficient *h*=10 W/m²K. Thickness of the plate was *d_s*= 0.7 mm.
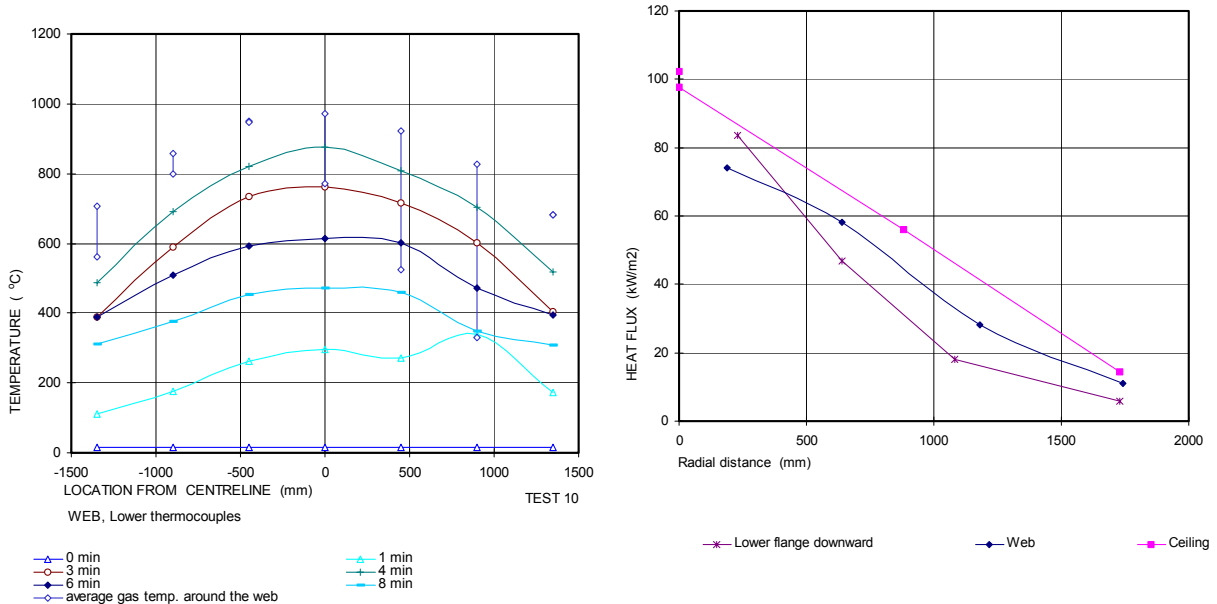
a)   *b)*

Fig. 5: Results of test 10; a) temperature distribution in web of the beam and time average of gas temperature around the web, b) flux distribution to the bottom surface of lower flange, web and ceiling as a function of radial distance from the stagnation point.

4. HASEMI'S METHOD

It has been shown (Hasemi et al. 1995), that the heat flux q_s at the stagnation point is dependent on the dimensionless length L_f / H, where L_f is the length of the visible flame and H is the vertical distance of the ceiling from the fire source. The size of the flame is dependent on the dimensionless heat release rate

$$\dot{Q}^* = \dot{Q} / \rho_\infty c_p T_\infty g^{1/2} D^{5/2} \qquad (2)$$

where $\dot{Q}$ is the heat release rate, c_p the specific heat of air and ρ_∞ the density of the air at ambient temperature T_∞, g is gravitational acceleration 9.81 m/s² and D the diameter of the fire source (m).

In the tests on flat ceilings, Hasemi et. al discovered an increasing heat flux q'' when the ratio of the flame length calculated from equation

$$L_f = 3.5 \ Q^{*N} D \qquad \text{where } N=2/5 \text{ when } Q^* \geq 1 \text{ or } N=2/3 \text{ when } Q^* < 1. \qquad (3)$$

and the distance from the fire source to the ceiling increased from $L_f/H = 1{,}0$ to $L_f/H = 2{,}5$. With the distance H_B scaled flame length L_f/H_B in VTT tests was in the same interesting range; from 1,43 to 3.39. (see Table 1).

Hasemi and Tokunaga have presented a following equation for the virtual origin of the fire source.

$$z' = 2.4 \ D \ (\dot{Q}^{*2/5} - \dot{Q}^{*2/3}) \qquad \dot{Q}^* < 1.$$

$$z' = 2.4 \ D \ (1 - \dot{Q}^{*2/5}) \qquad \dot{Q}^* \geq 1. \qquad (4)$$

The horizontal length of the flames engulfing the beam can be calculated using the correlation equations (Wakamatsu,Hasemi,Yokobayashi, Ptchelintsev 1996)

$$L_{HB} = H_B \left(2.3 \ \dot{Q}^{*0,3}_{HB} - 1 \right)$$

$$L_{HC} = H_C \left(2.9 \ \dot{Q}^{*0,4}_{HB} - 1 \right) \qquad (5)$$

where L_{HB} is the length of the flame at the height of bottom flange and L_{HC} at the height of the upper flange. The dimensionless heat release rates were calculated from equations

$$\dot{Q}_{HB}{}^* = \dot{Q} / \rho_\infty c_p T_\infty g^{1/2} H_B{}^{5/2}$$

$$\dot{Q}_{HC}{}^* = \dot{Q} / \rho_\infty c_p T_\infty g^{1/2} H_C{}^{5/2} \qquad (6)$$

where H_B and H_C are the vertical distances of the bottom flange and the ceiling from the fire source. Equations (6) were obtained by Wakamatsu using observations of videotape recordings.

5. THE HEAT FLUX CORRELATIONS

5.1 Correlation equation by Wakamatsu

Wakamatsu et al. (Wakamatsu et al. 1996) have shown that the heat flux to the downward surface of the lower flange can be presented as a function of a normalized distance of the studied point from virtual fire source; $x = (r + H_B + z') / (L_{HB} + H_B + z')$. Wakamatsu presents in his PhD thesis (Wakamatsu 1999) an exponential correlation for the heat flux towards the downward bottom surface of the lower flange

$$\dot{q}_S^{"} = 518.8 \ e^{-3.7x} \ \text{(kW/m}^2\text{)} \tag{7}$$

In this study the heat flux towards the downward surface of the lower flange was derived from the measured temperatures of the plate thermometers located under the lower flange. Figure 6a shows the average of the heat flux during the time when the burning rate keeps approximately constant. It can be seen that the measured fluxes in VTT tests are reasonably close to the curve obtained from equation (7).

For the heat fluxes to the web, lower flange upward and upper flange downward surface Wakamatsu gives correlation equations where the dimensionless distance $x = (r + H_C + z') / (L_{HC} + H_C + z')$ is normalised by using distance of the fire source to the ceiling H_C. Figure 7b shows the heat flux to the web as a function of a dimensionless distance $x = (r + H_W + z') / (L_{HW} + H_W + z')$, where H_W is the distance of the centre of the web from the pool edge. The flame length L_{HW} at the height of the web centre is calculated using equation

$$L_{HW} = H_W (2.9 \ \dot{Q}_{HW}^{*\ 0.4} - 1), \text{ where } \dot{Q}_{HW}^{*} = \dot{Q} / \rho_\infty c_p T_\infty g^{1/2} H_W^{5/2} \tag{8}$$

The measured average fluxes to the web and upper flange beam during the steady state burning phase were considerably higher than in the tests of Wakamatsu and Hasemi. The correlation that Wakamatsu uses for the heat flux to the web; $\dot{q}_S^{"} = 148.13 \ e^{-2.75x}$, underestimates the heat fluxes when compared to VTT test results. It can be seen however, that the heat flux to the web in the VTT tests is rather well represented by the correlation equation (7).

Similar behaviour can be seen in Figure 7a where the measured fluxes to the upper flange downwards are compared to the Wakamatsu's correlation $\dot{q}_S^{"} = 100.48 \ e^{-2.85x}$ for heat flux to upper flange . Once again the correlation to the heat flux to the lower flange downward surface (7) seems to be the most suitable for the VTT test data.

5.2 Correlation equation by Franssen

Franssen assumes (Franssen 1998) that the whole I-section to be at the same temperature, and the horizontal length of the plume is calculated from the equation

$$L_{HB} = H_B (2.9 \ \dot{Q}_{HB}^{*\ 0.33} - 1) \tag{9}$$

and $\dot{Q}_{HB}{}^*$ from Equation 6a. These equations were developed by Hasemi et al. (1995) for the flux on a flat ceiling.

The correlation between the heat flux $\dot{q}_s''$ (kW/m^2) and parameter x was given by Franssen in the ECSC report (Draft Final Report 1997) in a form

$$\dot{q}_s'' = 100$$
$$\dot{q}_s'' = 136.3 - 121x \ , \text{ if } x<1 \tag{10}$$
$$\dot{q}_s'' = 15x^{3.7}$$

where x is calculated from the equation

$$x = (r + H_B + z')/(L_{HB} + H_B + z') \tag{11}$$

The flux given by Franssen´s correlation equations (10) is compared to the VTT test results in Figure 6 b. It can be seen that Franssen´s equations give values that are on the safe side when compared to the fluxes measured in the tests.
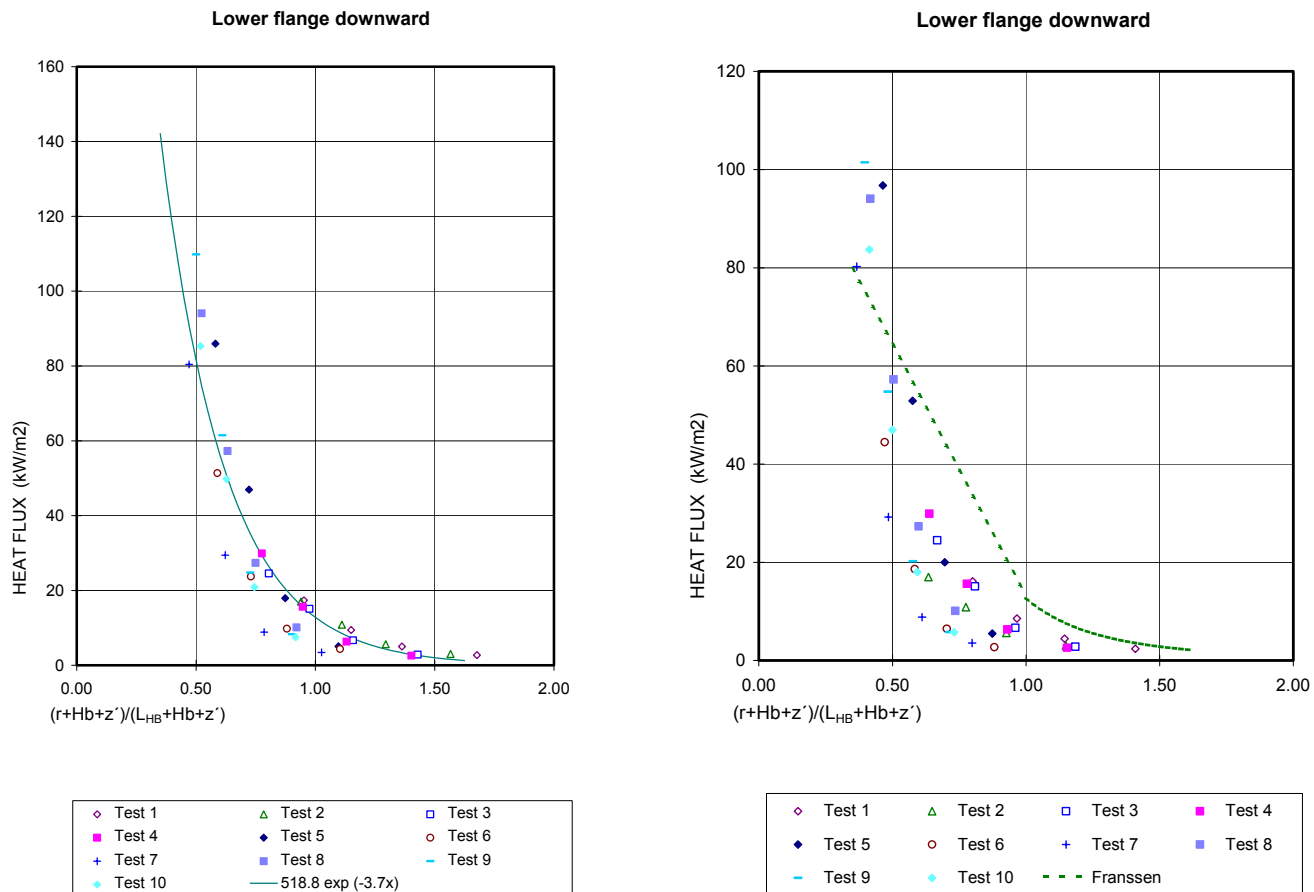
a)   *b)*

Fig. 6: Heat flux to the lower flange downward surface compared to a) exponential correlation of Wakamatsu and b) correlation function of Franssen. Note that L_{HB} is not the same in the two correlations.

a)   *b)*
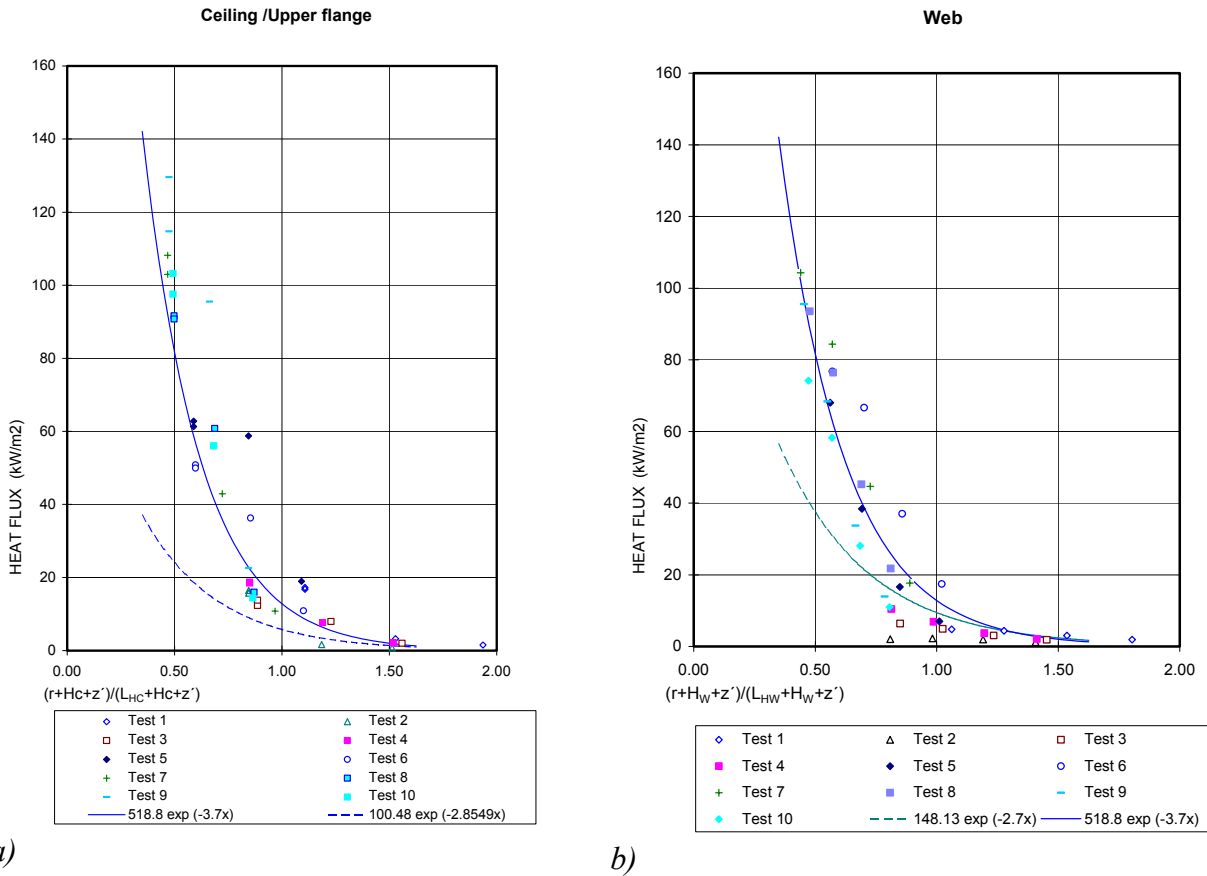
Fig. 7: Heat flux to the a) upper flange downward surface b) and to the web. Correlations of Wakamatsu are also shown.

6. COMPUTATION OF STEEL BEAM TEMPERATURE

The temperatures of the lower flange and the web of the steel beam have been computed using the equation

$$\dot{T}_s = \dot{q}_{net}^{"} \frac{F}{\rho_s \, c_s \, V} \tag{12}$$

where specific heat of steel c_s = 540 J/kg/K , density of steel ρ_s = 7850 kg/m³ and the section factor for lower flange was $F/V=(B+t)/(Bt)$, where B and t are the width and thickness of the flange. For web section factor was $F/V=2/d$, where d is the thickness of the web. Net flux to the lower flange and for web was calculated from equations (Myllymäki, Kokkala 1999)

$$\dot{q}_{net"} = \left[1 - (1 - \varepsilon)\gamma\right]\dot{q}"_S \; - h_c(T_S - T_\infty) \; - \sigma\varepsilon(T_s^4 - T_\infty^4). \qquad \text{when } \dot{Q}^* > 0 \tag{13}$$

$$\dot{q}_{net"} = - h_c(T_S - T_\infty) \; - \sigma\varepsilon_r(T_s^4 - T_\infty^4). \qquad\qquad \text{when } \dot{Q}^* = 0 \tag{14}$$

where convection coefficient $h_c = 10$ kW/m^{2}K and steel emissivity $\varepsilon = 0.85$ and T_∞ is the ambient temperature.

Factor γ taking into account assumed radiant part of the total flux has been assumed to be 0,8. When the fire has stopped ($\dot{Q}^* = 0$) a resultant emissivity[1] $\varepsilon_r = 0.5$ is used in equation (14). For the web the following total flux was used

$$\dot{q}''_{S,W} = 518.8 \ e^{-3.7x}, \text{ where } \quad x = (r + H_W + z') / (L_{HW} + H_W + z') \tag{15}$$

For the lower flange the total flux was taken as a sum of flux to upper surface of the flange
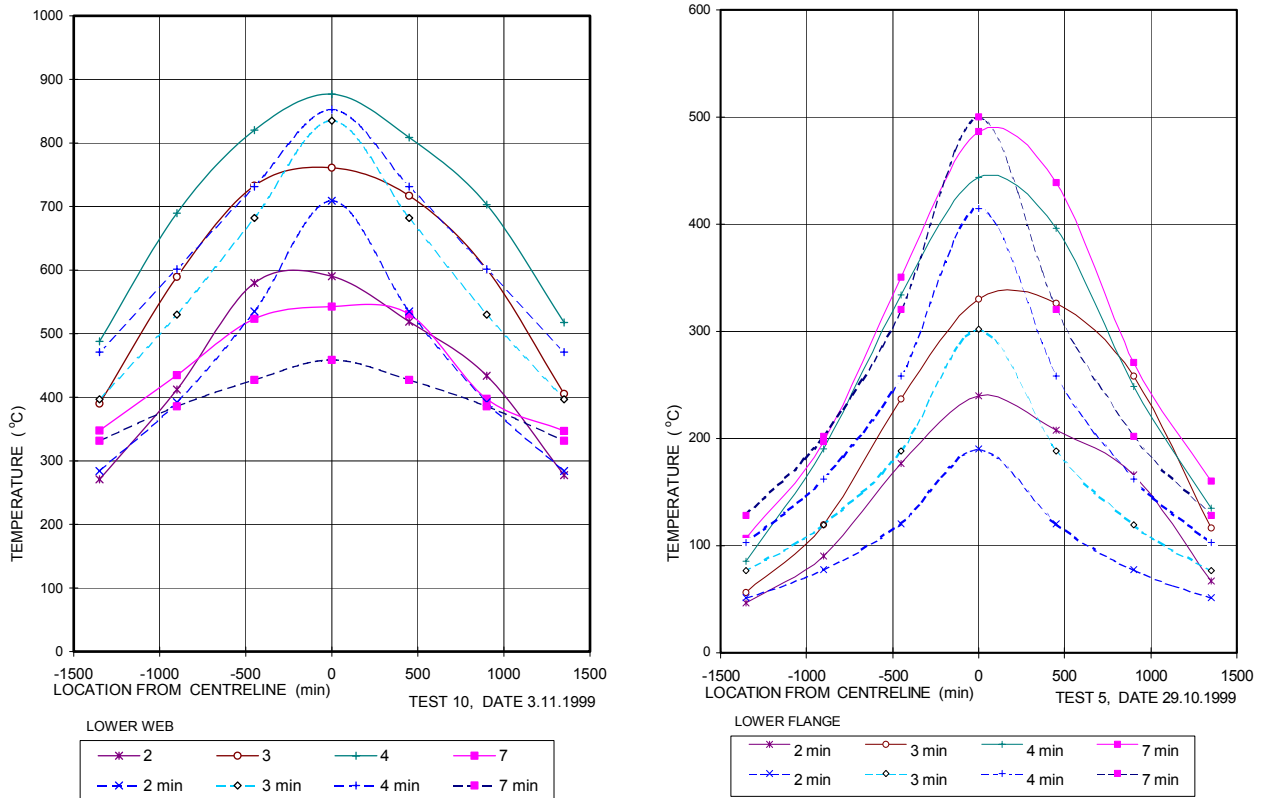
a)

b)

Fig. 8: Temperature distribution a) in web, test 10 and b) in lower flange, test 5 as a function of radial distance, dashed lines are calculation results, solid lines are results of tests. Note the asymmetry of test results.

and flux to the to the downward surface of the flange. Flux to upper surface of the flange was assumed to be same as for web.

$$\dot{q}''_{S,F} = \dot{q}''_{S,W} + 518.8 \ e^{-3.7x}, \text{ where } \quad x = (r + H_W + z') / (L_{HW} + H_W + z') \tag{16}$$

---

[1] The resultant emissivity takes into account the fact that part of the surfaces seen by the web is in a higher temperature than the ambient.

Computation results of temperature are shown in Figure 8 as a function of radial distance from the centre of the beam (stagnation point). In Figure 9 the evolution of temperature of the lower flange and web at centre of the beam in the test 5 are presented. In Figure 10 the temperature of the lower flange and web in the test 10 are given at the distance 1.35 m from the stagnation point. A reasonable accuracy can be achieved.
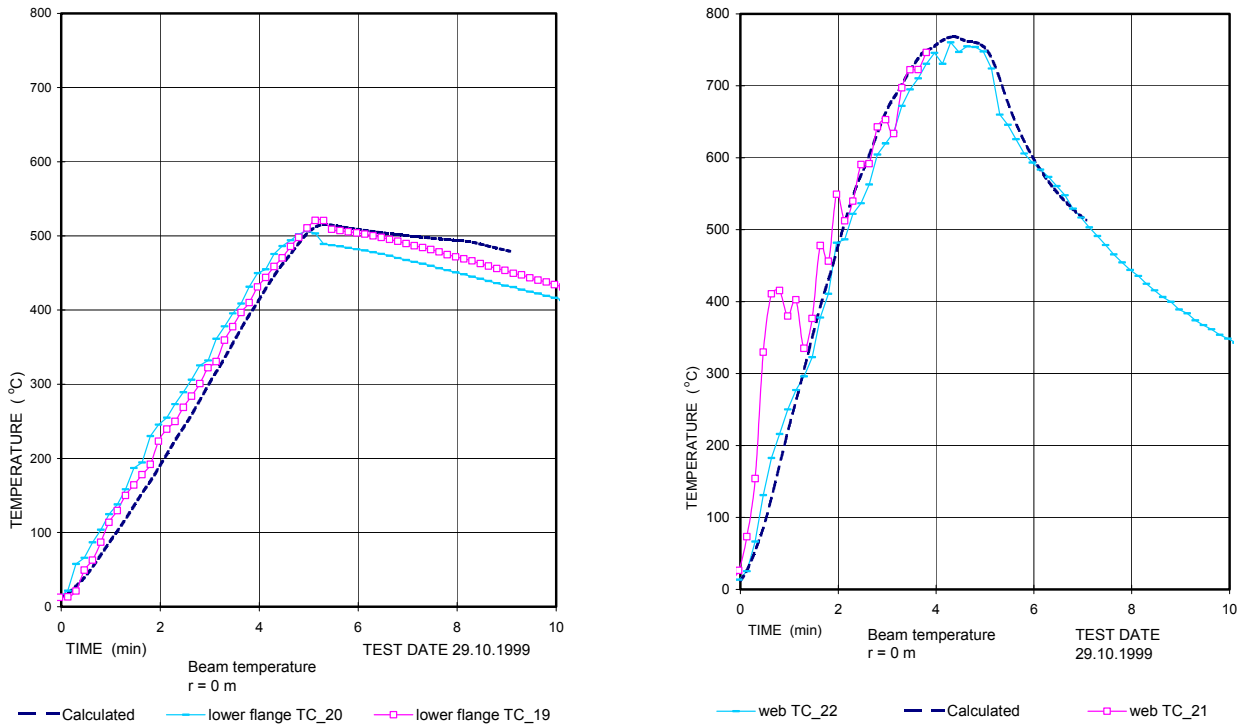
a)   *b)*

Fig. 9: Beam temperature at a) lower flange and b) web. Calculated (dashed bold line) compared to the measured temperatures (dotted lines) in test 5.

7. CONCLUSIONS AND ACKNOWLEDGEMENTS

Temperature and heat flux variations along the span of a steel beam connected to a lightweight concrete slab and exposed to a localized fire source have been measured. The following conclusions can be drawn:

In the case of small pools (smaller flames), the heat flux to the downward surface of the lower flange was about 30 % higher than the flux to web and upper flange. With larger pools (larger flames) the heat flux to web and upper flange was higher than the heat flux to the lower flange. With a smaller heat source and smaller beam Hasemi et al. have obtained fluxes to the lower flange that are 2 times or more higher than fluxes to the upper flange. The results of VTT show that the correlations of fluxes to the web and upper flange presented by Wakamatsu and Hasemi are not on the safe side for the case of larger fire sources. With slight modifications of correlations reasonable results are obtained.

The study also shows that when the temperature of the unprotected beam is computed using lumped model temperature of the flanges and webs should be calculated separately. Use of the

calculated temperature of the lower flange as a critical temperature is not a safe assumption at least not in a case when the thickness of the web is much smaller than the thickness of the lower flange.

a)

b)
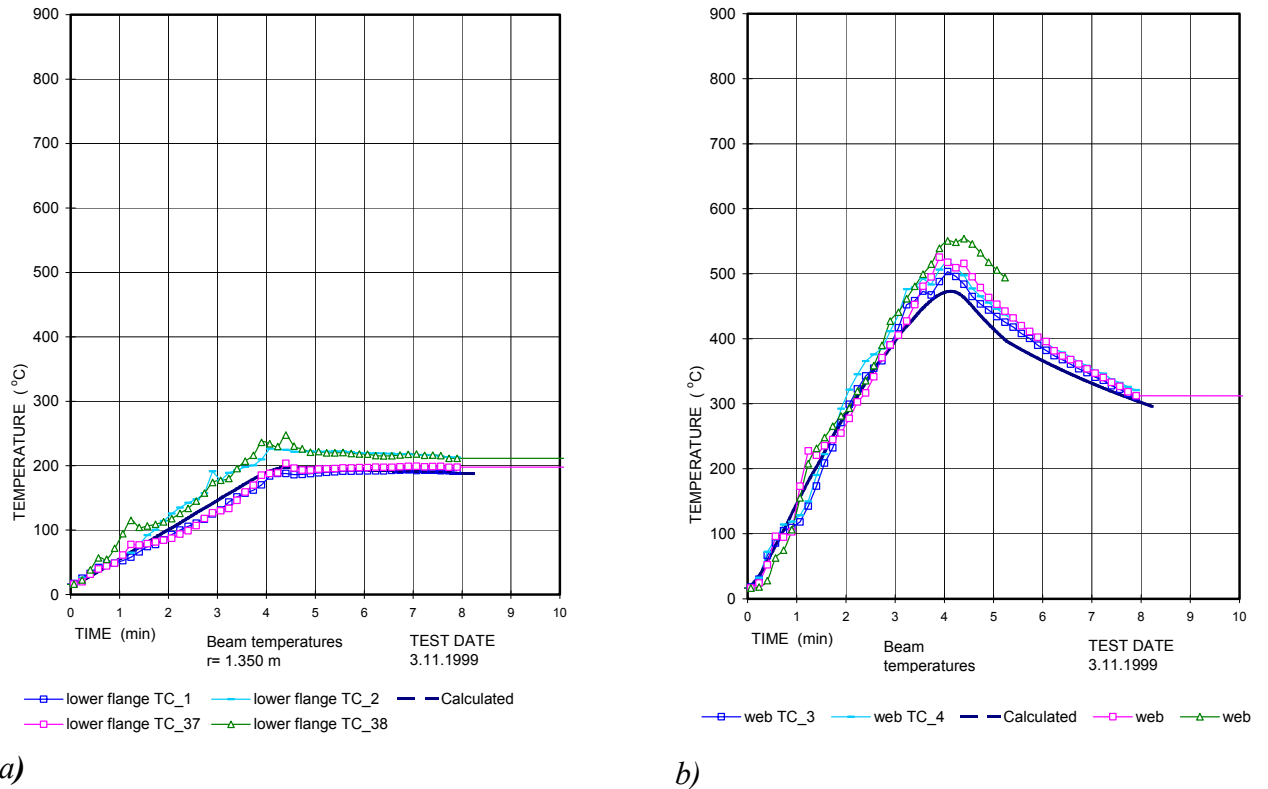
Fig. 10: Beam temperature at a) lower flange and b) web at distance r=1.35 m. Calculated (dashed bold line) compared to the measured temperatures (dotted lines) in test 10.

9. REFERENCES

Draft Final Report. March 1997. *Development of design rules for steel structures subjected to natural fires in closed car parks.* ECSC.

Franssen, J.-M. 1998. *Contributions a la modelisation des incendies dans les batiments et de leurs effets sur les structures.* Universite de Liege, Faculte des Sciences Appliquees. 1997-1998.(in French).

Hasemi Y, Yokobayashi S., Wakamatsu, T., Ptchelintsev A.V. 1995 , *Firesafety of Building Components Exposed to a Localized Fire*, ASIAFLAM 95. Hong Kong 1995.

Myllymäki, J., Kokkala, M. 1999. *Teräsrakenteiden lämpötilan laskenta paikallisessa palossa.* Palotutkimuksen päivät, Helsinki 25.-26.8.1999. Hki, Palotutkimusraati, 10 p. (in Finnish).

Wakamatsu, T. 1999. *Personal communication*, September 1999.

Wakamatsu, T., Hasemi Y., Yokobayashi Y., Ptchelintsev A.V. 1996. Experimental study on the heating mechanism of a steel beam under ceiling exposed to a localized fire. *Conference Proceedings Interflam 96. Seventh International Fire Science and Engineering Conference 26-28.3.1996.* Cambridge. England, 509-518.

EVALUATION OF FIRE RESISTANCE OF OPEN CAR PARK UNDER NATURAL FIRE CONDITION WITH ADVANCED CALCULATION MODELS

ZHAO B. and JOYEUX D.
C.T.I.C.M., France

ABSTRACT

In France, a ISO fire rating of either 30 minutes or 90 minutes is imposed on structures of car parks (open or closed) by the authorities. Nevertheless, in case of open car parks, the risk of a structure collapse will be largely reduced by several positive factors such as:

- very good ventilation condition so no risk of a generalised fire and then localised heating of structure ;
- easiness for firefighters to find and extinguish the fire quite quickly.

As a consequence, the fire protection of open car parks with steel structure can be avoided if an appropriate design procedure, taking account of both possible real fire scenarios and global structure behaviour, is applied.

In the paper, this kind of design procedure will be presented in detail through a real project of open car park in France.

The structure of this car park is designed with steel columns and composite steel and concrete beams. With the application of fire engineering procedure, it is shown that local collapse of the initially designed structure would happen under real car fire. In order to avoid the use of fire protection on this structure, some modifications are proposed to improve its fire resistance. The investigation with advanced calculation models show a much better fire resistance of the modified structure under real car fire. Even with severe fire scenario (fire spread between several cars), the unprotected structure remains stable.

The results of such analytical procedure have been fully accepted by French authority to build this park with unprotected steel structure.

- -

Towards a Performance Based Design Approach for Fire Resistance Grading of Buildings

Faller G, (MSc Eng, MIEI, MIStructE, MIFireE), Associate - Arup Fire Ireland, Arup Consulting Engineers, 10 Wellington Road, Ballsbridge, Dublin 4, Ireland

Abstract

In developing the fire strategy design for a building in Spain, the application of the local code by Arup Fire suggested that a 3 hour fire resistance period was required for compartmentation and stability of the structure in the event of a fire. The designers felt that this was too onerous a requirement for the building and it impacted negatively on the design objectives.

Alternative methods for calculating a more appropriate fire resistance period were explored and the t-equivalent method proposed by Eurocode 1 [6] was adopted. In order to convert the t-equivalent period into a fire resistance period, the adjustment factors suggested by the UK National Application Document [8] (NAD) were used. The outcome was that a much reduced fire resistance period was required that was more appropriate to the fire load and ventilation conditions in the building under consideration.

The adjustment factors proposed by the NAD are derived on a fairly arbitrary basis. Subsequent to the exercise described above, Arup Fire was commissioned by the British Standards Institute to prepare draft proposals for the construction issues related to fire safety for a new BS9999 code. Our proposals included a method for a performance based approach to determining the fire resistance grading of buildings.

The t-equivalent approach used for the design of the Spanish building was developed further with special emphasis being given to the factors used to convert the equivalent time period to a fire resistance period for the structure. The quantification of the factors was done by applying a combination of engineering logic and simple risk-based models.

A sound basis for a performance based design approach to fire resistance grading is proposed, but it is stressed that a more rigorous risk-based approach should be developed to justify the adjustment factors.

Keywords

Fire resistance grading, Fire resistance period, T-equivalent method, Structures, Compartment ventilation, Performance based design.

1. Introduction

Traditionally fire resistance requirements for the structure and separating elements of buildings have been addressed in codes by means of tabulated values, the fire resistance being a function of building use and height above ground level.

The Spanish fire safety code is no exception. Arup Fire developed a fire strategy for a 30m high building in La Coruña, Spain recently. The building's principal use is that of a gallery to display the Caixa Galicia Bank's collection of artworks, but also has two levels of offices on the top floors. Based on its height and occupancy, the recommended code value for the fire resistance period to the structure was 180 minutes.

The 3 hour fire protection was considered by the design team to be very onerous with regards to fire protection. Moreover an important design objective for the architect, Nicholas Grimshaw and Partners, was to bring natural light down into the galleries at all levels. This was to be achieved via an atrium, with a fully glazed separation between atrium and exhibition areas. In order to prevent fire spread between compartments at different levels, the authorities stipulated that the separation of the accommodation from the atrium should have a fire resistance of half that required for compartmentation. This implied that the glazing to the atrium had to achieve a fire resistance rating of 90 minutes.

However it was obvious from the outset that the galleries had a low fire load, and there was potentially a large percentage of ventilation into the atrium; in other words conditions very different to those assumed in deriving the tabulated fire resistance values in the codes. It has always been recognised that there are many factors other than occupancy and height that influence the fire resistance requirements. In general other contributory factors are taken into account on a fairly arbitrary basis, and are 'built into' the tabulated values. Given the manner in which the grading system has evolved over time, it is difficult to identify the influence of these other factors and impossible to quantify them.

For the design of the Caixa Galicia building it was felt that a more rational method for determining the fire resistance requirements for this building was needed. This paper describes the approach used for the building, which has since been developed further to provide the basis for a performance based design approach for fire resistance grading of buildings. The aim was to develop a method that was as simple as possible, while at the same time recognising all the major contributory factors and providing a transparent way of taking them into account.

2. Background to grading systems

Early studies of fires in compartments in the 1920's [1], together with practical experience of fires in buildings, produced a notional relationship between the standard fire resistance test and fire load, which was expressed as:

$$t_e \quad = \quad L/A_f \qquad \qquad \textbf{(1)}$$

where t_e = equivalent severity of fire in minutes of the standard test
L = mass of fire load in wood equivalent (kg)
A_f = floor area (m^2)

In the UK this relationship was used to derive assumed equivalent severities of fires in the post war building studies Report No.20 - Fire Grading of Buildings [2]. The values given below in Table 1 have been taken from that Report, expressed as a timber equivalent:

Table 1 – Fire ratings from Fire Grading of Buildings Report [2]

Fire Load Density	L_f	t_e
	(kg/m^2)	(minutes)
Low	Less than 60	60
Moderate	60 – 120	120
High	120 - 240	240

The t-equivalent results derived in this manner do not predict fire behaviour in a building, but can and traditionally have been, used as a basis for fire grading of structural elements.

3. Ventilation effects

Later studies of experimental fires in compartments revealed the importance of ventilation conditions and it became obvious that compartment ventilation had to be introduced into the grading system. Based on a series of international CIB experiments[3], and modified using the calculated temperature-time curve of Magnusson and Pettersson[4], the following relationship was derived[5]:

$$t_e \quad = \quad 1.24\, L/A_t[A_v h^{\frac{1}{2}}/A_t]^{\frac{1}{2}} \tag{2}$$

where
L = mass of fire load in wood equivalent (kg)
A_t = internal area of the compartment enclosure, including openings (m^2)
A_v = ventilation area of vertical openings (m^2)
h = height of the ventilation opening (m)

Using equation 2 with input values corresponding to:
- a ventilation area taken as 10% of the floor area, as suggested by the CIB Report[3] to give the maximum temperatures for ventilation controlled fires in large compartments,
- a compartment height equal to 2.75m,
- an opening height h = 2m, and
- large compartment floor areas,

we get the following relationship between the t-equivalent, fire load and compartment size:

$$t_e \quad = \quad 2.3\, L_f \tag{3}$$

where L_f = fire load density in wood equivalent (kg/m^2)

This relationship forms the basis for the tabulated values in many codes today. Using equation 3 for fire grading purposes, the values of fire resistance corresponding to fire load are:

Table 2 – Fire Grading based on revised t equivalent formula

Fire Resistance (minutes)	L_f (kg/m²)
30	13
60	26
90	39
120	52

Seen from a designer's point of view, it means that given a fire load density in wood equivalent of 26 kg/m², it could be assumed that a fire resistance of 60 minutes would be required to withstand total burnout of the fuel in a large compartment.

With a heat of combustion for timber of 18MJ/kg, the fire load given above equates to a fire load density of 470 MJ/m². This is similar to the characteristic fire load density of 500 MJ/m², typically specified for occupancies such as flats, dwellings, institutional buildings and offices. Therefore, 60 minutes would be an appropriate fire resistance period for an office building, if fire load and compartment geometry were the only aspects to be considered.

But fire resistance periods given in national regulations take into account factors other than fire load and ventilation - ease of escape, access for fire-fighters, the probability of a fully developed fire occurring and the consequence of structural failure. For the same value of fire load, a higher period of fire resistance is required for a tall building or one where people live and sleep than for a low-rise commercial building.

The 'built in' values in the codes are not transparent at all, and the designer would not know how or on what basis the adjustment factors have been derived.

4. The Eurocode approach

The Eurocode[6] allows the use of a time equivalence approach as a basis for calculating fire resistance periods, which takes the following form:

$$t_{e,d} = q_{f,d} \times k_b \times w_t \tag{4}$$

where
$t_{e,d}$ = equivalent time of fire exposure (minutes)

$q_{f,d}$ = design fire load density (MJ/m²)

k_b = conversion factor for thermal properties of enclosure

w_t = ventilation factor

4.1. Design fire load density, $q_{f,d}$

Characteristic fire load densities have been derived for different occupancies based on several European surveys and presented in the CIB report[3]. DD 240[9] has used the results of this report to assign average fire load densities to different occupancies.

For the UK it is recommended [9] that for design purposes the 80% fractile value should be used as the characteristic fire load. The 80% fractile value gives a fire load for a particular occupancy that would not be exceeded in 80% of cases, based on a mathematical distribution around the data obtained from fire load surveys [3]. These values can be used or alternatively, the fire load densities can be calculated from first principles by the use of methods such as that given in DD240.
Some typical values for fire load densities are given below:

Table 4 – Fire load densities

Occupancy	Fire load densities (MJ/m²)
Office	570
Industrial (non flammables)	470
Assembly (entertainment)	750
Shops and Commercial	900
Car Park	300

4.2. Thermal Properties of enclosure, k_b

The thermal inertia of the compartment is represented by the factor k_b. The value of k_b may be related to the thermal property $b = (\Delta c\delta)^{\frac{1}{2}}$. The Eurocode[6] recommends values for k_b ranging from 0.04 for a high thermal value to 0.07 for low values, which it also takes as the default value.

The value of k_b can quite easily be calculated once some basic fitting out details are known. As an alternative to the calculated method it is proposed that the Eurocode default value of $k_b = 0.07$ be used, as it represents a good approximation of a worst case value for most practical applications.

4.3. Ventilation factor, w_f

Once the geometry of the compartment is known, the ventilation factor can readily be calculated from the formula given in the Eurocode:

$$w_t = (6.0/H)^{0.3} [0.62 + 90(0.4 - \forall_v)^4 / (1 + b_v\forall_h)] \qquad (5)$$

where
H = height of the fire compartment
$\forall_v$ = area of vertical openings in the façade A_v related to A_f
$\forall_h$ = area of horizontal openings in the façade A_h related to A_f
A_v = ventilation area of vertical openings (m²)
A_h = ventilation area of horizontal openings (m²)
A_t = compartment floor area (m²)

In the Eurocode[6] however there is no link between the t-equivalent values calculated using equation 4 and the fire resistance period required, and it could be inferred from this document that they are one and the same thing. To do that would ignore the other factors that traditionally have influenced fire resistance grading for structures.

5. The UK National Application Document

The National Application Document[8] (NAD) for use with the Eurocode[6] in the UK, suggests risk and consequence adjustment factors in an attempt to bring the fire resistance periods, calculated using the Eurocode t-equivalent approach, to take into account factors other than fire load and ventilation conditions. The values given for office buildings are as follows:

Factor quantifying risk of failure	=	1.2
Factor quantifying consequence of failure		
for buildings less than 5m high	=	0.5
for buildings between 5 and 20m high	=	1.1
for buildings between 20 and 30m high	=	1.6
for buildings greater than 30m high	=	2.2

These adjustment factors were developed specifically to ensure that the Eurocode t-equivalent method gave results similar to those given in the Approved Document 'B'[7] (AD 'B'), and as such

have no deeper scientific basis. They do however illustrate the concept that 'raw' t-equivalent values should be adjusted in some way when determining fire resistance periods.

Assuming an office fire load density of 500 MJ/m^2 and applying these risk and consequence factors to the values calculated from the t-equivalent Equation 3, we would get the fire resistance periods for unsprinklered offices shown in the middle column of Table 4.

Table 4 – Fire Resistance periods

Building Height (m)	Nominal Fire Resistance Period (minutes)	ADB Fire Resistance Period (minutes)
Less than 5m	38	30
5 – 20m	84	60
20 – 30m	122	90
Greater than 30m	168	-

For example, on this basis the t-equivalent for an office building with a height of between 5 and 20m would be:

$$t_e \quad = \quad 2.3 \times 500/18 \times 1.2 \times 1.1 = 84 \text{ minutes}$$

Applying the risk and consequence values in this manner, with the most onerous ventilation conditions and a fire load density for offices of 500 MJ/m^2, we get values in excess of those obtained using the ADB. On the other hand, for well ventilated areas, the same approach could give fire resistance periods much lower than those required by the ADB.

In calculating the ventilation factor it is normally assumed that all permanent openings and glazed areas contribute to the ventilated area. Although it is very difficult to predict the exact temperature at which a glazed unit will fail, it is reasonable to assume that under the flashover conditions being modelled by the t-equivalent approach, the glazing will fail. If it does not fail the heating of the compartment will be less than assumed for the calculation procedure.

6. Application to the Caixa Galicia building

In many modern buildings the amount of glazing that forms a compartment enclosure can be much greater than would have been assumed by regulators a few decades ago, and this may have a significant effect on compartment heating in a fire. It is for this reason that the compartment ventilation conditions should be taken into account in assessing fire resistance requirements for buildings such as the Caixa Galicia building.

The NAD [8] approach, using the Eurocode t-equivalent formula and UK adjustments factors, were proposed for use in the Caixa Galicia building and the proposal was accepted by the local Fire Officer in Galicia.

The building has 6 floors above ground, with an enclosed circulation route, or 'street' at the base of a central atrium. At Ground Floor are several occupancies that are directly accessible to the public off the 'street'. Most of these areas at Ground Floor are open to the 'street' and atrium.

Above the 'street' the atrium extends the full height of the building, dividing the accommodation at the upper levels in two. The two zones are linked by means of open bridges across the atrium void. The accommodation above ground is dedicated to gallery and office use. The accommodation spaces are generally long and narrow, having relatively small floor areas. The longer side is glazed with ½ hour fire resistant glass along the side facing onto the atrium.

Atrium view in the Caixa Galicia building, La Coruña, Spain

A t-equivalent calculation was done for each of the compartments facing onto the atrium, as illustrated by the sample calculations given below:

6.1.   Upper Floors – Galleries

The fire load for the Galleries is relatively low, and from statistical data [3]

$$q_{f,d} \quad = 250 \text{ MJ/m}^2$$

The geometry of the rooms, assuming that only the door openings provide ventilation, is shown below:
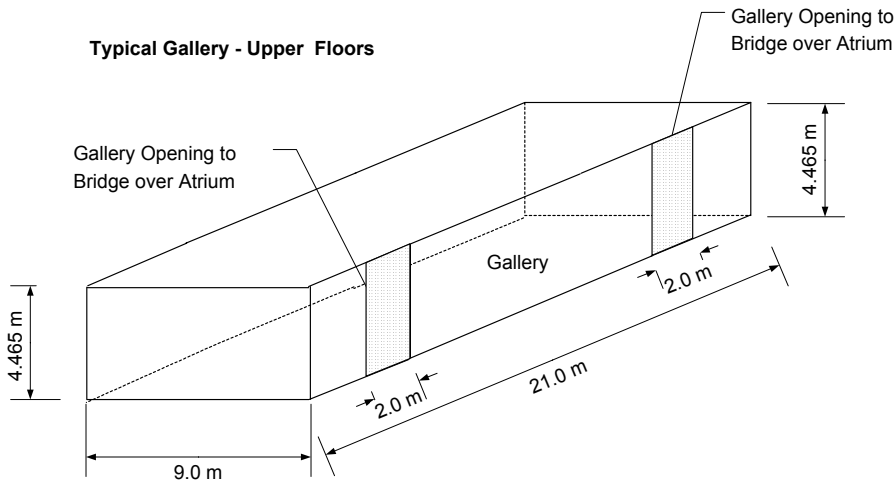
Typical Gallery - Upper Floors

Floor, internal surfaces and ventilation areas are as follows:

A_f = 9 x 21 = 189 m^2

A_v = 2 x 2 x 4.465 = 18 m^2

A = (2 x 189 + 2 x 9 x 4.465 + 2 x 21 x 4.465) – (2 x 2 x 4.465)

= 628 m²

Eurocode formula for equivalent time of exposure:

$t_{e,d}$ = $q_{f,d}$ x k_b x w_t

k_b = 0.07

w_t = $(6.0/H)^{0.3}$ [0.62 + 90(0.4 - $\forall_v$)^4 / (1 + $b_v \forall_h$)]

where H = height of the fire compartment

$\forall_v$ = area of vertical openings in the façade A_v related to A_f

= A_v/A_f = 18/189 = 0.095

This lies between the Eurocode formula limits for the ventilation factor of 0.025 # $\forall_v$ # 0.25

Therefore,

$t_{e,f}$ = 250 x 0.07 x $(6/4.465)^{0.3}$ [0.62 + 90(0.4 – 0.095)^4]

= 250 x 0.07 x 1.528

Equivalent time = 27 minutes.

This implies that the maximum temperature in a structural element for this compartment fire would be the same as that experienced by the element under consideration after an exposure time in the standard fire resistance test of 27 minutes.

6.2.   Upper Floor Offices

The fire load in the Offices is taken as, $q_{f,d} = 500 \text{ MJ/m}^2$
The geometry of the largest office on the 5th Floor is as shown below. It is assumed that the glazing to the atrium will break at elevated temperatures, providing the following geometry:
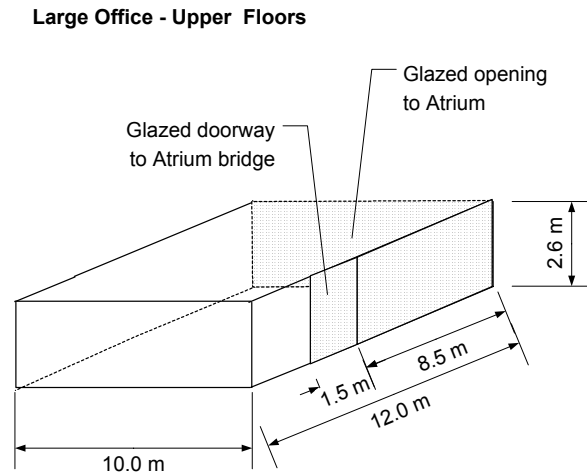
Large Office - Upper Floors

Floor, internal surfaces and ventilation areas are as follows:

A_f	=	10 x 12	=	120 m^2
A_v	=	2 x 10 x 2.6	=	52 m^2
A	=	(2 x 120 + 2 x 10 x 2.6 + 2 x 12 x 2.6) - (20 x 2.6)		
	=	302 m^2		

Eurocode formula for T-Equivalent

$\forall_v$ = A_v/A_f = 52/120 = 0.433

This lies outside the Eurocode formula limits of 0.025 # $\forall_v$ # 0.25, and therefore a value of 0.25 will be used:

$t_{e,f}$	=	$500 \times 0.07 \times (6/2.6)^{0.3} [0.62 + 90(0.4 - 0.25)^4]$
	=	$500 \times 0.07 \times 0.855$
	=	30 minutes

6.3.   Adjusted Fire Resistance periods

As discussed above the fire resistance grading is not only dependant on fire load and ventilation conditions, but also on issues such as ease of escape, the risk of a fully developed fire occurring and the consequence of structural failure. The values derived from the t-equivalent calculations are now adjusted applying the NAD risk factors, some of which are shown in Table 5 below:

Table 5 – T-Equivalent values adjusted using Eurocode risk factors

Occupancy	Height (m)	T-Equivalent (minutes)	Risk Factors $(\otimes_1, \otimes_2)$		Adjusted Value (minutes)
			Consequence	Failure	
Ground Fl Cafeteria	0.00	25	0.8	0.8	16
Ground Floor Gallery	0.00	33	0.8	0.8	21
Upper Levels Gallery	20.50	27	1.1	0.8	24
Upper Levels Offices	26.75	30	1.6	1.2	58

The calculations demonstrate that for all the areas examined on Ground Floor and above, a fire resistance of 60 minutes would be appropriate.

It should also be pointed out that all the calculations above are based on fully developed fires, for which there is a total burnout of the available fire load. In practice not all the fire load would be consumed. A conservative assumption for offices is that about 30% remains unburned. Therefore it could be argued that a further reduction could be applied to the values given above.

The practical effect of this exercise on the Caixa Galicia building was that it allowed a reduced fire protection to the structure, as well as a 30 minute separation from the atrium, which was easy to achieve using laminated glass.

It enabled us to achieve one of the principal design objectives - that of introducing natural lighting into all gallery areas without compromising on fire safety.

7. Further development of the t-equivalent approach

As we have seen, the Eurocode(6) does not give any guidance as to whether, or how, the probability of fire, the effects on rescue operations or consequence of structural failure should be taken into account.

Arup Fire have proposed a method based on the 't-equivalent' for consideration by the BS9999 committee in the UK and which we expect to find its way into the new code in some form or other. It is the formalisation and further development of the method used for the Caixa Galicia building and applied successfully to a number of other buildings.

The method is based on the approach outlined above, but proposes a more rational approach to the definition and quantification of the factors used to adjust the values derived from the t-equivalent calculation. The proposed factors are defined as;

- γ_p to reflect the probability of a fire given a specific occupancy,
- γ_c to reflect the consequence of failure due to fire, and
- γ_n to take into account the effect of sprinklers.

An alternative ventilation factor for use in the t-equivalent expression is also proposed and discussed briefly below, followed by a discussion on the adjustment factors.

7.1. Ventilation factor, w_f

A review[10] of the different formulae for the t-equivalent calculations revealed that the Eurocode [6] formula for ventilation effects does not always correlate well with test data, and that the formulae that best matched the experimental data were those of Law, Pettersson, Harmathy and Mehaffey.

A detailed analytical assessment of the results obtained using the different t-equivalent formulae was undertaken, using varying percentages of ventilation and compartment geometries. Simplifying assumptions made for this exercise were that all ventilation openings were on the vertical sides ie. no horizontal openings, and that the length to depth ratio of the compartment was kept constant at unity.

The Pettersson formula, although empirical, has a recognised scientific basis and was found to correlate well with test results[10]. It also compared well with the results obtained using the other formulae, being slightly on the conservative side for most practical cases.

The Pettersson t-equivalent formula can be expressed as follows:

$$t_e = 1.21(k_f)^{1/2} L_f A_f / [A_v(h)^{1/2} A_t]^{1/2} \tag{6}$$

where L_f = fire load density in wood equivalent (kg/m^2)

k_f = factor for thermal properties of compartment

A_f = floor area of the compartment (m^2)

A_t = internal area of the compartment enclosure, incl. openings (m^2)

A_v = ventilation area of vertical openings (m^2)

h = height of the ventilation opening (m)

Using a calorific value of 18 MJ/m^2 for wood, and adjusting for the default thermal insulation factors, the following expression for w_f has been derived:

$$w_f = 0.96 A_f / [A_v(h)^{1/2} A_t]^{1/2} \tag{7}$$

Using appropriate values for the fire load density, insulation properties and ventilation effect from Equation 7 ($q_{f,d}$, k_b and w_f), the value for t_e can be calculated as before using the Eurocode relationship given in Equation 4.

7.2. Adjustment factors

The t-equivalent value gives an approximation of the maximum heating effect that a structural element will be subjected to in the event of a given compartment fire. There are a number of other considerations that have traditionally influenced the required fire resistance period.

These factors have been identified and grouped into three categories, and an attempt has been made to quantify them using risk based methods, as outlined below:

7.3. Probability of occurrence factor ($_p$

The NAD[8] suggests values for a factor to quantify the risk of a fully developed fire occurring in different occupancies and another factor to reflect the consequence of such a fire. The factors given to reflect risk are in the range of 0.8 to 1.2 for most occupancies (other than car parks which has a factor of 0.4).

It would make more sense to regard this factor as a probability of a fully developed fire occurring, rather than a risk. The risk would then be determined from the product of the frequency-based probability and the consequence factors.

DD 240[9] gives values for probabilities of fires occurring in different occupancies in Table B1. Using these values as a means of weighting, probability factors in the range of 0.8 to 1.2 are suggested for the different occupancies. The following are some typical values for ($_p$:

Table 6 – Probability of occurrence factor ($_p$

Occupancy	Probability factor ($_p$
Office	0.8
Industrial (low fire risk)	0.8
Assembly (high fire risk)	1.2
Shops and Commercial	1.0
Car parks	0.8

7.4. Consequence of failure factor ($_c$

A probability weighting for fire growth has been given and now factors are needed to take account of the consequence of an uncontrolled fire.

It appears that the basis for increasing fire resistance with height and depth (both in UK and US) have been made on a somewhat arbitrary basis.

There is general agreement that the consequence factors should reflect:
- Ease of evacuation (stair and perimeter evacuation, stairs only, evacuation time, simultaneous or phased evacuation)
- Ease of fire fighting (internal and perimeter, internal only, fire spread to adjacent compartments).
- Potential for failure to damage in the immediate vicinity of the building.

Ease of evacuation and firefighting have traditionally been related to depth below grade and storey height. Given the requirements in modern building codes for more reliable provisions for escape and firefighting, the influence of items 1 and 2 as they affect fire resistance provisions for the structure may have diminished.

The potential to threaten life and cause damage on adjacent properties has been considered as the overriding influence on the magnitude of the consequence factor.

An attempt was made to relate the risk of failure to the number of floors using a simple analytical model, based on an increasing risk with number of floors. The values obtained indicated a factor of 3 between the risk for a high building as opposed to that for a low building. The consequence factors given in Table 7 were derived by applying this range to a base value of 0.5, to bring the results more into line with tabulated ADB values:

Table 7 – Consequence of failure factor

Height above access level	Consequence factor ($_c$
Not more than 11m	0.5
Not more than 30m	1.0
Greater than 30m	1.5

In an informal report done for British Steel in 1994 [11], a similar method for fire resistance grading was explored, the factor for consequence of structural failure being based on amount of floor area supported by any particular element. Resulting from this analysis, the relative consequence of failure factors were proposed as 2.5 for a 30-storey building as opposed to 0.8 for a 1-storey building, which again differ by a factor of approximately 3.

There seems to be general agreement that fire resistance requirements should be influenced by consequence of failure, and that the consequence increases with height or depth of a building. However the methods presented above to quantify these factors and to take into account the increased risk with height, lack a solid scientific basis and there is clearly a need to develop a more rigorous risk-based analysis technique to quantify appropriate risk factors.

The values given in Table 7 recognise the factors that influence the consequence of failure and will give results that do not differ very much from the existing prescriptive tabulated values.

It is the intention of Arup Fire to develop a more rigorous risk based expression to quantify how the consequence factor should vary with storey height (and depth).

7.5. Effect of sprinklers factor γ_n

It is not the intention of this paper to discuss the appropriate reduction factor for the effect of sprinklers on compartment fires, other than to note that numbers between 0.5 and 0.75 are referred to in the literature and used by different regulators. It is proposed that an adjustment factor $\gamma_n = 0.6$ be used to take into account the effect of sprinklers, which is in accordance with the value given in the Eurocode [6].

8. Application of the t-equivalent fire resistance grading method

The fire resistance period required for a building or part of a building can be calculated from the expression given below:

$$FR = t_e \times \gamma_p \times \gamma_c \times \gamma_n \tag{8}$$

where

FR	=	fire resistance period required (minutes)
t_e	=	time equivalent period (minutes)
γ_p	=	factor for probability of fire
γ_c	=	factor for consequence of fire
γ_n	=	factor for the effect of sprinklers

In order not to unnecessarily complicate the process of determining an appropriate fire resistance period, a t-equivalent methodology adopting the principles described above was proposed for the draft BS9999 code using a three-tiered approach:

1. Assumptions could be made as to the ventilation conditions of a typical compartment, and values could be calculated for all combinations of occupancy and height. The fire resistance periods could then be presented in the tabulated form, in the same format as it is in the ADB at present. The three variables for this table would be occupancy, height and whether the compartment is sprinklered or not.

2. For the designer who does not want to do any detailed calculation, but wants to be able to benefit from the ventilation conditions of a particular building, only the ventilation factor w_f need be calculated. Two tables, one each for the sprinklered and unsprinklered condition, could be produced. The designer would then read off a fire resistance value from a table based on occupancy, height and ventilation factor.

3. Designers who have sufficient data at their disposal and wanted to take full advantage of the actual conditions, could calculate the fire resistance period from an expression such as Equation 8, for a particular building or section of building.

For practical reasons it is not proposed at this stage that the fire grading system be changed from the present 30, 60, 90 and 120 minute periods. Rather the system would be used to justify the use of, for example, a 30 minute fire resistance period for a well ventilated compartment, as opposed to a 60 minute period obtained from code tables. When the method has been further developed and verified it may be possible to use it to justify the introduction of a 45 or 75 minute fire resistance into the grading system.

An implication of using a methodology such as that outlined above is that different fire resistance periods could be derived for different floors of the building. Based on the fact that the consequence factor is intimately related to height or depth of building, it follows that columns should be considered as more critical elements than beams.

Using this logic, a general rule could be applied, which stipulates that the fire resistance period for columns and transfer beams supporting columns, should not be decreased down the height of the building. Once the restraining effect of beams and slabs on columns is better understood, it may be possible to apply a different consequence factor to columns.

A better alternative may be to set the consequence of failure factor at 1.0 for all elements other than columns, and then have only the factor for columns increase with height or depth of building.

Failure due to loss of load bearing capacity of a structural element in the fire condition is very unusual. The question of probability of structural failure has been considered but is not addressed in this paper, because there is no evidence of buildings having collapsed to demonstrate that the t-equivalent approach inherent in the present grading system is unsafe.

Conclusion

The traditional way of determining the fire resistance requirements of a structure is to read off a value from a table in a code, which is dependent on occupancy and height of building.

Methods such as the t-equivalent method exist and allow designers to calculate the heating effect within a given compartment, given the fire load, internal linings and compartment geometry. It is a more rational approach to fire resistance requirements, which takes into account the compartment ventilation conditions.

The calculated t-equivalent can then be adjusted to give a fire resistance period, but the adjustment factors given in the literature have no transparent scientific basis. The practical effect of the weighted t-equivalent process described above does not radically change the fire resistance requirements from those obtained from tabulated code values for normally ventilated spaces. It does however differentiate between well and poorly ventilated areas that were in all other aspects identical.

An alternative performance based method, also based on the t-equivalent approach, has been presented, and an attempt has been made to provide a rational basis for the quantification of the adjustment factors. The quantification of the factors has been done by applying a combination of engineering logic and simple risk-based models. The method proposed is a sound basis for a performance based design approach to fire resistance grading, but it is recognised that a more rigorous risk-based approach should be developed to justify the numbers derived for the adjustment factors**.**

The determination of the 'political' factors such as the consequences to life safety, fire fighting and damage to adjacent properties for a fire in buildings of different height, are somewhat subjective in nature. Therefore the scientific risk based quantification process should not take place in isolation from the views and experiences of the building control authorities and fire officers. The fire engineer should lead the process and develop the risk model in which the various concerns can find expression.

References

1. Ingberg SH. *Tests of the Severity of Buidling Fires*, Quarterly, National Fire Protection Association, Vol:42, 1928.

2. *Fire Grading of Buildings – Part 1. General Principles and Structural Precautions*, Post-War Building Studies No.20. Ministry of Works, London, HMSO, 1946.

3. CIB W14 Workshop. *Design Guide – Structural Fire Safety*, Fire Safety Journal, March 1986.

4. Magnusson, SE, Pettersson, O and Thor, J. *Fire engineering design of steel structures*, Swedish Institute of Steel Construction, Publication 50, Stockholm, 1976.

5. *Fire safety in constructional steelwork*, CECM-III-74-2E, European Convention for Constructional Steelwork, 1974.

6. Eurocode 1: *Basis of Design and Action on Structures, Part 2.2 – Actions on Structures Exposed to Fire*, ENV 1991-2-2:1995, European Committee for Standardisation.

7. *The Building Regulations 1991, Approved Document B – Fire Safety.*

8. BSI, National Application Document, Eurocode 1: *Basis of Design and Action on Structures, Part 2.2 – Actions on Structures Exposed to Fire for use in the UK*, DD ENV 1991-2-2:1996.

9. BSI Draft for Development, *Fire safety engineering in buildings, Part 1 – Guide to the application of fire safety engineering principles,* DD 240: Part 1: 1997.

10. Law, M. *A Review of Formulae for T-Equivalent*, Fire Safety Science – Proceedings of the Fifth International Symposium, pp 985 – 996, International Association for Fire Safety Science, 1997.

11. Newman, GM. A system of grading the Fire Resistance of Structural elements: Report to British Steel, Revision 0, March 1994 - incomplete and not published.

WITH PERFORMANCE CODES WHO NEEDS STRUCTURAL FIRE RESISTANCE?

William E. Koffel, P.E.
Koffel Associates, Inc., Ellicott City, Maryland, USA

ABSTRACT

Historically, structural fire resistance has been regulated by prescriptive code requirements that link the construction of the building to risk factors such as the height and area of the building and the occupancy of the building. Additionally, fire resistance requirements were based upon the need to separate certain spaces within the building to protect the egress path or to separate hazards and to protect against fire spread to adjacent areas, floors or buildings. However, today if a project is designed using a performance code and the building is to be protected with an automatic sprinkler system, do we still need structural fire resistance?

The paper will discuss issues such as system reliability and safety factors and how they will impact the need for structural fire resistance. Examples will be provided using the performance design option contained in the NFPA Life Safety Code, NFPA 101-2000 and the proposed International Performance Building Code being developed in the USA.

ABOUT THE AUTHOR:

William Koffel is President of Koffel Associates, Inc., a fire protection engineering and code consulting firm with offices in the United States. Mr. Koffel has been active in the development of prescriptive and performance based codes in the United States. He is a member of BOCA, ICBO, NFPA, SBCCI, SFPE and is currently a Vice-President of the SFPE.

An Analysis of the Behaviour of the First Cardington Test Using Stress-Resultant Shell Elements.

M. Gillie and A.S Usmani

School of Civil and Environmental Engineering

University of Edinburgh, Edinburgh, EH9 3JN

United Kingdom

Abstract

This paper presents a finite element analysis of the first Cardington test using shell elements to model the concrete floor slab. The behaviour of these elements is defined using FEAST, a program that allows the behaviour of the shell elements to be defined within the commercial finite element package ABAQUS, using stress-resultants. The model of the test is described and the assumptions that were made are noted and justified. The results of the analysis indicate that the response of the structure is overwhelmingly dominated by the effects of thermal expansion and that material degradation and gravity loading are of secondary importance.

Keywords: Cardington, finite element analysis, FEAST, fire conditions

Introduction

The behaviour of composite structures in fire conditions, such as the office buildings found in many European cities, is extremely complex. In recent years it has been accepted that the traditional methods of fire safety engineering have been developed from an inadequate understanding of the behaviour of heated structures. This has led to the application of expensive fire protection that may have been unnecessary in many cases. To allow the behaviour of structures in fire conditions to be studied, a series of tests were performed on a full scale, eight storey, steel-framed building in 1995 at Cardington, UK.[1–3] These experiments produced a huge

amount of experimental data and it was intended that this data be used to develop a detailed understanding of the physical phenomena which dominate structural behaviour under fire loading. This paper is concerned with gaining some of this understanding. The Cardington tests, together with recent advances in computing power and modelling techniques, have allowed a new generation of numerical models of heated structures to be developed. Previous research into modelling isolated structural elements and simple frames has shown that it is difficult to obtain accurate models even with experimental data available for verification. Clearly, attempting to model 3-dimensional structures with no experimental data would not have produced reliable predictions. The availability of the Cardington experimental data prompted a number of groups to attempt to model the fire tests and to obtain an understanding of the structural behaviour based on the results of their models.

Workers at Sheffield University have produced numerical models of the fire tests[4–7] conducted at Cardington using the VULCAN[6] finite element program, previously known as INSTAF.[5] Analysts at Imperial College, London have used the ADAPTIC[8] finite element package to model the Cardington tests. ADAPTIC only includes beam elements and so the analyses have been performed by descretizing the Cardington tests in the form of a grillage. The results were reported in 2000 by Elgazhouli.[9] British Steel has developed a number of numerical models to investigate aspects of the Cardington tests.[10–12] Models of the floor slab using linear elastic shell elements with discrete hinges where yield lines were expected to develop were produced for the first, third and fourth tests. A group at Edinburgh University has used the commercial finite element package, ABAQUS,[13] to model the Cardington tests.[11, 12, 14–17] The group used beam elements with fully non-linear material behaviour to represent the steel frame and a grillage of beam elements defined using a stress-resultant approach to model the floorslab.

To date all numerical work on analysing the Cardington structure has been lacking in one or more areas. Work using shell elements to represent concrete floors has tended to either use very simple material behaviour and include various *ad hoc* assumptions, or has not included numerical representation of key phenomena such as geometric non-linearity. Work that has not been deficient in these respects has resorted to using a grillage of beam elements to represent a continuous floor slab. While all these models have been useful in gaining new insights into the behaviour of structures in fire conditions, it is clearly necessary for a more rigorous

numerical model to be developed before any firm conclusions can be drawn. The need for such a model is made more important by the move towards performance based fire safety design codes. In addition, most previous work has concentrated on modelling the tests and obtaining accurate matches with experimental data. This is clearly necessary but a clear understanding of the key structural phenomena is also required. Unless engineers have a good understanding of how heated structures behave, they will not be able to take full advantage of modern design codes.

This paper presents an analysis of the first Cardington test using the FEAST program. FEAST is a user-defined subroutine that can be used with ABAQUS to specify the behaviour of shell elements using stress-resultants. The use of FEAST means that the analysis accounts for full material and geometric non-linearity as well as thermal expansion, thermal curvature and non-linear thermal gradients. To date no other analysis has included all these aspects while using shell elements to model the Cardington floor slab. Full details of FEAST have been given elsewhere.[18,19] The combination of FEAST and ABAQUS has the added advantage of using the highly optimised and well verified ABAQUS numerics. As well as describing the numerical model that was used, the paper also presents information on the forces that developed in the structure and attempts to disentangle the complex structural response.

The Finite Element Mesh

The layout of a typical floor of the Cardington frame showing the position of each of the tests is shown in Fig. . Test one consisted of heating an internal secondary beam and the associated area of floor slab above it; the columns at each end of the beam were protected. The figure shows that in the test there was a considerable area of cold structure separating the heated compartment from the edge of the building on all sides. This cold area remained very stiff in comparison to the heated compartment and so the compartment was well restrained laterally. As a result, it was not necessary to model the entire floor for a realistic finite element mesh to be developed because the lateral restraint could be accurately represented by rigid horizontal boundary conditions. The symmetrical nature of the test was exploited in the finite element mesh. This approach resulted in the area of slab modelled extending from the middle of the heated compartment to the

column in the direction of the heated beam and to mid-span in each of the unheated bays adjacent to the heated compartment. This is shown in schematic form in Fig. 2 and the finite element mesh is shown in Fig. 3. Eight noded, reduced integration, 3-dimensional shell elements were used in a 30×30 regular grid. At each of the boundaries vertical displacement and rotation about an axis parallel to the line of the boundary were allowed while all other degrees of freedom were fixed. This arrangement produced a symmetry condition at all edges of the slab. FEAST was programmed to model the slab using the concrete behaviour specified in Eurocode 2.[20] The floorslab was orthotropic, due to ribs running perpendicular to the tested joist, and FEAST was programmed to take account of this.

The beams and column were modelled as I-section, 2-noded linear beam elements. This meant that the local flange buckling that was seen to take place in the Cardington experiment would not be captured in the model. However it was shown by O'Connor[10] that this local behaviour did not effect the overall predictions of numerical models. By using beam elements rather than shell elements considerable computational time and resources were saved. As with the slab, where the beam elements coincided with the edge of the mesh, symmetry boundary conditions were used. The column was modelled from one floor below the floor on which the test took place to one floor above it, also with 2-noded linear beam elements. The bottom end of the column was fully fixed whilst at the top only vertical deflections were permitted. The behaviour of the steel in the beams and columns was that defined in Eurocode 3.[21]

In the experiment the beam to beam and column to column connections were half-depth end plates.[3] Such connections can be assumed to have little or no moment capacity so pinned connections were used in the finite element model to represent this condition. The slab was connected to the beams by shear studs that provided a very high degree of restraint and so rigid connections were specified numerically.

There were two kinds of load applied during the Cardington experiment; a static load and a thermal load. The total static load was 5.48 kN/m^2 and this was straightforward to apply numerically. The thermal loading was less easy to define. The Cardington floor slab had ribs on its under-surface meaning that the temperature varied depending on the section being considered as shown in Fig. 4. In the analysis the temperature-time curve for the slab was obtained from the temperature sensor placed 75mm below the top

surface, over a rib. The joist temperature-time curve was obtained from a sensor located on the web. These temperature profiles are shown in Fig. 5. The loading was applied in two stages. First the static load was applied while the structure was unheated. The structure was then heated according to the temperature-time curves described above with the static load remaining unaltered.

Analysis of the Structure

It is clear from even a casual study of the analysis of the experimental load case that the behaviour of the Cardington frame during test 1 is extremely complex (Figs. 6 to 14). This section will analyse the behaviour of structure as it was heated and identify the key structural events. So that the order of these events is clear, the tested beam lower flange temperature will be used as a reference temperature.

General Points

Before discussing the physical behaviour of the structure it is worth emphasising the relationships between thermal, mechanical and total strains. At ambient temperature total strains and mechanical strains are equal and so lead to both stresses and deflections. This is no longer the case in heated structures where strains are related according to the following equations:

$$\epsilon_t = \epsilon_m + \epsilon_T \tag{1}$$

$$\epsilon_T = \alpha \Delta T \tag{2}$$

$$\text{where:} \quad \epsilon_t = \text{total strain}$$

$$\epsilon_m = \text{mechanical strain}$$

$$\epsilon_T = \text{thermal strain}$$

It is still true that total strains lead to deflections but it is now mechanical strains that lead to stresses. That this is the case can be most clearly seen by considering the simple example of a uniformly heated fixed ended beam. As the beam is heated the thermal strains are completely cancelled out by mechanical strains

of equal magnitude but opposite sign. The total strain and the deflections remain zero whilst stresses are induced as a result of the mechanical strain. If the fixed ends were now replaced with rollers, the mechanical strains and hence the stresses would be zero. Meanwhile the total strains and deflections would increase. These ideas have important consequences when it comes to considering deflections in heated structures. It is no longer necessarily the case that large deflections imply large stresses, or that the structure is close to failure, as is the case with structures at ambient temperature.

Total curvatures, thermal curvatures and mechanical curvatures are linked in a similar manner to strains:

$$\phi_t = \phi_m + \phi_T \tag{3}$$

$$\phi_T = \alpha \Delta G \tag{4}$$

where: $\phi_t =$ total curvature

                 $\phi_m =$ mechanical curvature

                 $\phi_T =$ thermal curvature

                 $G =$ thermal gradient (assumed linear)

Deflections

The steel joist had a low thermal capacity and high thermal conductivity and so its temperature remained close to the atmosphere temperature throughout the test. By contrast the concrete slab had a high thermal inertia and so it was only later in the test that its mean temperature started to rise significantly (Fig. 5). A consequence of this slow rise in the slab temperature was that the deflection behaviour in the early part of the test was controlled by the beam. As the beam temperature rose its thermal expansion was restrained directly by the cooler slab. The resultant thrust was eccentric to the composite slab-beam section and so forced the section into sagging curvature, thus producing deflections. This behaviour was dominant until about 120C.

At around 120C the tested beam yielded in compression (see below and Fig. 11) so expansion no longer resulted in increasing axial force and the beam ceased to drive deflections. As the beam temperature

continued to increase beyond 120C the axial force decreased (Fig. 11) as a result of the declining material properties of the steel. If the sole cause of deflections beyond 120C had been the thermal expansion of the steel beam, then the deflections would have stopped or even started decreasing as soon as the beam axial force began to reduce because the eccentric thrust would no longer have been sufficient to maintain the deformed shape.

There were a number of mechanisms that drove deflections after the tested joist yielded, all of which depended on rises in the slab temperature. At the time of the joist yielding the lower surface of the slab was starting to heat significantly while the upper surface remained cool, as can be seen in Fig. 4. This resulted in thermal gradients and hence thermally induced curvatures, both parallel and perpendicular to the ribs, which gave rise to increasing deflections. At higher temperatures still the thermal expansion of the slab parallel to the tested joist was sufficient to drive the deflections. This mechanism was resisted somewhat by tensile forces that developed in the ribs (Figs. 8 and 9). At the same time the temperature of the lower surface of the slab was becoming hot enough for degradation of material properties to reduce the slab's moment capacity, thus reducing its resistance to increasing deflections.

The changing importance of the different effects driving the deflections can be seen in Fig. 7. The figure shows the predicted deflections when the steel coefficient of thermal expansion is assumed to be zero and also when the concrete coefficient of thermal expansion (and therefore thermal gradient) are assumed to be zero. When the concrete's thermal expansion is taken as zero, the predicted deflections approximate the test deflections quite well up to 200C at which point the steel joist has yielded; beyond this the deflections are almost constant and have no relation to the test deflections. This behaviour is in line with the explanation given above. When the steel thermal expansion is assumed to be zero there is almost no predicted deflection before around 500C, at which point deflections grow very rapidly. The behaviour can be likened to the Euler buckling of columns, although in this case there is no instability because the ends of the compressive member are fixed and so the deflected shape is effectively defined. Above around 800C the behaviour of the model with no steel thermal expansion approximates the test behaviour fairly well. At such temperatures the steel has lost almost all its strength so the effects of the steel's thermal expansion are almost negligible.

Behaviour of Ribs

The behaviour of the ribs (i.e. the slab perpendicular to the tested beam) is shown in Figs. 8 to 10. These figures show forces per unit width plotted against distance from the edge of the numerical model. The symmetry in the model is exploited so on the x-axes the unheated secondary beam is at 1500mm, the edge of the heated compartment at 3000mm and the tested joist at 4500mm.

At mid-span (Fig. 8) the force in the ribs was tensile throughout the test and increased with increasing temperature. This tensile force is explained by compatibility. Since the length of the heated compartment was greater than its width, the increase in length in the ribs' direction due to thermal expansion was less than that in the direction of the heated joist. As a result tensile forces were produced in the ribs in areas of high deflection. The rib force at 850C at mid-span was approaching the ultimate capacity of the ribs. As positions progressively nearer to the column are considered (Figs. 9 and 10) the tensile forces in the ribs can be seen to decrease until at one-eighth span the ribs were subject to increasing compression as the temperature increased. This is because nearer the column deflections were less than at mid-span but the amount of thermal expansion in the ribs was the same. The increase in length of the ribs due to changes in geometry was now less than the increase due to thermal strains and so compressive forces resulted.

Behaviour of the Tested Joist

The force in the tested beam is plotted against temperature at various sections in Fig. 11. Until 120C the force increased linearly with temperature indicating that the beam was subject to restrained thermal expansion while remaining in its elastic range. The gradient of the plot in this region for all the heated parts of the beam is about (-)$11800N/C$. For fully restrained expansion the expected value of this gradient can

be obtained from the standard relationship:

$$\delta = PL/EA \qquad (5)$$

where in this case: $\quad \delta = \alpha L = 1.3 \times 10^{-5} \times 9000 = 0.117mm$

$$E = 210000N/mm^2$$

$$A = 5160mm^2$$

$$L = 9000mm$$

This gives a value of $14087N/C$ for P. The discrepancy between the two figures can be explained by remembering that the beam in the numerical model was not fully restrained but deflected downwards. This resulted in a geometric lengthening of the beam and so a reduced increase in force per unit temperature rise. The thermal expansion forces produced in the tested beam by even fairly modest increases in temperature were sufficient to swamp the forces in the beam resulting from the composite action of the slab-beam section. This can be seen by comparing the curves at 0C and 200C in Fig. 11. The figure shows that there was a fundamental change in the pattern of axial force in the beam during the first 200C degrees of heating, which resulted from restrained thermal expansion. Beyond this initial phase the changes in axial force resulted from declining material properties and were smoother and more gradual. Figure 11 demonstrates that a fairly small temperature rise can lead to dramatic changes in structural behaviour.

From 120C onwards the deformations of the joist were entirely plastic and so could not be recovered when the temperature dropped. Although the cooling phase of the test was not modelled numerically, the large plastic deformations of the beam explain the failure of the connections between the beam and columns that occurred during cooling in the test. On cooling the plastified beam would have attempted to contract and thus produced huge tensile forces over its entire length and through the connections.

Behaviour of the Heated Composite Section

To understand the behaviour of a composite structure it is useful to think in terms of the behaviour of composite members. In test 1 the behaviour of the heated joist and associated area of slab is clearly crucial to understanding the structural behaviour. Since the concrete slab was continuous between secondary beams a suitable width of slab that was deemed to act with the steel joist had to be determined. In this analysis an effective width of 2250mm was chosen, in line with the Eurocode design recommendations.

The force in the width of slab acting compositely, the force in the composite section and the moment over the section are shown in Figs. 12 to 14. The composite moments were calculated about an axis mid-way between the geometric centroid of the steel section and a point 70mm up from the lower surface of the ribs. All these graphs show abrupt changes in value near the column. These abrupt changes resulted from numerically predicted hot spots that occurred in the slab near areas that were unheated and highly restrained. The hot spots are likely to be more marked in the numerical model than in reality and it is suggested that the values very near the column are treated with a degree of scepticism.

The force in the slab increased until about 400C before decreasing as the slab's material properties declined (Fig. 12). At ambient temperature the pattern of forces was determined by the deflected shape of the slab with tensile forces occurring near the column and compressive forces at mid-span. In a similar way to the tested beam, this pattern changed soon after the heating began. By 200C the forces in the slab were almost uniform along the entire heated length and were produced almost entirely by restrained thermal expansion. At higher temperatures the force at mid-span was slightly less than near the column. The pattern of the composite axial forces (Fig. 13) followed similar trends to the slab forces but, because the joist was heated more quickly than the slab, two peaks occurred. One occurred when the joist force peaked at around 120C and the second when the slab force peaked between 400C and 600C.

The moments in the composite section are shown in Fig. 14. As expected, at ambient temperature the moments were governed by the curvature of the composite section; hogging was present near the column and sagging at mid-span. The axial forces in both joist and section of slab acting compositely have been shown to quickly become dominated restrained thermal expansion. Since the composite moments were determined

by these forces, they too resulted from thermal expansion at even quite modest temperatures. By 200C the composite moment for all three effective widths had changed from the ambient temperature distribution and had become almost uniform along the full length of the beam. The joist yielded by 200C so from this point onwards the changes in composite moments are largely governed by changes in the force in the slab section; it can be seen that the changing composite moment follows a similar trend to the changing slab force (this ignores the declining force in the joist due to material degradation).

Discussion

At ambient temperature the only loads on the structure were gravity loads. The way these were carried is well understood by structural engineers and it is tempting to assume the response of the structure continues to be dominated by gravity loads at high temperatures. However, it is clear from the figures that this is not the case. The forces and deflections in the structure developed largely as a result of restrained thermal expansion and were relatively independent of gravity loading. This point is shown clearly in Fig. 15 which shows the test deflections, the numerically predicted deflections and the predicted deflections with the gravity loading tripled. The difference in predicted deflections is almost uniform throughout the test showing that it is only at ambient temperature that the magnitude of gravity loading is important.

Test 1 was an extremely restrained test in a highly redundant building. This meant the effect of declining material properties on deflections was complex. The degree to which the structure deflected has been shown to be largely dominated by restrained thermal expansion. Any thermal expansion not absorbed by elastic or plastic mechanical straining had to produce deflections. A consequence of this observation is that a reduction in material properties could actually reduce deflections by allowing a greater proportion of the thermal expansion to be absorbed by mechanical straining. This effect was strongly apparent in Fig. 7 – when the concrete coefficient of thermal expansion was taken as zero, the declining strength of the steel meant that the deflections stopped increasing. The traditional assumptions about declining material properties are very much at odds with this argument. It is normally thought that a reduction in strength leads to increasing deflections until the structure no longer has the means to withstand the applied loads, and collapses. In very

simple determinate structures this is clearly the case and will also be the case in redundant structures once all alternative load carrying mechanisms have been used. The results from this analysis indicate however that the structure was some way from collapse and that the declining material properties were not responsible for significant increases in deflection.

Conclusions

It is concluded from this investigation that for well restrained compartment fires in highly redundant buildings:

- The effects of the thermal expansion are dominant in producing deflections and forces.

- Material degradation and gravity loading have only a minor effect on deflections and forces.

- Tensile membrane action plays an important role in supporting the structure.

References

[1] P.N.R. Bravery. Cardington Large Building Test Facility. Technical report, iki, c1993.

[2] D.M. Martin, B.R. Kirby, and M.A. O'Connor. Behaviour of a Multistorey, Steel Framed Building Subjected to Natural Fire Effects, Final Report. Technical report, British Steel, 1998. Confidential report.

[3] B.R. Kirby. The Behaviour of a Multi-storey Steel Framed Building Subjected to Fire Attack, Experimental Data. Technical report, British Steel, 1998.

[4] C.G. Bailey, I.W. Burgess, and R.J. Plank. Computer Simulation of a Full-scale Structural Fire Test. *The Structural Engineer*, 74(6):93–100, March 1996.

[5] P.S. Rose, I.W. Burgess, R.J. Plank, and C.G. Bailey. The Influence of Floor Slabs on the Structural Behaviour of Composite Frames. In Lee, editor, *Structures in the New Millennium*, 1997.

[6] Z. Huang, I.W. Burgess, and R.J. Plank. Nonlinear Analysis of Reinforced Concrete Slabs Subjected to Fire. *ACI Structural Journal*, 96:127–135, Jan-Feb 1999.

[7] Z. Huang, I.W. Burgess, and R.J. Plank. Three-dimensional Modelling of Two Full-scale Fire Test on a Composite Building. *Proceedings of the Institute of Civil Engineers, Structures and Buildings*, 134(1):243–255, 1999.

[8] B.A. Izzuddin and A.S. Elnashai. *ADAPTIC: A program for Adaptive Dynamic Analysis of Space Frames, User Manual*. Imperial College, London, 1989.

[9] A. Y. Elgazhouli. PIT Project Research Report MD15: Models of all the Cardington tests using ADAPTIC. Technical report, British Steel, 2000.

[10] M. O'Connor. PIT Project Research Report MD7: BS/Test2 ABAQUS model using shell elements for the beam and beam general section for the slab. Technical report, British Steel, 2000.

[11] A.M. Sanad. BS/Test3 reference ABAQUS model using beam general section. Technical report, University of Edinburgh, 2000.

[12] A.M. Sanad, J.M. Rotter, and M.A. O'Connor. Finite element modelling of fire tests on the cardington composite building. In *Proceedings Interflam'99*, volume 2, 1999.

[13] Hibbet, Karlson and Sorenson, Providence, Rhode Island, USA. *ABAQUS Users' Manual,Vols I to III, Ver 5.8*, 1998.

[14] J.M. Rotter, A.M. Sanad, A.S. Usmani, and M. Gillie. Structural Performance of Redundant Structures under Local Fires. In *Proceedings of Interflam '99*, volume 2, Scotland, 1999.

[15] A.M. Sanad. BS/Test1 reference ABAQUS model using beam general section. Technical report, University of Edinburgh, 2000.

[16] A.M. Sanad. PIT Project Research Report AM1: Analysis of results from BS/TEST1 models, Part A Grillage Models. Technical report, University of Edinburgh, 2000.

[17] A.M. Sanad. PIT Project Research Report AM6: Analysis of results from BS/TEST3 models, Part A Grillage Models. Technical report, University of Edinburgh, 2000.

[18] M. Gillie. Modelling Heated Composite Floorslabs with ABAQUS using a UGENS subroutine. In *ABAQUS Users' Conference 2000*. Hibbett, Karlsson and Sorenson, INC, 2000.

[19] M. Gillie, A.S. Usmani, and J.M. Rotter. Modelling of Heated Composite Floor Slabs with Reference to the Cardington Experiments. *Fire Safety Journal*, 2000. submitted.

[20] ENV. *Eurocode 2, Design of concrete structures*, 1992.

[21] ENV. *Eurocode 3, Design of composite steel and concrete structures*, 1994.
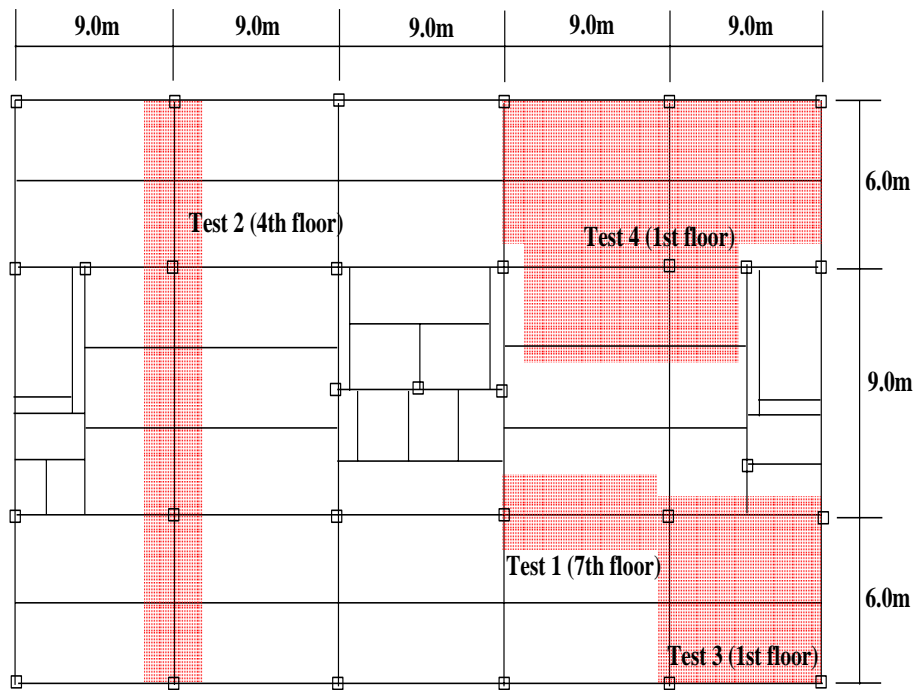
Figure 1: Layout of a typical floor of the Cardington frame showing the locations of the various tests. It should be noted that the tests were carried out on different floors.
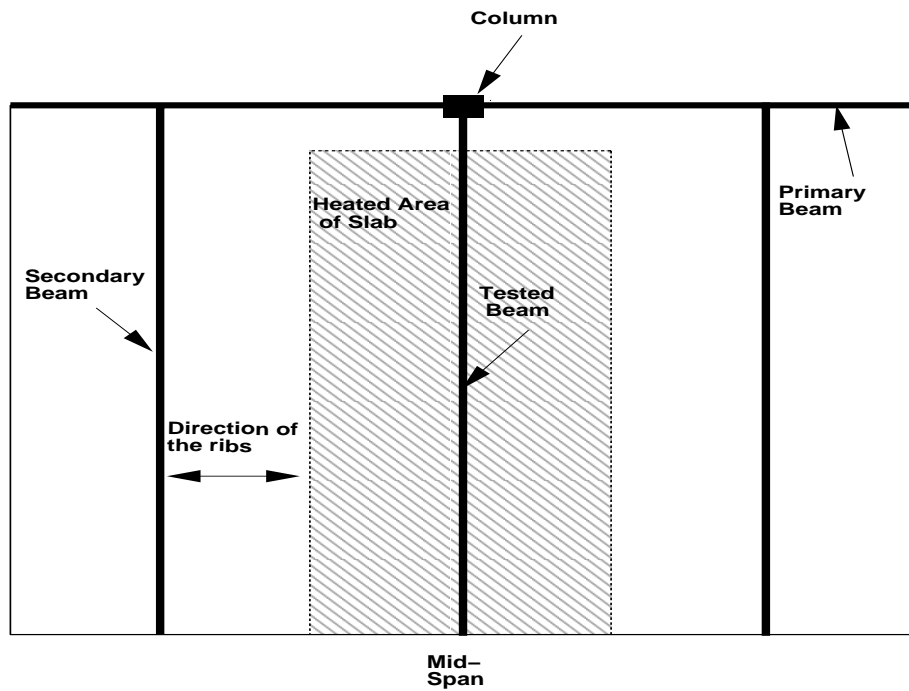
Figure 2: Schematic plan view of the area of the Cardington frame modelled for the analysis of test 1.
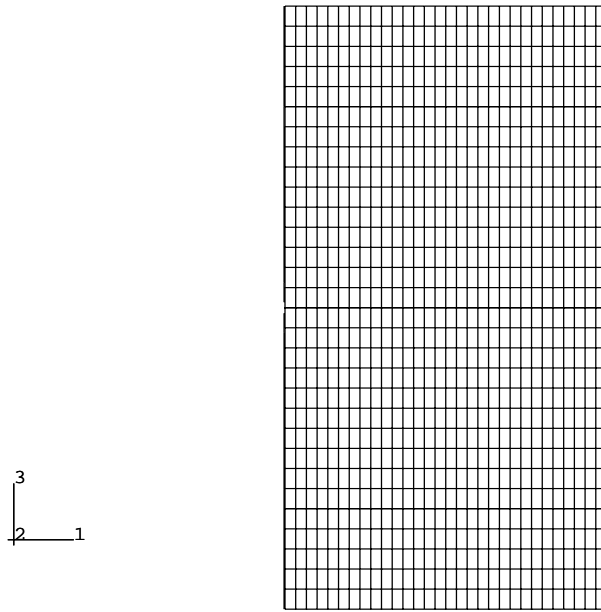
Figure 3: Plan view of the mesh used for the analysis of test 1.
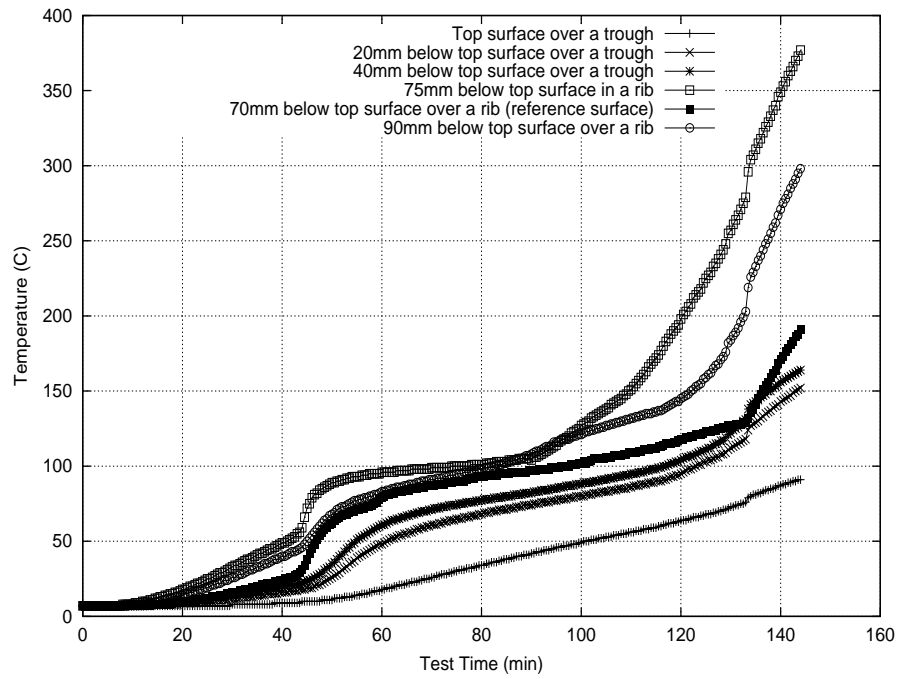
Figure 4: Variation of the slab temperature with time at various locations through its depth at a typical location.
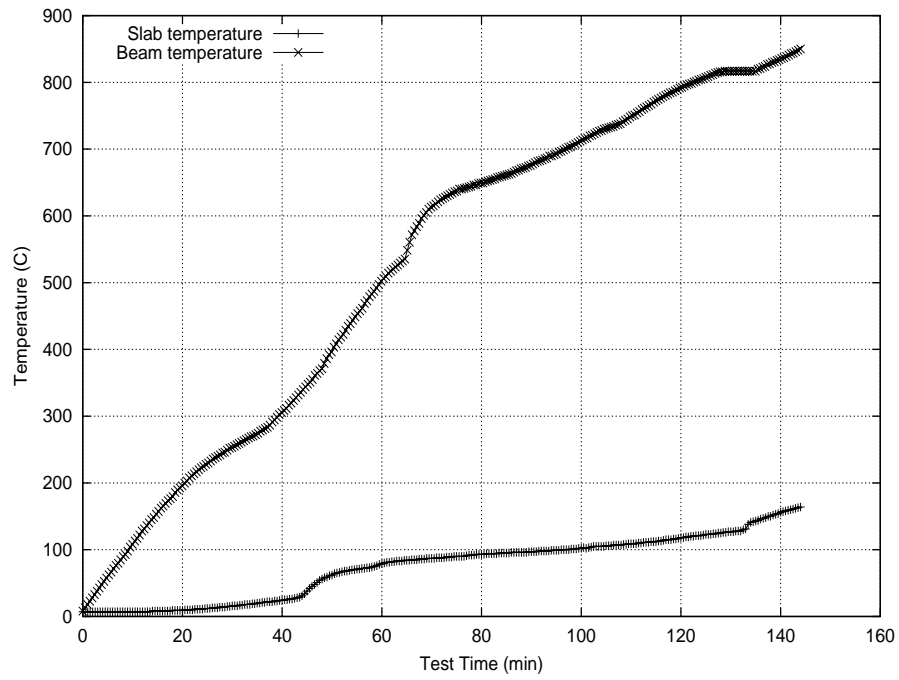
Figure 5: Slab and beam temperature-time curves used during the analysis of test 1.
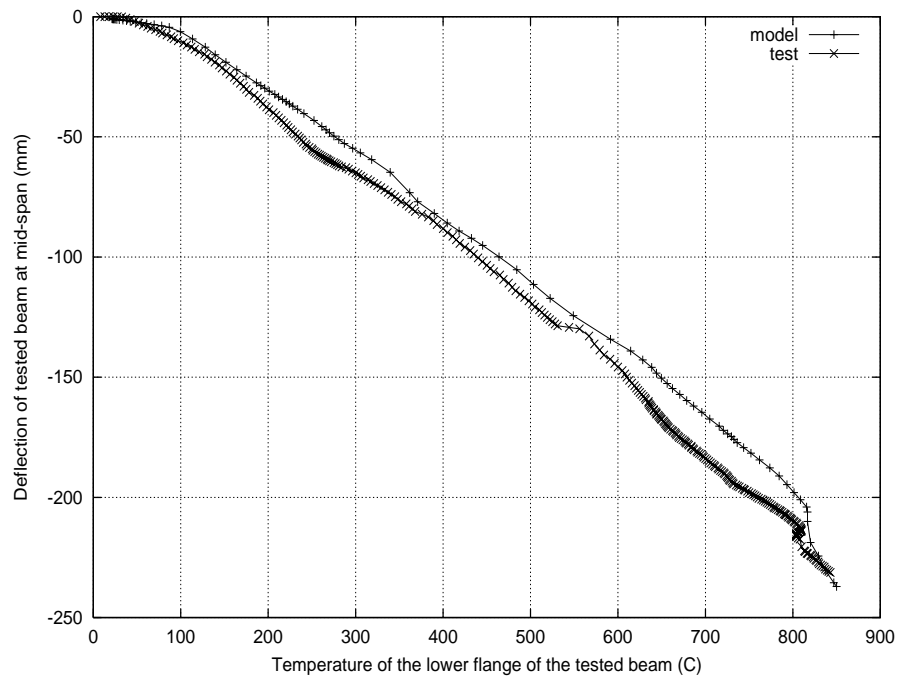
Figure 6: Comparison of deflections at midspan.
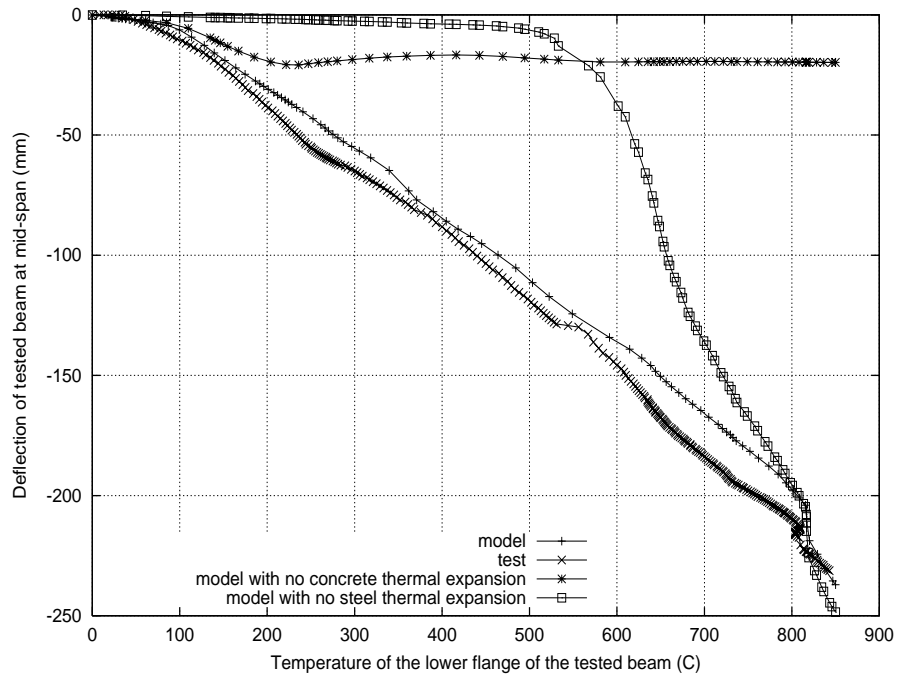
Figure 7: Comparison of the predicted deflections when the thermal expansion of the steel and concrete are assumed to be zero.
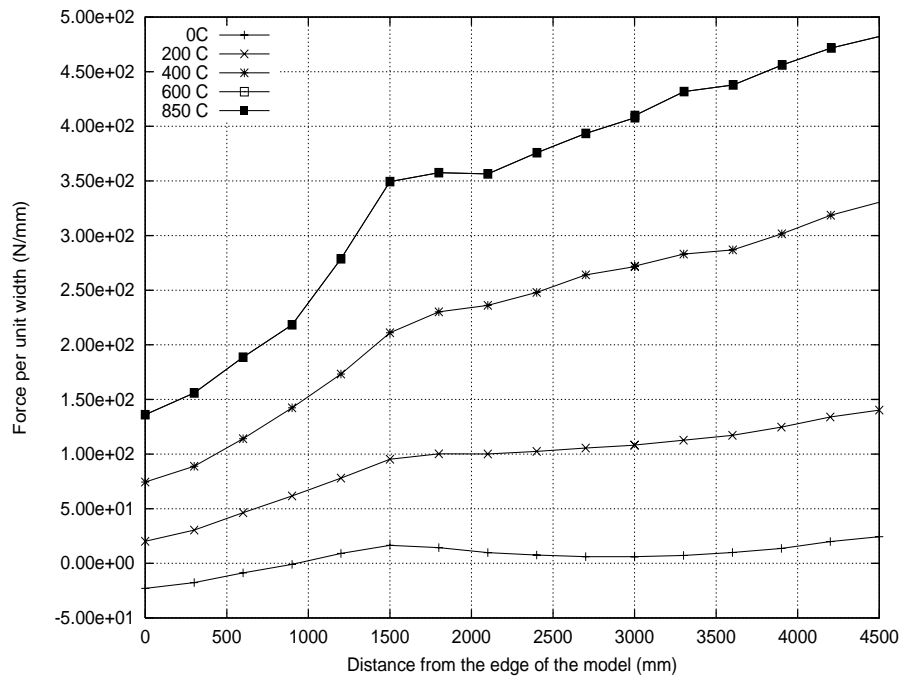
Figure 8: Force per unit width parallel to the ribs at mid-span.
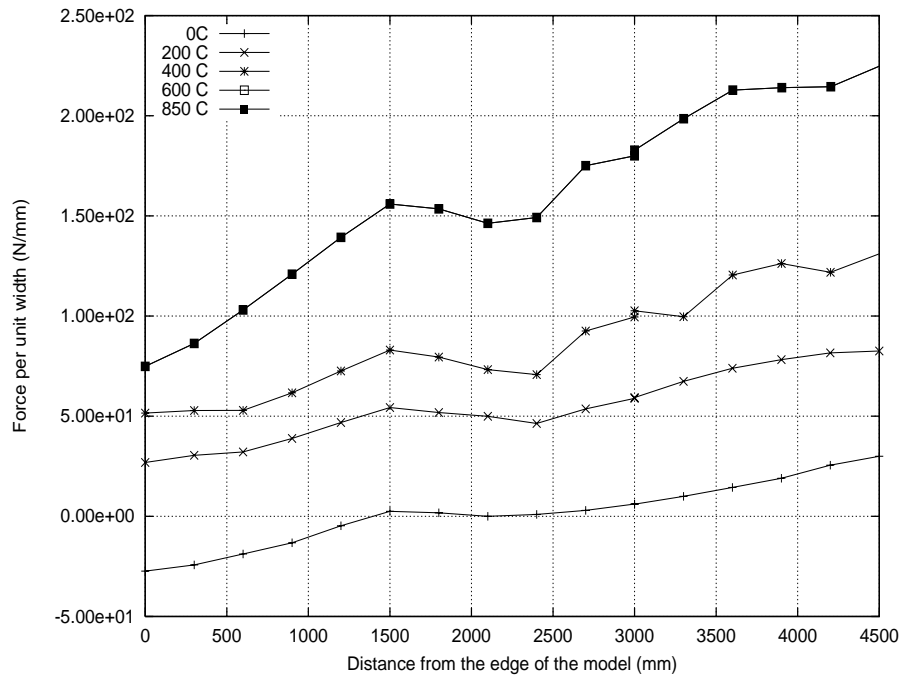
Figure 9: Force per unit width parallel to the ribs at one-quarter span.
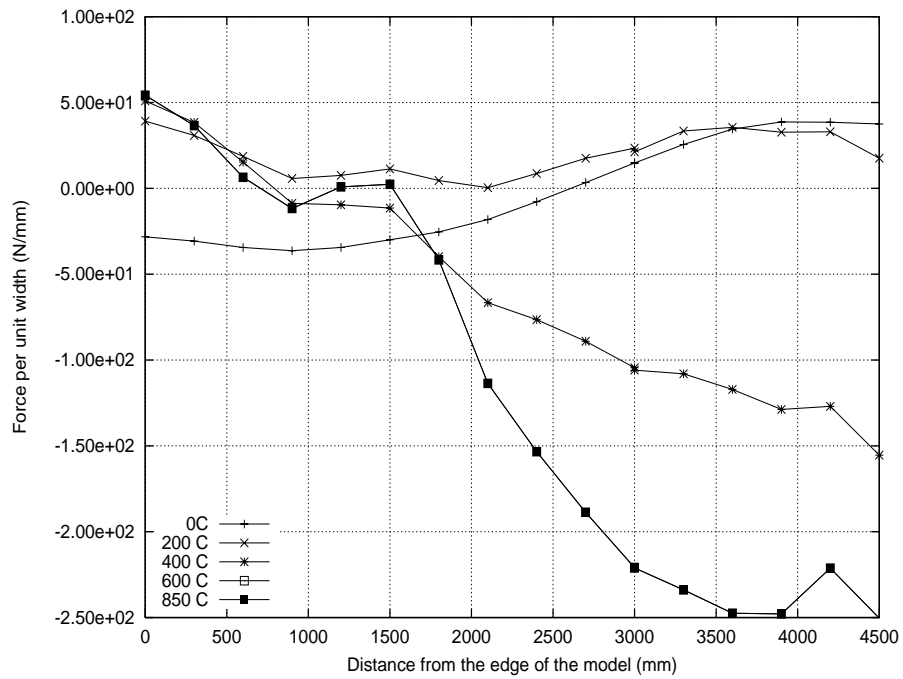
Figure 10: Force per unit width parallel to the ribs at one-eigth span.
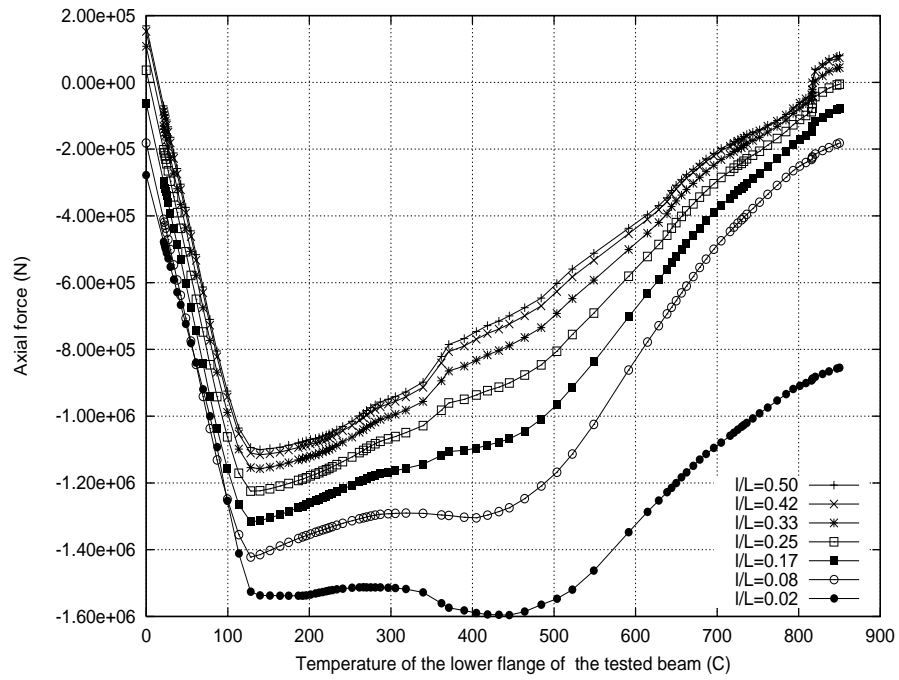
Figure 11: Axial force against temperature at various sections in the tested joist.
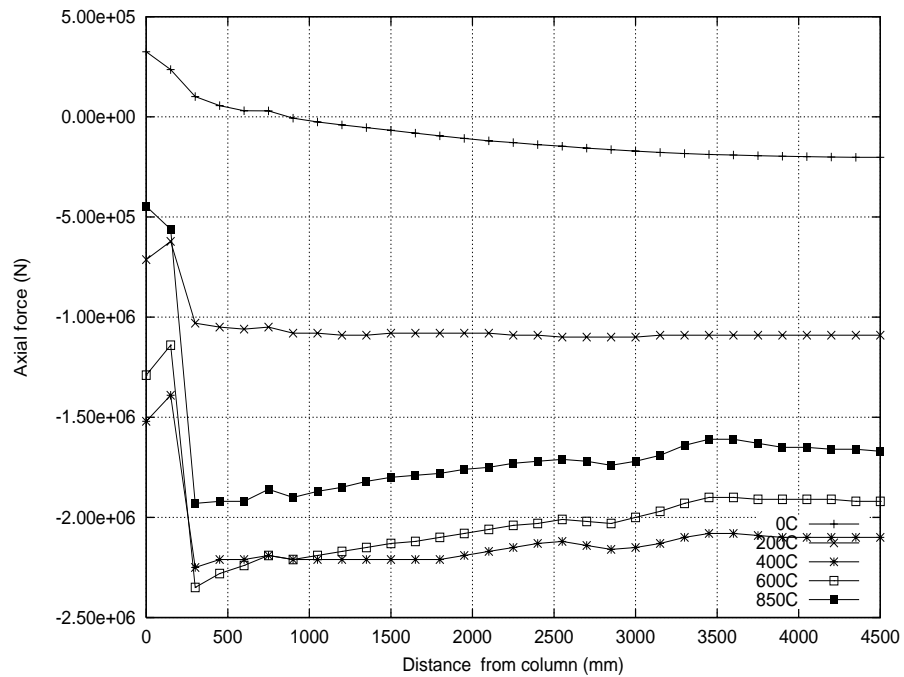
Figure 12: Slab force acting compositely at various temperatures assuming an effective width of 2250mm.
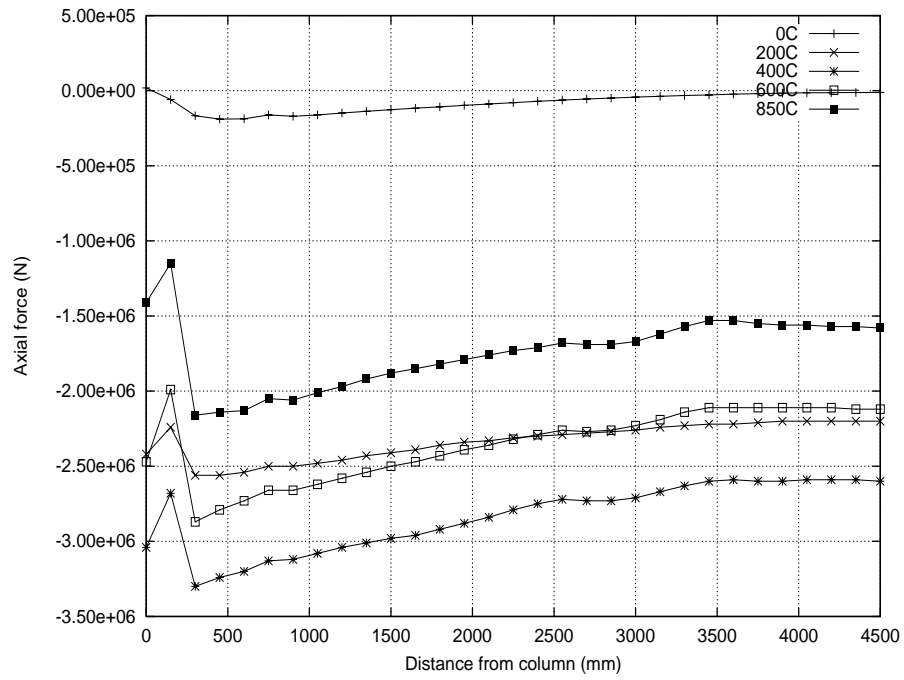
Figure 13: Composite force at various temperatures assuming an effective width of 2250mm.
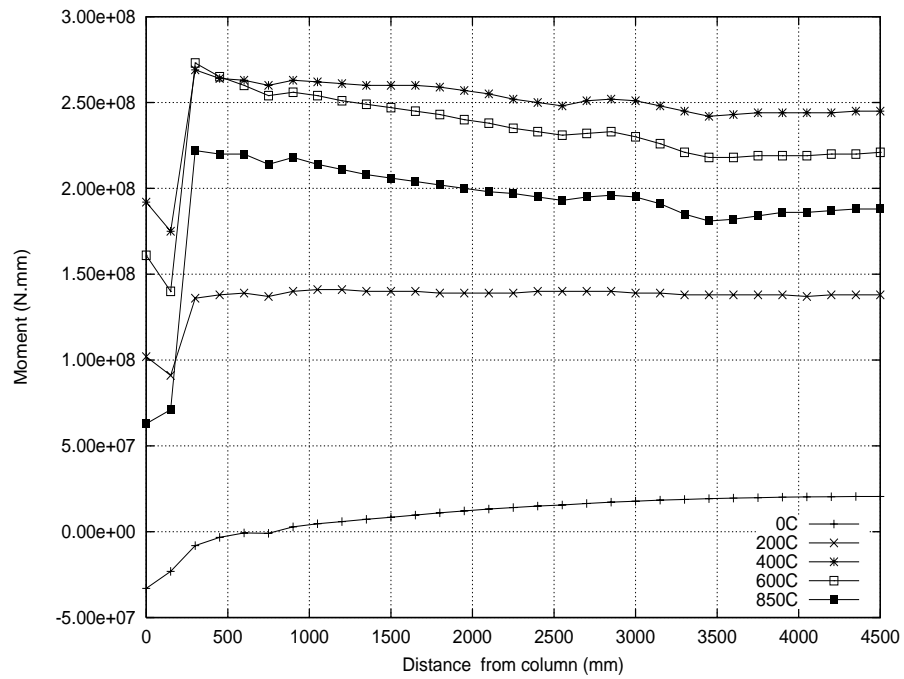
Figure 14: Composite moment at various temperatures assuming an effective width of 2250mm.
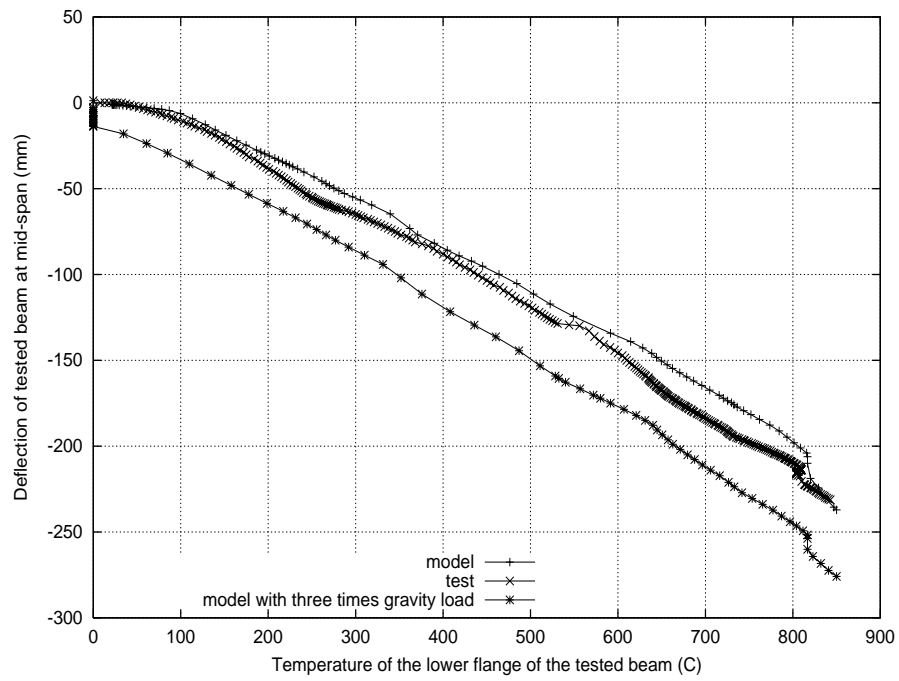
Figure 15: The effect of tripling the gravity load on deflections.

A STUDY FOR THE DEVELOPMENT OF THE DESIGN OF STEEL STRUCTURES IN FIRE CONDITIONS

Outinen, J., Kaitila, O., Mäkeläinen, P.
Laboratory of Steel Structures, Helsinki University of Technology, P.O.Box 2100, FIN-02015 HUT, Finland
Fax : +358-9-4513826
Email: jyri.outinen@hut.fi

SUMMARY

A study for the development of the design of steel structures in fire conditions has been started 1999 in the Laboratory of Steel Structures at Helsinki University of Technology. The objective of this project is to develop the fire engineering design of steel and steel-concrete composite structures using as a starting point the research done at the Technical Research Centre of Finland (VTT) on fire models for different types of buildings. The development of temperature increase in steel structures is studied. Material models in fire conditions based on experimental results are used to determine the load-bearing capacity of structures in fire. The point is to make use of the possibility of performing a more thorough and exact fire design given by, e.g. the Finnish design standards.

In connection to the above, an extensive experimental research program has been carried out during the years 1994-2000 in the Laboratory of Steel Structures at Helsinki University of Technology for the investigation of the mechanical properties of various structural steels at elevated temperatures. The latest research has concentrated on structural steel S355J2H. The tests are carried out for cold-formed material taken from rectangular hollow sections. The purpose of this research is to study the behaviour of this cold-formed steel material at fire temperatures using both transient state and steady state tensile test methods. The test results for this material and also for structural steels with yield strength 355N/mm^2 and 460N/mm^2 and for structural sheet steel with yield strength 350N/mm^2 are presented shortly in this paper.

KEYWORDS

Steel, structural steel, mechanical properties, strength, fire, high-temperature, elevated temperature, cold-formed, material model.

INTRODUCTION

Basic material research of structural steel materials is becoming more important as the significance of fire engineering design of steel structures is growing and new steel materials, including high-strength steels and stainless steels are going to be used more widely in steel structures in the near future. Extensive experimental research has been carried out during the years 1994-2000 in the Laboratory of Steel Structures at Helsinki University of Technology in order to investigate mechanical properties of several structural steels at elevated temperatures by using mainly the transient state tensile test method. Furthermore one austenitic stainless steel grade and one aluminium alloy have been studied with the same test method. Another method, the steady-state method has also been used in order to create a proper basis for the analyses of the test results.

In this paper the experimental test results for the mechanical properties of the studied steel grades S350GD+Z, S355 and S460M at fire temperatures are presented with a short description of the testing facilities. A test series is also carried out for cold-formed material taken from rectangular hollow sections.

The test results are used to determine the temperature dependencies of the mechanical properties, i.e. yield strength, modulus of elasticity and thermal elongation, of the studied steel materials at temperatures up to 950°C. The test results are compared with the material model for steel according to Eurocode 3: Part 1.2. The test results are presented as simple figures and graphs of the reduction factors of the mechanical properties, i.e. modulus of elasticity, yield strength and the other calculation parameters that are needed in the Eurocode 3 (EC3) model. Some modificatations to existing fire design codes are suggested based on the test results for the mechanical properties of the studied materials.

STUDIED STEEL MATERIALS

S350GD+Z

The studied material was cold-rolled hot dip zinc coated structural steel S350GD+Z (Z35) manufactured by Rautaruukki Oyj. Test pieces were cut out from a cold-formed steel sheet with nominal thickness of 2mm, longitudinally to rolling direction. Steel material is in accordance with requirements of the European standard SFS-EN 10 147.

S355

The steel grade used in this part of the research was hot-rolled structural steel S355 manufactured by Rautaruukki Oyj. Test pieces were cut out from a cold-rolled steel sheet with nominal thickness of 4mm, longitudinally to rolling direction. Structural steel material is in accordance with the requirements of the European standard SFS-EN 10 025 (1993) for structural steel grade S355.

S460M

The tests for structural high-strength steel S460M were carried out using test specimen that were made from 20mm thick steel plate. The pieces were cut out longitudinally to rolling direction. The material fills the requirements given in standard SFS-EN 10113 for structural steel S460M.

S355J2H

The tensile tests for structural steel S355J2H were carried out using test specimens that were cut out from SHS-tubes 50x50x3, 80x80x3 and 100x100x3 longitudinally from the middle of the face opposite to the welded seam. The material is in accordance with the requirements given in standard SFS-EN 10219-1.

TESTING FACILITIES

Test pieces

The tensile test specimens were in accordance with the standard EN 10 002-5 (1992). Strain was measured from the middle of the test piece. The gauge length was 25mm.

The test pieces for base materials were cut out from virgin steel plates. The nominal plate thickness for S350GD+Z was 2 mm , for S355 (base material) it was 3 mm, for high-strength steel S460 it was 20 mm and for the square hollow sections (structural steel S355J2H) the thickness was 3mm.The test pieces were cut out longitudinally to rolling direction.

The test pieces for cold-formed structural steel S355J2H were cut out longitudinally from the middle face opposite to the weld seam of square hollow sections 50x50x3, 80x80x3 and 100x100x3.

Testing device

The tensile testing machine used in the tests is verified in accordance with the standard EN 10 002-2 (1992). The extensometer is in accordance with the standard EN 10 002-4 (1992). The oven in which the test specimen is situated during the tests was heated by using three separately controlled resistor elements. The air temperature in the oven was measured with three separate temperature-detecting elements. The steel temperature was measured accurately from the test specimen using temperature-detecting element that was fastened to the specimen during the heating.

Test methods

Transient-state test method

In transient-state tests, the test specimen was under a constant load and under a constant temperature rise. Temperature and strain were measured during the test. As a result, a temperature-strain curve was recorded during the test. Thermal elongation was subtracted from the total strain. The transient-state test method gives quite a realistic basis for predicting the material's behaviour under fire conditions. The transient-state tests were conducted with two identical tests at different stress levels. Heating rate in the transient state tests was 20°C min^{-1}. Temperature was measured accurately from the test specimen during the heating.

Steady-state test method

In the steady-state tests, the test specimen was heated up to a specific temperature. After that a tensile test was carried out. In the steady state tests, stress and strain values were first recorded and from the stress-strain curves the mechanical material properties could be determined. The steady state tests can be carried out either as strain- or as load-controlled. In

269

the strain-controlled tests, the strain rate is kept constant and in the load-controlled tests the loading rate is kept constant.

MECHANICAL PROPERTIES AT ELEVATED TEMPERATURES

Structural sheet steel S350GD+Z

The behaviour of structural steel S350GD+Z at elevated temperatures was studied with 30 high-temperature tests. The test results were combined with an earlier test series that was carried out in the same laboratory. The aim was to add the test results of the mechanical properties at temperatures from 700°C to 950°C to the earlier test results. On the basis of these test results a suggestion concerning the mechanical properties of the studied material was made to a Finnish norm concerning the material models used in structural fire design of unprotected steel members. The suggested reduction factors for modulus of elasticity and yield strength are illustrated in Table 1.

TABLE 1
REDUCTION FACTORS FOR ELASTICITY MODULUS AND YIELD STRENGTH OF STRUCTURAL SHEET
STEEL S350GD+Z AT TEMPERATURES 20°C-1000°C

Steel temperature [°C]	$E_{a,\theta} / E_a$ EC 3:Part 1.2	$E_{a,\theta} / E_a$ Proposal	$f_{y,\theta} / f_y$ EC 3:Part 1.2	$f_{y,\theta} / f_y$ Proposal
20	1.0000	1.0000	1.0000	1.000
100	1.0000	1.0000	1.0000	0.970
200	0.9000	0.9000	1.0000	0.932
300	0.8000	0.8000	1.0000	0.895
400	0.7000	0.7000	1.0000	0.857
500	0.6000	0.6000	0.7800	0.619
600	0.3100	0.3100	0.4700	0.381
700	0.1300	0.1300	0.2300	0.143
800	0.0900	0.0900	0.1100	0.105
900	0.0675	0.0675	0.0600	0.067
1000	0.0450	0.0450	0.0400	0.029

The mechanical properties were determined from both transient and steady state test results. In Figures 1 and 2 the measured yield strength and modulus of elasticity are compared with yield strength given in different design codes.

270
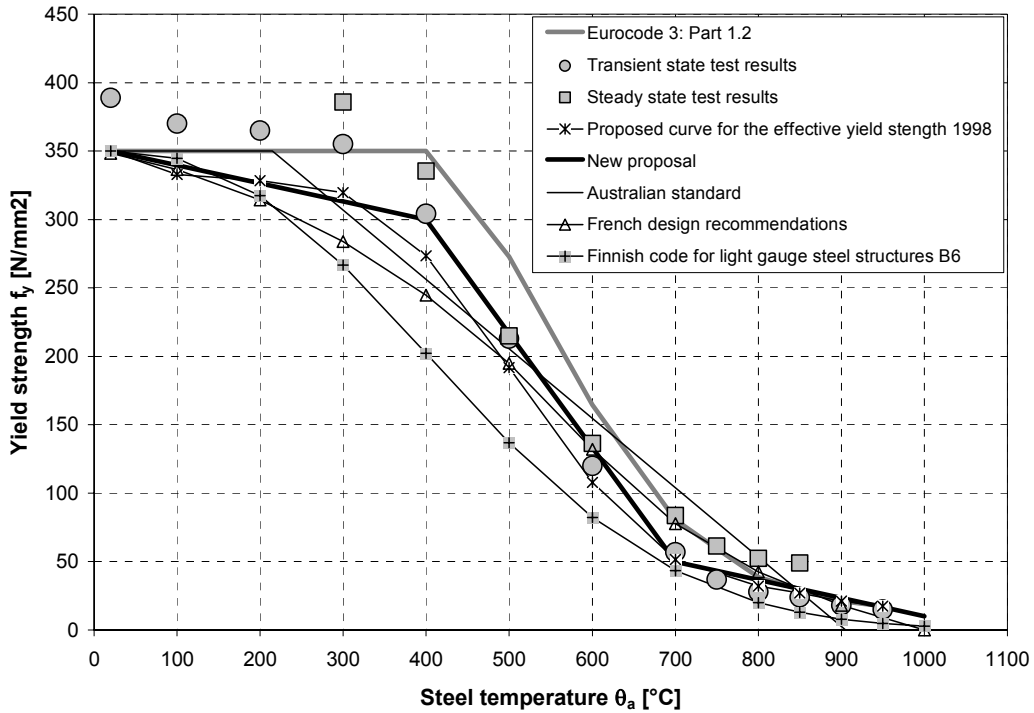
Figure 1:Yield strength of structural steel S350GD+Z determined from test results compared with yield strength given in different design codes.
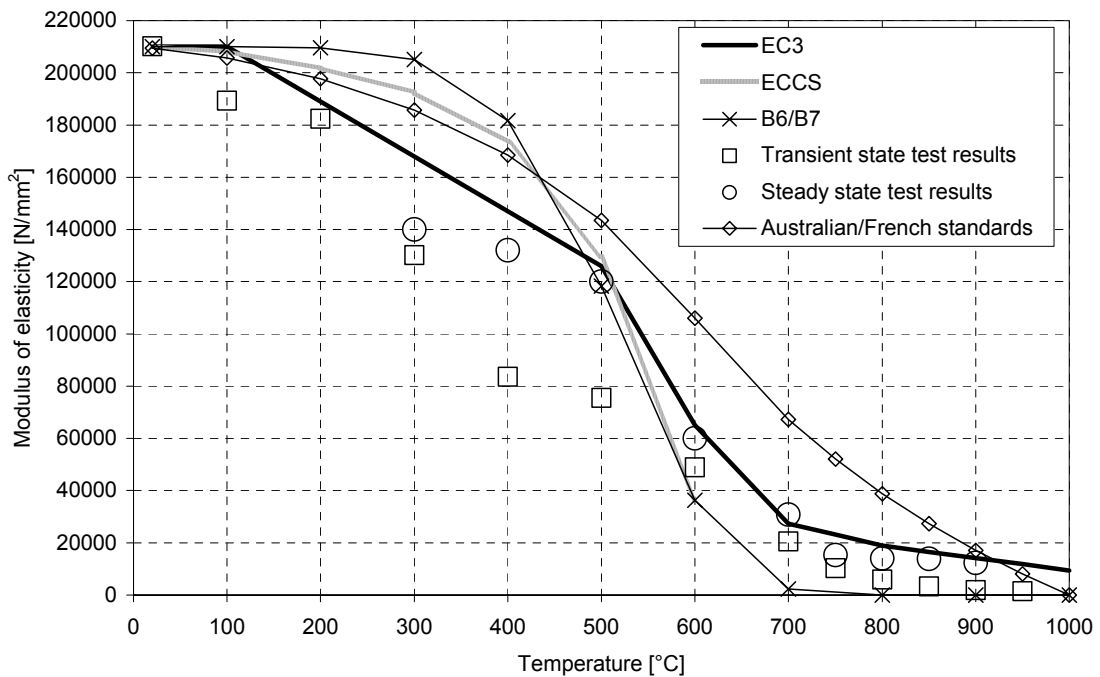
Figure 2: Modulus of elasticity of structural steel S350GD+Z determined from test results compared with yield strength given in different design codes. Structural steel S355

The high-temperature behaviour of structural steel S355 at elevated temperatures was studied with 30 tensile tests. The test results were combined with an earlier test series that was carried out in the same laboratory. The mechanical properties of sructural steel S355 determined from the transient state tests are illustrated in Table 2.

TABLE 2

MECHANICAL PROPERTIE S OF STRUCTURAL STEEL S355 AT TEMPERATURES 20°C - 950°C

Temperature [°C]	Modulus of elasticity [N/mm2]		Yield strength f_y [N/mm2]	
	EC3: part 1.2	Test results	EC3: part 1.2	Test results
20	210000	210600	355	406
100	210000	200070	355	375
200	189000	197964	355	375
300	168000	170586	355	365
400	147000	128466	355	360
500	126000	98982	276.9	300
600	65100	61074	166.85	190
700	27300	42120	81.65	95
750	23100	18900	60.35	58
800	18900	10500	39.05	44
850	16537.5	5250	30.175	32
900	14175	4200	21.3	22
950	11812.5	3780	17.75	20
1000	9450		14.2	

The tested thermal elongation of structural steel S355 is compared in the next figure with thermal elongation given in Eurocode 3 (EC39. The test results seem to be very near the EC3 values.
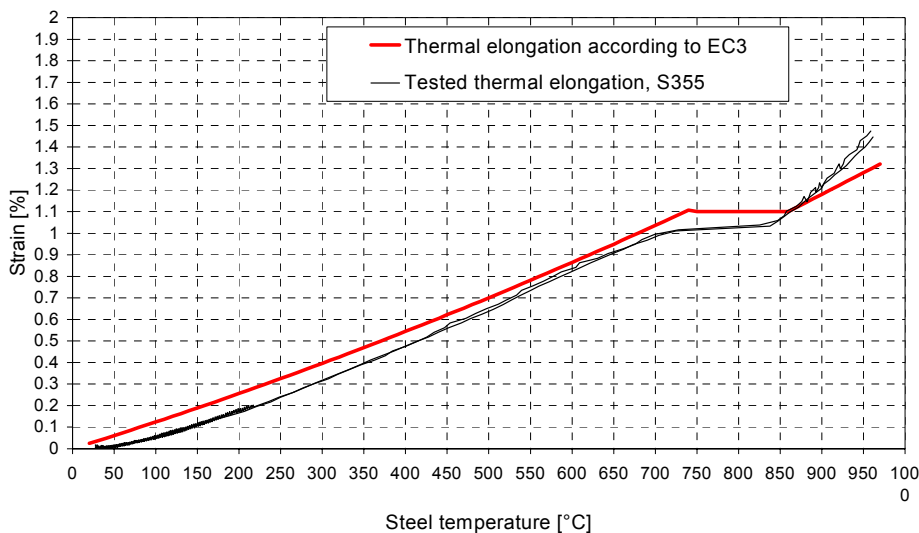
Figure 3: Thermal elongation of structural steel S355 at temperatures 20°C - 950°C

The behaviour of modulus of elasticity and yield strength at elevated temperatures is illustrated in Figures 4 and 5.
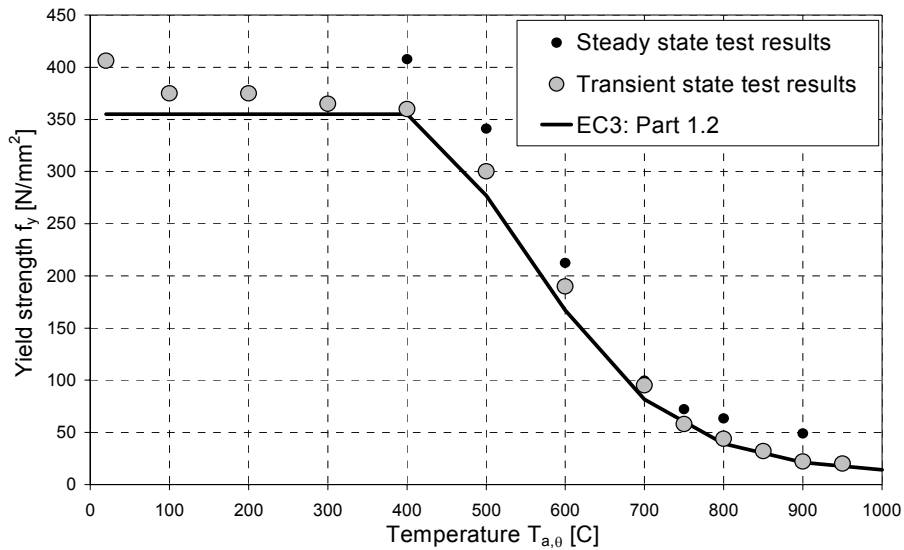
Figure 4: Yield strength of structural steel S355 at temperatures 20°C - 950°C
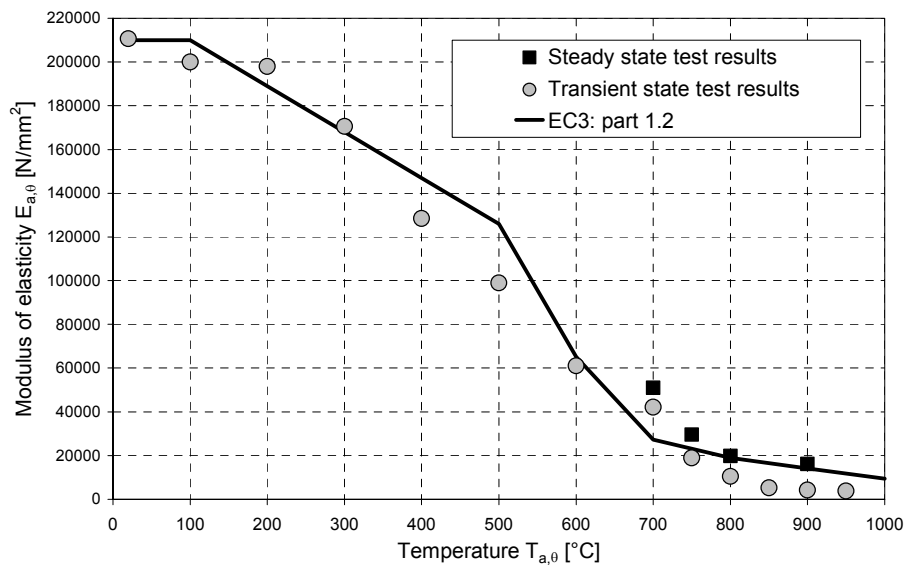
Figure 5: Modulus of elasticity of structural steel S355 at temperatures 20°C - 950°C

The effect of heating rate which also affects the strain rate during tests was studied by carrying out transient state tests at a low stress level. Three different heating rates were used varying from 10°C/min to 30°C/min. The test results within these temperature rates for structural steel did not differ much from each other. In Figure 6 the test results are illustrated as temperature-time curves.
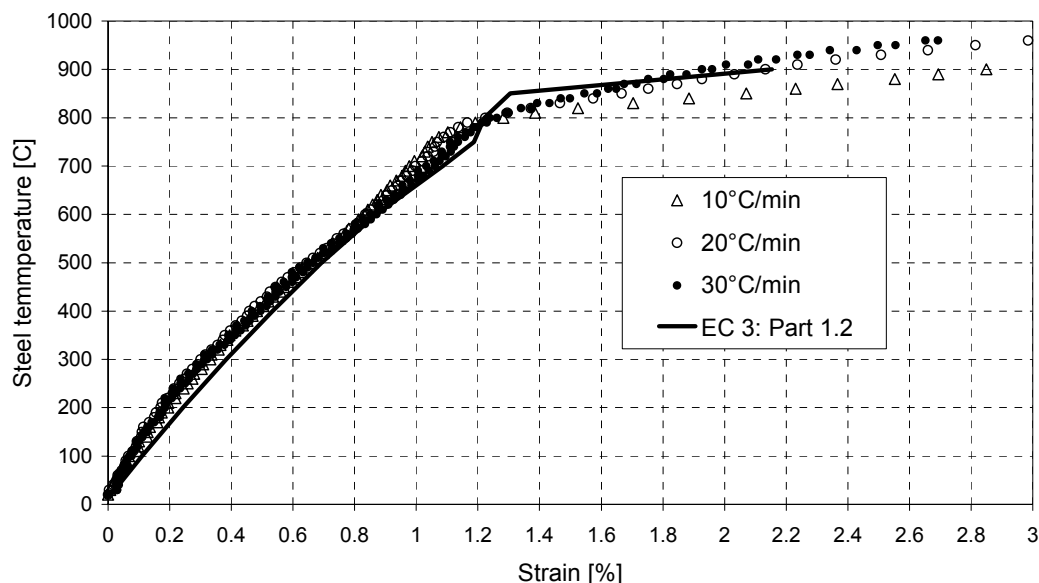
Figure 6: Transient state test results at stress level 20N/mm2 for structural steel S355 with heating rates 10-30°C/min.

The behaviour of structural steel S355 analyzed on the basis of transient state test results seem to be very near the material model given in Eurocode 3: Part 1.2. It can be concluded that within the limits that are given for that model in Eurocode 3 (EC3), the use of it for structural steel S355 is well-grounded in structural fire design of steel structures.

Structural steel S460M

The tests for structural high-strength steel S460M were carried out using test specimen that were made from 20mm thick steel plate. The pieces were cut out longitudinally to rolling direction. The material fills the requirements given in standard SFS-EN 10113 for structural steel S460M. The test pieces were in accordance with the testing standard SFS-EN 10002-5.

A series with 60 test specimen was carried out to study the behaviour of the mechanical properties of structural high-strength steel at elevated temperatures. The tests were carried out using transient state test method. Some steady state tests were also made at temperatures 700°C - 900°C.

The mechanical properties were determined from the stress-strain curves that were converted from the transient state test results.

The yield strength determined on the basis of the test results seems to differ significantly from the Eurocode 3 values at temperatures up until 500°C. At higher temperatures the behaviour follows quite well the Eurocode 3 values.

The experimentally determined modulus of elasticity follows the EC3 values at temperatures up until 500°C. At higher temperatures there is a notable difference between the test results and EC3. The reduction factors for the modulus of elasticity and yield strength are illustrated in Figures 7 and 8.
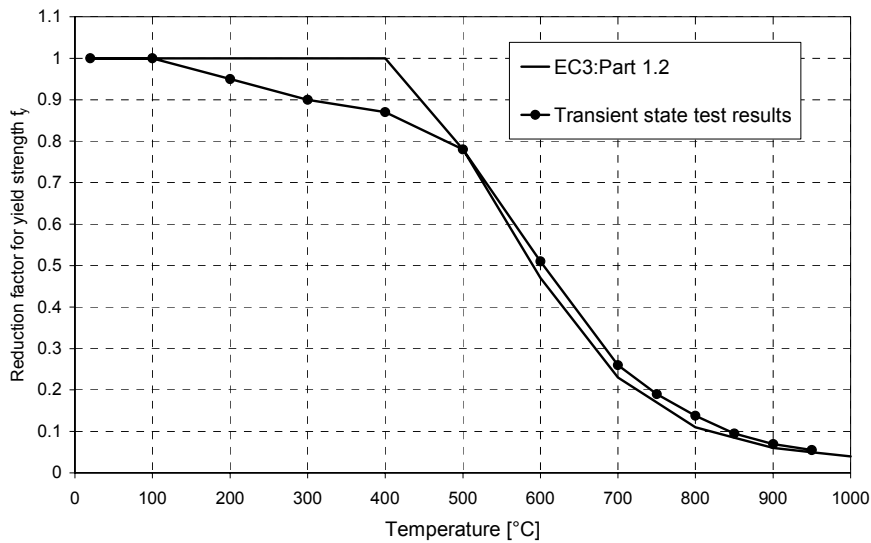
Figure 7: The behaviour of yield strength of structural steel S460M at high temperatures
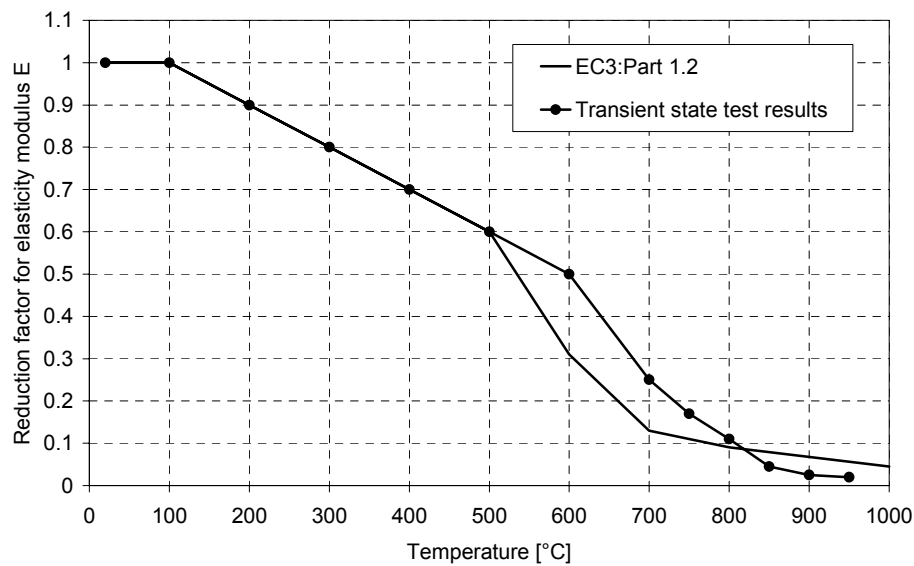
Figure 8: The behaviour of modulus of elasticity of structural steel S460M at high temperatures

The strain rate in the transient state tests before yielding is about 0.004 - 0.001 min^{-1}. In the high-temperature testing standard SFS-EN 10002-5 the strain rate limit is set to $0.003min^{-1}$. Some steady state tests were carried out to check the effect of the strain rate to test results. In figure 12 it can clearly be seen that the test results from tests with a high strain rate are significantly higher than the test results determined according the European standard. The strain rate in these tests varies between 0.006..0.01 min^{-1} in the elastic range. The test results are illustrated in Figures 9-11.
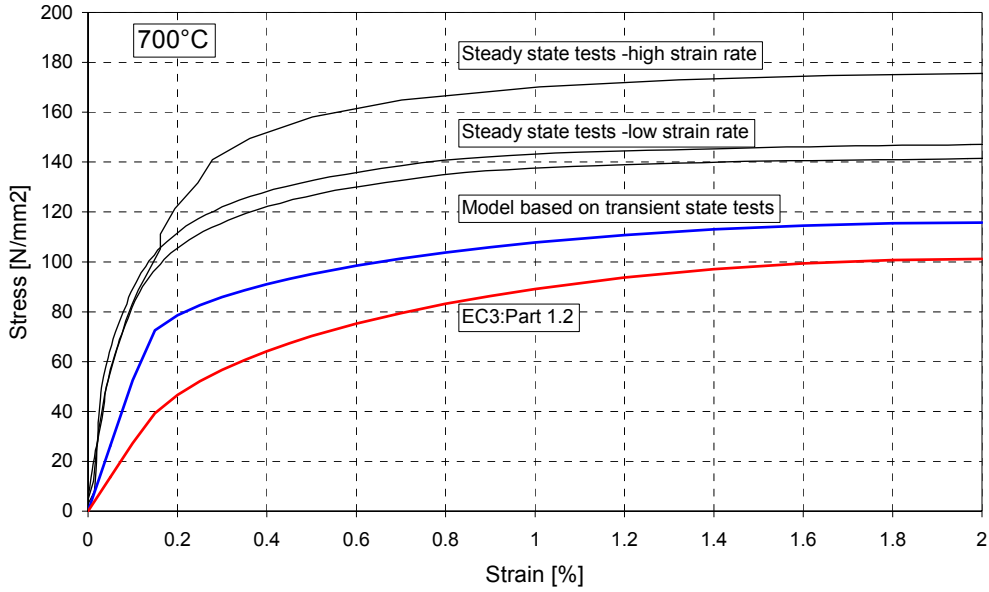
Figure 9: Steady state test results of structural steel S460M at temperature 700°C compared with the transient state tests and Eurocode 3: Part 1.2
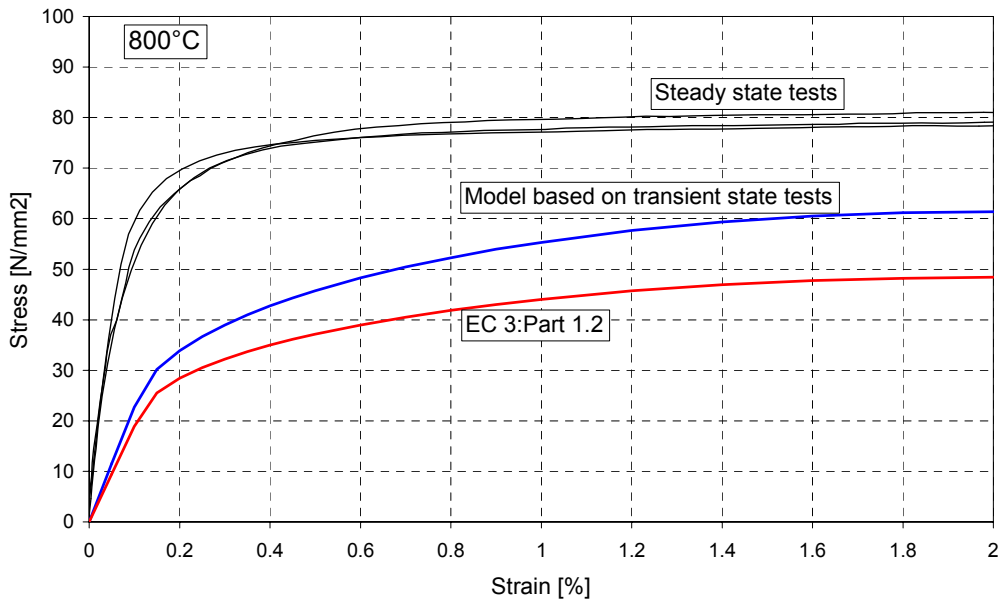
Figure 10: Steady state test results of structural steel S460M at temperature 800°C compared with the transient state tests and Eurocode 3: Part 1.2
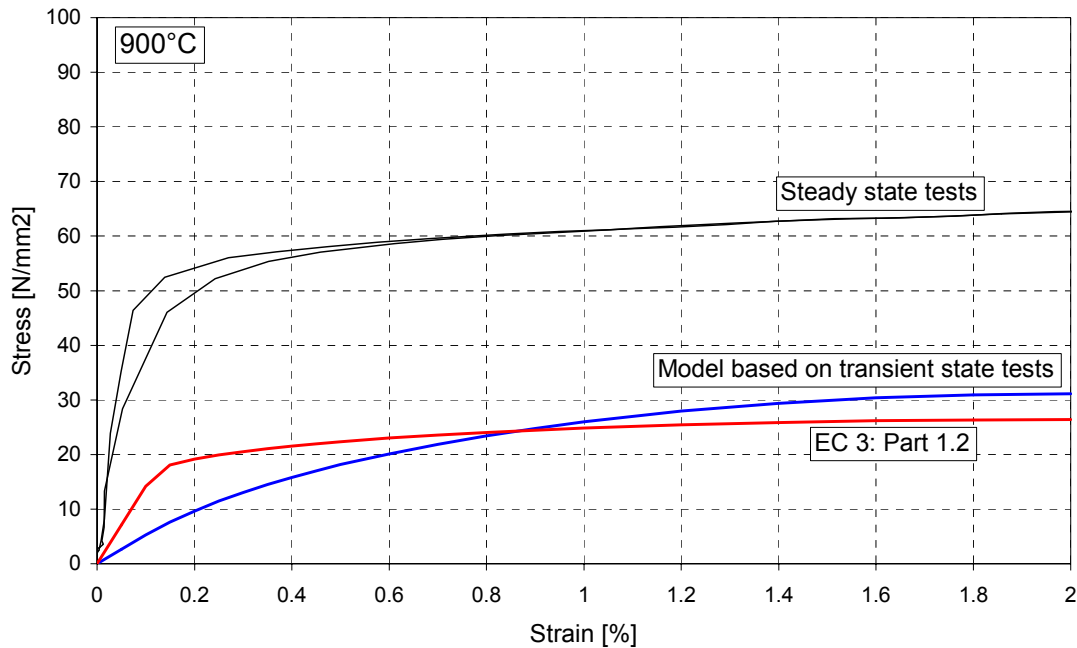
Figure 11: Steady state test results of structural steel S460M at temperature 900°C compared with the transient state tests and Eurocode 3: Part 1.2

Structural steel S355J2H

Most of the transient state tests for this material have been carried out for the material taken from SHS 50x50x3. A few tests have also been performed to the materials taken from SHS 80x80x3 and SHS 100x100x3. The heating rate in the tests was 20°C/minute. Some tests were also carried out with 10°C/minute and 30°C/minute.

The transient state tests have so far been carried out with stress levels 5…460N/mm^2 for the material taken from SHS 50x50x3. Two tests have also been performed for the material taken from SHS 80x80x3 and for SHS 100x100x3 at stress level 100N/mm^2.

The test results have been fitted into the EC3: Part 1.2 material model using the calculation parameters determined from the transient state tests. The modified stress-strain curves are presented in the next Figures 12 and 13.
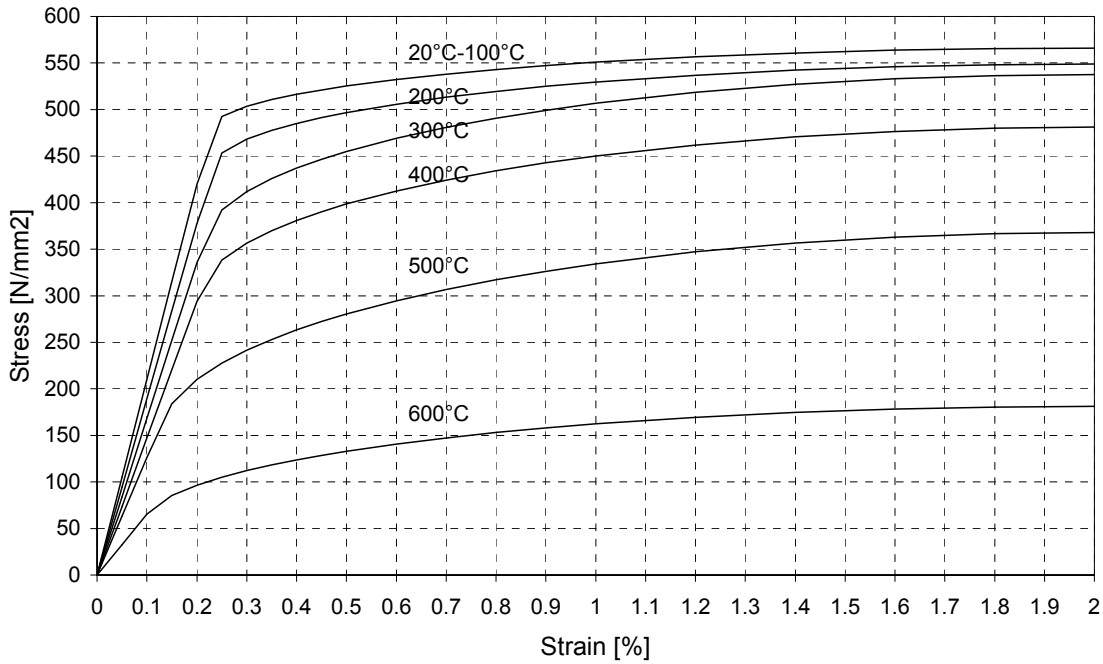
Figure 12: Stress-strain curves of structural steel S355J2H at temperatures 20°C - 600°C. Test pieces taken from SHS 50x50x3.
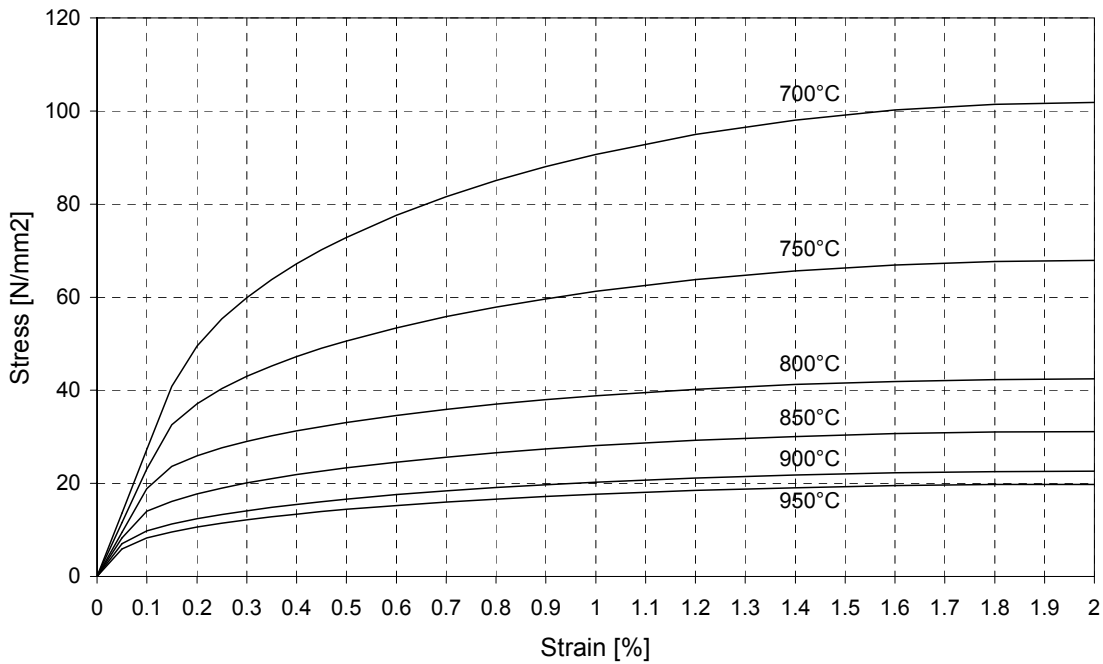
Figure 13: Stress-strain curves of structural steel S355J2H at temperatures 700°C - 950°C. Test pieces taken from SHS 50x50x3.

278

The test results for yield strength f_y, $R_{p0.2}$ and $R_{t0.5}$ determined from the transient state tests are compared with EC3 material model in the next figure.
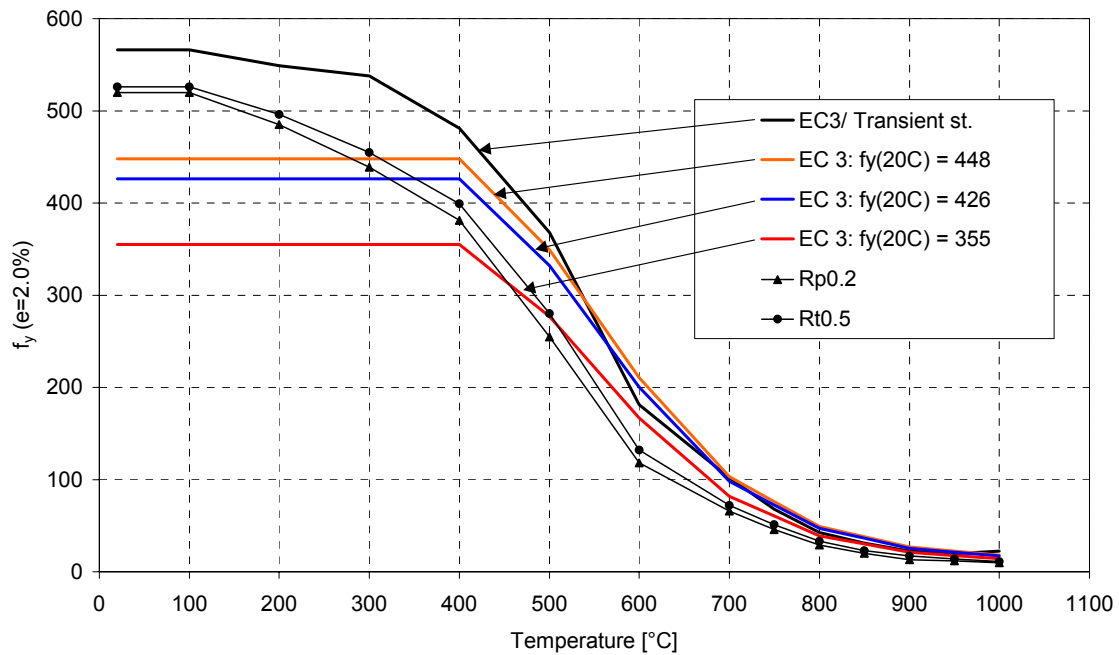
Figure 14: Yield strength of structural steel S355J2H at temperatures 20°C - 950°C (Test pieces taken from SHS 50x50x3)

TABLE 3
MECHANICAL PROPERTIES OF STRUCTURAL STEEL S355J2H AT ELEVATED TEMPERATURES
TEST PIECES TAKEN FROM SHS 50x50x3

Temperature	Modulus of Elasticity E	Proportional limit f_p	Yield strength f_y	Yield strength $R_{p0.2}$	Yield strength $R_{t0.5}$
20	210000	481.1	566	520	526
100	210000	481.1	566	520	526
200	189000	441.48	549.02	485	496
300	168000	367.9	537.7	439	455
400	147000	311.3	481.1	381	399
500	126000	169.8	367.9	255	280
600	65100	67.92	181.12	118	132
700	27300	39.62	101.88	66	72
750	23100	28.3	67.92	46	51
800	18900	19.81	42.45	29	33
850	16537.5	11.32	31.13	20	23
900	14175	6.792	22.64	13	17
950	11812.5	5.66	19.81	12	14
1000	9450	14.15	22.64	10	11

Transient state tests at stress level 100N/mm2 were carried out with three different heating rates; 10°C, 20°C and 30°C/min. The test results fom these tests are illustrated in the next figure.

279
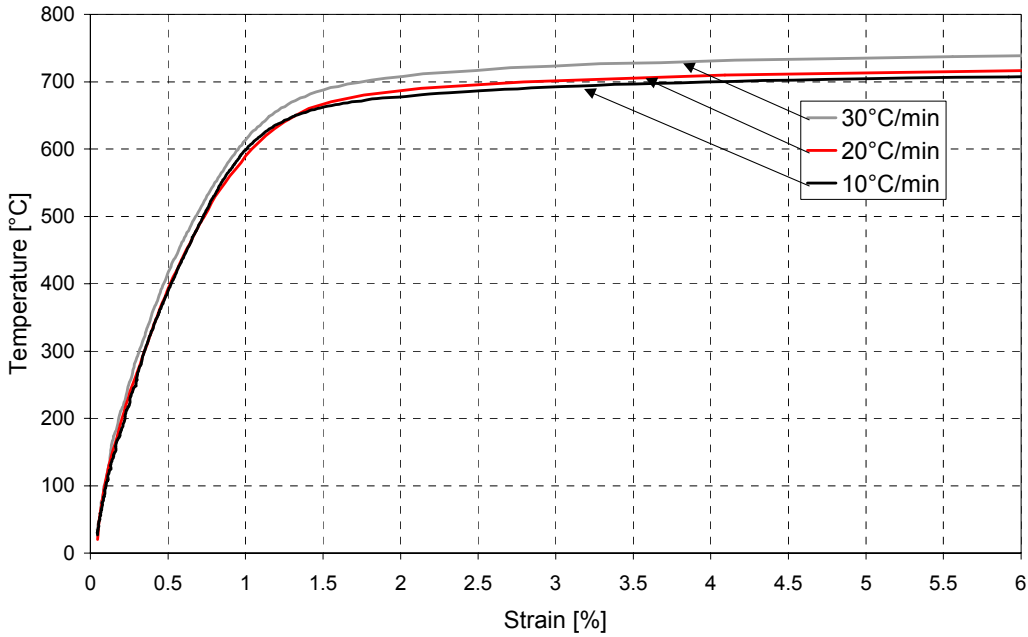
Figure 15: Temperature-strain curves of structural steel S355J2H at stress level 100N/mm^2 with heating rates 10°C, 20°C and 30°C/min. Test pieces taken from SHS 50x50x3.
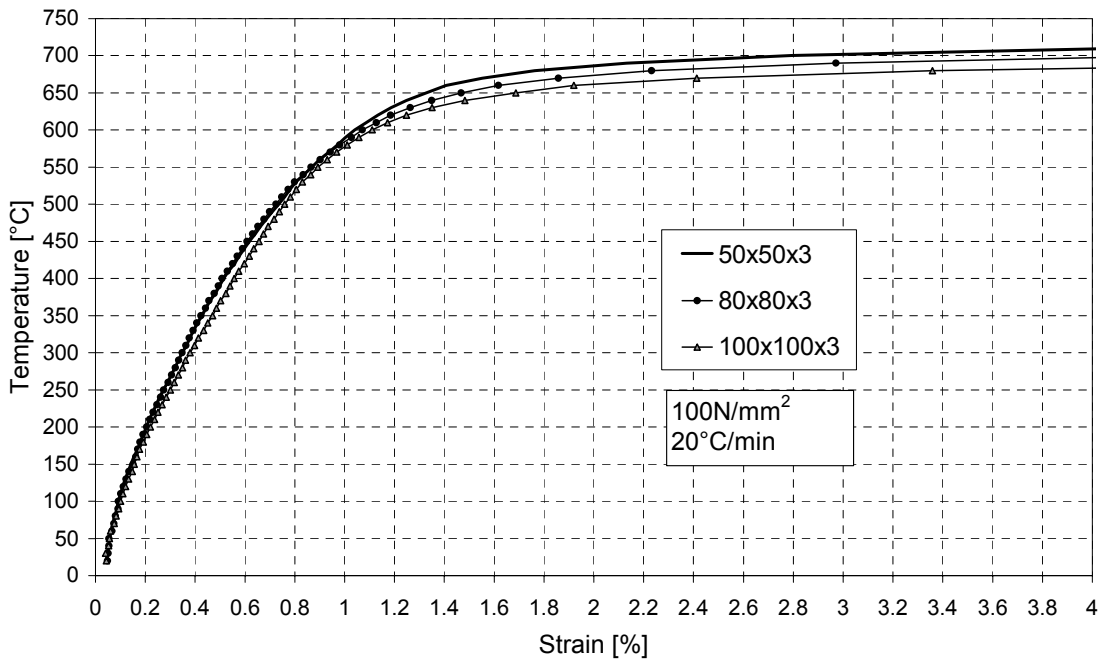
Figure 16: Temperature-strain curves of structural steel S355J2H at stress level 100N/mm^2. Test pieces taken from SHS 50x50x3, 80x80x3 and 100x100x3.

CONCLUSIONS

An overview of the test results for structural steels S350, S355, S460 and S355J2H is given in this paper. It has to be noted that the test results are going to checked and analyzed moro thoroughly by the end of his project. Also more tests are going to be carried out.

The test results show clear differences in the behaviour of these steel grades at elevated temperatures. For structural sheet steel S350GD+Z a new proposal for the behaviour of the yield strength was given. For structural steel grades S355 and S460 the material model given in EC3 seems to be quite good.

The behaviour of the mechanical properties of cold-formed steel seemed to be very promising. The increase of strength due to cold-forming seemed to remain quite well at elevated temperatures. This should naturally be taken into account when estimating the behaviour of cold-formed steel structures. More tests concerning the strength of the studied material after heating and the high-temperature behaviour of the corner parts of the square hollow sections are going to be carried out.

ACKNOWLEDGEMENTS

REFERENCES

European Committee for Standardisation (CEN), Eurocode 3: Design of steel   structures, Part 1.2 : Structural fire design, Brussels 1993.

SFS-EN 10002-1*:* Metallic materials. Tensile testing. Parts 1-5

Standard SFS-EN 10 025: Hot-rolled products of non-alloy structural steel (in Finnish), Helsinki 1993.

Standard SFS-EN 10 113-3: Hot rolled products in weldable fine grade structural steels. Delivery conditions for thermomechanical rolled steels. (in Finnish), Helsinki 1993.

Standard SFS-EN 10 147: Continuously hot-dip zinc coated structural steel sheet and strip. Technical delivery conditions. (in Finnish), Helsinki 1992.

SFS-EN 10219-1 Cold formed welded structural hollow sections of non-alloy and fine grain steels. Parts 1-2: 1998.

Outinen J., Mechanical properties of structural steels at elevated temperatures, Licentiate Thesis, Helsinki University of Technology, Laboratory of Steel Structures, Espoo 1999.

A Survey of a System of Methods for Fire Safety Design of Traditional Concrete Constructions

K. D. Hertz : head of the Department of Buildings and Energy at the Technical University of Denmark, Lyngby.

ABSTRACT

During the years since 1978 the author has been developing a series of calculation methods and supporting test methods for the fire safety design of concrete constructions. The basic methods have been adopted in the fire chapters of the Eurocode ENV1992-1-2 and in the Danish code for concrete constructions DS411. And the bases for many of the methods have been distributed as CIB W14 reports. But a survey of all the methods in coherence has never been presented, and much of this documentation and the additional documentation produced for the work with the codes needs still to be printed in papers.

It is the aim of this paper to give a coherent presentation of the design methods, their degree of documentation and the available references in order to facilitate the application of them.

By means of the calculation methods load bearing capacity and deflections can be found of any concrete construction made of any traditional material composition at any time of any fire exposure.

It is the intention that the calculations for fire connects continuously with similar methods for ordinary cold design when the fire is varied towards no fire. It is also the intention that standard fires as well as fully developed fire courses can be applied, which means that the methods are prepared for the introduction of performance based design requirements.

It is finally the intention that the methods should be applicable for hand calculation, so that they can be adopted by codes, and so that the user has a chance to understand the background of them, and thereby be able to apply them correctly to the actual problem.

The methods are applicable for dry constructions made of traditional concrete, which means concrete not densified by means of ultra fine particles smaller than the cement grains such as silica fume. Dry means less than 3-4 weight pct. moisture which usually is found in constructions exposed to an indoor climate for more than 6 months. The reason for this limitation is the increased risk of spalling for the new dense concrete qualities and the lack of quantitative knowledge on these phenomena.

Keywords*: concrete constructions, fire, design, structural codes, beams, shear, columns, anchorage, deflections.*

MATERIAL PROPERTIES

Data and a profound understanding of the material properties of concrete and reinforcing steel at high temperatures and the corresponding residual properties after cooling are important for the derivation and for the use of design methods for fire exposed concrete constructions.
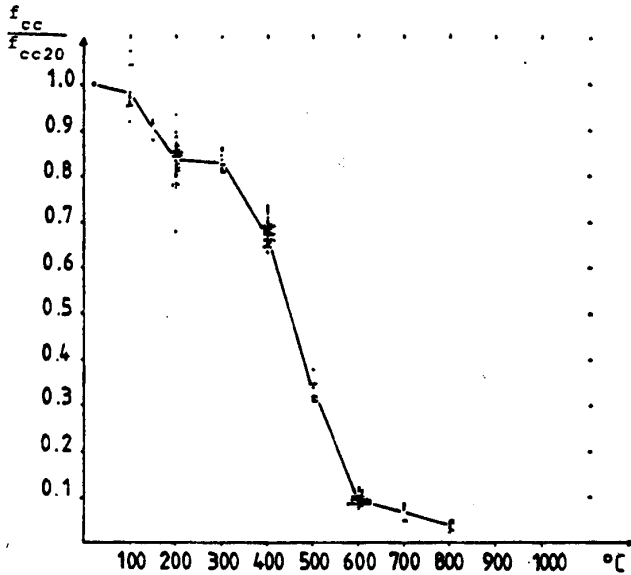
Residual compressive strength of concrete with Danish sea gravel, w/c = 0.87, f_{cc20}= 19.5 MPa. Hertz [2].
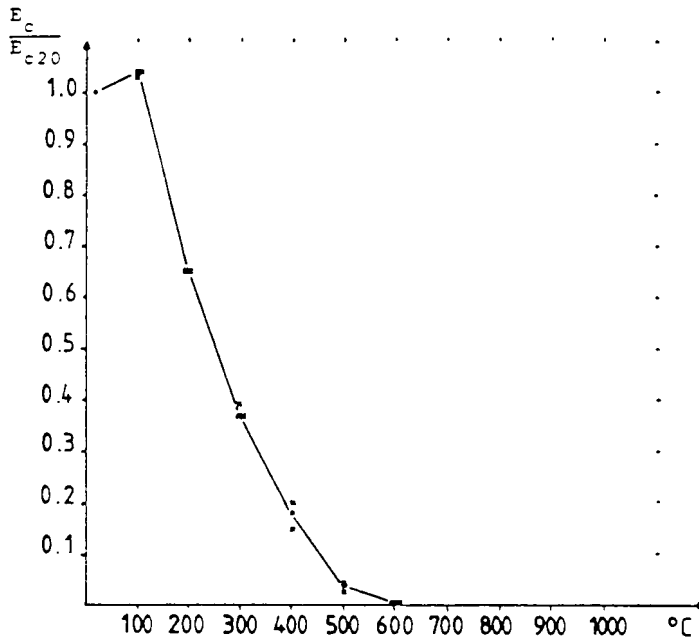
Residual modulus of elasticity of concrete with Danish sea gravel, w/c = 0.87, E_{c20}= 27.9 GPa. Hertz [2].

Strength and strains

At the late nineteen seventies, where the development of the present design methods began, a number of test series on compressive strength and E-modulus were known from the literature for various concretes. And especially the work on strain and transient strain properties made by Anderberg and Thelandersson [1] in Lund contributed to the knowledge of the behaviour of the materials.

In addition to that the author had to perform a substantial test program in order to establish a basis for the work. The literature study and the test series were reported in the Ph.D. thesis Hertz [2], [3] and [4].

Anchorage
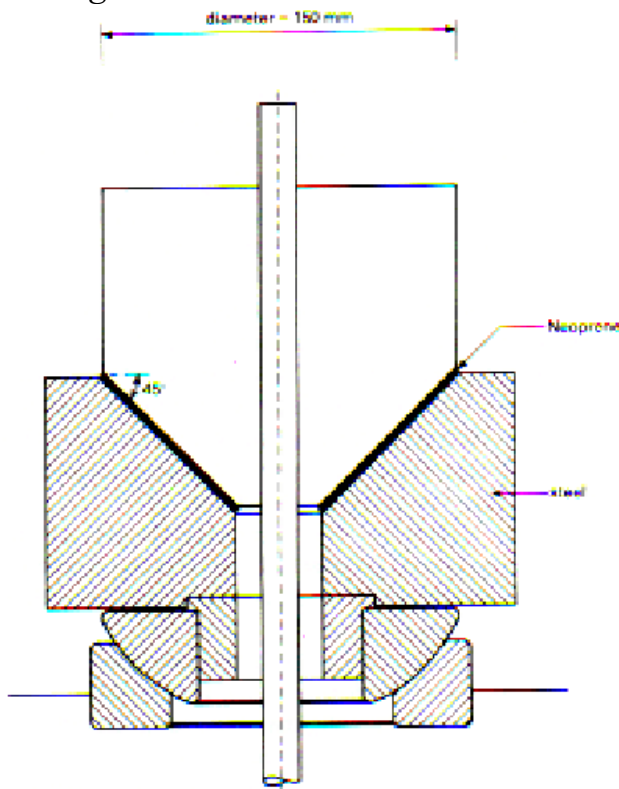
Bond strength test method.

During this work a new test method was developed for measuring the bond strength of reinforcing bars in concrete with or without fire exposure. And a complete method for estimating the anchorage capacity as the minimum of a bond capacity and a splitting capacity was developed and reported in Hertz [5].

A comprehensive test series confirmed that the measured value of the bond strength measured as a shear strength at the surface of the bar correspond to the theoretical value

$$\tau = 0.65 * f_{cc20}$$

where f_{cc20} is the concrete compressive cylinder strength at 20°C, and it is seen to be equal to

$$\tau = \cos\alpha * \sin\alpha * 1.30 * f_{cc20}$$
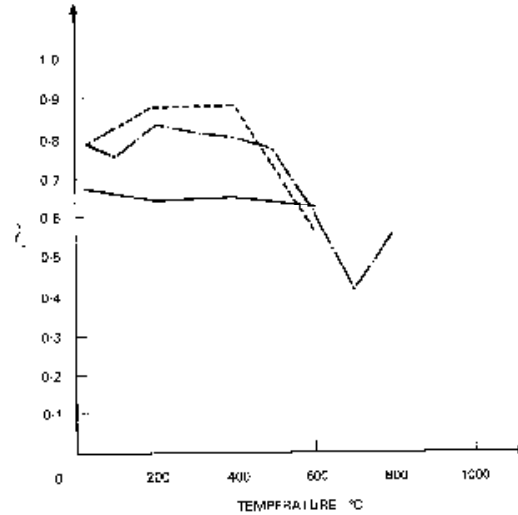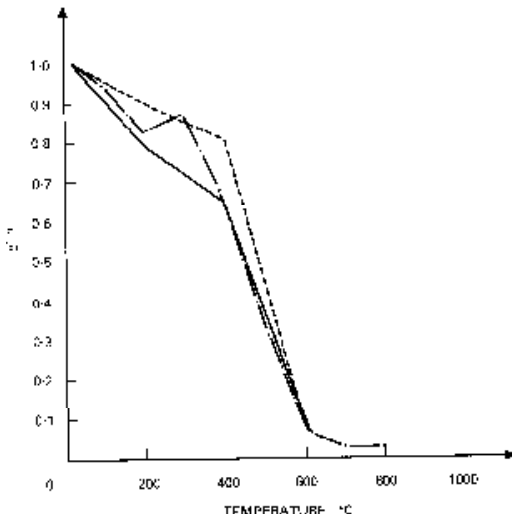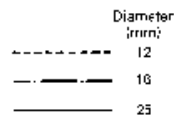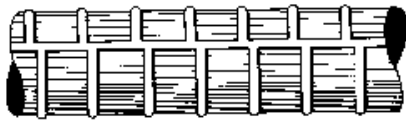
Variation of bond strength with temperature.   Variation of the relation between bond strength and compressive strength.

where α is the inclination of the compressive stresses related to the bar, which can be shown is 45° at the moment of failure, and $1.30*f_{cc20}$ is the compressive strength of the concrete with hindered transverse expansion.

By means of these new design methods the anchorage length has been reduced by a factor up to 10 compared to the code requirements in a large number of constructions designed by the author and by many other practising engineers.

Rapid heating

Further new test methods were developed in order to find the properties of concrete heated rapidly. The problem was that concrete specimens must have a certain size such as diameters of 100 mm, but this lead to a limit for the heating rate, which can be applied, to 1-2°C per minute. And this heating rate is not representative for concrete within 50 mm from a fire-exposed surface or in a slender construction. The Author therefore developed methods using microwave power to heat the specimens Hertz [6]. Testings at a heating rate of 10°C per minute showed less strength reductions for maximum temperatures between 200 and 500°C and larger reductions between 500 and 700°C compared to values for slow heated concretes. This means that in stead of the well-known S-shaped curve for the reduction a straight line was the result.

286

Spalling

The first good explanation of the phenomenon of explosive spalling was given by Harmathy and Berndt [7] mainly as a steam explosion of wet traditional concrete.

The author was the first to discover that high strength concrete has a much higher risk of spalling than traditional concretes Hertz [8]. Since then a number of tests have been made in order to investigate the phenomenon and especially the fires in the Great Belt tunnel and in the Channel tunnel have set focus on this reason for damage.

For a closer discussion of these phenomena see Hertz [9], where an argumentation for safe limits for the problem is made as covering indoor constructions (with a moisture content of less than 3 % by weight) and not densified by small particles like silica fume.

For the time being a new material test method is developed at the authors lab indicating which concretes will suffer from spalling. In connection with this work it has been concluded that hindered thermal expansion is a precondition for spalling of a number of concretes. And this may explain some of the randomness, which have seemed to be in the results of the tests performed.

Hopefully we will now be able to divide concretes into two groups: those, which are free of spalling and those, which may spall if the necessary stress conditions are met.

As the first aid of design it will be safe to use the non-spalling materials, where further documentation must be required for the particular applications of the materials which are deemed to be prone to spalling. And since we are not at present able to provide such further reliable documentation, we must stop using these materials until we can provide it, unless full scale test procedures are developed, where the moisture profiles and the hindered thermal expansions are modelled correctly.

REDUCED CROSS SECTIONS

The first presentation of the reduced cross section was an answer to a question raised by the censor Ove Pettersson at the defence of the Ph.D. thesis December 1980. The principle is to establish a cross section with the same average compressive strength or E-modulus as expected in the fire-exposed construction by means of removing a damaged zone and reducing the strength and E-modulus of the residual part equal to the reduction at the centre of such a section. (In order to be precise, the reduced zone and the properties at the centre are defined as equal to those for a two-sided exposed wall of a thickness equal to the smallest dimension of the cross section) Hertz [10], [11].
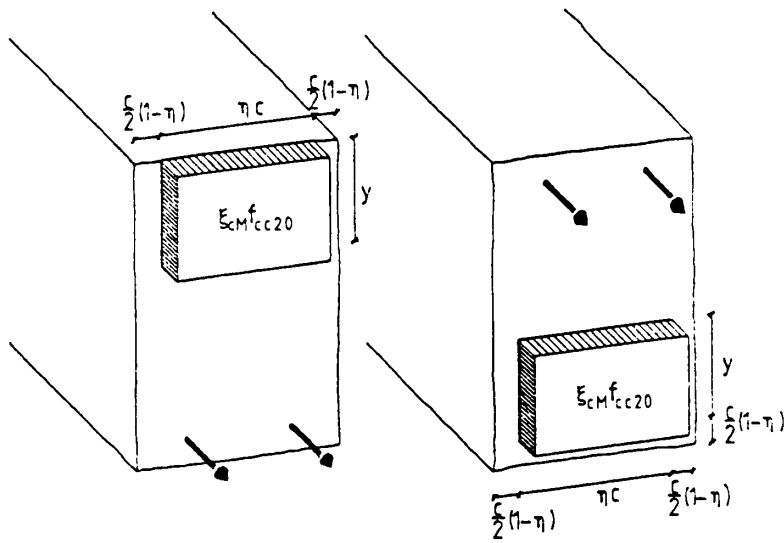
Positions of concentrated stress blocks within reduced cross sections.

Later the design methods were extended also to comprise calculation of deflections of constructions with slack and prestressed reinforcement and analyses of cracked cross sections using curved lined stress strain curves Hertz [12].

The report [12] presents several simplified calculation methods and compare these to results of full-scale tests reported in the literature. For columns, 4 full-scale tests are included. These and a description of the derivation of the methods are later included in the Eurocode [13] and in a supporting document for it Hertz [14]. During the work with the Eurocode from 1991 to 1993 the project team CEN/TC250/SC2/PT10 held 6 meetings and the simplified calculation methods were discussed and related to other methods. In between the meetings there was a closer corporation with Professor Dotreppe (Université de Liége) on material properties, with Mr. Gerritse (Stichting CUR) on temperature calculations, with Professor Tattoni (Dipart. di Ingegneria Strutt. Milano) on general aspects of calculations including deflections, with dr. Richter (TU Braunschweig) on transient materials data and full scale tests etc. and especially with Mr. Whittle (Ove Arup and Partners) on the reduced cross sections. Dr. Litzner (Deutscher Beton-Verein), chairman of SC2, participated in all the meetings and made very qualified contributions to the formulation of the methods. The fire chapter of the Eurocode [13] and the background document containing Hertz [14] was presented at a meeting in SC2 in Berlin January 1994, where the chapter was accepted for the ENV by voting.

The methods allows the concrete quality to vary, so that the considerable effect of the local aggregates can be taken into account, and so that the designer can choose to improve the fire resistance of his concrete by changing its composition.

The methods also allow calculations at any time of any fire exposure, and are thus not restricted to be used at a fixed time of a standard fire exposure. Therefore the methods can utilise the fully developed fire courses which are now included in the action code of CEN and in many national codes such as the Danish, and the methods are thereby prepared for the introduction of performance based requirements.

These were the main reasons why the methods were adopted in the Eurocode.

288

Lately a project team dealing with the revision of the Danish code of Practise [15] has discussed the technical content of the methods. During this work column calculations have become of a special importance, because the column examples of the Danish Building Regulations have been corrected and thereby their field of application became more restricted. Therefore the number of column calculations compared to full scale tests has been extended by 4 and later by 45 column tests in order to show the validity of the column calculation method Hertz [16].

The reduced cross section for a fire exposed column is derived to model the reduced flexural and axial stiffness of a cross section. This already represents some evidence for its applicability.

In order to extend this evidence results of full-scale tests have been compared to the results of the method.

As mentioned 50 tests have been recalculated representing variations in column length, cross section dimensions, reinforcement, concrete quality, axial load and eccentricity of load and of fire exposure.

The results are shown in the figure below.

45 of the tests are reported in Hass [17]. (Two column tests have been neglected because the test results were very deviating from the test results of columns with almost the same properties and load, and obviously some test error must have occurred). 2 columns are from Lie et.al. [18]. 2 tests are from Seekamp et.al. [19]. 1 three sided exposed column is from Anderberg and Forsén [20].

The first 45 columns are all calculated by the same spreadsheet and thus are results of the same algorithm.

The other 5 tests have been calculated by hand using the same basics formulas.

Generally the calculation results for the 50 columns are on the safe side compared to test results, and a reasonable agreement is observed. It must therefore be concluded that the calculation method is suitable for design purpose.

> Average fire resistance at test in minutes 80
> Average deviation in minutes 6,9
> Standard deviation in minutes 11,7
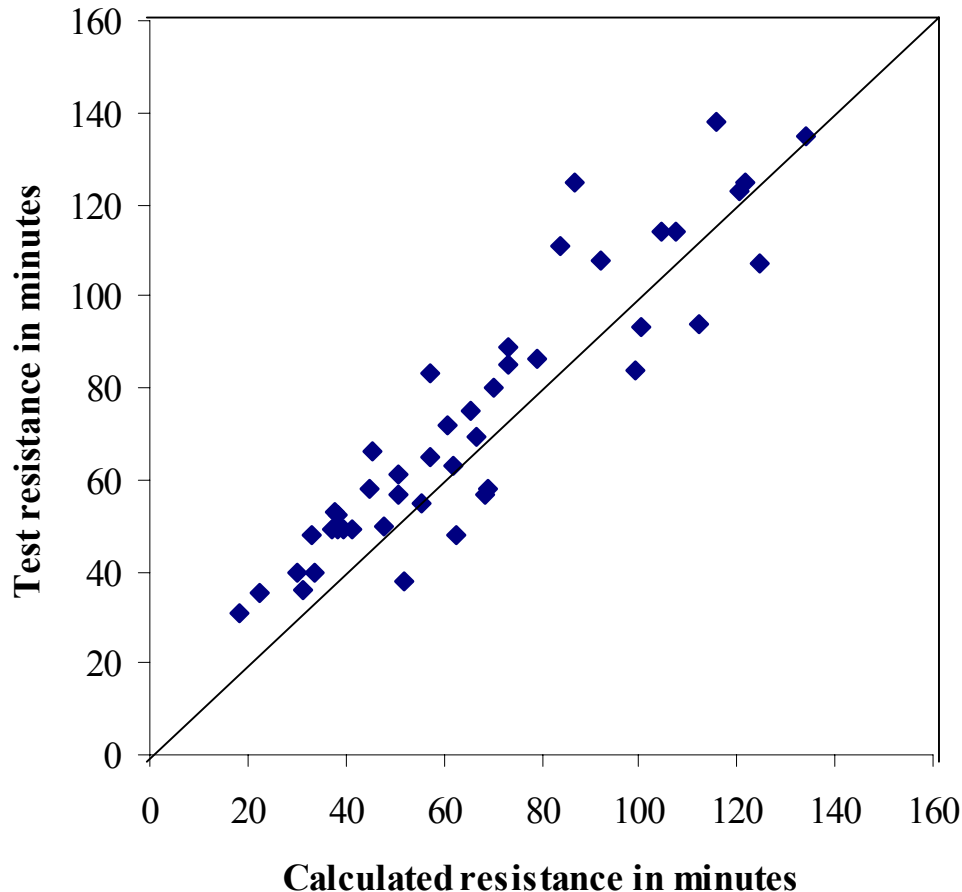
Comparison between calculations and 50 full-scale tests of concrete columns.

CONCLUSION

By means of the methods presented in this paper and in the papers and reports referred to it will be possible to estimate the load bearing capacity of about 95 % of the traditional concrete constructions in practice. The methods can not only be applied to estimate a standard fire resistance of constructions made of one single concrete quality, but can be applied for any time of any fully developed fire exposure as well, and they allow the designer to take the properties of the actual concrete into account.

The methods are therefore prepared for a performance based fire safety design of buildings, and because all calculations in principle can be made by hand they are suitable for use by a wide range of engineers and for adoption in the structural codes.

Further the methods are coherent with methods applicable for ordinary cold design of the same constructions, so that they fit smoothly with a cold design, if the fire is varied towards no fire.

It is a precondition for the application of the calculation methods that spalling will not occur, which at present can be ensured only by excluding some of the newest dense concrete qualities.

In case these new undocumented materials should be used for construction, full scale tests with the right border conditions with respect to moisture profiles and hindered thermal expansion seems to be the only alternative, and such tests have not been made so far.

REFERENCES

[1]   Anderberg, Y. Thelandersson, S.: Stress and deformation characteristics of concrete at high temperatures. 2. Experimental Investigation and Material Behaviour Model. Bulletin 54, Lund Institute of Technology. Lund 1976.

[2]   Hertz, K.D.: Betonkonstruktioners brandtekniske egenskaber. (Properties of Fire Exposed Concrete Structures) Part 1 and 2 of Ph.D. Thesis. Report No. 140. Institute of Building Design, 210p in Danish. Technical University of Denmark. Lyngby July 1980.

[3]   Hertz, K.D.: Armeringsståls forankring ved høje temperaturer. (Anchorage of Reinforcing Steel at High temperatures) Part 3 of Ph.D. Thesis. Report No. 138. Institute of Building Design, 103p in Danish. Technical University of Denmark. Lyngby July 1980.

[4]   Hertz, K.D.: Reference List on Concrete Constructions Exposed to High Temperatures. Part of Ph.D. Thesis. Report No. 141. Institute of Building Design, 63p. Technical University of Denmark. Lyngby July 1980.

[5]   Hertz, K.D.: The Anchorage Capacity of Reinforcing Bars at Normal and High Temperatures. Magazine of Concrete Research Vol.34, No.121, pp.213-220. December 1982.

[6]   Hertz, K.D.: Residual Properties of Concrete Heated Rapidly. ACI Special Publication SP-92 pp. 143 - 152. American Concrete Institute, Detroit 1986.

[7]   Harmathy, T.Z. Berndt, J.E.: Hydrated Portland Cement and Light weight Concrete at Elevated Temperatures. Journal of the ACI Vol.63, No.1, pp.93-112. Research Paper No. 280. Division of Building Research. Ottawa 1966.

[8]   Hertz, K.D.: Heat-Induced Explosion of Dense Concretes. Report No. 166. Institute of Building Design, 20p. Technical University of Denmark. Lyngby February 1984.

CIB W14/84/33 (DK).

[9]   Hertz, K.D.: Limits of Spalling of Fire Exposed Concrete. Research Paper, Department of Buildings and Energy. 11p. Technical University of Denmark. Lyngby November 1998.

[10] Hertz, K.D.: Stress Distribution Factors. Report No.160. Institute of Building Design,

Technical University of Denmark. Lyngby 1981. 60p. CIB W14/81/14 (DK).

[11] Hertz, K.D.: Design of Fire Exposed Concrete Structures. Report No.160. Institute of Building Design, Technical University of Denmark. Lyngby 1981. 50p. CIB W14/81/20 (DK).

[12] Hertz, K.D.: Analyses of Prestresssed Concrete Structures Exposed to Fire. Report No. 174, Institute of Building Design, Technical University of Denmark. 1985. CIB document W14/85/9 (DK).

[13] CEN: ENV 1992-1-2. Design of Concrete Structures; General Rules, Structural Fire Design. Secretariat of CEN/TC 250/SC 2. 1994.

[14] Hertz, K.D.: Simplified Calculation Method for Fire Exposed Concrete Structures. Supporting Document for CEN PR-ENV 1992-1-2. Report No. 203, Institute of Building Design, Technical University of Denmark. 1993. Published by CEN together with ENV 1992-1-2.

[15] Danish Standardisation Organisation: DS411ver. 4.1. Danish Code of Practice for Concrete Constructions. DS, 1999.

[16] Hertz, K.D.: Comments on Simplified Calculation Method for Fire Exposed Columns. (As found in ENV 1992-1-2 chapter 4.3, and in the proposal for Danish code of Practise DS411 chapter 9). Department of Buildings and Energy, 20p + addition 21p. Technical University of Denmark. June 1998.

[17] Hass, R.: Zur Praxisgerechten Brandschutztechnischen Beurteilung von Stützen aus Stahl und Beton.Heft 69. Institut für Baustoffe, Massivbau und Brandschutz der Technishen Universität Braunschweig. Braunschweig 1986.

[18] Lie, T.T. Allen, D.E. Abrams, M.S.: Fire Resistance of Reinforced Concrete Columns. DBR Paper No. 1167. National Research Council Canada. Ottawa 1984.

[19] Seekamp, H. Becker, W. Struck, W.: Brandversuche an Stahlbetonfertigsäulen. Deutscher Ausschuss für Stahlbeton. Heft 162, Teil 1. Wilhelm Ernst und Sohn. Berlin 1964.

[20] Anderberg, Y. Forsén, N.: Fire Resistance of Concrete Structures. Nordic Concrete Research No.1. Oslo 1982.

Calculation and testing of Factory-made Concrete Elements

Niels E. Andersen M.Sc., Ph.D, Danish Institute of Fire Technology

The background for this project is the development of a new Danish design code for concrete structures DS 411 as well as the development of the Eurocode EC2.

The section on calculation of fire resistance of concrete elements and structures caused strong disagreement between experts on fire and concrete in Denmark

The first basic problem was the question: How can you calculate the load bearing capacity of an element if you can not accurately predict the amount of spalling, which takes place?

It was also felt, that the knowledge about a number of other problems such as shear and anchorage might be insufficient.

Finally it was very difficult to make the concrete experts realise, that with higher utilisation of materials in the cold state, the fire design could become the determining part of the design of concrete elements and structures.

It was decided by DIFT to draw up a balance sheet in which the best available knowledge was used by experts to calculate the fire resistance of a number of elements and to compare the calculations with test results.

The project contained the following phases:

- Design of a number of concrete elements
- Calculation of fire resistance time based on actual material properties and loading conditions
- Fire testing
- Comparison of results from calculations and tests

It is important to realise that it is not within the scope of this project to perform standard fire test for classification purposes, but to compare the results of calculations and tests performed under identical and well-controlled conditions.

In many countries the classification of the fire resistance of concrete elements is based on tradition rather than on testing of the actual performance, and there is an enormous shortage of available and relevant test results. So it will be natural to look at the results of these tests also for assessment of the standard fire resistance of these elements.

Such comparisons of calculations and test results have been done before, but we felt that previous work had some shortcomings:

- Older tests are often performed with elements made from materials with lower strength
- Concrete elements from other countries may be manufactured from other types of cement powder and aggregates
- The fire test methods have been improved due to the attempts to achieve harmonised test results within the European community
- The test results were <u>not</u> known at the time of the calculations

The project comprised the following concrete elements:

- 3 TT Roof Slabs, pre-stressed, pre-tensioned, length 6,36 m
- 3 Pre-stressed, pre-tensioned Hollow Core Slabs, height 18, 22 an 27 cm, length 6,36 m
- 7 Load bearing walls, thickness 120 mm and 150 mm, height 4,5 m
- 4 Columns exposed to fire on one side, 200x200 mm and 240x240mm, height 4,5 m.

The elements were not designed for any specific fire resistance time. They were designed for cold load bearing capacity – as in practice. Such elements are frequently used in Denmark without any further proof where 60 minutes fire resistance is required.

Participants. It was important to get the co-operation from as many experts on calculation of fire exposed concrete structures as possible, so invitations were sent to a number of European institutions. The response was not quite satisfactory, and we only got a Nordic representation. The participants were:

Mr. Erik Steen Pedersen, M.Sc.
DTI, Danish Institute of Technology, Building Division

Professor Kristian Hertz, M.Sc., Ph.D.
DTU, Technical University of Denmark,Department of Building and Energy

Per J. Knudsen M.Sc.
Danish Standards Organisation, S417-U02

Dr Yngve Anderberg, M.Sc.
FSD, Fire Safety Fire Design, Sweden

DTI and FSD have developed finite-element programs, FIRE 2-D and TEMPCALC, which are both being sold commercially.

 Design of test specimen.   Some concrete elements can not be tested in full size. The fire test standards require that horizontal elements shall be tested with at least 4 m exposed length. In our floor furnace at DIFT we can test horizontal elements with an exposed length of 6 m, but even this is much smaller than the length of some of the longest TT-Roof Slabs, which have a length of about 30 m. So down-sizing and re-design of the elements is necessary. For this project we decided that the following parameters should not be changed when going from 30 m to 6 m test specimens:

- The total load on the element and the reaction at the supports
- The stress in the strands
- The location of the centre of gravity of the strands

We had to accept, that some other factors could not be reproduced:

- The number of strands had to be reduced from 11 to 4
- The pressure in the pressure zone, which is affected by the total pre-stress force
- The 'column-length' and the stability of the pressure zone

Elements of Fire Design. The complete determination of the behaviour of a load-bearing element in fire can traditionally be divided into four parts:

1. Determination of the temperature field around the element
2. Calculation of the temperature distribution inside the element

3. Calculation of the reduced load bearing capacity caused by the elevated temperature
4. Determination of the design load in fire

This project showed that for members under compression a fifth factor could be critical:

5. Determination of the effect of the load, i.e. eccentricity caused by thermal and second order deflection of the element.

The first part is easily dealt with; all tests and calculations use the ISO 834 standard time temperature curve.

Three participants used a finite element method for calculation of temperature inside the elements. The fourth calculation is a simplified method, which explicitly gives the temperature $\theta_{x,t}$ at time t and at distance x from the exposed surface. Equations are given in DS 411 for one-, two and three-sided exposure. Surface heat transfer conditions are not considered explicitly. Instead the surface temperature is assumed to follow the curve:
$T_0 = 312 * \log(8*t +1)$ and the temperature at depth x is calculated from.

$$\theta_{x,t} = T_0 * e^{-1,9*k(t)*x} * \sin(\pi/2 -k(t) *x); \quad k(t) = \sqrt{(\pi \rho c_p/(750\lambda t))}$$

Dr. K. Hertz (DTU) used this method.

Heat transfer parameters used for the calculations are listed in the table below:

	DTI	DTU	FSD	PJK
Emissivity	0,56	-	not stated	0,56
Coeff. of convective heat transfer	25	-	not stated	25
Configuration factor	1,0	-	-	1,0/0,5
λ0 [W/m/K]	1,4	0,75	1,5	1,44
λ200	1,0	0,75	0,8	1,0
λ500	0,75	0,75	0,6875	0,75
λ800	0,6	0,75	0,575	0,6
λ1000	0,6	0,75	0,5	0,6
c [J/kg/K]	1000	1000	1000	1000

Reduced Load Bearing Capacity. The calculations of the load bearing capacity can have different levels of sophistication.

1. Plastic rupture model using only temperature dependant yield strength or ultimate strength
2. Calculations, in which actual strain is considered, can be divided in:
   - Linear elasto-plastic model with reduced ultimate strength and E-modulus
   - Non-linear elasto-plastic model with reduced stress-strain relationship

The last method requires that also thermal strain be taken into account, because in a concrete section with non-uniform temperature distribution, the non-uniform thermal strain will be added to the mechanical strain. This is taken in account by the finite element program FIRE-2D.

The thermal expansion of concrete is a very complex matter. It depends not only on the actual values of temperature and stress but also on temperature/stress-history. There is very little help to be found in the design codes.

In EC2 (ENV 1992-1-2, Nov. 1995) only a stress-independent value is given:

$$\Delta l/l = 1{,}2 \cdot 10^{-5}\, \theta \quad \text{or} \quad 1{,}8 \cdot 10^{-5}\, \theta$$

In the Danish draft design code DS 411 the following expression was suggested:

$$\Delta l/l = 1{,}1 \cdot 10^{-5} * \{1 - 2{,}35 * \sigma/f_{cd,20}\} \qquad [°C^{-1}]$$

The term $-1{,}1 \cdot 10^{-5} * 2{,}35 * \sigma/f_{cd,20}$ is frequently referred to as 'transient strain'. In this equation, there is nothing 'transient' about this term. The total strain is a function of the instantaneous combination of temperature and stress and independent of the temperature/stress history.

The DTI calculations use the equation in a differential form where

$$d\varepsilon_{therm} = 11 * 10^{-6} * dT$$
$$d\varepsilon_{trans} = -2{,}35 * \sigma/f_{cd,20} * d\varepsilon_{therm}$$

When these equations are applied to the actual construction and load conditions and integrated over time and temperature, they give a truly transient expression for the strain.
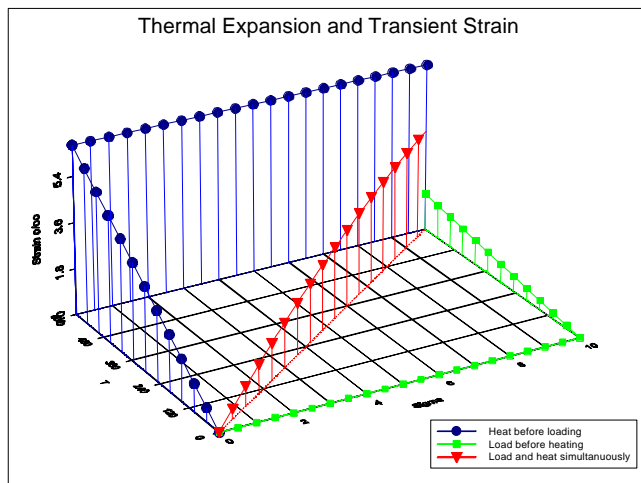
Change of Load Effect. A wall or a column with non-symmetrical heating will have a non-uniform temperature distribution and a non-uniform thermal strain, which causes bending of the member. This will cause the wall or column to bend toward the exposed side, and an axial load will have an eccentricity relative to the centre of the section. That will also happen when the mechanical properties of parts of the section are degraded because of increased temperature. The centre of the remaining section will move away from its original position and thereby change the load eccentricity.

Determination of design load in fire. The load reduction factor η_{fi} depends on the national partial safety factors and the actual combination of load types. At the time when the project was started, the Danish partial safety factors were: $\gamma_{f,G} = 1$ and $\gamma_{f,Q} = 1{,}3$ (ultimate limit state) and $\gamma_{f,fire} = 1$ (fire). The combination of permanent and variable load was assumed to be typical for the actual type of element:

Type of element	Permanent load	Variable load	Danish η_{fi}	EC η_{fi}
TT-Roof Slab	74%	26%	0,93	0,72
Hollow Core Slab	Own weight	5 kN/m²	0,84-0,85	0,70
Wall	67%	33%	0,91	0,91
Column	67%	33%	0,91	0,71

It should be noted, that the boxed values in Eurocode gives much lower design load in fire.

Mechanical Properties: The reduction factors for mechanical properties, which were used by all participants, were much like those, which can be found in EC2.

Calculation Methods. The table shows some of the main characteristics of the calculation methods employed by the experts for calculation of horizontal and vertical members

Calculation of Slabs	DTI (FIRE 2-D)	DTU	FSD	PJK
Reduction of tensile strength of strands	+ Entire stress-strain curve is considered	+	+	+
Transient strain	Yes	-	-	-
Reduction of pressure zone	Finite element	Reduced section	Finite element	No reduction because of low pressure load
Shear	-	Diagonal compression force method, θ=45° and variable	-	Diagonal compression force method, θ=26-45 °
Spalling	No	No	No	No
Anchorage	-	Method by K. Hertz	-	Draft DS 411, 9.2.6 (14)
Other	Deformation	-	-	-

The DTI calculation gives a physically correct calculation of moment capacity but ignores other failure modes. The calculations by DTU and PJK are based on simplified methods, but shear and bonding failure are also considered. The FSD calculations are simple calculations of moment capacity.

Calculation of Walls and Columns	DTI FIRE 2-D	DTU	PJK manual	PJK computer aided FIRE 2D
Reduction of tensile strength of reinforcement	Entire stress-strain curve is considered	+	+	Entire stress-strain curve is considered
Reduction of E-modulus of reinforcement		+ $E_\theta = E_{0,\theta}(1-\sigma/f_{u,\theta})$	+	
Transient strain	Yes	Pseudo	Pseudo	Yes
Reduction of pressure zone	Finite element Entire stress-strain curve is considered	Yes	Yes	Finite element Entire stress-strain curve is considered
Deflection	Based on finite element equilibrium	Based on linear temperature gradient in undamaged zone	Based on linear temperature gradient in undamaged zone	Based on finite element equilibrium
Second order defl.	Yes	Yes	Yes	Yes
Interpolation of second order deflection	By time-stepping	No	No	By time-stepping
Horizontal deflection	$\kappa*l^2 / 8$	$\kappa*l^2 / 8$	$\kappa*l^2 / 8,5$	$\kappa*l^2 / 8,5$

κ is the curvature at mid height of the wall.

All calculations of load bearing capacity of walls and columns are rather simple calculations of moment capacity. The important difference between the methods is the way thermal expansion, transient strain and bending is treated. The simple methods are based on the temperature-stress-strain at a fixed time. The F-E method calculates the entire history of temperature-stress-strain.

Test Arrangement. The tests were performed in accordance with the draft versions of the CEN standards. This particularly means that great care has been taken to use the same length of the supports as in practice.

The figure shows the arrangement of hollow core slabs within the loading frame. Notice that the total length 6,36 m is only 16 cm longer than the span. This figure is typical for the practical use of hollow core slabs and TT-roof slabs. The next figure shows the load arrangement that distributes the load to four load beams on each slab. A similar arrangement was used for TT-roof slabs.
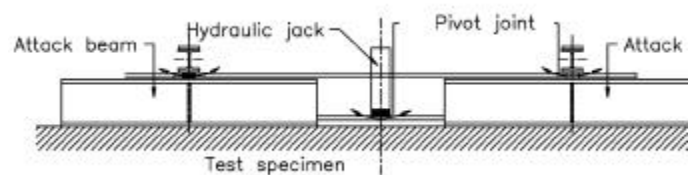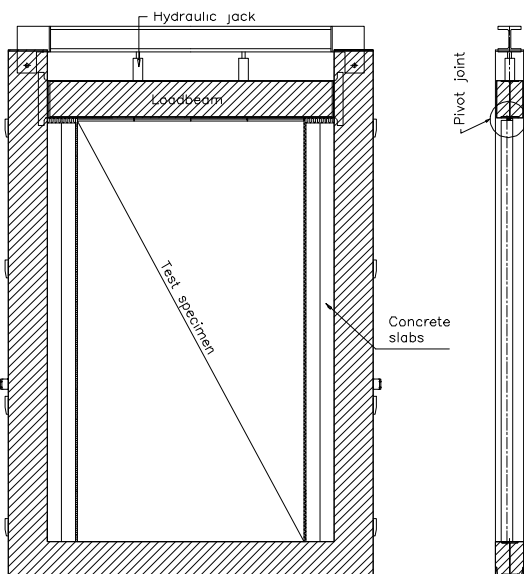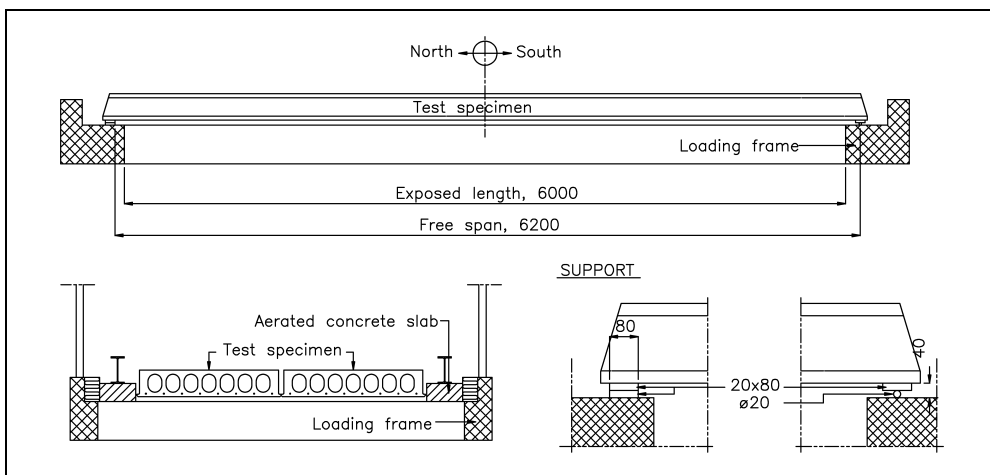
The test arrangement for walls is shown in the figure to the left.

The wall was mounted in a U-shaped test frame with fixed and movable load beams: Both beams were guided in vertical grooves inside the frame. The load was transmitted to the wall through a pivot joint along the top of the wall. The eccentricity was established by displacing the wall relative to the frame. The eccentricity was 35 mm for the 120 mm wall and 50 mm for the 150 mm wall.

Load eccentricity towards the furnace (i.e. wall displaced away from the furnace is designated load type A)

The columns were tested in much the same way as the walls. The columns were mounted in the same frame and were exposed to fire on one face and on half of the two sides.
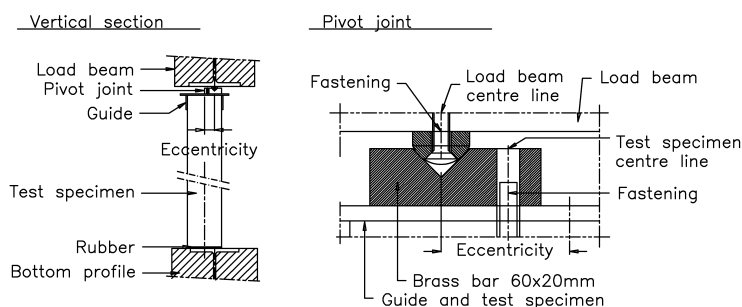
Test Results

The following tables show the calculated and measured fire resistance time for TT roof slabs and hollow core slabs. When experts have calculated more than one failure mode, the time to failure for each mode is listed in the table.

TT Roof Slabs		Moment Failure	Shear failure	Anchorage Failure	Fire Resistance Time, min.
DTI	Type 1	47	-	-	47
	Type 3	37	-	-	37
PJK	Type 1	52	50	> 60	50
	Type 3	45	40	> 60	40
DTU	Type 1	56	91	110	55
	Type 3	39	40	24	(24)/38
FSD	Type 1	77	-	-	77
	Type 3	63	-	-	63
Test	Type 1	No	42	42-	**42**
	Type 3	-No	-41	41	**41**

Hollow core Slabs		Moment Failure	Shear Failure	Anchorage failure	Fire Resistance Time, min.
DTI	SP 22	44	-	-	44
	SP 27	64	-	-	64
PJK	SP 22	55		(46)	46
	SP 27	74		(63)	63
DTU	SP 22	65	802	None	64
	SP 27	109	668	1121	108
FSD	SP 22	50	-	-	50
	SP 27	78	-	-	78
Test	SP 22	No	26	26	**26**
	SP 27	-No	21	21	**21**

The results from Type 2 TT-slab have been left out because the test had to be interrupted when integrity failure in the connecting slab threatened to destroy the loading equipment. The results from 18 cm hollow core slab have been left out because the test conditions were not correct.

The failure mode was in all cases bonding failure combined with shear failure. The strands were observed to contract from the ends of the elements. The cracks appeared 0,5 – 0,75 from the supports and the cracks under approximately 45°. Only the 27 cm hollow core slab was different. Here the failure occurred directly over one of the supports.

The tables show that the fire resistance time was generally overestimated in calculations.

The photographs show the cracks in the beam of one of the TT-roof slabs
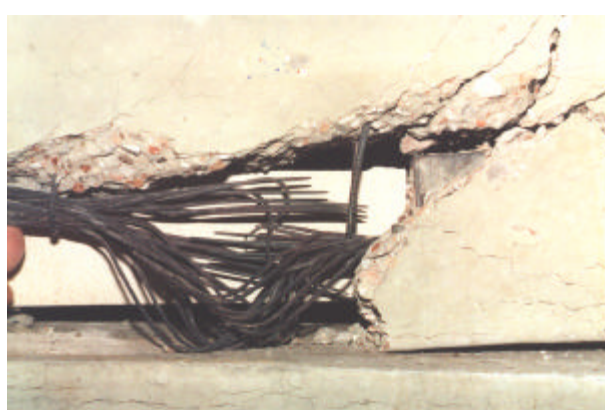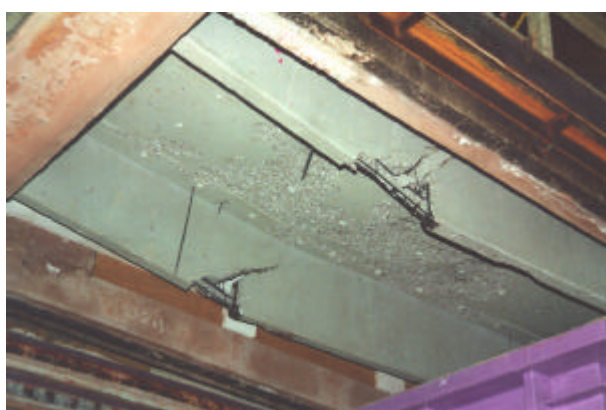
Walls and columns. The next tables show the calculated and measured fire resistance time for walls and columns. The failure mode is bending failure at mid height. The tables also show the horizontal deflection at mid height. A positive value is in the direction towards the furnace. Where two values are given, they indicate the maximum deflection and the deflection at the time of failure.

Walls	Test		DTI		DTU		PJK, Manual		PJK, Computer aided	
	t, min	δ, mm	t, min	δ, mm	t, min	δ, mm	t, min	δ, mm	t, min	δ, mm
1200 A1	32	234	23	103	118	120	23	148	22	103
1200 A2	33	239								
1200 B	25	195	12,5	85	19	123	7,2	93	5,4	78
1500 A	64	217	47	99	200	89	44	145	54	109
1500B	26	183	17	80	19	94	6,9	72	5,4	60
1501 A	72	257	89	145	200	90	143	168	148	147
1501 B	32	197	23	100	18	157	0	88	0	37

Co-lumns	Test		DTI		DTU		PJK, Manual		PJK, Computer aided	
	T, min	δ, mm	t, min	δ, mm	t, min	δ, mm	t, min	δ, mm	t, min	δ, mm
200 A	75	170	141	34,5/16	-		51,3 66 222	-88,5* 155	104*** 142 222	40/3 56/43 78/69
240 A	97	45/34	104	2,5/-52	-		57	-70,5	95 118 141	+1/-40 +15/-40 +30/-30
240 B	64	122	34	103	-		32,5	93	32 29 25	103 98 94

*   The simple calculation method allows two different equilibrium conditions. Only 'real time' calcula-tion can show which one will actually occur.
 *** The influence of a 9 mm imperfection has been investigated, (upper and lower lines)

The 200 B test is left out because of malfunction of the loading equipment.

The tables show that the horizontal deflection was generally underestimated. In the graph the horizontal deflection of the walls is shown. All walls break when the deflection reaches 200 – 240 mm. The second graph shows the expansion of the walls. There is a distinct difference between the two load cases. When thermal eccentricity and load eccentricity work in the same direction (Load case B) the horizontal deflection becomes large and there is very little thermal expansion.
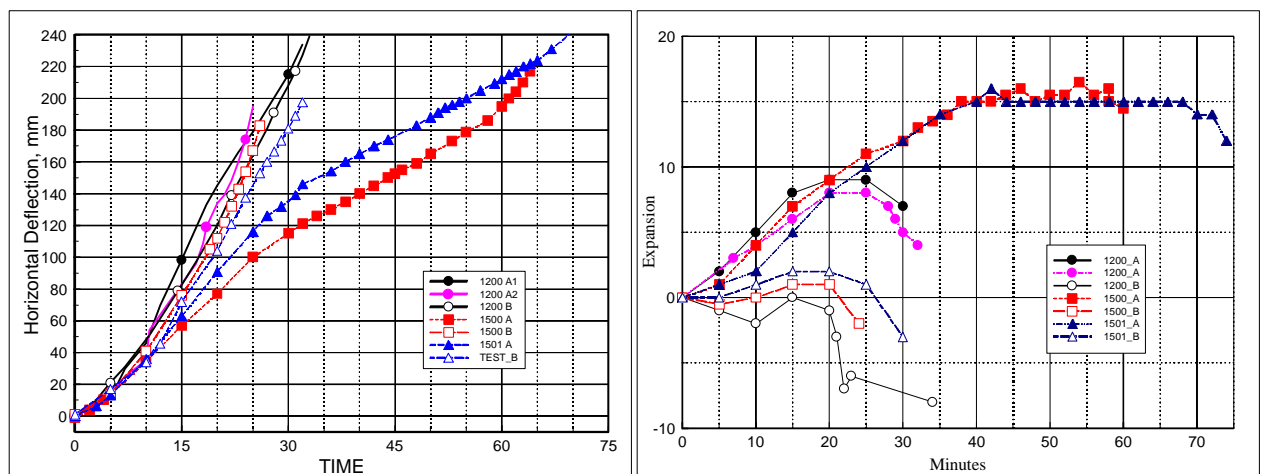
This situation also gives the shortest fire resistance time in test. The calculated fire resis-tance time in these cases is even lower and has generally been underestimated.

The photograph shows one of the walls shortly before it collapses. Notice the deflection towards the furnace.
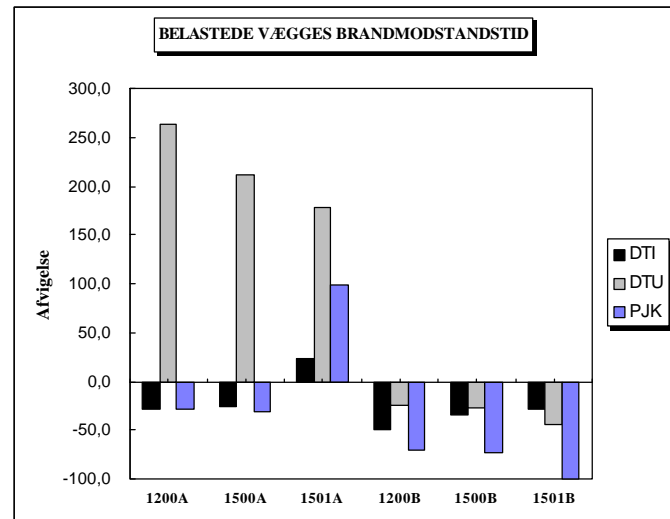
The graph shows the ratio between calculated and measured fire resistance time.

The behaviour of the columns is much like that of the walls and shall not be treated in detail.

Conclusions about the calculation methods

Horizontal elements: The calculations were not able to predict the failure modes that actually occurred, i.e. shear failure and bonding failure. Where attempts were made to calculate these modes, the accuracy was poor. For this type of elements the moment capacity, which can be calculated fairly easily, was not the critical factor

Vertical elements: The calculations could not predict the thermal load eccentricity with sufficient accuracy. This holds for the theoretically more correct finite element method as well as for the simplified methods. The horizontal deflection, and therefore the bending moment at the time of failure, was larger than predicted. This means that the walls have some extra moment capacity that has not been accounted for, such as tensile strength of the concrete.

Consequently, the final version of the design code for concrete structures DS 411 does not give any guidance on how to calculate

- Thermal expansion of concrete
- Anchorage
- Shear and torsion
- Spalling

The same subjects have been treated lightly or not at all in the Eurocode 2, so obviously these are areas where much more research is needed.

Conclusions about pre-fabricated concrete elements

The tests have shown that all elements have a shorter fire resistance period than the one for which they are generally used. At least this is true when they are loaded according to present practice, where the elements are designed for the cold ultimate limit state and are assumed to have 60 minutes fire resistance.

The type of elements with the most serious shortcomings are the hollow core slabs, which are only found to have 21 and 26 minutes fire resistance when tested as described.

Ever since these results were first reported, we have received a lot of flak from industry for having tested the hollow core slabs as simply supported slabs and without reinforcement and concrete in the longitudinal joint.

We find that this criticism is misplaced. The purpose of the entire project was to test the calculation methods, and this has been done by calculation and testing of the same arrangement. Furthermore the present Danish approval of these slabs does not require the slabs to be continuous, so the test arrangement is not quite unrealistic.

Future development

It has been realised, that much more work need to be done to improve the calculation methods for fire exposed concrete structures, so a project team has been formed with representatives from industry, universities and research institutes. The Danish Ministry of Housing has promised some financial support, so hopefully it will become possible to improve the calculation methods.

Improved calculations will not increase the fire resistance time of those elements which failed to meet the requirements, but improved calculations can be a useful tool in the re-design and development of those elements in the future.

INVESTIGATION IN EUROCODE FOR CONCRETE COLUMNS

Dr Eng. SAYED ATTIA
BRANSCHUTZPLANUNG KLINGSCH; GERMANY
s-attia@bpk-mail.de

1.   Introduction:

The idea of this paper is based on the new Eurocode (Eurocode 2, Part 1.2) for concrete in fire design, which is developed only since five years. This code will be applied in the different europiean countries gradually. In Germany, where this investigation was performed, the code will be applied in the next two years but it will not be used instead of the DIN-Code (national code).

Now, the different new Eurocodes are not easy and a great effort is needed to analysis and understand the different parts and it's combinations.

The main part of Eurocode 2 which is included here:

-Eurocode 2, Part 1.2: For fire resistance of concrete structures

This part deals with the design of concrete structures in the fire situation. It provides the difference between this case and the design of structures at room temperature. Part 1.2 applies on structures, which must fulfil the following criteria in the fire situation:

-prevent premature collapse,

-limit fire spread beyond the designated areas.

2.   Some definitions from Eurocode 2, Part 1.2:

To make the Eurocode 2-Part 1.2 usable, a borrow of some parts from DIN 488, DIN 1045, DIN 1055 and DIN 4227 are necessary. The design concept of EC 2 does not differentiate between prestressed and non-prestressed structural members.

EC 2 divided into „principles" and „applications". However, principles comprise defined general requirements (such as structural stability), to which no alternative is permitted. The application rules are generally recognised (such as detailing rules) and follow the „principles" and satisfy their requirements.

Conceivably, it is permissible to use alternative design rules provided that these rules agree with the relevant principles and at least equivalent to those in EC 2.

DIN 1045 gives the methods of analysis which is based on the elastic theory. On the other hand for example EC 2 permits more redistribution of bending moments than in DIN 1045 (15% due to DIN 1045 and more than 30% due to EC 2).

Eurocode 2, part 1.2 has divided the failure criterion of members in the fire situation as follows:

criterion „**R**" (Resistance): The structure shall be designed and constructed to maintain it's load bearing function during the relevant fire exposure,

criterion „**E**" (Enclosure): The structure shall be designed that no integrity due to cracks or holes which are large enough to cause fire penetration by hot gases or flame.

criterion „**I**" (Insulation): The structure shall be designed that the average temperature rise during the standard fire exposure at the unexposed surface not exceed 140° K and the maximum rise at the unexposed surface not exceed 180° K.

3.   Structural fire design:

The Eurocode 2, part 1.2 has suggested 3 calculation procedures:

a) tabulated data; level 1,

b) simply calculation method; level 2,

c) advanced calculation model for simulating the behaviour of the member in fire; with physical and non- linearities, level 3 (computer program) .

The load level μ under normal situations is defined by the following equation:

$$\mu = E_d / R_d \; < \; 1{,}0$$

where:

E_d is the design effect of actions for normal temperature design,

R_d is the design load bearing resistance for normal temperature design.

The previous load level μ can also be defined in fire as $\mu_{fi,t}$ by the following equation:

$$\mu_{fi,t} = E_{fi,d,t} / R_d$$

where:

$E_{fi,d,t}$ is the design effect of action in the fire situation at time t.

The load bearing capacity „R" in the different analysis is reached, when the design load in fire case $R_{fi,d,t}$ is equal to the design effect of actions in fire $E_{fi,d,t.}$:

$$t_u = (R_{fi,d,t} = E_{fi,d,t})$$

4.   Fire Characteristics:

In order to obtain a basis of comparison for the effect of fire on a structural element, the fire is defined as a time-temperature relationship by ISO 834 fire curve (figure 1).
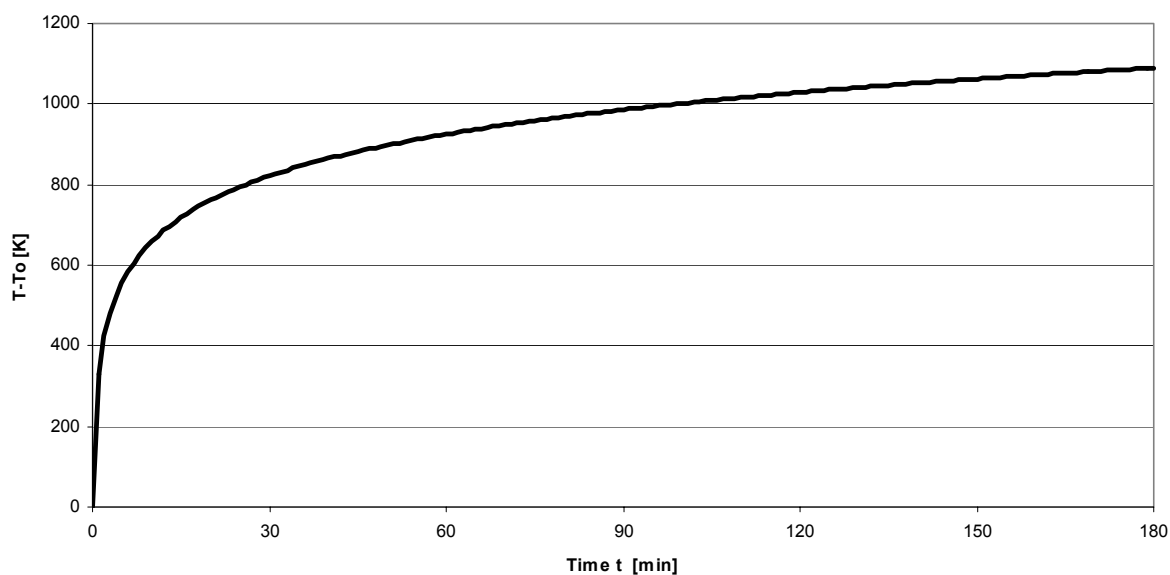
Figure 1: Temperature-Time curve (ISO 834). [33]

5.   Comparison of the material laws:

The standard fire conditions are defined between 20°C and 1200°C and within this range the properties have been defined.

Material properties dealt with are divided into mechanical and deformation and thermal properties. The material law which has been used in ENSA is taken from [17]

Table (1) shows the concrete grade and it's different mechanical properties which are applicable in the fire situation design of concrete structures. The classification of concrete eg. C20/25 refers to cylinder/cube strength of concrete at 28 days.

Table 1: Concrete strength classes for normal temperature, characteristic strength f_{ck} (cylinder), average of the tensile strength f_{ctm} and secant modulus of elasticity E_{cm} of concrete (in N/mm^2): [11]

Strength Class of Concrete	C12/15	C16/20	C20/25	C25/30	C30/37	C35/40	C40/50	C45/55	C50/60
f_{ck}	12	16	20	25	30	35	40	45	50
f_{ctm}	1,6	1,9	2,2	2,6	2,9	3,2	3,5	3,8	4,1
E_{cm}	26	27,5	29	30,5	32	33,5	35	36	37

6.   Mechanical and deformation properties of concrete in the case of fire:

The main effective concrete mechanical property is the stress-strain relationship at elevated temperatures. The stress-strain relations in figures 2   (as example) is defined by two parameters:

- the compressive strength $f_{c(\theta)}$,
- the strain $\varepsilon_{cu(\theta)}$ corresponding to $f_{c(\theta)}$.

The stress-strain relations include in an approximate way the effect of the high temperatures creep.

To be at the safe side the tensile strength of concrete may be assumed zero. But if it is taken into account, it must be not exceed than 10 % of the corresponding compressive strength.

Figures 2 shows this relation at different temperatures (100°C and 500°C) from ENSA and Eurocode 2. From this figure, it is noted that there is a difference in the trend of the relations and in defining the range of strain.

Figure 3 shows a comparison of concrete density at elevated temperatures from ENSA and Eurocode 2. In ENSA, it is considered that the density decreases with the increase of temperature, while in Eurocode 2 the density does not depend on the concrete temperature and for non-reinforced normal concrete it will be taken 2300kg/m^3.
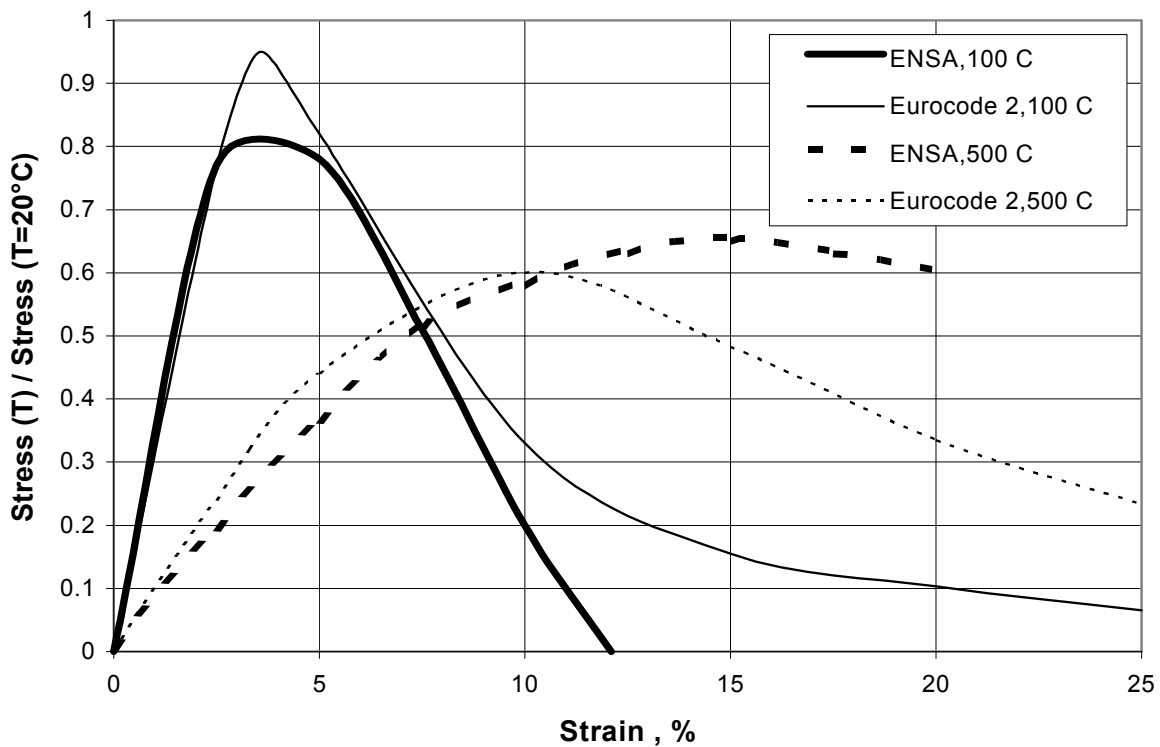
Figure 2: Comparison between the influences of temperatures on the stress-strain relationships of concrete (temperatures are 100°C and 500°C) from ENSA and Eurocode 2.
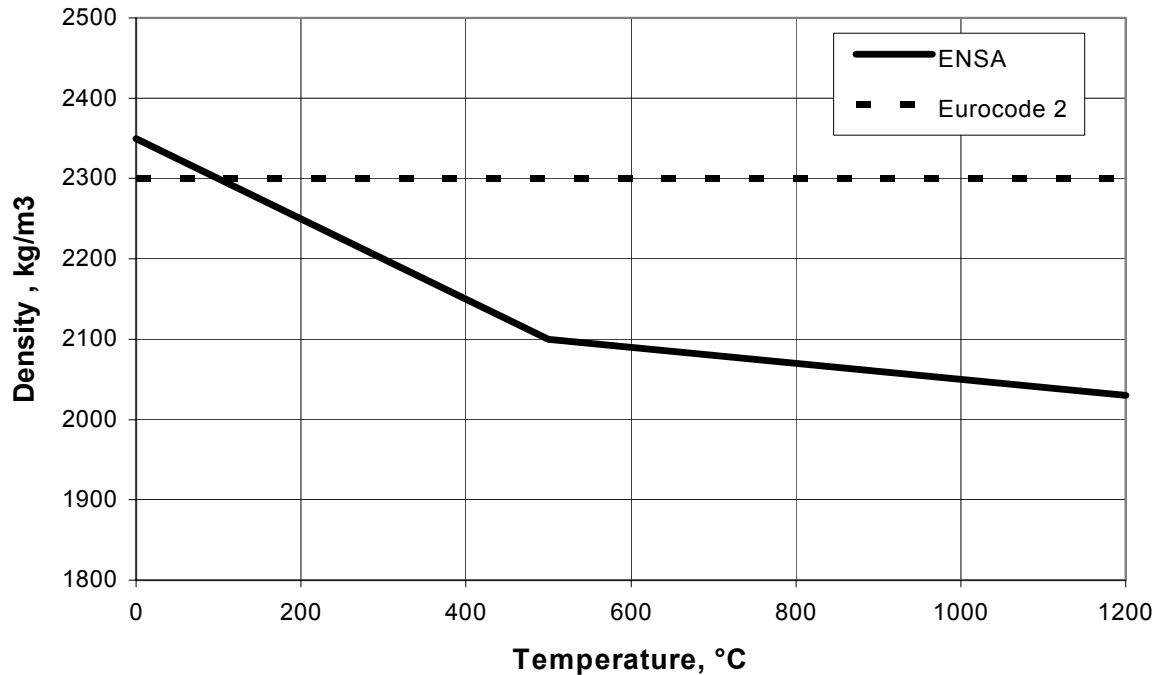
Figure 3: Comparison between concrete densities in fire case from ENSA and Eurocode 2.

7. Thermal properties of concrete in the fire case:

a) Thermal elongation (Δl/l):

In Eurocode 2, it may be determined from the following equations:

$$\Delta l/l = -1{,}8 \times 10^{-4} + 9 \times 10^{-6}\,\theta_c + 2{,}3 \times 10^{-11}\,\theta_c^{3} \qquad \text{for } 20°C \leq \theta_c \leq 700°C$$

$$\Delta l/l = 14 \times 10^{-13} \qquad \text{for } 700°C \leq \theta_c \leq 1200°C$$

where:

l   is the length at 20°C of the concrete member,

Δl   is the temperature induced elongation of the concrete member,

θc   is the concrete temperature.

b) Specific heat (Cc)

In Eurocodes 2, it may be determined from the following equation:

$C_c = 900 + 80\,(\theta_c/120) - 4\,(\theta_c/120)2$ J/kgk   for $20°C \leq \theta_c \leq 1200°C$

c) Thermal conductivity (λc)

In Eurocode 2, it may be determined from the following equation:

$\lambda_c = 2 - .0{,}24\,(\theta_c/120) + 0{,}12\,(\theta_c/120)^{2}$ W/mk   for $20°C \leq \theta_c \leq 1200°C$

8.   Computer calculation method

The computer program (ENSA) has been deliberately chosen as a tool for calculations in the present work.

Most finite element programs are based on a linear elastic material behaviour. Through these programs, thermal and mechanical results can be obtained. The equilibrium and deformation interaction (second order theory) are taken into account. It is necessary to adjust the internal forces to the load depended deformations and forces.

There are two groups of computer programs for structural fire design:

a- The direct method: modelling the element by a corresponding number of 3 dimensional finite elements, leads very fast to the rate of computer capacity.

b- The indirect method: a fibre model which uses the single component stiffness of the cross section reduced to an integrated stiffness.[30]

The method of integrated stiffness [31] was developed to get a more economic method. This means that the single component stiffness of the cross section are be reduced to an integrated stiffness of the whole cross section and is based on a realistic thermal and mechanical cross section analysis by two dimensional discretisation.[1]

With helping the computer program **ENSA** („**E**bene **N**ichtlineare **S**ystem **A**nalyse", in German language which means in English „Non-linear System Analysis in Plane"), it is possible, mainly, to analyse the load bearing capacity for different kinds of materials (concrete-steel-composite) and for different structural elements (slab-beam-column) and this with sufficient accuracy [7].

The concept of calculation with resulting stiffness uses the assumption of Bernoulli, that means plain cross section remains plain.

The most used cross sections are stored with its discretisiering in a special subroutine .

This method provides a realistic analysis of elements exposed to fire. It is based on fundamental physical behaviour leading to a reliable approximation of the expected behaviour of the relevant structural component under fire conditions.

This method uses separate sub-models for the determination of:

a) the development and distribution of the temperature within the cross section; thermal response model . It will be used computer program (Fires-T). [29]

b) the mechanical behaviour of the structural member; mechanical response model. It will be used computer program (ENSA) to calculate the ultimate load bearing capacity.

Figure 4 shows the main skeleton of the calculations combination of the previous two computer programs, where:

- **E1, E2, E3** are the input files of the computer programs,

- **A1, A2, A3** are the output files of the computer programs,

- **E1** contains the section geometry (dimensions, thicknesses), materials kind (concrete, steel) and the discritisation of the section,

- **E2** contains thermal properties (conductivity , specific heat and density) for steel and concrete, the elements which exposed to fire and the desired fire duration,

-**E3** contains the mechanical properties (buckling length, eccentricity, compressive strength , tensile strength, creep, modulus of elasticity, yield strength) for steel and concrete,

- **A1** contains the co-ordinates value of the cross section's nodes in y-direction (horizontal) and z-direction (vertical),

- **A2** contains centre of gravity for the different elements, area of the elements, temperature at the previous desired fire duration,

-    **A3** contains the ultimate load bearing capacity of the considered structural member at the previous desired fire duration.

-

```
                        ┌─────────┐
                        │   E 1   │
                        └────┬────┘
                             │
   ┌─────────────────────────┴──────────────────────────┐
   │   Program for discretition of cross section into elements   │
   └──────┬──────────────────────────────────┬──────────┘
          │                                  │
     ┌────┴────┐                        ┌────┴────┐
     │   A 1   │                        │   E 2   │
     └────┬────┘                        └────┬────┘
          │                                  │
   ┌──────┴──────────────────────────────────┴──────────┐
   │   Program to calculate the different element        │
   │   temperatures                                      │
   └──────┬──────────────────────────────────┬──────────┘
          │                                  │
     ┌────┴────┐                        ┌────┴────┐
     │   A 2   │                        │   E 3   │
     └────┬────┘                        └────┬────┘
          │                                  │
   ┌──────┴──────────────────────────────────┴──────────┐
   │   Program to calculate the non-linear ultimate load │
   │   bearing capacity                                  │
   └──────────────────┬──────────────────────────────────┘
                      │
                 ┌────┴────┐
                 │   A 3   │
                 └─────────┘
```
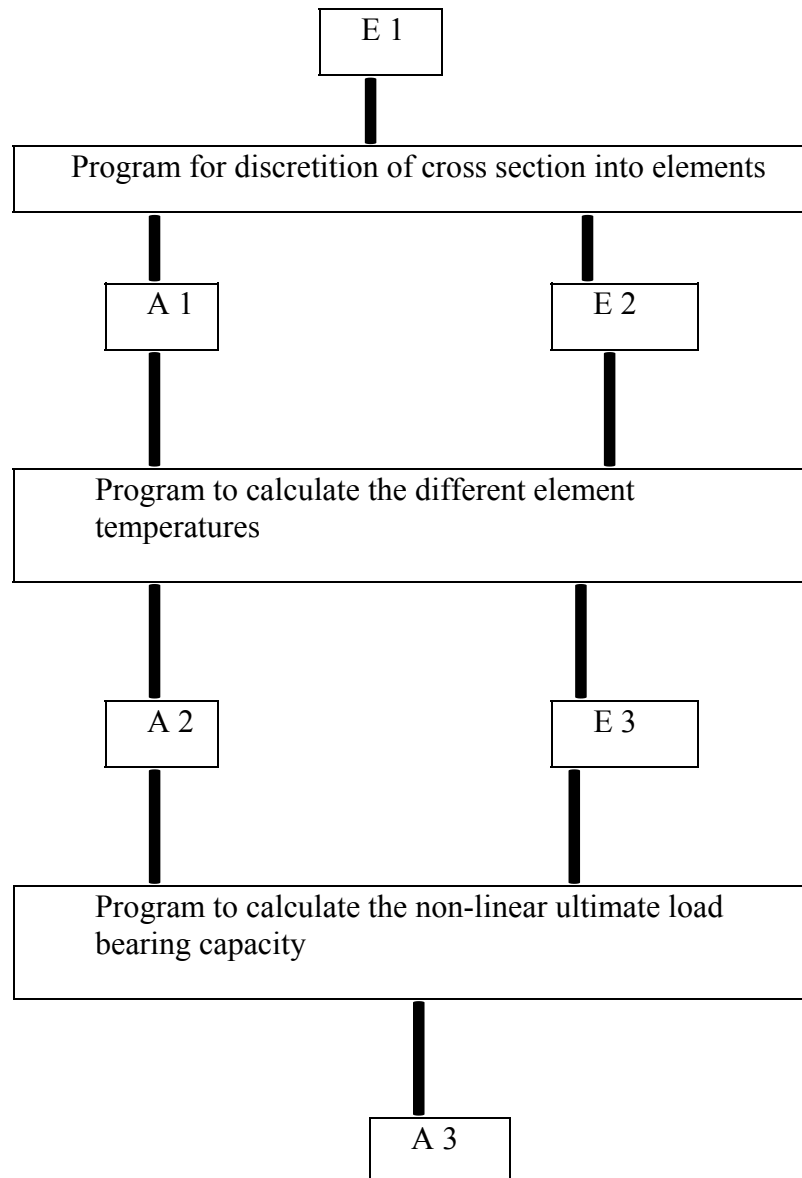
Figure 4: The main skeleton of the calculation's combination of the Fires-T and ENSA. [29]

9. Analysis of concrete columns

It will be compared the calculated results for some concrete column sections designed for fire resistance using different design methods. However, how good is the approximated calculation by level 1 and 2 which are given in EC2,1.2. The results from level 1 will be compared with those from level 2 and with those from ENSA as an „exact „ calculation of level 3 quality.

Table 2: Description of analysed concrete sections *

Section	Fire Duration	Description**	
		level 1	level 2
Square reinforced concrete column	R 60 R 90 R 120	h=b=200x200mm+4ϕ16mm a=30mm h=b=240x240mm+4ϕ16mm a=35mm h=b=280x280mm+4ϕ16mm a=40mm	$h_{red.}=b_{red.}$=249x249mm +4ϕ16mm, a=30mm $h_{red.}=b_{red.}$=227x227mm +4ϕ16mm, a=35mm $h_{red.}=b_{red.}$=209x209mm +4ϕ16mm, a=40mm
Circular reinforced concrete column	R 60 R 90 R 120	ϕ=200mm+6ϕ16mm a=30mm ϕ=240mm+6ϕ16mm a=35mm ϕ=280mm+6ϕ16mm a=40mm	$ϕ_{red.}$=249mm+6ϕ16mm a=30mm $ϕ_{red.}$=227mm+6ϕ16mm a=35mm $ϕ_{red.}$=209mm+6ϕ16mm a=40mm

*The suggested cross sections from level 1 either square or circular are different from those which suggested from level 2, because in level 1 the minimum cross sections for every fire duration are suggested from EC2, 1.2. While in level 2 the original cross sections are supposed (30x30 cm and ϕ 30 cm) for all fire durations and then these cross sections will be reduced according to EC 2, 1.2.
**For all fire durations : C35/45, S 500, $γ_M$ = 1.0.

Table 3: Partial safety factors for material properties for fundamental combinations. [32]

Structural steel	Concrete	Reinforced steel
$γ_a$ = 1.1	$γ_c$ = 1.5	$γ_S$ = 1.15

10. Level 1 of calculation, tabulated data

It is a method in which the fire resistance of a load bearing element or structural assembly, under standard fire conditions, is determined in terms of time equal to or exceeding the time of fire duration required by the building regulations.
The requirements are expressed as a required time of fire duration, i.e. the fire resistance time, directly related to the standard fire.
The tables which will be used, applies for the standard fire exposure. These tables are based on an empirical basis confirmed by experience and theoretical evaluation of tests.
The tables in ENV 1992, 1.2 apply to normal weight siliceous concrete, taking into account requirements to prevent explosive spalling and no further check is required. Generally, linear interpolation between the values given in the tables is allowed.
By using table 4, the concrete column may be classified according to:
-the minimum cross section dimension (b or d),

312

-the minimum axis distance reinforcement bars (a),
-number of sides at which the column is exposed to fire (one side or more).

Table 4: Reinforced concrete columns; square or circular section. [32]

Standard fire Resistance	Minimum dimensions (mm)			
	Column width b/axis distance a			
	Column exposed on more than one side			Exposed on one side
	$\mu_{fi} = 0.2$	$\mu_{fi} = 0.5$	$\mu_{fi} = 0.7$	$\mu_{fi} = 0.7$
1	2	3	4	5
R 30	150/10*	150/10*	150/10*	100/10*
R 60	150/10*	180/10*	200/10*	120/10*
R 90	180/10*	210/10*	240/35	140/10*
R 120	200/40	250/40	280/40	160/45
R 180	240/50	320/50	360/50	200/60
R 240	300/50	400/50	450/50	300/60
• Normally the cover required by ENV 1992-1-1 will control				

The previous calculations of the load bearing capacities, when the slenderness ratio (λ) of the considered column is greater than 50, then the column must be checked with second order analysis and the imperfection effects will be taken into consideration. To get the column's ultimate load bearing capacity, the N-M interaction diagrams [34] will be used.
Table 5 shows the minimum dimensions of square and circular sections and it's load bearing capacity at different fire duration.

Table 5: Minimum dimensions considered for square and circular columns with it's load bearing capacity at different fire durations. (level 1)[+]

Concrete Column	Buckling length[++] (m)	Load bearing capacity					
		R 60*		R 90**		R 120***	
		N_u (-kN)	M_u (kNm)	N_u (-kN)	M_u (kNm)	N_u (-kN)	M_u (kNm)
Square Column with μ_{fi}= 0,7	lo= 0,5	1114	---------	1481	--------	1914	--------
	lo= 0,7	1114	---------	1481	--------	1914	--------
	lo= 1,0	1114	---------	1481	--------	1914	--------
	lo= 1,5	467	13	1481	--------	1914	--------
	lo= 2,0	354	17	604	24	1914	--------
	lo= 2,5	298	23	497	31	585	30
	lo= 3,0	280	31	403	36	548	41
	lo= 4,0	149	29	268	42	475	63
Circular Column with μ_{fi}= 0,7	lo= 0,5	1077	---------	1364	--------	1705	--------
	lo= 0,7	1077	---------	1364	--------	1705	--------
	lo= 1,0	1077	---------	1364	--------	1705	--------
	lo= 1,5	290	8	1364	--------	1705	--------
	lo= 2,0	180	9	410	16	470	16
	lo= 2,5	130	10	210	13	310	16
	lo= 3,0	85	9	145	13	205	15
	lo= 4,0	45	9	90	14	125	17

+for all fire durations and cross-sections: C35/45, S 500,

++the buckling lengths are always equal to column lengths,

*the considered square cross-section is 200x200mm+4ϕ16mm with 30mm concrete cover (a) and the considered circular cross-section is ϕ200+6ϕ16mm with 30mm also concrete cover (a),

**the considered square cross-section is 240x240mm+4ϕ16mm with 35mm concrete cover (a) and the considered circular cross-section is ϕ240mm+6ϕ16mm with 35mm also concrete cover (a),

***the considered square cross-section is 280x280mm+4ϕ16mm with 40mm concrete cover (a) and the considered circular cross-section is ϕ280mm+6ϕ16mm with 40mm also concrete cover (a),

11. Level 2 of calculation, simple calculation method

It is a method, in which the fire resistance of a load bearing element or structural assembly under standard fire conditions is determined analytically. The design criterion is that the analytically-determined fire resistance is equal to or exceeds the "effective fire duration", a quantity which relates a non-standard or natural fire exposure to the standard fire.

The non-standard or natural fire exposure is related to the standard fire by the concept of the "effective fire duration". The effective fire duration is a function of the fire load, the geometry and the ventilation conditions of the fire compartment and replaces the time of fire duration fixed in the building regulations. This method shall only be used for columns in braced frames.

This method consists of three steps :

1)Determine the temperature profile of the cross section,

2)Reduce the concrete cross section, the strength and the short time E-modulus of concrete and reinforcement,

3)Calculate the ultimate load bearing capacity of the structure (or member) with the reduced cross section.

Again for pre-calculation of load bearing capacities, the column must be checked for second order analysis and the imperfection effects will be taken into consideration, if slenderness ratio (λ) of the considered column is greater than 50. To get the column's ultimate load bearing capacity, the N-M interaction diagrams [28] will be used.

In the previous mentioned second step, it is assumed that the isotherms in the compression zone of a rectangular cross section are parallel with the sides. The fire damage of part of cross- section is represented by a reduced cross section within the concrete is considered uniformly damaged. The cross section is geometrically reduced by ignoring a damaged zone of thickness at the fire exposed surfaces. The reinforcement is taken into account using reduced strength and E-modulus according to the temperature of each bar, even if it is placed outside the reduced cross section. The ultimate load bearing capacity with the reduced section can be calculated in accordance with ENV 1992, 1.1. [11]

Siliceous-aggregate concrete C35/45 and reinforcement-bars S 500 will be used in this level of calculation. The different cross-sections; square and circular, which are considered in level 1 at R 60, R 90 and R 120 will be calculated another time with level.

Table 6 shows the reduced considered cross section and it's ultimate load bearing capacity at R 60, R 90 and R 120 for columns.

Table 6: The reduced considered column and it's load bearing capacity at different fire durations. (**level 2**)[+]

Concrete Column	Buckling length (m)[++]	Load bearing capacity					
		R 60*		R 90**		R 120***	
		N_u (-kN)	M_u (kNm)	N_u (-kN)	M_u (kNm)	N_u (-kN)	M_u (kNm)
Square Column with μ_{fi}= 0,7	lo= 0,5	2279	---------	1844	--------	1569	--------
	lo= 0,7	2279	---------	1844	--------	1569	--------
	lo= 1,0	2279	---------	1844	--------	1569	--------
	lo= 1,5	2279	---------	1844	--------	1569	--------
	lo= 2,0	650	23	504	20	407	19
	lo= 2,5	535	29	444	28	326	24
	lo= 3,0	467	37	366	33	275	29
	lo= 4,0	405	57	252	41	132	25
Circular Column with μ_{fi}= 0,7	lo= 0,5	1976	---------	1525	--------	1249	--------
	lo= 0,7	1976	---------	1525	--------	1249	--------
	lo= 1,0	1976	---------	1525	--------	1249	--------
	lo= 1,5	1976	---------	420	10	320	8
	lo= 2,0	510	18	260	10	185	9
	lo= 2,5	260	14	170	11	120	9
	lo= 3,0	180	14	120	11	80	8
	lo= 4,0	105	15	70	11	60	11

+for all fire durations and cross-sections: C35/45, S 500,

++the buckling lengths are always equal to column lengths and the original cross-section either in square or circular is 300x300mm+4ϕ16mm or ϕ 300mm+6ϕ16mm,

*the considered reduced square cross-section is 249x249mm with 30mm concrete cover (a) and the considered reduced circular cross-section is ϕ249 with 30mm also concrete cover (a),

**the considered reduced square cross-section is 227x227mm with 35mm concrete cover (a) and the considered reduced circular cross-section is ϕ227mm with 35mm also concrete cover (a),

***the considered reduced square cross-section is 209x209mm with 40mm concrete cover (a) and the considered reduced circular cross-section is ϕ209mm with 40mm also concrete cover (a).

12. Level 3 of calculation, general calculation method (computer program ENSA)

This method may include separate sub-models to determine:

-Development and distribution of the temperature within structural members (thermal response model),

-Mechanical behaviour of the structure or of any part of it (mechanical response model).

Thermal response model shall be based on the main principles and assumptions of the heat transfer theory. The influence of moisture content in concrete may conservatively be neglected.

While the mechanical response model shall be based on the main principles and assumptions of structural mechanics theory, it will be taken into account the changes of the mechanical properties with temperature.

The calculation method offers solutions to two problems in the structural fire design:

(1)Determination of state of equilibrium and deformation of a structure at any time ($_{ti}$) and at given temperature/time development in the environment of the structure, a given load level and a given support conditions,

(2)For structural fire design, the maximum load level (N_u, M_u) of structure can be obtained for a given temperature/time development in it's environment and for a given fire time.

The deformations at ultimate state determined by the calculation method are be limited as necessary to ensure that the compatibility is maintained between all parts of the structure.

The load bearing capacity of individual members, sub-assemblies or entire structures exposed to fire may be determined by the plastic analysis.

In the analysis of individual member or sub-assemblies, the boundary conditions shall be checked and detailed to avoid failure due to the loss of adequate support to the members.

The ultimate load bearing capacity of different members are calculated at R 60 , R 90 and R 120 by ENSA based on the considered cross section of level 1 and another time based on the considered cross section of level 2.

From figures 6 and 7 it can be indicated that, when the minimum square cross-section is considered, the most results from level 1 at R 60 are smaller than those from ENSA, while at R 90 are greater than those from ENSA. The most results from level 2 for all considered fire durations are smaller than those from ENSA.

From figures 8 and 9 it can be indicated that, when the minimum circular cross-section is considered, the most results from level 1 at R60 and R90 are smaller than those from ENSA, but greater than those in level 2. The results from level 2 for all considered fire durations are smaller than those from ENSA.
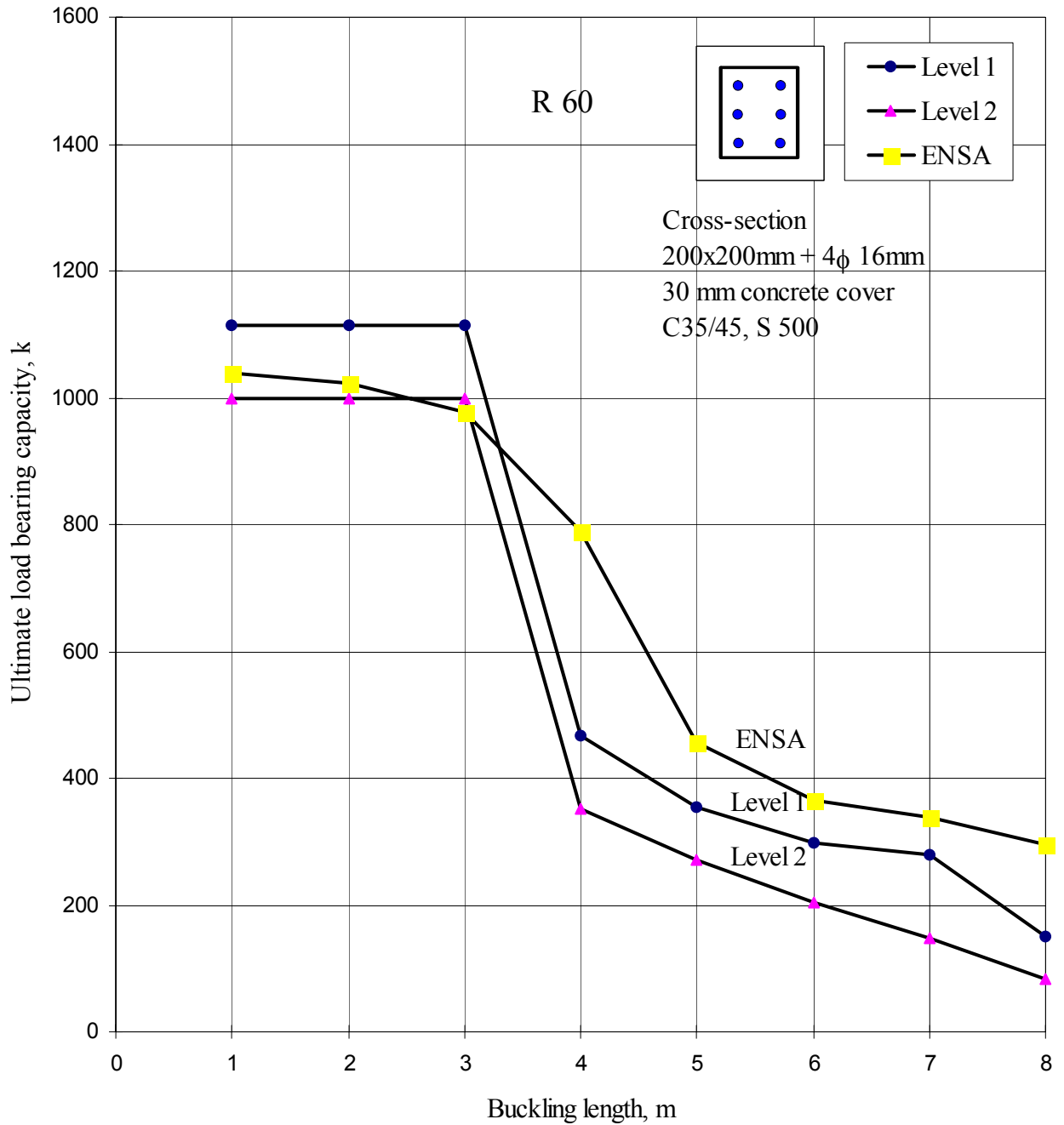
Figure 6: Comparison between level 1, level 2 and ENSA for square reinforced concrete column at 60 minutes when the minimum cross-section suggested in level 1 is considered.
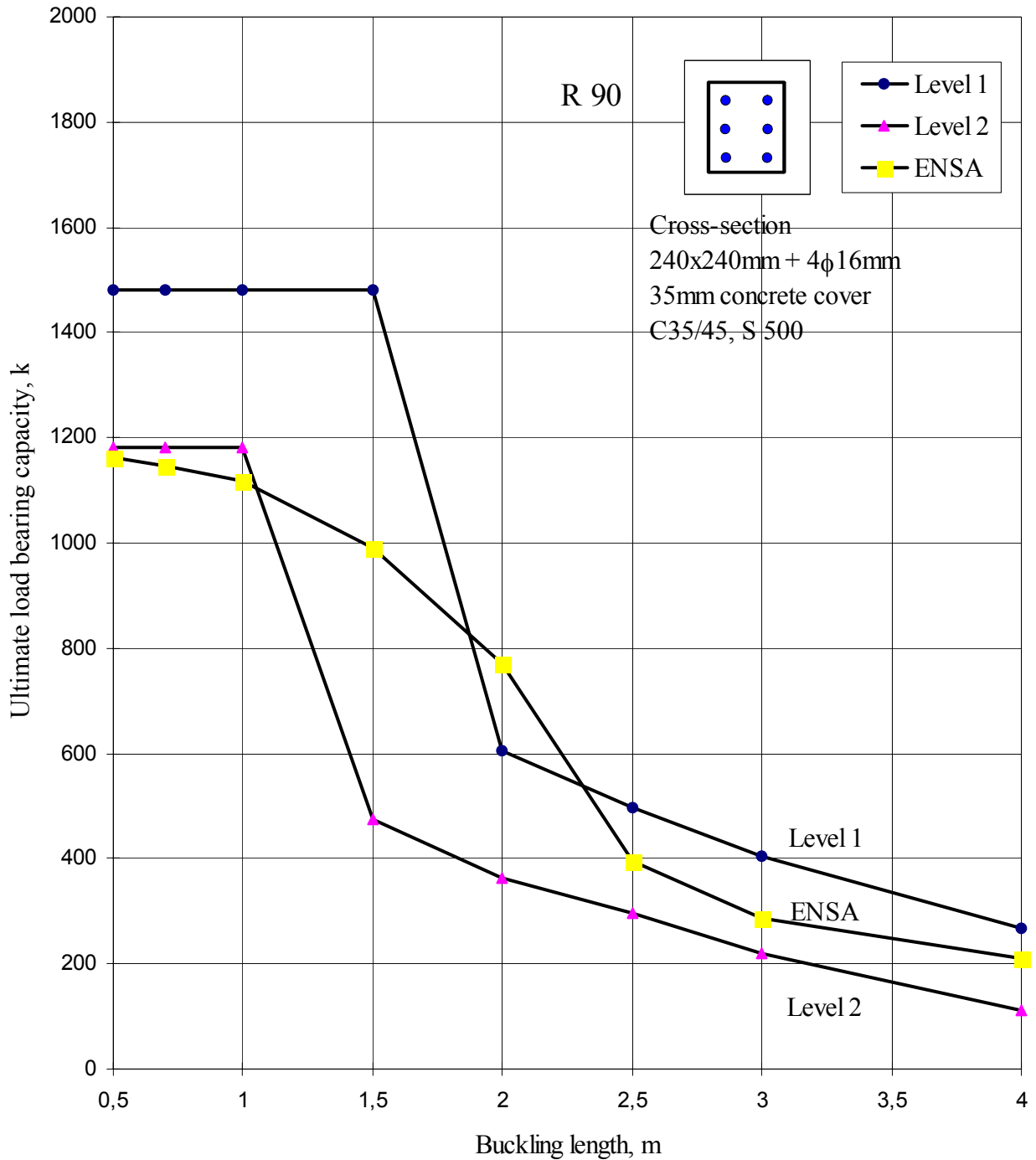
Figure 7: Comparison between level 1, level 2 and ENSA for square reinforced concrete column at 90 minutes when the minimum cross-section suggested in level 1 is considered.
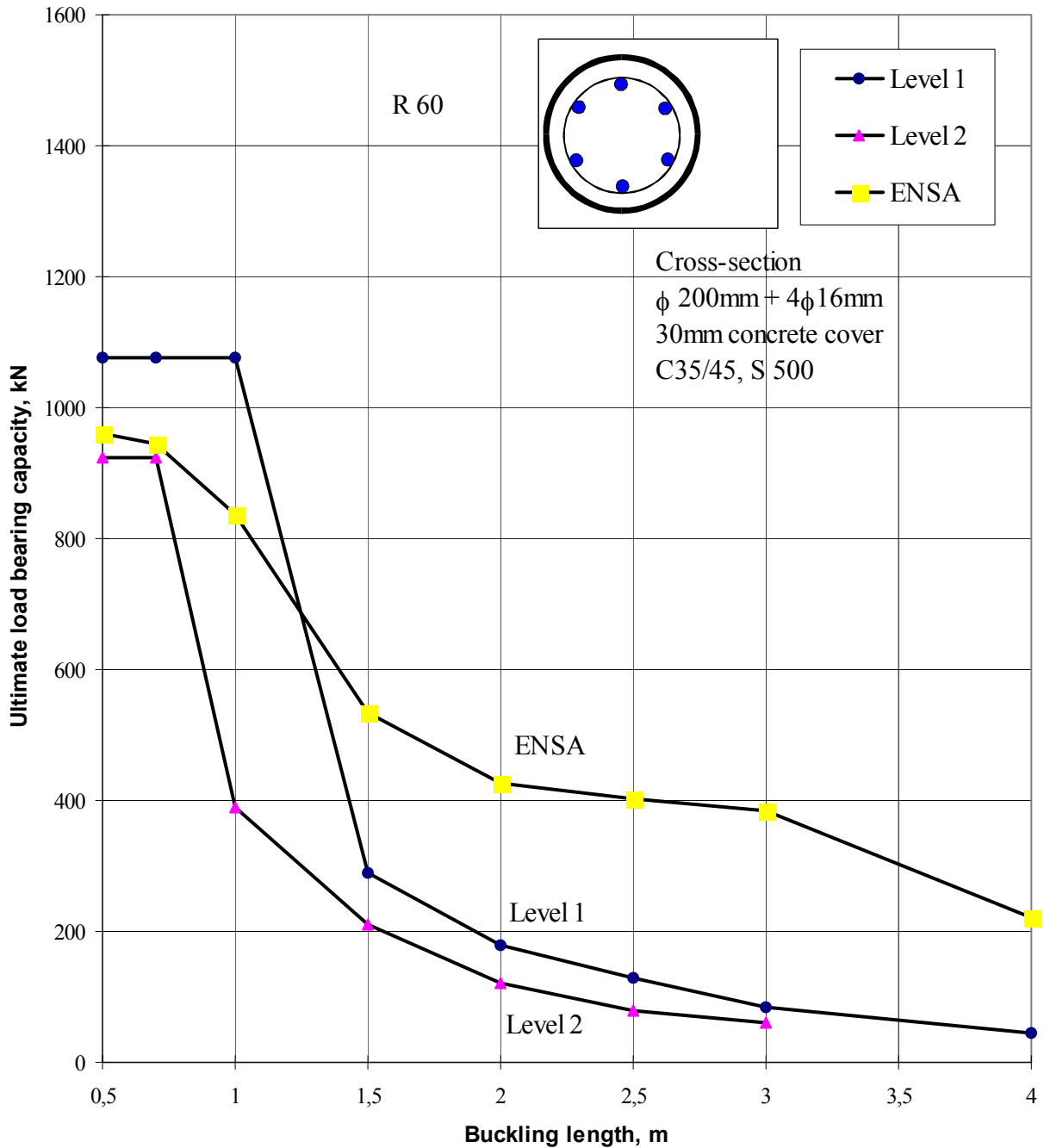
Figure 8: Comparison between level 1, level 2 and ENSA for circular reinforced concrete column at 60 minutes when the minimum cross-section which suggested in level 1 is considered.
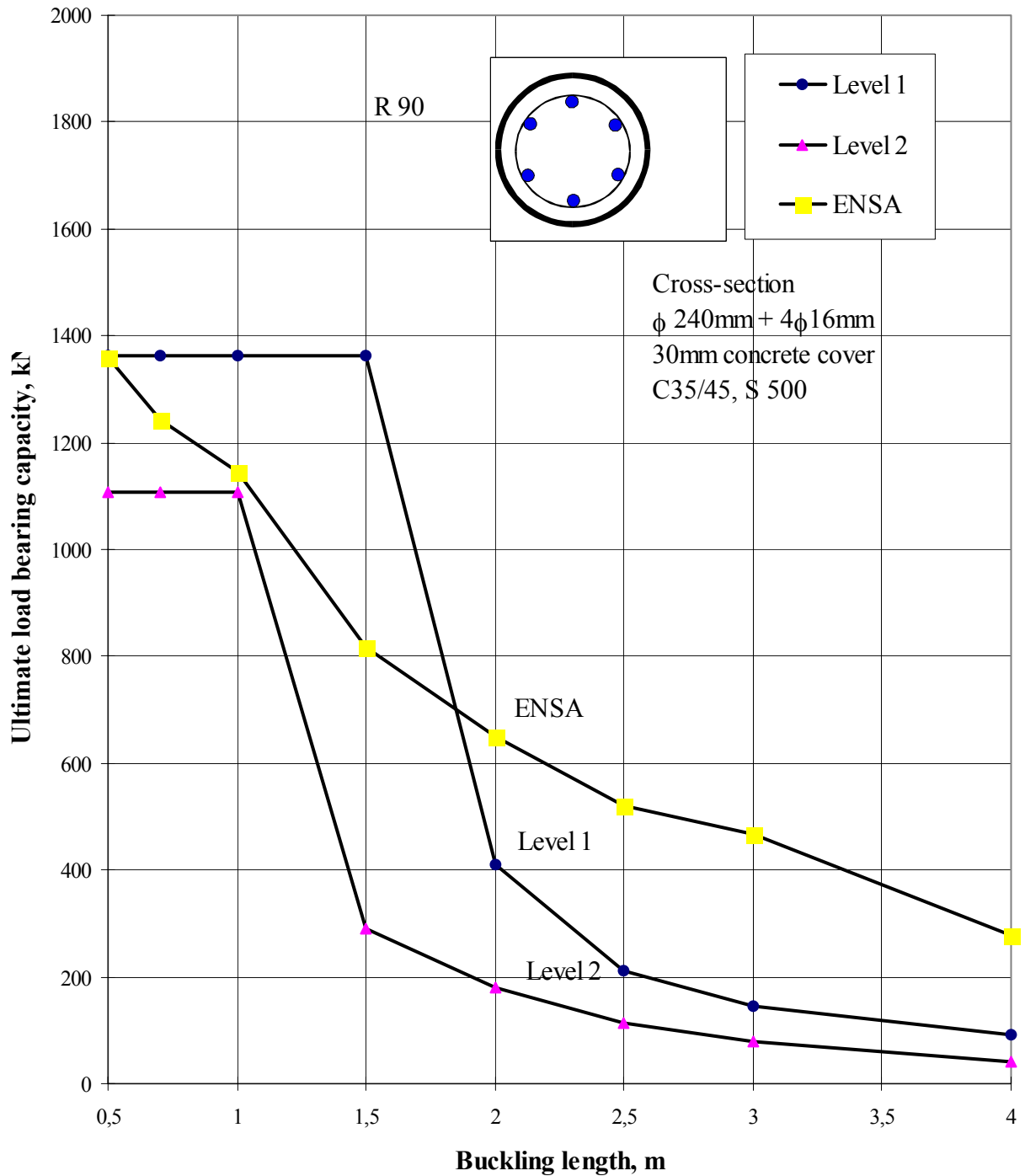
Figure 9: Comparison between level 1, level 2 and ENSA for circular reinforced concrete column at 90 minutes when the minimum cross-section which suggested in level 1 is considered.

13. Conclusion:

This investigation dealt with a detailed study on the methods incorporated in the Eurocode as regards the design of reinforced concrete columns columns for resisting fire at different fire durations.

It is necessary to cover different topics relevant to the components of reinforced concrete. Some of it's basic characteristic properties; mechanical and thermal and how far they can affected by heat or fire. The time-temperature relationship, which as considered by ISO 834, is also defined.

This investigation referred to the principles of design of reinforced concrete columns as quoted in the Eurocode regarding design for fire.

As one of the calculation methods (level 3) is based on a computer program (ENSA) which is, to some extent complicated.

The next phase of this investigation dealt with extensive calculations based on the code and covering wide range of parameters: different temperatures, different periods of fire exposure, different element properties and different buckling lengths.

As the data are too many and for space limitation, the results have been given, mainly, in the form of figures and discussions dealt with these figures.

As general, the difference between the results from both level 1 and level 2 to those from ENSA is not from the used materials law. There is no significant difference between the materials law which used in level 1 and level 2 and ENSA.

The previous difference between the results is may be attributed to the suggested approximate methods in both level 1 and level 2. Now 4, it can be said or suggested that these approximate methods in level 1 and level 2 must be reworked in order to get a smaller difference between level 1, level 2 and a proved computer program (for example ENSA).

As regards the methods recommended for design for fire comparisons and analyses have pointed out that while some of these methods can be applied successfully others suffer from lack of accuracy within some ranges of applications. Such inaccuracy is sometimes accompanied by non-safety.

It remains of importance, that the Eurocode user or reader should be acquainted with the findings of the present investigation in the form of recommendations and/or limitations and/or design procedures and/or precautions.

References

[1] Klingsch W., Wittbecker F.-W.: "Numerical analysis of complete frame structures in fire cases", International Meeting of Fire Research and Test Centres 1986.

[2] Klingsch W., Wittbecker F.-W.: "Structural fire engineering of complex frames by means of Micro-Computer Application", 2nd I.A.F.S.S. Symp. , Tokyo 1988.

[3] Litzner H.-U.: "Design principles according to Eurocode 2 with regard to the specific aspects of precast concrete elements", Betonwerk und Fertigteil Technik Journal 1993.

[4] Petzold A. , Röhrs M. :"Concrete for high temperatures", 1970.

[5] Pagni P.-J., Grant C.-E.: "Fire safety Science", 1rst I.A.F.S.S. Symposium, U.S.A. 1986.

[6] Grant C.-E.: "Fire Safety Science", 2nd I.A.F.S.S Symp. 1989.

[7] Rußwurm D., Bunke N., Krampf L.: "Bauen in Europa", Weiterbildungsseminar, Institut für Baustoffe, Massivbau und Brandschutz der T. U. Braunschweig 1990.

[8] Eurocode No.2 Part 10: "Structural Fire Design for Concrete Structures", 1990.

[9] Eurocode Actions Chapter 20: "Actions on Structures exposed to Fire", 1990.

[10] Jensen und Chenoweth: "Applied strengths of materials", 1975.

[11] Eurocode No.2 Part 1: "Design of Concrete Structures; General Rules and Rules for Building", 1989.

[12] Raymond C.-R.: "Structural Engineering Handbook", 1968.

[13] Malhorta H.L.: "Design of Fire Resisting Structures", 1982 .

[14] Lohmeyer G.: "Stahlbetonbau". Bemessung, Konstruktion, Ausführung, 1990.

[15] Anderberg Y. and Thelandersson S.: "Stress and deformation characteristics of concrete at high temperatures", Lund Institute of Technology, Division of structural mechanics and concrete construction, Bulletin 54, Lund 1976.

[16] DIN 1045: "Beton und Stahlbeton". Bemessung und Ausführung, 1978.

[17] Klingsch W.: "Numerical analysis of structures in fire case for micro computer application, 1989.

[18] Institution of Structural Engineers: "Design and detailing of concrete structures for fire resistance". The Concrete Society, London, 1978.

[19] Kordina K. und Klingsch W.: "Failure load of slender reinforced concrete columns under elevated temperature using a two and three dimensional discretisation", International Symposium on Discrete Methods in Engineering, C.I.S.E-Segrate, Milan, 1974.

[20] Sargin M.: "Stress-strain relationships for concrete and analysis of concrete sections", Study No.4, Solid Mechanics Division, University of Waterloo, Ontario, Canada 1971.

[21] Cruz C.R.: "Elastic properties of concrete at high temperatures", Journal of PCA, Research and Development Laboratories, 1966.

[22] Allen D.E., Lie T.T.: "Calculated fire resistance of reinforced concrete walls and rectangular columns", 1976.

[23] Tulin L.G., Gerestle H., Sanez L.: "Equation for stress- strain curve of concrete" ACI Journal, Proceedings Vol. 61, No.9 1964.

[24] Eurocode 2: "Design of concrete structures, Part 1-2: Structural fire design", October 1993.

[25] Hertz K.: "Design of fire exposed concrete structures", Institute of building design . Report No. 160, Technical University of Denmark, 1981.

[26] Lösert B., Löser H., Wiese H., Stritzke J.: "Bemessungsverfahren für Beton - und Stahlbetonbauteile", 1986.

[27] Wommelsdorff O.: "Stahlbetonbau, Bemessung und Konstruktion, Teil 2 Stützen und Sondergebiete des Stahlbetonbaus", 1993.

[28] Grasser E., Kordina K. und Quast U.: "Bemessung von Beton-und Stahlbetonbauteilennach DIN 1045", Deutscher Ausschuß für Stahlbeton, Heft 220, Dezember 1978.

[29] Becker F., Bizri H. and Bresler R.: "Fires-T-A computer program for the fire response of structures thermal. Report No. UCB FRG 74-1", Brekely, U.S.A., 1974.

[30] Klingsch W.: "Traglastberechnung instationär thermisch belasteter schlanker Stahlbetondruckglieder mittels zwei- und dreidimensionaler Diskretrisierung", 1976.

[31] Klingsch W., Muess und Wittbecker F.-W.: "Ein baupraktisches Nährungsverfahren für die brandschutztechnische Bemessung von Verbundstützen", Springer Verlag 1988.

[32] Elsevier: "European Convention for constructional steelwork, recommendations for the fire safety of steel structures, calculation of the fire resistance of load bearing elements and structures assemblies exposed to the standard fire", 1983.

[33] Klingsch W. und Würker K.G.: "New developments in fire resistance of hollow section structures", Symposium on hollow structural sections in building construction, September 1985.

[34] Grasser E., Kordina K. und Quast U.:"Bemessung von Beton- und Stahlbetonbauteilen nach DIN 1045", Deutscher Ausschuß für Stahlbeton, Heft 220, Dezember 1978.

DESIGN OF CONCRETE COLUMNS BASED ON EC2 TABULATED DATA - A CRITICAL REVIEW

Jean-Marc FRANSSEN
Univ. of Liege, 1, Chemin des Chevreuils, 4000, Liège 1, Belgium
jm.franssen@ulg.ac.be

ABSTRACT

ENV 1992-1-2, the fire part of the concrete Eurocode, proposes different tables for the design of simple concrete elements submitted to the ISO fire. Table 4.1 is the table valid for concrete columns. For six fire resistance times R_f = 30, 60, 90, 120, 180 and 240 minutes, and for three load ratio μ_{fi} = 0.2, 0.5 and 0.7, an acceptable solution is given in term of the minimum dimension of the section b_{min} and axis distance a from the re-bar to the edge of the section.

The application of this table is not as easy as one could believe at first glance especially when it comes to assessing the fire resistance time of existing elements which are different from the recommended solutions. This is because a double interpolation has to be done, on R_f and on μ_{fi}, because the criteria is based on 2 different variables, b_{min} and a, and because the load ratio is not available from the room temperature design (not to mention the complication created by clause 4.2.3 (6)). In this paper, a graphic is presented that allows an easier application of this table 4.1.

This table has been compared with experimental test results from the University of Braunschweig, the University of Gent, the University of Liege and the National Research Council of Ottawa. It appears that virtually no correlation exists between the results predicted by the table and the results of the tests. Even more alarming is the fact that there is a systematic tendency of the table to yield unsafe results.

An alternative table is presented here, accompanied by a simple calculation equation that allows to easily derive the fire resistance for situations that are different from the ones proposed in the table.

KEYWORDS: *fire resistance, concrete, column, reinforced concrete, Eurocode, fire test*

INTRODUCTION

Three different levels are proposed in the Eurocodes for structural fire design: the tabulated data, the simplified calculation method and the general calculation method. Tabulated data provide detailing according to recognised design solutions that are valid for member analysis and for the standard fire exposure. According to the Eurocodes,

"The tables have been developed on an empirical basis confirmed by experience and theoretical evaluation of tests. Therefore, this data is derived from approximate conservative assumptions…".

Unfortunately, there are several sections in several of the fire Eurocodes for which such a thing as a fully documented and generally accepted background presented in a publication submitted to a peer review is simply non existent.

This is the situation for Table 4.1 of Eurocode 2 Part 1-2 [1] presented as a tabulated data for reinforced concrete columns. It is therefore difficult to judge on the validity and on the conservative character of this table. In fact, on the base of a limited number of comparisons with test results, some doubts were raised about the fact that the results provided by this table are conservative.

This paper presents the results of an extensive analysis in which the results provided by Table 4.1 have been compared to the results of experimental tests.

WHAT IS TABLE 4.1 FOR REINFORCED CONCRETE COLUMNS?

The table gives minimum section dimensions b_{min} and axis distance of the re-bars a for different load levels μ_{fi} and different fire resistance times R_f. As far as columns exposed on more than one side are concerned, Table 4.1 of Eurocode 2 is summarised in Table 1 of this paper.

R_f	$\mu_{fi} = 0.20$	$\mu_{fi} = 0.50$	$\mu_{fi} = 0.70$
30 min.	150 / 10*	150 / 10*	150 / 10*
60 min.	150 / 10*	180 / 10*	200 / 10*
90 min.	180 / 10*	210 / 10*	240 / 35
120 min.	200 / 40	250 / 40	280 / 40
180 min.	240 / 50	320 / 50	360 / 50
240 min.	300 / 50	400 / 50	450 / 50

Table 1 : tabulated data for reinforced concrete column

The symbol * in this table means that *"Normally the cover required by ENV 1992-1-1 will control"*. It is desirable here to chose a value of the axis distance a_{req} which represents what would normally be required by ENV 1992-1-1. According to Table 4.2 of ENV 1992-1-1, the concrete cover cannot be less than 15 mm in a normally dry building, i.e. class 1a according to Table 4.1.

- For 12 mm longitudinal re-bars and 6 mm stirrups, this yields a_{req} = 15+6+12/2 = 27 mm. This is the smallest possible value of a_{req}.
- For 25 mm longitudinal re-bars, the cover must not be smaller than 25 mm. With a tolerance of construction of 5 to 10 mm, the value of a_{req} recommended by ENV 1992-1-1 could be as high as 40 mm.

In this paper, a fixed value of a_{req} = 35 mm will be considered as the value required by ENV 1992-1-1. Table 2 can therefore be used instead of Table 1.

R_f	$\mu_{fi} = 0.20$	$\mu_{fi} = 0.50$	$\mu_{fi} = 0.70$
30 min.	150 / 35	150 / 35	150 / 35
60 min.	150 / 35	180 / 35	200 / 35
90 min.	180 / 35	210 / 35	240 / 35
120 min.	200 / 40	250 / 40	280 / 40
180 min.	240 / 50	320 / 50	360 / 50
240 min.	300 / 50	400 / 50	450 / 50

Table 2 : tabulated data for reinforced concrete column, a_{req} taken into account

The value of a_{req} is important not only in the cases where the symbol * was present in Table 1, but also because of clause 4.2.3 (6) of ENV 19929-1-2. This clause says:

> *"Where the actual width ... b of column is at least 1.2 times the minimum value b_{min} given in Table 4.1 the axis distance a may be reduced to a value not less than a_{req}. Linear interpolation of a may be used for values b/b_{min} between 1 and 1.2".*

Figure 1 is a graphical expression of the admissible solution for a fire resistance R_f of 120 minutes and a load ratio μ_{fi} of 0.50. The solution is based on 250 / 40 and on clause 4.2.3 (6) in which a_{req} = 35 mm has been taken into account. This clause says that a can be as low as a_{req} = 35 mm, provided that b is greater than 1.2 b_{min} = 1.2 x 250 = 300 mm. The linear interpolation is clearly seen as cutting the corner of the curve. Every solution in the upper right part of the figure can be considered as yielding a fire resistance of 120 minutes or more.
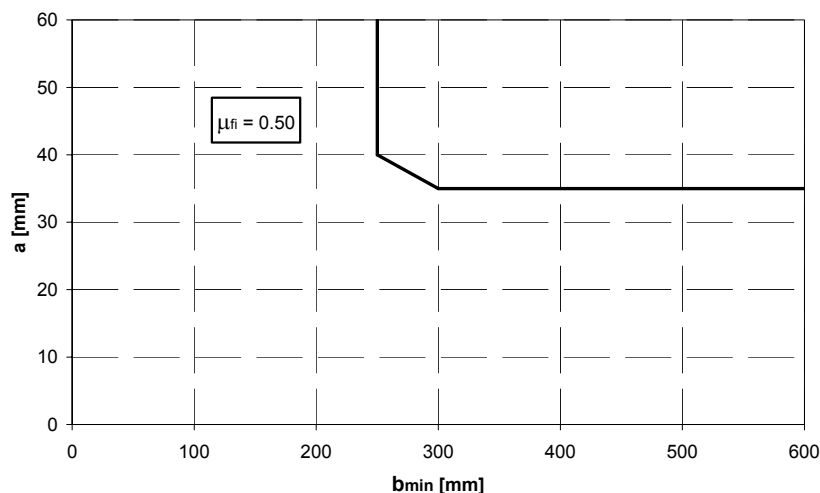
FIGURE 1 : Solution for R_f = 120 min.

Figure 2, 3 and 4 give, for load ratio μ_{fi} = 0.2, 0.5 and 0.7, the different zones leading to different fire resistance times. Other graphs can be made for other load ratio, for example 0.3, 0.4, and 0.6, assuming also a linear variation of the parameters as a function of the load ratio.
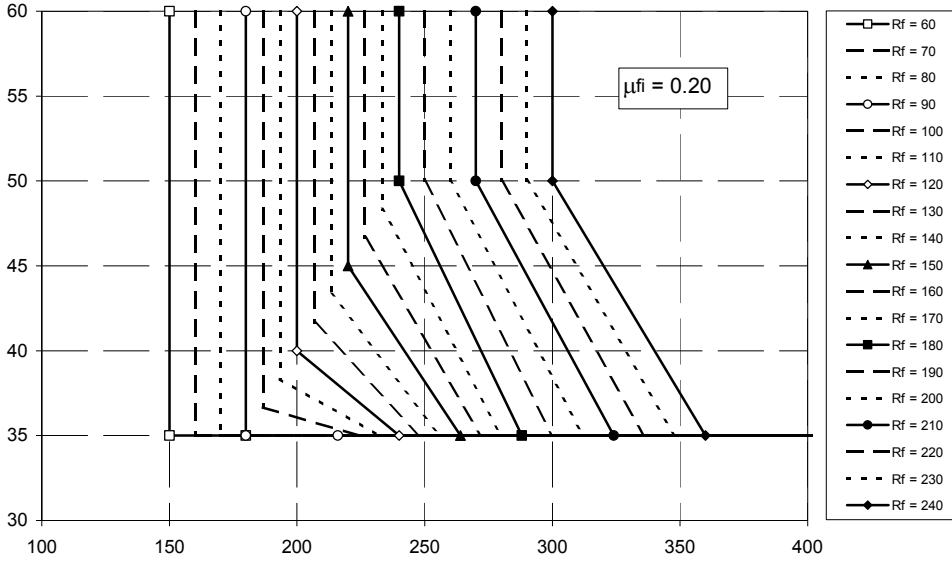
FIGURE 2 : Solution for μ_{fi} = 0.20.
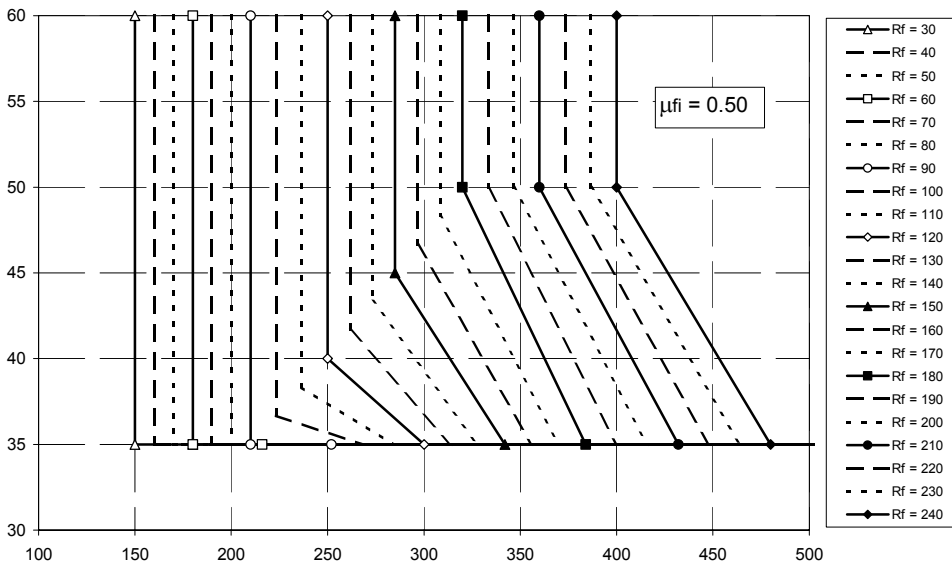
FIGURE 3 : Solution for μ_{fi} = 0.50 .
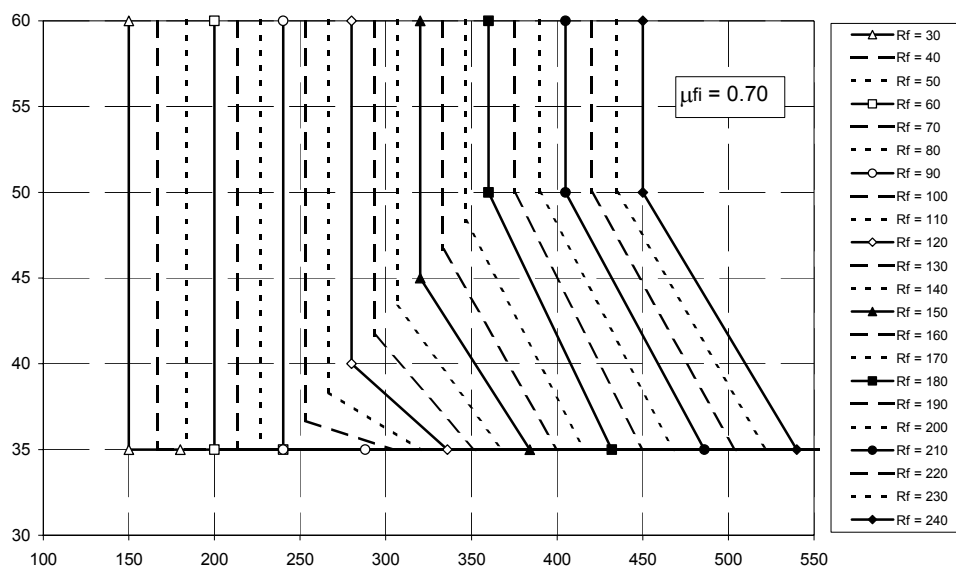
FIGURE 4 : Solution for $\mu_{fi} = 0.70$.

It is essential to have a clear idea of the correct definition of μ_{fi} . It is defined by equation 1.

$$\mu_{fi} = E_{d,fi} / R_{d,fi}(0) \tag{1}$$

with $\quad E_{d,fi} \quad$ design effect of actions in the fire situation,

$\quad\quad R_{d,fi}(0)$ design load bearing capacity (resistance) in the fire situation at time $t = 0$.

This ratio may appear as the most rational choice for expressing the variable supposed to influence the fire resistance time. It has yet to be recognised that it is based on a quantity, $R_{d,fi}(0)$, which is not directly provided by the design of the structure at room temperature. A specific calculation is required in order to obtain this value and it can only be made by one of the calculation methods, hopefully the simplified calculation method, whereas the main purpose of the tabulated data is to avoid any calculation! If the author of the project has to calculate $R_{d,fi}(0)$ at time $t = 0$ in order to use the tabulated data, he might as well directly apply the same simplified calculation method at time t in order to calculate $R_{d,fi}(t)$!

Table 3 shows the comparison between the load ratio μ_{fi} which is proposed in the Eurocode and the load ratio υ_{fi} that will be used in the alternative method proposed in the next section of this paper. This comparison is made in Table 3 for the very simple case of a centrally loaded short column. The calculations would of course be much more complex if the load is applied with an eccentricity or if the slenderness of the column has to be taken into account, see appendix 1.

	EC2 - Part 1-2	New proposal
Variable	μ_{fi}	υ_{fi}
Definition	$\mu_{fi} = E_{d,fi} / R_{d,fi}(0)$	$\upsilon_{fi} = E_{d,fi} / R_d$
with	$E_{d,fi}$ = design effect of actions in the fire situation	$E_{d,fi}$ = design effect of actions in the fire situation
and	$R_{d,fi}(0)$ = design resistance in the fire situation at time $t = 0$	R_d = design resistance for normal temperature design
Example for short column	$R_{d,fi}(0) = A_s f_y + A_c f_{c,k}$	$\begin{aligned} R_d &= A_s \frac{f_y}{\gamma_s} + A_c\, 0.85 \frac{f_{c,k}}{\gamma_c} \\ &= A_s \frac{f_y}{1.15} + A_c\, 0.85 \frac{f_{c,k}}{1.5} \end{aligned}$

Table 3 : comparison between two different load ratio

COMPARISON BETWEEN EUROCODE AND EXPERIMENTAL RESULTS

The results provided by Table 4.1 of Eurocode 2 have been compared with the results of experimental tests made in Belgium, University of Liege and Gent [2], in Germany, Technical University of Braunschweig [3], and in Canada, Fire Research Station in Ottawa [4]. A total of 82 test results have been considered. The result of this comparison is shown on Figure 5. On this figure, it is quite clear that the tests made in Belgium were calibrated to investigate the fire resistance period of 2 hours where a gap existed between the German tests, usually around one hour, and the Canadian tests, three to four hours. It can be seen that the application of the recommendations of Table 4.1 leads to results on the unsafe side. The average value of all the ratio R_f(EC2) / R_f(Test) is 1.71. It means that the existing calculation method based on Table 4.1 overestimates the fire resistance of columns by a factor which, in the average, has a value of 1.71. The standard deviation of the population is 0.69, leading to a coefficient of variation of $0.69/1.71 = 0.41$.
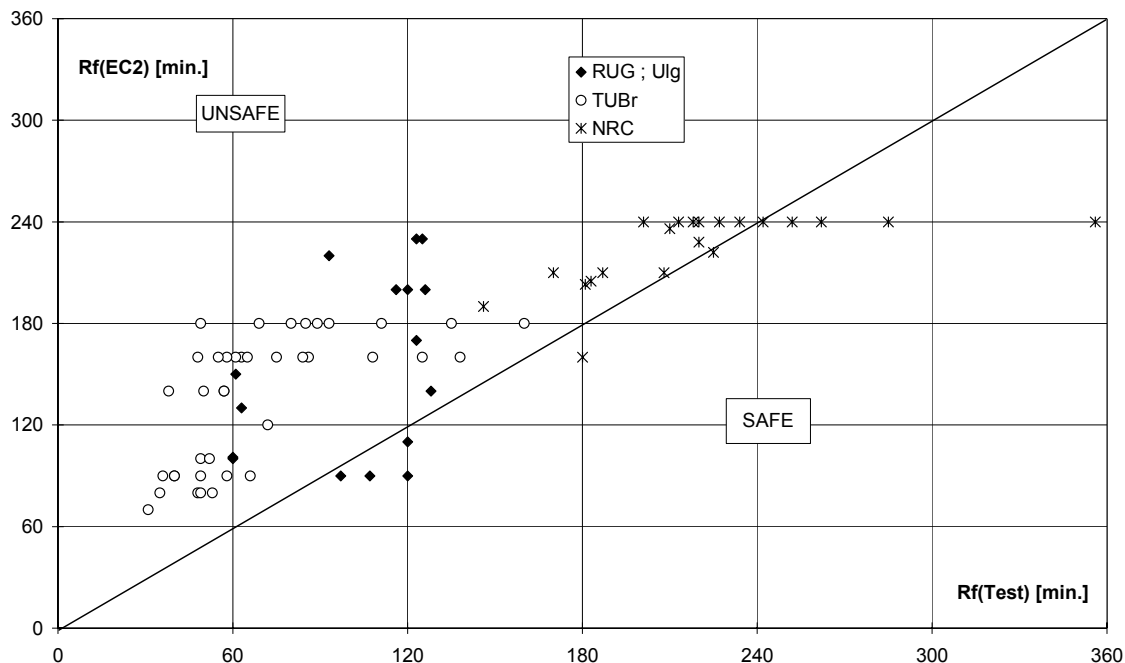
FIGURE 5 : Comparison between EUROCODE and tests

NEW PROPOSAL

The situation depicted in Figure 5 motivated a research project having as an objective to present an alternative design method. The methodology was the following.

1. An extensive parametric investigation was first performed with the numerical code SAFIR of the University of Liege [5] in order to highlight the influence of different parameters on the fire resistance.

2. Additional experimental programs were performed in Belgium, [6] and [7], in order to investigate some effects on which it was impossible to conclude from other previously performed tests (the results of these new test series are incorporated in Figure 5). Most of the tests have been performed at the University of Gent on columns 3.95 m high, while a few tests on 2.10 m high columns have been performed at the University of Liege. The following parameters have been examined : load level, massivity (dimensions of the cross sections), length, diameter of the longitudinal reinforcement and structural detailing, concrete cover, load eccentricity, concrete strength. A lot of observations could be made from these test results.

   - Columns including reinforcement with a large diameter (ϕ = 25 mm) present fire resistance times much smaller than those expected from theoretical estimation, mainly because of extensive corner spalling occurrence. Such premature failures have practically not been observed with ϕ 16 or ϕ 12 reinforcement. It has also been noticed that the use of 8 ϕ 16 instead of 4 ϕ 25 leads to a substantial improvement.

   - Experimental results displayed a rather wide scatter.

   - Corner spalling has been observed in many tests, more frequently in Gent than in Liege. In this latter case, very few spalling was detected, but large cracks along the

bearing reinforcements could often be seen. The length of the columns and the end conditions, not similar in Gent and in Liege, can partly explain these differences.

- The influence of the load level, the massivity and the length corresponds to what could be expected : the increase of the load level and of the length, and a decrease of the cross-section lead to a decrease of the fire resistance.
- The increase of concrete cover has a positive effect on the fire resistance or on the admissible load level. This influence, however, seems less important than the one resulting from FIP/CEB Recommendations and Eurocode 2.

3. A simple model was established which took account of all most sensitive parameters.

4. The model was calibrated on the base of the experimental results.

The new model for assessing the fire resistance R_f of reinforced concrete columns is based on the following formula :

$$R_f = 120 \left[\frac{R_{f,\upsilon} + R_{f,a} + R_{f,L} + R_{f,b'} + R_{f,n}}{120} \right]^{1.8} \tag{2}$$

in which

$$R_{f,\upsilon} = 83 \left(1 - \upsilon_{fi} \right) \tag{3}$$

$$\upsilon_{fi} = \frac{E_{d,fi}}{R_d} \tag{4}$$

υ_{fi} takes into account the load ratio, in which the crushing strength of the column is included, as well as the effects of bending and second order effects.

$$R_{f,a} = 1.6 \left(a - 30 \right) \tag{5}$$

with *a* the axis distance in mm of the steel to the nearest exposed surface, see Fig. 6.
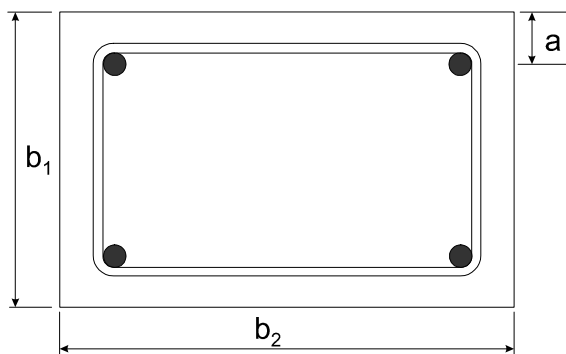
FIGURE 6 : Definition of *a*, *b₁* and *b₂*

$$R_{f,L} = 9.6 \left(5 - L \right) \tag{6}$$

with L the buckling length of the column in m.

$$R_{f,b'} = 0.09 \, b' \tag{7}$$

with $b' = \frac{4A}{p}$ in mm.

For Fig. 6, $b' = \dfrac{2 b_1 b_2}{b_1 + b_2}$

$R_{f,n} = 0$ for n ≤ 4   (8)

$R_{f,n} = 12$ for n > 4

with n the number of longitudinal bars.

Figure 7 presents the comparison of the results obtained by the new model and the results of the experimental tests. The average value of the ratio R_f(model) / R_f(test) is equal to 1.01 and the standard deviation is equal to 0.23
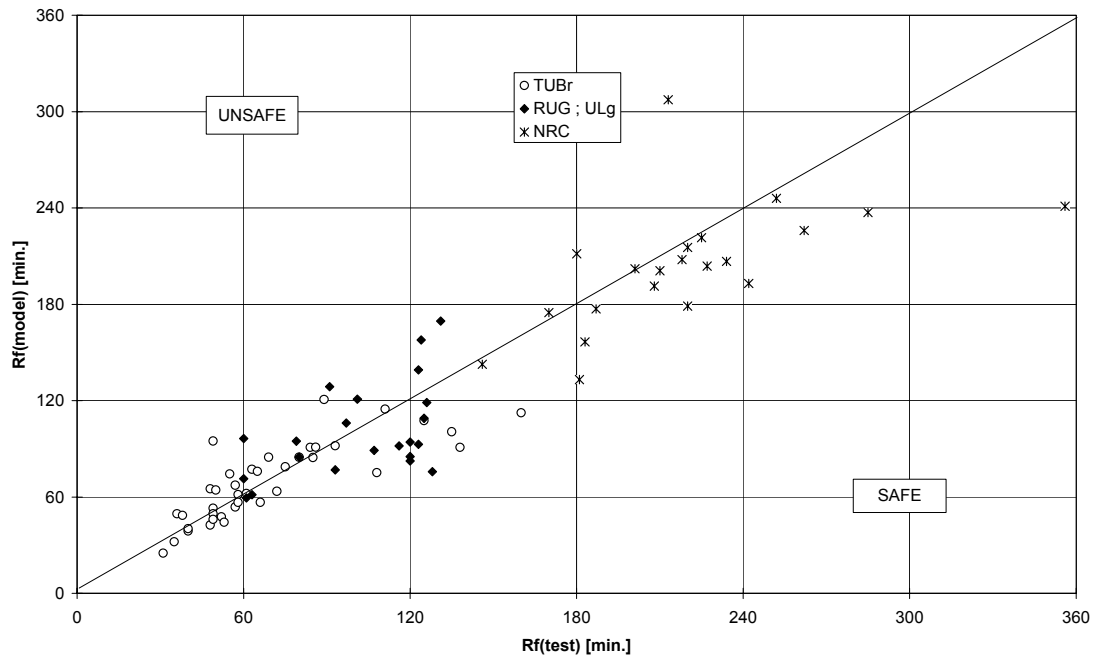
FIGURE 7 : Comparison between new model and tests

Even if an equation is proposed, see Eq. 2, which allows the calculation of the fire resistance for any combination of the parameters, the proposed model must anyway be seen as belonging to the family of the *tabulated data*. Indeed, the proposed equation is just a best fit equation; it is not based on any consideration of equilibrium. In this sense, the field of application of this model is restricted, for each parameter, to the range in which experimental values exist. Allowing anyway very limited extrapolations on some parameters, the field of application is:

Load level	$0.15 \le \upsilon_{fi} \le 0{,}80$
Dimensions of the section	$200 \le b' \le 450$ mm
	$b_2 \le 1.5\, b_1$
Concrete cover	$25 \le a \le 80$ mm
Length of the column	$1.50 \le L \le 6.00$ m

Reinforcement ratio	$0.9\,\% \leq A_s/A_c \leq 4.0\,\%$
Concrete strength	$24 \leq f_{cm} \leq 53$ MPa
Eccentricity	$e \leq 15$ cm
Diameter of the bars	$\phi < 25$ mm

It has been verified that the model gives a safety level which is not dependent of either the load level, the width of the section, the concrete cover or the length of the column. It can be noticed that the linear best regression among the points is virtually equal to the horizontal line at level R_f(model) / R_f(test)= 1.00 in all figures from Fig. 8 to Fig. 11
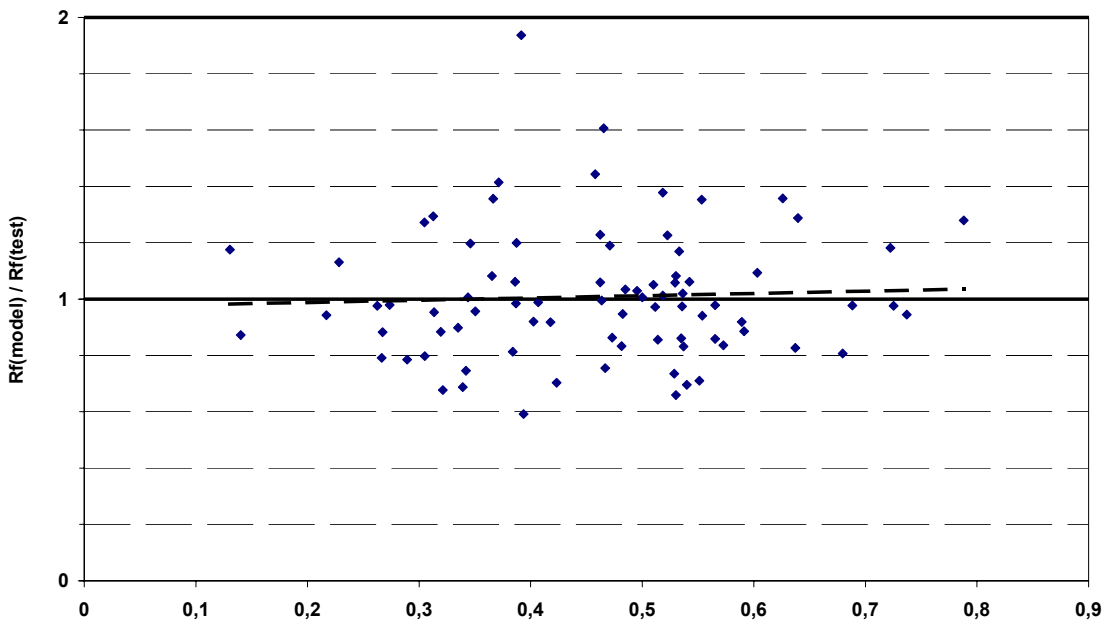
FIGURE 8 : R_f(model) / R_f(test) as a function of υ_{fi}
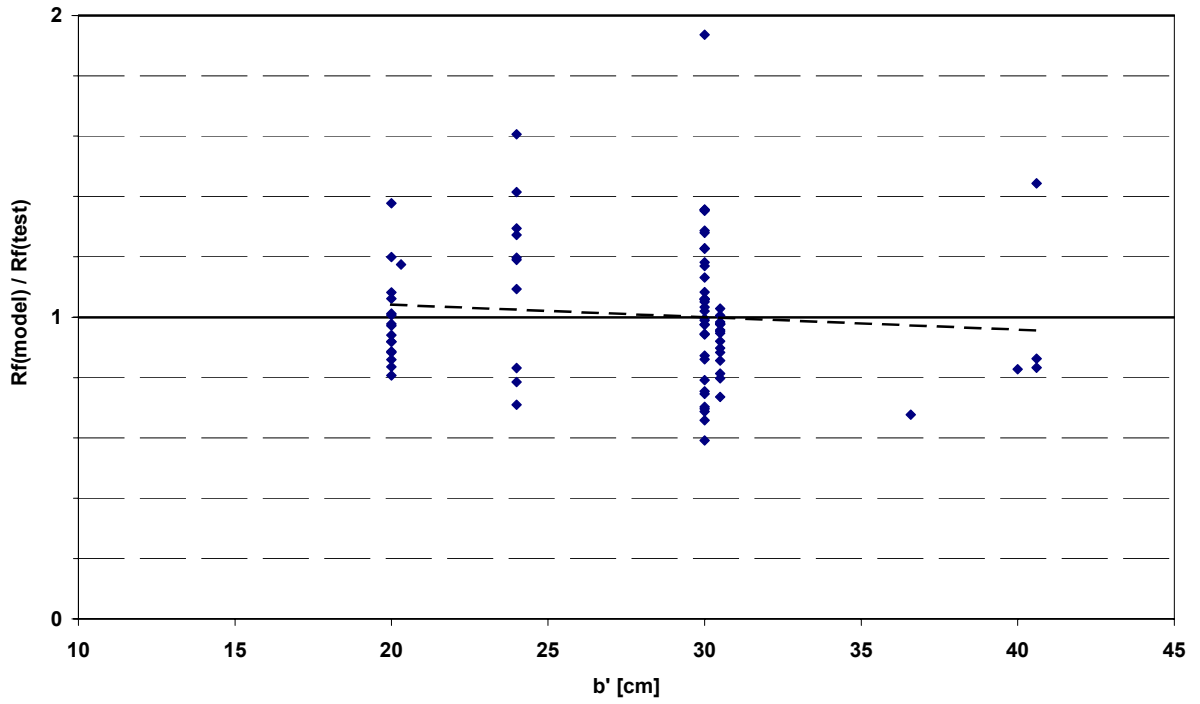
FIGURE 9 : R_f(model) / R_f(test) as a function of $b\,'$
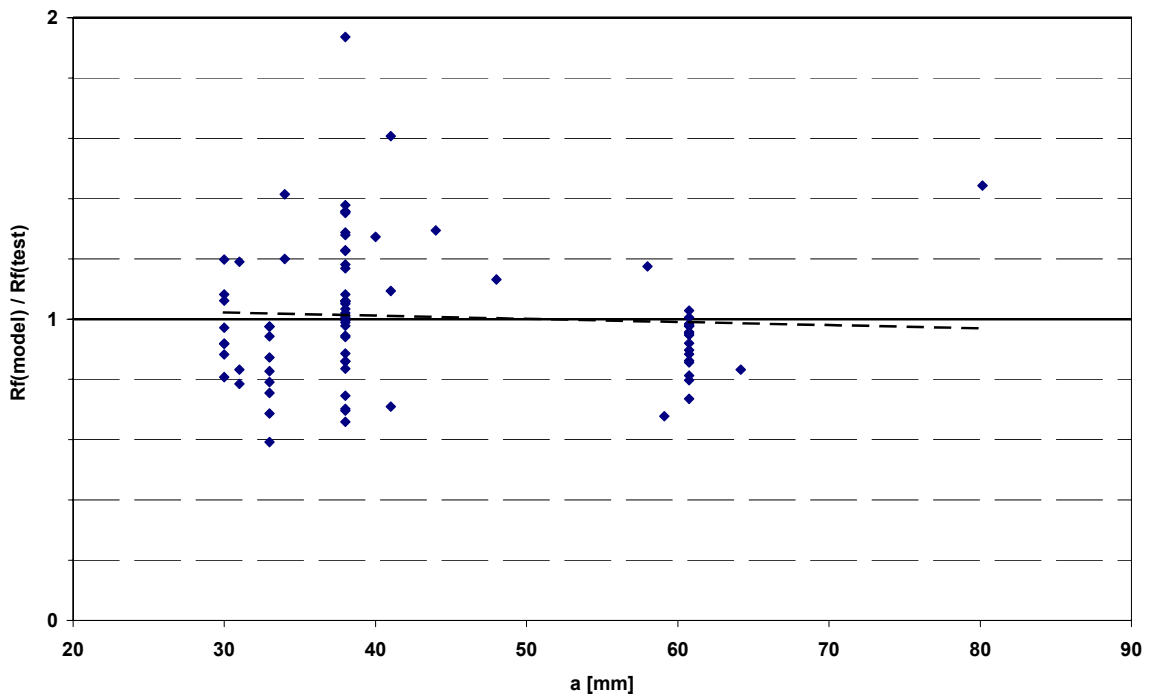
FIGURE 10 : R_f(model) / R_f(test) as a function of a
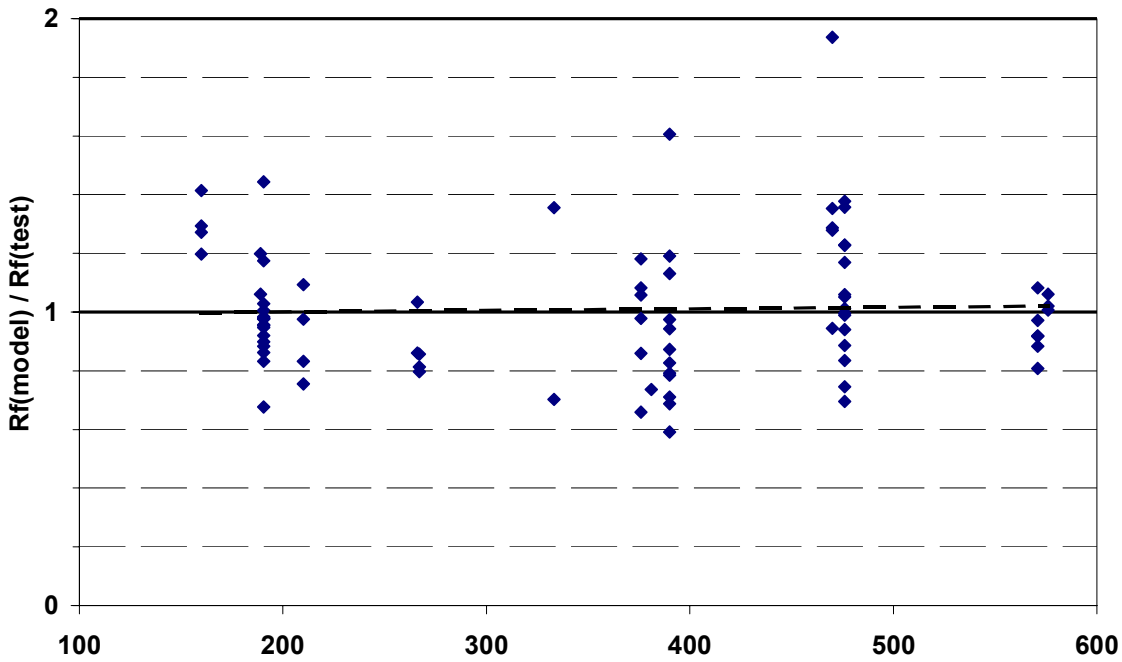
FIGURE 12 : R_f**(model) /** R_f**(test) as a function of** *L*

Notes :

1. *In the interpretation of the tests which has been made in order to calibrate the model and to draw figures 5 and 8, the* <u>measured average values</u> *of the mechanical properties of concrete and steel have been taken into account. In a normal design process, the* <u>characteristic values</u> *of these properties shall be used and this will introduce, in the average, an additional safety margin.*

2. *A new series of tests has been recently performed in Liege on 4 short columns with a circular section. The diameter was 30 cm and 2 columns had 6 φ 12 and 2 had 6 φ 20. The resistance times were, expressed as (model ; test), the following*

   (166 ; 156)

   (143 ; 131)

   (179 ; 187)

   (160 ; 163)

In order to retain the simplicity of the presentation of the tabulated data, a table similar to table 1 or 2 of this paper, i.e. table 4.1 of the Eurocode, can be established with the new model. This is table 4 presented here bellow, valid for a buckling length *L* of 3 meters. In this table, two different possibilities have been proposed for several of the combinations fire resistance – load level. One solution is a wide section with a normal concrete cover, the other one is a normal section with a more important concrete cover.

Standard fire resistance	Minimum dimensions (mm) Column width b_{min}/axis distance a of the main bars			
	Column exposed on more than one side			Exposed on one side
	$\upsilon_{fi} = 0.2$	$\upsilon_{fi} = 0.5$	$\upsilon_{fi} = 0.7$	$\upsilon_{fi} = 0.7$
R 30	200/25	200/25	200/25	140/25
R 60	200/25	200/35 250/30	200/45 300/30**	140/25
R 90	200/30 300/25	300/40 350/30**	300/45** 450/35**	140/25
R 120	250/40 300/30**	300/45** 450/35**	350/50** 450/45**	160/35
R 180	350/45**	350/60**	450/65**	210/55
R 240	350/60**	450/70**	450/80**	270/70
** Minimum 8 bars				

Table 4 : tabulated data for reinforced concrete column – new proposal

It is not easy to compare table 2 and table 4 because they are based on a different definition of the load ratio. Anyway, under the realistic following hypotheses:

$A_s = 0.0085 \ A_c$

$f_y = 500$ Mpa

$f_c = 25$ Mpa

one obtains the following relation that gives an idea of the ratio that might exist between the two different definition of the load level

$\mu_{fi} = 0.6 \ \upsilon_{fi}$

Thus, column 3 of Table 2, for example, should be compared with column 4 of Table 4. It can be observed that the new proposal is by far more severe.

CONCLUSIONS

The comparison which has been made between experimental test results and the tabulated data proposed in Eurocode 2 shows that there is very little correlation and that the results proposed by the Eurocode are almost systematically on the unsafe side.

A model has been proposed which has a good correlation with the results of a series of 82 experimental tests. The new model allows to determine the solution very easily even for a combination of the parameters which is different from the one proposed in the table. This is achieved by a simple interpolation equation.

REFERENCES

[1] ENV 1992-1-2, *Eurocode 2: Design of concrete structures - Part 1-2: General rules - Structural fire design*, CEN, Brussels, November 1995.

[2] Dotreppe J-C., Baus R., Franssen J.-M., Brüls A. & Vanderzeypen, Y., *Dimensionnement des colonnes en béton armé en considérant le problème de la résistance au feu*. Rapport de Clôture, Convention F.R.F.C. N° 29010.90/F, Service des Ponts et Charpentes, Université de Liège, 1995.

[3] Hass R., *Zur Praxisgerechten Brandschutztechnischen Beurteilung von Stutzen aus Stahl und Beton*, Inst. für Baustoffe, Massivbau und Brandschutz der Technischen Universität Braunschweig, Heft 69, 1986.

[4] Lie T. T. & Woolerton J. L., *Fire resistance of reinforced concrete columns - Test results*, Int. Report N°569, National Research Council, Institute for Research in Construction, Ottawa, 1988.

[5] Franssen J.-M., Kodur V. K. R. & Mason J., *User's Manual for SAFIR (Version NZ). A Computer Program for Analysis of Structures Submitted to the Fire*, Univ. of Liege, Ponts et Charpentes, Rapport interne SPEC/2000_03, 2000

[6] Dotreppe J.-C., Franssen J-M., Brüls A., Baus R., Vandevelde P., Minne R., Van Nieuwenburg D. & Lambotte H., *Experimental research on the determination of the main parameters affecting the behaviour of reinforced concrete columns under fire conditions*, Magazine of Concrete Research, 49, N° 179, Thomas Telford Ltd, London, pp. 117-127 (1997).

[7] Aldea C.-M., Franssen J.-M. & Dotreppe J-C. *Fire tests on normal and high strength reinforced concrete columns*, Proceedings of the International Workshop on Fire Performance of High Strength Concrete, NIST-National Institute of Standards and Technology, Gaithersburg, Maryland, USA, pp. 109-124 (1997).

APPENDIX

I   Basic equations for the calculation of the resistance of the column

The method is the method called *model column* and explained in Eurocode 1 Part 1-1. It goes as follows.

First order eccentricity of the load $e_0 = 0,6\ e_1 + 0,4\ e_2 \geq 0,4\ e_1$

Accidental eccentricity $e_a = \dfrac{v\,L}{2}$

with $v = \dfrac{1}{100\sqrt{L/100}} \geq \dfrac{1}{200}$

External equilibrium $e_{ext} = e_0 + e_a + \dfrac{\chi\,L^2}{10}$ (I.1)

Internal equilibrium $e_{int} = \dfrac{M_{int}(N_{int},\chi)}{N_{int}}$ (I.2)

Equation I.1 and I.2 are solved with the use of a spreadsheet:

- The straight line corresponding to equation I.1 is first drawn in a (χ ; e) plan.

- For successive and increasing values of N_{int}, the curves corresponding to equation I.2 are drawn in the same plane. For each value of N_{int}, different points of the curve are found by giving successive and increasing values to χ and computing with the spreadsheet the value of M_{int} and, hence, of e_{int}.

- The ultimate load is the one that yields a curve I.2 which is tangent to the line I.1.

II   Main parameters of the experimental tests

Lab.	As	a	b1	b2	L	fcm	fym	e_sup	e_inf	N_d,fi	R_d	υ_{fi}	Rd,fi(0)	μ_{fi}	Rf Test	Rf Model
	cm²	mm	cm			kN/cm²		cm		kN	kN		kN	□	min.	
TUBr	9.2	30	20	20	571	4.2	48.0	10.0	10.0	140	206	0.68	252	0.56	31	25
TUBr	9.2	30	20	20	571	4.2	48.0	5.0	5.0	172	292	0.59	371	0.46	35	32
TUBr	12.6	38	20	20	476	3.1	46.2	2.0	2.0	240	463	0.52	630	0.38	36	50
TUBr	18.9	38	30	30	470	3.5	50.5	0.5	0.5	1 548	1 964	0.79	2 988	0.52	38	49
TUBr	12.6	38	20	20	576	3.2	44.3	1.0	1.0	208	416	0.50	590	0.35	40	40
TUBr	9.2	30	20	20	571	4.2	47.7	1.0	1.0	245	479	0.51	712	0.34	40	39
TUBr	12.6	38	20	20	476	2.4	48.7			340	575	0.59	799	0.43	48	43
TUBr	18.9	38	30	30	476	3.8	40.4	0.5	0.5	1 224	1 956	0.63	3 105	0.39	48	65
TUBr	12.6	38	20	20	476	3.1	46.2	1.0	1.0	280	540	0.52	766	0.37	49	50
TUBr	12.6	38	20	20	476	3.1	46.2	6.0	6.0	170	307	0.55	390	0.44	49	46
TUBr	18.9	38	30	30	470	3.2	50.3	15.0	15.0	280	715	0.39	923	0.30	49	95
TUBr	9.2	30	20	20	571	4.2	48.2	1.0	1.0	175	479	0.37	712	0.25	49	53
TUBr	18.9	38	30	30	470	3.2	52.6	15.0	15.0	465	727	0.64	941	0.49	50	64
TUBr	9.2	30	20	20	571	4.2	48.5	5.0	5.0	122	292	0.42	371	0.33	52	48
TUBr	12.6	38	20	20	476	3.1	46.2	10.0	10.0	130	227	0.57	282	0.46	53	44
TUBr	18.9	38	30	30	470	3.2	50.3	1.0	1.0	970	1 753	0.55	2 654	0.37	55	74
TUBr	18.9	38	30	30	376	4.2	45.2	0.5	0.5	1 695	2 347	0.72	3 723	0.46	57	67
TUBr	18.9	38	30	30	470	3.2	52.6	1.0	1.0	1 308	1 775	0.74	2 662	0.49	57	54
TUBr	18.9	38	30	30	576	2.4	48.7			800	1 475	0.54	2 126	0.38	58	62
TUBr	12.6	38	20	20	376	2.4	48.7			420	743	0.57	1 027	0.41	58	57
RUG	6.8	31	30	20	390	3.1	49.3	2.0	2.0	300	637	0.47	986	0.30	60	71
RUG	6.8	41	30	20	390	3.3	49.3	2.0	2.0	283	608	0.47	972	0.29	60	96
RUG	8.0	33	30	30	390	3.4	57.6			950	1 773	0.54	2 858	0.33	61	59
TUBr	18.9	38	30	30	576	2.4	48.7	3.0	3.0	600	1 119	0.54	1 564	0.38	61	62
Ulg	8.0	33	30	30	210	2.9	57.6			1 270	1 751	0.73	2 840	0.45	63	61
TUBr	18.9	38	30	30	476	2.4	48.7	3.0	3.0	650	1 244	0.52	1 809	0.36	63	77
TUBr	18.9	38	30	30	476	3.1	46.2	15.0	15.0	362	679	0.53	878	0.41	65	76
TUBr	12.6	38	20	20	376	2.4	48.7			420	743	0.57	1 027	0.41	66	57
TUBr	18.9	38	30	30	476	3.1	46.2	3.0	3.0	650	1 406	0.46	2 115	0.31	69	85
TUBr	9.2	30	20	20	571	4.2	47.8	1.0	1.0	128	479	0.27	712	0.18	72	64
TUBr	18.9	38	30	30	476	3.1	46.2	9.0	9.0	460	902	0.51	1 288	0.36	75	79
RUG	10.2	34	20	20	189	5.1	22.0			468	1 208	0.39	2 030	0.23	79	95
RUG	3.1	30	20	20	189	4.7	22.0			385	997	0.39	1 729	0.22	80	85
TUBr	18.9	38	30	30	476	3.1	46.2	3.0	3.0	650	1 406	0.46	2 115	0.31	80	85
TUBr	18.9	38	30	30	376	2.4	48.7			930	1 754	0.53	2 616	0.36	84	91
TUBr	18.9	38	30	30	476	3.1	46.2	1.5	1.5	740	1 596	0.46	2 434	0.30	85	85
TUBr	18.9	38	30	30	376	2.4	48.7	3.0	3.0	710	1 341	0.53	2 003	0.35	86	91
TUBr	18.9	38	30	30	333	4.3	54.4	15.0	15.0	355	969	0.37	1 282	0.28	89	121

Lab.	As cm²	a mm	b1 cm	b2 cm	L	fcm kN/cm²	fym	e_sup cm	e_inf cm	N_d,fi kN	R_d kN	υ_fi	Rd,fi(0) kN	μ_fi	Rf Test min.	Model min.
RUG	15.3	34	30	20	160	4.0	22.0			558	1 503	0.37	2 491	0.22	91	129
RUG	16.1	33	40	40	390	3.0	57.6	2.0	2.0	1 650	2 590	0.64	4 240	0.39	93	77
TUBr	18.9	38	30	30	476	3.2	49.9	-1.5	1.5	735	1 807	0.41	2 725	0.27	93	92
Ulg	6.8	41	30	20	210	2.7	49.3			620	1 028	0.60	1 649	0.38	97	106
RUG	4.7	30	30	20	160	4.5	22.0			457	1 321	0.35	2 280	0.20	101	121
Ulg	6.8	31	30	20	210	3.1	49.3			611	1 138	0.54	1 837	0.33	107	89
TUBr	18.9	38	30	30	476	2.4	48.7			880	1 630	0.54	2 400	0.37	108	75
TUBr	18.9	38	30	30	266	3.3	45.8	3.0	3.0	845	1 743	0.48	2 732	0.31	111	115
RUG	8.0	33	30	30	390	2.9	57.6			422	1 584	0.27	2 525	0.17	116	92
RUG	8.0	33	30	30	390	3.5	57.6			622	1 834	0.34	2 967	0.21	120	82
RUG	6.8	31	30	20	390	3.0	49.3	2.0	2.0	178	615	0.29	947	0.19	120	94
RUG	6.8	41	30	20	390	3.2	49.3	2.0	2.0	334	606	0.55	970	0.34	120	85
RUG	8.0	48	30	30	390	3.7	57.6	2.0	2.0	349	1 528	0.23	2 466	0.14	123	139
Ulg	8.0	33	30	30	210	2.9	57.6			803	1 720	0.47	2 782	0.29	123	93
RUG	4.7	40	30	20	160	4.5	22.0			457	1 499	0.30	2 595	0.18	124	158
RUG	8.0	33	30	30	390	3.7	57.6	2.0	2.0	220	1 568	0.14	2 525	0.09	125	109
TUBr	18.9	38	30	30	266	3.3	41.8	5.0	5.0	780	1 458	0.53	2 275	0.34	125	108
RUG	16.1	33	30	30	390	3.6	57.6	2.0	2.0	370	1 704	0.22	2 682	0.14	126	119
RUG	8.0	33	30	30	390	3.3	57.6	-2.0	2.0	664	1 687	0.39	1 584	0.42	128	76
RUG	15.3	44	30	20	160	4.9	22.0			558	1 785	0.31	2 987	0.19	131	170
TUBr	18.9	38	30	30	476	3.8	44.9	-3.0	3.0	645	1 886	0.34	2 946	0.22	135	101
TUBr	18.9	38	30	30	376	2.4	48.7			930	1 754	0.53	2 616	0.36	138	91
NRC	20.4	61	31	31	191	3.5	44.4			1 778	2 583	0.69	4 073	0.44	146	143
TUBr	18.9	38	30	30	333	3.1	43.3	1.5	1.5	735	1 737	0.42	2 711	0.27	160	112
NRC	20.4	61	31	31	191	3.7	44.4			1 333	2 691	0.50	4 264	0.31	170	175
NRC	12.6	58	20	20	191	4.2	44.2			169	1 295	0.13	2 017	0.08	180	212
NRC	20.4	61	31	31	381	4.0	44.4	2.5	2.5	1 000	1 892	0.53	2 987	0.33	181	133
NRC	20.4	61	31	31	267	3.8	44.4	2.5	0.0	1 178	2 292	0.51	3 650	0.32	183	157
NRC	20.4	61	31	31	191	3.8	44.4			1 333	2 763	0.48	4 392	0.30	187	177
NRC	20.4	61	31	31	191	4.4	44.4			1 044	3 037	0.34	4 874	0.21	201	202
NRC	20.4	61	31	31	191	3.6	44.4			1 067	2 650	0.40	4 191	0.25	208	191
NRC	20.4	61	31	31	191	3.5	44.4			916	2 614	0.35	4 128	0.22	210	201
NRC	65.5	80	41	41	191	4.6	41.4			2 978	6 504	0.46	10 026	0.30	213	307
NRC	20.4	61	31	31	191	3.4	44.4			800	2 552	0.31	4 019	0.20	218	208
NRC	20.4	61	31	31	191	3.5	44.4			711	2 598	0.27	4 100	0.17	220	215
NRC	20.4	61	31	31	267	3.9	44.4			1 000	2 604	0.38	4 138	0.24	220	179
NRC	40.9	61	31	31	191	3.7	44.4			1 333	3 447	0.39	5 144	0.26	225	221
NRC	20.4	61	31	31	191	5.3	44.4			1 178	3 516	0.34	5 720	0.21	227	204
NRC	20.4	61	31	31	191	5.0	44.4			1 067	3 341	0.32	5 411	0.20	234	207
NRC	20.4	61	31	31	267	4.0	44.4			800	2 623	0.30	4 172	0.19	242	193
NRC	40.9	61	31	31	191	4.3	44.4			978	3 724	0.26	5 603	0.17	252	246
NRC	40.9	61	41	41	191	3.9	44.4			2 418	5 112	0.47	8 051	0.30	262	226
NRC	65.5	64	41	41	191	3.8	41.4			2 795	5 804	0.48	8 792	0.32	285	237
NRC	31.0	59	31	46	191	4.3	41.4			1 413	4 397	0.32	7 074	0.20	356	241